Monolithic beam to external column joints in reinforced concrete.

Jubin Motamed

School of Architecture and the Built Environment

Monolithic Beam to External Column Joints in Reinforced Concrete

By

Jubin Motamed

A thesis submitted to the University of Westminster

in partial fulfilment of requirements for

the degree of Doctor of Philosophy

Department of Architecture

School of Architecture and the Built Environment

University of Westminster

35 Marylebone Road, London NW1 5LS

United Kingdom

February 2010

This thesis is dedicated to people who support research

“The most imposing analyses have often shown an excellent correlation with known results but have failed to predict behaviour under untested circumstances”. Regan, P.E. [1-1]

Declaration

I hereby declare that this thesis is a result of my own independent endeavours and investigation, except where I have acknowledged other sources.

I further declare that this thesis has not been accepted or submitted for any other degree.

Candidate’s name: Jubin Motamed

Candidate’s signature:

Date of declaration:

Acknowledgements

I would like to thank all the staff of the University of Westminster who provided me with the opportunity to continue my postgraduate studies, in particular Jon Davis in the Construction Hall who made it possible for me to enjoy this research work during its experimental stage.

I would like to express my deepest gratitude to my supervisor Dr Abbas Al-Hussaini for his guidance, constructive criticism and highly professional help and support in all aspects of the project. I am also grateful to Professor Emeritus Paul E. Regan for his guidance and his research which stimulated my initial interest in the shear behaviour of concrete.

Finally, I wish to express my greatest appreciation to my family and friends for their care and concern throughout the duration of this work.

List of frequently used symbols and abbreviations

a	shear span from the centre of a concentrated load to the centre of a support (mm)
A_s	area of beam steel (mm^2)
A_{sje}	the cross-sectional area of the joint stirrups within the top $^5/_8$ of the beam depth below the main beam reinforcement (mm^2)
b	breadth of the beam (mm)
b_e	is the average of the beam and column widths (mm)
b_w	web width of the beam (mm)
d	effective depth of the beam (mm)
d_b	diameter of dowel bars (mm)
BCJ	beam column joints
C_{cent}	compression force balancing strut formed by the CVB (N)
C_{col}	compression force balancing strut formed by column load on the rear side (N)
C1	factor involving unknown effect of combined stresses
C_1	compressive force balancing struts formed by the uncracked part of the beam (N)
C'_1	compressive force balancing struts formed by the cracked part of the beam (N)
C_s	compressive force balancing struts formed by the stirrups (N)
C_{stir}	the compression force balancing struts formed by stirrups (N)
C_t	the compression force balancing strut formed by tension reinforcement at the bottom (N)
CVB	central vertical bars
C_w	the compressive force balancing strut fromed by HWB (N)
d	effective depth to tension reinforcement (mm)
d_b	diameter of each HWB (mm)
D_{cr1}	dowel force in a single HWB (N)
f	distance from the crack to the first stirrup (mm)
f_c	cylinder compression strength of concrete (N/mm^2)
f_c'	cylinder compression strength of concrete (N/mm^2)
f_{ct}	indirect tensile strength (N/mm^2)
f_{cu}	cube compression strength of concrete (N/mm^2)
FE	finite element ,
f_y	yield stress of reinforcement (N/mm^2)
l_a	lever arm between C_1 and T_1 (mm)
L_b	lever arm between T_w and T_1 (mm)
I	moment of inertia of the structure from the transformed section (mm^4)
J_v	moment of inertia of dowel bars + concrete cover directly below bars. (mm^4)
h_b	section depth of beam (mm)
h_c	section depth of column (mm)
H	height of column between points of inflection
HSC	high strength concrete
HWB	horizontal web bars
M	beam moment at the column face (Nmm)
M_{dw}	dowel moment resisted by HWB in the shear span (Nmm)
n	is number of dowel bars,
NSC	normal strength concrete
STM	strut and tie model
T_1 & T	tension in the beam reinforcement at centre of flexural span (N)
T_2	tension in the beam reinforcement at centre of shear span (N)
T_{dw}	tension in the beam HWB at centre of flexural span (N)
T_b	tension in the beam reinforcement (N)

TBCJ	transfer beam column joints
T_{cent}	tension in the column central reinforcement (N)
T_{col}	tension in the column rear reinforcement (N)
V_a	strut formed to balance aggregate interlock in direction of shear crack (N)
V_{ax}	strut formed to balance aggregate interlock in horizontal direction at shear crack (N)
V_{ay}	strut formed to balance aggregate interlock in vertical direction at shear crack (N)
V_{col}	horizontal shear force across the column (N)
V_{du}	dowel force (N)
V_{dw}	strut formed by HWB dowel action to resist shear in direction of shear crack (N)
V_{dwx}	strut formed by HWB dowel action to resist shear in horizontal direction at shear crack (N)
V_{dwy}	strut formed by HWB dowel action to resist shear in horizontal direction at shear crack (N)
$V_{Rd,c}$	calculated design shear resistance of a member without shear reinforcement (N)
V_{Rk}	calculated characteristic shear resistance (N)
$V_{Rk,c}$	calculated characteristic shear resistance of a member without shear reinforcement (N)
V_s	struts formed to balance the tension in the stirrups (N)
V_t	strut formed to balance tension steel at the bottom (N)
Vu	experimental ultimate shear force (N)
V_w	strut formed to balance web bar at the centre (N)
V_j	beam column joint shear (N)
Vjc	joint shear force due to beam loading at failure (N)
V_{jd}	Design value of jont shear force (N)
Vje	joint shear due to beam load (N)
V_{jo}	uniaxial joint shear strength (N)
V_{jv}	vertical joint shear force from the equilibrium of the stress resultants (N)
Z	flexural lever arm (mm)
λ	steel strength factor = 1.25
$\phi_{m,min}$	minimum mandrel bent diameter for anchorage of the beam bar (mm)
ϕ	bar diameter when designing minimum mandrel bent diameter for anchorage (mm)
σ_{be}	design bearing stress (N/mm^2)
ρ_l	ratio of tension reinforcement (A_s/bd)
ρ'_l	ratio of compression reinforcement (A'_s/bd)
ρ_w	ratio of web reinforcement (vertical stirrups)
α	is conservatively taken as 0.2 $MPa^{0.5}$ and is dependent on factors depending on column load, concrete strength, stirrup index and joint aspect ratio
β	is 0.9 for U detail beam reinforcement and 1 for L bent down

ABSTRACT

The benefits of high strength concrete (HSC) in the construction of multi-storey buildings are commonly acknowledged. Past researchers have investigated the suitability of design codes for the use of HSC [1-2]. However, there are concerns about the shear behaviour of HSC beams and BCJ used in the construction of these buildings. HSC beams have equal or less shear resistance compared to normal strength concrete (NSC) beams [1-3], and the brittleness of HSC material could be unsuitable for BCJ as confinement stirrups may not be as effective as NSC in the column due to a smaller Poisson's ratio.

This research investigates the behaviour of HSC beams, BCJ and transfer beam column joints (TBCJ), and develop appropriate design modifications to improve their shear capacity.

HSC beams were strengthened with horizontal web bars (HWB), while TBCJ were strengthened with central vertical bars (CVB).

Finite element (FE) models were developed for these structures and the numerical results were compared with those of the published experimental results, concluding that good agreement had been achieved. Beam span/depth (a/d) ratio of $1.5 \leq a/d \leq 3.02$ and BCJ of beam to column depth (d_b/d_c) ratio of $1.33 \leq d_b/d_c \leq 3.1$ were analysed. The FE models were compared with published test results and further ones were developed to carry out various parametric investigations.

Struts and ties were mechanically modelled for beams with HWB and for TBCJ with CVB are used to recommend design equation modifications for the design of HSC beams with HWB and TBCJ with CVB.

It was found that HWB and CVB are effective in beams and BCJ only with HSC as they have little influence when they were used with NSC. Using HWB in HSC beams and CVB in HSC TBCJ improved the shear capacity of these structures by 130% and 31% respectively.

Contents

LIST OF FIGURES

LIST OF TABLES

Chapter 1
Introduction

1.1 Preface

Failure of corner BCJ due to shear failure in multi- storey reinforced concrete frames is a common occurrence when severe blast, impact or seismic loadings are applied to the frame, therefore, international codes of practice recommend closely spaced confinement stirrups reinforcement at BCJ to resist large shear forces when exposed to severe lateral loading.

The lower Poisson ratio of HSC means that confinement stirrups are less strained and are therefore less effective in HSC compared to NSC. Also the face of cracks in HSC are smoother than in NSC because of aggregate fracture. Hence shear resisting mechanisms involving aggregate interlock are less in HSC than in NSC. In spite of the mentioned disadvantages, HSC has become a popular material for the construction of high rise buildings in the industrialised world.

The aim of this research is to introduce an alternative shear reinforcement made of CVB placed in HSC columns at BCJ to improve shear resistance and to avoid the need for excessive stirrups. Congestion of stirrups can often leads to obstruction of the poker vibrator's head and full compaction of the column cover which leads to 'honey combing' in the cover and therefore weaker concrete column sections.

The presence of CVB in HSC columns reduces the lateral inter-storey drift and therefore delays the collapse of the structure when lateral loading is applied to the RC frame providing additional time for occupants to leave the building.

Lighter HSC columns produce less gyration forces and smaller lateral drift from severe lateral loading compared to the larger and heavier NSC columns. The use of HSC enables more economical foundations and more floor space.

1.2 Background

Morsch truss analogy

The idea of dowel action in tension reinforcement influencing shear resistance in

reinforced concrete was first recognised by Morsch [1-4] at the beginning of the twentieth century. The element shown in Figure 1-1 is assumed to be at the neutral axis of a concrete beam, and has shear stresses acting on faces AC and BD.

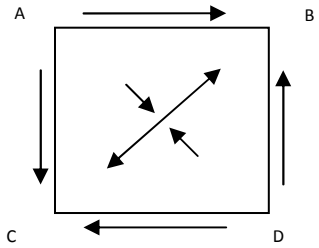

Figure 1-1: Acting shear stresses

For equilibrium, complimentary shears of the same magnitude must act on faces AB and CD in such a direction as to prevent rotation of the element, Figure 1-1. The strength of materials theory shows that the effect of these stresses is to produce tensile and compressive forces acting on the diagonal planes BC and AD. These are the principal stresses, and are of the same magnitude as the original shear stresses.

Application of this theory to concrete sections would therefore suggest that the presence of shear stresses in a concrete section causes tensile cracking in the concrete at an angle of 45° to the neutral axis . This is the basis of the Morsch truss analogy.

The origin of shear cracking in beams was anticipated from the stress distribution shown in Figure 1-2(a). When the longitudinal stresses are missing, the constant shear, $\tau = V/bz$, underneath the neutral axis gives rise to equal principal tensions and compressions, and the tensions cause diagonal cracks when they approach the tensile strength of concrete. Morsch understood that some of the transverse force could be carried by inclination of the main compression, while the ribs of concrete between flexural cracks would bend and produce dowel forces in the main steel, Figure 1-2(b).

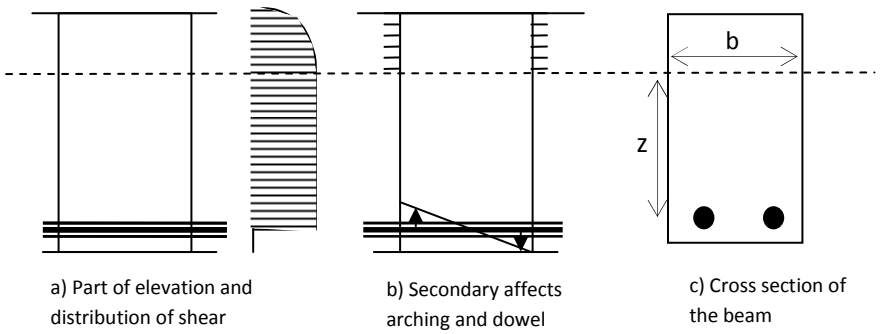

Figure 1-2: Stress distribution on the width and secondary effects

Beams with stirrups are treated by truss analogy with the web compression at 45° to the longitudinal axis, Figure 1-3.

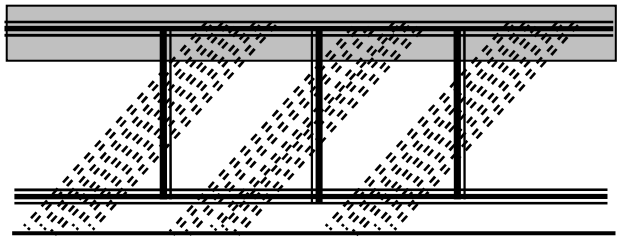

Figure 1-3: Truss analogy with the web compression at 45° to the longitudinal axis

In general, when considering shear reinforcement made of vertical links, the basic theory assumes that the reinforced section behaves in a fashion similar to that of a pin-jointed truss, with concrete taking the compressive forces and the reinforcement providing the tensile support**,** Figure 1-4. However, a 45° truss model produces a conservative solution as it makes no allowance for the effects of the uncracked concrete in the compression zone, aggregate interlock, or dowel action from the longitudinal reinforcement. It presumes that once the concrete has cracked as a result of the diagonal tension, no contribution can be expected from the concrete and all tensile and shear forces should be carried by the reinforcement.

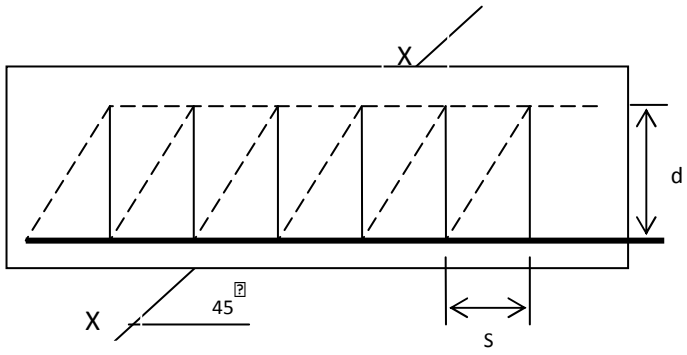

Figure 1-4:Members of a pin jointed truss with concrete (---) compression and steel (__) tension. α = 45°

Mechanism of shear transfer

Shear failure of reinforced concrete, more properly called diagonal tension failure is difficult to predict accurately. In spite of a century of experimental research [1-4] and use of analytical Finite Element software, it is not yet fully understood. Furthermore, if a beam or BCJ without appropriately designed shear reinforcement is overloaded to failure, shear collapse is expected to happen suddenly, with no advance warning of the failure.

This sudden mode of shear failure is totally different from the mode of flexural failure,

which is, for a typically under reinforced beams, failure starts with gradual yielding of the flexural steel, together with apparent cracking of the concrete and large sagging, giving abundant safety warning and providing the opportunity to retrofit the beam..

The four mechanisms of shear transfer are: shear stresses in uncracked concrete, interface shear transfer, often called "aggregate interlock" or "crack friction", the dowel action of the longitudinal reinforcing bars, and arch action. The 1998 ASCE-ACI Committee 445 Report highlights a new mechanism, residual tensile stresses, which are transmitted directly across cracks. Opinions vary about the relative importance of each mechanism in the total shear resistance, resulting in different models for members without transverse reinforcement.

Analogy of short beams to BCJ

Taylor [1-5] investigated the similarity of the shear behaviour of short beams with that of BCJ. He concluded that the relation between shear on a short beam and shear in a BCJ zone is such that the shear span to effective depth ratio (a/d) in a short beam is analogous to the ratio of the beam lever arm to the column effective depth in a BCJ (z_b/d_c).

Experimental tests

The experimental research investigated was comprised of three series of tests: two short beams without stirrups [1-6], twelve beams of HSC and NSC with stirrups and HWB [1-8], and two BCJ [6]. The tests were carried out under static concentrated loads and were supplemented with a large number of strain measurements in reinforcement and concrete struts.

1.3 Aims and Objectives

Aim:

To investigate the behaviour of monolithic beam to external column joints in reinforced concrete multi-storey building frames and the influence of CVB on the shear behaviour of joints.

Objectives:

1. to study the shear behaviour of HSC beams with HWB and stirrups.
2. to verify and validate FE modelling of the behaviour of HSC beams with HWB and shear stirrups
3. to investigate the behaviour of BCJ and influence of CVB on shear capacity.

4. to develop strut and tie model
5. to develop modified design equation for HSC BCJ
6. to verify and validate FE modelling for BCJ
7. to carry out parametric investigation on factors influencing the behaviour of the joint.

1.4 Present work

This research is concerned with studying the effects of CVB in HSC columns at external TBCJ.

To carry out this investigation, FE models and STM were developed to analyse the behaviour of the beams and TBCJ and to study the parameters influencing their behaviour in the following sequence:

- Numerical modelling of two NSC short beams [1-6] with different size support plates (a/d=1.5) and three NSC and HSC beams [1-8] with and without HWB (a/d=3.02) to verify and validate FE modelling of beam with experimental tests.
- Numerical modelling of two NSC BCJ [1-6] with and without stirrups to verify and validate FE modelling of BCJ with experimental tests.
- STM were developed for HSC beams with HWB of a/d=3.02 and were extended to similar HSC TBCJ with CVB of d_b/d_c=3.11.
- A FE parametric study for four TBCJ of NSC and HSC, with and without CVB, was completed.

1.5 Research methodology

To achieve the aims and objectives of the research programme, a number of different research methods were used.

- Initially, a review was carried out to study related up to date research projects and published materials on the subject. The results of this are given in the literature review in Chapter 2 which facilitated compilation of the objectives and the focus of the research direction.
- A detailed review of the experimental work completed for testing to failure of beams of a/d=3.02 [1-8] and short beams a/d=1.5, and BCJ [1-6] are presented in order to verify and validate the FE numerical models with the experiments in relation to failure loads, displacements, crack propagation and strain in the location of interest.

- To develop STM for HSC beams with stirrups and HWB of a/d=3.02, and after validating the predicted STM results with the experimental test results, the STM model for the beam was considered to be analogous to HSC TBCJ with CVB and stirrups .
- The data collected from past experiments on 56 BCJ specimens are used to investigate parameters effecting shear behaviour of BCJ. The data is used to examine the validity of existing design rules from codes and past researchers. The results obtained from this analysis are used to develop a design rule for HSC external BCJ with CVB.
- FE parametric investigations were performed to explore the effect of CVB and HSC on the behaviour of TBCJ [1-7].

1.6 Thesis presentation

Results of the research are presented in nine chapters as follows:
Chapter 1 contains background information on the topic, aims and objectives and research methodology.

Chapter 2 covers a general literature review of the past research on shear behaviour in RC beams. Actions and parameters influencing shear behaviour are discussed with special attention given to the past research on the influence of dowel action and aggregate interlock on shear behaviour. International codes and their recommendations for shear design are discussed.

Chapter 3 covers a detailed review of this writer's experimental tests on12 beams of NSC and HSC with shear links and various shear spans and diameter size for HWB[1-8]. There is a detailed analysis and discussion of the shear behaviour of the tested NSC and HSC beams with comparison of shear resistance from dowel action in NSC and HSC beams.

Chapter 4 begins with a literature review on nonlinear finite-element analysis of shear characteristics of reinforced concrete beams. An introduction of the experimental work two short beams a/d=1.5 [1-6] was followed with FE numerical modelling the beams, with different size support plates without links. Three beams with HWB in NSC and HSC with and without HWB of a/d=3.02 which were experimentally tested [1-8] were FE modelled. Results obtained from FE models for strains on the reinforcement are compared with those recorded from strain gauges [1-8].

Chapter 5 is a reviews of the principals of STM and develops STM for HSC beams of a/d=3.02 with links and HWB, and a solution was proposed for all the tensile forces in the

reinforcement and compressive forces in concrete struts of the beam STM was investigated. This investigation was further extended for a similar external HSC-TBCJ with CVB of d_b/d_c=3.11 [1-9] .

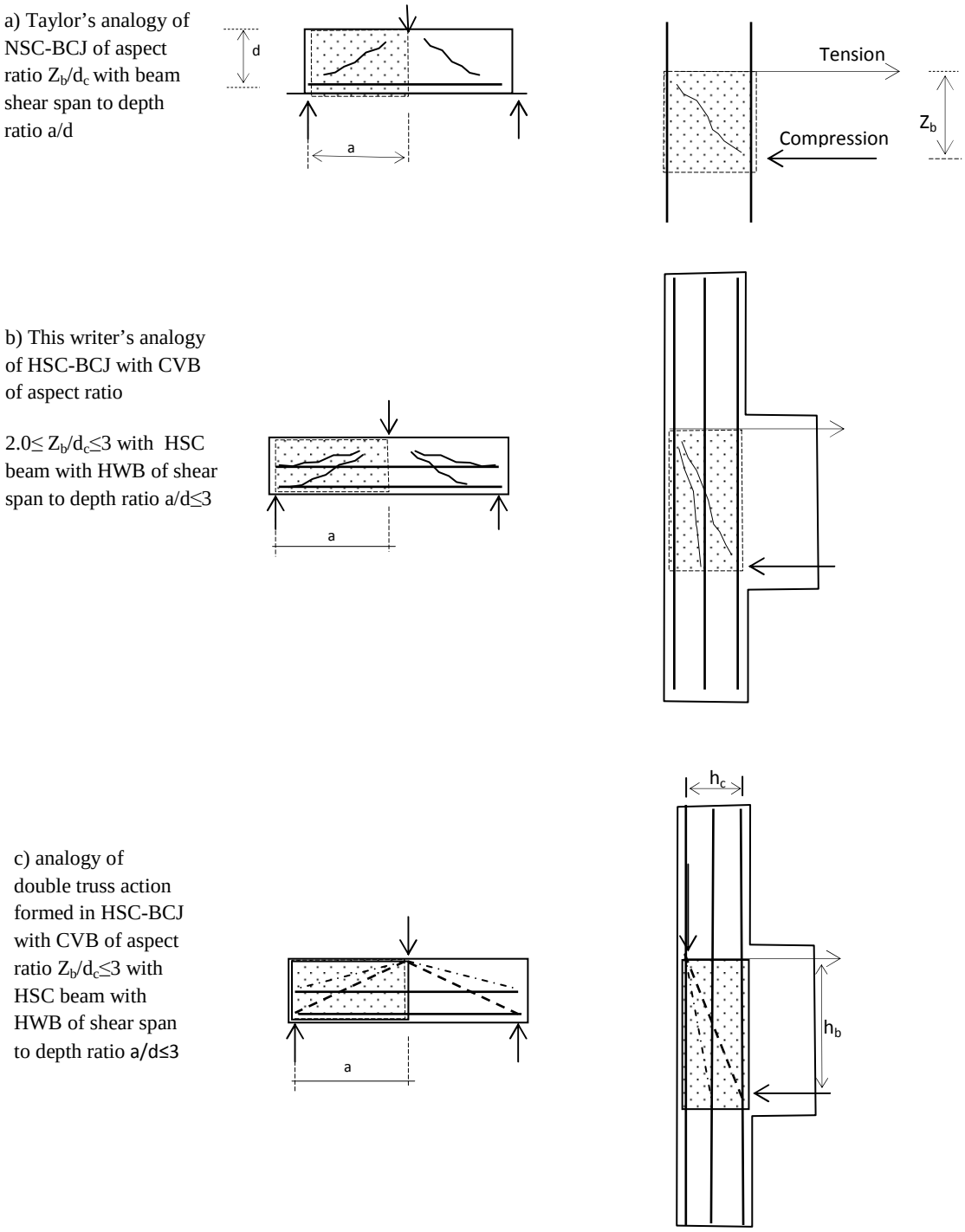

Figure 1-5: Types of NSC and HSC beams with and without HWB analogous to NSC and HSC-BCJ with and without CVB.

Chapter 6 the tests on BCJ are reviewed, and existing design rules for shear prediction of BCJ are discusses and a shear design rule is proposed by taking into consideration the improvement in joint shear resistance due to dowel action from CVB performing jointly with the confinement stirrups to prevent BCJ failure under extreme loading which has been recorded.

Chapter 7 is a review of experimental work on BCJ of aspect ratio 1.33 [1-6], FE numerical modelling of two NSC-BCJ, with and without stirrups. The strain recordings of reinforcement from the FE models are validated and verified with those of strain gauge readings from the experimental tests.

Chapter 8 covers the FE parametric investigation for four TBCJ, d_b/d_c=3.11, of HSC and NSC with stirrups, with and without CVB. Detailed study of the strain development along the reinforcement for NSC and HSC with and without CVB under loading up to failure demonstrates the influence of CVB and HSC in TBCJ.

Chapter 9 is a summary and conclusion of the results by analytical modelling of shear behaviour in HWB and CVB, comparing results obtained from numerical modelling and STM with those from the experimental tests and making suggestions for future research.

1.7 References

1-1 Regan, P. E. 'Research on shear: a benefit to humanity or waste of time?'. The Structural Engineer, Volume 71/No 19/5 October 1993.

1-2 Regan, P. E., Kennedy -Reid I. L., Pullen, A. D., Smith, D. A. 'The influence of aggregate type on the shear resistance of reinforced concrete' – The Structural Engineer. 6 December 2005. p 27-32.

1-3 Al-Hussaini, A. Motamed, J. 'HSC beams with combination of links and horizontal web steel as alternative shear reinforcement'. 6th International Symposium on Utilization of High Strength/High Performance Concrete, Leipzig, June 2002. p 611-619 http://www.jmotamed.spaces.live.com

1-4 Morsch, E. 'Der Eisenbetonau'. Published in English as 'Concrete-Steel construction'. New York, Engineering News Publishing Co. 1909, 3rd ed (1908).

1-5 Taylor, H.P.J. 'The Behaviour of In Situ Concrete Beam column Joints', Cement and Concrete Association, May 1974, Technical Report no. 42492, 33p.

1-6 Reys de Ortiz, I. 'STM of reinforced concrete short beams and beam column joints'. PhD thesis, 1993, University of Westminster.

1-7 Motamed, J. Al-Hussaini, A. 'Influence of central vertical bar on the behaviour of high strength concrete transfer beam-column joints' . Third International Conference on Concrete and Development.p.485-496 May 2009
http://www.irb.fraunhofer.de/CIBlibrary

1-8 Motamed, J. 'Shear in normal strength and high strength reinforced concrete beams with stirrups and horizontal web bars'. University of Westminster, MSc Dissertation, 1997

1-9 Motamed, J, Al-Hussaini, A. 'Strut-and-tie model for high strength concrete beams with combination of links and horizontal web bar'. 2nd International conference on recent advances in railway engineering, 27-28 Sept 2009, Iran University of Science and Technology, Iran

Chapter 2
Literature review

2.1 Introduction

This chapter starts with a short review of the history of shear with an emphasis on the most relevant early studies, experiments and analysis of shear behaviour in beams.

Available literature on different actions influencing the total shear strength are reviewed and the contribution of arching, dowel action and aggregate interlock towards shear resistance is discussed in detail.

International codes and their recommendations for shear design for beams with and without shear reinforcement are discussed. The design rules for shear in codes of practice are, at present, based mainly on experimental tests on NSC. Tests providing the basic data for these equations were conducted on members whose concrete strengths were mostly below 40 MPa. To ensure the safety and serviceability of HSC concrete, certain essentially empirical design procedures and equations based on the characteristics of concrete of lower strengths are reviewed.

A review of research on the adverse shear material property of HSC in particular when the aggregate is limestone is discussed and remedial measures to overcome the undesirable shear behaviour of HSC are proposed with the introduction of horizontal web bars (HWB) as shear reinforcement in the beam.

2.2 Shear behaviour of reinforced concrete

2.2.1 History of shear research

The first concrete structure is the Pantheon in Rome, which has a dome of 43 m in diameter, constructed during the 1st century AD. The dome becomes thinner as it rises, with its coffers becoming smaller towards the top. It is of lightweight concrete of pumice stone. It is an example of durable, high plasticity concrete. The gravitational load path is transferred through the dome by arching action to its supporting vaults.

The Pantheon dome has three layers of concrete of cement and aggregate as follows:

lower ring (1) brick fragments, middle ring (2) blocks of tufa and brick fragments, and the top ring (3) is pumice stone and blocks of tufa. The dome is a perfect hemisphere. The concrete for the walls of the rotunda supporting the dome is made from tufa and travertine chippings and the foundation supporting the wall is of 4.5m thick concrete with travertine chippings[2-1], Figure 2.1.

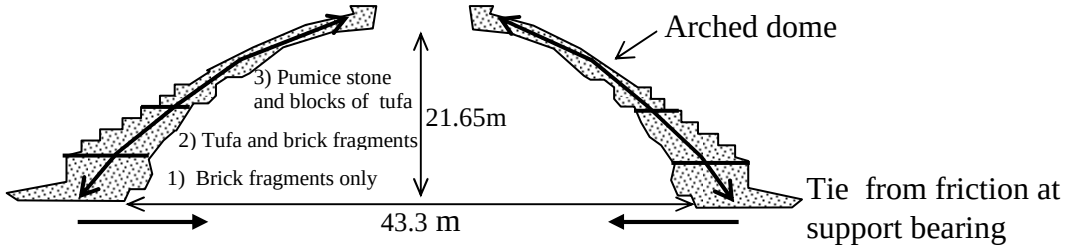

Figure 2.1: Section of Pantheon dome with 3 rings of different density concrete, showing the load path of the strut and tie

The first patented applications of reinforced concrete appeared in France and England between 1850-1860, and the first method of theoretical computation of slabs was devised by Koenen in Berlin in 1886 and Coignet and Tedasco in 1894. These theories assumed a linear variation of concrete stress with distance to neutral axis and the existence of an internal couple equilibrating the external loads. In 1897 Thullie, and two years later Ritter, advanced the ultimate strength theories based on non-linear stress distribution.

Design for shear in concrete beams by applying the horizontal shear approach was adopted based on the theory of elasticity. It was assumed that failure would occur when shear becomes greater than the shear capacity of the concrete. In an elastic homogeneous beam the horizontal shear stress at a distance y from the neutral axis is:

$$q_n = V \cdot \frac{A \cdot \bar{y}}{I \cdot b} \quad \textbf{2-1}$$

where:

V = shear force on the section.

A $\bar{y}$ = first moment of area about the neutral axis of the part section between the extreme fibre and a line distance y from the neutral axis.

I = moment of inertia of the entire section about the neutral axis.

b = width of the cross-section at a distance y from the neutral axis .

In the case of a rectangular section the equation defines a parabolic distribution of shear stress with its maximum value of 1.5V/bd at mid-height.

2.2.2 Pioneering analysts in the first half of 20th century

2.2.2.1 Ritter-Morsch analysis of shear

In 1899, the Swiss researcher Ritter suggested the concept of diagonal tension but his findings were largely ignored and overshadowed by horizontal shear theory [2-2].

In 1902, Emil Morsch [2-3] for the first time experimentally tested reinforced concrete beams failing in shear in the laboratory. In 1902, he published his tests of four reinforced concrete beams designed to study the action of vertical and inclined stirrups as well as bent-up bars. His paper indicated diagonal action as the cause of shear failures and introduced the truss analogy to describe the action of web reinforcement [2-3].

In 1902, Morsch analysed the shear stress distribution for a reinforced concrete beam containing flexural cracks. He predicted that shear stress would reach its maximum value at the neutral axis and would then remain constant from the neutral axis down to the flexural steel . The value of this maximum shear stress is:

$\tau = V/b_wZ$

where V is the total shear force and b_w is the web width and Z the flexural lever arm.

Morsch recognised that this was a simplification, as some of the transverse force could be resisted by an inclination in the main compression, which would cause the ribs of the concrete between flexural cracks to bend, producing dowel forces in the main steel.

By the turn of the century, Ritter [2-2] introduced the 'Truss analogy' for solving shear forces in beams, this analogy was further consolidated by Morsch [2-3].

Sewell suggested in 1903 that experimental tests demonstrated the creation of cracks along the lines of principal tensile stress and he called for a justifiable method to design stirrups to resist these principle stresses. Nevertheless, Thacher, in 1903, asserted that stirrups and bent-up bars in reinforced concrete beams were 'utterly useless'.

The newly proposed 'diagonal tension' and the older approach of 'horizontal shear' were the subjects of debate mainly in Europe and to some extent in America for almost ten years until the 'Ritter-Morsch' approach was finally accepted.

The traditional Ritter-Morsch proposal for distribution of shear stresses in beams without web reinforcement was derived as follows:

AB and A'B' are two adjacent sections d*l* apart between which on the plane C-C' there act shearing stresses balancing the difference between the normal forces on AC and A'C', Figure 2.2(a) & (b).

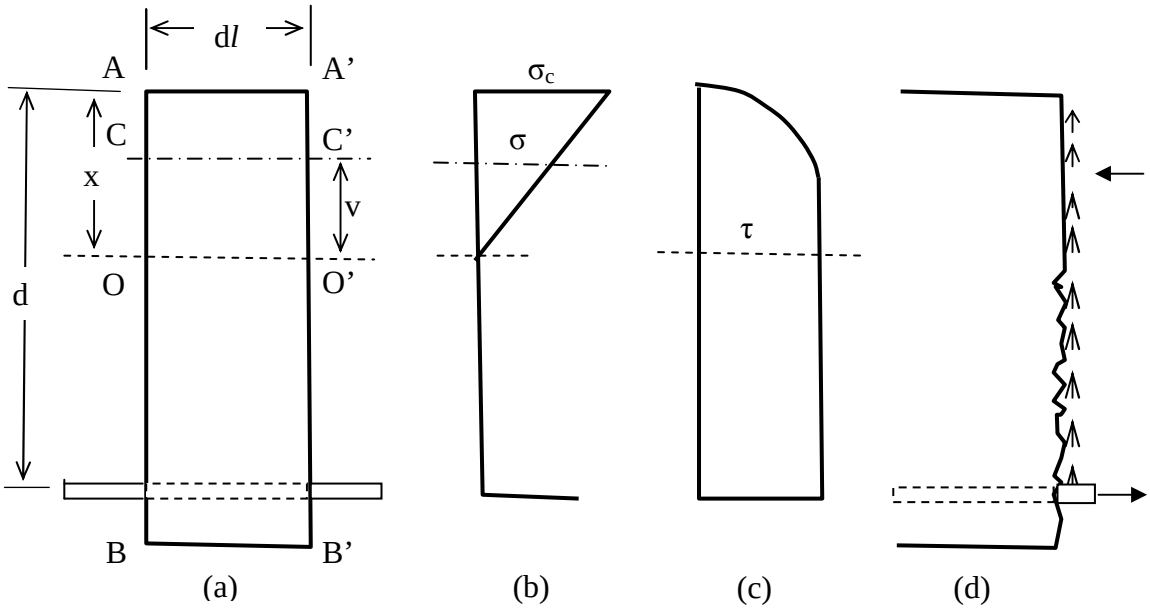

Figure 2.2: Traditional Ritter-Morsch shear theory:(a) Beam element of length d*l* in the shear span, (b) Longitudinal flexural forces, (c) The shear stress distribution and (d) Shear and flexural forces acting on the section along a flexural crack

Source: Morsch, E. 1908 [2-3]

Considering forces in plane of C–C'

$$\tau \cdot b \cdot dl = \int_{v}^{x} b \cdot d\sigma \cdot dv \qquad \textbf{(a)}$$

Where b is the beam width

Taking moment about the steel level

$$\sigma_C = \frac{2 \cdot M}{b.x(d - \frac{x}{3})}$$

$$\frac{d\sigma_C}{dl} = \frac{2 \cdot dM}{dl \cdot b.x(d - \frac{x}{3})} \qquad \textbf{or} \quad = \frac{2 \cdot V}{b.x(d - \frac{x}{3})} \qquad \textbf{(b)}$$

Where V represents the applied shear force shown in Figure 2.2 (d).

$$d\sigma = \frac{v}{x} \cdot d\sigma_C \qquad \textbf{(c)}$$

Substitute b and c in a

$$\tau \cdot b \cdot dl = \int_{v}^{x} b \cdot v.dv \cdot \frac{2V \cdot dl}{bx^2 \cdot \left(d - \frac{x}{3}\right)}$$

From which:

$$\tau = \frac{V(x^2 - v^2)}{bx^2(d - \frac{x}{3})} \qquad \textbf{2-2}$$

The above equation demonstrates that where v = x, the shearing stress is zero and it then increases towards neutral axis to:

$$\tau_o = \frac{V}{b(d - \frac{x}{3})} \qquad \textbf{2-3}$$

It is assumed that no normal stress acts in the concrete below the neutral axis, the whole tensile force being taken by the reinforcement . With this assumption, the shearing stress τ_o is constant between the line OO' and the reinforcement, Figure 2.2. It is then evident that the shearing stress τ_o balances the difference in the tensile stress between two adjacent sections of the reinforcement.

Therefore it follows that:

$$\tau_o \cdot b \cdot dl = dT \qquad \textbf{(d)}$$

But

$$T = \frac{M}{(d - \frac{x}{3})}$$

From which

$$\frac{dT}{dl} = \frac{dM}{dl.(d - \frac{x}{3})} \quad \text{or} \quad = \frac{V}{(d - \frac{x}{3})} \qquad \textbf{(e)}$$

Substituting (d) and (e) results in:

$$\tau_o = \frac{V}{(d - \frac{x}{3})}$$

Which is identical to $\tau_o = \frac{V}{b(d - \frac{x}{3})}$ 2-3

The value of $b.\tau_o$ also represents the total effective adhesive (bond) stress on a unit length of the circumference of the steel, and consequently the adhesive stress τ_1 is:

τ_1= b τ_o / total circumference of the reinforcement

The above derivation is reproduced from the third edition (1908) of Professor Morsch's pioneering book 'Concrete-steel Construction'. In 1909 this book was translated into English and was published in London and New York. Its first German edition was in 1902.

This derivation was based on zero longitudinal tensile stress in the tension zone, because of Morsch' s awareness of the existence of the flexural cracks, although he accepted a transverse uniform shear resistance in the tension zone. This, therefore, must mean that he was satisfied with the 'inevitable' availability of this resistance, τ_o , in the tension zone whether the section is taken between two adjacent cracks or at one of them, Figure 2.2d.

2.2.2.2 Morsch's concept of dowel action

Morsch [2-3] referred to the dowel action of the longitudinal reinforcement on many occasions. Although he did not mention the terms 'concrete teeth' and 'dowel action', his understanding of these two important concepts can be recognized from the following paragraphs which were written in his book [2-3]:

"On the concrete of a rib between two cracks must act the difference ΔZ of the tensions in the steel at the two cracks, this difference being the total frictional resistance between steel and concrete of the corresponding length. Further, the concrete exerts bending stresses on the reinforcing rod, as shown in Figure 2.3 a which counteract the deformation in the piece of concrete, which would be caused by ΔZ".

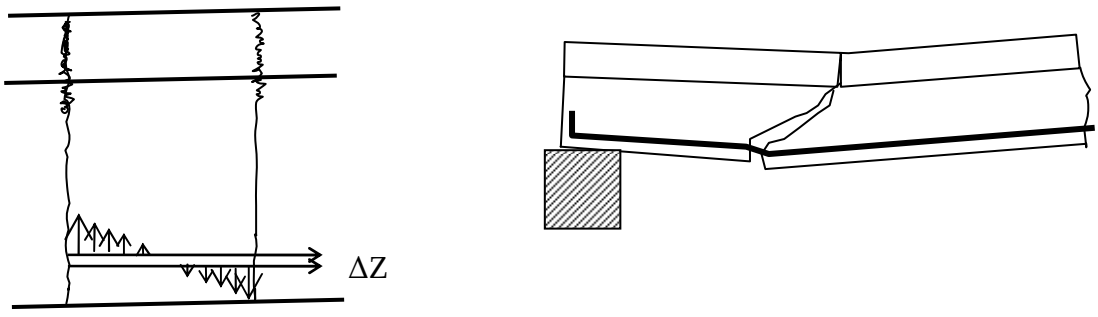

Figure 2.3: (a) the cantilevered concrete teeth. (b) dowel action of the main reinforcement

Source: Redrawn from Morsch, E. 1909 [2-3]

In another paragraph , he identified dowel action clearly and associated it with the tensile strength of the concrete beneath the bar. He proposed his concept as follows: "The turning of the two parts of the beam resulting from the opening of the cracks will cause

reinforcement on the right end of the left hand part of the beam to press downward, Figure 2.3 b , so that at that point in the steel a downward force will act which naturally can not be larger than the tensile strength between the concrete beneath the reinforcement and that in the rib above it".

Morsch tested 12 beams, out of which three beams had stirrups in one of the two shear spans only. He stated, in his description of the failure of one of the beams which had a single bent up bar in one span and stirrups on the other, that "failure resulted from a widening of the diagonal cracks and downward pressure of the reinforcement near the supports". Moreover, Morsch even emphasised the effect of the stirrups on this 'downward pressure' of the reinforcement in his studies of some other tests carried out by Carl von Bach and Otto Graf in1907 [2-4] on continuous rectangular and I-beams designed primarily for bond investigations. These tests were also fully discussed by Morsch who also stated that the "tensile strength of the stirrups prevented the downward pressure of the reinforcing rods near the supports after the appearance of diagonal cracks".

2.2.2.3 Other relevant research

In America, in 1909, Talbot [2-5] presented a study of 188 beams. His main conclusions regarding beams without web reinforcement were that the nominal shear strength increases with cement content, age of concrete, amount of longitudinal reinforcement and decreasing span of beam for the same cross-section.

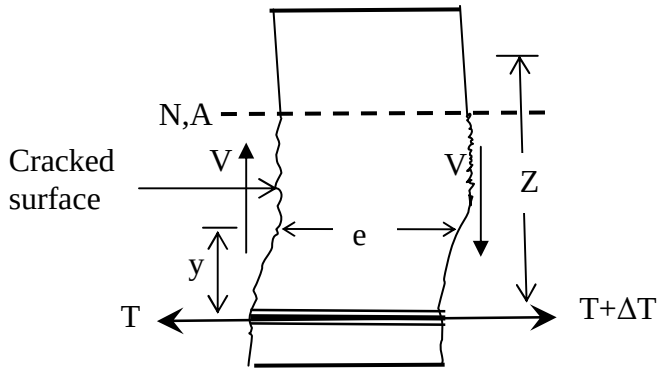

Figure 2.4: An element of a reinforced beam between two adjacent shear cracks
Reproduced from: Bjuggren, U. [2,6] 1948

The beginning of understanding of shear in beams without web reinforcement can be considered to be when the Swedish engineer Ulf Bjuggren [2-6], in 1948, made a specu1ative reconsideration of Morsch's 'teeth', Figure 2.3 a, and developed the concept

shown in Figure 2.4. His revised model resulted in an awareness of the likelihood of shear transfer across cracks.

From, Figure 2.4, by taking moment about the centre of concrete in compression, he derived that the difference of tensile forces in the tension steel is:

$$\Delta T = \frac{V.e}{Z} \quad \textbf{2-4}$$

This force gives a bending moment on the concrete between the cracks. In a horizontal section at a vertical distance y from the reinforcement this bending moment , M_t is:

$$M_t = \Delta T \cdot y = \frac{V \cdot e \cdot y}{Z} \quad \textbf{2-5}$$

Section modulus is = $\frac{be^2}{6}$

Corresponding to a flexural stress f_{ct} in the concrete:

$$f_{ct} = \frac{6 \cdot M_t}{b \cdot e^2} = \frac{6 \cdot V \cdot y}{z \cdot b \cdot e} \quad \textbf{2-6}$$

$$f_{ct} = \frac{6 \cdot y \cdot \tau}{e} \quad \textbf{2-7}$$

Where τ represents the maximum intensity of vertical shearing stress for rectangular beams.

At high steel stresses, when using steel with good bond, e can be smaller than 100mm, and it is easily seen that these bending stresses can be many times the computed shearing stresses. The concrete should break if no other forces counteract the mentioned bending moment. Bjuggren carried out his logical argument that such forces can only appear in the shape of shearing stresses between adjacent crack surfaces and they will appear only if the cracks are sufficiently small. Then he summarised the conditions required for a cracked reinforced, concrete beam to act as a true beam, i.e. for the steel stresses to vary substantially with the bending moment:

1. The bond between the steel and concrete shall be sufficient that the difference ΔT of the tensile forces can be transferred to the concrete.
2. The cracks shall be narrow enough so that the required shearing stresses can be developed in the crack surfaces.

By 1950, the number of tests on beams had reached around 1,000.

2.2.3 Recent research on shear in beams

This section is a review of general research on the understanding of shear in beams without stirrups.

In 1962, Moe [2-7] in a short discussion recalled attention to Bjuggren's [2-6] argument. Moe stated that in an arbitrarily chosen beam which was reported to have failed in inclined tension it was found that the vertical tensile stresses f_{ct} exceeded the nominal shearing stresses $\tau = V/bz$ by more than 100% , even when V_r, Figure 2.5, was assumed to be as high as 72% of the shear force V_t assigned to the cracked zone proportion of the beam according to the classical theory. He concluded that according to the established formulae

$$V_t = \tau \cdot b \cdot \gamma \cdot d = V \frac{\gamma}{j}$$

it appears reasonable to assume that the amount of shear transmission across the bending cracks decreases gradually as the widths of the cracks increase. At the same time the shearing stresses in the compression zone increase, Figure 2.5 (c). At a certain value of the crack width, the stresses in the cantilever become high enough to cause failure.

Figure 2.5 shows : a) The cantilever encastre near the neutral axis of the beam in the compression zone; b) Shear stresses according to the classical theory; c) Moe's suggested distribution of shear stresses.

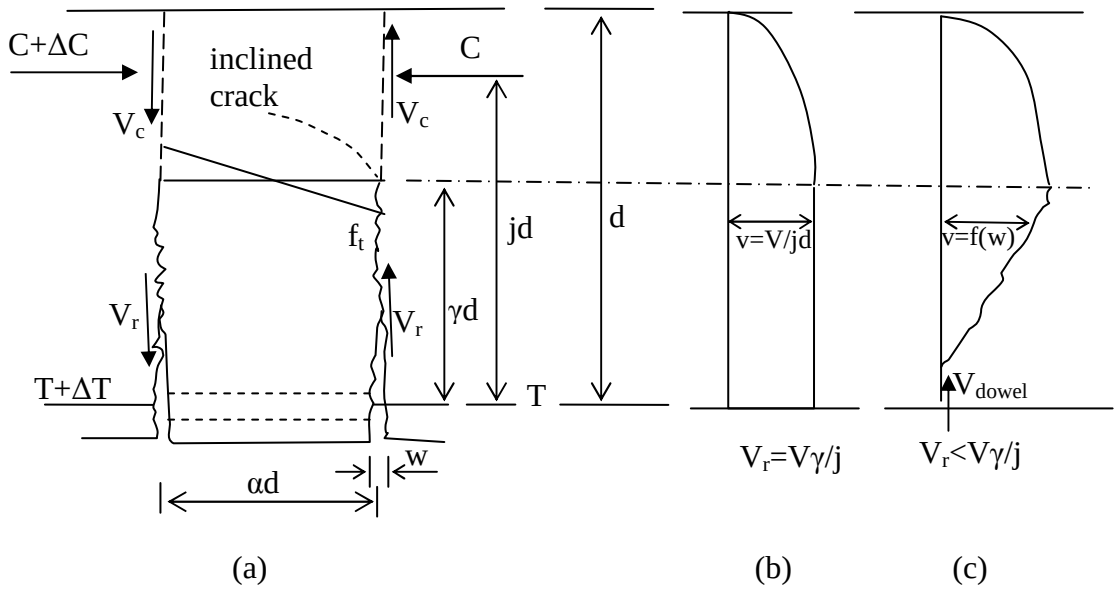

Figure 2.5: Suggested mechanism of inclined cracking in case of a/d>2.5

Moe's model does not give enough attention to Bjuggren's [2-6] first recommendation emphasing that bond between the steel and concrete should be sufficient that the difference ΔT of the tensile forces can be transferred to the concrete.

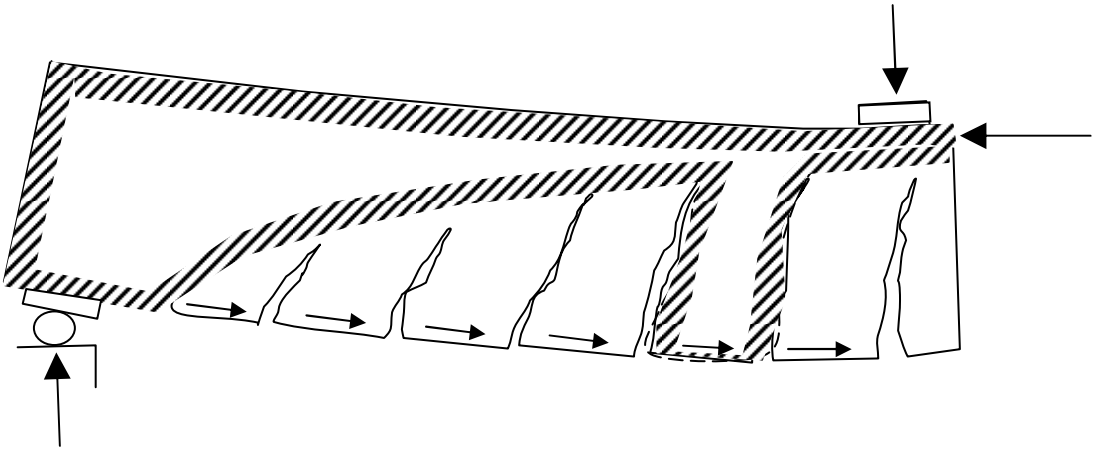

Figure 2.6: Comb-like cracked beam

In 1965, Lorentsen [2-8] proposed an analysis regarding the function of concrete teeth, Figure 2.6. By making the assumption that the teeth between cracks were infinitely narrow, he produced a function for dT/ds, the rate of change of tensile force along the beam, at which the teeth would fail.

According to his theory the shear is carried partly by beam action, partly by arch action. The theory led to an equation in which the shear strength of beams without web reinforcement may be expressed as a function of the strength of the crack lamina, the shear span, and the flexural cracking moment. The lamina strength being the sum of two components, k_a, the shear force carried by the reinforcement by dowel action and k_b the force carried by the compression zone. Thus: $k = k_a + k_b$. He then carried out a limited series of dowel tests to determine k_a and some splitting tests on, and analyses of, concrete plates to determine k_b. In his theory, not only the interlock forces were ignored, but the bond equation also was not realistic, since too much arch action was assumed prior to diagonal cracking.

In 1964, a similar presentation of a comb-like structure, Figure 2.6, was presented by Kani [2-9] by addressing the problem of the bending of the 'teeth' of the concrete between flexural cracks. The concrete between two adjacent flexural cracks was considered to be analogous to a tooth in a comb.

The concrete teeth were assumed to be free cantilevers fixed in the compression zone of the beams and loaded by the horizontal shear from bonded reinforcement. Although this theory did not cover most of the shear transfer mechanisms, it was probably the start of more rational approaches.

His analysis was based on Bjuggren's [2-6], $f_{ct} = \frac{6 \cdot M_t}{b \cdot e^2} = \frac{6 \cdot V \cdot y}{z \cdot b \cdot e}$ 2-6 which with Kani's notation is:

$$f_t' = \frac{M}{S} = \frac{6 \cdot \Delta T \cdot s}{b \cdot (\Delta x)^2} \qquad \textbf{2-8}$$

where:

S = The section modulus of a tooth

ΔT = The bond force as defined by Morsch, Figure 2.3 a.

s = Crack height

b = Beam width

Δx = Crack spacing.

f_t' = The tensile strength of concrete.

From this formula,

if ΔT/Δx , the rate of change of the steel force along the beam is assumed to be T/a, where a is the shear span; a relationship for the ultimate moment for the beam may be derived:

$\frac{T}{a} = \frac{f_t'}{6} \cdot \frac{\Delta x}{s} \cdot b$ assuming that lever arm is 7d / 8

$$M = \frac{f_t'}{6} \cdot \frac{7}{8} .b.d^2 \cdot \frac{\Delta x}{s} \cdot \frac{a}{d} \qquad \textbf{2-9}$$

This analysis ignores shear transfer by aggregate interlock and dowel action. Taylor [2-10] pointed out that "without the strengthening effect of the shear transferred across the cracks, Kani found that his theory would give good results only if very short teeth (very small S values) were used".

In 196, Fenwick and Paulay [2-11], working with 'tooth' models, pointed out the significance of the forces transferred across cracks in normal beams by crack friction. Taylor (1974) [2-14], also evaluating Kani's model, found that for normal test beams the components of shear resistance were: compression zone shear (20-40%), crack friction (35-50%) and dowel action (15-25%).

In 1975, based on extensive experimental work on interface shear, Hamadi [2-26] and Regan [2-25] proposed an analysis of the tooth model. It was assumed that the cracks were vertical and that their spacing was equal to half the effective depth of a particular beam. Their analysis will be discussed in detail in section. 2.2.7.5.

In 1982, Schlaich [2-12] suggested a refined strut and tie model (STM) approach that includes concrete tension ties. In 1991, Reineck [2-13] showed that such truss models comply with the tooth model he had proposed. Taking all the shear transfer mechanisms into account, carrying out a full nonlinear calculation including compatibility. Reineck [2-13] derived an explicit formula for the ultimate shear force based on his mechanical model which matched with the results of the test as well as with those of many empirical formulas.

In Chapter 5, the STM approach will be discussed and a a new model is developed to demonstrate that in HSC beams with HWB, the dowel moment, deflects the inclined diagonal compression strut in the STM to develop a better arching action.

With regards to Lorentsen [2-8] and Kani [2-9] neglecting the importance of the aggregate interlock and dowel action, this writer's experimental results in chapter 3, a graph in Figure 3-37 and six graphs in Figure3-39, demonstrate that strains in the links at the centre of shear span in HSC beams after the diagonal tension crack has widened and caused the stirrup resisting the crack opening to exceed well over its yield, the dowel (HWB) and arching action due to presence of HWB in HSC beam provides the final 40% shear resistance, that is from 90 to 150 kN shear force.

2.2.4 Influence of shear span to depth ratio (a/d)

Beam behaviour in resisting shear can be classified in various ways. The most popular parameter used to define boundaries between modes of action is the 'Shear span /effective depth' or a/d ratio, i.e. the distance from the support to the load over the effective depth. Beams are defined with $a/d \leq 1$ as deep, $1 < a/d \leq 2.5$ as short and $a/d > 2.5$ as normal or slender.

For $a/d > 2.5$ the tension steel ratio ρ_t affects the shear behaviour as an increase of ρ_t means a reduction of the flexural crack width resulting in an increase in crack friction, and

also means a decrease in the length of the cracks which in turn increases the uncracked compression area resulting in a higher shear capacity.

2.2.5 Actions influencing the total shear strength

This section investigates the four mechanisms of shear transfer which are: shear stresses in uncracked concrete, aggregate interlock, the dowel action of the longitudinal reinforcing bars, and arch action. These are the fundamental actions which influence the shear behaviour of the reinforced concrete elements. Proportion of shear resistance taken by each action is discussed in detail in this section.

Fenwick and Paulay [2-11] carried out some displacement measurement on cracks in few beams. Some of these beams had preformed, smooth, diagonal cracks to avoid aggregate interlock forces and some had a cushion of foam rubber to eliminate dowel forces.

They concluded that there are two ways in which shear displacement may occur. The first is by the rotation of the compression zone between adjacent concrete cantilevers. This requires curved cracks. The second way is by bending within the concrete cantilevers.

Taylor [2-14] tested shear transfer by aggregate interlock (or surface shear) and by dowel action and derived load /displacement relationships from them. He then used these relationships, together with measurements of movements at cracks in beams, to assess the separate contributions to the total shear resistance. At stages close to shear cracking the proportions taken by the different actions are shown in Table 2.1.

	% of total shear resistance provided by different action in NSC			
	Fenwick & Paulay	Taylor [2-14]	Hamadi and Regan [2-25]	
	Aggregate unchanged	Aggregate unchanged	Natural Gravel	Expanded Clay
Compression zone	20	20-40	37	40
Aggregate interlock	60	35-50	44	26
Dowel action	200	15-25	19	34

Table 2.1: Fenwick and Paulay [2-11], Taylor [2-14], Hamadi and Regan [2-25]tests for separate contributions to the total shear resistance

Hamadi and Regan [2-25] reviewed Taylor's [2-14] above mentioned experiments with 14 beams of dense and light aggregate concrete, and measured aggregate interlock and dowel action and derived load /displacement relationships from them. These relationships were then used together with measurements of movements at cracks in beams to assess the separate contributions to the total shear resistance. Details of their approach are described in sections 2.2.7.5 and 2.2.8.2. At stages close to shear cracking the proportions taken by the different actions by Hamadi and Regan [2-25] correlated with Taylor's [2-14] results and were found to be as shown in Table 2.1.

The inclined cracking load is a function of the tensile strength $f_{ct.}$ of the concrete. The stress state in the web of the beam involves the biaxial principal tension and compression stresses. The flexural cracking that precedes the inclined cracking disrupts the elastic stress field such that inclined cracking occurs at principal tensile stress roughly at half of f_{ct} for theuncracked section in NSC.

2.2.6 Shear resistance from arch action

If, for some reason, the transfer of bond forces is entirely destroyed along the full length of a beam, it will either suddenly fail or transform almost immediately into an arch-dome only if a/d<1, Figure 2.1. Arch action means that the shearing resistance is provided by the inclined compressive thrust between load and support. In such a mechanism , usually when 1<a/d < 2.5, the main reinforcement acts as a simple tie.

Arch or strut and tie action normally occurs in beams without stirrups when the shear span /effective depth ratio a/d <2.5. There is a load path direct to the support by a compression arch or strut held in equilibrium by a horizontal tension tie formed by the longitudinal reinforcement. The loading capacity is decided by the concrete strut's compression strength, the strength of the tension ties or that of their connection, i.e. the main steel anchorage.

There was some initial research on beams with stirrups by Oscar Faber [2-15] published in 1924 which drew attention to the possibility of arch as opposed to truss action. However, the first major change of approach was in the work of Borishanski [2-16] who made tests in which shear reinforcement was omitted from limited lengths of shear spans and who derived an expression for the shear resistance of such zones. Borishanski's work has been

very effective in Eastern Europe and is still the basis for Russian codes [2-17].

Generally, an increase in the compressive strength of the concrete means an increase in its tensile strength which in turns results in an increase in diagonal cracking strength. With a low a /d ratio the compression arch or strut is directly dependent on the compressive strength of the concrete. Therefore, assuming the tie is strong enough, an increase of the compressive strength results in a proportional increase of the shear capacity.

Arch action is present in deep beams (a/d<1) from the start of loading. In beams of $1 \leq a/d \leq 2.5$, the inclined crack is generally the result of a flexural crack which suggests that prior to the formation of the shear cracks, beam action predominates. In this kind of beam, a transformation to the arch action usually occurs at the later stages of loading.

In section 3.2.12, it will be demonstrated that arching action fully develops in HSC with HWB of a/d=3.02, after stirrups pass their yield, whereas when HWB is absent in the same beam no arching action develops at all.

2.2.7 Shear resistance from dowel action of reinforcement

The development of dowel action in beams is a result of the longitudinal reinforcement taking some shear force in a crack, initiated by the vertical movement of two opposite crack surfaces. On the contact area of the concrete and the steel there are stresses that are perpendicular to the longitudinal reinforcement. Dowel failure occurs with the formation of a crack next to the steel bar and in the same direction as the bar.

The shear force in the bar increases proportionally to the vertical crack displacement, therefore an appreciable dowel force develops only towards the ultimate load, when shear cracks are actually opening.

In practice, dowel action occurs in reinforced concrete at both flexural and shear cracks and the forces against the cover are decisive for the failure of the dowel action. Dowel bars may also act against the core of concrete, resulting in a bending of the bar and local crushing of the concrete or, alternatively, may cause splitting in the plane of the bar if the cover is small. If the cover is large, failure occurs at the final stage of loading as a result of diagonal tension cracking of the inclined compression strut, Figure 3-15.

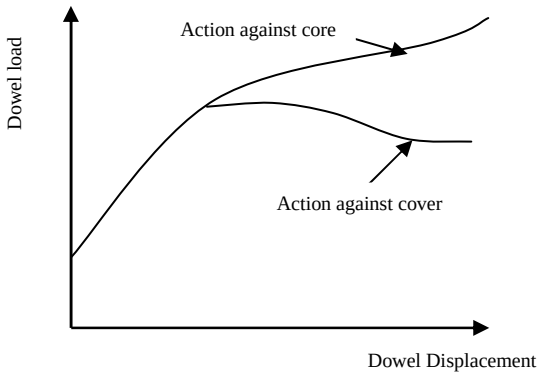

Figure 2.7: Dowel load in relation to the action against core concrete as compared to the cover

Source: Baumann,T.,Rusch, H. [2-23] 1970

The resistance of a dowel acting against the core concrete is greater than that of a dowel acting on the cover. Figure 2.7 shows the dowel load in relation to the action against the core concrete as compared to the cover.

The dowel action is primarily dependent on the tensile strength of the concrete. Therefore, an increase in tensile strength produces a proportional increase in the dowel capacity.

In this section past research on the dowel action on the tension reinforcement is reviewed in detail and past research on dowel action resulting from horizontal web bars (HWB) of the beams is investigated and compared with this writers research.

As discussed in section 2.2.2.2, it seems that Morsch was the first to recognise the existence of dowel forces.

2.2.7.1 Background to research on dowel action

In 1954, the Swedish researcher Forssell [2-18] was the first to make tests of dowel action in beams, Figure 2.8.

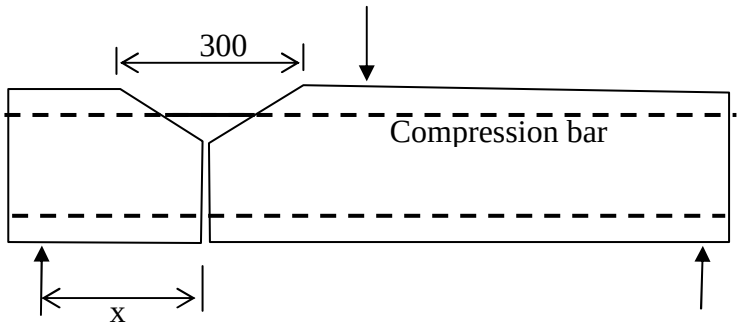

Figure 2.8: Dowel action test set up by Forssell [2-18] and Lorentsen [2-19]

In 1956, Jones [2-20] made tests to investigate dowel forces in beams with stirrups. He tested three divided beams especially designed and instrumented to study dowel action. Dowel forces were computed from the flexural stresses observed in the longitudinal reinforcement and were evaluated to be 30 % of the applied transverse forces.

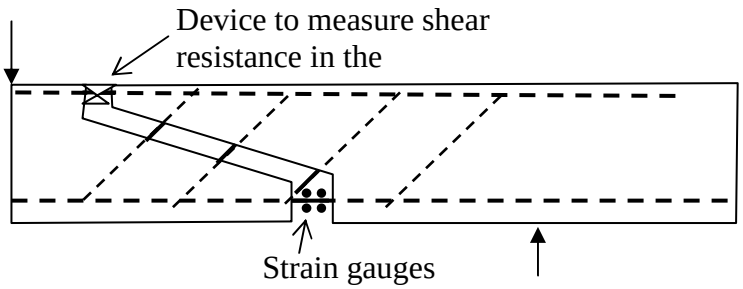

Figure 2.9: Test set up by Jones [2-20] to measure the dowel action

Jones considered the distribution of shear in doubly reinforced concrete beams with inclined stirrups, and presented data from which he evaluated the proportions of the total shear carried by the concrete, the stirrup and the longitudinal steel. He concluded that longitudinal steel functions as a dowel and contributes substantially to shear resistance at failure.

Jones [2-20] concluded that for beams where the bars are relatively close to the concrete surface, dowel resistance depends on other factors such as bar size, amount of cover below the bars, beam depth, the net width of concrete at the level of the longitudinal steel, concrete tensile strength and the moment of inertia of the structure (from the transformed section).

In 1964, Lorentsen [2-19], tested two divided reinforced beams with set up test pieces similar to those used by Forssell [2-18],
Figure 2.8.

2.2.7.2 Krefeld and Thurston's treatment of dowel action

In 1966, Krefeld and Thurston [2-21] carried out nine tests on divided beams in which the tension zone was cast separately from the compressive zone, Figure 2.10. The dowel was tested by pulling the centre section of the beam downward, therefore the main steel was in

tension throughout the test. The dowel shear force and the tensile stress are related to each other by the geometry of the test specimen.

Following successful experimental tests on 7 beams, it was proposed that when the limit of tensile strain in the concrete is reached, vertical flexural cracks form from the tension surface of the beam at intervals along the span according to the magnitude of the bending moment. The composite action is modified, a redistribution of stress starts at the cracked sections with increased stresses in the steel and concrete, and the rate of deflection of the beam increases.

After the flexural cracks have extended upward a short distance above the longitudinal reinforcement, they become inclined at sections subjected to shear as well as bending. Since the tensile stresses in the concrete due to bending moments decrease approaching the neutral axis, the inclined extensions are due largely to the influence of shear producing diagonal tension. The progressive changes in the steel and concrete stresses as the inclined cracks extend upward constitute a second redistribution of stresses.

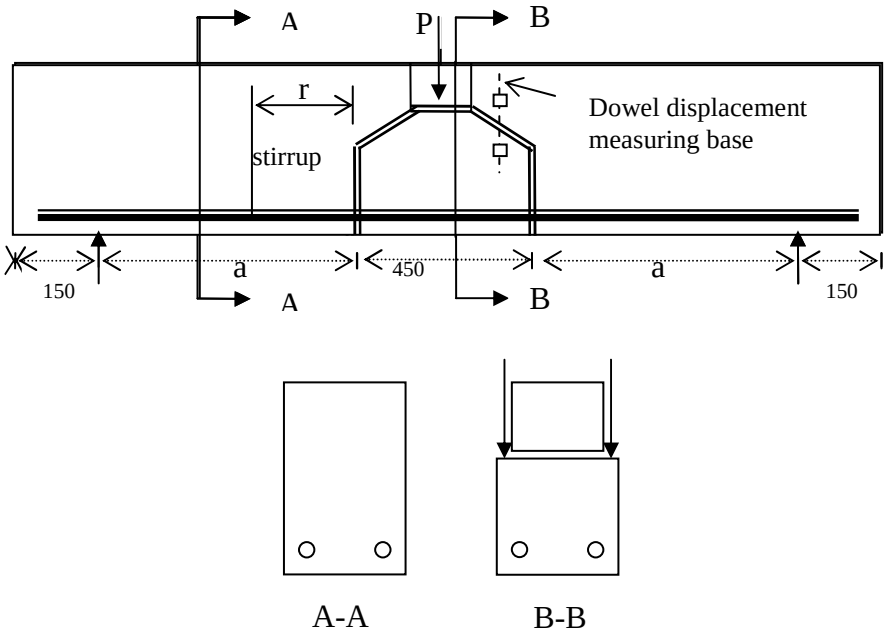

Figure 2.10: Test arrangement and the test pieces used by Krefeld and Thurston [2-21], Baumann [2-24] and Taylor [2-22]

Source: Redrawn from a sketch by Baumann, T, Rusch H. 1970 [2-23]

Based on an assumed inclined crack in a reinforced concrete beam and the empirical data from a series of tests, the following expression was derived:

$$V_1 = C_1 \sqrt{f_c} (d\, I\, b^3)^{3/4} \qquad \textbf{2-10}$$

where C_1 is a factor, involving unknown effects of combined stresses, and *I* is the moment of inertia of the structure from the transformed section. This is the same form of equation as that derived by Jones [2-20] except that it is expressed in terms of a $\sqrt{f_c}$ and b whereas Jones used f_t (the ultimate tensile strength of the concrete) and b' (the net width of concrete at the level of the longitudinal steel). While this theoretical expression does not include the location of the crack as a variable, their test data indicated that the value of V_1 decreases as the distance of the crack from the support increases.

2.2.7.3 Baumann's treatment of dowel action

In 1968, Baumann [2-24] tested 31 beams of which 26 had similar pieces to those used by Krefeld, Thurston [2-21] in 1966 and Taylor [2-22] in 1969. The arrangement and the test pieces are shown in Figure 2.10. Their preferred arrangement was different from Forssell [2-18] and Lorentsen's [2-19] tests which had beams divided in two sections, Figure 2.8.

Loading was applied to a part of the tensile zone of a simply supported beam. The concrete of this part was divided from that of the rest of the beam by a preformed artificial crack. The only element transferring load between the two parts was the main reinforcement (the dowel).

The effects of the following variables were studied:-

1.Width of preformed crack
2.Breadth of beam
3.Depth of beam
4.Thickness of bottom cover
5.Distance from preformed crack to support
6.Distance from preformed crack to a stirrup supporting the dowel
7.Number of stirrups supporting dowel
8.Diameter of main reinforcement
9.Number of bars in main reinforcement
10.Steel type (main reinforcement)
11.Number of layers of main reinforcement
12.Concrete strength

The diameter of the stirrups supporting the dowel was also varied but this parameter was not treated systematically. Baumann presented his test results in the form of tables of shear (dowel) forces at where cracking commenced along the line of the main steel in the outer (unloaded) part of the beam, and the vertical deflections Δ corresponded to these cracking loads.

At small dowel forces, the longitudinal reinforcement is considered to be suspended from the upper part of a beam by vertical tensile stresses in the concrete, Figure 2.11. When the maximum tensile stress reaches the tensile strength of concrete, the first horizontal dowel-crack starts. The load, V_{cr}, at this stage is given by:

$V_{cr} = l_z \cdot b_n \cdot f_t'$

where

l_z = length, shown in Figure 2.11

b_n = net width of beam = $b - \sum \phi$

ϕ = bar diameter.

f_t' = tensile strength of concrete (axially) = $0.53\, f_{cu}^{2/3}$

f_{cu} = cube crushing strength (kgf/cm^2).

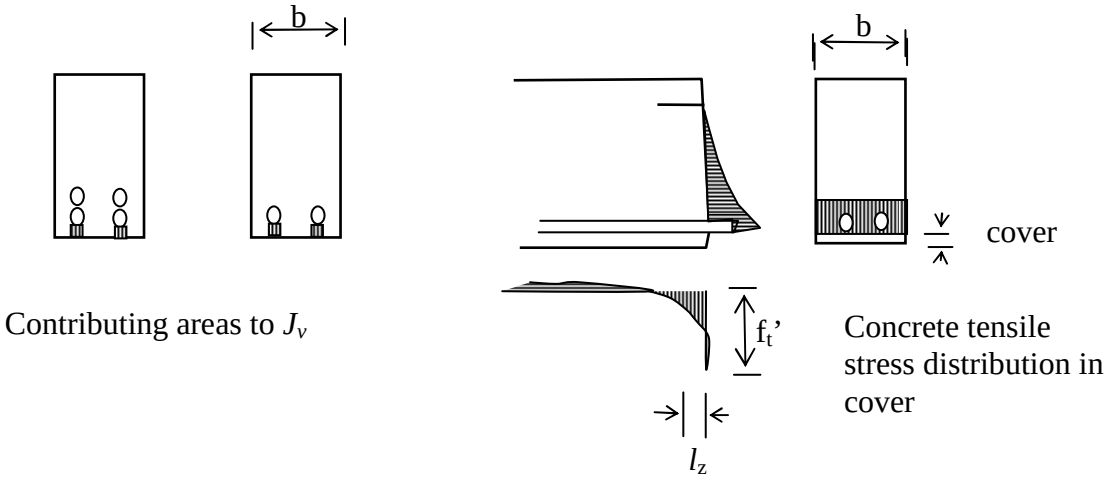

Figure 2.11: Stress distribution under dowel loads.

The length l_z, Figure 2.11, characterises the distribution of vertical tensile stresses in the concrete along the reinforcing bar. It is mainly influenced by the diameter of longitudinal reinforcement, the number of reinforcing layers and to a lesser extent by the concrete strength. They also stated that the cross-section of the beams, the concrete cover, the number of reinforcing bars in one layer and any stirrups did not influence l_z in these tests.

Accordingly, they established the following empirical expression for one layer of longitudinal reinforcement in cm:

$$l_z = 14.3 \times \frac{\phi}{f_{cu}^{1/3}}$$

Therefore:

$$V_{cr} = 7.6 \times \phi \times b_n \times f_{cu}^{1/3} \quad \text{in kgf}$$

In Newtons

$$V_{cr} = 3.1 \times \phi \times b_n \times f_{cu}^{1/3} \quad \text{2-11}$$

For two layers of longitudinal reinforcement l_z was given by:

$$l_z = 4 + 0.032 J_v$$

where J_v is the combined bending rigidity of the longitudinal bars and a part of the bottom cover, Figure 2.11.

The load-displacement relationship before dowel cracking was given as:

$$V_d = V_{cr} \cdot \frac{\Delta_d}{0.08}$$

where Δ_d is the dowel displacement at the dowel force V_d.

Cracking behaviour was presented in the form of graphs of 'dowel force V deflection' for most of the beams. An example in Figure 2.13 shows overall characteristics for a beam with stirrups and Figure 2.14 shows a detail for low loads.

All the results were tabulated, the post-cracking behaviour being given by the values of the dowel force corresponding to fixed increments of deflection.

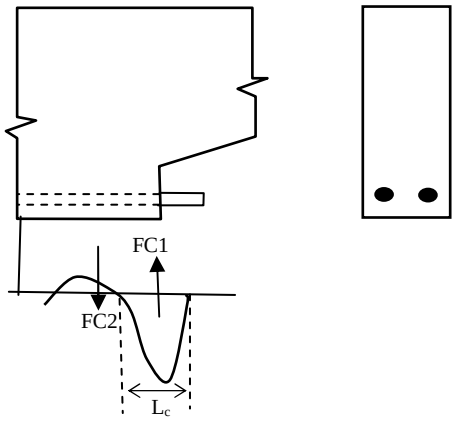

Figure 2.12: Stress due to dowel action

Source: Redrawn from a sketch by Baumann, T, Rusch, H. 1970 [2-23]

In the early stages of loading, prior to dowel cracking, the load transferred by the dowel is supported by the concrete under bars which is in turn supported by vertical tension in the concrete above. Stresses due to dowel action are shown in Figure 2.12.

The condition of equilibrium for dowel force where the main reinforcement is in single layers is:

$D_{cr1} = Kb_n d_b f_{cu}^{1/3}$ 2-12

where net breadth of the cross section (b_n) is the beam breadth after deduction of diameter of dowel bars (d_b).

$V=Kf_{ct}\, b_n L_c$ **2-13**

The general equation where the main reinforcement is in up to 2 layers is:

Before dowel cracking occurs, the dowel deformation Δ results initially from pressure caused by the bars to the concrete cover below. The tensile strain of the concrete above the dowel makes little contribution to Δ.

$\Delta \approx 0.08$ mm (D/D_{crack})

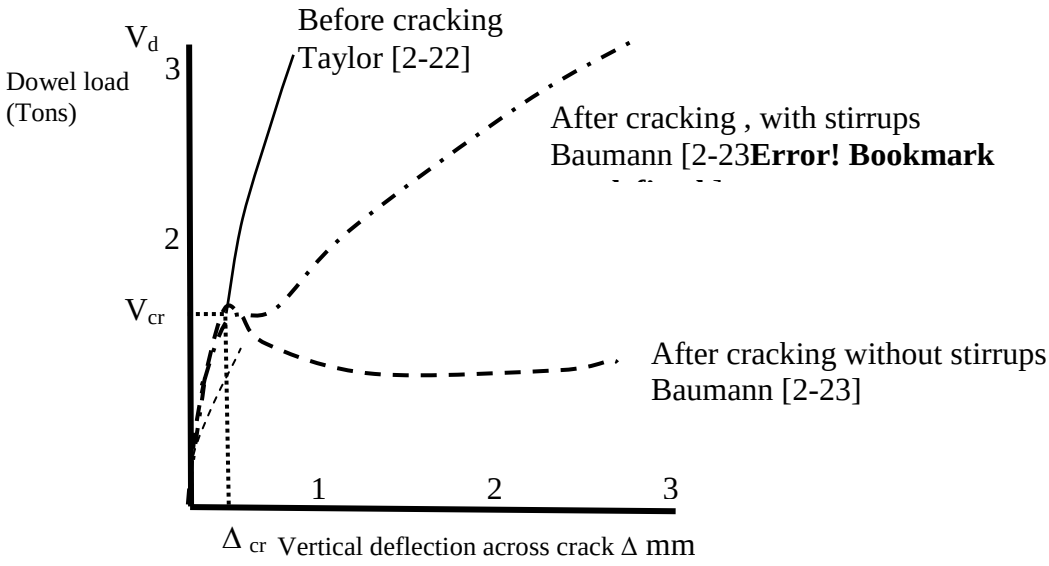

Figure 2.13: A graph for a beam with and without stirrups. Curve equation approximation $\Delta=\gamma V2$

Source: Redrawn from a sketch by Baumann T, Rusch H, 1970 [2-23]

After dowel cracking the dowel force D_{cr} can increase only when the longitudinal reinforcement is supported by a stirrup near the diagonal crack. In this case, at first loading

the relation between D_{cr} and Δ follows a parabola

Δ (mm)= γD_{cr}
where γ= constant and is a factor of (r^2/J_v)

r= distance from the crack to the first stirrup in mm.

J_v =moment of inertia of dowel bars + concrete cover directly below bars.

Also an expression was given for the load-displacement relationship after dowel cracking, Figure 2.13. It is dependent on the distance between the stirrup and the diagonal crack and also on J_v.

Baumann investigated the accuracy of his equation for the dowel cracking loads of beams with single layer reinforcement to compare with his own test results and others reported by Krefeld and Thurston, Lorentsen, and Fenwick's tests in 1966 on 67 dowel specimens, where the steel was in compression which did not exactly represent the behaviour of dowel steel under tension in beams.

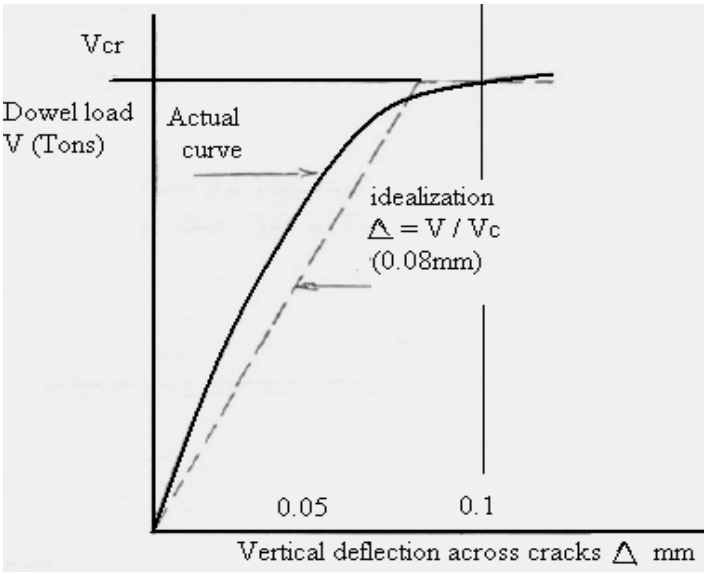

Figure 2.14: Detail for low loads
Source: Redrawn from a sketch by BaumannT, Rusch H, 1970 [2-]

2.2.7.4 Taylor's tests on dowel action

In 1969, based on his experimental results, Taylor[2-22] proposed a load displacement relationship before cracking which is a curve compared with the straight line proposed by Baumann. The end co-ordinates of this curve are (V_{cr}, Δ_{cr}). Taylor experimentally tested 34 model beams of scale 2:7 and 12 prototype beams. He investigated the following parameters:

1. Concrete tensile strength
2. Net width b_n
3. Cover thickness
4. Two layers of reinforcements
5. Distance from the support

The displacement Δ_{cr} was evaluated to be 0.17mm, a figure derived from a survey of all his test data including both the models and the prototypes. A multiple regression analysis defined the dowel cracking load (kN) at this displacement (mm) as:

$2V_{cr} = 9.1 + 0.001\ b_n^2\ f_t'$ 2-14

where:

b = Net width (mm)

f_t'= Concrete tensile strength, (kN/mm^2)

The curve in the continuous line in Figure 2.13 was represented by the following equation:

$V_d = 1.55 \cdot \Delta_d^{0.25} \cdot V_{cr}$ **2-15**

Taylor's results were essentially identical to those obtained by Baumann when stirrups were present, Figure 2.13. He also concluded that, for the equivalent non-divided beams tested, the dowels carried between 9% and 20% of the total shear force on the section at failure.

2.2.7.5 Hamadi and Regan's research on dowel action

In early seventies, Hamadi [2-25&26] tested divided-beam specimens of the type used in previous studies similar to Baumann's, with the difference that the load was applied via a steel plate passing through the opening, Figure 2.15, with the loaded section cast first and with the bars projecting from it as compared to Baumann's test set up shown in Figure 2.10.

The simply supported beams were tested with load applied to the precast section via a steel plate passing through an opening below the in situ compression zone. Tests were made

with the gravel and expanded clay aggregate concrete for each of the bar arrangements used in the main tests. The ultimate loads are given in Table 2.2.
The results of these tests and other published data on dowel strengths were compared with a slightly modified form of Baumann equation, for simplicity, called Baumann-Hamadi's equation for the dowel resistance of a single layer of bars:

$$V_d^{'} = 4.12 \cdot \phi^{2/3} \cdot b_n \cdot \sqrt[3]{f_{cu}} \quad \text{2-16}$$

in units of N and mm, where φ is the bar diameter and b_n is the net breadth of the section at the level of the bars (= b - ∑φ). Analysis of these tests and that of Baumann-Hamadi gives the results in Table 2.2.

In total 14 beams were tested, 400 x 100 mm in cross-section, and two continuous bars were used as flexural reinforcement. Variables were the type of aggregate, the percentage of main steel and the 'shear-span/effective depth' ratio.

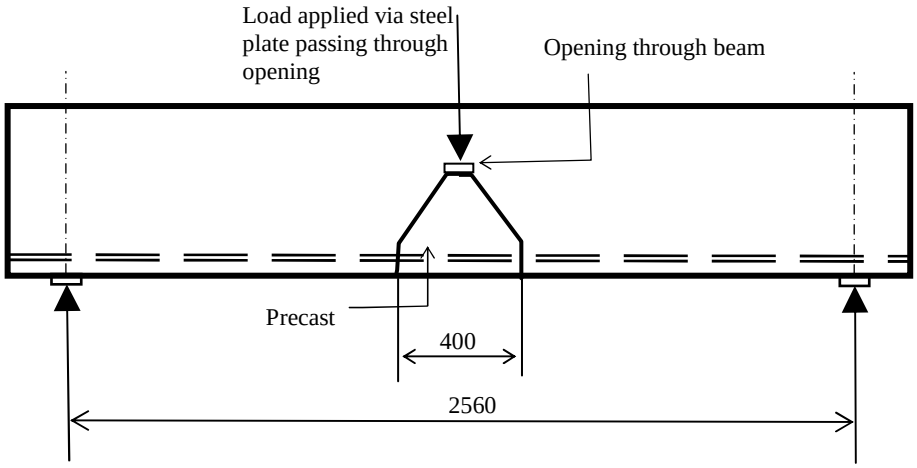

Figure 2.15: Beam arrangement with load applied via steel plate passing through opening

Source: Hamadi Y.D and Regan P.E, June 1980 [2-25]

The 6 beams discussed are most related to this review because of their span to depth ratio (a/d)=3.4. The last column of Table 2.2 shows 128%, 119% and 108% improvement for calculated dowel resistance for bars T20, T16 and T12 respectively.
The force-displacement relationship can be expressed as:

$$\frac{V_d^{'}}{V_d} = 2\left(\frac{S}{0.08}\right) - \left(\frac{S}{0.08}\right)^2 \quad \textbf{2-17}$$

where s is the vertical displacement across the crack or beam division at the level of the dowel bars and is in mm. The expression is plotted in Figure 2.17.

Beam	Reinforcement		f_{cu}	$V'_{d\ test}$	$V'_{d\ Baumann-Hamadi}$	$V'_{d\ Baumann-Hamadi} / V_{d\ test}$	Failure $2V_u$
	Number & diameter	100As / bd	N/mm^2	kN	kN		kN
GD-1	2Y20	1.70	35.0	6.00	5.96	0.99	89.0
GD-2	2Y16	1.08	58.0	7.00	6.89	0.98	89.5
GD-3	2Y12	0.60	34.3	5.60	5.33	0.95	75.4
LD-1	2Y20	1.70	23.6	5.00	5.23	1.04	50.0
LD-2	2Y16	1.08	24.4	4.75	5.16	1.09	42.5
LD-3	2Y12	0.60	25.1	4.65	4.81	1.03	30.0

Table 2.2: Beam with span to depth ratio a/d=3.4 . G and L series were made of light and gravel aggregates. Baumann-Hamadi's equation predicts the experimental failure within the standard deviation of 0.03

Source: Hamadi Y.D and Regan P.E, June 1980 [2-25]

$\frac{100A_s}{bd}$	x_1 (mm)	x_2 (mm)	y (mm)	$\frac{y_o}{y}$
1.70	790	800	240	0.54
1.08	815	870	255	0.57
0.60	610	635	190	0.58

Table 2.3: Position of a crack in position shown in Figure 2.19

Source: Hamadi, Y.D and Regan, P.E, June 1980 [2-25]

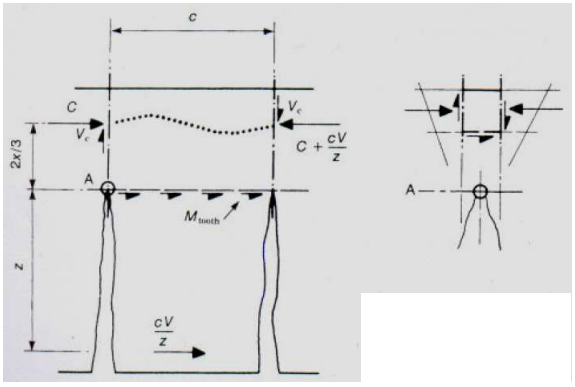

a) Forces involved in over-all equilibrium

b) Local equilibrium determining shear stress distribution

Figure 2.16: Shear resistance of a horizontal compression zone showing forces in over-all and local equilibrium

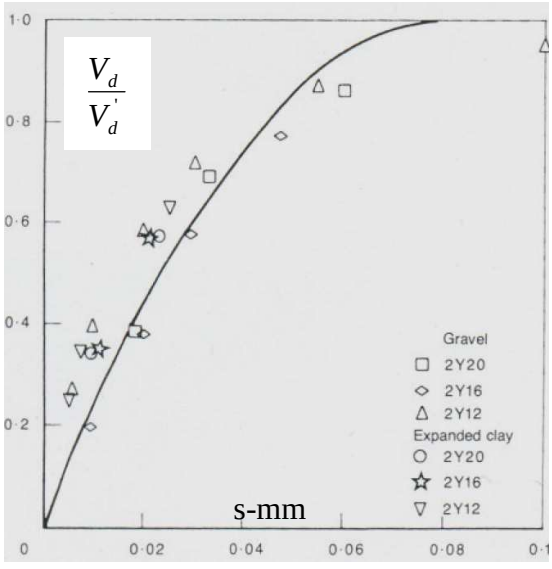

Figure 2.17: Comparison between the experimental dowel-force V displacement relationship

Source: Hamadi, Y.D and Regan, P.E, June 1980 [2-25]

Taking moment about A from Figure 2.16:

$$V_c = \frac{2Vx}{3Z} + \frac{M_{tooth}}{C} \qquad \textbf{2-18}$$

Mesurements recorded in conjunction with the force-displacement relationships obtained from the push-off and divided-beam specimens (equations 2.26 and 2.16) to evaluate the shear carried by interlock and dowel forces at cracks V_g and V_d. The total shear in the compression zone was then found as

$V_c = V - V_g - V_d$.

The value of V_c thus obtained was always greater than the classical Morsch value of *2Vx / 3z.* This is consistent with the equilibrium of the element of Figure 2.16 (a), where the moment M_{tooth} arises because the shears across the cracks do not fully balance the moment *Vcl/z* due to the bond force. The vertical stresses from the tooth moment cause the deflection of the thrust line.

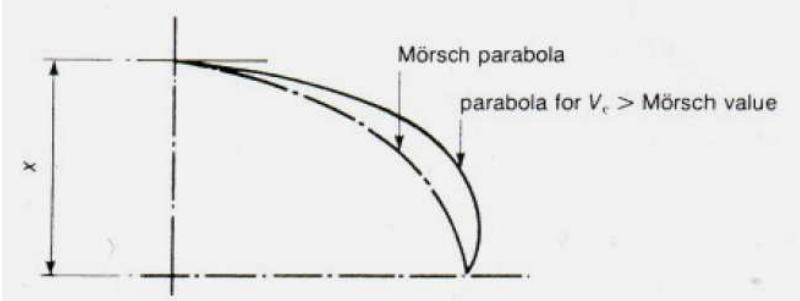

Figure 2.18 : Shear stress distribution of a horizontal compression of the tooth shown in Figure 2.16

Source: Hamadi Y.D and Regan P.E, June 1980 [2-25]

The local equilibrium of elements such as that in Figure 2.16 (b) determines the variation of shear stresses over the depth of the compression zone. If the distributions of longitudinal stresses are linear, as shown, that of the shear is necessarily parabolic. The compression zone shear distributions of Figure 2.18, and in other figures produced from other beams which they had tested, are parabolas drawn to coincide with the classical shear value at the neutral axis, as this was consistent with the distribution of shear across cracks.

Figure 2.23 shows the structure of a shear span with flexural cracks. The elements of concrete between cracks are subjected to bond forces near their lower ends and are fixed to the compression zone above. The moments of the bond forces are resisted partly by couples between the vertical interlock and dowel forces at the cracks and partly by flexure of the elements or teeth.

The flexure of the teeth produces vertical tensile stresses and strains at the level of their attachment in the compression zone, and it seems that inclined cracking is generally the result of a combination of this tension and the shear in a tooth. The failure criterion is thus somewhat complex, but over a wide range it is a reasonable approximation to express it solely in terms of the tensile stress or strain.

The loading of a tooth may be divided into two component systems. The first comprises a part of the bond forces together with the interlock and dowel forces and produces shear deformations but no vertical strains. The second is the remainder of the bond force and the moment at the head of the tooth.

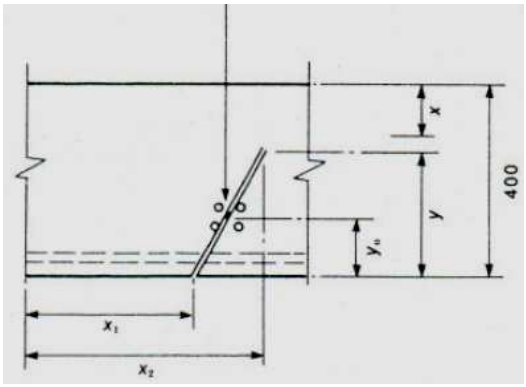

Figure 2.19: Position of a crack for data shown in Table 2.3

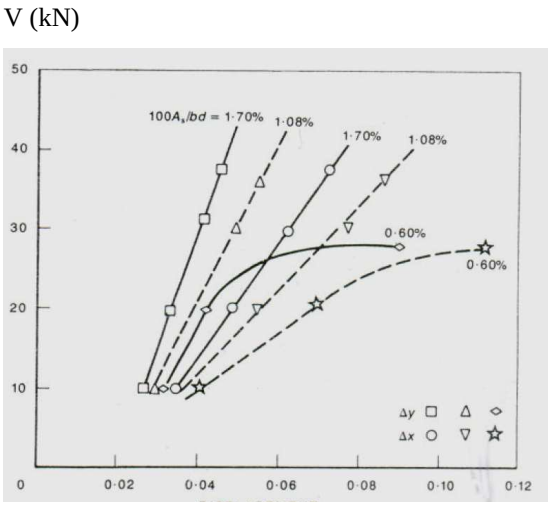

Figure 2.20: Development of the crack displacement in the gravel concrete beams for beam listed in Table 2.2

Source: Hamadi, Y.D and Regan, P.E, June 1980 [2-25]

For the second component, the tooth acts as a cantilever and the loading can be approximated to a uniform shear *F/bc*, where *F* is the bond force and c the tooth width or crack spacing. The longitudinal deflection of the extreme fibres at the loaded end of such a cantilever is given by elastic theory as:

$$u = \frac{Fc}{2EI}\left[\frac{3l^2 - (1+1.25\nu)}{6}\right] \quad \textbf{2-19}$$

where *l* is the span (height of tooth from steel level to top of crack), *v* is Poisson's ratio and *EI* is the rigidity of the tooth.

The extreme fibre longitudinal strain at the encastre end is

$$\varepsilon = \frac{Flc}{2EI} \quad \textbf{2-20}$$

Substituting between these two expressions to remove *F*, we get

$$u = \varepsilon\left[\frac{3l^2 - (1+1.25\nu)}{6}\right] \quad \textbf{2-21}$$

The corresponding crack width can be evaluated as follows. For a point-loaded shear span, the strain in the main steel at a distance *x* from a support is

$$\varepsilon_{sx} = \frac{Vx}{A_s E_s z} \qquad \textbf{2-22}$$

If the stiffening effect of the concrete between cracks is ignored, the total elongation of the steel in the shear span is thus

$$\int_0^a \varepsilon_{xx} dx = \frac{1}{2} \cdot \frac{\mathrm{Va}^2}{\mathrm{A_s} E_s z} \qquad \textbf{2-23}$$

It has been observed that the distribution of crack widths along a shear span, in which diagonal cracking can occur, does not follow the external moment diagram, and it seems reasonable to work simply in terms of an average crack width:

$$a_{cr} = \frac{1}{2} \cdot \frac{\mathrm{Vac}}{\mathrm{A_s} E_s z} \qquad \textbf{2-24}$$

Taking moments about point A in Figure 2.21 with $\Delta T = Vc/z$ gives

$$\frac{Vc}{z} l = (V_g + V_d)c + \frac{\sigma_t b c^2}{6} \quad \textbf{2-25}$$

The measurements of vertical displacements at the level of the main steel indicated values of about 0.08 mm at failure in all cases. In view of equation $\frac{V_d'}{V_d} = 2\left(\frac{S}{0.08}\right) - \left(\frac{S}{0.08}\right)^2$ 2-17, the dowel force at inclined cracking can thus be taken as V'_d according to equation

$$V_d' = 4.12 \cdot \phi^{2/3} \cdot b_n \cdot \sqrt[3]{f_{cu}} \quad \textbf{2-16}$$

Similarly, with the criterion of failure taken as one of a limiting vertical tension, σ_t can be equated to the tensile strength of the concrete.

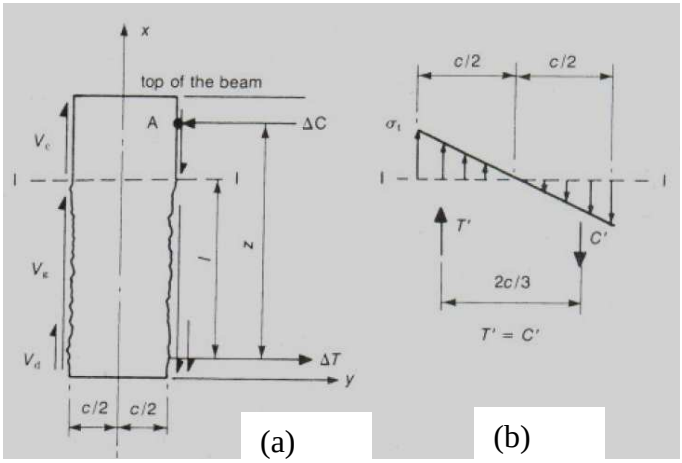

Figure 2.21: The concrete cantilever equilibrium conditions. (a) The concrete cantilever, which is fixed in the compression zone, and the forces associated with it (b) Distributions of internal bending stresses created at section I-I of (a)

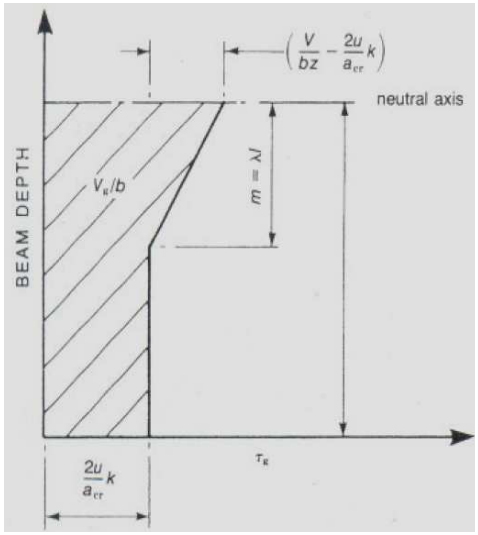

Figure 2.22: Distribution of shear transfers tress due to aggregate interlock.

Source: Hamadi Y.D and Regan P.E, June 1980 [2-25]

To evaluate the interlock component V_g, from comparison of shear stress distribution at the crack section of the tested beams can be idealized to that of Figure 2.22, the value at the top being a consequence of Figure 2.16.

$$V_g = lb\left[\frac{k}{a_{cr}}s + \tfrac{1}{2}\lambda\left(\frac{V}{bz} - \frac{k}{a_{cr}}s\right)\right] \qquad \textbf{2-26}$$

where *s* is the vertical displacement across the crack at the level of the steel. Since one crack surface moves up and the other moves down, the displacement is twice the end movement of the cantilever tooth (*s* =2*u)*, whilst from the tests λ is approximately constant at 0.4, making

$$V_g = 0.2lb\left[8k\frac{u}{a_{cr}} + \frac{V}{bz}\right] \qquad \textbf{2-27}$$

Substituting for *u* from equation $u = \varepsilon\left[\frac{3l^2 - (1+1.25\nu)}{6}\right]$ 2-21 and for from equation

$$a_{cr} = \frac{1}{2}\cdot\frac{\mathrm{Vac}}{\mathrm{A_s}E_s z} \qquad 2\text{-}24$$

and considering ultimate conditions, we get:

$$V_g^{'} = 0.2lb\left[8k\frac{\varepsilon_t^{'}[3l^2 - c^2(1+1.25\nu)\ ]}{6l}\frac{2A_sE_sz}{V_uac} + \frac{V_u}{bz}\right] \qquad \textbf{2-28}$$

Equation $\frac{Vc}{z}l = (V_g + V_d)c + \frac{\sigma_t bc^2}{6}$ 2-25, then gives

$$V_u = \frac{z}{L}\{\frac{\varepsilon_t^{'}E_cbc}{6} + 0.2lb\left[8k\frac{\varepsilon_t^{'}[3l^2 - c^2(1+1.25\nu)\ ]}{6l}\frac{2A_sE_sz}{V_uac} + \frac{V_u}{bz}\right] + 4.12\times10^{-3}\phi^{2/3}b_n\times\sqrt{f_{cu}}\} \qquad \textbf{2-29}$$

where V_u is in kN if E_e and E_s are in kN/mm^2, f_{cu} is in N/mm^2 and all dimensions are in mm. Some of the terms in this equation can be given conventional approximate values:

$z \approx \frac{7d}{8}$

$l \approx \frac{5d}{8}$

$\varepsilon_t^{'} \approx 120\times10^{-6}$

And $\nu \approx 0.2$

Study of a considerable number of crack patterns suggests that for major cracks c may be taken as $d/2$.

Finally, E_c can be estimated as $E_c = 4.5\cdot\sqrt{f_{cu}}$ for dense concrete [2-27] and for Leca aggregate this writer proposes $E_c = 2.15\cdot\sqrt{f_{cu}}$ for concretes in the range of f_{cu} = 20 - 25 N/mm^2.

Substituting , the above equation can be re-expressed as:

$$\frac{V_u}{bd} = \tfrac{1}{2}\left[q_1 + \sqrt{q_1 + q_2}\right] \qquad \textbf{2-30}$$

Where $q_1 = 1.75\left[E_c\times10^{-5} + \tau_d\right]$

$$q_2 = 67.4\times10^{-7}kE_s\frac{d}{a}\times\frac{100A_s}{bd}\times\frac{100A_s}{bd}$$

and

$\tau_d = \frac{V_d^{'}}{bd}$ ($V_d^{'}$ from $V_d^{'} = 4.12\cdot\phi^{2/3}\cdot b_n\cdot\sqrt[3]{f_{cu}}$ 2-16)

All units in N and mm

Hamadi and Regan's [2-25] compare their proposed equations, $\frac{V_u}{bd} = \tfrac{1}{2}\left[q_1 + \sqrt{q_1 + q_2}\right]$ 2-30, with their own test results, Figure 2.24, and others, Figure 2.25, reported in the

literature [2-28,2-29, 2-30, 2-31, 2-32, 2-33, 2-34, 2-35 and 2-36]. The beams included had the following in common:

(1) the ratio a/d was not less than 3.0;

(2) the cube strength of the concrete was not less than 20 N/mm2;

(3) the diameter of the main steel was not less than 10mm;

(4) the main steel was in a single layer;

(5) with the exception of the present tests, all the concretes had natural dense aggregates.

Although, on the whole, good correspondence is apparent, Figure 2.24 shows somewhat better agreement with the equation than Figure 2.25. The reason is probably that the beams in the former had only two main bars, as in virtually all dowel tests, whereas those in the second Figure had more bars.

Their more detailed analysis of the test results provided further information on the behaviour of concrete members in shear. Their analysis presented appeared to be a relatively successful attempt to make direct numerical use of the increasing knowledge of interlock and dowel actions. However, Baumann-Hamadi's [2-25] equation is proportional to the power of $2/3$ diameter of the longitudinal dowel bar and contribution from increasing the number of dowel bars is not included in their design rule.

From this writer's experimental work, Baumann-Motamed's equation will be introduced in chapter 3, section 3.9 which is directly proportional to the diameter of the longitudinal dowel bar, similar to Baumann's original equation, but in addition, a proportionality to the power of $1/4$ for the number of bars is introduced. This writer's revised equation will provide 12% improvement in accuracy of prediction compared to Hamadi and Regan's [2-25].

Two conclusions directly from the results of the their experimental work were; Firstly the shear strength of a lightweight-aggregate member made with Leca aggregate without shear reinforcement can be as low as about 50% of the strength of an equivalent member in dense concrete with the same cube strength. They concluded that the relative reduction in strength depends upon the type of aggregate, and CP110 [2-37] approach, using a general 20% reduction for all lightweight aggregates, is undesirable. Secondly the tests of pre-cracked shear spans show that vertical displacements and thus interlock forces are

developed even at vertical cracks and the actions are not reliant upon the cracks being curved as has been assumed in some previous work.

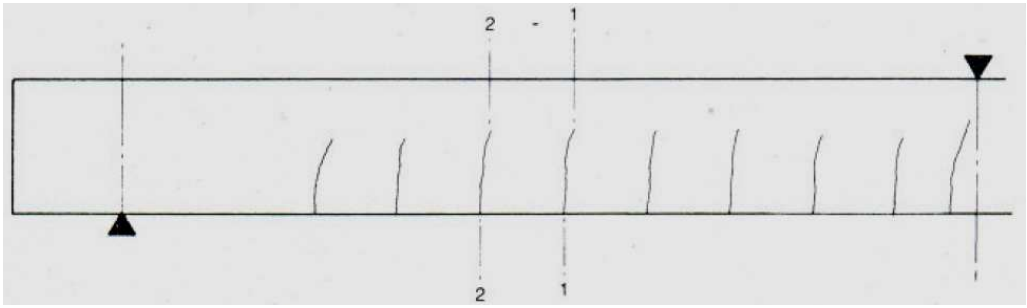

(a) Typical cracked shear span of a beam subjected to *bending and shear*

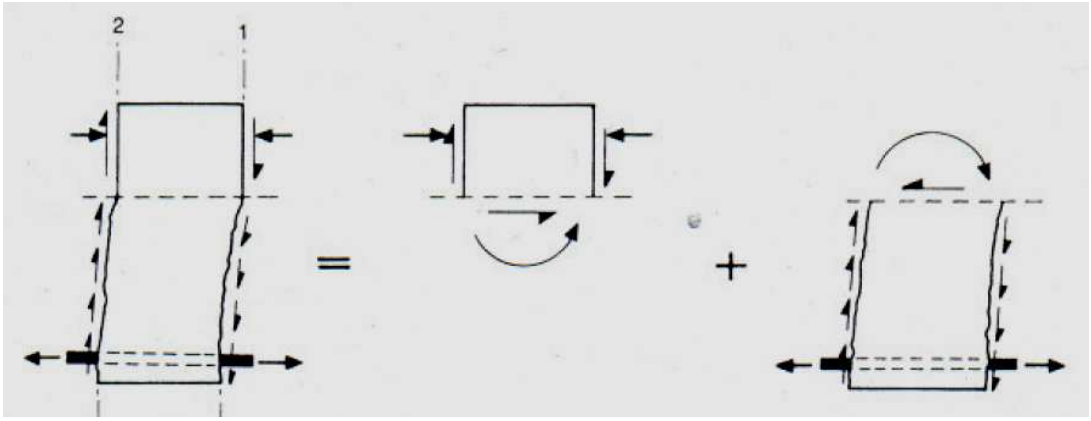

(b) Equilibrium conditions of a portion of the above shear span, between sections 1 *and* 2

Figure 2.23: Shear span with flexural cracks.

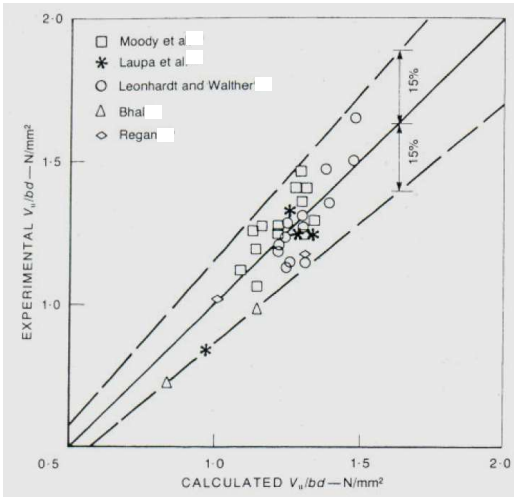

Figure 2.24: Comparison between test results and proposed equation. Beams with two bars of main steel in one layer.

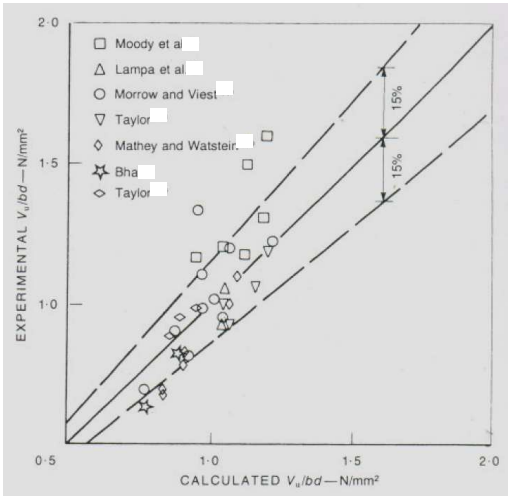

Figure 2.25: Comparison between test results and proposed equation. Beams with other than two bars in one layer of main steel.

Source: Hamadi, Y.D and Regan, P.E, June 1980 [2-25]

2.2.7.6 Houde and Mirza's investigation of inclined cracks

In 1974, Houde and Mirza [2-38] proposed a theoretical solution of the shear strength of reinforced concrete beams which involved numerical procedures using a finite element approach by applying successive approximation taking into account the non-linear behaviour of the concrete and its progressive cracking.

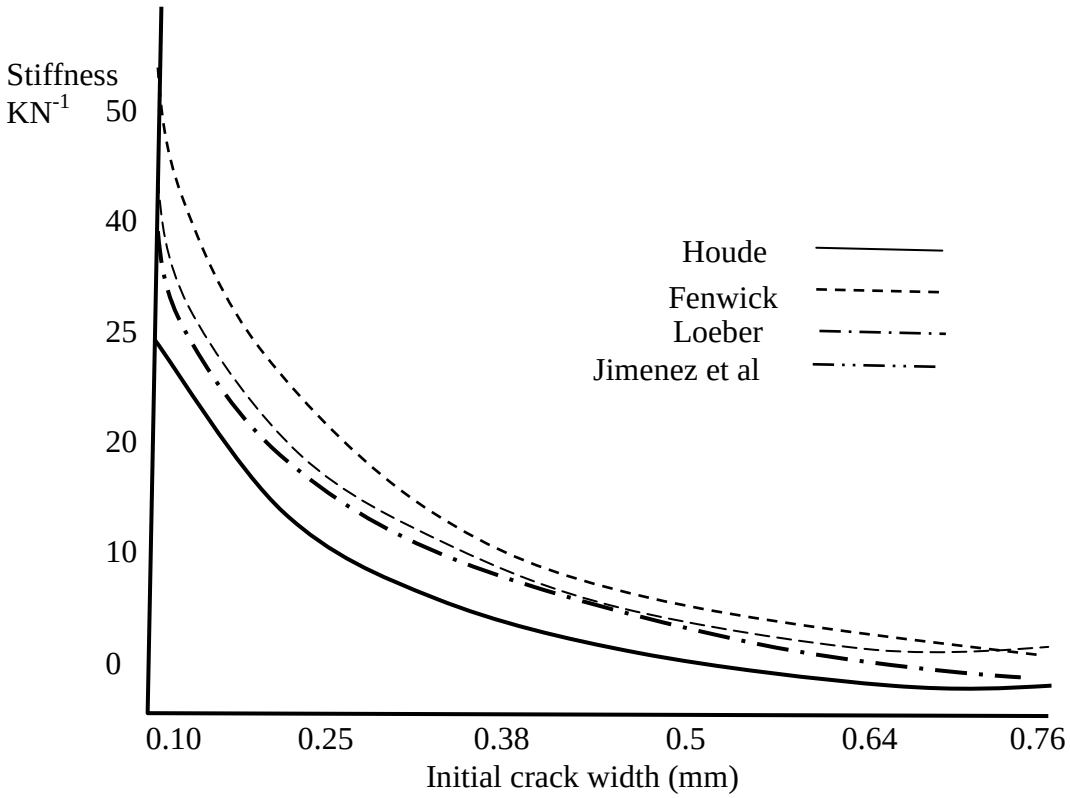

Figure 2.26comparison on the relation of crack shear stiffness initial crack width in different studies

Adopted and converted units from Buyukozturk [2-39]

They presented a finite element idealisation of a beam which was divided into a finite number of discrete elements rigidly connected at the nodes except at the steel-concrete interface and along an assumed main inclined crack path in the shear span where spring assemblies were introduced to correspond to aggregate interlock, dowel action and bond of the main steel. Stiffnesses for these were calculated experimentally, and by using their proposed equation for the aggregate interlock. The response of concrete was assumed to be linear in tension and nonlinear in compression.

The finite element technique provided a wide range of information in its output. Although

Houde and Mirza's [2-38] model was an idealisation, their inclusion of the different resisting mechanisms must have promoted their output. The most important weakness in this model is that the aggregate interlock was introduced along a pre-defined path corresponding to the diagonal crack frequently observed in failures. It is, therefore, hard to imagine that appreciable interlock forces would be possible along such flat cracks as the shear displacement along them must be small in comparison with the normal displacements. These cracks only occur at failure, therefore, no information was provided on crack formations from other load increments.

Buyukozturk [2-39] showed the comparison on the relation of crack shear stiffness initial crack width in different studies by Houde and Mirza [2-38], Fenwick, Loeber and Jimenez et al.

2.2.7.7 Chana's study on the role and importance of dowel action

Chana [2-40] experimented on the role and importance of dowel action. In his investigation of the mechanism of shear failure of reinforced concrete beams, crack widths at critical locations in the shear span were monitored. Chana's [2-40] tests demonstrate that at peak load, the diagonal crack width varies from zero at the tip of the crack to 0.25mm at the level of the main steel, while the dowel crack is 0.08 mm. The displacements at which the dowel splits as measured by other researchers were: 0.17mm by Taylor, 0.06mm by Fenwick, 0.02mm by Houde and Mirza and 0.08mm by Baumann and Rusch. In Chana's research , the dowel forces which are represented by gauge recording on links are responsible for 47% of the total shear force.

In his investigation of the mechanism of shear failure of reinforced concrete beams, crack widths at critical locations in the shear span were monitored. This was done continuously by means of a high speed tape recorder in conjunction with electrical demountable strain transducers and related to the load history approaching failure.

It was shown that beam failure is preceded by splitting at the level of the steel; this is identified to be the primary cause of shear failure for slender beams. The cracks formed as a result of the above tests are shown at three successive stages, Figure 2.27 (a), (b) and (c). The internal force system after the formation of diagonal cracks is shown in Figure 2.27(d).

The shear force is shown to be resisted by the compression zone, aggregate interlock and to some extent by dowel action of the main steel. As the shear force is increased, the diagonal crack opens up, giving rise to tensions in the surrounding concrete and an increase in the dowel force. This, in turn, produces splitting cracks in the concrete along the line of the reinforcement with an associated loss of bond.

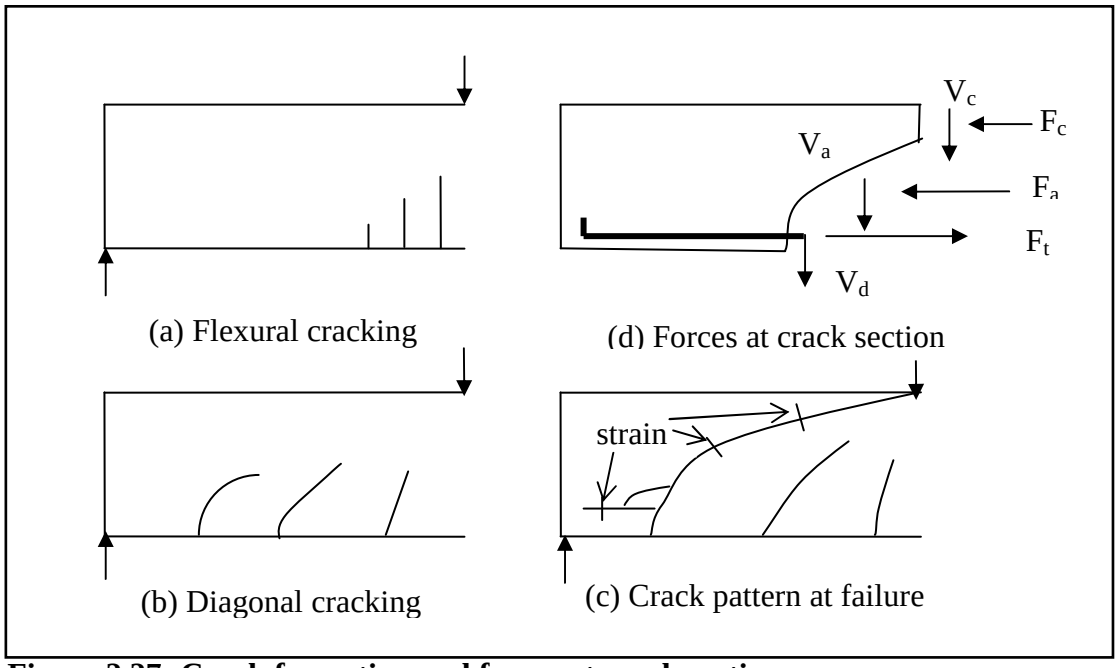

Figure 2.27: Crack formation and forces at crack section
Source: Reproduced from sketch by Chana, Dec 1987 [2-40]

The second stage of redistribution of stresses starts at the onset of dowel cracking. Due to loss of dowel stiffness, the rotation of the two beam segments is hindered (to a lesser extent) by the dowel action of the tension steel. Once dowel cracking has started, the rate of opening of the dowel crack increases steadily.

Average diagonal and dowel crack width at peak load were derived from the trace records for the beam on which the portal gauges were accurately positioned as shown in Figure 2.27(c). Peak load is attained when either or both of mechanisms of aggregate interlock or dowel action reach their limiting value.

Tests demonstrate that at peak load the diagonal crack width varies from zero at the tip of the crack to 0.25mm at the level of the main steel, while the dowel crack is 0.08mm. Chana's analysis of the forces at the cracked section, Figure 2.27d, does not take the presence of moment in the compression zone into account. This moment resists opening of the two beam segments and results in less dowel crack opening compared to a complete

precast concrete set-up of experimental beams such as Baumann's. However, the dowel crack which measured 0.08mm is the same as Baumann's figure.

2.2.7.8 Desai's research on horizontal web bars

Desai's [2-41] research explores the possibility of using horizontal bars in the web to increase shear resistance. He proposes that longitudinal bars placed towards the centre of a beam or a slab perform two functions:

1. As reinforcement improving the resistance of the surrounding concrete to the progress of a shear crack into the compression block.
2. As a dowel, resisting rotation about the tip of the crack.

Desai points out the benefit of using horizontal web steel to offset some proportion of links in order to ease congestion and improve detailing of reinforcement. He suggests that fire resistance of a beam or slab is improved when central bars with larger cover are used instead of links which are placed close to the surface of the concrete.

Tests were carried out on 200 x 300 mm simply supported beams loaded at midspan. Specimens with span 1 of 1400 mm, Table 2.4 and Table 2.5,were tested at the BCA Laboratory and those with span of 2100 mm were carried out by Vollum R. L at the Imperial College,Table 2.6.

Desai adopts the BS8110 [2-42] expressions for a design rule, section for the contribution of the central steel.

Error! Reference source not found.$V_{Rk=}V_{Rk.c} + \rho_w f_y bd$ 2-31

This gives Desai's expression $V_d= V_{Rk}+ V_b$

where V_b is the contribution of a central bar to V_d.

The details of specimen types were chosen to represent various percentages of tension reinforcement: 1.2% (2T20), 1.8% (3T20) and 2.8% (3T25). 1400 mm and 2100 mm spans were chosen to have variation in the shear span ratio of 2.6 for 1400 mm span and 4.0 for 2100 mm span. For all specimen types, the top steel was 2T12.

Based on a test programme of the beams with 6mm links at 200 mm centres, a design rule is proposed suggesting that there appears to be a limit to the maximum contribution of a central bar. Up to this limit the contribution of a central bar to ultimate shear resistance is taken to be directly proportional to the contribution of the concrete to shear resistance, Figure 2.28.

$V_b= 0.4\ V_{Rk,c}.\rho_b$ 2-32

where ρ_b is the percentage ($100A_b/bd$) of central web steel and $V_{rk,c}$ is the shear resistance of a similar beam without horizontal web steel.

The contribution of links to the ultimate shear resistance of the section is given by the BS8110 rule, excluding the partial factor γ_m.

$V_l = A_{sw} d f_{yv} / s$ 2-33

where A_{sw} is the cross-sectional area of a link, s is the spacing of links and f_{yv} is the yield stress for the link.

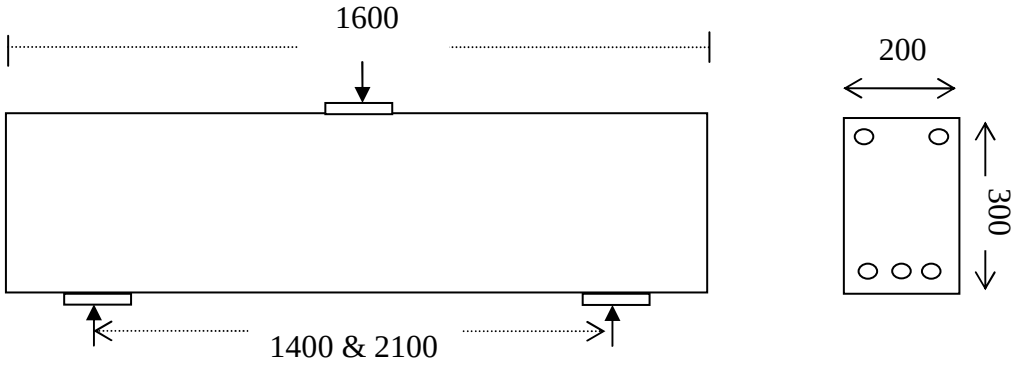

Figure 2.28: Test specimen, with 3T20 tension bars and 2T12 compression reinforcement

Source: Redrawn from Desai, S., June 1995 [2-41]

$V_d = V_{Rk,c} (1+0.4 \rho_b) + V_l$ *2-34*

The geometry and cross-section of the beams are shown in Figure 2.28**.** Test specimen**,** have 3T20 tension bars and 2T12 compression reinforcement with the central load applied over a 75 mm wide plate and support plates 75mm wide, over roller bearing. The beam in Table 2.4, had stirrups. The contribution of links to ultimate shear resistance V_l is 34.5 kN for all the beams.

Desai's expression for shear resistance appears to be empirical . From the tests on NSC it seems likely that the main effect produced by HWB is an additional dowel action of about 30%. It is difficult to follow the reason why the ratio of main reinforcement affects the contribution of the horizontal web bars (HWB), and also why there is an upper limit to dowel action.

Beam	Centre Steel	ρb	f_{cu} N/mm²	V_{fu} kN	V_{cu} kN	V_{lu} kN	V_{bu} kN	V_{du} kN	$\frac{V_{fu}}{V_{du}}$
C1		0	32	119	61	34.5		95.5	1.25
C1a		0	32	128	61	34.5		95.5	1.34
D1	2T10	0.29	32	132	61	34.5	7	102.5	1.29
D1a	2T10	0.29	32	141	61	34.5	7	102.5	1.38
D2	1Y16	0.38	28	146	58	34.5	9	101.5	1.44
D2a	1Y16	0.38	28	154	58	34.5	9	101.5	1.52
D3	1Y20	0.59	26	130	57	34.5	14	105.5	1.23
D3a	1Y20	0.59	26	130	57	34.5	14	105.5	1.27
D4	1Y23	0.93	26	134	57	34.5	21	112.5	1.19
D4a	1Y25	0.93	26	133	57	34.5	21	112.5	1.18

Table 2.4: 1400mm span beams with the bottom steel of 3T20 and top steel of 2T12, and 6mm links at 200 mm centres

Source: Table from Desai, S**.** June 1995 [2-41]

Specimen	Tension steel	Centre steel	ρ_b	f_{cu} N/mm²	V_{FU} kN	V_{CU} kN	V_{FU}/V_{CU}
AI	2T20	_	0	28	55	51	**1.**08
Ala	2T20	_			63		1.24
A2	2T20	2Y8	0.19	36	67	55.4	1.21
B1	3T20	_	0	27	58	57.6	1.01
Bla	3T20	_			60		1.04
B2	3T20	2T10	0.29	27	65	57.6	1.13
B2a	3T20				68		1.18
B3	3T20	1T16	0.38	28	81	58.3	1.39
B3a	3T20				88		1.51
B4	3T20	1T20	0.59	33	101	61.6	1.64
B4a	3T20				110		1.78
B5	3T20	1T25	0.93	33	90	61.6	1.46
B5a	3T20				96		1.56
El	3T25	_	0	28	72	67.3	1 .07
Ela	3T25	_			75		1.11
E2	3T25	2T10	0.30	34	80	71.9	1.11
E2a	3125				92		1.28
E3	3T25	2T12	0.43	34	90	71.9	1.25
E3a	3T25				84		1.17
E4	3T25	1T16	0.38	35	75	72.6	1.03
E4a	3125				88		1.21

Table 2.5: 1400mm span beams without stirrups. NB: The test on specimen A2a was abandoned due to faulty application of the test loads

Source: Table from Desai, S**.** June 1995 [2-41]

.

Specimen	Tension steel	Centre steel	ρ_b	f_{cu} N/mm^2	V_{FU} kN	V_{CU} kN	V_{FU}/V_{CU}
F1	3T20	_	0	43	69	67.3	1.03
F1a					75		1.11
F2	3T20	1T12	0.21	44	80	67.8	1.18
F2a					82		1.21
F3	3T20	1T16	0.38	46	76	68.8	1.10
F3a					82		1.19
F4	3T20	1T20	0.59	44	86	67.8	1.27
F4a					79		1.17
F5	3T20	1T25	0.93	43	82	67.3	1.22
F5a					80		1.19

Table 2.6: Vollum's tests at Imperial College for 2100mm span beams without stirrups

Source: Table from Desai, S. June 1995 [2-41]

2.2.8 Shear resistance from aggregate interlock

The term' aggregate interlock' is used to refer to the action by which shear forces are transmitted across the rough surfaces of cracks in concrete. Aggregate interlock is also called "interface shear transfer", "crack friction", or "surface shear". The possible importance of such an action in beams subjected to shear was understood earlier by Bjuggren [2-43]. Research by Fenwick [2-11] , Taylor [2-50], Hamadi [2-26], this writer [2-47], Albajar [2-44] and others has demonstrated that the effects of this action is considerable and has done much to clarify the patterns of deformation and internal stresses in cracked members.

2.2.8.1 Walraven's model

Walraven's [2-52] research on force transfer shows the influence of the maximum size of the aggregate, especially where cracks are relatively wide.

Walraven made numerous tests and developed a model that considered the probability that aggregate particles, idealised as spheres, would project from the crack interface. As slips develop, the matrix phase deforms plastically, coming into contact with projecting aggregates. The stresses in the contact zones are comprised of a constant pressure, σ_p and a constant shear, $\mu\ \sigma_p$ .The geometry of the crack surface is described statistically in terms of the aggregate content of the mix and the probabilities of particles projecting out at different degrees.

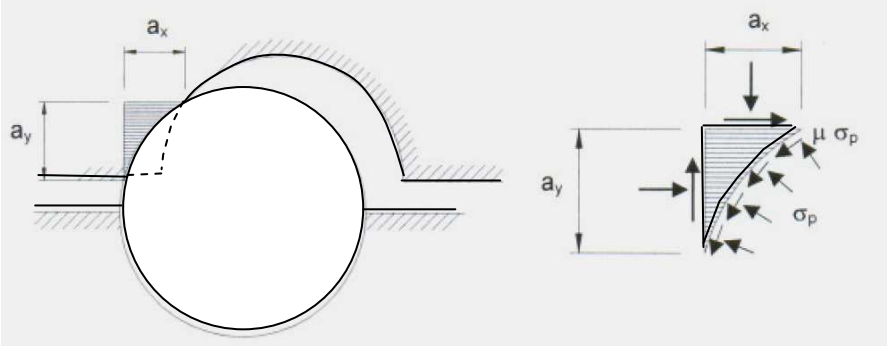

Figure 2.29: Walraven's model of crack friction

Source: Walraven [2-52] 1979

As the size or diameter of the coarse aggregate increases, the roughness of the crack surfaces increases, allowing higher shear stresses to be transferred across cracks.

Walraven [2-52] concluded that shear transfer in the interface was due primarily to 'aggregate interlock', and hence caused by those aggregates that protruded from the crack surface and provided resistance against slip. However, as cracks go through the aggregate in lightweight and high-strength concrete yet still have the ability to transfer shear, he considered the term 'friction' to be more appropriate andconcluded that the four basic parameters involved are the crack interface shear stress, normal stress, crack width, and crack slip.

2.2.8.2 Hamadi and Regan's research on lightweight and dense concrete

Hamadi and Regan[2-25] investigated the influences of different types of aggregate by applying push-off tests to gravel concrete, expanded slate concrete, and expanded clay concrete. The effect of the reduction in aggregate interlock due to aggregate fracture was studied.

Three types of test were made. Push-off specimens and divided beams were used to find load deformation characteristics for aggregate interlock and dowel actions. The aggregates used were natural gravel and sand, expanded slate (Solite) and expanded clay (Leca). Leca coarse and fine aggregates were used and no natural sand was included in the lightweight mixes. Only one mix was used for each aggregate and the mixes were designed to give reasonably similar cube strengths.

The push-off tests were made on blocks which were pre-cracked along their shear planes.

The cracking was produced by line loads applied through round bars resting in V-grooves in opposite faces of the specimens. Total separation at this stage was prevented by external bolts.

After cracking, the specimen was installed in the shear-test rig (Figure 2.30) and the bolts were removed, leaving the shear plane almost free from normal stresses. The area of the shear plane was 350 x 120mm and there was no reinforcement across it. Nominal reinforcement was provided in the remainder of the specimen.

With both lightweight aggregates, tensile failures occurred in the particles, eliminating much of the surface irregularity although random over-all undulations remained. At a smaller scale, there was a difference between the slate and clay aggregates, the fracture surfaces through the former being rough but through the latter almost plane. Similar characteristics were observed in the failure cracks of the beams described below.

Figure 2.31 shows the principal data from these tests as a graph of secant interlock stiffness E_g (= shear stress/shear displacement = τ_g / S) versus crack width. The figure includes the results of eleven tests – six with gravel and five with expanded clay (Leca) aggregate. The stiffnesses obtained with the slate aggregate were only marginally lower than those for the gravel.

The results of these tests can be interpreted approximately in terms of the very simple expression

$$E = \frac{k}{a_{cr}} \qquad 2\text{-}35$$

where a_{cr} is the crack width at the stage in question and k is a dimensional constant having the following values:

k = 1.2 N/mm^2 for gravel concrete;

k = 1.1 N/mm^2 for expanded slate concrete;

k = 0.4 N/mm^2 for expanded clay concrete.

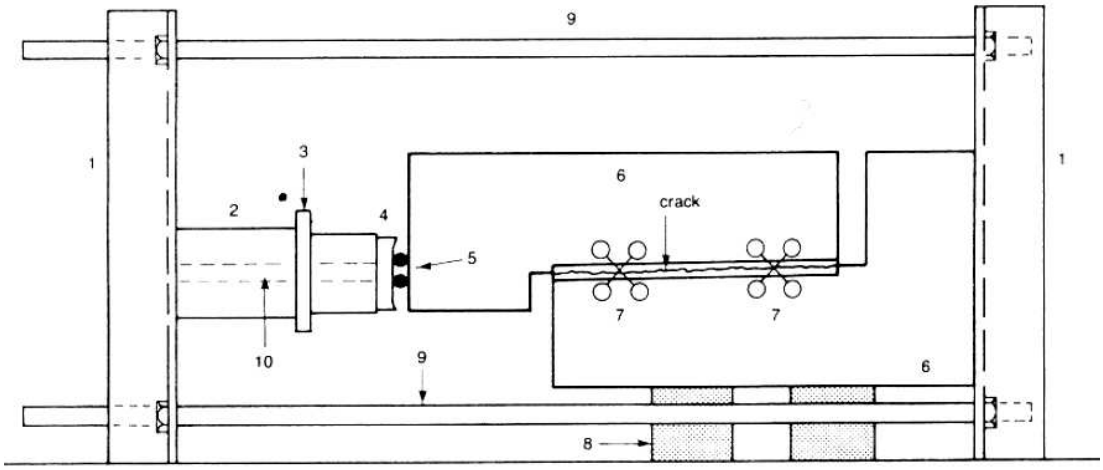

1: End supports (steel channels)
2: Hollow ram jack
3: Plate
4: Load-cell (25 kN capacity)
5: Rollers
6: Demec crosses
8: Timber supports
9: Rods tightened to the vertical channels by nuts. The lower rod passes through the timber support (8)
10: Horizontal plain bar fixed to the channel to hold the assembly (2, 3 and 4)
11: Laboratory floor

Figure 2.30: Push-off specimen (700 x 300 x 150 mm) to be tested
Source: Hamadi and Regan [2-25] 1980

The data here are all for concretes with cube strengths of 25-30 N/mm^2, but it is unlikely that variations of cube strength would have much effect upon interlock at low normal stresses, where the phenomenon is essentially a function of crack geometry and frictional effects. Even at higher stresses, tests by Fenwick [2-11] showed that, with a crack width of 0.2 mm, for a large range of shear stresses the displacements were increased by only about 20% as the cube strength varied from 56 to 33 N/mm^2.
The results in Figure 2.31 are of limited scope and are scattered within themselves.
The form of equation

$$E = \frac{k}{a_{cr}} \qquad \textbf{2-35}$$

however, is consistent with more numerous data from tests [2-26] of specimens with reinforcement or external compression across the shear plane.

2.2.8.3 Aggregate interlock in high strength concrete

In spite of all its economical advantages, the main weakness of HSC is its brittle behaviour and reduced shear resistance due to aggregate interlock.

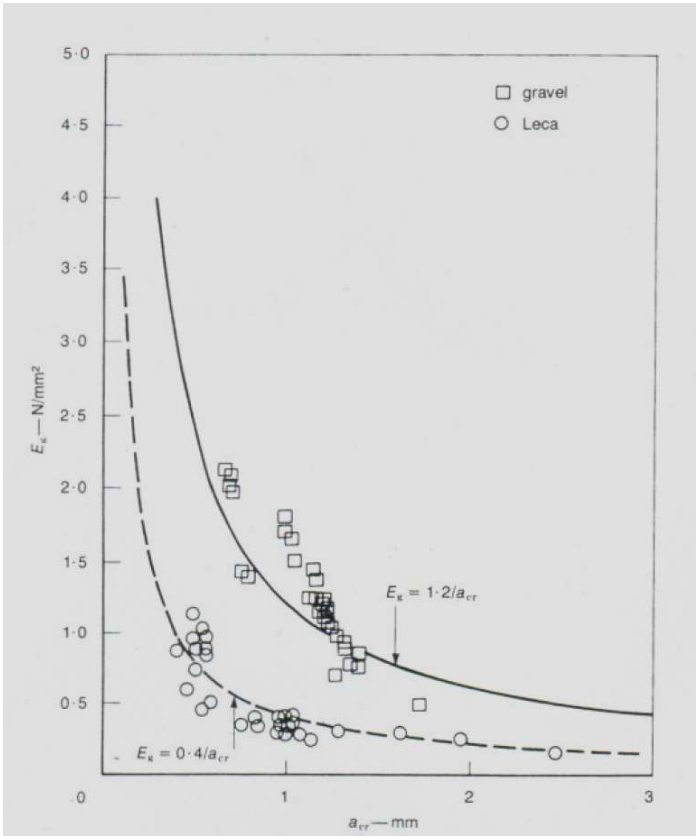

Figure 2.31 :Relationship between aggregate interlock stiffness E_g and crack width a_{cr}
Source: Hamadi and Regan [2-25] 1980

Both cement paste and natural aggregates are brittle materials. The NSC concrete made up of more ductile cement matrix materials has an obvious improved ductility behaviour compared to HSC as a result of the difference in rigidity that normally exists between the two types of NSC and HSC cement pastes with the aggregate. This difference will result in stress concentrations in the contact zones. Consequently, at a certain overall stress level, a distributed micro crack pattern will begin to form.

As the overall stress increases, an increasing part of the applied energy will be consumed as the crack pattern develops and at higher stress, the stress-strain curve tends to deviate from the linear-elastic course. As the ultimate stress level is reached, the newly developed micro crack pattern causes an abrupt failure. In HSC the failure is more abrupt, Figure 2.32. HSC has reduced ductility. The embrittlement of the HSC increases with strength. In HSC, when the maximum stress is reached a sharp reduction in stresses is measured.

Aggregate interlock is the result of the roughness of cracks in concrete. This roughness occurs when the aggregate in the concrete is stronger than the cement matrix as is the case with NSC. However, when the cement matrix is strong as in HSC, aggregate interlock

becomes relatively a less significant factor [2-45, 46&47] . In NSC where cracks travel around the unbroken aggregates that are clamped in the cement matrix, the aggregates produce a very rough surface that can transfer shear stresses and displacement along the shear interface develops this 'friction'. In NSC fracture travels along the grain surface but in HSC the fracture passes through the grain, Figure 2.33.

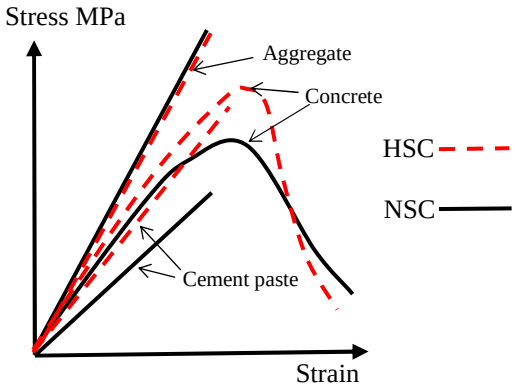

Figure 2.32: Principal stress-strain curves for cement paste, aggregates and concrete in compression

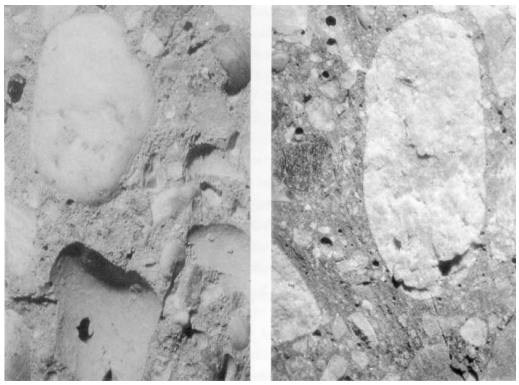

NSC **HSC**

Figure 2.33: Aggregate interlock resulting from the roughness of cracks in concrete
Source: Mathias, B. - 2008 [2-48]

Crack friction depends on the aggregate strength and size as well as the difference of strength between the aggregate and the cement matrix. When cracks travel through the aggregate which normally occurs in HSC or in lightweight NSC, the roughness of the concrete is reduced which reduces the crack friction capacity.

2.2.8.4 Regan et al's research on high strength concrete

Regan et al [2-45] analysed test results from a number of experiments on HSC beams made with limestone aggregate. It was found that the shear strengths of members without shear reinforcement are often below characteristic resistances calculated according to EC 2 [2-49] and other up-to-date guidelines. A considerable percentage of the experimental strengths were found to be below design resistance, which was greatest where HSC beams had relatively large effective depths.

The same trend seems to occur to a lesser degree in other aggregates. Members with shear reinforcement are also likely to be affected but not as much as that of those without.
In reinforced concrete members without shear reinforcement, shear resistance is mainly affected by the transfer of shear forces across cracks, in which a large part of the applied

shear is carried across flexural cracks. The force transfer across early 45°cracks develops a resistance greater than those anticipated for 45° truss models for elements with shear steel.

The magnitude of the shear transferred across a crack depends on the roughness of the crack surfaces and the widths of the cracks. In typical element design equations, the second influence is treated by depth or size factors.

Regan et al [2-45] reviewed differences in the behaviour of dense concrete made with different aggregates and discussed research completed by Taylor [2-50] , KaWar [2-51], Walraven [2-52] , Al-Hussaini and this writer [2-46 & 2-47] on aggregate interlock and referred to this writer's tests, Table 3.5, in which the shear transfer strength of specimens made with limestone aggregate failed to increase with increasing concrete strength and produced the graph shown in Figure 2.34.

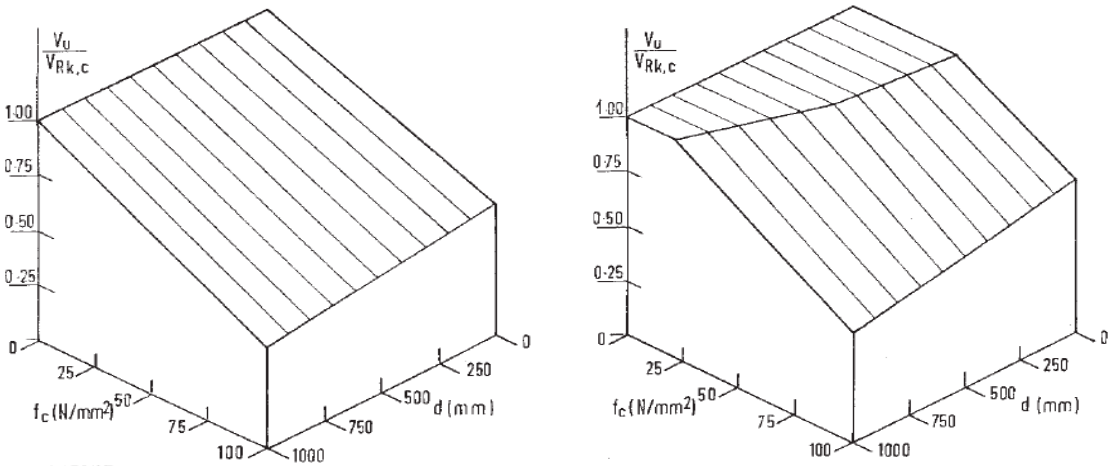

Limestone aggregate Gravel aggregate

Figure 2.34: Relation between V_u/V_{Rk} and concrete strength(f_c) and beam depth (d)

Source: Regan et al [2-45], 2005

Figure 2.34 provides a three dimensional graph of the influences of concrete strength and beam depth on $V_u/V_{Rk,c}$ calculated with no restrictions on f_{cu} to EC2 [2-49]. Regan et al [2-45] outline that "The graphs are somewhat subjective lower-bounds, where the inclined lines are sections through the solids of Figure 2.34. Although empirically reasonable in the ranges of concrete strengths and member depths normally considered, however, the linear reductions of $V_u/V_{Rk,c}$ are not physically possible as for very large members or very high concrete strengths because the strengths tends to become zero".

2.2.8.5 Albajar's research on aggregate interlock

Albajar's [2-44] research included a total of seven push-off tests, Figure 2.30. The specimens were cast in two groups; one group made with limestone aggregate concrete and another group made with normal gravel aggregate. The limestone aggregate fractured completely at the crack unlike the gravel, where the crack went round the aggregate.

Push-off tests were carried out by using gravel and limestone aggregates which showed that considerable shear stresses could be transmitted through the crack in the limestone specimens. This was surprising since the limestone aggregate had fractured completely at the crack in these specimens. In addition, the friction parameter μ estimated from linear regression of the experimental data according to the shear friction formula ($\tau = C + \mu \sigma$), was very similar between the gravel and limestone push-off tests ($\mu \sim 1.0$).

Albajar [2-44] concluded that his estimated value of the friction coefficient was considerably larger than those usually obtained experimentally for light-weight aggregate, ($\mu = 0.3$), by Hamadi & Regan [2-25] or those recommended in EC2 [2-49] for very smooth surfaces ($\mu = 0.5$).

It is worth noting that Hamadi & Regan [2-25] tested two types of lightweight concrete which were expanded clay aggregate (LECA) and expanded slate (Solite). Their[2-25] research demonstrated the inherent shear weakness of LECA, with a dimension constant of $k=E_g a_{cr}$, $k=0.4$ N/mm^2, only had 50% of the shear resistance of normal strength concrete of similar crushing strength made with gravel aggregate whereas Solite had $k=1.1$ N/mm^2 which is close tothat of gravel . LECA is no longer used in reinforced concrete as the result of their research [2-25] and is presently used for thermal insulation, light blocks, etc.

After detailed investigation of several models, Albajar [2-44] chose Hamadi & Regan's [2-25] model due to its simple formulation and the linear aggregate interlock relationship presented, for his analysis of shear cracks for the beam tests in the final chapters of his thesis.

The predictions of the shear stresses in the push-off tests using these two models seemed sensible for crack slips of up to around 1mm. This was acceptable for the analysis of cracks in beam tests, since the crack slips measured in this case were usually lower than 0.5mm.

2.2.9 Other factors influencing shear behaviour

Factors such as overall depth and axial forces have some influence on the shear behaviour. A brief description of their influences is discussed in this section.

2.2.9.1 Size of the beam

An increase in the overall depth of a beam without stirrups results in a decrease in the shear at failure for the given concrete strength, tension reinforcement ratio and span to depth ratio. The width of an inclined crack depends on the product of the strain in the reinforcement crossing the crack and the spacing of the crack. With increasing beam depth, the crack spacing and the crack widths tend to increase. This leads to a reduction in the maximum shear stress that can be transferred across the crack by aggregate interlock.

Kani raised the size effect subject in 1967, when he demonstrated that as the depth of the beam increases the shear stress at failure decreases. As the depth of the beam increases, the crack widths at points above the main reinforcement tend to increase. Some authors think that this leads to a reduction in the aggregate interlock across the crack, resulting in earlier inclined cracking. In 1999 Collins and Kuchma [demonstrated that the size effect disappears when beams without stirrups contain well-distributed longitudinal reinforcement. This was partly due to research at the University of Westminster in 1996.

2.2.9.2 Axial forces

Axial compressive forces tend to increase the inclined cracking load. As the axial compressive force is increased , the start of formation of flexural cracking is delayed and cracks do not penetrate as far into the beam. Axial tensile forces tend to decrease the inclined cracking because they increase the stresses and strains in the tension reinforcement. This causes an increase in the inclined crack width which results in a decrease in maximum shear stress that can be transmitted across the crack. This reduces shear failure load. The opposite is true for axial compressive forces.

2.3 Design Codes for beams without shear reinforcement

For BS8110 [2-42] and EC 2 [2-49]**,** the following equations are the two basic expressions for the characteristic shear resistances of slender rectangular members without shear reinforcement:

The resistance of a rectangular reinforced concrete beam with shear reinforcement can be assessed by the BS8110 [3-**Error! Bookmark not defined.**] equation, with eliminating safety factors.

$$V_{du} = 0.27(100\,\rho_i f_{cu})^{1/3}\,(400/d)^{1/4}\,bd + \rho_w f_y\,bd \qquad \textbf{2-36}$$

EC 2 [2-49]

$$V_{Rk,c} = 0.18(100\rho_i.f_c)^{1/3}\,(1+\sqrt{200/d})b.d \qquad \textbf{2-37}$$

both in N and mm units.

Present UK recommendations, BS 8110 [2-42] restricts concrete strength to 40N/mm^2 on the value of f_{cu} to be used in equation (2-21). The Concrete Society's recommendations of 1998 [2-53] had a restriction on concrete strength of 100N/mm^2, but this has been reduced to 60N/mm^2, by an amendment made in 2004 [2- 45], partly motivated by this research work detailed in Table 3.5.

The above two equations differ slightly from one another, as the characteristic level the EC 2 resistances are a little above those from equation (2-21), EC 2 applies a partial safety of 1.5 to obtain design resistances, whereas the BS 8110 factor is only 1.25. At design level, EC 2 shear resistances given by equation (2-32) are about 10% below those from BS8110, equation (2-21), although the difference is, in result is reduced by the UK's slightly higher load factors.

The shear expression in BS 5400 [2-54] is practically the same as that of BS 8110 [2-42] . The coefficient 0.18 in equation (2-32) is the recommended value, but it may be modified in National Annexes. In EC 2, there is a limit of $f_c \leq 90$N/mm^2 [2- 45], however, the UK National Annex has given a limit of $f_c \leq 50$N/mm^2.

However, when related experimental work demonstrate that a higher value f_c can be safely used for the HSC, then use of higher strength concrete is permitted. This research experimentally demonstrates, Table 3-13, that shear resistance of HSC beams of a/d=3, $f_c \leq 90$ N/mm^2, with HWB can be safely predicted when this writer's proposed design rule to include dowel action for HWB is applied, section 3.9.

In the ACI building code [2-55] the expression which is typically used to estimate the nominal shear strength of non-prestressed RC members without stirrups when considering shear failure for the practical range of reinforcement 0.0075 to 0.025 is:

$V_c = b_w d(\sqrt{f'_c}/ 6)$ **2-38**

although this equation over-estimates the shear with a small percentage of tension steel. When the tension steel ratio is small, flexural cracks extend higher into beam and open wider, and an increase in crack width causes a decrease in the maximum component of dowel action from the tension reinforcement and the aggregate interlock.

In using the expression in equation (2-3) to estimate the shear strength of members made from high-strength concrete, the term $\sqrt{f'_c}$ is limited to a value of 8.30 MPa .

2.4 Review of Codes for shear reinforcement in beams

The shear failure of a beam without stirrups is sudden and brittle, therefore codes recommend a minimum amount of stirrup reinforcement. The shear failure loads predicted by codes are widely different from one another.

The treatments of members with shear reinforcement are different in BS 8110 and EC 2[2-45]. In BS 8110 the shear resistance is taken as the sum of $V_{Rk.c}$ and the yield forces of (vertical) stirrups within a length equal to d:

$V_{Rk} = V_{Rk.c} + \rho_w f_y bd$ 2-31

$V_{Rk.c}$, the calculated characteristic shear resistance of a member without shear reinforcement, can only be explained as a force transferred across cracks at approximately 45°. ρ_w is the ratio of vertical stirrups, f_y is yield stress of reinforcement.

Both of these approaches rely upon the transfer of shear forces across well-formed cracks, and it is thus probable that the characteristics of the aggregate have an influence on behaviour and ultimate strength. The influence is probably less than that in members without shear reinforcement as the effective depth is a less relevant factor when shear reinforcement provides a control over crack widths.

2.4.1 BS8110 approach for shear link design

Although the truss analogy still forms the basis of the BS8110 [2-42] treatment of shear of reinforced concrete sections, it is now modified to the extent that the shear strength of the concrete is assumed to make some contribution to the overall strength of the section.

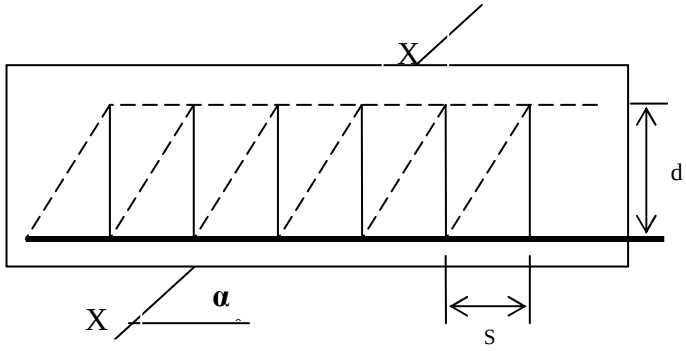

Figure 2.35:Members of a pin jointed truss with concrete (---) compression and steel (__) tension.

The stirrups and the main reinforcement represent the tensile members of a truss, and the concrete acts as the compression members. Even assuming that the concrete has cracked in diagonal tension, the aggregate interlock factors provide some shear resistance, v_c in the concrete. At shear collapse, therefore, the external shear force on the section is resisted by forces in the shear reinforcement and the shear resistance of the cracked concrete so that, considering the vertical equilibrium of the section to the left of the diagonal tension crack X-X, Figure 2.35,

$$v_{bd} = [\ (As_v\ f_{yv} / \gamma_m\ )\ .\ (d/s_v\ ).\ \cot\alpha\ ] + v_c bd \qquad 2\text{-}39$$
$$\qquad\quad (1) \qquad\qquad (2) \qquad\qquad (3)$$

where

v_{bd} = external shear

expression (1) = force in one stirrup

expression (2) =number of stirrups

expression (3) = shear resistance of cracked concrete

Note that the number of stirrups cut by the section line depends on the spacing of the

stirrups, the depth of the beam and the angle of the tension crack which, for design purposes, may be taken as being 45° (Figure 1-2).

Rearranging

vbd= [(Asv fyv / γm) . (d/sv). cot α] + vcbd

and putting the partial safety factor for the shear reinforcement γ_m =1.15.

gives

$As_v / s_v = b(v-v_c) / 0.87 f_{yv}$ 2-40

Permitting the required area of vertical stirrups to be found. If bent-up bars are used then the procedure is as above except that, as vertical components of the forces in the bars are required, the angle of inclination of the bars is included in the basic equation.

The angle of inclination should not be less than 45° and, as experimental evidence suggests that an inclined bar system is not efficient in resisting shear unless additional reinforcement in the form of stirrups is provided, it is now recommended that a maximum of 50 per cent of the shear reinforcement be in the form of bent-up bars, the remainder being vertical stirrups.

0.5 v_c and $(v_c + 0.4)$ N/mm^2. As with the designed shear reinforcement, the stirrup spacing is limited to a maximum of 0.75 d.

$As_v / s_v = 0.4b / 0.87 f_{yv}$ **2-41**

For a design shear stress greater than $(v_c + 0.4)$ N/mm^2, shear reinforcement should be provided to

$As_v / s_v = b(v-v_c) / 0.87 f_{yv}$ Asv / sv = b(v-vc) / 0.87 *fyv* **2-40**

2.4.2 Shear design of links in Eurocode 2

Eurocode 2 [2-49] recommends that for members requiring shear reinforcement, their design is based on a truss model. For members with vertical shear reinforcement, the shear resistance $V_{Rd,s}$, should be taken to be the lesser of the following:

$V_{Rd,s} = (A_{sw} / s) Z. f_{ywd} \cot\Theta$ 2-42

or

$V_{Rd,max} = \alpha . b_w . Z.v. f_{cd} / (\cot\Theta + \tan\Theta)$ 2-43

The recommended limiting values for cot Θ are given by the expression

$1 \leq \cot \Theta \leq 2.5$

where

Z = is the inner lever arm , its approximate value may be taken as 0.9d

A_{sw} is the cross-sectional area of the shear reinforcement,

s is the spacing of the stirrups,

f_{ywd} is the yield strength of the shear reinforcement,

v may be taken to be 0.6 for 60 MPa, and 0.9 for high-strength concrete beams,

α = 1, for non-prestressed structures.

2.4.3 Shear design of web reinforcement in ACI code 318

Section 11.4.1.2 of ACI code 318 [2-55] allows shear reinforcement for non-prestressed beams and a variety of shapes such as stirrups or ties, welded fabric, stirrups inclined at 45º and combination of spirals, circular ties and hoops are acceptable. Section 11.4.6.1 of ACI code 318 requires a minimum amount of stirrup reinforcement to be provided if the applied shear force, V_u, exceeds half of the factored inclined cracking shear, ǿ ($0.5V_c$) where ǿ=0.75 (ACI Code Section 9.3.2.3) is the strength-reduction factor .

There are exceptions for certain types of beams where load redistributions can occur in the transverse direction or in relation to size –effect or beams with steel fibre –reinforced concrete.

The minimum stirrup reinforcement requirement (ACI Code Section 11.4.6.3) from ACI equation 11-13 is:

$$A_{v,min} = \frac{1}{16} \times \frac{b_w}{f_{yt}} \times s \times \sqrt{f_c'} \qquad \textbf{2-44}$$

But not less than

$$A_{v,min} = \frac{1}{3} \frac{s b_w}{f_{yt}} \qquad 2\text{-}45$$

In seismic regions, web reinforcement is required in most beams, because V_c is taken equal to zero if earthquake-induced shear exceeds half the total shear.

2.5 Conclusion

A review of background to shear analysis and factors influencing shear resistance was discussed. Actions influencing the total shear strength was discussed and a detailed study

on past research on dowel action was performed. It was shown that Baumann's and Hamadi-Regan's proposals were a more rational approach for predicting the dowel forces compared to other researchers.

Past research on aggregate interlock with various type of aggregate for light weight, normal weight concrete was investigated. This was further extended to discuss the performance of aggregate type in HSC.

Guidance from international codes of practice for shear design and shear reinforcement in beams was investigated.

From this study the main conclusion is as follows:

- Shear performance of HSC beams made with limestone aggregate need further investigation due to reduced aggregate interlock action. In the next chapter the experimental testsbeams are experimentally tested to examine the aggregate interlock in the HSC beams of a/d=3 is described.

- The dowel resistance of NSC and HSC beams with HWB of a/d=3 will be experimentally tested in the next chapter to developed an improved formulae to predict dowel resistance. Baumann's and Hamadi-Regan proposal for prediction of dowel action will be modified to a new empirical formulae for the prediction of dowel resistance of HWB in the next chapter.

- The proposed Baumann modified formulae will be added to BS8110 and other international code shear design formulae to predict total shear resistance including the contribution of HWB. The proposed design predictions will be compared with the beams tested by this writer as well numerous beams tested by other researchers.

2.6 References

2-1 Liberati, A.N, Bourbon, F. 'Rome, Splendours of an Ancient Civilization'. Thames & Hudson

2-2 Ritter, W. "Die Bauweise Hennebique (Construction Techniques of Hennebique)", *Schweizerische Bauzeitung*, Zürich, Vol. 33, No. 7, pp. 59-61, 1899.

2-3 Morsch, E. 'Der Eisenbetonau, seine Theorie und Anwendung'. Published in English as 'Concrete-Steel construction'. New York, Engineering News Publishing Co. 1909 & McGraw-Hill Book Company, New York, 368pp translated from 3rd (1908) German edition. German publication of first edition (1902).

2-4 Bach, C., Graf, O. 'Versuche mit Eisenbetonbalken, namentlich Zur Bestimmung des Gleitwiderstandes'. Mitteilungen uber Forschung sarbeiten auf dem Gebiete des Ingenieurwesens, No 72-74, Verein dentscher Ingenieure, Berlin (1909). Summarized by Slater, W.A. as 'Tests of Bond Resistance in Reinforced Concrete Beams'. Engineering News-Record, Vol.94, June 25, 1925, pp. 1050-1053

2-5. Talbot, A.N. 'Test of reinforced concrete beams: resistance of web stresses series of 1907 and 1908', Bull. 29, University of Illinois, Engineering Experiment Station, Urbana, I11. 1909

2-6 Bjuggren, U. 'Bond and Anchorage'. Translated and summarised from Swedish by Mylrea, T. D. Journal, Am, Concrete Institute, March 1948, Proceedings, Vol 44, pp.521-552

2-7 Moe, J. 'Discussion of ACI-ASCE Committee 326', Journal of the American Concrete Institute, Proceedings, Vol. 59, No. 9, pp. 1334-1339, 1962

2-8 Lorentsen, M. 'Theory for the combined action of bending moment and Shear in reinforced and prestressed concrete beams reinforced and prestressed concrete beams'. ACI Journal, Volume 62, issue 4, pp 403-420, April 1, 1965

2-9 Kani, G.N.J. "The Riddle of Shear Failure and its Solution," Journal of the American Concrete Institute, Proceedings, Vol. 61, No. 4, pp. 441-466, 1964

2-10 Taylor , H.P.J. 'The Fundamental Behavior of Reinforced Concrete Beams in Bending and Shear'. ACI special publication, Vol 42, pp 43-78, Jan 1974

2-11 Fenwick, R.C., Paulay, T. 'Mechanisms of shear resistance of concrete beams'. Proceedings of the American Society of Civil Engineers. Vol.94, No. ST 10. October 1968. pp 2325-2530

2-12 Schlaich, J, Weischede, D. "Detailing of Concrete Structures" (in German), Bulletin d'Information 150, Comite Euro-International du Beton, Paris, March 1982, 163 pp

2-13 Reineck, K.H. “Ultimate shear force of structural concrete members without transverse reinforcement derived from a mechanical model.’’ ACI Struct. J., 1991, 88-51, 592–602

2-14 Taylor, R.P.J. 'Fundamental behaviour in bending and shear of reinforced concrete.' PhD. thesis. University of London. 1971.316pp

2-15 Faber, O. : ‘Reinforced Concrete beams in bending and shear’. London. Concrete Publications, Ltd. 1924

2-16 Borishanski, M. S. : 'Calculations for reinforced concrete members subjected to transverse force'.(exact reference uncertain). 1946

2-17 SNIP 2.03.01 : Plain and reinforced concrete structures (English language version). Moscow. Gosstroy, USSR.1991

2-18 Forssell, C. ‘Tests of Shear Strength and Shear Reinforcement of Concrete Beams,’ Transactions, Swedish Cement and Concrete Research Institute at the Royal Institute of Technology, Stockholm, Sweden, No. 78, 1954

2-19 Loreston, M. ‘Shear and bond in prestressed concrete beams without shear reinforcement’. Handlingar Nr 47, Stockholm, Statens Rad for Byggnadsforskning, 1964

2-20 Jones, R. ‘The Ultimate Strength of Reinforced Concrete Beams in shear’. Magazine of Concrete Research (London), V.8, No. 23, Aug. 1956,PP. 69-84

2-21 Krefeld, W.J., Thurston, C.W. ‘Studies of the shear and diagonal tension strength of simply supported reinforced concrete beams’. Columbia University, New York, 1962. (April 1966, ACI Journal)

2-22 Taylor, H. P. J. ‘Investigation on the dowel shear forces carried by the tensile steel in reinforced concrete beams’. London, Cement & Concrete Association, 1969, Technical Report 42.431.

2-23 Baumann, T., Rusch,.H.'Versuche zum Studium der Verdubelungswirkung der Biegezugbewehrung eines Stahlbetonbalkens, (Tests studying the dowel action of the flexural tensile reinforcement of reinforced concrete beams.) Berlin, Wilhelm Ernst und Sohn, 1970, Deutscher Ausschuss fur Stahlbeton, Heft 210. pp. 42-82

2-24 Baumann, T. “Tests to Study the Dowel Action of the Bending Tension Reinforcement of Reinforced Concrete Beams,” *Bericht Nr. 77*, Munich Technischen Hochschule, (English Translation by PCA), 1968

2-25 Hamadi, Y.D, Regan P.E ‘Behaviour in shear of beams with flexural cracks’. Magazine of Concrete Research: Vol. 32, No 111: June 1980

2-26 Hamadi, Y.D. ‘Force transfer across cracks in concrete structures’. PhD thesis, Polytechnic of Central London, May 1976. pp. 503

2-27 Ramdane, K.E. ‘ Properties and structural behaviour of high strength concrete’. University of Westminster , PhD thesis, 2000, p.317

2-28 Leonhardt, F.,. and Walther, R . ‘The Stuttgart shear tests 1961’. Translated by c. V.Amerongen from Beton und Stahlbetonbau, Vol. 56, No. 12. 1961. Vol. 57, Nos. 2, 3, 6,7 and 8.1962. London, Cement and Concrete Association Liabrary,1964. Translation Cj 111.

2-29 Moody, K. G., Viest, I, M., Elstner R. C., and Hognestad, E. ‘Shear strength of reinforced concrete beams. Part 1 – Tests of simple beams’. Journal of the American Concrete Institute. Proceedings, Vol. 51, NO.4. December 1954. pp. 317-33

2-30 Laupa, A, Siess, C. P., and Newmark, N. M.’The shear strength of simple span reinforced concrete beams without web reinforcement’. Urbana, University of Illinois, 1953. Civil Engineering studies, Structural Research Series No. 52.

2-31 Bhal, N. S. ‘Uber den Einfluss der Balkenhohe auf die Schubtragfahigkeit van einfeldrigen Stahlbetonbalken mit und ohne Schubbewebrung’. (On the influence of beam depth on the shear strength of simple span reinforced concrete beams with and without shear reinforcement.) Thesis submitted to the University of Stuttgart for the degree of Dring. 1968. pp. 123

2-32 Regan, P. E. ‘Shear tests of beams with low percentages of high yield main reinforcement’. Unpublished tests at the Polytechnic of Central London, 1975.

2-33 Morrow, J., and Viest, I. M. ‘Shear strength of reinforced concrete frame members without shear reinforcement’. Journal of the American Concrete Institute. Proceedings Vol. 53, No.9. March 1957. pp. 833-869.

2-34 Taylor, R. ‘Some shear tests of reinforced concrete beams without shear reinforcement’. Magazine of Concrete Research. Vol. 13, No. 36. November 1960. pp. 145-154.

2-35 Mathey, R.G., Walstein, D. ‘Shear strength of beams without web reinforcement containing deformed bars of different yield strengths’. Journal of the American Concrete Institute. Proceedings Vol. 60, No.2. February 1963. pp. 183-205.

2- 36 Taylor, H. P. J. ‘The shear strength of large beams’. Proceedings of the American Society of Civil Engineers. Vol. 98, No. STl1. November 1972. pp. 2473-2490

2-37 CP110, Structural use of concrete, Part 1.Code of practice for design and construction, British Standards Institution, London, 1972

2-38 J. Houde and M.S. Mirza ‘A Finite Element Analsis of Shear Strength of Reinforced Concrete Beams’ Journal ACI Proceedings, volume 42, 1 January, 1974, pp.103-128

4-39 Fardis, M. N., and O. Buyukozturk. "Shear Transfer Model for Reinforced Concrete." Journal of The Engineering Mechanics Division, ASCE 105, no. EM2 (1979): 255-274.

2-40 Chana, P.S. 'Investigation of the mechanism of shear failure of reinforced concrete beams'. Magazine of Concrete Research: Vol. 39, No 141: December 1987

2-41 Desai, S.B. ‘Horizontal web steel as shear reinforcement’. Magazine of Concrete Research, Vol.47. No.171.June 1995.pp. 143-152

2-42 BS8110: Structural use of concrete, part 1. code of practice for design and construction , British Standards Institution, London , 1985

2-43 Bjuggren, U. ‘Discussion of a paper on bond and anchorage’, Journal of the American Concrete Institute. Proceedings Vol.20, No.4. Part 2, December 1948. pp. 552-1-4.

2-44 Albajar, J.S. ‘The influence of aggregate fracture on the shear strength of reinforced concrete beams’, Thesis submitted to the Imperial College London, University of London, for the degree of PhD, Sept 2008, pp. 409

2-45 Regan, P. E., Kennedy -Reid I. L., Pullen, A. D., Smith, D. A. ‘The influence of aggregate type on the shear resistance of reinforced concrete’ – The Structural Engineer. 6 December 2005

2-46 Al-Hussaini, A., Motamed, J. ‘HSC beams with combination of links and horizontal web steel as alternative shear reinforcement’. 6th International Symposium on Utilization of High Strength/High Performance Concrete, Leipzig, June 2002

2-47 Motamed, J. ‘Shear in normal strength and high strength reinforced concrete beams with stirrups and horizontal web bars’. University of Westminster, MSc Dissertation, 1997

2-48 Mathias B, 'History and Development of Concrete'. Opus Concrete architecture & Design, issue 3, 2008

2-49 Eurocode 2: Design of concrete structures, Part 1-1, General rules and rules for buildings, BS EN 1992-1-1:2004, British Standards Institution, London, Dec 2004
2-49 Allan, A.H, ‘Reinforced Concrete Design to BS8110 Simply explained’. E & F. Spon Ltd, published 1988, p 49 to 51

2-50 Taylor, H. P. J. 'Investigation of the forces carried across cracks in reinforced concrete beams in shear by interlock of aggregate', Tech. Rep. 42.447, Cement and Concrete Association, London, Nov 1970

2-51 Kawar, A.N. N. 'Punching strength of plain concrete', Dissertation, University of Birmingham, Dept. of Civil Engineering, 1980

2-52 Walraven, J.'Experiments on shear transfer in cracks in concrete, Part II: Analysis of test results', Report 5-79-1 0, Dept of Civil Engineering, Delft University of Technology, Nov 1979

2-53 Concrete Society: ‘Design guidance for high strength concrete’, *Tech. Rep. No 49*, Slough, The Concrete Society, 1998.(amended 2004)

2-54 BS 5400: Steel, concrete and composite bridges, Part 4. Code of practice for design of concrete bridges, British Standards Institution, London 1990.

2-55 ACI Committee 318, Building Code Requirements for Structural Concrete (ACI 318-08) and commentary (ACI 318R-08), American Concrete Institute , Formington Hills, MI, 2008, 465 pp

Chapter 3
Experimental work

3.1 Introduction

The experimental tests by this writer on twelve beams are discussed, Table 3.4, strain gauge recordings on the reinforcement of the specimen are interpreted and the influence of HWB and its contribution to both NSC and HSC beams are explored.

A theoretical mechanism of internal shear forces by considering the proportion of shear resistance taken by different actions in HSC with HWB based on reduced contribution of aggregate interlock and improved contribution of dowel action due to HWB is developed and internal shear forces are diagrammatically shown, Figure 3.39.
This writer's proposed design equation is applied to experimental tests completed by others and its accuracy of prediction of the shear resistance is compared with the design rules proposed by other researchers.

Design rules proposed for predicting dowel action by other researchers are investigated and a new and improved design rule is proposed to take into account the number of dowel bars resisting shear forces.

This writer's proposed design rule for the prediction of the quantity of HWB that compensates for the inherent weakness in HSC is discussed in section 3.6, and its application within the existing design rules for current codes of practice including BS8110 [3-9] , EC2 [3-10], CEB FIP90 [3-1] and ACI318 [3-2] for members with and without shear links is investigated.

General theories for the analysis of beams subjected to bending and shear are reviewed and extended to develop a design rule for prediction of shear based on experimental results with values calculated using semi-empirical formulae.

3.2 This writer's experimental tests on twelve beams

Twelve HSC and NSC beams with links and varying amounts of horizontal web steel at the centre of the cross-section of the members were tested to shear failure. They were simply supported beams loaded with point loads and therefore subjected to bending and shear.

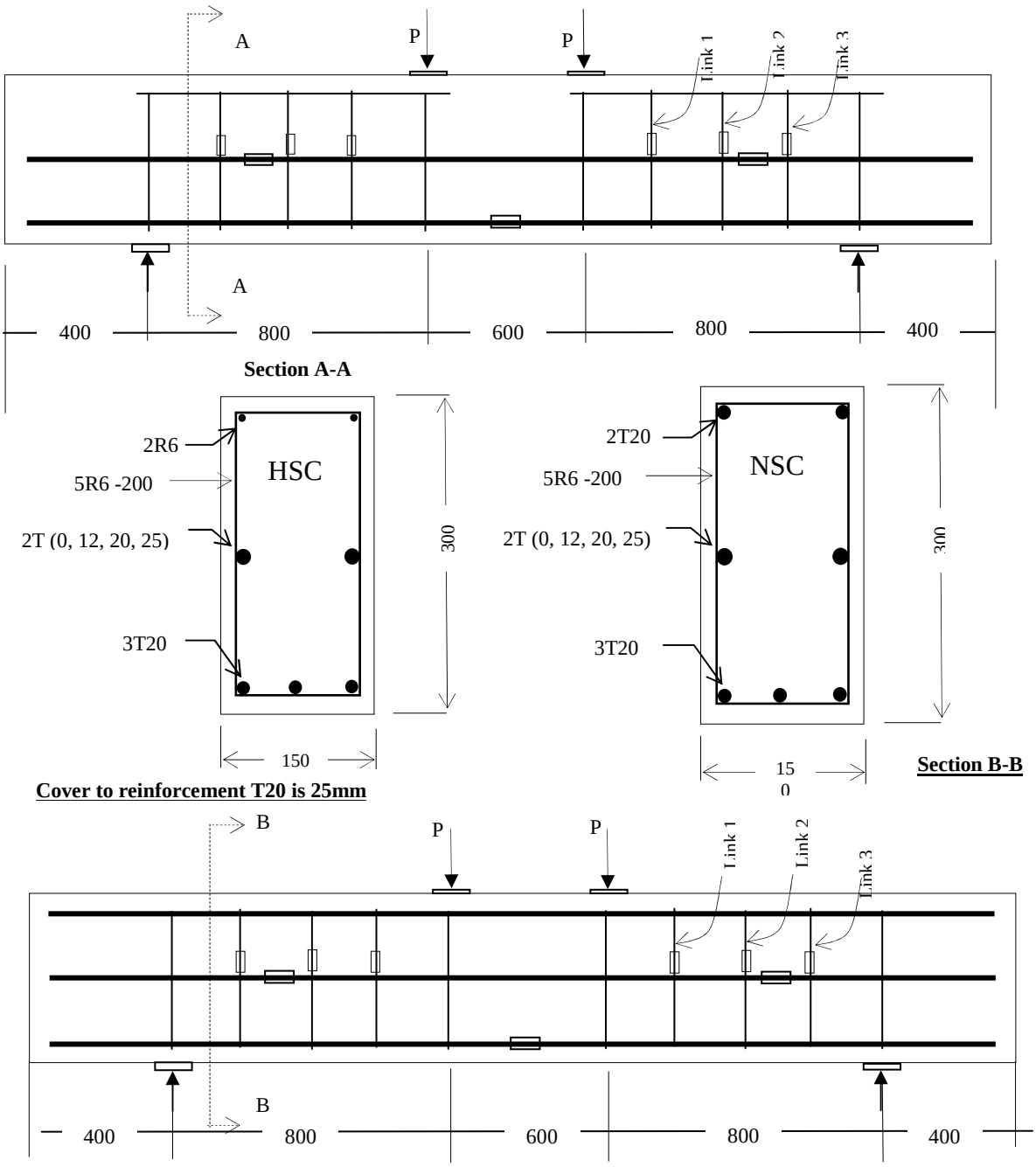

Figure 3.1: Reinforcement details and position of strain gauges for HSC and NSC test specimens.

The parameters varied in the test series were:

- Type of concrete (normal strength and high strength).
- Compression steel.
- Horizontal web steel.
- Distribution and strength of vertical reinforcement (beam NSCL was different).
- Shear span (beam BJ2 was different).

The experiments were performed in order to study the effect of horizontal web reinforcement on the shear capacity of rectangular normal and high strength concrete beams with stirrups. In the next section tests of four identical NSC beams without stirrups with HWB, completed in the Construction Hall of the University of Westminster [3- 23] during the same period as this writer's experiment, are discussed.

The beams were intended to have practical dimensions, thus avoiding excessive size effects. Eight of the beams of HSC and NSC of a/d=3.02 with links and HWB were tested to failure in order to investigate the dowel action contribution of the HWB to shear resistance of the beams.

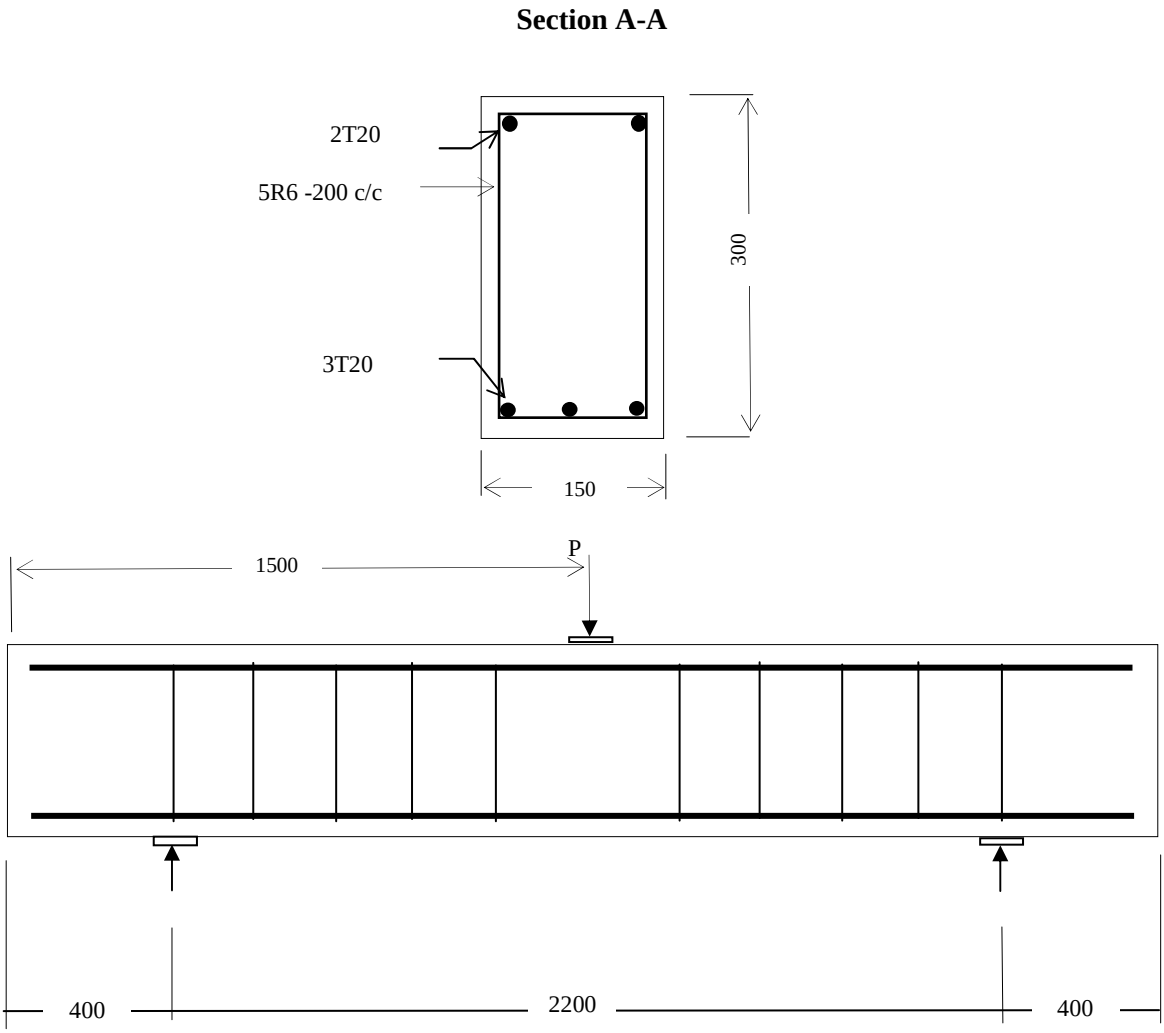

Figure 3.2 : Reinforcement details for the HSC test specimen BJ-2 with point load in the mid-span, Shear span to depth ratio=4.15

3.2.1 Design of beams for shear failure

From the proposed design equation

Vdu = 0.27(100 ρi.fcu)1/3 (400/d)1/4 bd + ρw fy bd + 1.64.bn.db.4√n. *fcu1/3* 3.13

let us predict shear failure load for the typical beam shown with geometry and reinforcement detailing in Figure 3.1 with stirrups and 20mm HWB, and. assume concrete strength of f_{cu}= 40 MPa for NSC and f_{cu}= 100 MPa for HSC steel of f_y= 460 MPa for tension as well as compression and f_y= 250 MPa for stirrups.

Let us predict shear resistance for beam of NSC with HWB of 25mm with stirrups as V_{du}= 82.76 kN for NSC and and V_{du}= 105.64 kN for HSC or totals loading of 165.5 for NSC and 211.3kN for HSC

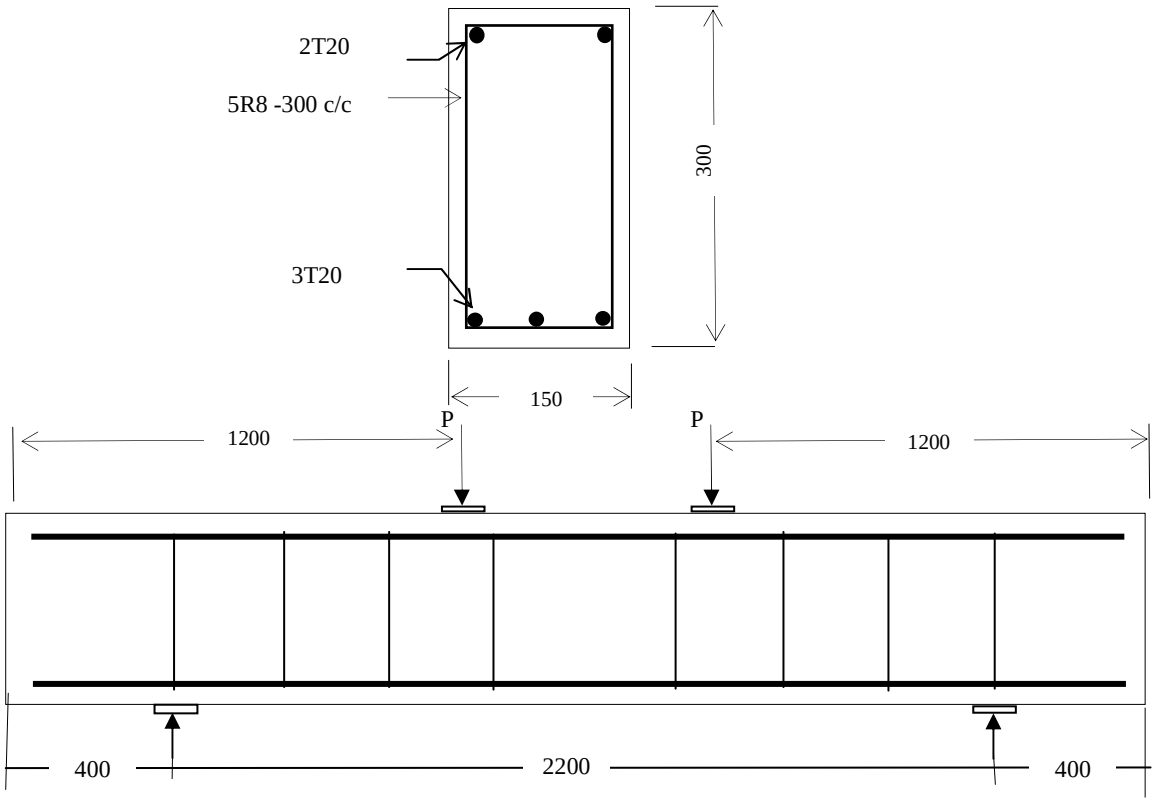

Figure 3.3: Reinforcement details for the NSC test specimen NSCL with link in the flexural span near supports. Shear span to depth ratio =3.02

To ensure shear failure, design the beam to have flexural resistance for 200kN loading for NSC.

From the condition of equilibrium for BS8110, clause 3.4.4.4, consider the simplified stress block for concrete with rectangular section, Figure 3.4.

Force from flexural steel

$T=0.87f_yA_s$ **3.1**

Concrete force is

$C=(0.67/1.5)f_{cu}b(0.9x)=0.402f_{cu}bx$ **3.2**

Equating forces to find x, and from z= d- 0.45x an expression for z in terms of A_s is obtained [3-3]:

$z =d(1-0.97f_yA_s/f_{cu}bd)$ **3.3**

Taking moments for the tensile force about the centre of compression

$M=0.87f_yA_sz.$ **3.4**

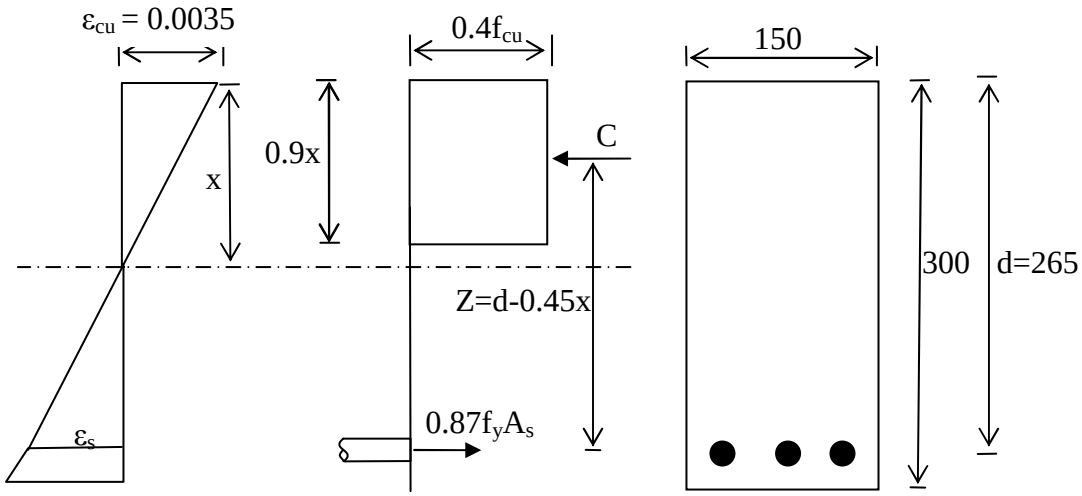

Figure 3.4: Strain and stress distribution at failure for singly reinforced NSC beams

From the above two equations

$z/d= [0.5 +\sqrt{(0.25 -K/0.9)}]$ **3.5**

where

$K=M / (bd^2f_{cu})$ **3.6**

K=1.9 for beam in Figure 3.4

Having calculated z we can now find the reinforcement required from equation

M=0.87fyAsz. 3.4

Above equation can be rearranged as

$A_s=M/0.87f_yz$

The upper limit for K for singly reinforced sections is derived as follows:

Taking moments for the compressive force about the centre of tension, we obtain

$M= (0.67/1.5)f_{cu}b(0.9x)z$ **3.7**

The area of reinforcement to balance the concrete force $C = K' f_{cu} bd^2 / z$

$0.87 f_y A_s = K' f_{cu} bd^2 / z + 0.87 f_y A_s'$ **3.8**

Taking moment about the centre of tension reinforcement :

$M = K' f_{cu} bd^2 / 0.87 f_y A_s'(d - d')$ **3.9**

In NSC, the total area of tension steel required is 898mm^2 or just under 3T20, with 2T20 compression steel. If compression steel is not used the area of tension steel required would increase to 973 mm^2, which would mean more than 3T20 tension which cannot be used because of the restriction to the width of the beam due to the cover size and spacing required.

BS8110 limits concrete strength to 40 MPa, however, for HSC beams, a similar approach is adopted by following EC2 [3-10] guidance.

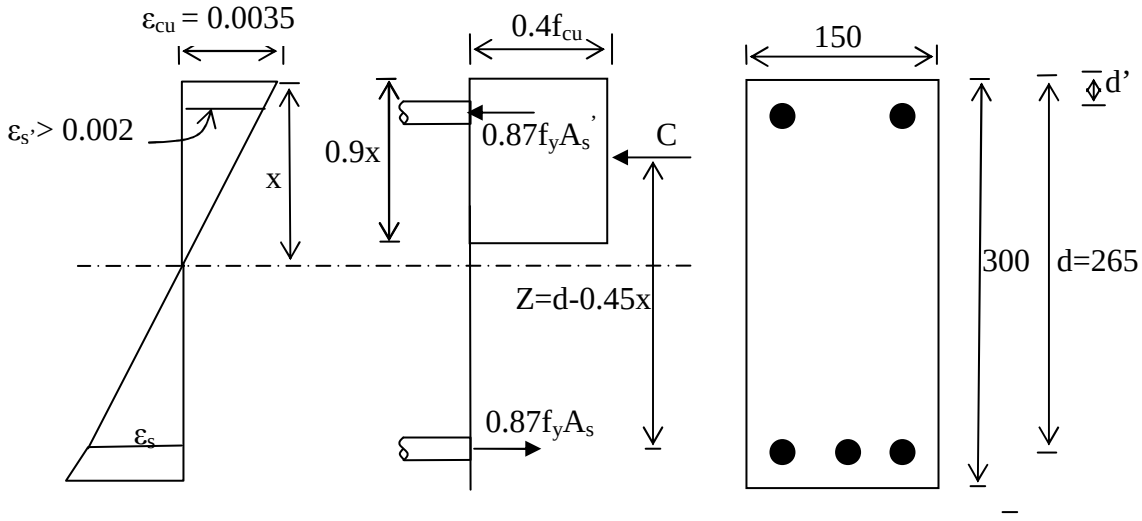

Figure 3.5: Strain and stress distribution at failure for doubly reinforced NSC beams

3.2.2 Geometry of the beams

The size and length of the test specimens were chosen to make the beams fail in shear and to ensure that the specimens were sufficiently large to simulate real structural elements.

All twelve beams were rectangular in section with a breadth of b=150mm, overall depth of 300mm, effective depth d=270mm, and a length of 3000mm. The span was 2200mm for all the beams, eleven of which had a shear span to depth ratio (a/d)=3.02, Figure 3.1 and Figure 3.3, and BJ-2 was the only one with a/d=4.15, Figure 3.2. All the beams other than BJ-2 had two vertical point loads applied at 300mm from the mid-span. One vertical point load was applied to the centre of BJ-2. All the support and load plates were 20mm thick, extended throughout the breadth of the beam and were 100mm wide. The shear span of BJ-2 was 1100 mm whereas the rest of the beams had a shear span of 800mm.

3.2.3 Concrete

Concrete density varies due to the type and content of aggregates. The NSC weighed 2280 kg and HSC weighed 2477 kg per cubic metre. Furthermore, by reducing w/c ratio for HSC and introducing silica fume into the concrete as an addition or replacement to cement, permeability is reduced [3-4& 3-5] due to blocking of the capillaries by ultra-fine silica particles, therefore, leading to fewer voids in the dense concrete.

Beam	Splitting strength fsp (N/mm^2)	Cube strength fcu(N/mm^2)	Cylinder strength fc(N/mm^2)
NSCL	3.38	44.2	35.36
NSC1	2.98	43.2	34.56
NSC2	3.01	41.0	32.80
NSC3	3.22	47.7	38.16
NSC4	2.97	43.3	34.64

Table 3.1: Results of control tests for the author's NSC. See Figure 3.3, Table 3.4, for details of the beams.

Beam	Splitting strength fsp(N/mm^2)	Cube strength fcu(N/mm^2)	Cylinder strength fcu(N/mm^2)
BJ-2	6.26	118.1	94.48
HSC1	4.34	112.5	90.00
HSC2	5.20	109.3	87.44
HSC3	4.21	109.0	87.20
HSC4	4.34	112.5	90.00

Table 3.2: Results of control tests for the author's HSC. The properties of beams HSC1-2 & HSC1-3 were assumed to be the same as HSC1.

The splitting tensile tests for the indirect tensile strength of this writer's concrete specimens were carried out in accordance with BS1881, Part 117/836. Two cylinders, 150×300mm, were tested and the results given are the average for each beam specimen shown in Table 3.1 and 3-3. It is notable that a two fold increase in tensile strength has been achieved in HSC as compared with NSC. The results of indirect tensile strength as a function of cube strength from this writer's experimental relation for dense HSC and NSC as calculated from Table 3.1 for indirect tensile strength f_{ct} is:

$f_{ct} = 0.47 \sqrt{f_{cu}}$

Description of constituent of concrete	Normal Strength (kg)	High Strength (kg)
Cement	360	550
Sand	660	560
Gravel Aggregate (0-10mm)	360	-
Gravel Aggregate (10-20mm)	720	-
Limestone (5-10mm)	-	1140
Water	180	160
Superplasticiser	-	12.1
Silica fume	-	55

Table 3.3:The mix proportions by weight developed from volumetric equation per cubic metre of concrete used for testing author's beams

3.2.4 Reinforcement

All the beams have 3T20 tension steel and the ratio was ρ=2.33%. Beams BJ-2, NSCL, NSC1, HSC1, HSC1-2 and HSC1-3 had no HWB, horizontal web bars, whereas the rest of the beams had two HWB at 100mm from the centre of the tension steel. The HSC beams other than BJ-2 have no compression steel, only 2R6 in shear span to hold the cage. The NSC beams and BJ-2 have 2T20.

Shear links were R6 at 200mm centres in the shear spans for ten beams, except for NSCL which had 4R8 at 300mm. Both NSC and HSC series beams were tested without and with horizontal web steel of 2T12, 2T20 and 2T25.

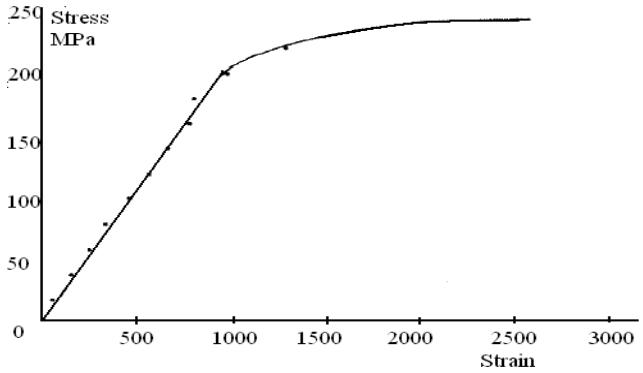

Figure 3.6: Stress v strain for 6mm mild steel which was tested in the laboratory.

Tests were carried out on three specimens representing the steel in the links, Figure 3.6, and the average value f_{yv} was 250 N/mm^2 according to BS4449 [3-7]. The reinforcement used for the top, bottom and horizontal web steel was high yield, hot rolled deformed bars with a guaranteed yield value f_{yl} of 460 N/mm^2 according to BS4449 [3-7]. The beam notation, reinforcement detailing, concrete strengths f_{cu} and f_{sp} and failure loads are given in Table 3-8.

3.2.5 Test procedures

All the beams were supported by a rocker bearing at one end and a roller bearing at the other end on two concrete blocks resting on the concrete slab floor.

The loading was applied by a 1000 kN capacity hydraulic jack and except for BJ-2 was distributed to two load points by an RHS spreader supported on one roller and one rocker bearing. The jack was supported on a steel frame and controlled by an Amsler loading cabinet.

3.2.6 Instrumentation

At each load increment, the vertical deflection were recorded by the mechanical gauge positioned at mid-span, Figure 3.7. An optical micrometer was used to measure the width of the shear cracks. The development of cracks were observed and recorded. Figure 3.8 to Figure 3.15. All the angles of the cracks are the measured angle of the tangent to the inclined crack to longitudinal line along the axis of the centroid at half the depth of the beam.

Electrical strain gauges were placed in pairs on the links, the tension reinforcements and the horizontal web bars of 8 beams to measure the strain in the reinforcement, Figure 3.1.

All horizontal web steel bars were strain gauged near the centre of the shear span. Out of three tension steel bars in each beam, the central bar and one side bar were strain gauged.

In HSC, at 180 kN, 2 - T25 HWB develop gradual strain until 220 kN and then strain rapidly at 220 kN and continue to 2400 EU, Figure 3.28. This is due to the stabilising arching effect of HWB, as the 2 - T25 have strain gauges at the centre of the diagonal strut.

Figure 3.7: With beam NSC2, the opening and closing of cracks was investigated with crack monitoring binoculars.

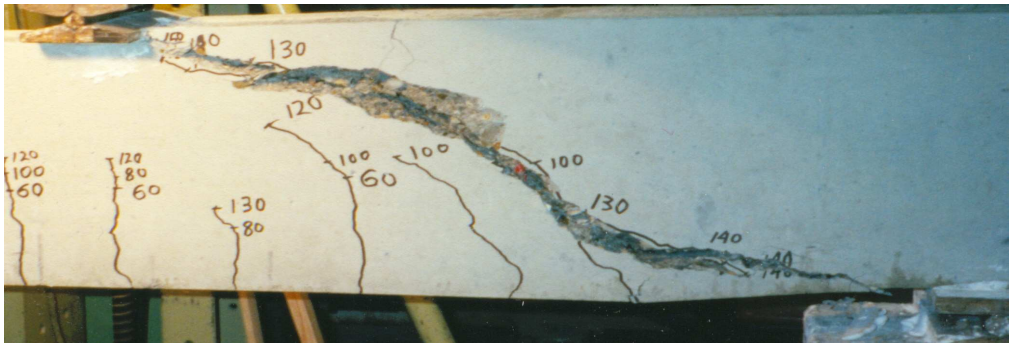

Figure 3.8: Normal Strength Beam (NSC1) with the angle of crack at about 35°

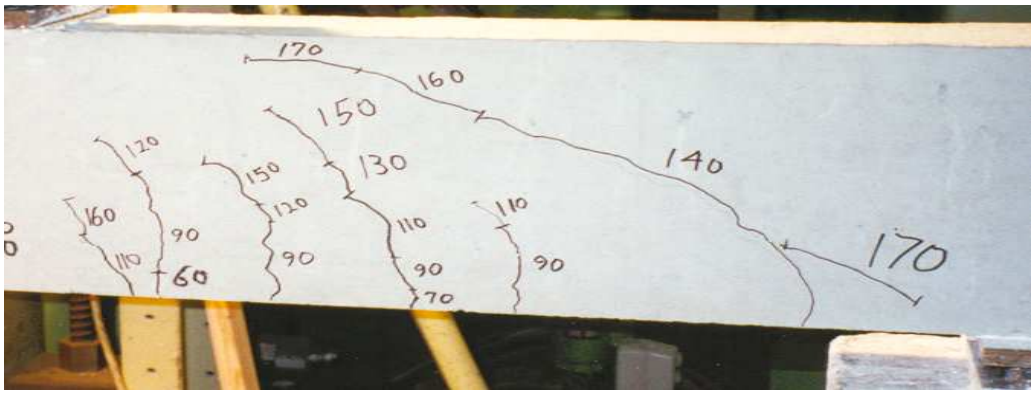

Figure 3.9:Normal Strength Beam (NSC2) with the angle of crack at about 28°

Figure 3.10: Normal Strength Beam (NSC3) with the angle of crack at about 27°

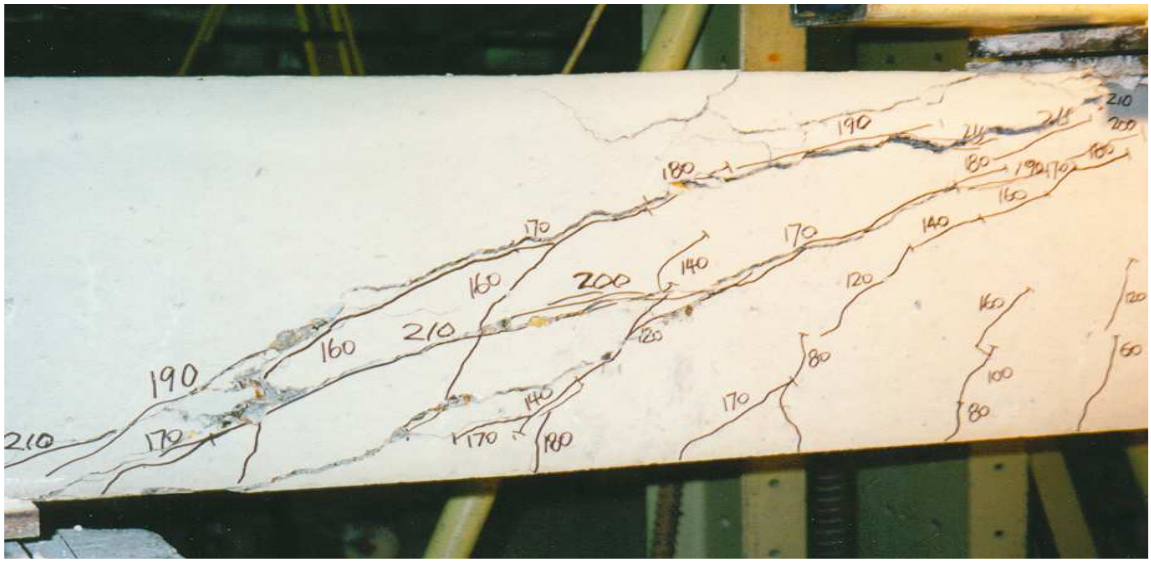

Figure 3.11:Normal Strength Beam (NSC4) with the angle of crack at about 27°

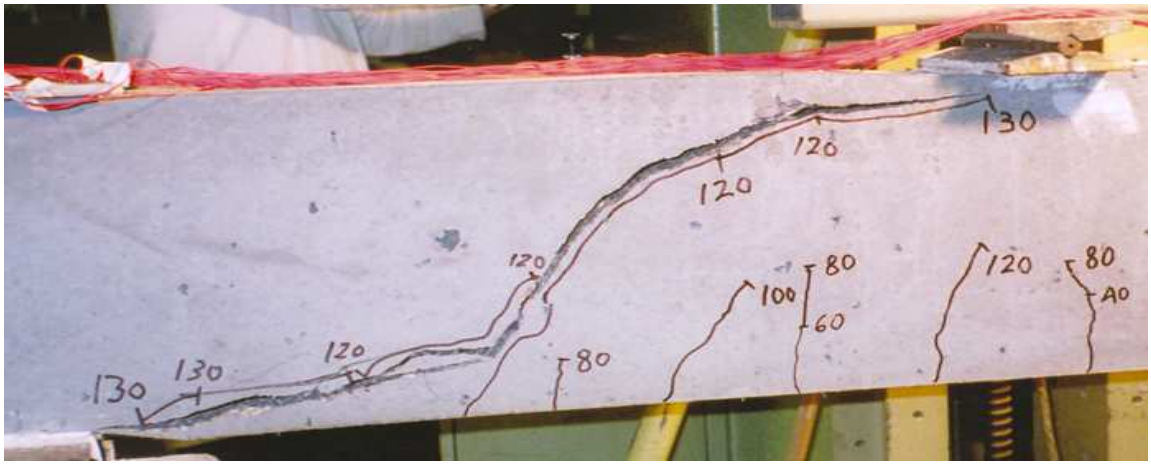

Figure 3.12: High Strength Beam (HSC1) with angle of crack of about 50°

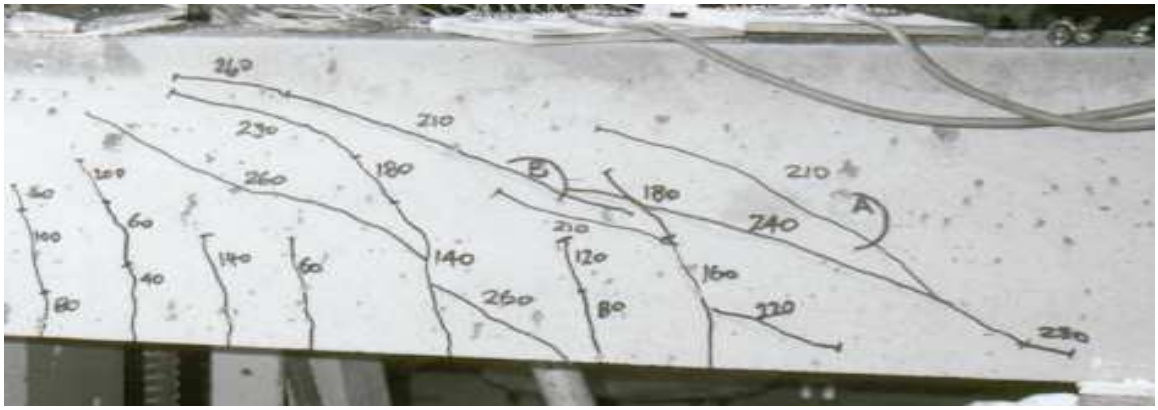

Figure 3.13:High Strength Beam (HSC2) with the angle of crack at about 43°

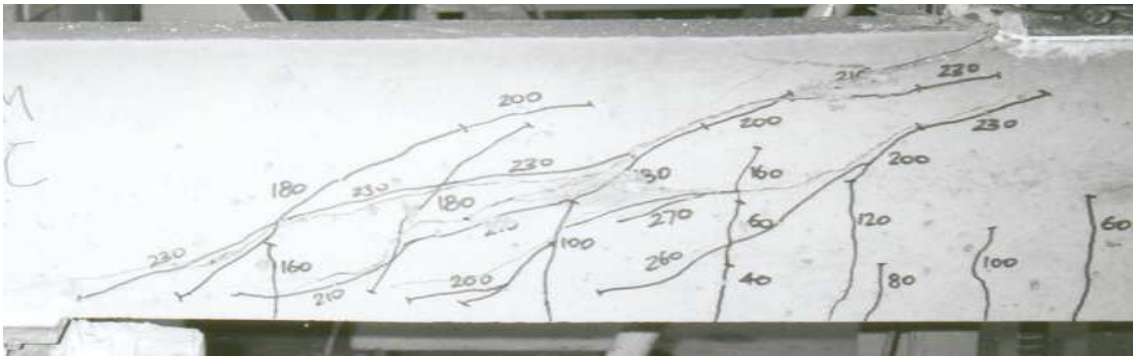

Figure 3.14: High Strength Beam (HSC3) with the angle of crack at about 45°

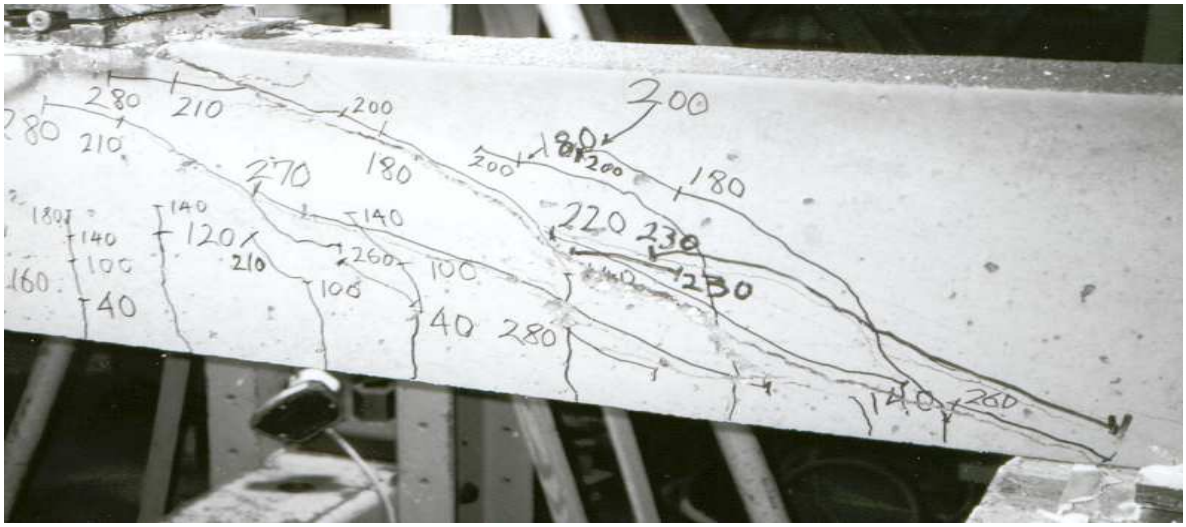

Figure 3.15: High Strength Beam (HSC4) with the angle of crack at about 42°

Beam No	Top Steel	Link	Space (mm)	Horizontal web bar (HWB)	Cube Strength (f_{cu}) N/mm^2	Splitting strength (f_{sp}) N/mm^2	Ultimate load ($2V_u$) kN
NSC1	2T20	2R6	200	0	43.2	2.98	160
NSC2	2T20	2R6	200	2T12	41.0	3.01	203
NSC3	2T20	2R6	200	2T20	47.7	3.22	200
NSC4	2T20	2R6	200	2T25	43.3	2.97	210
HSC1	2R6	2R6	200	0	109.0	4.21	140
HSC1-2	2R6	2R6	200	0	101.2	-	143.3
HSC1-3	2R6	2R6	200	0	106.6	-	160.0
HSC2	2R6	2R6	200	2T12	109.3	5.20	265
HSC3	2R6	2R6	200	2T20	112.5	4.34	280
HSC4	2R6	2R6	200	2T25	112.5	4.34	300
NSCL	2T20	2R8	300	0	44.2	3.06	250
BJ-2	2T20	2R6	200	0	118.1	4.3	142

Table 3.4: Data for beams tested by this writer. All beams are of shear span to depth ratio of a/d=3.02 other than BJ-2 which has a/d= 4.15

A summary of the test specimen details and results is given in Table 3-8. In the following sections the discussion are presented in four following sub-sections: shear failure loads, crack propagation, load-deflection behaviour, and load-strain behaviour.

3.2.7 Shear failure of the beams

The first HSC1 failure load of 130 kN (fcu = 109 N/mm2) appeared low, the second HSC1-2 failure load of 140 kN (fcu = 101.2 N/mm2) was also low and the third HSC1-3 failure load of 160 kN (fcu=106.6 N/mm2) was just under that of NSC1. The average ultimate load carried by these three similar HSC1 beams was 143.3 kN(fcu=105.6 N/mm2) as compared to the ultimate load of beam NSC1 which was 160 kN (fcu=43.2 N/mm2). The links were similar in all and none contained any horizontal web steel. NSC1 had 1.55% of compression reinforcement which was not present in HSC1.
The inclination of the critical shear crack was much steeper in HSC1 at about 50°, Figure 3.12, as compared with approximately 35° in NSC1, Figure 3.8. The surprising reduction of shear resistance with increasing concrete strength found for beams NSC1 and HSC1 was reversed when horizontal web steel was provided. With two 25mm HWB in both, the ultimate loads for HSC4 (fcu=112.5 N/mm2) and NSC4 (fcu=43.3 N/mm2) were 300 KN and 210 kN respectively.

The major increase of shear strength for the HSC beams occurred between HSC1 (no HWB) and HSC2 (2T12) with ultimate loads of 130 kN and 265 kN. The rises with increasing horizontal web steel were much more modest - HSC3 (2T20) carried 280 kN and HSC4 (2T25) took 300kN.

With ordinary concrete the influence of horizontal bars was modest: NSC1 (no web bars)-160kN, NSC2 (2T12)-203kN, NSC3 (2T20)- 200kN and NSC4 (2T25)-210kN. The results for the four HSC beams with horizontal web steel demonstrated that no limit to improvement in shear resistance as the result of increasing the area of horizontal web reinforcement was reached. When the diameter of the web bars was increased from 20 to 25mm a further 7% improvement was recorded. The inherent weakness in shear behaviour of HSC was first noticed in 1986 [3-8]. The relationship of frictional resistance to concrete strength was rather uncertain until around 1995 when it was demonstrated that the ratio of the ultimate shear to characteristic resistance for HSC beam , calculated by the BS equation without a limit on f_{cu} and ignoring the requirement on $\rho_w f_y$, was as low as 0.69

when compared with an identical NSC beam, or 31% lower, Table 3.4. This reduction in frictional resistance in HSC was later demonstrated to be as low as 35%, Table 3.5, and it was attributed to the material properties of aggregate.

It has been demonstrated that overall reserve shear strength diminishes after diagonal tension cracking in HSC. To compensate for this reduced ductility and aggregate interlock and to improve shear strength after diagonal tension cracking in the shear span, this thesis proposes HWB in beams and CVB in BCJ to improve shear performance. It is demonstrated experimentally that HWB improve shear performance by 130%, Table 3.4, and in Chapter 7, by using a FE parametric model, it is demonstrated that the contribution of CVB to HSC- TBCJ is 35%.

3.2.8 Comparison of accuracy of BS8110 design rules for NSC and HSC beams

In the existing formulae relating shear capacity to concrete properties, only concrete compression strength is considered since these are empirically derived from test data of NSC. The power to which f_c is incorporated in expressions for V_c varies from 1/3 in BS81109 to 2/3 in Eurocode EC2 [3-10].

A group of tests detailed in Table 3.5, gives an indication of a potential problem with high strength limestone aggregate concrete. In considering these results, it should be observed that the amount of shear reinforcement used in the HSC beams was below the minima of both EC 2 and the Concrete Society recommendations, which are $\rho_w f_y \geq 0.08$ and $\rho_w f_y \geq 0.039 f_{cu}^{2/3}$. Nonetheless, it is quite striking that the ratio of the ultimate shear to the characteristic resistance, calculated by the BS equation without a limit on f_{cu} and ignoring the requirement on $\rho_w f_y$, was as low as 0.69 with beam HSC1.

The ultimate strengths of three of the four HSC beams were below both that of a reference beam with gravel aggregate and a modest value f_{cu} and the resistances were calculated ignoring the shear steel.

Values of V_{rkc} and V_{rk} have been calculated ignoring limits on f_{cu} and $\rho_w f_{yw}$, since,

f_{cu}=100 N/mm^2 to EC2 minimum $\rho_w f_{yw}$ =0.74 N/mm^2 and to Concrete Society minimum $\rho_w f_{yw}$ =0.84 N/mm^2. All beams failed in shear. The aggregate was 20mm gravel in NSC-1 and 10mm limestone in all other beams. B=150mm, d=265mm, h=300mm, ρ_1= 2.37%.

Comparing the mean shear failure load V_u of 71.7 kN for HSC1, HSC1-2 and HSC1-3 with NSC1 which had a shear failure load V_u of 80 kN, it is concluded that on average HSC beams have 11.6% less shear resistance compared to equivalent NSC beams.

Beam No.	ρ_i %	**a/d**	f_c (N/mm^2)	V_u (kN)	V_{rkc} (kN)	V_u/V_{Rk}, equ 2.9	$V_u/V_{VRk,c}$ equ 2.10
NSC1	1.58	3.02	34.6	80	51.6	1.08	1.44
HSC1-1	0.14	3.02	94	65	71.9	0.69	0.86
HSC1-2	0.14	3.02	86.2	70	69.9	0.76	0.95
HSC1-3	0.14	3.02	91.6	80	71.3	0.85	1.06
BJ-2	1.58	4.15	103.1	71	74.2	0.74	0.90

Table 3.5:Published tests by this writer with reference to BS8110 equations. Details of the beams are described in Table 3.4.

The ratio of empirical values of ultimate shear resistance is compared to the predicted value from BS8110 for beams without HWB. All beams have stirrups, $\rho_w f_{yw}$ = 0.47 N/mm^2 or V_s=18.72 kN.

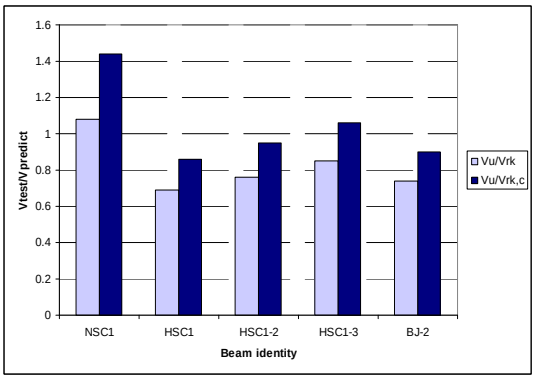

Figure 3.16: Comparison of accuracy of BS8110 design rule to experimental values

3.2.9 Crack propagation

At loads of 40 kN, small flexural cracks appeared in HSC beams at the bottom surface in the region of constant bending moment, whereas in NSC beams similar small flexural cracks appeared at 60kN. This could be due to the presence of compression steel in NSC which resulted in a reduction of deflection at mid span at early loading stage.

As the load was increased, new flexural cracks appeared in the shear spans spreading from the load application sections towards the supports. These cracks tended to become somewhat inclined. This was followed by the sudden occurrence of a wide shear crack in one of the shear spans, which lead to failure.

A crack angle was defined as the angle between a tangent to the crack at the centre of the depth of the beam and its x-axis. The angle of the failure crack for the beam HSC1, Figure 3.12, was around 50° compared to the 35° for the beam NSC1, Figure 3.8. Beams HSC2, HSC3, , and HSC4, had respective angles of cracks of about 43°, 45° and 42°, and NSC2, NSC3 and NSC4 with angles 28°, 27° and 27° respectively. HSC1, and NSC1, had dowel cracks at the level of the bottom steel. These cracks were formed at 120kN (92% Vu) and 140kN(64% Vu). NSC3 may possibly have had dowel cracks in mid-web formed at 170kN (85% Vu) and HSC4 did have a dowel crack at 230kN (77% Vu). HSC3 and NSC4 developed web dowel cracks at 270kN (96% Vu) and 200kN (95% Vu). Figure 3.8 to Figure 3.15.

HWB resist initiation and widening of crack width at mid depth in the shear span for HSC beams, due to the tensile strength of the concrete which is double of NSC.

3.2.10 Deflection

Mid-span deflections were measured by a single gauge mounted on the laboratory floor and include any settlements of the supports. The deflection of beam HSC1 was similar to that of NSC1, Figure 3.17. Both beams were without any horizontal web reinforcement. Initially, the deflection of HSC1 is slightly higher than NSC1**.** The 1.55% of compression reinforcement, present in NSC1, reduced its deflection but the higher strength and elastic modulus of the concrete in HSC1 with no compression steel counter-weighed the compression steel in NSC1 .

The deflection of beam NSC1 was greater than for NSC4 (2T25) at equal loads and NSC1's deflection near failure was the greater, Figure 3.18. The deflections of NSC2, NSC3 and NSC4 did not change by more than 15% as the area of horizontal web steel was increased in NSC beams.

The presence of 2T20 compression steel bars in NSC1 at initial stages of loading contributes to reduced deflection of NSC1 compared to HSC1. However, as load increases, the higher modulus of elasticity of HSC1 results in NSC1 deflecting more than HSC1. This is a beneficial property for HSC when used in columns of tall buildings where less deflection due to lateral loading means less sway and inter-storey drift, Figure 3.17.

Deflection of the beams reduces as the diameter of HWB in the beam increases, Figure 3.18.

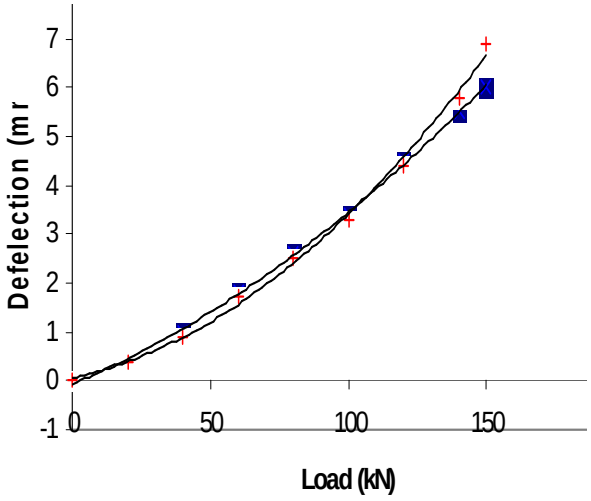

Figure 3.17: Load-deflection at midspan for NSC1 (squares) and HSC1 (crosses) beams.

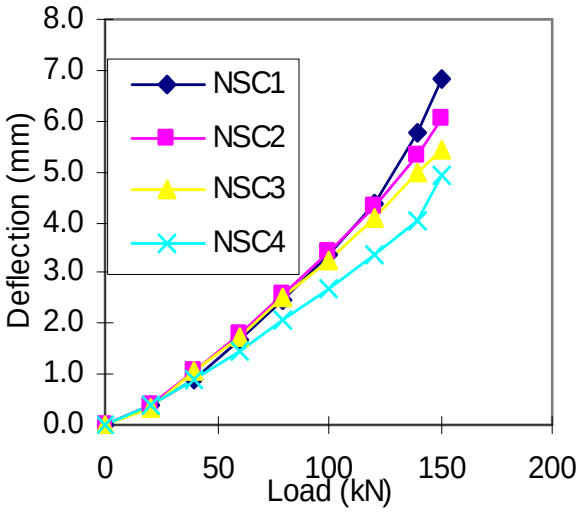

Figure 3.18: Load-deflection at midspan for NSC, the presence of HWB reduces deflection

In Chapter 6 the ability of CVB to reduce side drift (deflection) of BCJ is considered beneficial, because the CVB would reduce lateral displacement or sway of the building, resulting in less side drift, therefore a reduced load on the foundations and less damage to the cladding and the building from excessive lateral loading.

3.2.11 Load-strain behaviour

A comparison can be made between strains in links beams HSC4 and NSC4, Figure 3.19. Both beams had 2T25 horizontal web reinforcement. In beam NSC4, links 1, 2 and 3 yielded at 200 kN, whereas in HSC4 link 3 yielded at 200 kN and links 1 and 2 remain elastic. This shows that the strain difference between HSC and NSC is relatively small at link 3, close to the support, compared to the greater difference in yielding for link

2 and significant difference for link 3. This indicates that HWB restrain width of the diagonal shear cracksBeam HSC4 continued to sustain load for an increment of 100 kN after links 2&3 yielded and an increment of 70 kN after link 1 yielded. The horizontal web reinforcement (2T25) of HSC4 yielded at 270 kN, Figure 3.20. A possible explanation is that the horizontal web reinforcement in beam HSC4 was stabilising arching which resulted in yielding of the links and increased the forces in the main steel near supports. This tie effect of the tension steel continued until the tension reinforcement reached 90% of its yield strain at 300 kN when the beam failed, Figure 3.21**.**

The difference between HSC and NSC beams is partly in terms of the loads at which stirrups yielded. As Figure 3.19 shows, this difference for beam HSC4 compared to NSC4 could amount to a maximum load difference of 70 kN.

In beam HSC1, as Figure 3-28 shows, link 2 yielded at about 100kN and link 3 reached 80% of its yield at 110kN. Shear failure occurred with a crack positioned between links 2 and 3. When failure occurred, link 1 had not yet reached 40% of its yield and the strain at mid-span of the tension steel had reached only 40% of its yield.

The average strain in the centre of tension bars for the beam HSC2 reaches nearly 80% of its yield value, demonstrating that this tension has developed as the result of STM action in the beam with the HWB stabilising arching effect added to the resistance of the diagonal compression strut, Figure 3.26.

Yield strain in tension bars for the beam HSC4, Figure 3.29, is higher than HSC2, Figure 3.26, demonstrating that the larger diameter of HSC4 has produced a larger stabilizing arch effect. This tension has further developed as a result of STM action in the beam when the central dowel bar has improved the compressive strength of the diagonal strut, therefore giving higher shear resistance, Figure 3.21.

When no horizontal web reinforcement is present, tension reinforcement yield is about 40% for both NSC and HSC beams, Figure 3.27 & Figure 3.25.

The dowel action on the T25 HWB in HSC4 is visible in Figure 3.28 when the load exceeds 220 kN. The lower surface part takes the tension up to 350(UE) then as the top surface experiences sudden tension with an increase of 1000 (UE), the bottom surface

simultaneously experiences a sudden bend from tension of 350(UE) to compression of 650 (UE). The beam is about to fail at 280 kN when this compressive force is released.

Figure 3.20 shows that strain in links 1,2& 3 reaches yield point at about 230kN loading but the dowel action in the web bar creating stabilising arching action resists the shear forces for a further 70 kN loading until loading reaches 300 kN, at which point the HWB (2T25) also yield. Stirrups are mild steel.

Figure 3.19 shows that at 200 kN loading all the links for beam NSC4 yield and it fails at 210 kN, whereas for beam HSC4 link 1 is only strained at less than 200 UE and link 2 is close to yield and will continue carrying loads up to 300 kN, as shown in Figure 3.20.

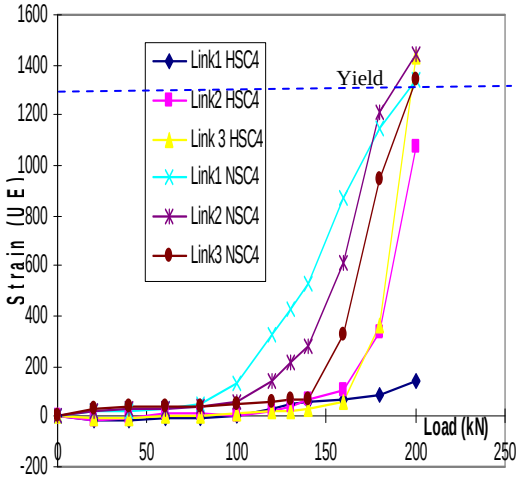

Figure 3.19: Comparison of strain in links for HSC 4

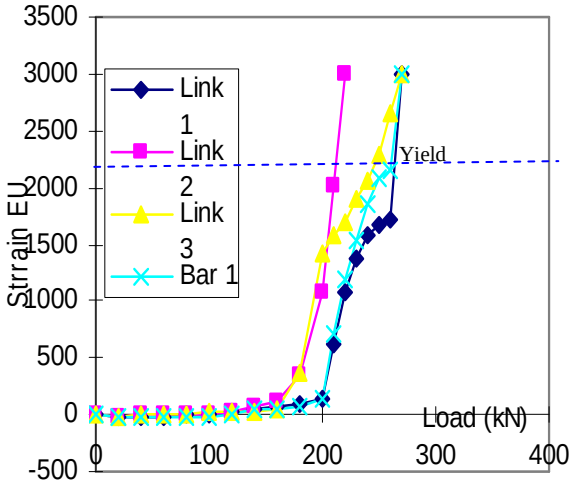

Figure 3.20:In beam HSC4, strain in links 1,2& 3.

Figure 3.21 shows the stabilising arching action causes tension bars to almost yield. The HWB 3-T25 contributing to stabilising arching action also almost yield.

In HSC4 beam, 2T25 web bars act as tie within compression strut, and provide a successful shear resisting model with links resisting vertical shear forces in tension while HWB acts as stabilising arch acting as tension tie to make the beam behave in a similar way to a short beam exposed to arch-like diagonal compression strut and tension reinforcement nearly yielding in tension as the tie.

HSC1 at small load of 130 kN without presence of HWB its link 3 yields suddenly after 120 kN loading, Figure 3.22. Split in concrete is sudden along the tension steel , diagonal tension cracks travel at a steep angle directly to the top and failure occurs. At 130 kN links

1 & 2 are strained to 700 UE and 400 UE and link 3 yields and suddenly fails whereas for NSC1 , Figure 3.24, at 170 kN links 1 & 2 are strained only to 100 UE .

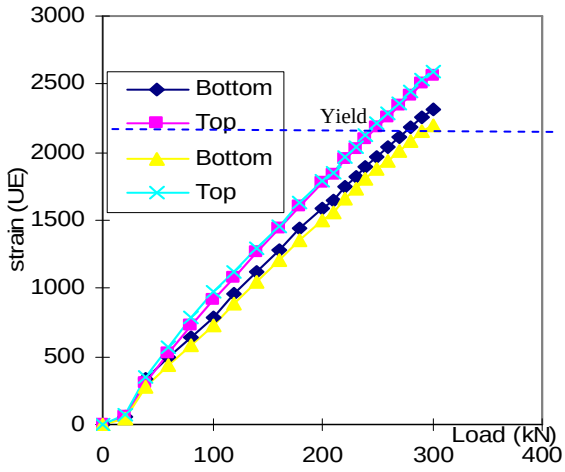

Figure 3.21: HSC4, strain in the centre of tension bars (3-T20)

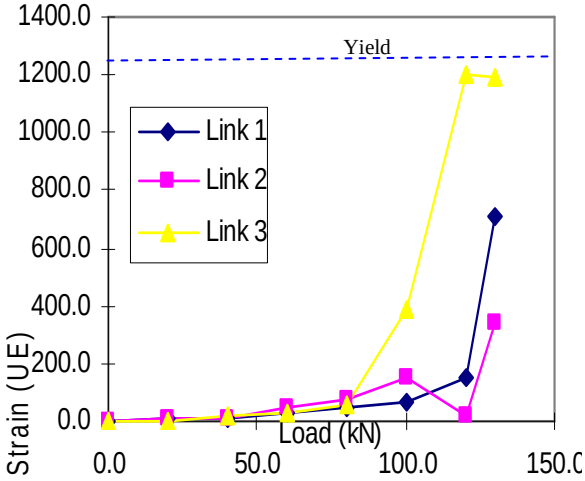

Figure 3.22: Strain in links 1, 2 and 3 for beam HSC1.

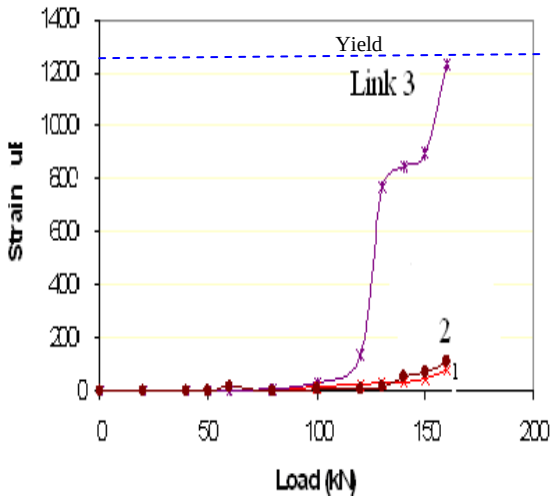

Figure 3.23: Strain in links 1, 2 and 3 for beam NSC1.

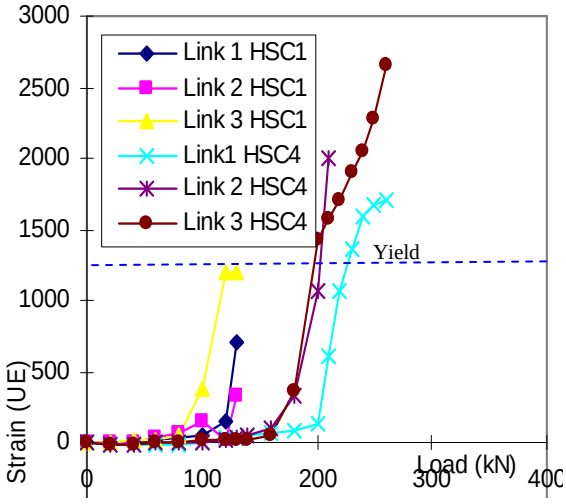

Figure 3.24: Strain in links for beam HSC1 compared to HSC4

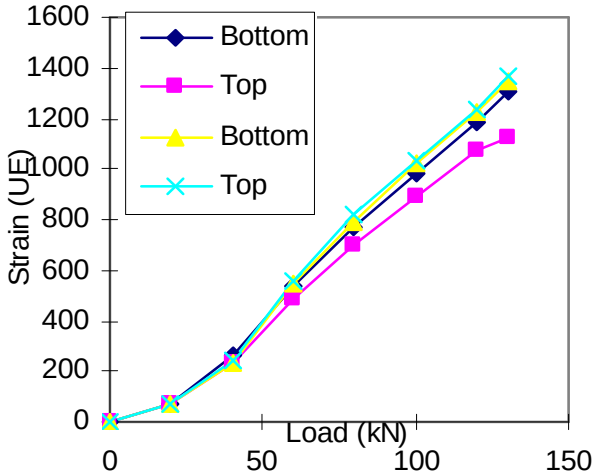

Figure 3.25: Strain at the centre of tension bars for the beam HSC1.

Figure 3.23 shows strain in links 1, 2 and 3 for NSC1. Presence of aggregate interlock improves shear resistance in NSC1 as compared to HSC made with lime stone aggregate which has less aggregate interlock. Between loading of 130 kN to 150 kN while strain in all the links remain within elastic range, aggregate interlock in NSC improves shear, whereas, in HSC1, Figure 3.24, the absence of aggregate interlock results in sudden failure of the beam at lower load compared to HSC1.

Figure 3.24 shows the strain in links for beams HSC1 as compared to HSC4 which has 2T25 HWB. HSC4 shear resistance is more than double that of HSC1 and all its links fully yield. The sudden split along the tension bar at 130 kN (HSC1) results from absence of aggregate interlock in concrete. In HSC4, 2T25 web bars contribute to stabilising arch action, therefore, transfer the shear resisting forces to the 3T20 tension bars at the bottom making them almost yield.

Strain is at the centre of tension bars for the beam HSC1, Figure 3.25. As the result of the absence of HWB, tensile strain does not reach one third of steel yield value, therefore no stabilising arch effect takes place, and a STM is not developed. STM can be applicable to HSC beams of shear span to depth ratio of 3 which have HWB as shear reinforcement, such as HSC2, HSC3 & HSC4.

Average strain against load for HSC2 is at the centre of tension bars for the beam, Figure 3.26. The strain in the tension bar is nearly 80% of its yield value, demonstrating that this tension has developed as the result of stabilising arch action in the beam due to 2 T20 central web bars. The strain in the tension bars in HSC2 is double that of HSC1, solely due to presence of 2 horizontal web bars.

Average strain at the centre of tension bars against load (kN) for NSC1 is shown in Figure 3.27. In HSC4 with 2 T25-HWB, Figure 3.29, and HSC2 with 2 T12-HWB, Figure 3.26, the HWB result in tension bars reaching strain of 2400 UE which is double that of NSC1 of 1400 UE. NSC1 has 2 T20 compression bars, HSC4 and HSC2 have none.

In HSC4, there is strain on the T25 HWB when load exceeds 220 kN, Figure 3.28 the lower surface part (blue triangles) takes tension up to 250(UE), the top surface (squares) experiences tension up to 350(UE) with a sudden increase to 2000 (UE), and simultaneously the bottom surface experiences a sudden bend from tension of 250(UE) to

compression of 850 (UE). The 2T25 behave like arches during loading from 200kN to 300 kN with tensile strain on top of it and compressive strain at bottom.

Beam HSC4, average strain in bottom tension steel 3T20 bars reach 85% of their yield as the beam fails in shear, Figure 3.29 .

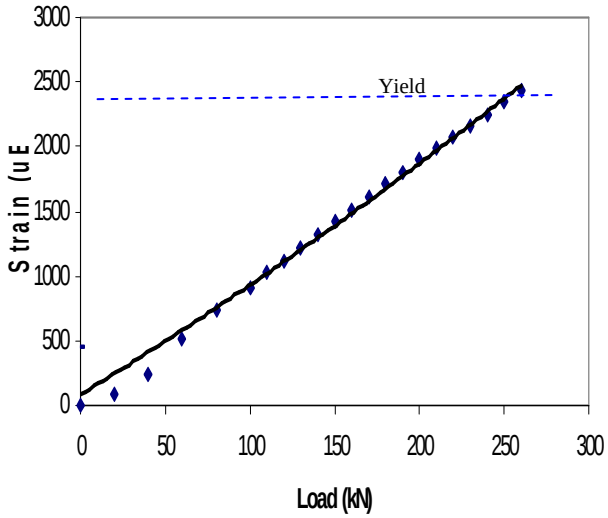

Figure 3.26: Average Strain V Load (kN) for HSC2 at the centre of tension bars

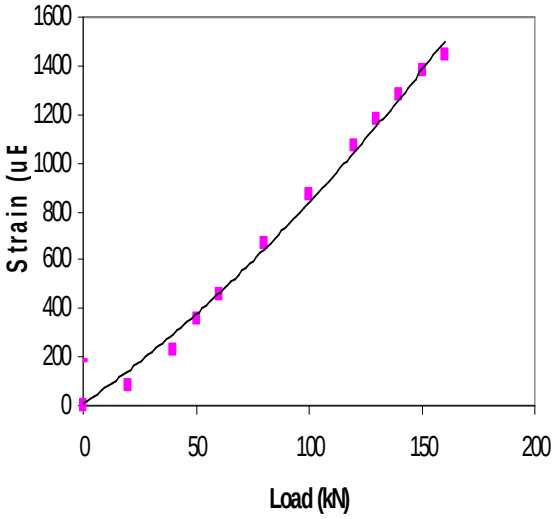

Figure 3.27: NSC1, Average Strain at the centre of tension bars V Load (kN)

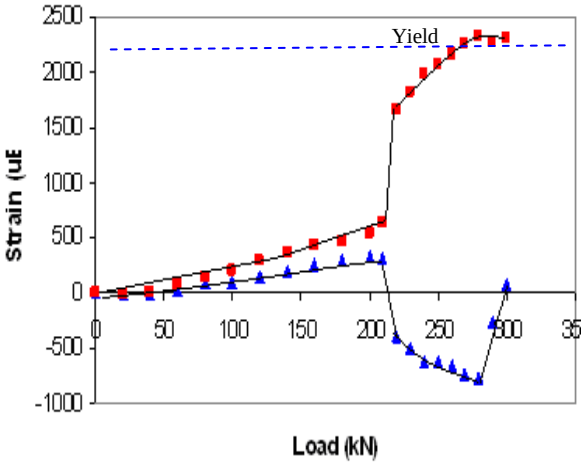

Figure 3.28: In HSC4 beam, sudden change in strain on the T25 HWB when load exceeds 220 kN,

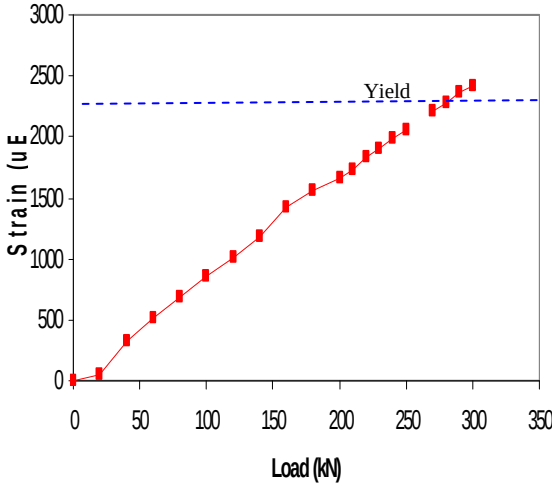

Figure 3.29: Beam HSC4, average strain in bottom tension steel 3T20

3.2.12 Arching action in HSC beams of a/d=3.02 with HWB

Verification that HSC beams of a/d=3.02 with HWB develop stabilising arching to form STM is shown in this section, follwing which an analogy to HSC- BCJ with CVB with aspect ratio=3 can be developed.

It is demonstrated that HSC beams of a/d≤3 have sufficient plasticity for the tension bar to yield thereby developing STM .

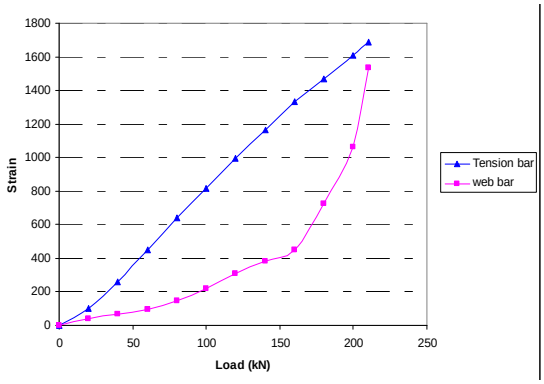

Figure 3.30: Micro-strain in tension bar (T20) and strain W_t on top of web bar (T25) for beam NSC4.

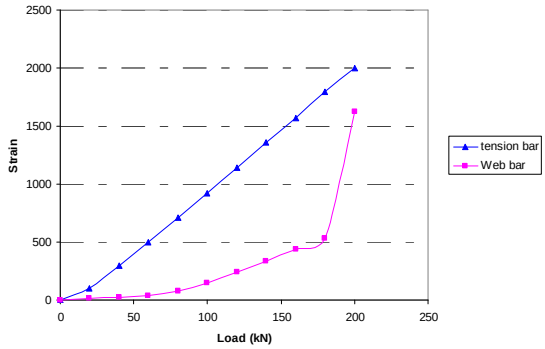

Figure 3.31: Micro-strain in tension bar (T20) and strain W_t on top of web bar (T20) for beam NSC3

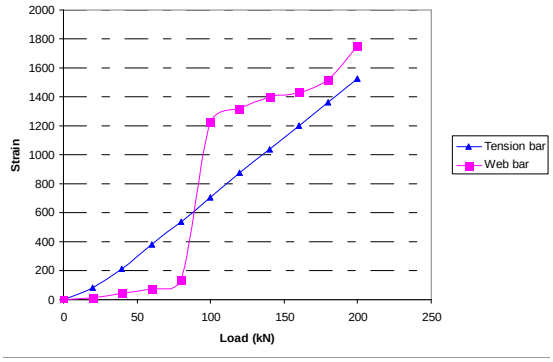

Figure 3.32: Micro- strain in tension bar (T20) and strain W_t on top of web bar (T12) for beam NSC2.

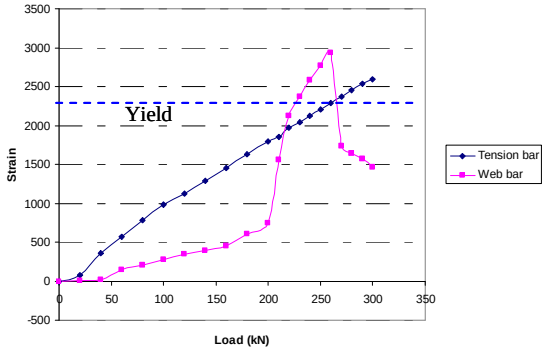

Figure 3.33: Beam HSC4 with web bar T25 and tension reinforcement T20 yielding.

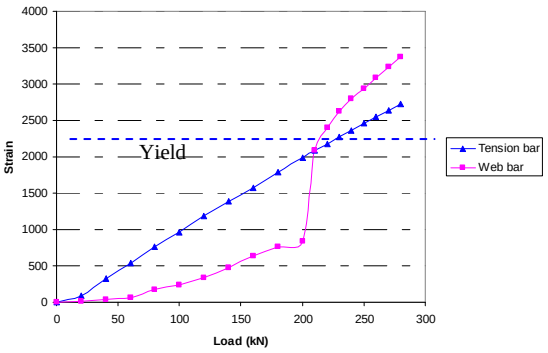

Figure 3.34: HSC3 with web bar T20 and tension reinforcement T20 yielding.

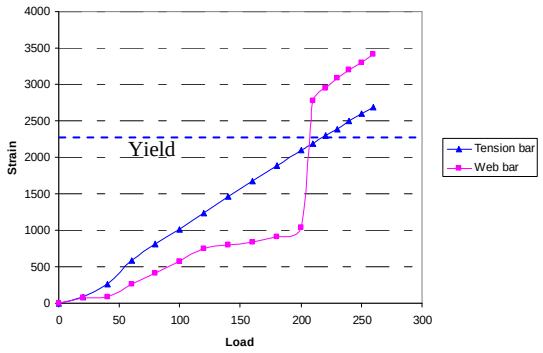

Figure 3.35: HSC2 with web bar T12 and tension reinforcement T20 yielding.

Past research [3-11& 3-23] has shown, however, that the HWB has little, if any, effect on the shear strength of NSC beams. This is due to the comparatively low crushing strength of NSC which crushes before reaching sufficient plasticity to bring the tension bar to yield.

This writer's experimental work is in agreement with past research [3-11& 23] demonstrating for NSC of a/d=3.05 with HWB, Figure 3.30 to Figure 3.32, that the arching action does not develop enough to bring HWB or tension bar to yield.

The reinforcement used had a yield strength of 460 MPa, yielding beyond 2,300 micro-strains. However, the experiment shows that HSC beams of a/d=3.05 with HWB provide sufficient plasticity to bring the tension bar to yield, Figure 3.33 to Figure 3.35. For details of the beams see Table 3.4.

In the NSC beams a/d=3.02, due to comparatively low crushing strength of concrete the tension steel or tie does not reach its yield. The concrete strut crushes before tension reinforcement yielded, Figure 3.30 to Figure 3.32. Therefore, for NSC beams with a/d=3 with HWB, STM is applicable for a/d≤2.5 and not for 2.5<a/d≤3.

In beam NSC4, crack initiate as inclined tension cracks and at 160 kN inclined web cracks rapidly develop up to 200 kN. Strain on the bottom face of web bar W_b increase$_s$ corresponding to readings on top face W_t until 160 kN loading, after this load W_b remains constant, Figure 3.30**.**

In beam NSC3, inclined web cracks develop at 170 kN. Strain on the bottom face of web bar W_b increase corresponding to readings on top face W_t until 160 kN loading, after this load W_b remains constant, Figure 3.31.

In beam NSC2, strain on the bottom face of web bar W_b increase corresponding to readings on top face W_t until 130 kN loading, after this load W_b remains constant, Figure 3.32.

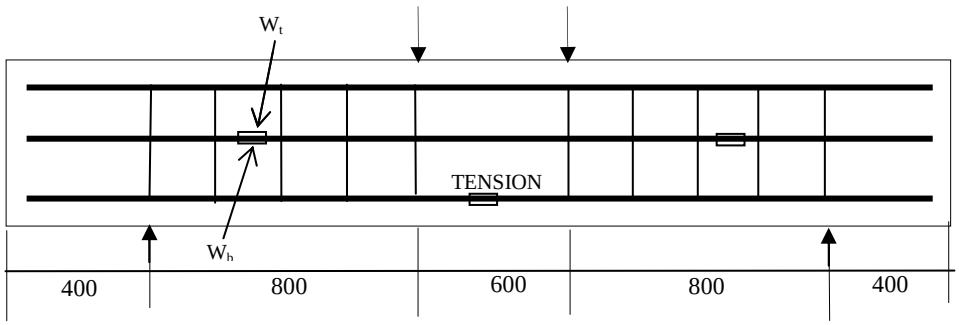

Figure 3.36: Position of strain gauges on tension reinforcement (TENSION) and on HWB

In beam HSC4, Strain W_t on top of web bar, shown as web bar, begins to yield at 225 kN when Strain on the bottom face of web bar W_b does not increase more than 300μ (not shown). The dowel action improves the arching and restricts opening of the inclined web crack. Inclined cracks develop between 200and 210 kN, with large increase of strain on top W_t. At 250 kN a sudden dowel crack near the web bar results in a drop in strain reading W_t on top, Figure 3.33.

In beam HSC3, inclined cracks develop between 200 and 210 kN, with large increase of strain on top W_t, Strain on the bottom face of web bar W_b (not shown) does not increase more than 600μ when W_t yields at 210 kN. The dowel action improves the arching and restricts opening of the inclined web crack, Figure 3.34.

In beam HSC2, inclined cracks developed between 200and 205 kN. Strain on the bottom face of web bar W_b, does not increase more than 600μ when W_t yields at 205 kN. The dowel action improves the arching and restricts opening of the inclined web crack, Figure 3.35.

The tie action in the 3T20 tension bars develops close to yield. 2T25 web bars produce dowel resistance and stabilising arching affect which produce higher tensile strains in the 3T20 tension bars. Comparatively in NSC4 at 210 kN , just before failure, the average of four strain readings in the middle of tension bars reach 1742 UE which is 70% of strain in tension bars of HSC4 (Figure 3.29).

3.2.13 Influence of dowel action on links at the centre of the shear span

Strain fluctuation in the centre link for beams NSC1, NSC3, HSC1 and HSC3 is shown in Figure 3.37 a& b. Beam NSC3 has a rate of increase in strain of 0.0042×10^{-3} per kN up to 140 kN, followed by a rate of increase of 0.0243×10^{-3} per kN from 140 kN to 160 kN and then at 0.16×10^{-3} per kN up to 6.77×10^{-3} strain. FE cannot model strains when element separation has occurred and strains have passed the yield point many times over.

It was recorded experimentally, Figure 3.37d, that after HSC3 has passed its yield value of 1.3×10^{-3} several times over reaching 9.9×10^{-3} at 200 kN, at this stage a significant shear crack has made the centre link obsolete but the dowel action from HWB is the only means of resisting the shear forces from 200 kN to 280 kN which demonstrates that only

dowel action from HWB was resisting the final 80kN (40%) loading.

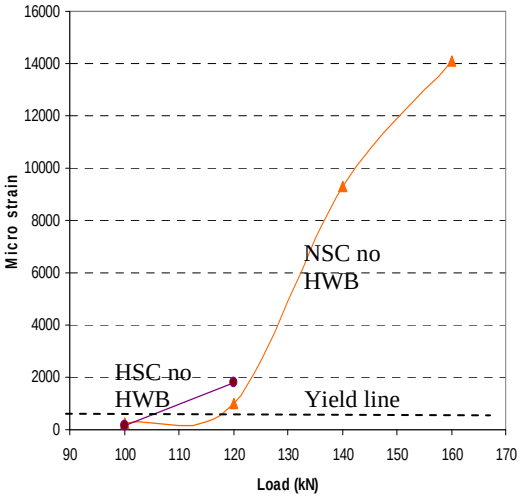

a) Strains in NSC1 & HSC1 to 160 kN

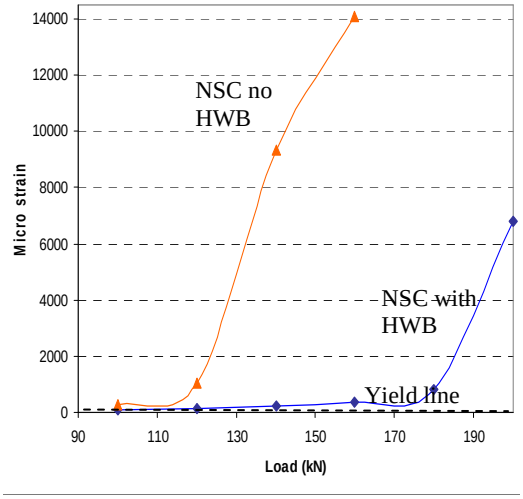

b) Strains in NSC1 and NSC3 to 200 kN

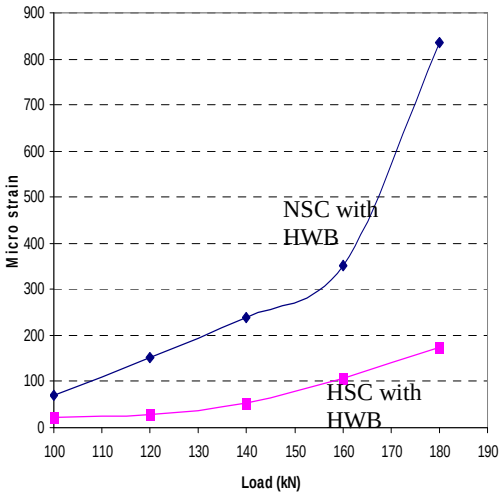

c) Strains in NSC3 and HSC3 to 180 kN

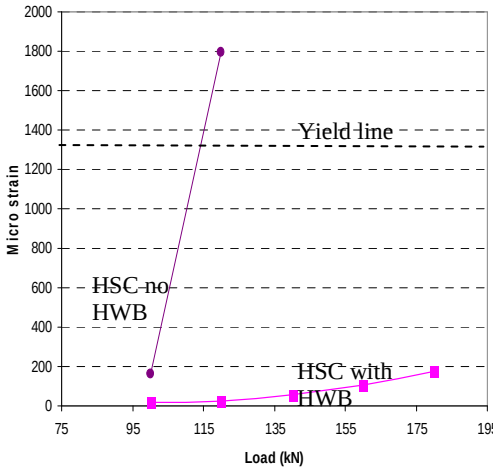

d) Strains in HSC1 and HSC3 to 180 kN

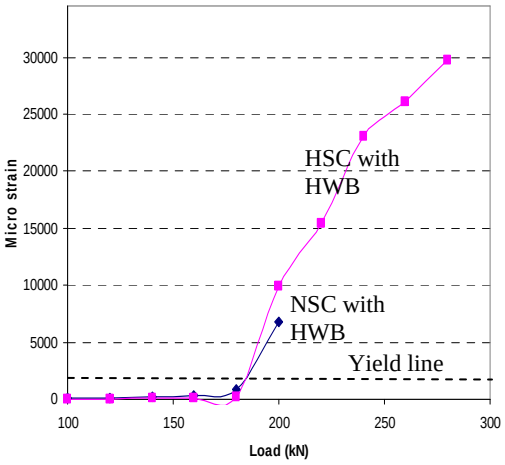

e) Strains in NSC3 and HSC3 to 280 kN

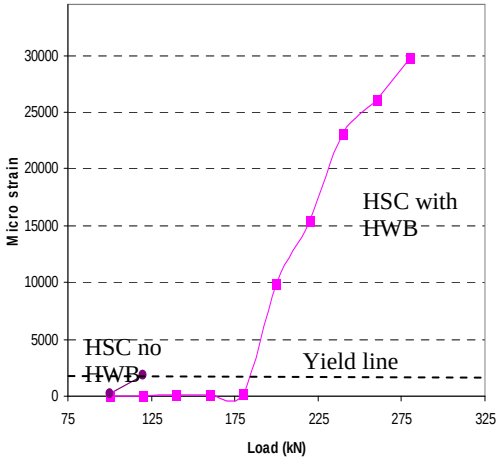

f) Strains in HSC1 and HSC3 to 280 kN

Figure 3.37: Strains in the centre link for beams of a/d=3.02

Further research is needed to investigate whether Finite Difference or Applied Element methods which model element separation can simulate the experimental beam HSC3, Figure 3.37d, which demonstrated the significant contribution (40% to load bearing capacity) from dowel action from CVB after element separation has occurred and centre link has passed its yield many times over and has become obsolete.
For beam NSC3, the presence of HWB does not make much difference in strain on the centre link until 120 kN, Figure 3.37 b, after which NSC1, which has no HWB, has a very high strain increase at 0.033×10^{-3} until its failure. The strain passes 9.3×10^{-3} (more than 700% yield) after 140 kN, and the dowel action from HWB resists shear until failure load of 170 kN.

The experimental results for beams HSC1 and HSC3show that after 120 kN as the strain in centre link of HSC1 reaches 1.8×10^{-3} , 138% of its yield value, the beam abruptly fails, whereas when HWB is present, the strain in centre link remains as little as 0.17×10^{-3}, 13 % of its yield value , up to 180 kN loading. However, due to the formation of large shear cracks the centre link reaches strain of 9.9×10^{-3} (760% of its yield) at 200 kN, but at this stage the HWB resists the shear forces for another 80kN or a further 40% increase in loading, Figure 3.37f.

3.3 Comparison of span/depth ratio with the tested beams

Figure 3.38 shows how the failure shear strength of a simply-supported reinforced concrete beam loaded with two-point loads changes as the shear span changes. For these series of beams, tested by Kani [3-12], the ultimate shear strength was reduced by a factor of about 6 as the a/d ratio increased from 1 to 7. As the beams contained a large amount of longitudinal reinforcement, flexural failures at mid-span did not become critical until a shear span-to-depth ratio of about 7.

This writer's tested beams, in Table 3.4, are transposed and compared with Kani's beams when considering relation between shear index (V/bdf_c') and shear span index (a/d). When HWB is present in NSC beams a/d =3.02, the shear index ($V/bdf_c'\approx0.11$) improves slightly compared to similar NSC beams but without HWB ($V/bdf_c'\approx0.09$), Figure 3.38.
The observed shear strength of the 3 beams of HSC without HWB of a/d =3.02 with ($V/bdf_c'\approx0.035$) fall even below the predicted value using sectional model, demonstrating

that for HSC without HWB of a/d =3.02, the arching action is absent and the aggregate interlock is also low, [3-13].

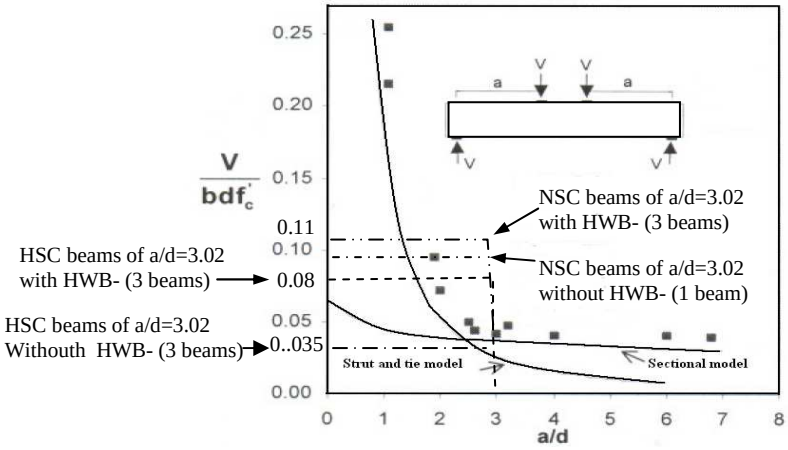

Figure 3.38: Predicted and observed strengths of a series of reinforced concrete beams tested by Kani (square) compared with ten beams tested by this writer (dotted lines)

Source: Collins and Mitchell 1996 [3-31]

From Figure 3.38 when comparing the experimental results of this writer's ten beams with Kani's prediction, it is demonstrated that Kani's graph does not compare well regarding the behaviour of HSC beams with a/d=3.0. Kani's prediction ignores the reduction of aggregate interlock in HSC and the significance of the contribution of dowel action from HWB in HSC for a/d≈3.02, Table 3.4, transposes results for 6 beams of a/d=3.02, the only difference being the presence of two HWB in three of them. Shear index (V/bdf_c') is 0.035 for the three without and 0.11 for those with HWB, which is more than 310% higher than shear index of those without HWB. HSC beams of a/d=3.02 with HWB have shear index (V/bdf_c') expected from shear span (a/d) of 1.5 according to Kani's graph, Figure 3.38, or 100% discrepancy in prediction.

The relative importance of the arch action is directly related to the shear span-to-depth Ratio. With an a/d ratio of less than 2.5, inclined crack develops and, after a redistribution of internal forces, are able to carry an additional load due in part to arch action. However, as shown in 3.2.12, full strut and tie action develops in all beams of a/d=3.05 made of HSC with HWB.

3.4 Mechanism of forces in HSC beams with HWB

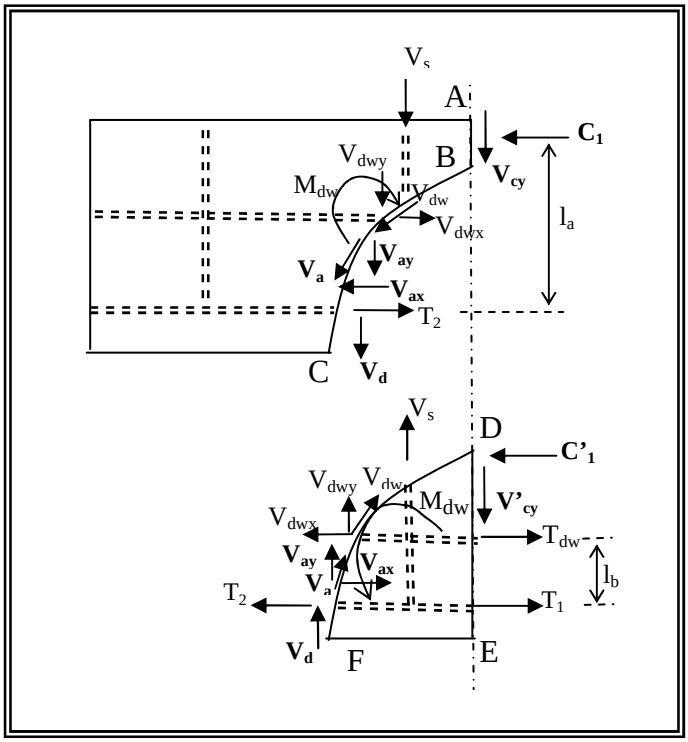

Figure 3.39: Internal forces in a cracked HSC4 beam with stirrups and HWB.

At loading between 210 kN and 300 kN, across the line A-B-C after cracks are wide enough to make the stirrup strain several times its yield and become plastic, where V_s remains constant, the moment M_{dw} from the HWB starts to resist the higher shear loads on its own, Figure 3.28. In beam HSC4 which has two HWB of T-25, as the result of this moment the strain on the top surface of HWB is strained to 2,320 micro-strain, just passing yield, whereas strain on the bottom surface is compressive and reaches 770 micro strain, Figure 3.28.

The idealised model for the internal shear forces mechanism demonstrating the influence of HWB in HSC beam is shown in Figure 3.39, the forces transferring shear across an inclined crack act at an angle of 50º, Figure 3.12, compared to 35º for NSC, Figure 3.8, therefore the crack travels between stirrups if no HWB is present. However, when HWB is present the angle of inclined crack reduces to 45º, Figure 3.14.

Considering the forces acting about the tension reinforcement, M_{dw} is the counter balancing moment which is the product of C_1 and the lever arm l_a. HSC-4 produces a large force C_1 which in turn bends the two T-25 HWB to strain its top surface beyond yield, to

resist the external additional 90 kN loading. The beam fails at 300 kN, and the last 90 kN is due to HSC acting as C_1. In NSC, C_1 would have given up and crushed at a failure load of 210 kN, Figure 3.11, Table 3.4. This moment M_{dw} from HWB acting in HSC is responsible for deflecting the diagonal inclined compression strut.

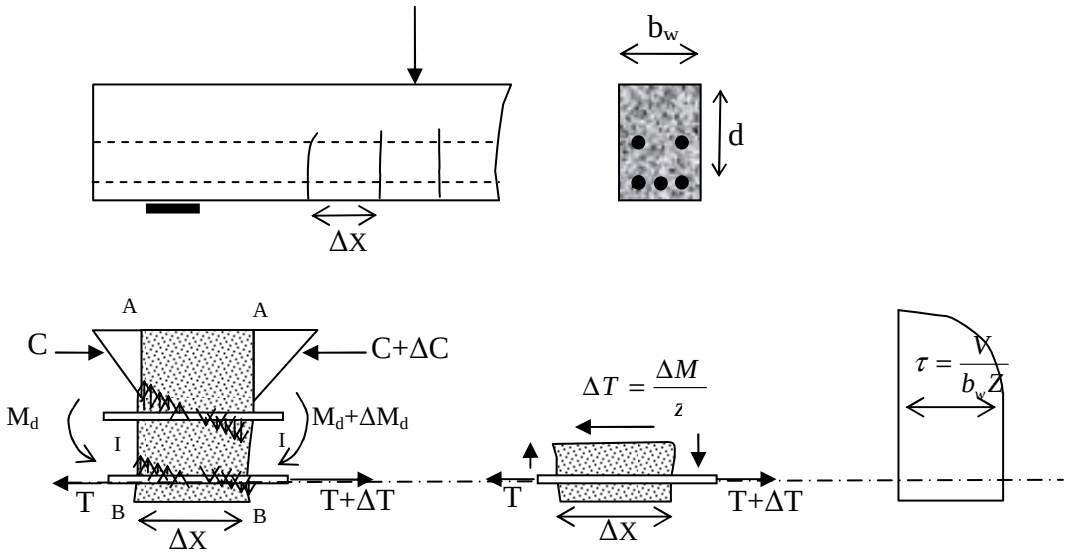

Figure 3.42: Shear stress distribution in a beam HSC3 with HWB exposed moment M from dowel action after inclined diagonal tension cracks are formed. N.B: Action of stirrups are not shown

At loading between 210 kN and 300 kN, across the line A-B-C, taking moment about C_1 , a product of T_2 and lever arm l_a counter balance M_{dw} due to HWB, therefore, 3-T20 tension bars in HSC4 are strained beyond their yield, Figure 3.21. This phenomena of strain beyond yield of T_2 and deflection of the diagonal inclined compression strut will be discussed in detail in Chapter 6 on STM.

At the D-E-F line, at lower loading below 210 kN, considering the part of the beam below the crack, total moments about the tension reinforcement at E, resulting from V_d and V_{dwy} and V_s and T_{dw} must balance C'_1, but at 210 kN, Figure 3.39, large dowel cracks on the tension bar and inclined tension cracks appear, dowel action from tension bar (V_d) disappears and tensile strain in stirrup (V_s) reaches several times its yield and becomes plastic, therefore, $T_{dw} \times l_b = C'_1 \times l_a$, Figure 3.37. As a result T_{dw} reaches yield. In Chapter 4, the FE modelling this action will be analysed for the vector force T_{dw} in HSC3.

Therefore, forces V_{dw} from HWB remain to resist forces from the inclined diagonal compression strut, and reinforcement tension resists the inclined diagonal strut produced

by C'_1 which is HSC, but when C'_1 reaches its maximum capacity , compression failure occurs, Figure 3.39.

Horizontal forces on section ABDE are $T_1 + T_{dw} = C_1 + C'_1$ and also $T_1 + T_{dw}$ and $C_1 + C'_1$ must balance the external moment at this section. Therefore, strain in T_1 reaches 2600 passing its yield strain of 2300 micro-strain, producing the tie action, Figure 3.21.

In HSC as the crack opens in diagonal tension, V_s is strained to several times its maximum yield within initial 60% loading. The dowel moment from M_{dw} and V_{dwx} resists the final 40% of the loading therefore the compression force C_1 provides a substantial resistance. This horizontal compression force C_1 is balanced with the the inclined diagonal compression strut C'_1 which is balanced with the tension force in the flexural reinforcement T_1 in an arch action.

At loading between 120 kN and 200 kN, the shear transferred across the line A-B-C by the shear in compression zone (V_{cy}) is about 20 to 25% smaller than in NSC because the vertical components of the shear transferred across the crack by interlock of the aggregate particles on the two faces of the crack (V_{ay}) are about 20% less than NSC, Table 3.6, and the dowel action of the longitudinal tension reinforcement V_d takes about 20% of the shear. V_s takes between 30-40% of the shear.

3.5 Contribution of various actions to total shear in the tested beams

This writer attempts to present an approximation to the percentage proportion of shear resistance taken by different actions in HSC beams of a/d <3 with HWB as shown in Table 3.6.

To this writer's knowledge, past research has not investigated the percentage of total shear resistance provided by different action in HSC beams with and HWB.

Comparing the proportion of different actions allocated by three groups of researchers, it can be concluded that the experimental work by Taylor [3-14] and Hamadi and Regan [3-15] were much more extensive than that of Fenwick and Paulay [3-16]. Taylor [3-14] and Hamadi and Regan [3-15] findings agree with one another but are significantly different to those from Fenwick and Paulay [3-16]. Hamadi and Regan's [3-15] guideline are concise and within the range of Taylor's [3-14]. The aggregates used in this writer's

experiment for NSC beams are the same as those used by Hamadi and Regan[3-15], Table 3.3.

	% of total shear resistance provided by different action			
	NSC Without HWB	NSC With HWB	HSC Limestone	HSC Limestone With HWB
Compression zone	37	32	39	21
Aggregate interlock	44	38	39	21
Dowel action, tension bar	19	17	22	12
Dowel action from HWB	0	13	0	45

Table 3.6: This writer's tests evaluation of separate contribution to the total shear resistance from experimental tests on 12 beams. Contribution of stirrups is about 20% of the total shear resistance for all beams.

From the above it is assumed it is justified for this writer to take Hamadi and Regan's [3-15] results as to be correct for this writer's NSC beams without HWB. Following these results , this writer established data for NSC beam without HWB, and began a detailed investigation on the mechanism of forces is performed in section 3.4, and is shown in Figure 3.39, in order to develop proportions for HSC beams with and without HWB.

From Table 3.4, comparing the failure load of HSC to NSC without HWB, a drop in shear resistance of 9.3% in shear due to limestone aggregate . This is also comparable to Albajar's [3-17] push off tests on HSC made with limestone aggregate.

The experimental tests by this writer on twelve beams are discussed, Table 3.4, strain gauge recordings on the reinforcement of the specimen are interpreted and the influence of HWB and its contribution to both NSC and HSC beams are explored.

A theoretical mechanism of internal shear forces by considering the proportion of shear resistance taken by different actions in HSC with HWB based on reduced contribution of aggregate interlock and improved contribution of dowel action due to HWB is developed and internal shear forces are diagrammatically shown, Figure 3.39.
This writer's proposed design equation is applied to experimental tests completed by others and its accuracy of prediction of the shear resistance is compared with the design rules

proposed by other researchers.

Design rules proposed for predicting dowel action by other researchers are investigated and a new and improved design rule is proposed to take into account the number of dowel bars resisting shear forces.

This writer's proposed design rule for the prediction of the quantity of HWB that compensates for the inherent weakness in HSC is discussed in 3.6, and its application within the existing design rules for current codes of practice including BS8110 [3-9] , EC2 [3-10], CEB FIP90 [3-18] and ACI318 [3-2] for members with and without shear links is investigated.

General theories for the analysis of beams subjected to bending and shear are reviewed and extended to develops a design rule for prediction of shear based on experimental results with values calculated using semi-empirical formulae.

3.6 This writer's proposed design rule for dowel action

In this section after reviewing the background of this writer's proposed design rule an improved Baumann [3-19] modified rule is proposed. This rule will be referred to as Baumann-Motamed rule in order to simplify future references to improved Baumann [3-19] modified rule.

When considering dowel action component, V_d, three terms are to be understood in order to analyse this action which are :

1. Dowel cracking force, V_d'
2. Dowel displacement at cracking, Δ_d'
3. Dowel force-displacement (V_d/Δ_d) relationship up to dowel cracking.

There is noticeable inconsistency in opinion amongst the researchers with regarding the above three terms. The range of suggested dowel cracking displacements, Δ_d', are from 0.013 suggested by Houde and Mirza [3-20] to 0.170 mm by Taylor [3-21] . However, from extensive experimental tests Baumann[3-19], Hamadi and Regan [3-15], and Chana [3-22] suggested 0.080mm as an average value for Δ_d', which was based on comparatively

large number of experimental tests on divided beam specimens, and compares well with the values from the experimental data of the full scale divided beams of similar specimens tested at the University of Westminster by Hamadi and Regan [3-15].

Also, the dowel force-displacement relationship, V_d/Δ_d , before cracking varies from straight lines of significantly different slopes to a parabolic curve. For example, Taylor's parabola does not give agreement with the experimental data of the full-scale divided beam specimens tested by Hamadi and Regan [3-15]. Therefore, it was judged that Baumann-Rusch [3-19] and Hamadi – Regan [3-15] had the most reasonable approach for the purpose of this thesis.

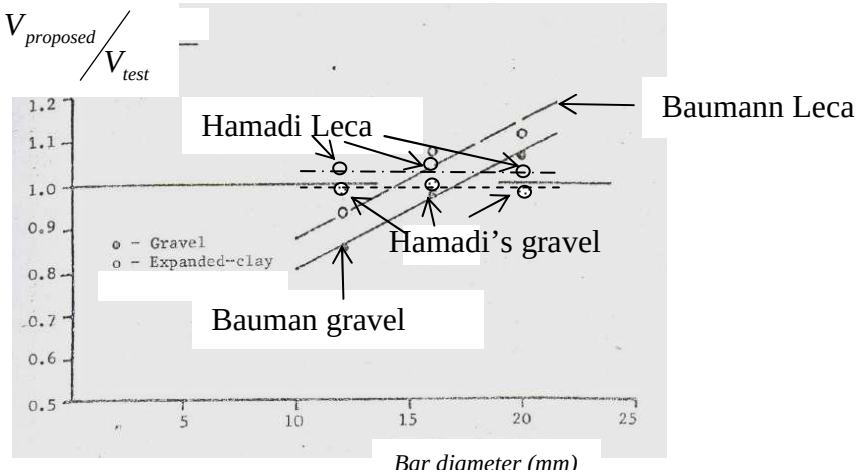

Figure 3.43: Comparison between the reported dowel action tests on divided beams specimens by Hamadi and Regan [3-15], Table2-2 , and comparing Baumann's dowel action formulae and Hamadi's proposed formulae

Baumann's [3-19] equation [Section: 2.2.7.3] for the cracking force V_{cr} was checked with the tests detailed in Figure 3.43. Hamadi and Regan [3-15] considered that the direct proportionality of V_{cr} with the bar diameter ϕ in Baumann's [3-19] equation may be unrealistic as most past researchers had not even included ϕ in their equation [Section;2.2.7.5]. He sensed a slight modification in this respect was necessary, and as a result he suggested his equation.

From

Figure 3.43, it can be seen that Baumann's proposed design rule is not safe for dense concrete with gravel or for LECA. However, from results produced in Table 2-2

[Section;2.2.7.5] , it may be concluded that Hamadi-Regan's [3-15] formulae for modified Baumann's equation, which will be called Baumann-Hamadi for convenience, is also not safe for dense concrete but gives a safe prediction for Leca. Therefore, there is an urgent need to propose a design formulae for modified Baumann's equation which safe for dense concrete.

A more accurate assessment can be obtained by considering the effect of the number of dowel bars. Baumann 's fundamental way to expose dowel cracking resistance (D_{cr}) is as follows:

D_{cr}= Tensile strength of the concrete × Net breadth of beam × Primary bearing length

The primary bearing length *L*c ', is correspondent to the following:

$\approx \sqrt[4]{}$(Flexural stiffness of dowe1/ Modulus of support)

when there are n dowels:

Flexural stiffness of total dowel= n × stiffness of one bar

The modulus of support in practice ought to be independent of the number of bars.

This would suggest a change in Baumann's equation as follows:

From

$D_{cr1} = K.b_n.d_b.\ f_{cu}^{1/3}$ 2.11

to

$D_{cr1} = K.b_n.d_b.\sqrt[4]{n}.\ f_{cu}^{1/3}$ **3.10**

where d_b= diameter of dowel bars *and* b_n = net breadth = (b_n- d_b)

One way of assessing the total shear resistance of a member with a single layer of horizontal web steel is to add its dowel resistance to the above V_{Rk} using Baumnann's dowel cracking expression with the condition of equilibrium for dowel force where the main reinforcement is in single layers is:

In order to check if the movements of cracks were correct for the mobilisation of D_{cr}, reference was made to published measurements by Baumann[3-19], Hamadi and Regan [3-15], and Chana [3-22] of vertical movements at flexural cracks that developed into shear cracks. It was clear that the movements are large enough for dowel resistance to be fully achieved as it is limited by the tensile strength of the concrete, and a movement of about 0.1mm can adequately mobilise it.

The general equation where the main reinforcement is in up to 2 layers is:

$V=Kf_{ct}\, b_n L_c$ 3.11

where

b_n = net breadth

V=Dowel force

f_{cu}=Cube crushing strength of concrete of 200mm cubes in N/mm^2

Kf_{ct} = Average vertical tensile stress in concrete at the level of the bars along the primary bearing length

f_{ct}=Uniaxial tensile stress in concrete (may be taken as $0.245f_{cu}^{2/3}$ where both are in N/mm^2)

L_c=Primary bearing length of dowel.

From the test results the following formulae for L_c were determined:

Where the main reinforcement is in one layer.

Substituting for L_c and the tensile stress in the concrete

$f_{ct} = 0.24\, f_{cu}^{2/3}$

gives the dowel force causing cracking V_{cr} or D_{cr}.

Hence if D_{cr} is mobilised, the suggested formulation for the shear strength of the beam with stirrups and horizontal web reinforcement (HWR) to the revised proposed Baumann's is called Baumann-Motamed for convenience, which is;

$D_{cr1} = 1.64.b_n.d_b.\sqrt[4]{n}.\, f_{cu}^{1/3}$ **3.12**

The resistance of a rectangular reinforced concrete beam with shear reinforcement can be assessed by the BS8110 [3-9] equation, with eliminating safety factors.

$V_{du} = 0.27(100\, \rho_i f_{cu})^{1/3} (400/d)^{1/4} bd + \rho_w f_y bd$ 2.22

in N and mm units

$V_{du} = 0.27(100\, \rho_i f_{cu})^{1/3} (400/d)^{1/4} bd + \rho_w f_y bd + 1.64.b_n.d_b.\sqrt[4]{n}.\, f_{cu}^{1/3}$ **3.13**

where V_{du} is the proposed calculated shear resistance of a member with stirrups and HWR.

When considering two bars

$Dcr1 = 1.95.b_n.d_b.\, f_{cu}^{1/3}$ **3.14**

The upper limit for d_b maximum steel percentage ρ_b= 2.2%

3.7 Influence of stirrups on dowel action resulting from HWB

3.7.1 Beams of a/d=3.02 with HWB without shear stirrups

Hejazi[3-23] tested four normal strength beams with 3T16 tension bars, with shear span to depth ratio of 3.02, without shear links. Three of the beams had HWB of 2T12, 2T20 and 2T25. Test results were compared to the design proposal of Desai and Baumann-Motamed for shear resistance of RC beams with web bars. This research concluded that horizontal web bars do not significantly improve shear performance of NSC beams.

Four normal strength beams without links, with horizontal web steel were tested to failure. The geometry of the beams is shown in Figure 3.44, concrete type for beams and failure loads are shown in Table 3.7.

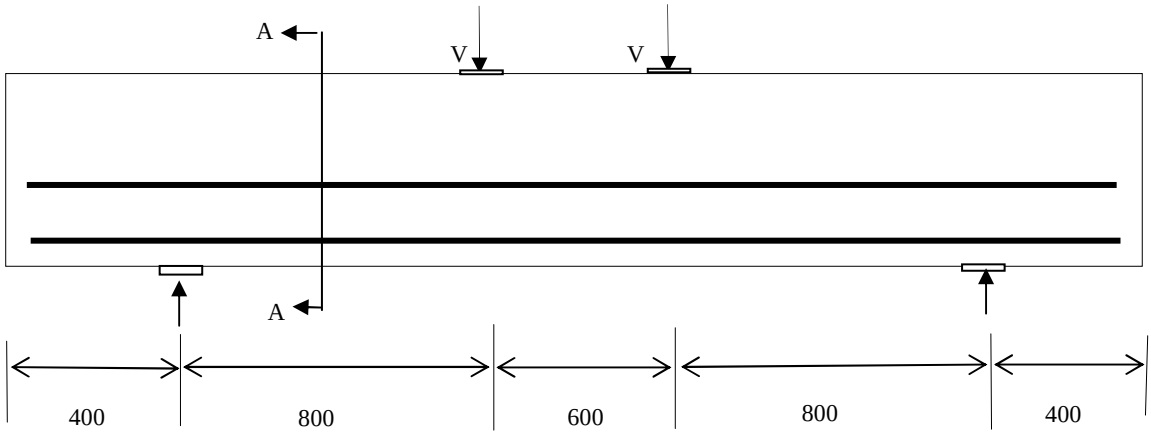

Figure 3.44: Hejazi's test arrangement for four beams of normal strength with different sizes of web steel. Geometry and reinforcement, excluding stirrups, is the same as Figure 3.1

Beam No	**BH1**	**BH2**	**BH3**	**BH4**
F_{cu} (N/mm^2)	40.3	42.2	37.7	40
Vtest (kN)	48.9	57.5	65	63.5
Web steel		2T12	2T20	2T25
Bau-Mot	-	10.59	14.30	17.21
Vtest / V des	1.01	0.96	0.87	0.66
Vtest / V Bau-Mot	1.01	1.06	1.02	0.95
ρb %	0	0.56	1.5	2.44
Tension steel	3T16	3T16	3T16	3T16

Table 3.7: Data for beams tested by Hejazi. All four beams are of shear span to depth ratio of a/d=3.02.

Source: Table from Hejazi, J.,1997[3-23]

This writer performed a comparative study of the failure loads on the four beams Hejazi tested to failure with all parameters being the same but with stirrups. In the comparison

the only parameter other than presence of stirrups which differed was the strength of concrete,Table 3.4. It is shown that for BH3 and NSC3 with HWB of 2T-20 their f_{cu} differs by 27%, and the difference in f_{cu} in other matching beams is limited from 0.03% to 0.08%.

A comparison was made of experimental results for 8 identical NSC beams of which four of the beams, NSC1 to NSC4, have stirrups, Table 3-8 and Figure 3.1, and have 3 different sizes of HWB, and four other identical beams, BH1 to BH4, which have no stirrups [3-23], Table 3.7 and Figure 3.44.

In Table 3.7, tests results are compared with Desai's prediction, , compared to Baumann-Motamed prediction, Section 3.6

Baumann-Motamed's design rule for shear prediction including the dowel action of the web bar remains conservative as the diameter of the web bar increases.

Web steel	NSC beams	2T12	2T20	2T25	Total
V_{test} / $V_{Bau\ (mot)}$	With Link (	1.21	1.08	1.15	3.44
V_{test} / $V_{Bau\ (hej)}$	No link	1.06	1.02	0.95	3.03
ρb %		0.56	1.5	2.44	
Tension steel		3T16	3T16	3T16	

Table 3.8: Comparison of shear performance of HWB in NSC when links are present, Table 3.7, with those in Table 3.4 from this writer's experimental tests.

The above table shows that V_{test} / $V_{Bau\ (Mot)}$ is 14% larger than V_{test} / $V_{Bau\ (Hej)}$, indicating that this difference is due to presence of stirrups which were used in this writer's tests on NSC as compared to Hejazi's with no stirrups. This agrees with Baumann's [3-19] experimental results shown in Figure 2-14.

Desai underestimates the contribution of the dowel bar as its diameter increases, see Table 3.7, and does not directly include concrete strength as a determining factor in his design rule.

3.8 The influence of stirrup on dowel action

Test results were compared with the predicted values by Desai and Baumann-Motamed,

Figure 3.45. Desai's design rule for shear prediction including the dowel action of the web bar becomes less conservative as the diameter of the web bar increases,Table 3.7.

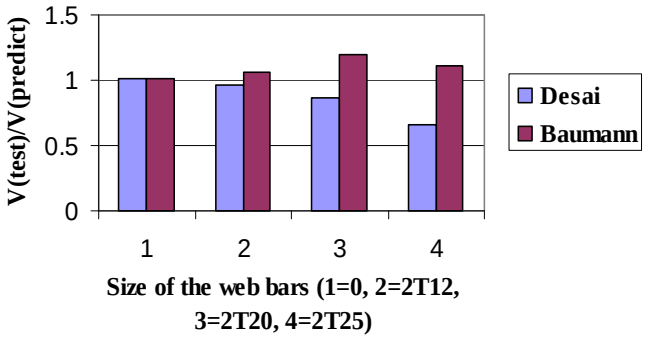

Figure 3.45: Comparative accuracy of predictions by Baumann-Motamed and Desai according to Hejazi's tests for normal strength beams without link

Chana's research, [Section 2.2.7.7], concludes that the dowel forces which are represented by gauge recording on links in NSC are responsible for 47% of the total shear. His beams had no stirrups and, he seems to overestimate the dowel contribution of the flexural steel in NSC beams because when considering the contribution of dowel action of HWB at half the depth of the NSC beam without stirrups, Hejazi's experiments[3-23] shows an improvement of 30%, Table 3.7. When stirrup are presents, the dowel resistance for NSC does not exceed more than 25%, Table 3.4, although, when HSC is considered the contribution is between 42% to 50% depending on the diameter of the dowel bar.

Tests by Baumann [3-19], Krefeld and Thurston [3-24], Taylor[3-21], and Hamadi and Regan [3-15] who completed their experiments in June 1980 are a useful guidance for exploring dowel forces at flexural cracks but they do provide limited information on the complex performance of dowel forces at inclined cracks, where they are bearing on comparatively weaker wedges of concrete. The beams tested are comparatively slender of a/d ≈3.5, therefore it is difficult to envisage that arch action develops in the beam.

The above mentioned tests do not clearly explore the support stirrups have towards improving the dowel action. Baumann makes some effort to investigate by changing the diameter of the stirrups supporting the dowels, but in his research this parameter was not treated systematically.

The action from these wedges are assumed to be transmitted into the main internal structural system to produce compression struts at 45º for NSC as shown in Figure 3.46.

But the true angle depends on the strength of the concrete as cracks for HSC occur at around 65º to horizontal.

As shown with Hejazi's tests in Table 3.8, a maximum 33% increase in shear resistance is recorded and this is the maximum improvement expected with NSC. However, in tests completed by this writer of HSC members with comparable amounts of longitudinal web reinforcement in beams with stirrups, an improvement of 102% was recorded Table 3.4.

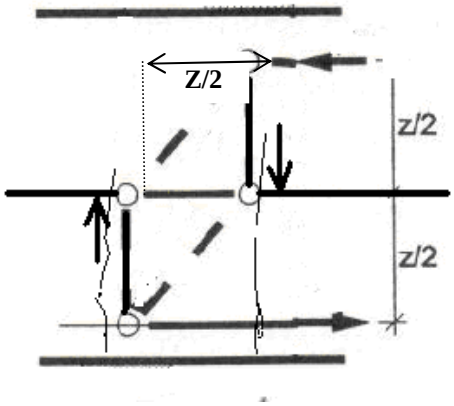

Figure 3.46: The action from these wedges is assumed to be transmitted into the main internal structural system to produce compression struts at 45º

Hejazi [3-23]	**Beam No:**	**BH1**	**BH2**	**BH3**	**BH4**
	F_{cu} (N/mm^2)	40.3	42.2	37.7	40
	V_{hej} (kN)	48.9	57.5	65	63.5
Motamed [Table 3.11]	**Beam No:**	**NSC1**	**NSC2**	**NSC3**	**NSC4**
	F_{cu} (N/mm^2)	43.2	41	47.7	43.3
	V_t (kN)	80	101.5	100	105
	V_s (kN)	18.72	18.72	18.72	18.72
	V_t-V_s (kN)	61.28	82.78	81.28	86.28
Both tests	**HWB**	0	2T-12	2T-20	2T-25
	V_t - V_s - V_{hej} (kN)	12.38	25.28	16.28	22.78
	Vstirrup support for dowel (kN)	0	12.9	3.9	10.4

Table 3.9: Calculation of average percentage of stirrup support for dowel

Baumann's approach proposing dowel action from the web bar is related to the strength of concrete $\sqrt[3]{f_{cu}}$ and gives a more realistic result compared to other proposals.
This additional internal structural system within the length of 0.5z can be assumed to increase the STM action from the conventional a/z=2.5 to 3.

3.9 Comparison of accuracy of the proposed equation with existing equations

In the following section the accuracy of the Baumann-Motamed equation will be compared with other proposed equations by other researchers or by codes of practice by comparing the predicted failure loads from the equations with the actual failure load to available experimental tests.

3.9.1 Comparison of Baumann, Baumannn-Hamadi and Baumann-Motamed equation

The proposed equations by Baumann [3-19], Baumann-Hamadi [3-15] and Baumann-Motamed for dowel forces are compared to tested beams, see Table 3.10.

Beam	HWB (mm)	f_{cu} MPa	Baumann-Hamadi KN	Baumann-Motamed KN	Baumann kN
NSC2	12	41	9.38	10.17	39.62
NSC3	20	47.7	12.11	15.56	60.64
NSC4	25	43	12.34	17.08	66.56
HSC2	12	109	13.00	14.08	54.89
HSC3	20	112.5	16.12	20.71	80.71
HSC4	25	112.5	17.00	23.53	91.72

Table 3.10: Dowel resistance predicted by equations from Baumann , Baumann-Hamadi and Baumann-Motamed compared to tested beams, Table 3.4

The comparisons in Table 3.10 indicate that while the original Baumann equation appears to overestimate the influence of dowel action from HWB, Baumann-Hamadi equation provides a safe prediction but does not take into consideration the changing number of dowel bars in one layer and also is not directly dependent on the diameter of the dowel bar, as originally proposed by Baumann.

In Baumann-Hamadi's equation, shear resistance from dowel action is proportional to the power of $^{2}\!/_{3}$ of the diameter of the longitudinal dowel bar and contribution from increasing the number of dowel bars in one layer is not included in the rule.

This writer's proposed equation provides the same degree of accuracy as Baumann-Hamadi's but considers the number of dowel bars in each layer and is directly proportional to the diameter of the dowel bar.

Beam	**NSC 1**	**NSC 2**	**NSC 3**	**NSC 4**	**HSC 1**	**HSC 2**	**HSC 3**	**HSC 4**
Description	1	2	3	4	5	6	7	8
f_{CU} N/mm$_2$	43.2	41	47.7	43.3	109	109.3	113	112.5
V_C kN	55.6	55.2	58	55.6	76.4	76.5	77.2	77.2
V_S kN	18.72	18.7	18.72	18.72	18.72	18.72	18.7	18.72
Web Steel	0	12	20	25	0	12	20	25
V_{du} Bau	0	39.6	60.6	66.6	0	54.9	80.7	91.7
V_{du} Bau-Ham	0	9.4	12.1	12.3	0	13	16.1	17
V_{du} Bau-Mota	0	10.2	15.6	17.1	0	14.1	20.7	23.5
V Bau	74.32	114	137.3	140.9	95.12	150.1	177	187.6
VBau-Hama	74.32	84.1	92.32	91.42	95.12	109.3	117	119.4
VBau-Mota	74.32	84.1	92.32	91.42	95.12	109.3	117	119.4
Vt (test)	80	102	100	105	65	132.5	140	150
ρb%	0	0.5	1.4	2.2	0	0.5	1.4	2.2
Vt/VBau	1.076	0.894	0.728	0.745	0.683	0.883	0.793	0.799
Vt/VBau-Hama	1.076	1.207	1.083	1.149	0.683	1.212	1.200	1.256
V /VBau-Mota	1.080	1.210	1.080	1.150	0.680	1.210	1.200	1.260

Table 3.11: Predictions by Baumann, Baumann- Hamadi and Baumann-Motamed compared to tested results, Table 3.4. All shear forces (V) are in kN

Following writer's experimental work, Table 3.4, Baumann-Motamed's equation is directly proportional to the diameter of the longitudinal dowel bar, similar to Baumann's original equation, but in addition, a proportionality to the power of $1/4$ for the number of bars is introduced and the empirical constant is accordingly adjusted.
This writer's revised equation gives similar accuracy of prediction to that of Baumann-Hamadi.

3.9.2 Hamadi & Regan's analysis of dowel action and aggregate interlock

Hamadi and Regan's [3-15] more detailed analysis of the test results provided further information on the behaviour of concrete members in shear. Their analysis appeared to be

a successful attempt to make direct numerical use of the increasing knowledge of interlock and dowel actions.

Applications of analytical procedure of prediction of shear forces proposed by Hamadi-Regan, from their equation 2-23 of section 2.2.7.5, with dowel action modified by using Baumann-Motamed equation instead of Baumann-Hamadi equation for this writer's tested beams are shown in Table 3.12.

It can be demonstrated that safe and comparatively accurate predictions with 35% and 53% safety margin can be obtained when using the analytical prediction approach proposed by Hamadi-Regan [3-15].

Beams	F_{cu} (N/mm^2)	E_c (kN/mm^2)	q_1 equation	q_2 equation	V_u (kN)	Vs (kN)	Dowel - Motamed	Vpredict (kN)	Vtesr (kN)	Vtest/ Vpredict
NSC1	43	29.508	0.696	0.004	31.03	34.5	0	65.53	80	1.22
NSC2	41	28.814	0.684	0.004	30.64	34.5	10.21	75.35	101.5	1.35
NSC3	47.7	31.079	0.722	0.004	31.89	34.5	15.6	81.99	100	1.22
NSC4	43	29.508	0.696	0.004	31.03	34.5	17.1	82.63	105	1.27
HSC1	109	46.981	0.975	0.007	39.80	34.5	0	74.30	74	1.00
HSC2	109	46.981	0.975	0.007	39.80	34.5	14.1	88.40	132.5	1.50
HSC3	112.5	47.730	0.986	0.007	40.15	34.5	20.7	95.35	140	1.47
HSC4	112.5	47.730	0.986	0.007	40.15	34.5	23.5	98.15	150	1.53

Table 3.12: Accuracy of Hamadi-Regan's [3-15] prediction with dowel action calculated by Baumann-Motamed equation for this writer's tested beams

3.9.3 Comparison of accuracy of Baumann-Motamed equation with Desai's rule

To improve assessment of shear resistance of beams with HWB, the test results from the present experimental work were compared with the prediction of Baumann-Motamed's modified equation (3-13) and Desai's equations with the upper limit which are:

As shown in Figure 3.47 for beams HSC 2 (no 6), HSC 3 (no 7) and HSC4 (no 8), Desai's design rule does not express influence of HWB in HSC as his prediction for shear resistance of HSC2 beam with HWB of 2T12 is the same as that for HSC4 beam with

HWB of 2T25. However, the proposed Baumann-Motamed rule allows for the improvement in shear resistance as HWB increases.

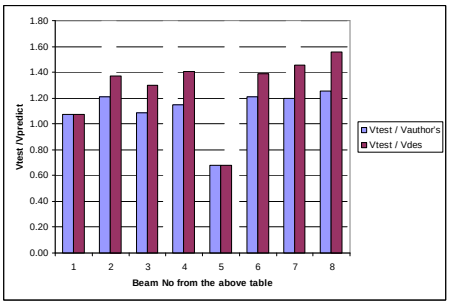

Figure 3.47:Comparison of Desai's and Baumann-Motamed's predictions of shear strength for beams tested by this writer. For beam numbering refer to Table 3.13

Beam	**NSC1**	**NSC2**	**NSC3**	**NSC4**	**HSC1**	**HSC2**	**HSC3**	**HSC4**
Description	1	2	3	4	5	6	7	8
f_{CU} N/mm^2	43.2	41	47.7	43.3	109	109.3	112.5	112.5
V_C kN	55.6	55.2	58	55.6	76.4	76.5	77.2	77.2
V_S kN	18.72	18.72	18.72	18.72	18.72	18.72	18.72	18.72
Web Steel	0	12	20	25	0	12	20	25
$V_{du\text{-}Bau\text{-}Mot}$ kN	0	10.2	15.6	17.1	0	14.1	20.7	23.5
$V_{Bau\text{-}Mot}$ kN	74.32	84.12	92.32	91.42	95.12	109.32	116.62	119.42
V_{test} kN	80	101.5	100	105	65	132.5	140	150
$V_{test}/V_{Bau\text{-}Mot}$	1.08	1.21	1.08	1.15	0.68	1.21	1.20	1.26
ρ_b%	0	0.5	1.4	2.2	0	0.5	1.4	2.2
V_{Des} kN	74.3	74.0	76.9	74.6	95.1	95.3	96.1	96.3
V_{test} / V_{Des}	1.08	1.37	1.30	1.41	0.68	1.39	1.46	1.56

Table 3.13: Ratio of empirical values of ultimate shear resistance compared to predicted value from Baumann-Motamed's and Desai's equations for tested beams

Beam	**NSC2**	**NSC3**	**NSC4**	**HSC2**	**HSC3**	**HSC4**	**Mean**
V_{cu}	55.2	58	55.6	76.5	77.2	77.2	
Vt	101.5	100	105	132.5	140	150	
V_s	34.5	34.5	34.5	34.5	34.5	34.5	
$(Vt- V_s)/Vcu$	1.21	1.13	1.27	1.28	1.37	1.50	1.29

Table 3.14: Shear resistance increase compared to V_{cu} (not including resistance from stirrups) due to presence of HWB

It is difficult to follow why the ratio of main reinforcement ought to affect the contribution of the web bar as proposed in Desai's design rule described in the literature review. In

Desai's design rule he restricts the upper limit for contribution of HWB to 0.4Vcu, whereas in the experimental tests of this writer's beams the corresponding increase due to the presence of HWB was 0.5Vcu, for beam HSC4, Table 3.14, or 25% higher than Desai's proposed upper limit for the contribution of HWB.

3.9.4 European, American and Canadian codes with Baumann-Motamed rule

In this section the accuracy of prediction of European [3-10], American [3-2] and Canadian [3-32] codes guidance when Baumann-Motamed rule is added to the guidance is investigated.

In the ACI building code [3-2] the expression for the shear prediction is :
$V_c = b_w d(\sqrt{f'_c}/ 6)$.

BEAM	h mm	b mm	d mm	Fcu (kN)	%ρ dow	%ρ bott	%ρv 103	V_d (kN)	V_L (kN)	Shear span	Vmaci (kN)	Vexp (kN)	Vexp/Vmaci
NSC1	300	150	265	43.2	0	2.37	1.9	0	18.72	3.02	47.4	80	1.29
NSC2	300	150	265	41	0.56	2.37	1.9	10.04	18.72	3.02	67.7	101.5	1.43
NSC3	300	150	265	47.7	1.50	2.37	1.9	15.36	18.72	3.02	86.8	100	1.26
NSC4	300	150	265	43.3	2.44	2.37	1.9	16.91	18.72	3.02	96.4	105	1.33
NSCL	300	150	265	44.2	0	2.37	2.2	0	22.19	3.02	51	125	1.89
HSC1	300	150	265	109	0	2.37	1.9	0	18.72	3.02	57.6	65	0.88
HSC2	300	150	265	1093	056	237	19	1388	1872	302	851	1325	1.52
HSC3	300	150	265	112.5	1.50	2.37	1.9	20.39	18.72	3.02	107	140	1.49
HSC4	300	150	265	112.5	2.44	2.37	1.9	23.17	18.72	3.02	122	150	1.55
HSC1-2	300	150	265	101.2	0	2.37	1.9	0	18.72	3.02	56.6	70	0.95
HSC1-3	300	150	265	106.6	0	2.37	1.9	0	18.72	3.02	57.3	80	1.09
BJ-2	300	150	265	118.1	0	2.37	1.9	0	18.72	4.15	58.6	71	0.97

Table 3.15: Comparison of this writer's experimental beams with revised modified MACI design rule using Baumann-Motamed's design formulae.

ACI [3-2] design guidelines appear to be generally unsafe when HSC beams with a modest amount of tension reinforcement and links are considered. When considering a large percentage of longitudinal steel and regarding this writer's experiments on beams with HWB, ACI's [3-2] predictions are reasonably safe.

The EC2 [3-10], Figure 3.48, and CSA [3-32], Figure 3.49, design rules give a safe guideline when HSC beams with a modest amount of tension reinforcement and links are considered. However, with ACI [3-2] shown in Figure 3.48 out of all four HSC beams

without HWB including BJ2, HSC1, HSC1-2 and HSC1-3, only the HSC1-3 prediction are safe and higher than experimental failure. Considering the large percentage of longitudinal steel, and regarding the author's experiments on beams with HWB, EC2's predictions are conservative.

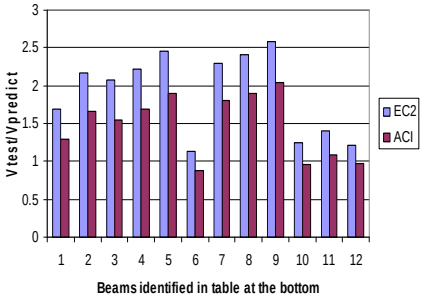

Beam type	NSC1	NSC2	NSC3	NSC4	NSCL	HSC1	HSC2	HSC3	HSC4	HSC1-2	HSC1-3	BJ-2
Beam No	1	2	3	4	5	6	7	8	9	10	11	12

Figure 3.48:Comparative accuracy of EC2 and ACI predicting shear strength for beams tested by this writer.

3.9.5 Collins and Kuchma

Collins and Kuchma [3-25] concluded that the current ACI shear design procedures are not conservative if applied to large, lightly reinforced members because ACI procedures do not recognize that as the size of such members increases, the shear stress required to cause failure decreases. Their paper which was published in 1999 experimentally evaluates the significant parameters which influence the magnitude of size effect in shear.

This paper also investigates the influence of reinforcement positioned in layers, or HWB. However, the percentage of HWB steel or layered steel is relatively small, therefore their influence is not as clearly demonstrated as explained in this writer's research which was completed in 1997 [3-13].

It was found that the reduction in shear stress at failure was related more directly to the maximum spacing between the layers of longitudinal reinforcement rather than the overall member depth. HSC members displayed a more significant size effect in shear than NSC members.

There is now substantial evidence from Kani [3-26], Bazanyt [3-27], Kuchma [3-28] and Shioya [3-29&30] that for members without stirrups the shear stress at failure decreases as

the member becomes larger and as the percentage of longitudinal reinforcement becomes lower.

BEAM	Vexp (kN)	Vec2 Con (kN)	Vec2 (kN) con+link	no	d_b mm	Vec2m Total (kN)	Vdow (kN)	Vexp/ Vec2	Vexp / Vec2 m
NSC1	80	28.63	51.60	0.00	0.00	47.36	0	1.55	1.69
NSC2	101.5	28.14	51.10	2.00	12.00	56.91	10.04	1.99	1.78
NSC3	100	29.59	52.50	2.00	20.00	63.67	1536	1.90	1.57
NSC4	105	28.66	51.40	200	25.00	64.29	16.91	2.04	1.63
NSCL	125	28.85	51.04	0.00	0.00	51.04	0	2.45	2.45
HSC1	65	38.86	57.58	0.00	0.00	57.58	0	1.13	1.13
HSC2	132.5	38.90	57.62	2.00	12.00	71.50	13.88	2.30	1.85
HSC3	70	39.27	57.99	2.00	20.00	78.38	20.39	2.41	1.79
HSC4	75	39.27	57.99	2.00	25.00	81.16	23.17	2.59	1.85
HSC1-2	70	37.92	56.64	0.00	0.00	56.64	0	1.24	1.24
HSC1-3	80	38.58	57.30	0.00	0.00	57.30	0	1.40	1.40
BJ-2	71	39.90	58.63	0.00	0.00	58.63	0	1.21	1.21

Table 3.16: This writer's experimental beams comparison with EC2 and revised modified EC2M design rule using Baumann-Motamed formulae.

Parameter	H (mm)	B (mm)	D (mm)	F_{cu} (kN)	% ρ_{dow}	%ρ_{bott}	% ρ_v (10^{-3})	Fy MPa	V_s (kN)	Shear Span	Vexp (kN)	Vaci (kN)	Vexp/ Vaci
Beam													
NSC1	300	150	265	43.2	0	2.37	1.9	250	18.72	3.02	80	62.09	1.288
NSC2	300	150	265	41	0.56	2.37	1.9	250	18.72	3.02	101.5	60.97	1.665
NSC3	300	150	265	47.7	1.50	2.37	1.9	250	18.72	3.02	100	64.29	1.555
NSC4	300	150	265	43.3	2.44	2.37	1.9	250	1872	3.02	105	62.14	1.69
NSCL	300	150	265	44.2	0	2.37	2.2	250	22.19	3.02	125	66.06	1.892
HSC1	300	150	265	109	0	2.37	1.9	250	18.72	3.02	65	73.49	0.884
HSC2	300	150	265	109.3	0.56	2.37	1.9	250	18.72	3.02	132.5	73.49	1.803
HSC3	300	150	265	112.5	150	2.37	1.9	250	18.72	3.02	140	73.49	1.905
HSC4	300	150	265	112.5	2.44	2.37	1.9	250	18.72	3.02	150	73.49	2.041
HSC1-2	300	150	265	101.2	0	2.37	1.9	250	18.72	3.02	70	73.49	0.953
HSC1-3	300	150	265	106.6	0	2.37	1.9	250	18.72	3.02	80	73.49	1.089
BJ-2	300	150	265	118.1	0	2.37	1.9	250	18.72	4.15	71	73.49	0.966

Table 3.17: This writer's' experimental beams comparison with ACI design rule

Collins et al proposed shear design procedures [3-31] based on the revised modified compression field theory, where the nominal shear strength of non pre-stressed reinforced concrete members without stirrups is given as:

$Vc = \beta b_w d_v \sqrt{f'_c}$

where d_v is the flexural lever arm which can be taken as 0.9d, and β is a parameter that indicates the ability of the concrete section to transmit stresses across diagonal cracks.

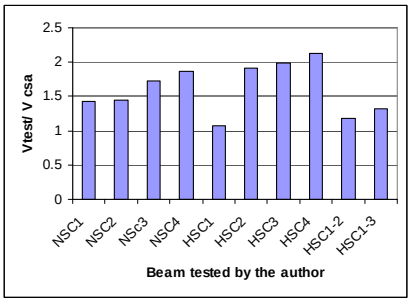

Figure 3.49:Comparative accuracy of Canadian CSA [3-32] code with author's test results

The values of β are derived from the revised modified compression field theory, where β is a function of a crack spacing parameter *se* and the strain in the flexural reinforcement εx. Charts are published in the paper for estimating the values of β. The parameter *se* accounts for the influence of the crack spacing *sx* and the maximum aggregate size a which is taken as zero for HSC because of absence of aggregate interlock in the following: $se = 35\ sx / (a+16)$ this was revised modified in 2008[3-33] to $se = 35\ sx / (a+15)$ *sx* is taken as 0.9 *d* for members that have only concentrated reinforcement near the flexural tension face, or as the maximum distance between the layers of longitudinal reinforcement if the member contains intermediate layers of crack control reinforcement . *sx* is taken as 0.9 *d* for members that have only concentrated reinforcement near the flexural tension face, or as the maximum distance between the layers of longitudinal reinforcement if the member contains intermediate layers of crack control reinforcement.

It is worth noting from this author's experiments that HWB, in addition to being layers of crack control reinforcement, more importantly stabilise the arching effect on the beam by contributing to diagonal compression strut action, therefore the STM action takes place in beams of a/d=3 with tension reinforcement almost reaching its yield.

For non-prestressed members with no axial load, the strain *εx* is given by

$\varepsilon_x = [(M / d_v) + 0.5 V \cot\Theta] / E_s A_s$

where, Θ is a function of a crack spacing parameter *se* and the strain in the flexural reinforcement ε_x, and *As* is the area of longitudinal reinforcement in the flexural tension half of the section. For determining εx, the moment at a distance of *dv* from the face of the support, or *dv* from the edge of the loading plate is used.

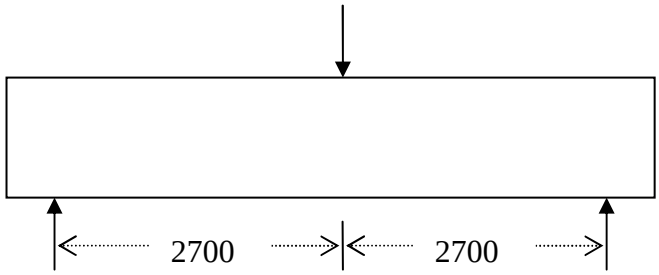

Figure 3.50: Loading arrangement for Collins et al beams

To study the factors influencing the shear strength of large, lightly reinforced flexural members, 22 specimens with a point load applied at mid-span of the beams were tested to failure.

Thirteen of the beams had an overall depth of 1000 mm, four had 500 mm, four had 250 mm, while one had 125 mm. The longitudinal reinforcement ratio varied from 1.19 % down to 0.50 % . All of the beams were made from concrete with a maximum aggregate size of 10 mm.

The revised modified compression field theory predicts that the size effect in shear depends on the distance between the layers of reinforcement rather than on the overall depth of the beam. In HSC, cracks pass through the aggregate, resulting in crack surfaces that are relatively smooth and in cracks whose roughness is not influenced by the maximum aggregate size.

To investigate the sensitivity of the failure shear to the bond characteristics of the flexural reinforcement, beam Bl00HE used epoxy coated reinforcement, beam Bl00L contained an array of three layers of small-diameter bars, and beam Bl00B had a bundle of large-diameter bars.

The revised modified compression field theory design method assumes that if a member obtains at least the required minimum area of stirrups, the reduction in shear failure stress with increasing member size will become insignificant.

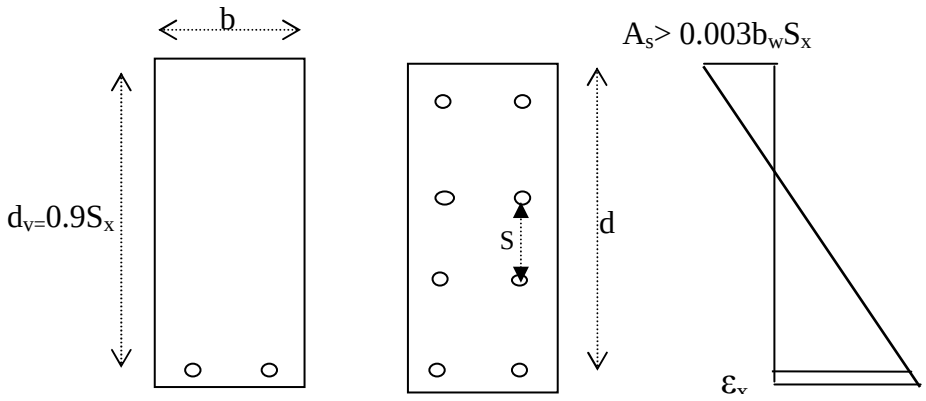

Figure 3.51: Showing S_x and flexural lever arm dv = 0.9d

All of the 22 beams tested in the series had a width of 300 mm. All the beams failed in shear prior to flexural yielding of the longitudinal reinforcement. For four of the beams, the shear span that failed first was reinforced with external clamps, and the beam was then retested. The results of all 26 tests, with the four retests being labelled R, are summarized in Table 3.18.

The proposed revised modified compression field design rule together with ACI prediction or Collins' revised modified ACI rule does not seems conservative when designing beams with central web steel such as beam BHD100.

The observed failure shear stresses for 20 beams that did not contain stirrups are shown in Table 3.18, and are compared to ten of this author's beams with links and six with HWB, Table 3.19.

One inherent weakness in Collins' modified compression field design rule is that this theory for reinforced concrete beams subjected to shear [3-34] was developed on the assumption that the average stress-strain relationships for the reinforcement and for the concrete will be completely independent of each other. This assumption needs careful review as RC beams' average stress/average strain relationship for reinforcement and for concrete are dependent on one another.

It was further assumed that the average shear stress on the plane normal to the reinforcement resisted by the reinforcement is zero. However, the presence of dowel action in the form of shear stress on the plane normal to the reinforcement is demonstrated in earlier

sections and in this writer's tests, and its existence is generally accepted.

Test specimen	h mm	bu mm	d mm	*fc' MPa*	As mm^2	ρx percent	ρvfy MPa	M/Vd*	Vexp kN	Vexp/ bud$\sqrt{f'c}$	Vaci kN	se mm	V_{maci} kN	V_{mcft} kN	Vexp/ Vaci	Vexp/V_{maci}	Vexp/ Vmcft
B100	1000	300	925	36.0	2800	1.01	—	2.92	225	0.135	278	1120	170	184	0.81	1..32	1.22
Bl00-R	1000	300	925	36.0	2800	1.01	—	2.92	249	0.150	278	1120	170	184	0.90	1.46	1.35
Bl00D	1000	300	925	56.0	3300	1.19	—	2.9	320	0.192	278	229	271	264	1.15	1.18	1..21
Bl00H	1000	300	925	98.0	2800	1.01	—	2.92	193	0.084	384	1820	182	200	0.50	1.06	0.96
B100HE	1000	300	925	98.0	2800	1.01	—	2.92	217	0.094	384	1820	182	200	0.56	1.19	1.08
Bl100L	1000	soo	925	39.0	2800	1.01	—	2.92	223	0.129	289	1120	177	189	0.77	1.26	1.18
Bl00LR	1000	300	925	39.0	2800	1.01	—	2.92	235	0.136	289	1120	177	189	0.81	1.33	1.24
Bl100B	1000	300	925	39.0	2800	1.01	—	2.9	204	0.118	289	1120	177	189	0.71	1.15	1.08
BNl00	1000	300	925	37.2	2100	0.76	—	2.9	192	0.113	282	1121	173	168	0.68	1.11	1.14
BN50	500	300	450	37.2	1100	0.81	—	3.0	132	0.160	137	545	111	99	0.96	1.19	1.33
BN25	250	300	225	37.2	600	0.89	—	3.00	73	0.177	69	273	65	58	1.06	1.12	1.25
BN12	125	300	110	37.2	300	0.91	—	3.07	40	0.199	34	133	35	32	1.19	1.14	1.24
BND	1000	300	925	37.2	2900	1.05	—	2.92	258	0.152	282	229	276	258	0.91	0.94	1.00
BND50	500	300	450	37.2	1500	1.11	—	3.00	163	0.198	137	108	146	144	1.19	1.12	1.13
BND25	250	300	225	37.2	884	1.31	—	3.00	112	0.272	69	54	76	82	1.63	1.48	1.36
BHl00	1000	300	925	98.8	2100	0.76	—	2.92	193	0.084	384	1821	182	179	0.50	1.06	1.08
BH50	500	300	450	98.8	1100	0.81	—	3.00	132	0.117	187	886	127	109	0.70	1.04	1.20
BH25	250	300	225	. 98.8	600	0.89	—	300	85	0.151	93	443	80	66	0.91	1.06	1.28
BHDl00	1000	300	925	98.8	2900	1.05	—	2.92	278	0.121	384	372	343	295	0.72	0.81	0.94
BHD1	1000	300	925	98.8	2900	1.05	—	2.92	334	0.145	384	372	343	295	0.87	0.97	1.13
BHD50	500	300	450	98.8	1500	1.11	—	3.00	193	0.172	187	175	189	167	1.03	1.O2	1.15
BHD50	500	500	450	98.8	1500	1.11	—	300	205	0.183	187	175	189	167	1.10	1.O8	1.22
BHD25	250	300	225	98.8	884	1.31	—	3.00	111	0.199	93	88	101	81	1.19	1. 10	1.37
BRL100	1000	500	925	94.0	1400	0.50	—	2.92	163	0.071	384	1821	182	154	0.42	0.89	1.06
BM100	1000	300	925	47.0	2100	0.76	0.40	2.92	342	0.180	429	1121	306	246	0.80	1.12	1.39
BM100	1000	300	925	47.0	2900	1.05	0.40	2.92	461	0.242	429	229	422	392	1.08	1.09	1.18

[1] *M/Vd* ratio given for maximum moment location.

*Load at significant diagonal cracking, failure load — 93 kN.

Note: *Vmaci*= modified ACI approach using Eq. (6) for *Vr*

Table 3.18: Collins' experimental programme, results, and predictions

Source: Extracted from the table in Collins, M.P. et al [3-25] -1999

Table 3.4 demonstrates that the shear resisted by the reinforcement in the form of dowel action , or shear in the plane normal to the axis of the bar in high strength reinforced concrete beams, increases by more than 100%.

Collins et al [3-25] conclude that as the members become deeper, the shear stress at failure decreases. Members with distributed longitudinal reinforcement fail at higher shear stresses than members with concentrated reinforcement and in terms of the ratio of failure shear stress to √fc' HSC beams fail at lower ratios than NSC beams.

This writer's experimental tests demonstrate, contrary to the above conclusion, that when reinforced concrete beams have a large percentage of HWB, HSC beams fail at a higher ratio than NSC beams, as shown in Table 3.4.

Collins' specimens with percentage longitudinal reinforcement, or HWB, are identified as D in Table 3.18. The percentage of tension reinforcement did not increase by more than 40% for layered or HWB reinforcement, whereas this writer's experiment the HWB increased by 104% compared to the tension bar and therefore this influence was fully investigated.

Collins et al [3-25] were concerned to note that 13 of the 20 beams failed at shears less than those predicted by the ACI Code equation, with four of these beams failing at less than 60 % of the ACI value and one beam, BRLl00, failing at 43 % of the ACI value. To emphasize the difference between what is predicted by the code and what was observed in the tests, the failure state of three beams are compared.

Note that beam Bl00H, for which fc= 98 MPa, failed at a lower shear force than the identically reinforced beam Bl00, for which fc = 36 MPa. Bl00D was identical to Bl00, except that it contained a small amount of distributed reinforcement over the depth of the member. As a result, Bl00D had more closely spaced shear cracks and had a shear strength 39 % higher than that of Bl00. In addition, Bl00D failed in a ductile manner while both Bl00 and Bl00H had sudden failures.

Collins et al [3-25] reconfirmed this writer's tests results on the contribution of HWB in HSC with their test specimen BHD25 which was made with HSC and HWB and had the highest V_{exp}/V_{aci} of 1.19 compared to their other specimens, demonstrating that the contribution of HWB in HSC is not fully utilised in ACI318 [3-2]

Premature failure of a HSC beam as compared to a corresponding NSC beam has also been recognised and identified by the following group of researchers since 1984:

- Andrew G. Mphonde and Gregory C. Frantz 'Shear Tests of High- and Low-Strength Concrete Beams Without Stirrups' ACI Journal Proceedings, 1984 - ACI
- Ashraf H. Elzanaty, Arthur H. Nilson, and Floyd O. Slate 'Shear Capacity of Reinforced Concrete Beams Using High-Strength Concrete' Journal ACI Proceedings, volume 83, issue 2 March 1, 1986
- Shuaib H. Ahmad, A. R. Khaloo, and A. Poveda 'Shear Capacity of Reinforced High-Strength Concrete Beams'. ACI Journal Proceedings.March 1, 1986
- Mark K. Johnson and Julio A. Ramirez. 'Minimum Shear Reinforcement in Beams With Higher Strength Concrete' Structural Journal, vol 86 issue 4, pages 376-382, July 1, 1989
- Thorenfeldt E and Drangsholt, G. 'Shear capacity of reinforced HSC beams.'ACI 2nd International Symposium on HSC, ACI SP 121.8, 1990.pp.129-154
- Roller J, J. and Russel H, G 'Shear Strength of High-Strength Concrete Beams With Web Reinforcement'. Structural Journal, vol 87, issue 2 p 191-198
- Sarsam K. F, Al-Musawi J.M.S, ' Shear Design of High- and Normal Strength Concrete Beams' with Web Reinforcement ACI Structural Journal, 1992
- Raghu S. P and Mendis P 'Experimental Study on Shear Strength of High-Strength Concrete Beams' Structural Journal July 1, 2000
- Angelakos. D, Bentz E. C, and Collins M. P.'Effect of Concrete Strength and Minimum Stirrups on Shear Strength of Large Members' Structural Journal. vol 98, issue 3, 1 May 2001
- Cladera .A.,. Marí .A.R 'Experimental study on high-strength concrete beams failing in shear' Engineering Structures 27, 2005, 1519–1527

3.9.6 Variation of failure shear stress ratio with beam depth

Stabilising the arching effect of horizontal web reinforcement HWR (layered reinforcement) over the depth in the HSC was demonstrated in this writer's tests in 1997 [3-13] .

Collins [3-25] in 1999 concluded that large, lightly reinforced concrete members that do not contain stirrups will fail in shear at loads considerably less than those predicted by the current ACI expressions. He conducted a series of tests with HWB and proposed an empirical design approach.

The EC2 design rule complemented with the Baumann-Motamed's revised modified design rule for dowel action give reasonable results for Collins' [3-25] beams compared with Collins' proposal which appears unsafe for shallow HSC beams of 500mm depth with layer (HWB) reinforcement.

BEAM	D mm	No dowels	d_{dow} mm	fcu N/mm	ρx% bott	M/vd	Vs kN	Vexp kN	Vexp/ bwd'√fc √fc≤10.5'	Vexp/ bwd'√fc √fc≤8.3
NSC1	265	0.00	0.00	43.2	2.37	3.02	18.72	80	0.23	0.23
NSC2	265	2.00	12.00	41	2.37	3.02	18.72	101.5	0.33	0.33
NSC3	265	2.00	20.00	47.7	2.37	3.02	18.72	100	0.30	0.30
NSC4	265	2.00	25.00	43.3	2.37	3.02	18.72	105	0.33	0.33
HSC1	265	0.00	0.00	109	2.37	3.02	18.72	65	0.11	0.14
HSC2	265	2.00	12.00	109.3	2.37	3.02	18.72	132.5	0.27	0.34
HSC3	265	2.00	20.00	112.5	2.37	3.02	18.72	140	0.29	0.36
HSC4	265	2.00	25.00	112.5	2.37	3.02	18.72	150	0.31	0.39
HSC1-2	265	0.00	0.00	101.20	2.37	3.02	18.72	70	0.13	0.15
HSC1-3	265	0.00	0.00	106.6	2.37	3.02	18.72	80	0.15	0.18

Table 3.19: Variation of failure shear stress ratio at beam depth 265mm.

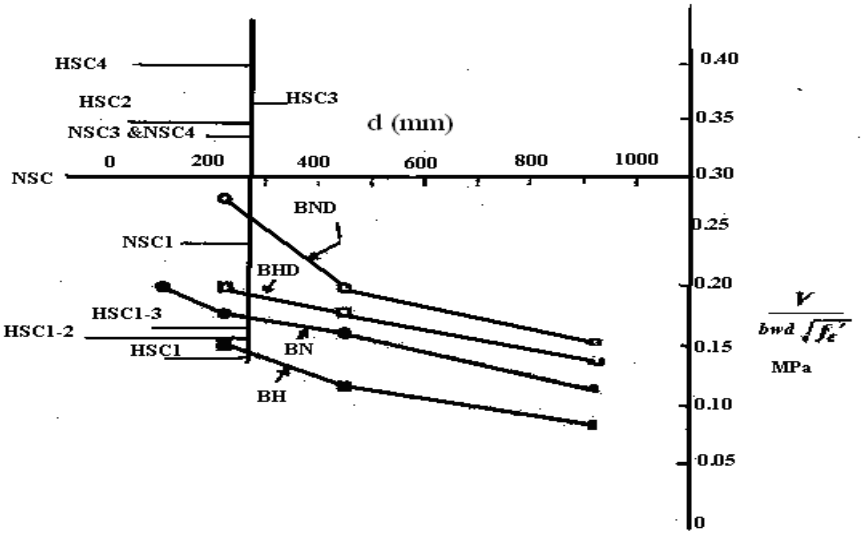

Figure 3.52: Variation of failure shear stress ratio with beam depth, comparison of author's beams and Collins et al beams for √fc≤8.3

Members 2000mm deep, made from 25 MPa concrete with 25mm maximum aggregate, or members l000mm deep, of 70MPa concrete with less than 1 % of flexural reinforcement may fail at less than 50 % of the predicted shear capacity.

Beam	εx 1/1000	Se mm	β	Vdow kN	V Con (kN)	Vmcft Tot kN	Vmmcft kN	Vexp kN	Vmcft /Vexp
NSC1	1.45	2.43	0.14	0	37.27	55.99	55.99	80	1.43
NSC2	1.59	97.2	0.14	12.7	38.7	56.01	70.49	101.	1.44
NSC3	1.83	97.2	0.14	13.30	39.16	56.03	78.03	100	1.73
NSC4	1.74	97.2	0.14	16.9	37.31	56.03	84.05	105	1.87
HSC1	1.29	601	0.1		42.28	61.01	61.01	65	1.07
HSC2	2.43	219	0.12	13.8k	50.81	69.53	82.78	132.5	1.91
HSC3	2.49	219	0.12	203	51.55	70.27	95.82	140	1.99
HSC4	2.42	219	0.12	23.17	51.55	70.27	105A	150	2.13
HSC1-2	1.29	601	0.1.	0	40.74	59.46	59.46	70	1.18
HSC1-3	1.29	601	0.1.	0	41.82	60.54	60.54	80	1.32

Table 3.20:Author's beams experimental comparison with Collins' MCFT design rule using Baumann-Motamed's formula for the web bars.

3.10 This writer's prediction rule applied to tests by others

3.10.1 Desai's tests

As series of tests carried out by Desai [3-35] at BCA laboratory on beams with bottom steel of 3T20 and top steel of 2T12, span/depth ratio 2.59, with 6mm diameter links at 200 mm centres, Table 3.21 and without link shown in Table 3.22

The tolerance for the proposed writer's rule is 27% and safe for all beams whereas Desai's is 31% for his beams tested of span/depth ratio 2.59 with stirrups.

When investigating the safety of this writer's prediction rule for beams tested in Table 3.22, the average proposed predictions are 1.03 for E2 type, 0.98 for B2 type, 1.02 for type E3 and 0.92 for type E4. In this writer's opinion there may have been a possible anchorage failure at HWB level in beams tested in Table 3.22.

The BS8110 clause 3.12.8.4 for design ultimate anchorage bar, f_{bu} , derived from equation 49 is

$f_{bu}=\beta\sqrt{f_{cu}}$ 3.15

Value β depends on the type and diameter of the bar. For E4 series with T16 bars of f_y=460 N/mm^2 and f_{cu}=35 N/mm^2 a minimum anchorage length of 34×16 or 544mm

length is required to provide f_{bu}=2.9 N/mm^2 ultimate anchorage bar stress to develop the tie action in the HWB and to resist the inclined diagonal compression forces resulting from presence of HWB.

Beam	No of bars	Diameter of HWB	ρb	f_{cu} N/mm^2	V_{fu} kN	V_{cu} kN	V_{lu} kN	$V_{bu\text{-}desai}$ kN	$V_{du\text{-}Baumann\text{-}Motamed}$ kN	V_{du} kN	V_{fu} / V_{desai}	$V_{Baumann\text{-}Motamed}$	Vfu/ $V_{Baumann\text{-}Motamed}$
C1	**0**		0	32	119	61	34.5	0	0	96	1.25	95.5	1.25
C1a	**0**		0	32	128	61	34.5	0	0	96	1.34	95.5	1.34
D1	**2**	10	0.3	32	132	61	34.5	7	11.15	103	1.29	106.6	1.24
D1a	**2**	10	0.3	32	141	61	34.5	7	11.15	103	1.38	106.6	1.32
D2	**1**	16	0.4	28	146	58	34.5	9	14.66	102	1.44	107.2	1.36
D2a	**1**	16	0.4	28	154	58	34.5	9	14.66	102	1.52	107.2	1.44
D3	**1**	20	0.6	26	130	57	34.5	14	17.49	106	1.23	109.0	1.19
D3a	**1**	20	0.6	26	130	57	34.5	14	17.49	106	1.27	109.0	1.19
D4	**1**	23	0.9	26	134	57	34.5	21	19.78	113	1.19	111.3	1.20
D4a	**1**	25	0.9	26	133	57	34.5	21	21.26	113	1.18	112.8	1.18
Average tolerance for all beams											1.31		1.27

Table 3.21: Proposed prediction rule applied to shear failure of Desai's [3-35] specimen

In Chapter 5 it will be demonstrated that presence of HWB improves arching action, by deflecting the inclined diagonal compression strut at the HWB level, therefore increasing the tensile force in HWB at supports. Also absence of stirrups exaggerates arching action for the tested beams which are span/depth ratio 2.59.

Similarly, for beam types B2, E2, and E3, minimum anchorage lengths of $40\times10 = 400mm$, $34\times10 = 340mm$ and $34\times12 = 408mm$ are required in order to transfer the force from the deflected inclined diagonal compression strut to the HWB at support level.

When stirrups are present, part of the forces from the inclined diagonal strut are carried by the stirrups therefore the strains at the support of the beam on the HWB bars are reduced.

But, in the absence of stirrups these strains remain high. There are no given dimensions for the length of the end anchorage for specimens in Table 3.22. However, from the diagram and the pictures available, it can be deducted that the anchorage is only about 100mm rather than the required 544mm for development of the full ultimate anchorage forces in the bars.

Specimen	**No of bars**	**Size of HWB**	ρ_b	f_{cu} N/mm^2	V_{FU} kN	V_{CU} kN	V_{FU}/V_{CU}	**Vdu** Baumann-Motamed	**Ratios**	
									Vfu /V Baumann-Motamed	**Vfu / Vdesai**
A1	0	0	0	28	55	51	1.08	0.00	1.08	1.08
Ala	0	0	0	28	63	51	1.24	0.00	1.24	1.24
A2	2	8	0.2	36	67	55.4	1.21	9.67	1.03	1.18
B1	0	0	0	27	58	57.6	1.01	0.00	1.01	1.01
Bla	0	0	0	27	60	57.6	1.04	0.00	1.04	1.04
B2	2	10	0.3	27	65	57.6	1.13	10.74	0.95	1.07
B2a	2	10	0.3	27	68	57.6	1.18	10.74	1.00	1.12
B3	1	16	0.4	28	81	58.3	1.39	14.95	1.11	1.33
B3a	1	16	0.4	28	88	58.3	1.51	14.95	1.20	1.44
B4	1	20	0.6	33	101	61.6	1.64	19.31	1.25	1.48
B4a	1	20	0.6	33	110	61.6	1.78	19.31	1.36	1.60
B5	1	25	0.9	33	90	61.6	1.46	23.47	1.06	1.15
B5a	1	25	0.9	33	96	61.6	1.56	23.47	1.13	1.24
El	1	0	0	28	72	67.3	1 .07	0.00	1.07	1.07
Ela	1	0	0	28	75	67.3	1.11	0.00	1.11	1.11
E2	2	10	0.3	34	80	71.9	1.11	11.60	0.96	1.05
E2a	2	10	0.3	34	92	71.9	1.28	11.60	1.10	1.21
E3	2	12	0.4	34	90	71.9	1.25	13.61	1.05	1.12
E3a	2	12	0.4	34	84	71.9	1.17	13.61	0.98	1.06
E4	1	16	0.4	35	75	72.6	1.03	16.10	0.85	0.99
E4a	1	16	0.4	35	88	72.6	1.21	16.10	0.99	1.15
Average ratio							1.27		1.07	1.18

Table 3.22: Proposed prediction applied to Desai's [3-35] beams without stirrups. NB: Test on specimen A2a was abandoned due to faulty application of the test loads.

In this writer's opinion, it could be possible that tests shown in Table 3.22 may have failed at bond anchorage of the horizontal web bar near support simultaneously with shear failure, resulting in lower shear failure load compared to the true shear failure load which would have occurred if sufficient bond anchorage had been provided for the HWB bars.

3.10.2 Vollum's tests

A series of tests were carried out by Vollum at the Imperial College laboratory on beams with the bottom steel of 3T20 and top steel of 2T12, with flexural span 2100mm and span/depth ratio 3.17, without link shown in Table 3.23.

Specimen	Tension steel	No of HWB	Diameter of HWB	ρ_b	f_{cu} $_2$ N/mm	V_{FU} kN	V_{CU} kN	V_{FU}/V_{CU}	Dowel force kN	$V_{fu}/V_{Baumann-Motamed}$
F1	3T20	0	0	0	43	69	67.3	1.03	0.00	1.025
F1a		0	0		43	75	67.3	1.11	0.00	1.114
F2	3T20	1	12	0.21	44	80	67.8	1.18	12.90	0.991
F2a		1	12		44	82	67.8	1.21	12.90	1.016
F3	3T20	1	16	0.38	46	76	68.8	1.1	17.09	0.885
F3a		1	16		46	82	68.8	1.19	17.09	0.955
F4	3T20	1	20	0.59	44	86	67.8	1.27	20.59	0.973
F4a		1	20		44	79	67.8	1.17	20.59	0.894
F5	3T20	1	25	0.93	43	82	67.3	1.22	24.83	0.89
F5a		1	25		43	80	67.3	1.19	24.83	0.868

Table 3.23:Vollum's [3-35] tests at Imperial College for 2100mm span beams without stirrups

Source: Table from Desai, S**.** June 1995 [3-35]

Table 3.23 demonstrates that dowel action does not develop in NSC beams of a/d=3.17 with no shear stirrups, which may indicate that the upper limit for applying the proposed dowel formulae is for beams of a/d=3.03.

3.10.3 Collins' tests

Collin et al [3-25] reported in their paper that structures made from HSC are more sensitive to the size effect in shear . This was demonstrated by experiments in which they considered the performance of layered crack control reinforcement and concluded that layer reinforcement or HWB influences the crack size in the shear diagonal cracks, and therefore improves the shear resistance of the beam. However, the experiment did not fully explore the stabilizing arching effect of the layer reinforcement in HSC.
In section 2.3.7 the strain fluctuation in the centre link of NSC1, NSC3, HSC1 and HSC3

are investigated in detail. This link is identified as number 2 in Figure 2.36 and since it is located in the middle of shear span, its strain fluctuations clearly demonstrate the contribution of HWB to resist shear forces.

Test specimen	H (mm)	Bu (mm)	*D* (mm)	fc' N/mm^2	As	Web radius mm	Web diam mm	Layer	Vd kN	Px	Vaci /Vexp	Vmaci /Vexp	Vmcft /Vexp	Vexp_/Vtot
B100D	1000	300	925	36	2100	9.8	19,6	1	32.87	0.008	1.15	1.18	1..21	1.73
BND100	1000	300	925	37.2	2100	8	16	1	27.88	0.008	0.91	0.94	1.00	1.42
BND50	500	300	450	37.2	1100	5.7	11.4	1	20.55	0.008	1.19	1.12	1.13	1.65
BND25	250	300	225	37.2	600	4.8	9.6	1	17.53	0.009	1.63	1.48	1.36	1.90
BHD100	1000	300	925	98.8	2100	8	16	1	38.6	0.008	0.72	0.81	0.94	1.10
BHD50	500	300	450	98.8	1100	5.64	11.3	1	28.17	0.008	1.03	**1.02**	1.15	1.42
BHD25	250	300	225	98.8	600	4.8	9.6	1	24.26	0.009	1.19	1. 10	1.37	1.36

Table 3.24: Table of comparison for author's design proposal with Collins' modified compression and modified ACI proposals for beams tested by Collins.

3.11 Summary and comments

In general, tests on HSC beams proved that HWB located towards the centre of the beam improve the shear resistance significantly. The results for beam HSC4 compared with those for HSC1 proved there is an enhancement of shear resistance of about 130% when horizontal web steel is provided.

HWB can provide added ductility and resistance to accidental loading. In particular, for design purposes, when considering fire exposure, to have their location protected by the surrounding concrete would be of some advantage.

According to the truss analysis method which is the proposed method of BS8110, although maximum allowable spacing between links is 200mm and in the experiment spacing of link for beam NSCL was 300mm, with less shear links (ρw fy bd=31.4 kN) tyhan NSC1 (ρw fybd=34.5 kN) , with all other parameters identical, surprisingly NSCL has an improved shear resistance of 70% compared to NSC1. The behaviour of compression horizontal strut in STM can be influenced by the presence of confinement

links in the flexural span near loading point. This phenomena is analysed in Chapter 6 in a parametric model.

When Baumann-Motamed's equation for shear resistance of HWB was applied to beams tested by Collins et al [3-25], the equation gave a satisfactory prediction when used in conjunction with shear design guidelines in BS8110, EC2, ACI and CSA codes.

3.12 Conclusion

Experimental and theoretical studies have shown that HSC can be used economically for column members of the structures, but its shear performance and its brittle inductile material property need to be taken into consideration.

Shear resistance of HSC is equal to and, in some cases, particularly with limestone aggregate, less than NSC.

The decrease in shear strength for HSC members with or without shear reinforcement has resulted in restrictions being imposed on the use of HSC in such codes as the Concrete Society is [3-36] and EC2-BS EN [3-10] which limit f_c and f_{cu} to 50 and 60 MPa respectively.

The proposed design rule to predict the contribution of HWB in resisting shear provides a reliable approach for shear design of HSC beams of $a/d \leq 3$.

In section 3.2.12 it was demonstrated that arching action fully develops in HSC with HWB of a/3=3.02, 3.2.12whereas when HWB is absent in the same beam no arching action develop at all. In the following chapter, F.E approach is used to analyse the forces and moments on the HWB to demonstrate that dowel action on HWB results in sufficient moment to produce full arching in the diagonal compression strut.

3.13 References

3-1 Comité Euro-International du Béton, CEB-FIP Model Code 1990, Thomas Telford Services, Ltd., London, 1993, 437 pp.

3-2 ACI Committee 318, Building Code Requirements for Structural Concrete (ACI 318-08) and commentary (ACI 318R-08), American Concrete Institute , Formington Hills, MI, 2008, 465 pp

3-3 Allan, A.H, 'Reinforced Concrete Design to BS8110 Simply explained'. E & F. Spon Ltd, published 1988, p 49 to 51

3-4 Franyois de Larrard, 'Formulation et Proprietes des Betons a tres Hautes Performances', Rapport de Recherche du Laboratoire Central des Ponts et Chaussees de Paris, No.149, Paris, Mars 1988.

3-5 Special Report, 'Les Fumees de Silice dans Ie Genie Civil. Applications aux Betons et Coulis', Annales de l'Institut Technique du Batiment et des Travaux Publiques. No.483, Mai 1990.

3-6 BS1881: Part 117-83, Method for Determination of the Tensile Splitting Strength.

3-7 BS 4449:1997: Specification for carbon steel bars for the reinforcement of concrete, British Standards Institution, 15-May-1997

3-8 Elzanaty, A.H, Nilson, A. H, and Slate, F, O, ' Shear capacity of of Reinforced Concrete Beams Using High Strength Concrete'. Journal ACI Proceedings, volume 83, issue 2 March 1, 1986.

3-9 BS 8110: Structural use of concrete, Part 1.Code of practice for design and construction, British Standards Institution, London, 1985

3-10 Eurocode 2: Design of concrete structures, Part 1-1, General rules and rules for buildings, BS EN 1992-1-1:2004, British Standards Institution, London, Dec 2004

3-11 Rogowsky, D. M , MacGregor, J.G. "Design of Deep Reinforced Concrete Continuous Beams," Concrete International : Design and Construction, Vol.8, No 8, August 1986, pp.49-58

3-12 Kani, G.N.J. 'Kani on Shear in Reinforced Concrete', Department of Civil engineering, University of Toronto, Canada, 1979

3-13 Motamed, J. 'Shear in normal strength and high strength reinforced concrete beams with stirrups and horizontal web bars'. University of Westminster, MSc Dissertation, 1997

3-14 Taylor, H. P. J. 'Investigation of the forces carried across cracks in reinforced concrete beams in shear by interlock of aggregate', Tech. Rep. 42.447, Cement and Concrete Association, London, Nov 1970

3-15 Hamadi, Y.D, Regan P.E. 'Behaviour in shear of beams with flexural cracks'. Magazine of Concrete Research: Vol. 32, No 111: June 1980

3-16 Fenwick, R.C., Paulay, T. ‘Mechanisms of shear resistance of concrete beams’. Proceedings of the American Society of Civil Engineers. Vol.94, No. ST 10. October 1968. pp 2325-2530

3-17 Albajar, J.S. ‘The influence of aggregate fracture on the shear strength of reinforced concrete beams’, Thesis submitted to the Imperial College London, University of London, PhD, Sept 2008, pp. 409

3-18 Comité Euro-International du Béton, CEB-FIP Model Code 1990, Thomas Telford Services, Ltd., London, 1993, 437 pp.

3-19 Baumann, T., Rusch,.H.'Versuche zum Studium der Verdubelungswirkung der Biegezugbewehrung eines Stahlbetonbalkens, (Tests studying the dowel action of the flexural tensile reinforcement of reinforced concrete beams.) Berlin, Wilhelm Ernst und Sohn, 1970, Deutscher Ausschuss fur Stahlbeton, Heft 210. pp. 42-82

3-20 Houde, J and Mirza, M.S, ‘A Finite Element Analsis of Shear Strength of Reinforced Concrete Beams’ Journal ACI Proceedings, volume 42, 1 January, 1974, pp.103-128

3-21 Taylor, H. P. J. ‘Investigation on the dowel shear forces carried by the tensile steel in reinforced concrete beams’. London, Cement & Concrete Association, 1969, Technical Report 42.431

3-22 Chana, P.S. 'Investigation of the mechanism of shear failure of reinforced concrete beams'. Magazine of Concrete Research: Vol. 39, No 141: December 1987

3-23 Hejazi, J. 'Horizontal web steel as shear reinforcement'. MSc dissertation, University of Westminster, 1997

3-24 Krefeld, W.J., Thurston, C.W. ‘Studies of the shear and diagonal tension strength of simply supported reinforced concrete beams’. Columbia University, New York, 1962. (April 1966, ACI Journal)

3-25 Collins, M. P,. and Kuchma, D.‘How Safe Are Our Large, Lightly Reinforced Concrete Beams, Slabs, and Footings?’ ACI Structural Journal. V. 96. No. 4. July-August 1999, p482-490

3-26 Kani, G. N. I. "How Safe Are Our Large Concrete Beams?," ACI JOURNAL Proceedings, V 64, No. 3, Mar. 1967, pp. 128-141.

3-27 Kuchma, D., Vegh, P., Simionopoulos, K., Stanik, B.; Collins, M. P. "The Influence of Concrete Strength, Distribution of Longitudinal Reinforcement and Member Size on the Shear Strength of Reinforced Concrete Beams," CEB Bulletin No. 237, 21 pp.

3-28 Bazant, Z. P., and Kazemi, M. T, "Size Effect on Diagonal Shear Failure of Beams without Stirrups," ACI Structural Journal, V 88, No. 3, May-June 1991, pp. 268-276.

3-29 Shioya, T.; Iguro, M. Nojirr, Y., Akiyama, H.; and Okada, T., "Shear Strength of Large Reinforced Concrete Beams," Fracture Mechanics- Application to Concrete, SP-118, Y C. Li and Z. P. Bazant, eds., American Concrete Institute, Farmington Hills, Mich., 1989, pp. 259-279.

3-30 Shioya, T. "Shear Properties of Large Reinforced Concrete Member," Special Report of Institute of Technology, Shimizu Corp., No. 25, Feb. 1989, 198 pp.

3-31 Collins, M. P.; Mitchell, D.; Adebar, P. E., Vecchio. F. J., ' General Shear Design Method." ACI Structural Journal, V 9.3, No. 1, Jan.-Feb. 1.9.96. pp. 36-45.

3-32 CSA Committee A23.3, ‘Design of concrete structures’, Canadian Standards Association, Mississauga, Ontario, Canada, 2004, 214pp.

3-33 Collins, M. P., Mitchell, D., Evans C.B. 'Shear Design of Concrete Structures" 20 May 2008, The Structural Engineer.

3-34 Frank., V., Collins, M. P. ‘The modified compression-field theory for reinforced concrete elements subjected to shear’. ACI Journal- March- April 1986

3-35 Desai, S.B. ‘Horizontal web steel as shear reinforcement’. Magazine of Concrete Research, Vol.47. No.171.June 1995.pp. 143-152

3-36 Concrete Society: ‘Design guidance for high strength concrete’, Tech. Rep. No 49, Slough, The Concrete Society, 1998.(amended 2004)

Chapter 4

Finite Element Analysis of NSC and HSC Beams with Horizontal Web Bar

4.1 Introduction

Advances in computer technology have facilitated solving engineering problems, however, can have the unfortunate side-effect of downplaying the importance of sound engineering knowledge. Although vital to current design practice, computer use, if not subordinated to design experience and engineering judgement, would be a recipe for disaster.

Different methods have been utilized to study the response of structural components. Experimental based testing has been widely used as a means to analyze individual elements, while experimental methods produce realistic and accurate results but they are costly and time consuming. There are presently several user-friendly non linear FE software packages available for researchers and designers in order to predict shear behaviour of RC structures.

To understand the capabilities of FE computer software, one must look to experimental data and simple analysis. Results obtained from a FE analysis packages are not reliable or useful unless the necessary steps are taken to understand what is happening within the model that is created using the software.

Non linear FE modelling of shear behaviour of brittle concrete structures involves processing large amount of constitutive models and parameters which are very complex to calibrate. Mesh properties, solver configurations or boundary conditions can also significantly influence the FE results. Executing the necessary checks along the way is the key to make sure that the output by the non linear FE software is valid.

The FE models are developed using ANSYS version 11 software package, which offers a large variety of constitutive models for concrete and reinforcement. Smeared, discrete and combined cracking models in reinforced concrete are investigated and the main features of the constitutive models are discussed. The nonlinear FE models developed by this writer is verified and validated by his experiments on beams described in this chapter and experiments

by others on short beams and BCJ in chapter 7 in order to validate proposed analytical methods for shear design. In Chapter 8 a non linear FE parametric investigation for TBCJ will be presented in order to validate the proposed design rule.

In this chapter, a non-linear FE computer program, ANSYS, is used to idealise experimentally tested RC beams with shear span/depth ratio of a/d=3.02. The results of the analysis are then compared with the experimental results to verify and validate the accuracy of the FE model. Furthermore, the FE model for HSC beams with HWB is used to develop and refine the nonlinear STM for the practical shear design and analysis in the HSC reinforced concrete beams with HWB and HSC beam column joints with CVB.

It is encouraging to note that reasonable agreement between predictions of the FE model of the experimental test data, covering a wide range such as variation in shear span ratios, influence of size of support plates, percentage of HWB reinforcement and concrete strength, has been found with no adjustments made to the theoretical model from problem to problem in order to make the theory match experiments.

Nonlinear techniques were employed to select, analyse and verify processes of STM in the FE analysis in order to eliminate the limitations of the conventional STM relating to the behaviour of reinforced concrete beams.

4.2 Objectives

The purpose of this chapter is to demonstrate that by proper amalgamation of the various first order factors it is possible to reliably predict the shear characteristics such as load -deflection or strains in reinforcement to load and ultimate failure load of reinforced concrete beams.

The objectives are achieved as follows:

1. To review FE material property models proposed by others for concrete and steel properties for the reinforced concrete structure.
2. To demonstrate that by proper amalgamation of the various first order factors it is possible to reliably predict the shear characteristics of reinforced concrete beams.

3. To FE model bond represent dowel action produced by longitudinal reinforcement showing the location of the occurrence of the maximum dowel. It is notable, that in this research the concrete-steel interface is assumed to be fully bonded. Whereas, in practice full bond slippage occurs. However, this compromise enabled identifying the location of the maximum moment on the HWB, which is the main objective for FE modeling in order to use the data for developing an STM while minimizing the possibility of early numerical instabilities associated with post-cracking behaviour.

4. To develop correct coefficients for FE model to analyse HSC beams of a/d=3.02.

5. To develop FE models to analyse nonlinearly NSC and HSC beams with HWB of a/d=3.02.

6. To compare the results obtained by FE analysis with those of this writer's experimental results from past research on beams of a/d=3.02.

The results obtained from nonlinear FE for HSC beam with HWB are later used to develop STM for HSC beam column joints with CVB.

The redistribution of internal forces due to material nonlinearity (concrete cracking, concrete softening and steel yielding) are allowed. The redistribution of internal stresses allows the reorientation of principal stresses, leading to a higher accuracy. It should be noted that to allow for the redistribution of internal forces due to material nonlinearity, FE setting of tolerance for displacement is eventually increased from 0.05 for convergence criteria.

The material and geometric nonlinearity of conventional STM usually does not fully take into account the tensile contribution of concrete. In nonlinear STM , the concrete tensile contribution could be either in plain concrete or reinforced concrete ties. Reinforced concrete ties are concrete ties that contain reinforcing bars inside, while plain concrete ties have no reinforcing bars. In plain concrete ties, after the concrete cracks, the tie strength drops very rapidly and becomes dependent mainly on the bridging tensile stress transferred across the crack surface, while in reinforced concrete ties the concrete between cracks still has the ability to contribute towards resisting tie deformations through the tension stiffening effect.

In FE analysis, geometrical nonlinearity is introduced by updating the displacements at every iteration and by computing the strains based on the most updated displacements. The new position of the member is used to compute the elongation, hence the current strain. In nonlinear analysis of statically indeterminate STM, the absorbed energy in potential plastic hinges in reinforcement allows internal redistribution of stresses and hence enables the utilization of higher load carrying capacities. It is concluded that the nonlinear STM allows more economical design than the conventional STM and eliminates uncertainties related to FE prediction of shear performance of RC structures.

It is notable that there is a general scarcity of reported experimental data for HSC components. To this writer's knowledge, no attempt has been made to apply FE and STM to the higher range of concrete strengths for beams with HWB as an additional shear reinforcement.

4.3 Review of finite element research on shear in RC beams

Over the last three decades, there has been significant activity in the area of analysis of concrete structures by the finite element method. For the recently reported nonlinear FE models to be reliable, such techniques must be capable of predicting a number of different failure mechanisms and must be sufficiently discriminating so that the critical failure mechanism which would occur in the real structure is that which the analysis predicts [4-1].

There have been numerous attempts to amalgamate various factors incorporated into the various proposed models in order to achieve the required reliability. However, with regards to non-linear FE analysis of structural concrete, there are still many remaining challenges to solve.

A set of 12 beams of real life scale RC beams were tested by Bresler and Scordelis [4-2] to investigate the problem of brittle shear failure with and without stirrups. Vidosa et al [4-3] report that those 12 beams have been used for more than half a dozen FE studies to investigate the complexities involved with non-linear modelling of brittle shear failure in RC beams. One example is a study by Blaauwendraad and Zheng [4-4] emphasized that at the

time of publication of their paper in 1992, there were major problems associated with the prediction of shear characteristics of simple RC beams when using numerical techniques.

Seraj, S. M, Korsovos, M. D. and Pavlovic, M. N. A. [4-5] applied a three-dimensional FE model for structural concrete, based on brittle constitutive relationships at the material level to the analysis of reinforced concrete members. The generality of the 'constant-parameter' FE model, previously established for NSC, was extended to high-strength mixes. A high-strength rectangular member was also considered.

The analysis of the various structural components was preceded by the modelling of a particular, normal-strength T-beam, which was studied by adopting a number of mesh discretizations in order to accomplish an economical solution without impairing the accuracy of the numerical predictions. What emerged from their investigation was that the existing FE model, applied in the past to NSC, is just as applicable to high-strength mixes. They recommended that the accuracy of FE material modelling could improve if the acceptable ratio of the model elements to aggregate size was kept to about 3. Based on their research, this writer's FE model has maintained meshing of concrete elements dimension with the minimum size of 50mm for NSC and HSC which is made with aggregates of 25mm and 10mm.

Kachlakev, et al [4-6] studied concrete beam members with externally bonded carbon fibre reinforced polymer (CFRP) fabric. Symmetry allowed one quarter of the beam to be modelled. At planes of symmetry, the displacement in the direction perpendicular to the plane was set to zero. A single line support was utilized to allow rotation at the supports. Loads were placed at third points along the full beam on top of steel plates. The mesh was refined immediately beneath the load. Reduction of the dimensions of elements size to smaller than aggregate size may misrepresent the properties of concrete [4-5].

The property model Link 8 chosen for the reinforcement in the analysis [4-6] does not model traverse forces acting on the reinforcement which result in bending or dowel action produced by the reinforcement. To improve modelling of the reinforcement , the property model for

reinforcement applied for this writer's FE numerical models is Beam 188 which models bending to model realistic representation of the dowel action in the reinforcement.

Zhang and Raoof [4-7] numerically modelled bond between steel and concrete and proposed an equation for tension stiffening in post cracking behaviour of the concrete . They proposed 2- D FE model for concrete properties in the biaxial stress failure envelope defined in three regions in the principal stress space, Figure 4.1, by amalgamation of Kupfer and Gerstle's [40-9] model under compression-compression and Balakrishnan and Murray [4-10] model under compression-compression state of biaxial loading.

Their model combines smear cracking with plasticity and propose bonds in the steel concrete interface to be made of spring like linkage element along the edge of the solid steel and concrete element in order to follow transition from zero slip to full-slip. Their model to represent bond slippage at steel concrete interface by introducing the linkage element along the edge of steel consists of two orthogonal springs connecting and transmitting shear and normal forces across two nodes with the stiffness in the two orthogonal directions assumed uncoupled , Figure 4.8. Their model is comparable to that of Houde and Mirza's [4-17] model which proposed tangential springs at crack and steel concrete interface, see section 2.2.7.6. They introduced a modified empirical equation order for tension stiffening based on Bhide's [4-8] equation in order to calibrate their FE model with Bresler and Scordelis [4-2] experimental results.

4.4 Material behaviour

4.4.1 Failure surface of concrete

Kupfer and Gerstle [4-9] proposed that in a plane stress state, the biaxial stress failure envelope is defined in three regions in the principal stress space, Figure 4.1, tension-tension, tension-compression, compression-compression and under tension-tension state of principal stresses. Concrete cracking normal to the direction of a principal stress takes place when the magnitude of the principal stress exceeds concrete tensile strength, f_t'.

Under compression-compression state of biaxial loading, the formulation originally proposed by Kupfer and Gerstle [4-9] is:

$$\sigma_{cu} = \frac{-1+3.65\alpha}{(1+\alpha)^2} \, f_c' \quad \textbf{4.1}$$

where

f_c' = uniaxial compressive strength of concrete (always +ve)

$\alpha = \sigma_1 / \sigma_2$, σ_1 and σ_2 are the principal stresses with σ_1 being greater or equal to σ_2

In the tension-compression zone, a bilinear failure envelope, Balakrishnan and Murray [4-10], shown in Figure 4.1, proposed two distinctly different types *(i.e.*either tension or compression) of failure, under tension-compression state of biaxial loading, can take place depending on the value of the parameters α_A and σ_A defined as

$$\alpha_A = -\frac{23 f_t'}{34 f_c'} \quad \textbf{4.2}$$

$$\sigma_A = 0.5 f_t' - 0.85 f_c' \quad \textbf{4.3}$$

where f_t' = uniaxial tensile strength with f_t' and f_c' (always +ve).

In the above two equations the parameters α_A and σ_A define the location of point A in Figure 4.1. For a value of $\alpha=\sigma_1/\sigma_2$ larger than α_A, a crushing failure of concrete takes place when the principal stresses reach the failure envelope between points A and C. For values of α less than α_A, tensile failure will occur for combinations of principal stresses σ_1 and σ_2 exceeding the failure envelope between points A and B. It is notable that in view of the very small magnitude of the angle θ in Figure 4.1, early divergence can take place for certain combinations of σ_1 and σ_2 in the near vicinity of point B.

To avoid such potential problems, for values of the principal compressive (or tensile) stress $|\sigma_2| < f_t'$ occurrence of the crack is assumed to be followed by gradual increases in the magnitude of the compressive (or tensile) stress parallel to the crack direction up to a limit of f_t' as dictated by the ascending part of the stress-strain curve for biaxial loading to be discussed in the next section. This model combines smeared cracking with plasticity.

A 3-D model proposed by William and Warnke [4-11] is capable of predicting failure for concrete materials. Both cracking and crushing failure modes are accounted for. The two input strength parameters, i.e., ultimate uniaxial tensile and compressive strengths, are needed to define a failure surface for the concrete. Consequently, a criterion for failure of the concrete due to a multiaxial stress state can be calculated.

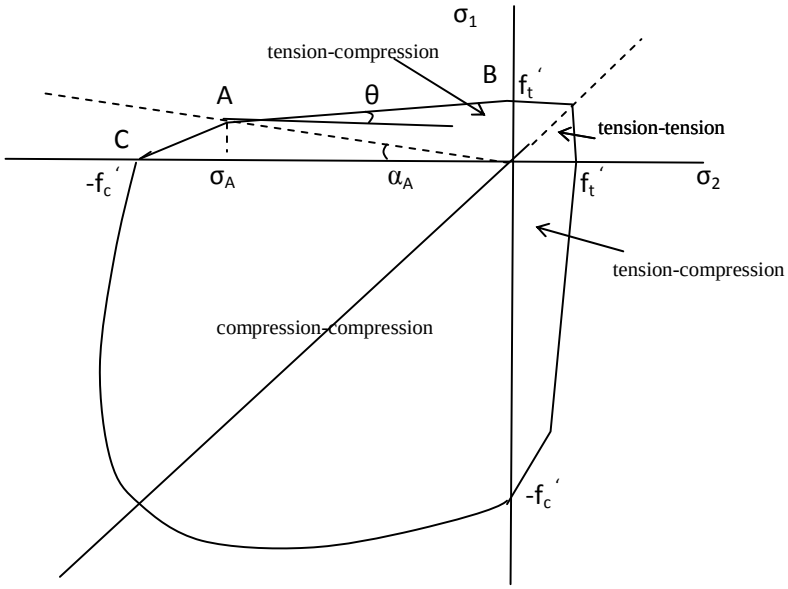

Figure 4.1: Failure surface of concrete in the two-dimensional principal stress plane

A three-dimensional failure surface for concrete is shown in Figure 4.2. The most significant nonzero principal stresses are in the x and y directions, represented by σ_{xp} and σ_{yp}, respectively. Three failure surfaces are shown as projections on the σ_{xp}-σ_{yp} plane.

The mode of failure is a function of the sign of σ_{zp} (principal stress in the z direction). For example, if σ_{xp} and σ_{yp} are both negative (compressive) and σ_{zp} is slightly positive (tensile), cracking would be predicted in a direction perpendicular to σ_{zp}. However, if σ_{zp} is zero or slightly negative, the material is assumed to crush [ANSYS v.11].

In a concrete element, cracking occurs when the principal tensile stress in any direction lies outside the failure surface. After cracking, the elastic modulus of the concrete element is set to zero in the direction parallel to the principal tensile stress direction.

Crushing occurs when all principal stresses are compressive and lie outside the failure surface; subsequently, the elastic modulus is set to zero in all directions, and the element effectively disappears.

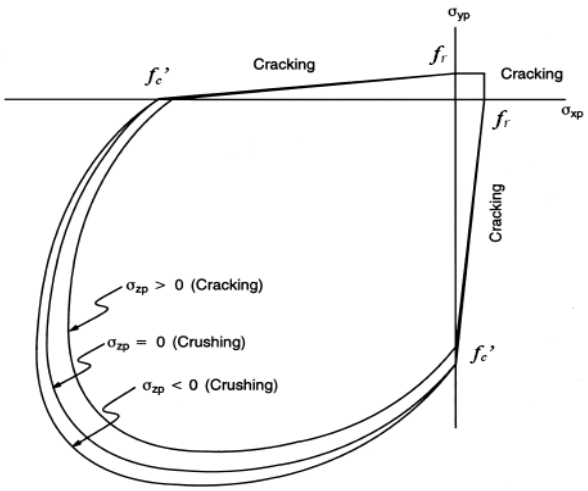

Figure 4.2: failure surface for concrete in 3-D, William and Warnke's [4-11] model

William and Warnke's [4-11] concrete material model predicts the failure of brittle materials. Both cracking and crushing failure modes are accounted for. this material model is accessed with the reinforced concrete element Solid 65 (described in section-----).

The criterion for failure of concrete due to a multiaxial stress state can be expressed in the form:

$$\frac{F}{f_c} - S \geq 0 \qquad \textbf{4.4}$$

where:

F = a function of the principal stress state (σxp, σ yp, σzp)

S = failure surface expressed in terms of principal stresses and five input parameters f_t, f_c, f_{cb}, $f_{1,}$ f_2 and f_c defined below

σ_{xp}, σ_{yp}, σ_{zp} = principal stresses in principal directions

If equation $\frac{F}{f_c} - S \geq 0$ 4.4 is satisfied, the material will crack or crush.

A total of five input strength parameters are needed to define the failure surface as well as an ambient hydrostatic stress state are:

f_t Ultimate uniaxial tensile strength

f_c Ultimate uniaxial compressive strength

f_{cb} Ultimate biaxial compressive strength

f_1 Ultimate compressive strength for a state of biaxial compression superimposed on hydrostatic stress state (σ_h^a)

f_2 Ultimate compressive strength for a state of uniaxial compression superimposed on hydrostatic stress state (σ_h^a)

σ_h^a hydrostatic stress state

However, the failure surface can be specified with a minimum of two constants, f_t and f_c. The other three constants default to [4-11]:

$f_{cb} = 1.2\ f_c$ **4.5**

$f_1 = 1.45\ f_c$ **4.6**

$f_2 = 1.725\ f_c$ **4.7**

However, these default values are valid only for stress states where the condition

$|\sigma_h| \le \sqrt{3} \cdot f_c$ **4.8**

σ_h=hydrostatic stress state = $\frac{1}{3}(\sigma_{xp} + \sigma_{yp} + \sigma_{zp})$ **4.9**

is satisfied. Thus condition $|\sigma_h| \le \sqrt{3} \cdot f_c$ 4.8 applies to stress situations with a low hydrostatic stress component. All five failure parameters should be specified when a large hydrostatic stress component is expected. However, if this condition is not satisfied and the default values shown in fcb =1.2 fc 4.5 through $|\sigma_h| \le \sqrt{3} \cdot f_c$ 4.8 are assumed, the strength of the concrete material may be incorrectly evaluated.

When the crushing capability is suppressed with f_c = -1.0, the material cracks whenever a principal stress component exceeds f_t.

In the following chapters of this thesis, William and Warnke [4-11] model is adopted in ANSYS v.11 for the analysis of 3-D failure surface for concrete while the crushing capability is turned off and cracking of the concrete control the failure of the FE models.

4.4.2 Stress-strain relationship up to failure

Concrete is assumed isotropic up to failure either by crushing in compression or cracking in

tension. Development of a model for the behaviour of concrete is a challenging task. Concrete is a quasi-brittle material and has different behaviour in compression and tension. The tensile strength of NSC is approximately 8-15% of the compressive strength, shows a typical stress-strain curve for NSC.

The uniaxial stress-strain curve for compression originally proposed by Saenz [4-12], using the notation of reference [4-13], the concrete compressive stress, f_c is given as:

$$f_c = \frac{E_c \times \varepsilon}{1 + (R + R_E - 2)(\frac{\varepsilon}{\varepsilon_o}) - (2R - 1)(\frac{\varepsilon}{\varepsilon_o})^2 + R\left(\frac{\varepsilon}{\varepsilon_o}\right)^3} \qquad \textbf{4.10}$$

In which

$$R = \frac{R_E(R_\sigma - 1)}{(R_\varepsilon - 1)^2} - \frac{1}{R_\varepsilon} \qquad \textbf{4.11}$$

$$R_E = \frac{E_c}{E_o} \quad \text{(b)}, \quad R_\sigma = \frac{f_m}{f_{cf}} \quad \text{(c)}, \quad R_\varepsilon = \frac{\varepsilon_f}{\varepsilon_o} \quad \text{(d)}, \quad E_o = \frac{f_m}{\varepsilon_o} \quad \text{(e)}$$

where the various terms are defined in Figure 4.3 with $f_m = f^c_m$ for compressive loading as decided by the failure surface.

Soltani [4-14] introduced an interesting post cracking constitutive laws and applications to nonlinear finite element analysis.

Bangash's [4-15] stress-strain curve, when concrete is in compression, is linearly elastic up to about 30 percent of the maximum compressive strength. Above this point, the stress increases gradually up to the maximum compressive strength, f_m^t. After this the curve descends into a softening region, and eventually crushing failure occurs at an ultimate strain ε_1 . In tension, the stress-strain curve for concrete is approximately linearly elastic up to the maximum tensile strength. After this point, the concrete cracks and the strength decreases gradually to zero. Bangash's [4-15] Stress-strain curve for concrete is used in ANSYS v.11.

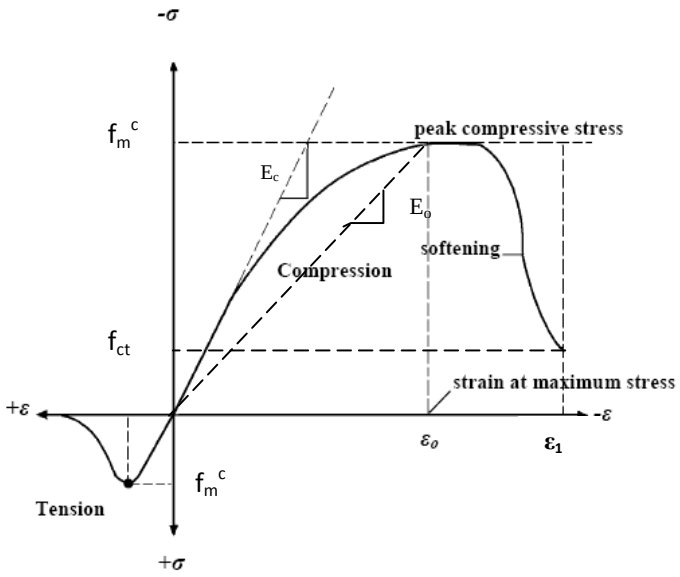

Figure 4.3: Stress-strain curve for concrete

4.4.3 Experimental measurement of the triaxial stress failure envelope

The Triaxial stress testing machine, Figure 4.4 measures 3-D failure surface in principal stress.

The Figure 4.4 shows stages of construction and the important components of the triaxial stress testing machine.

Figure 4.4 shows: a) Installation stage for the triaxial testing equipment at the department of Civil & Structural Engineering of University of Sheffield . b) Installation completed ready for operation . c) Detailed drawing of the position of the frame in relation to the 3-D co-ordinates. d) Loading plates for positioning the specimen.

Figure 4.5 shows critical locations for measurement which are as follows:
Path 0-7: arbitrary stress excursion which may be experienced by a material point in a structure.
Point 7: stress probes for direct identification of the stiffness matrix.
Grey zones (at 0 and 7): extent of elastic nucleus.

Figure 4.4: Triaxial stress testing machine at University of Sheffield, Department of Structural Engineering.

Point 8: direction of the normal to the yield surface and direction of a plastic strain rate during loading.

Point 9: starting hydrostatic stress state for a number of test paths.

Path 9-10:stair-step path parallel to σ_1 and σ_2 principal directions.

Path 9-11: proportional stress path with excursion parallel to hydrostatic axis.

Path 9-12: uniaxial stress paths in each of the three principal directions.

Path 13: circular locus within a single deviatoric plane.

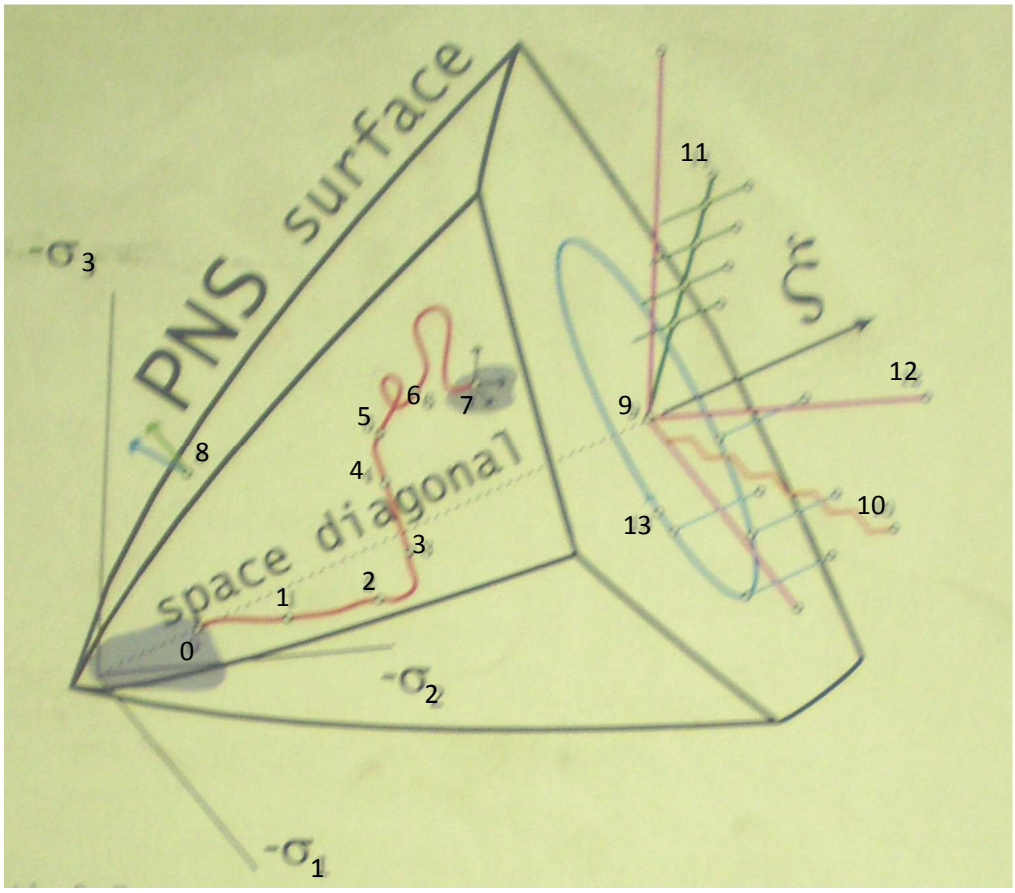

Figure 4.5: Critical locations for measurement of 3-D failure surface in principal stress space using triaxial stress testing machine

4.3.4 Cracks models

Considerable effort has been devoted in recent years to developing numerical methods and models to simulate the real behaviour of quasi-brittle material such as concrete. Traditionally, the numerical models are based on FE and are classified into two groups: “smeared” crack approach and “discrete” crack approach. In the smeared crack models the fracture or crack is represented as smeared over a finite area .

The above two methods, are in general, used to model cracking in nonlinear FE of reinforced

concrete structures. In the smeared crack method, cracking is smeared within the element in contrast to the discrete approach where a gap is introduced into the mesh after cracking. The discrete crack approach is more accurate than the smeared crack formulation but it is more complicated to implement in a FE model because change of the nodal connectivity is required as soon as the crack forms and the crack must follow the element edges. The smeared crack approach is an idealization that the cracked element is a band which leads to "stress locking" effects near the crack.

The general conclusion and recommendations for crack modelling with ANSYS drawn from the research published by a joint collaboration of Danish and Bulgarian universities based on the numerical results [4-16} are as follows:
Using 3D ANSYS modelling it is possible to properly simulate the nonlinear behaviour of R/C beams without shear reinforcement, with a moderate shear span size of a/d=3. ANSYS 3D concrete element is a very good model concerning the flexural and shear crack development but poor concerning the crushing state. However this deficiency could be removed by employing a certain multilinear plasticity option available in ANSYS.
The particular concrete FE does not consider one of the most important fracture mechanics parameter – the fracture energy G_F., which means that in the case of a concrete beam with no reinforcement it would not be possible to reach a proper solution.
The ANSYS smeared approach for beams with moderate shear span does not reproduce satisfactorily the softening due to big sliding emerging at the critical shear crack. That is likely to be more realistically achieved by a 2D discrete crack approach.
Further results and the parametric study, not given in the paper [4-16], suggest that some correction factors are needed to adjust the values of material parameters available from the experiment in order to convert them to effective parameters related to the particular modeling. Therefore, much more research is needed in order to develop a similar simulation for R/C deeper beams and to suggest reliable methods for adjusting the experimental material data to effective parameter data suitable to particular finite element models.

The above conclusion suggested that a new 2D "discrete" crack model should be developed in order to handle the big amount of sliding attributed to the development of the critical crack. The ANSYS program with its nonlinear options and capabilities is employed again to achieve

this aim, by introducing the model shown in Figure 4.6 which is similar to Houde and Mirza's [4-17] original model which proposed tangential springs at crack and steel concrete interface, section 2.2.7.6.

This research group [4-18] developed numerical models for nonlinear analysis of structures made from quasi brittle concrete materials using the fracture mechanics approach and concluded that:

- The present variant of the modelling is based on prescribing in advance discrete cracks and nonlinear translational springs at the crack interface, Figure 4.6. The discrete crack path is developed by the means of linear fracture mechanics and the results showed a good fit with the ones experimentally observed.
- In general, this 2-D numerical simulation is capable of successfully simulating the real behaviour of RC beams for different values of a/d ratio.
- The type of failure, the development of the critical shear crack, as well as the ultimate external load are captured well, but not the fitting with the experimental load-deflection curve within the full range of displacements.
- The plasticity in reinforcement and concrete in the compression zone is reproduced with sufficient accuracy including the final failure phase of the simulation.
- The main drawback of the suggested model is the way the constitutive data for the tangential springs is extracted. The existing and important relationship between the normal and tangential relative displacements is not modelled, therefore an important phenomena such as dilatation is not present in the model.

A new and improved constitutive mode, independent from those available in ANSYS, should be developed. Probably the new model should be based on the damage or softening plasticity theory. The relationship between normal and tangential stresses will be related through a "failure surface", so it is natural to get the proper displacements relationship. Therefore, the dilatancy phenomena may be handled and controlled properly.

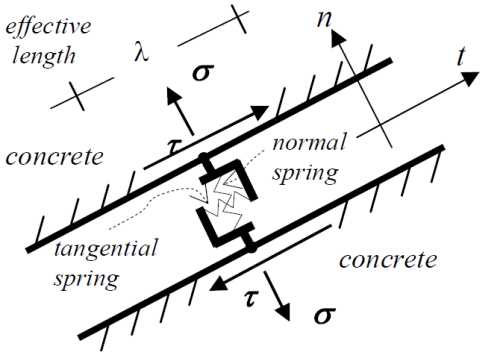

Figure 4.6: The normal and tangential nonlinear springs at the contact interfaces of the cracks to simulate the complex nonlinear processes which are happening in the cracks as the loading process is progressing.

Sagaseta [4-19] and Vollum [4-20] suggest that to implement the aggregate interlock phenomena into the calculations crack dilatancy models are used with constitutive laws that can be based on an empirical formulation proposed by Hamadi & Regan [4-21], obtained from experimental data from push-off tests whose stiffness parameter *k* was 5.4N/mm^2 and 2.7N/mm^2 for natural gravel and expanded clay aggregates respectively. According to equation ($\tau_{cr} = \frac{k}{\Delta w} \cdot \Delta s$ 4.12) the aggregate interlock stiffness depends only on the type of aggregate and crack width. Hamadi & Regan [4-21] used a shear friction type of formula ($\tau_{ult} = c + \mu\sigma$ 4.13) to obtain the shear capacity (τ_{ult}), in which the cohesion (*c*) and friction (μ) parameters need to be estimated, and τ_{cr} is the shear stress at the crack. Although this approach is commonly used in design codes, the influence of the crack width is neglected.

$$\tau_{cr} = \frac{k}{\Delta w} \cdot \Delta s \qquad \textbf{4.12}$$

$$\tau_{ult} = c + \mu\sigma \qquad \textbf{4.13}$$

Fanning [4-22] modelled the response of the reinforcement using both the discrete and smeared models for reinforced concrete beams. It was found that the best modelling strategy was to use the discrete model when modelling reinforcement. Another reason for not choosing the smeared model is that it assumes negligible contributions of aggregate interlock and dowel-action to shear capacity at peak load. Smeared model was not chosen partly in view of these findings [4-3].

In this thesis, the discrete model is used for modelling cracks in order to present the location of maximum moment on the HWB for further mechanical modelling with STM.

4.3.5 FE modelling of steel reinforcement

Tavarez [4-23] discusses the three existing techniques for modelling steel reinforcement in finite element models for reinforced concrete Figure 4.7, the discrete model, the embedded model, and the smeared model.

The reinforcement in the discrete model (a) uses bar or beam elements that are connected to concrete mesh nodes. Therefore, the concrete and the reinforcement mesh share the same nodes and concrete occupies the same regions occupied by the reinforcement. A drawback to this model is that the concrete mesh is restricted by the location of the reinforcement and bond slippage between concrete and steel is not taken into account and the volume of the steel reinforcement is not deducted from the concrete volume.

The embedded model (b) overcomes the concrete mesh restriction(s) because the stiffness of the reinforcing steel is evaluated separately from the concrete elements. The model is built in a way that keeps reinforcing steel displacements compatible with the surrounding concrete elements. When reinforcement is complex, this model is very advantageous. However, this model increases the number of nodes and degrees of freedom in the model, therefore, increasing the run time and computational costs. As a result, this model was abandoned.

Reinforcement elements are assumed to be embedded in plane stress main elements. Extra attention regarding the normal and shear stiffness must be given if the reinforcement is embedded in interface elements. This situation arises at discrete cracks crossed by reinforcement bars. A number of phenomena related to dowel action and bond-slip effects take place at the crack where it is crossed by reinforcement as outlined by Maekawa et al. [4-24] and Soltani et al. [4-25]. Bond stresses are decidedly influenced by deterioration of the concrete surrounding the reinforcement bar due to splitting and crushing of the concrete. In addition, if the reinforcement is at an angle to the shear plane, the deterioration length increases due to spalling of the concrete near the reinforcement bar at the crack [4-25].

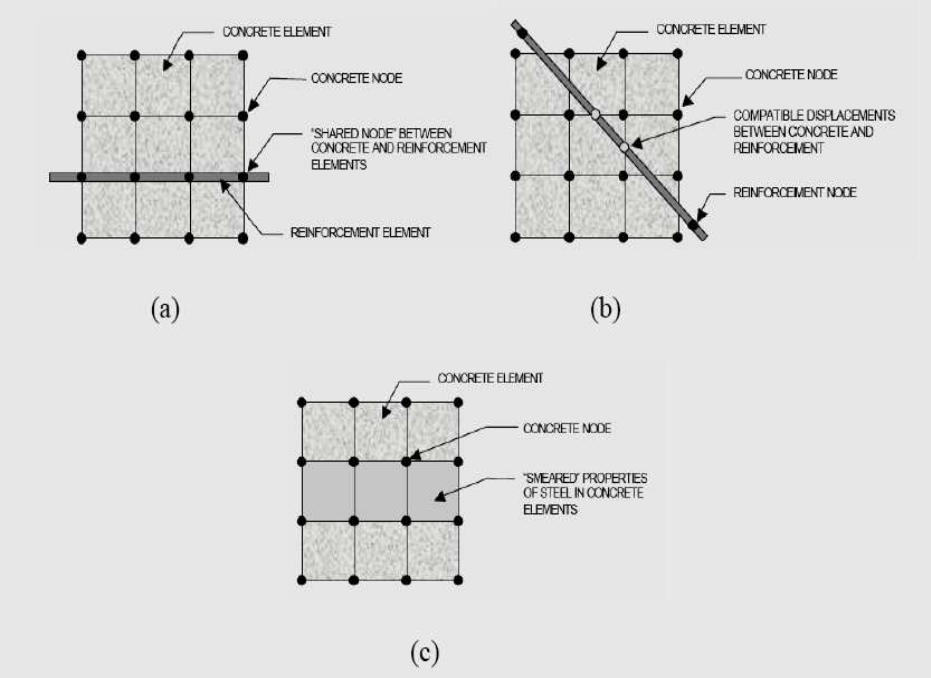

Figure 4.7: Models for Reinforcement in Reinforced Concrete Tavarez : (a) discrete; (b) embedded; and (c) smeared

Source: ANSYS 9: 2003

4.3.6 Bond at concrete steel interface

The present knowledge in structural analysis and numerical analysis is far ahead of the actual material characteristics. This is predominantly true for concrete materials and even more so for steel - concrete bond. Experiments attempting to determine ' bond stress-slip curves typically exhibit a large scatter of data [4-26] and such curves are not applicable to displacements between steel and concrete transverse to the reinforcement which would, then, require assignment of an arbitrary stiffness.

A detailed modelling of the localised bond behaviour between steel and concrete with realistic modelling of concrete between discrete cracks is also burdened with difficulties. Despite all these difficulties, the condition of full bond between steel and concrete elements assumed in this thesis for FE analysis in this chapter and chapter 7 and 8. This condition of full bond significantly reduces the true moments on the surface of the HWB at steel concrete interface.

If this full bond did not exist and bond slippage was allowed when the HWB yields at failure load, then much higher moments would have been recorded for the moments on the surface of the HWB, however, condition of full bond modelled results in producing much smaller moment at this interface for the HWB.

On way of improving the model is by using the fundamental idea for two dimensional modelling proposed is by introducing simple two-dimensional linkage elements [4-26] [4-27], Figure 4.8, along the edges of the solid steel and concrete elements in order to follow the transition from no-slip to full-slip (and beyond) at the steel/concrete interfaces in, admittedly, an approximate fashion. This technique should provide a reasonable insight into the validity of the extensively adopted assumption of full-bond.

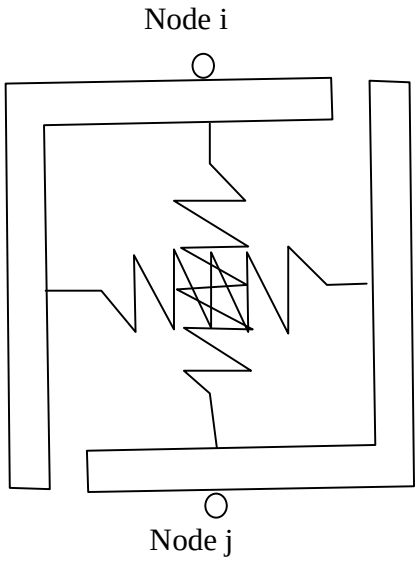

Figure 4.8: Two dimensional Link element
Source from: Zhang and Raoof [4-7]

The linkage element consists of two orthogonal springs which connect and transmit shear and normal forces between nodes i and j, Figure 4.8, with the stiffness in the two orthogonal directions assumed uncoupled, The spring element has no physical thickness in either tangential \or normal directions, and obviously this will lead to fictitious behaviour in the radial direction - i.e. for a compressive state of loading in the spring normal to the interface, the adjacent steel and concrete elements can interfere with associated changes in the relative position of two nodes, which are originally coincident. This interference may be reduced by

using a high value of the spring stiffness bearing in mind that if the spring is too stiff then numerical problems will result. In connection

with the numerical analysis of grouted tubular joints, Elnashai [4-28] suggested values of the normal stiffnesses En = 1000 N/mm^3 and E_{nt} = 100N/mm^3 in compression and tension, respectively. Such values of E_n and E_{nt} calibrated well with the, then, available

experimental data. Carroll [4-29], on the other hand, concluded that the range of values assumed for the normal compressive stiffness in the case of grouted tubular joints may vary from at least 100 N/mm^3 to 10,000 N/mm^3 without significantly affecting the results.

The Zhang and Raoof [4-7] carried out rather extensive numerical studies, based on a wide range of values of normal stiffnesses, on a number of reinforced concrete beams with full anchorage provided at the ends of the main reinforcing bars [4-30]. These studies strongly suggested the relative insensitivity of the calculated ultimate load bearing capacity to the assumed values of the normal stiffness, although, their extremely high (or low, depending on the mesh) values were found to lead to numerical difficulties.

Values of E_n = 10,000 N/mm^3 and E_{nt} = 1,000 N/mm^3 in general, provide reasonable results and was chosen for all the subsequent numerical results presented. The load bearing capacity of the normal spring is, on the other hand, limited by its tensile and compressive strengths (f_{nt} and f_{nc}). In compression, the spring strength is taken to be equal to the cube crushing strength of concrete (f_{cu}), while a value of $0.5(f_{cu})^{0.5}$ has been used in tension [4-31].

In the case of the tangential direction, a bilinear elasto-plastic stress-strain behaviour is assumed with the ultimate shear strength determined by Mohr-Columb criterion [4-32]- i.e.

$$\tau = \tau_0 + \gamma\sigma_n$$

Where = shear strength, σ_n = normal stress, γ = friction coefficient, and τ_0= intrinsic shear strength which represents plain bond strength. It must be noted that the actual functional relating the normal and bond stresses is unlikely to be linear in practice. However, the assumption of a linear relationship should suffice until more detailed experimental information

is available. It is assumed that τ_0= 1.12 N/mm^2 [4-31] and γ = 0.5. The tangential shear stiffness E_{S1} has been suggested to lie in the range $600 \geq E_{S1} \geq 10$N/mm^3 [4-28]. Numerical results on reinforced concrete beams with the main reinforcing bars firmly hooked at the ends, however, suggest the rather insensitive

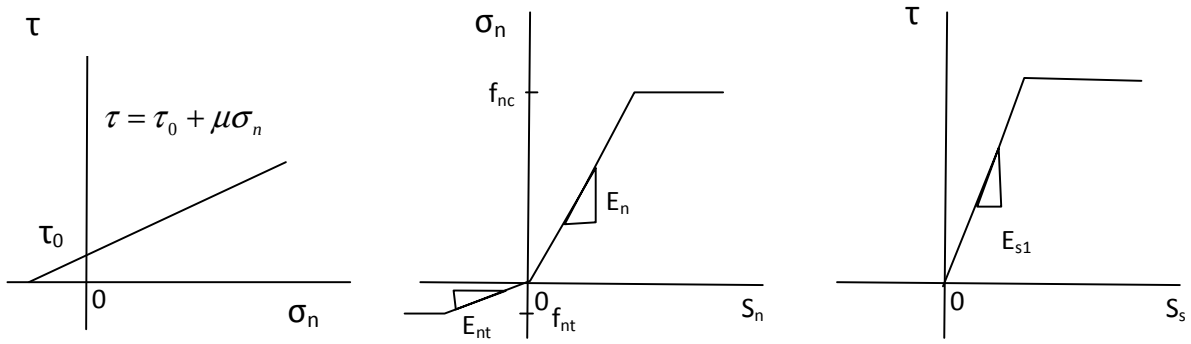

a) Failure surface b) Normal σ_n - S_n relationship c) Shear τ - S_s relation

Figure 4.9: relation between (τ) shear strength, (σ_n) normal stress, and tangential stiffness in the link

Source from: Zhang and Raoof [4-7]

variations of the load-deflection and / or ultimate load bearing capacity of beams to the exact value chosen for E_{S1}.

4.3.7 Material properties for steel

Properties, i.e., elastic modulus and yield stress, for the steel reinforcement used in this FEM study follow the design material properties used for the experimental investigation [4-33]. The steel for the FE models was assumed to be an elastic-perfectly plastic material and identical in tension and compression.

Poisson's ratio of 0.3 and elastic modulus, *Es* = 200,000 MPa was used for the steel reinforcement in this study [4-34]. Figure 4.10, shows the stress-strain relationship used in this study. Material properties for the steel reinforcement for all four models are as follows:

Steel plates were added at support locations in the FE models to simulate the experiment and provide a more even stress distribution over the support areas. An elastic modulus equal to

200,000 MPa and Poisson's ratio of 0.3 were used for the plates. The steel plates were assumed to be linear elastic materials.

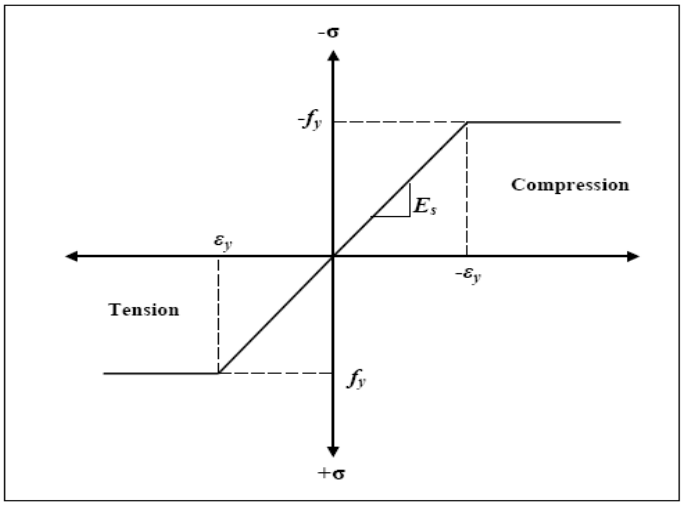

Figure 4.10: Stress-strain curve for steel reinforcement
Source: Ansys 9: 2003

4.4 Numerical modelling of the experimental tests

The literature review suggests that use of a finite element package to model reinforced HSC beams is indeed feasible. ANSYS (Version 11) is chosen for this. Reinforced concrete beams of normal and high strength with various types of reinforcement, using material property Beam 188, modelled discretely will be developed with results compared to the experimental work. The load-strain and load-deflection response, strain along reinforcement, post cracking and ultimate load of the experimental beam will be compared to the analytical predictions to calibrate the FE model for further use.

The FE calibration study in this chapter includes modelling a concrete beam with the dimensions and properties of corresponding beams experimentally tested by this writer listed in Table 3-1.

To create the FE model, there are multiple tasks that have to be completed for the model to run properly which will be explained in the following sections.

4.4.1 Material models

The descriptions for each element type are laid out in the ANSYS element library [4- 37]. An eight-node solid element, Solid65, was used to model the concrete. The solid element has eight nodes with three degrees of freedom at each node – translations in the nodal x, y, and z directions. The element is capable of plastic deformation, cracking in three orthogonal directions, and crushing. The geometry and node locations for this element type are shown in Figure 4.11.

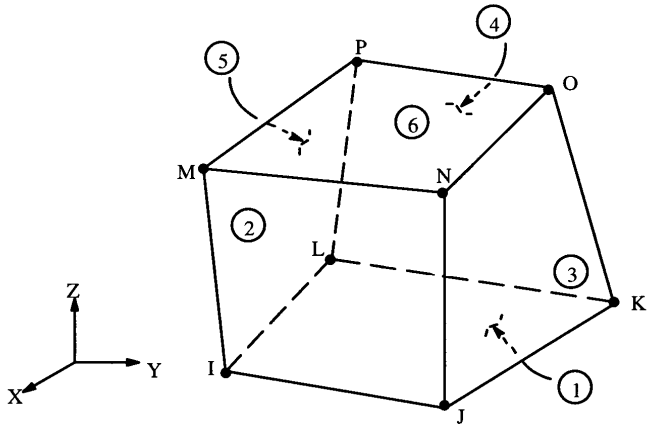

Figure 4.11: Solid 65 – 3-D reinforced concrete solid element and solid 45 element for loading and support plates. This element has eight nodes with three degrees of freedom at each node.

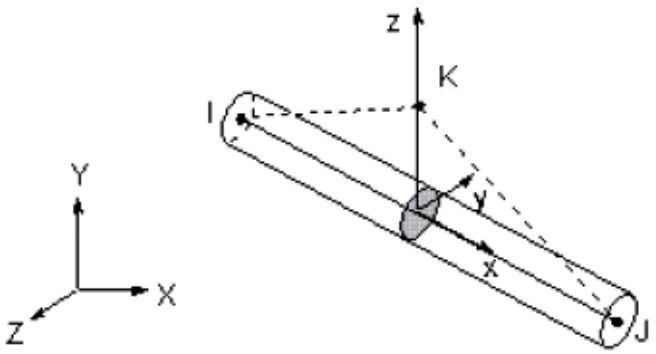

Figure 4.12: Beam 188 (reinforcement) element is used to model steel reinforcement. This element is a 3-D spar element and it has two nodes with three degrees of freedom

Source: ANSYS 9: 2003

Solid 45 element is well-suited for linear, large rotation, and/or large strain nonlinear applications, Figure 4.11. The cross sectional dimensions are scaled uniformly as a function of axial strain in nonlinear analysis such that the volume of the element is preserved.

Transverse shear strain is constant through cross-section, i.e., cross sections remain plane and undistorted after deformation.

Beam 188 element is used to model steel reinforcement. This element is a 3-D spar element and it has two nodes with three degrees of freedom**.** Figure 4.12

4.4.2 Material model for the tested beams

After introducing the Element Type, Solid 65 for concrete and Beam 188 for steel, the real constant for the two materials is introduced.
Material Properties are identified by modelling such that:

Material No 1 being concrete is modelled as structural-linear isotropic with E values dependent on whether it is high or normal strength.

Nonlinear behaviour of concrete is modelled as structural-nonlinear, inelastic, non-metal plasticity and concrete.

Material Model No 1 refers to the Solid 65 element. This element requires linear isotropic and multilinear isotropic material properties to properly model concrete. The multilinear isotropic material uses the Von Mises failure criteria along with the model [4-11] to define the failure of the concrete. EX is the modulus of elasticity of the concrete (E c), and PRXY is the Poisson's ratio (ν) which was assumed to be 0.2 for NSC and 0.24 for HSC. In the concrete model the descending branch is included.

The data for material properties of concrete is mainly obtained from the extensive past research on HSC in the Construction Hall at the University of Westminster [4-35]. However, the values for indirect tensile strength are chosen based on this writer's proposed rule

$f_{ct} = 0.47\sqrt{f_{cu}}$.

Parameters needed to define the material models can be found in Table 4-1. As seen in this table , there are multiple parts of the material model for each element.

For the beams tested by this writer two different material properties for HSC and NSC are considered for the two different yield strengths of the longitudinal bars and stirrups. In choosing beam sections for Beam 188, three different bar sections are considered, which are for longitudinal tension and compression (1), longitudinal web bars(2) and stirrups (3).
In the past, to this writer's knowledge, when ANSYS was used by other researchers [4-6] for FE analysis of reinforced concrete structure, material property model Beam 188 had not been developed at the time so Link 8 was utilised which only takes axial force to model the reinforcement. In this thesis, this writer uses model Beam 188 successfully to model bending moment due to dowel moments resisted by HWB and CVB in the reinforcement in the BCJ.
Implementation of the material model in ANSYS requires that different constants be defined. These are:

1. Shear transfer coefficients for an open crack
2. Shear transfer coefficients for a closed crack
3. Uniaxial tensile cracking stress
4. Uniaxial crushing stress (positive)
5. Biaxial crushing stress (positive)

Shear transfer coefficients are factors applied to shear modulus in the direction of cracking.

At the University of Westminster, extensive experimental work on properties of HSC were completed and published, [2-36] from which data for material properties of NSC and HSC is provided for this chapter.

Typical shear transfer coefficients range from 0.0 to 1.0, with 0.0 representing a smooth crack (complete loss of shear transfer) and 1.0 representing a rough crack (no loss of shear transfer). The shear transfer coefficients for open and closed cracks were determined using past research [4-6] as a basis. Convergence problems occurred when the shear transfer coefficient for the open crack dropped below 0.15 for HSC. The coefficient of friction enables concrete between cracks to be able to contribute in resisting tie deformations through the tension stiffening effect.

Numerical Model Number	Element Type	Material Properties		
1	**Solid 65**	Linear, Elastic, Isotropic		
		EX (NSC)	27,237 MPa	
		EX (HSC)	45,000 MPa	
		PRXY(NSC)	0.2	
		PRXY(HSC)	0.24	
		Nonlinear, Inelastic, Rate independent, Isotropic hardening plasticity, Mises plasticity, Multilinear Isotropic		
		NSC	Strain	Stress (MPa)
		Point 1	0.00036	9.8
		Point 2	0.0006	15.40
		Point 3	0.0013	27.52
		Point 4	0.0019	32.11
		Point 5	0.00243	33.10
		HSC	Strain	Stress (MPa)
		Point 1	0.00035	11.69
		Point 2	0.00242	85.05
		Point 3	0.00336	89.87
		Non linear, Inelastic, Non metal plasticity, Concrete		
		Definition of	NSC (a/d=3.02)	HSC (a/d=3.02)
		ShrCf-Op (1)	0.3	0.15
		ShrCf-Cl (2)	1	1
		UnTensSt (3)	3.11	4.87
		UnCompSt (4)	-1	-1

Table 4-1: Material Models no 1, Element type Solid 65 (concrete) . FE concrete models allows for falling branch for NSC.

Material model n0s 2 & 3 refer to the Beam 188 element which is used for all the steel reinforcement in the beam and is assumed to be bilinear isotropic. Bilinear isotropic material is also based on the Von Mises failure criteria. The bilinear model requires the yield stress (f_y), as well as the hardening modulus of the steel to be defined. The yield stress was defined as shown in Table 4-2.

The Beam Section is chosen in the Common Section. In Beam tool, identities are chosen according to the diameter of bars used for the longitudinal, stirrup or web reinforcement.

4.4.3 Modelling elements

<table>
<tr><th>Numerical Model Number</th><th>Elemet Type</th><th colspan="3">Material Properties</th></tr>
<tr><td rowspan="8">2

3</td><td rowspan="8">Beam188</td><td colspan="3">Linear, Elastic, Isotropic</td></tr>
<tr><td>EX (NSC)</td><td colspan="2">200,000 MPa</td></tr>
<tr><td>EX (HSC)</td><td colspan="2">200,000 MPa</td></tr>
<tr><td>PRXY</td><td colspan="2">0.3</td></tr>
<tr><td colspan="3"></td></tr>
<tr><td colspan="3">Non linear, Inelastic, Rate independent, Isotropic hardening plasticity, Mises plasticity, Bilinear Isotropic</td></tr>
<tr><td>Type</td><td>Reinforcement</td><td>Yield Stress MPa</td></tr>
<tr><td rowspan="2">Cold-drawn Mild</td><td>Main</td><td>460</td></tr>
<tr><td>Link</td><td>250</td></tr>
</table>

Table 4-2: Material Models, Beam 188

No mid-span deflection was recorded in the experimental work. However, strain in the mid-span on the tension reinforcement in X direction was recorded. This writer therefore uses experimental results from those readings to calibrate the FE models.

4.4.4 Meshing

To obtain good results from the Solid 65 element, the use of a rectangular mesh is recommended. Therefore, the mesh was set up such that square or rectangular elements were created. The overall mesh size is recommended to be about three times the size of the aggregate, therefore, NSC with 25mm aggregate is allocated larger mesh than HSC with 10mm maximum size aggregate. The meshing of the reinforcement is a special case compared to the volumes. However, the necessary mesh attributes as described above need to

be set before each section of the reinforcement is created.

Numerical Model Number	Elemet Type	Material Properties	
4	**Solid 45**	EX	200,000 MPa
		PRXY	0.3

Table 4-3: Material Models, solid 45, for support and loading plates

4.4.5 Nonlinear solving procedure

A nonlinear solving procedure in FE analysis is adopted using Newton –Ralphson's model in which a step-iterative procedure is followed until an acceptable convergence is obtained. The convergence criterion here is to minimize the unbalanced forces at the nodes. The essential steps in the analysis scheme are:

1) At the beginning of the analysis, the geometry, boundary conditions and the incremental load vector {f} are input to the solver.

2) The overall stiffness matrix [K] is calculated as a function of the initial stiffness of the constituent materials, i.e. stiffness at strain equals zero.

3) The system of equilibrium equations [K]{d}={f} is solved and the nodal displacement vector {d} is obtained.

4) Once the Nodal displacements are determined, the strain in each element is calculated from its end displacements, and consequently both the stress and the tangent stiffness can be calculated from the nonlinear constitutive laws of the constituent materials.

5) The force in each member is calculated by multiplying the stress by the cross-sectional area.

6) The Nodal force vector {f 1} that corresponds to the current displacement field {d} is then calculated. At each node, the Nodal forces are computed as the algebraic sum of the horizontal and vertical components of the forces in the element of the truss members meeting at the node of concern.

7) The unbalanced Nodal force vector {Δf} is determined by subtracting the compatibility Nodal force vector {f l} from the load vector {f}.

8) The convergence is checked for the unbalanced Nodal force vector {Δf} and if the convergence criterion is not met, another iteration is carried out.

9) In the new iteration, the tangent stiffness matrix [K] is calculated based on the current displacement field of the nodes {d}, and the equilibrium equations are again solved to get the displacement field {Δd} that corresponds to the unbalanced Nodal force vector {Δf} as

[K]{ Δd}={Δf}.

10) The deflection is then updated by summing up the displacement vectors {d} and {Δd}.

11) The unbalanced Nodal force vector {Δf} is determined again based on the most updated displacement vector {d} as explained above in steps 4, 5, 6 and 7.

12) The convergence is checked again for the unbalanced Nodal force vector {Δf} and if the convergence criterion is not met, another iteration is carried out, and so on until the proposed accuracy for the solution is obtained. When the convergence is fulfilled, the next load increment is analyzed and so on.

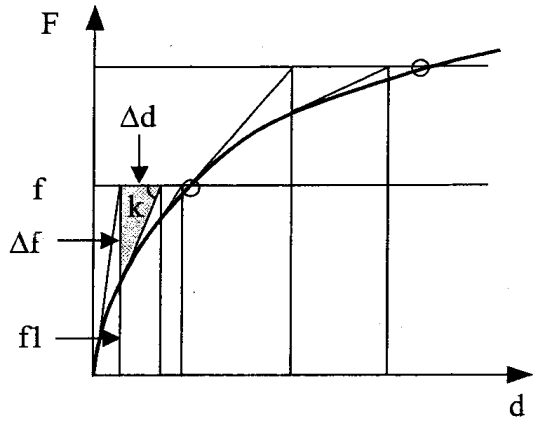

Figure 4.13: Nonlinear solving procedure as explained in steps 1 to 13.

13) FE principal strain vector output diagram can be used to determine the angle of the modified diagonal Strut to develop an alternative Strut-and-tie models. The nonlinear Strut-and-tie model NSTM may then be used for calculating the optimized amount of reinforcement as compared to the amount calculated by the linear Strut-and-tie STM.

For the verification and validation of the proposed model, the model results are compared to the experimental results of simply supported two point loaded short beams B1 and B2 of shear span to depth ratio (a/d) of 1.5 which are tested experimentally as described in the following section.

4.4.6 Evolution of crack patterns

In numerical analysis, outputs, i.e. stresses and strains, are calculated at integration points of the concrete solid elements. Figure 4.14 shows integration points in a concrete solid element. A cracking sign represented by a circle appears when the principal tensile stress exceeds the ultimate tensile strength of the concrete. The cracking sign appears perpendicular to the direction of the principal stress.

As shown in Figure 4.16(a), principal tensile stresses at the bottom of the beam at midspan occur mostly in the *x* direction (longitudinally). When the principal stresses exceed the ultimate tensile strength of the concrete, circles indicating cracking signs appear perpendicular to the principal stresses in the *x* direction. Therefore the cracking signs shown in the figure appear as vertical straight lines occurring at the integration points of the concrete solid elements. Hereafter, these will be referred to as flexural cracks.

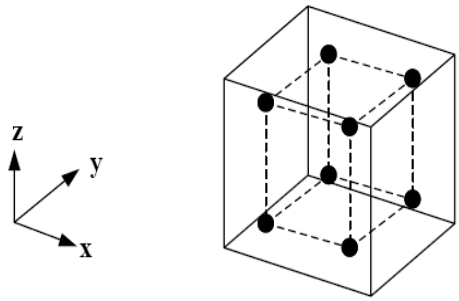

Figure 4.14: Integration points in concrete solid element

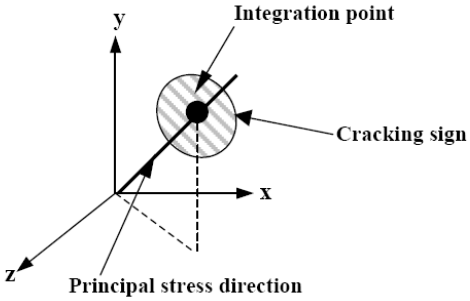

Figure 4.15: Cracking sign

Source: ANSYS Manual [4-37]

Figure 4.16 shows the type of cracking signs observed for concrete elements underneath the loading locations. The different types of concrete failure that can occur are flexural cracks, compression failure (crushing), and diagonal tension cracks. Flexural cracks (a) form vertically up the beam. Compression failures (b) are shown as circles. Diagonal tension cracks (c) form diagonally up the beam towards the loading that is applied.

For a concrete structure subjected to uniaxial compression, cracks propagate primarily parallel

to the direction of the applied compressive load, since the cracks result from tensile strains developed due to Poisson's effect [4-38 &39].

Similar behaviour is seen in the FE analysis. Loads in the *z* direction result in tensile strains in the *y* direction by Poisson's effect. Thus, the circles appear perpendicular to the principal tensile strains in the *y* direction at integration points in the concrete elements near the loading location. These will be referred to as compressive cracks. Figure 4.16(c) shows cracking signs where both normal and shear stresses act on concrete elements.
Tensile stresses generally develop in the *x* direction and shear stresses occur in the *xz* plane. Consequently, the direction of tensile principal stresses becomes inclined from the horizontal.

Once the principal tensile stresses exceed the ultimate tensile strength of the concrete, inclined circles appearing as straight lines perpendicular to the directions of the principal stresses appear at integration points of the concrete elements. Hereafter, these will be referred to as diagonal tensile cracks.

The ANSYS programme records a crack pattern at each applied load step. Figure 4.16 shows the evolution of crack patterns for each beam. In general, flexural cracks occur early at mid-span. When applied loads increase, vertical flexural cracks spread horizontally from the mid-span to the support. At a higher applied load, diagonal tensile cracks appear. Increasing applied loads induces additional diagonal and flexural cracks. Finally, compressive cracks appear at nearly the last applied load steps. These appear underneath the loading location.

The first crack at an integration point is outlined with a red circle, the second with a green, and the third with a blue.

Symbols shown at the element centroid are based on the status of all of the element's integration points. If any integration point in the element has crushed, the crushed (octahedron) symbol is shown. If any integration point has cracked or cracked and closed, the cracked symbol is shown at the element centroid.

If at least five integration points have cracked and closed, the cracked and closed symbol is shown at the element centroid. Finally, if more than one integration point has cracked, the

circle outline at the element centroid shows the average orientation of all cracked planes for that element. Cracking signs represented by a circle appear when the principal tensile stress exceeds the ultimate strength of the concrete.

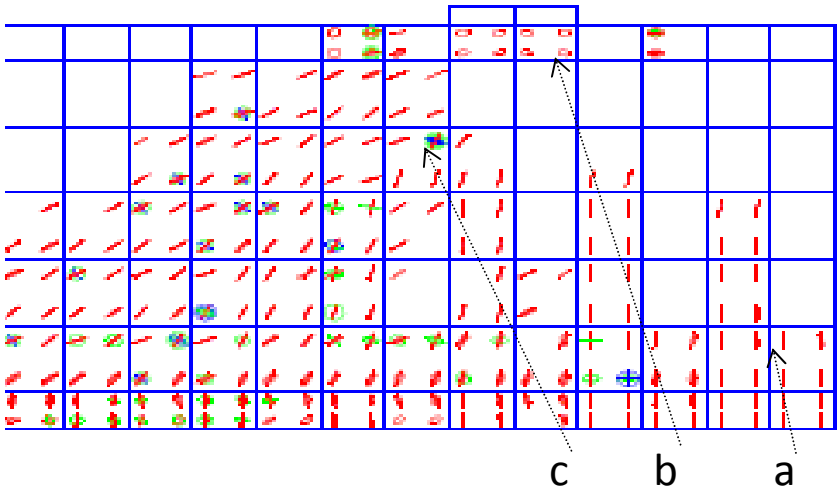

Figure 4.16: Typical cracking signs in FE models: a) Flexural cracks, b) Compressive cracks, c) Cracks which opened and closed

4.5 Influence of HWB in beams of shear span/depth ratio of 3.02

This section discusses the validation and verification of FE analysis for experimental tests on 3 beams of HSC and NSC which are HSC1, NSC3 and HSC3. Details of these beams are given in Figure 3-1 and Table 3-4 . These beams will be used for the purpose of validating and verifying the influence of limestone aggregate in HSC1 and the influence of dowel action from HWB on the shear behaviour of FE models beams NSC3 and HSC3. The data obtained will be used in Chapter 7 for FE modelling and analysis of the corresponding TBCJ.

4.5.1 Aims and objectives of analysis of beams of shear span/depth ratio of 3.02

Past research using FE analysis of shear tests as well as the behaviour of NSC with stirrups provides data for FE analysis of NSC beams with stirrups in this chapter. No FE analysis will be carried out for beam NSC1 but information available from past research [4-6] will be used in chapters 6 and 7 for current FE analysis of BCJ and TBCJ. However, although past research included FE analysis of the shear strength of HSC beams [4-40], the shear behaviour

of HSC beams made of limestone aggregate [4-41] which behave differently from other types of aggregate in HSC has not been modelled or investigated by FE analysis.

The four beams, NSC1, NSC3, HSC1 and HSC3 are of particular interest because they have shear span to depth ratio (a/d) of 3.02 which are analogous to TBCJ of aspect ratio 3.1.

The correct value for the coefficient of friction used in the FE analysis for open and closed cracks was chosen for the FE models with their corresponding experimental results for beams HSC1, NSC3 and HSC3.

4.5.2 Verification and validation of FE models for beams of a/d=3.02

Three RC beams which were experimentally tested by this writer and are directly related to the final objective of this thesis were FE modelled and results were compared with the results obtained experimentally in order to verify and validate the idealisation of the FE model for NSC and HSC beams with and without HWB. These beams are analogous to TBCJ with and without CVB, as will be discussed in Chapter 8.

One of the objectives of this comparison is to find out a realistic value for the "coefficient of friction" used in the FE idealisation to model cracking in concrete. This parameter will be used for FE modelling of different material properties of NSC and HSC.

This indicates that the FE model may predict greater failure load than the experimental model. However, the differences are greater in NSC and smaller in HSC, because the FE model assumes a rigid model and ignores material imperfections. Similarly HSC models are more rigid and experience less shrinkage than NSC models hence behave more like the FE model so have smaller differences with the numerical model.

HSC has lower shrinkage because the water cement ratio (W/C) was 0.25 for HSC beam as compared to 0.6 for NSC. This significant reduction in W/C for HSC means much smaller shrinkage or micro cracking for HSC, also higher tensile strength for HSC means less slippage at bond between concrete and reinforcement. FE does not include micro-cracking or bond slippage effect so models NSC as a stiffer structure compared to the experiment, whereas in

HSC because of lower micro-cracking and slippage, the FE model gives a closer prediction to the experimental results.

Section	Experimental test		FE analysis		Difference between experi ence &FE failure loads	Differ
Part	Test ID	Failure load (kN)	Model ID	Failure Load (kN)		
2A	HSC1	140	FE-HSC1	155	15	11%
2B	NSC1	170	FE-NSC1	230	60	35%
2C	NSC3	200	FE-NSC3	240	40	20%
2D	HSC3	285	FE-HSC	290	5	2%

Table 4-4: Experimental tests, details in Table 2-4 and Figure 2-5, and their FE models

The coefficient of shear friction for open cracks was taken as 0.15 for HSC compared to 0.3 for NSC. The sudden premature failure of HSC beam was therefore successfully modelled by FE resulting in a close prediction of the experimental value.

Experimental data on the analogous beams of a/d=3.02 for beams HSC1, NSC3 and HSC3 are shown in Figure 3-1 and Table 3-4. Verification and validation of the FE models is performed comparing the data obtained from strain gauges on tension steel, links and the measured deflection for experimental tests HSC1 and NSC3 with FE models FE-HSC1 and FE-NSC3, Table 4-4.

4.5.3 Numerical model for beam FE-NSC1

In NSC1, at initial loading, maximum strain occurs at quarter of the length from the bottom, but when loading reaches 200 kN the maximum loading changes location to the centre of the link. However, the lower part of the link is generally more strained. Whereas in link 2 from low loading, 120 kN, the maximum strain occurs at the centre and at 200 kN the strain is distributed almost evenly on both sides of the link. However, within 20 kN increase in loading, suddenly the maximum strain develops at three quarters of the length from the bottom followed by that at a quarter of the length. The maximum strain occurs in link 2 followed by link 1, Figure 4.19.

Link 3 almost reaches its yield at 220 kN loading. The maximum strain location changes from three quarters of length of stirrup from bottom to the centre point of the link after 180 kN loading. From 180 kN to 220 kN loading increment, or 28% increase in loading, the strain in the link is increased by 43%, Figure 4.20.

The strain in the tension bar up to 220 kN has two sudden jumps in value due to development of cracks. However, if these maximum readings are ignored, the true maximum strain would be the same as strain at 180 kN and 200 kN, indicating that no increase in tie action occurs with increase in loading, Figure 4.21.

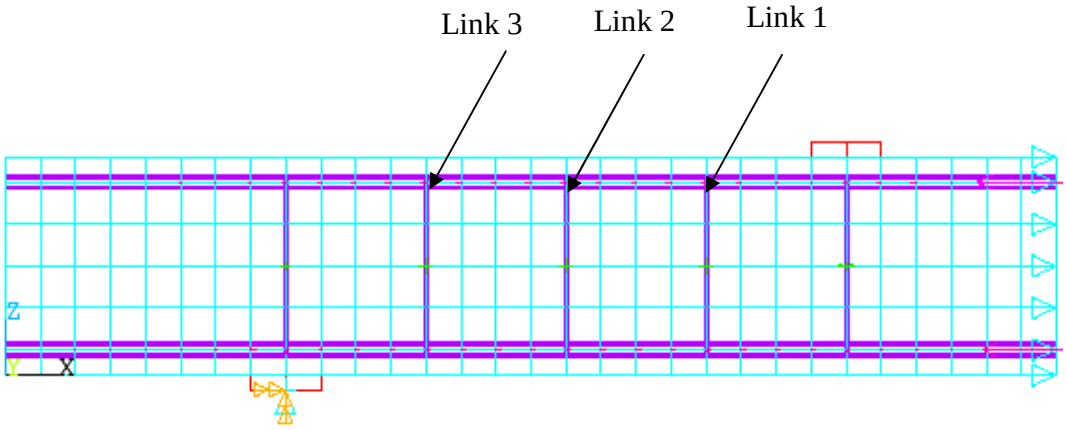

Figure 4.17: Model for FE-NSC1 beam, showing constraints for symmetry and support

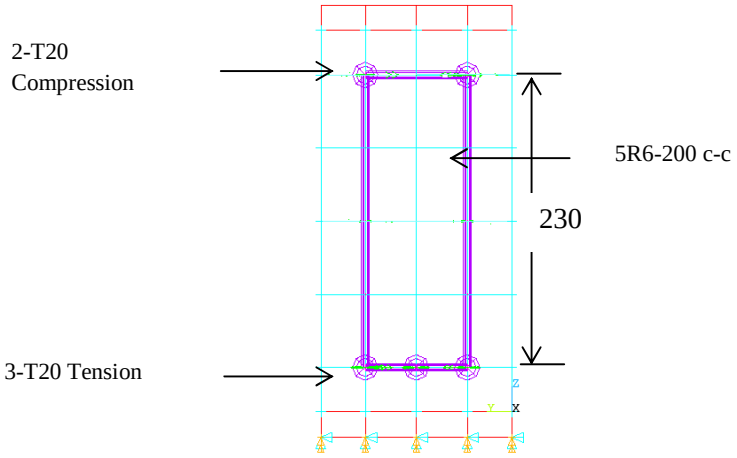

Figure 4.18: Section beam model for FE-NSC1 beam, showing 3-T20 tension, 2T20 compression and no horizontal web reinforcement, with 6mm links.

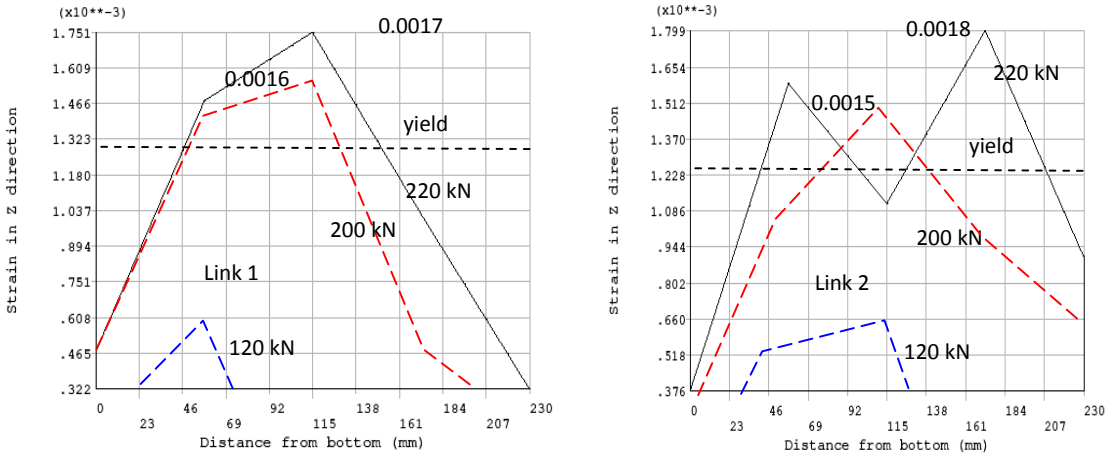

Figure 4.19: NSC1, Link 1, left, and Link 2, right, up to 220 kN loading.

The force from the inclined diagonal strut is lost as a result of the displacement produced from large shear cracks in the shear span at the link nearer to the loading plate.

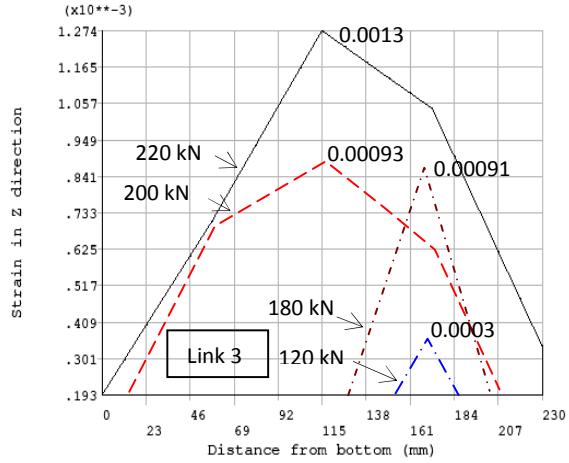

Figure 4.20: NSC1, Link 3 up to 220 kN, just before reaching yield at 220 kN.

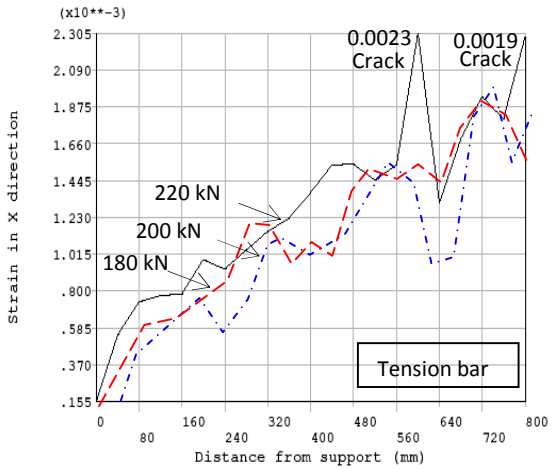

Figure 4.21: NSC1,Tension bar up to 220 kN

4.5.4 Numerical model for beam FE-HSC1

The model for FE-HSC1 was developed by including two R-6 bars extending over the shear span, Figure 2-5. In the experiment, two lengths of R6 were placed in the shear span to hold

the stirrups and the cage in position, however, in the FE model of FE-HSC1 it is assumed that 2-R6 are present in the compression zone along the length of the beam.

Since the compression zone of the beam is made of HSC concrete of 110 MPa, the presence of 2-R6 mild steel of f_y=240 MPa in the compression zone has an insignificant influence on the shear behaviour of the beam.

The FE mesh adopted for the volume of one half of the span for FE-HSC1 without reinforcement consists of 720 (ie. 30X6X4) elements. The supporting and loading plates each consist of eight elements. Each longitudinal reinforcement in tension is made up of 30 elements and each stirrup consist of 12 elements.

Links 1,2 and 3 are the inner links in the shear span with link 1 being nearest to the support plate.

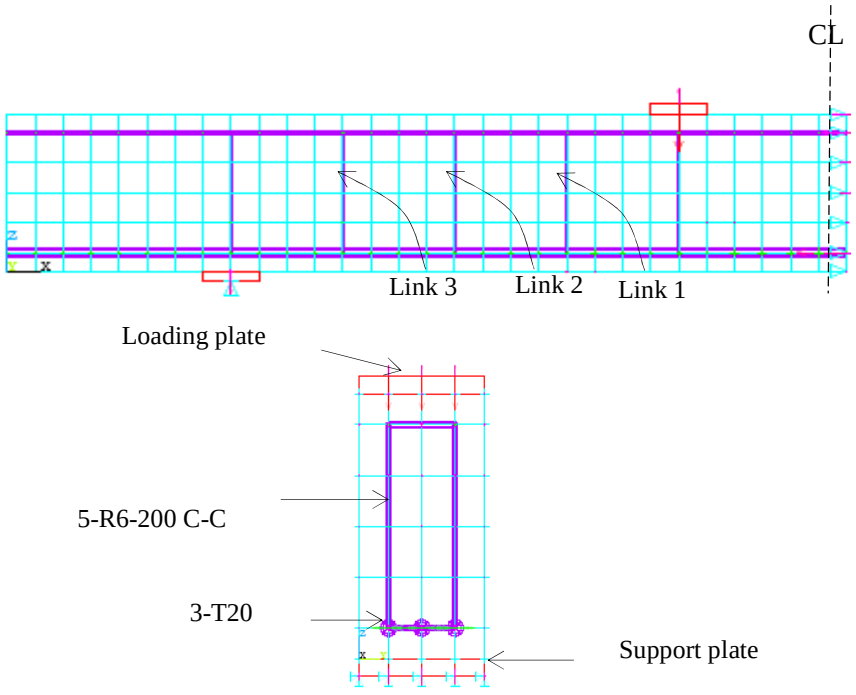

Figure 4.22: Elevation and section of FE-HSC1.

The first crack in the FE numerical model and the experimental test for beam FE-HSC1 cracks at he same loading of 50 kN which causes a strain of 0.65×10-3, Figure 4.25,

compared to HSC3 where the unopened crack has produced a maximum strain of 0.45×10^{-3}.

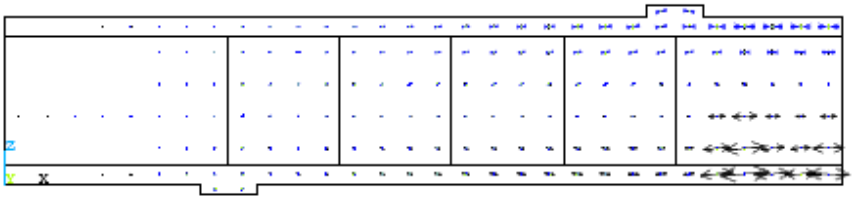

Figure 4.23: Principal strain vector development at first tensile crack formation at 40 kN.

Figure 4.28 shows a more or less linear relation until 100 kN. When cracks open after 100 kN, sudden non-linearity occurs and deflection is increased non-linearly. The FE model does not demonstrate this sudden nonlinearity due to opening of cracks, and assumes that some contact between elements always exists and does not taken into account element separation which occurs after cracks. This results in 15% less deflection recorded than that of the experiment, Figure 4.28.

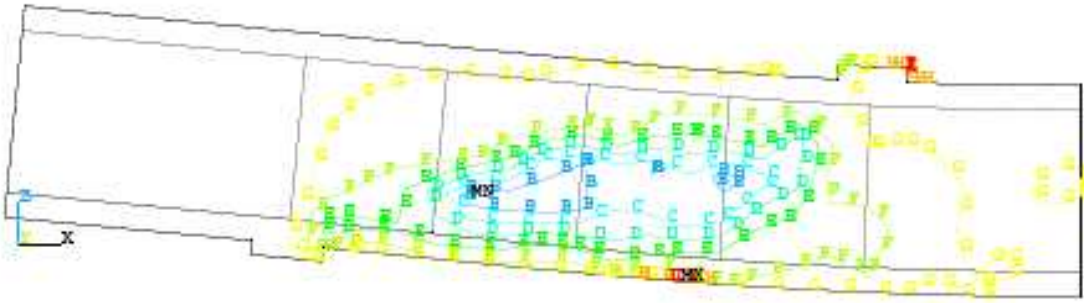

Contour	A	B	C	D	E	E
Strain (10^{-3})	-2.772	-2.456	-2.29	-0.90	-0.62	0.25

Figure 4.24: Nodal strain development in X-Z direction at 150 kN load just before failure at 155 kN.

In order to simulate the opening of cracks and model element separation more accurately it is recommended there be further research using the Finite Difference or the Applied Element method which simulate element separation.

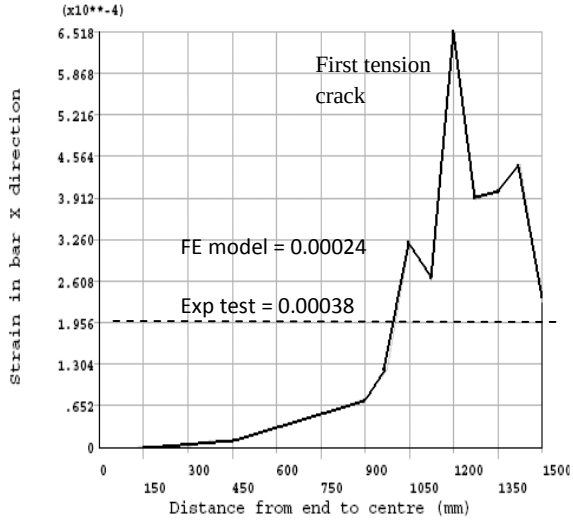

Figure 4.25: Strain in tension bar in FE-HSC1 at 50 kN with first tension crack

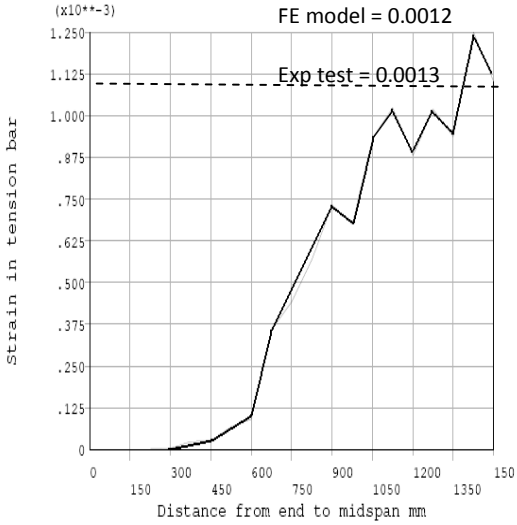

Figure 4.26: Strain in tension bar in FE-HSC1at 120 kN

Load (kN)	Bottom$_1$ x10^{-3}	Top$_1$ x10^{-3}	Bottom$_2$ x10^{-3}	Top$_2$ x10^{-3}	Average x10^{-3}	Deflection mm
0	0	0	0	0	0.0	0
20	68.8	67.9	67.2	74.9	69.7	0.3
40	267.0	235.3	232.9	246	245.3	1
60	537.2	487	551.7	557.6	533.4	1.7
80	774.2	701.7	803.5	825.9	776.3	2.5
100	987.2	893.4	1027.8	1034.4	985.7	3.2
120	1186.5	1074.6	1226.4	1230.8	1179.6	4.6
130	1305.7	1127.7	1344.1	1371.3	1287.2	0
0	317.2	281.6	314.9	337.4	312.8	0

Table 4-5: Experimental micro strain gauge reading for two T20 side tension bars (excluding the third bar placed in the centre) on top and bottom, and corresponding deflection in HSC1

4.5.4.1 Discussion on numerical model of FE-HSC1

It was concluded that the failure load of 155 kN for FE-HSC1 is 4.7% higher than the average failure load of 148 kN for 3 experimental tests on HSC1, HSC1-2 and HSC1-3, Table 3-1, which is the safety factor for the FE prediction. This is due, as noted before, to the rigid

idealisation of the FE model. It is assumed that the reinforcement and concrete are rigidly connected at the nodes and the cracking are not smear cracks.

Furthermore, the FE model assumes perfect bonding between aggregates and paste and no honey-combing in concrete, leading to a more rigid FE model than the experimental model. Another factor could be the inherent weakness in aggregate interlock of limestone in HSC in the experimental test.However, when comparing deflection of the numerical model compared to the experimental test, Figure 4.28, just before failure, they are within 18% tolerance.

Strain on the tension bar with FE strain on the tension bar in FE-HSC1 at 50 kN as the first closed tension cracks appear at 450mm from the centre of the beam, compared with the strain at mid-span for the FE model which is 0.00024 and the experimental test is 0.00038, Figure 4.25.

At 120 kN, when ignoring the sudden surge in strain in the model which is recording the strain due to large tension cracks near mid span, Figure 4.27, the strain reading from the FE model is about 0.0012 which is close to the experimental results of 0.0013, within 8.3% tolerance.

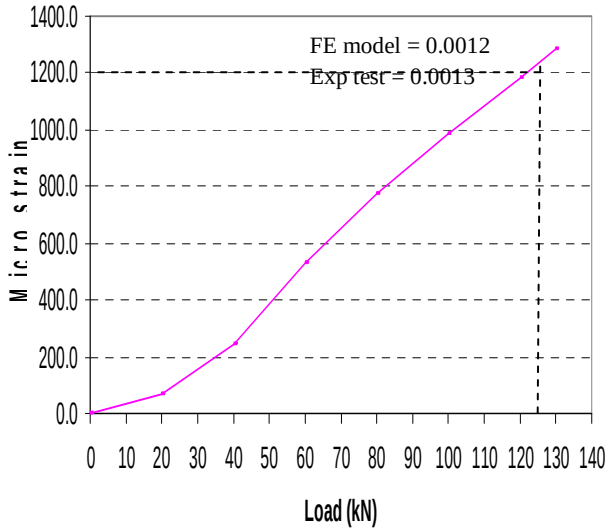

Figure 4.27: Strain development recorded experimentally and by FE model along the tension reinforcement T20 of HSC1,120 KN

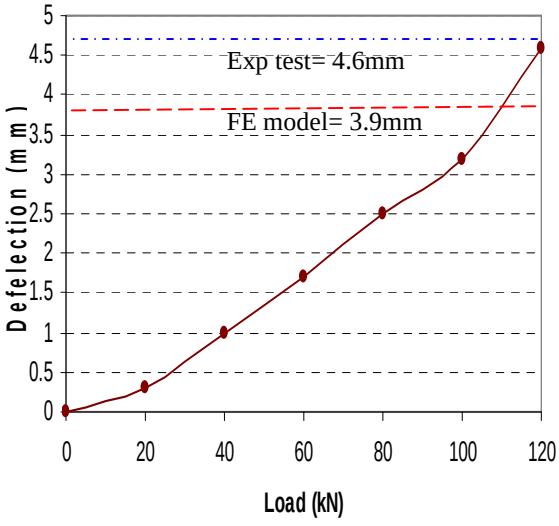

Figure 4.28: Comparison of deflection for FE model and experimental test for HSC1 analysis

It can be concluded that the shear cracking behaviour, strains in tension bar, deflection and the mode of failure of the experimentally tested beam HSC1 and those of an idealised FE model are quite satisfactory and the results developed by FE model, FE-HSC1, are within 5% of the experimental results.

4.5.4.2 Crack propagation in FE model FE-HSC1

The model FE-HSC1 was step loaded incrementally at 20 kN load steps until 140 kN, followed by step loads of 5 kN until failure load of 155 kN. Flexural cracks appear at 40 kN, Figure 4.29. At 90 kN inclined shear cracks appear, Figure 4.30. Cracks at 150 kN failure occur in the lower part of the beam, Figure 4.31. The compression part of the beam continues to sustain shear load until 155 kN when failure occurs. A description of signs is given in Figure 4.16.

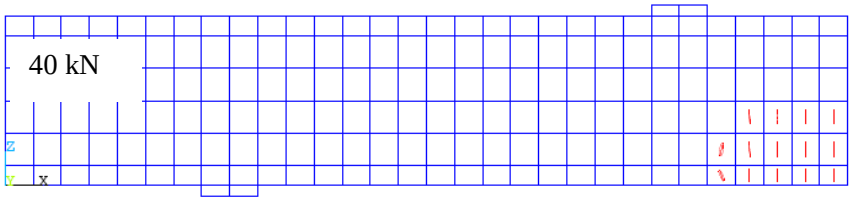

Figure 4.29: At early loading of 40 kN, tension cracks appear in the flexural span.

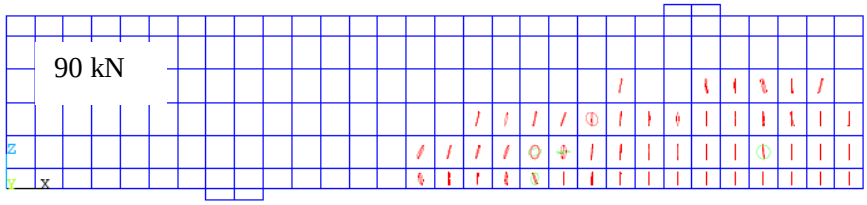

Figure 4.30: At 90 kN inclined shear cracks scatter in the shear span opening of the inclined crack within the shear span

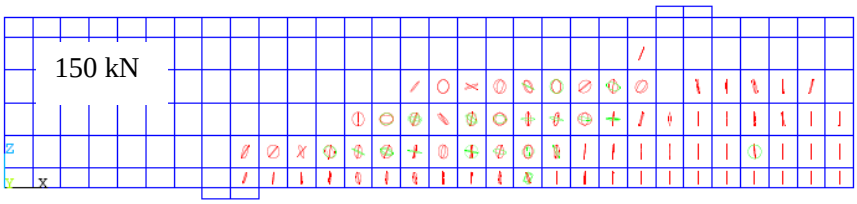

Figure 4.31: Cracks at 150 kN failure occur in the lower part of the beam

4.5.5 Numerical model for FE-NSC3

In this section the numerical model for FE-NSC3, Figure 4.34, which has HWB of 2-T12 is developed in order to validate and verify the influence of HWB in NSC beam of a/d=3.02.

This numerical analysis is performed as an initial investigation of the performance of HWB.

Mid-span deflection was recorded in the experimental work. Strains in the mid-span on the tension reinforcement in X direction and in the links were also recorded. The available experimental results are used to verify and validate model FE-NSC3.

At ultimate loading, the direction of principal vectors indicate the shear failure mode, Figure 4.33.

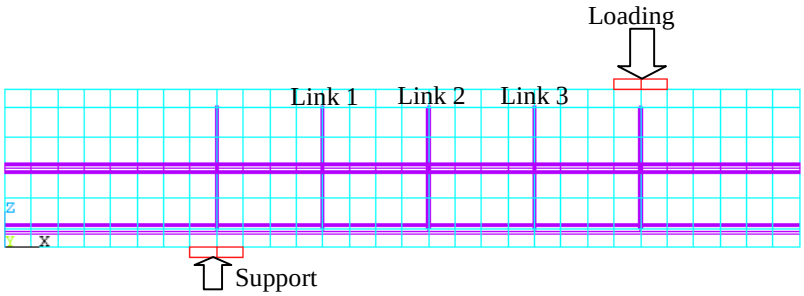

Figure 4.32: Elevation of beam FE-HSC3

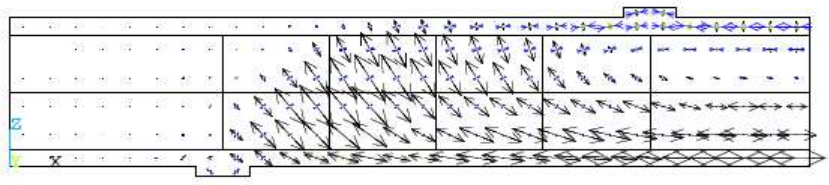

Figure 4.33: Direction of principal vectors just before failure at 180 kN in FE-NSC3

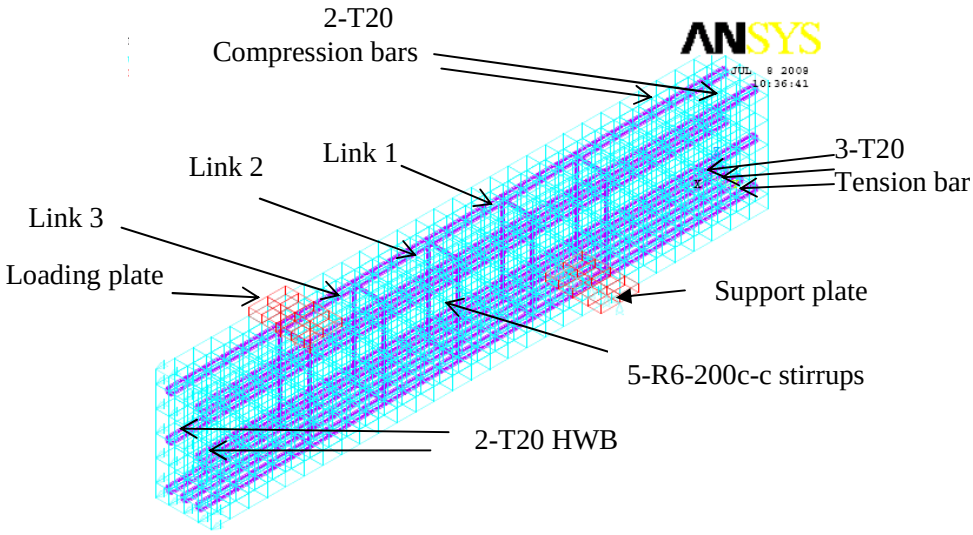

Figure 4.34: The symmetrical beam model for FE-NSC3 beam showing the end restraint in X direction for symmetry

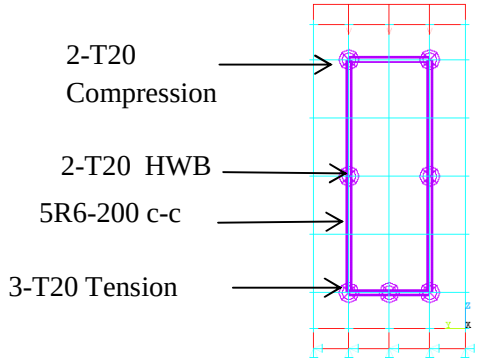

Figure 4.35: Section beam FE-NSC3

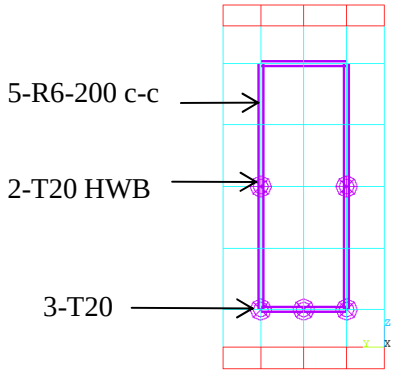

Figure 4.36: Section of beam FE-HSC3

4.5.5.1 Crack Propagation for Beam FE-NSC3

The main stages of the progressive cracking process of the beam FE-NSC3 under increasing load and the element centroid cracks are shown at various loadings, Figure 4.37.

The first crack recorded experimentally was at 50 kN. The experimental loading for the first four load steps were at 20 kN each step.

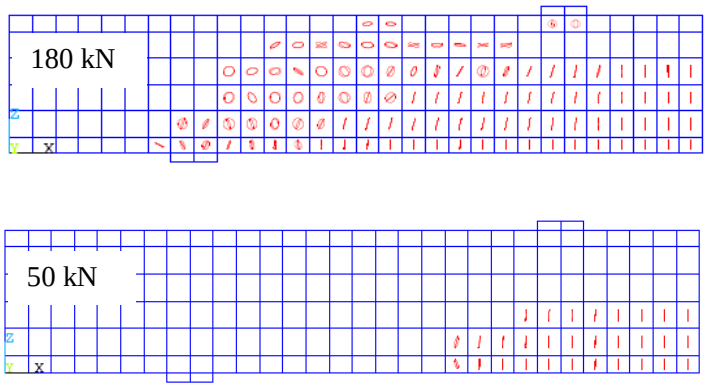

Figure 4.37: Beam FE-NSC3 at 50 kN loading when first inclined cracks are formed. Element centroid cracks are shown at 50 and 180 kN.

4.5.5.2 Strains in links of beam FE-NSC3

At failure load, Link 1, 200mm away from the support in the shear span, almost yields. In experiment, all strain gauges were fixed at the centre of link at 115mm from the top, and the test showed 0.86 (≈9) micro strain compared with FE numerical value of 1.36 (≈1.4) micro strain, Figure 4.38.

The link in the middle of the shear span, link 2, almost yields. In experiment the average strain at 115mm from top was 0.836 micro strain compared to the numerical value of 0.78. The link 200 mm away from loading plate is hardly strained. The average strain gauge reading at the middle of the stirrup in the experimental test was 0.78×10^{-3}, however, the numerical prediction at 115mm from top is 0.84×10^{-3}.

The strain gauge readings on either side of the length of link 3 on the side of the beam where failure occurred were 0.428×10^{-3} and 0.484×10^{-3} or an average of 0.456×10^{-3} (Appendix C). This could be assumed to be due to error in the experimental work from fixing the gauge 5 or 6 mm away from centre of the link. Based on that assumption the FE model reading of 0.00041 compares well with experimental results, Figure 4.39.

At 230 kN, just before failure, link 1 just reaches its yield whereas link 2 exceeds its yield by

21%. Increase of loading from 180 kN to 230 KN, or 28%, results in an increase in strain of 40%.

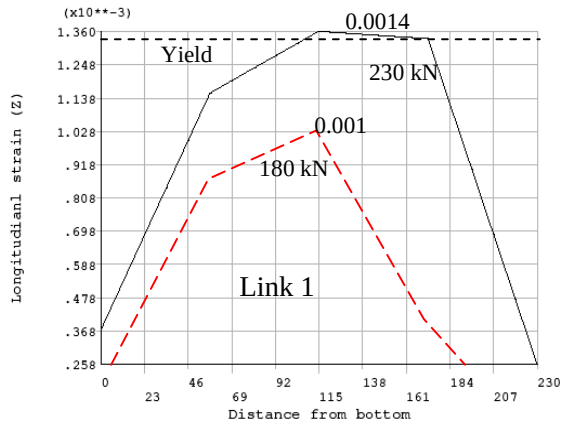

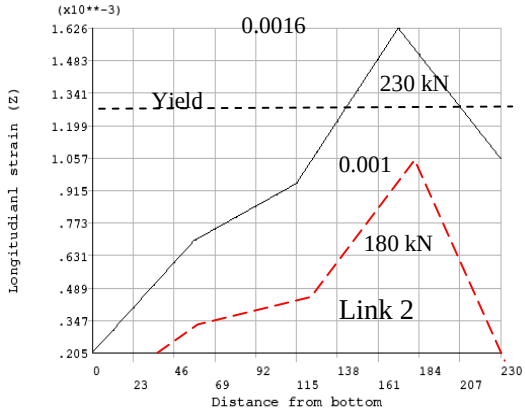

Figure 4.38: NSC3, strains in Link 1 and 2 at 180 kN and 230kN loading along the stirrup

in link 1 and 60 % in link 2. Link 1 has the maximum strain at centre of the link, whereas link 2 has its maximum at three quarters of the length of the link from bottom, **Figure 4.38**.

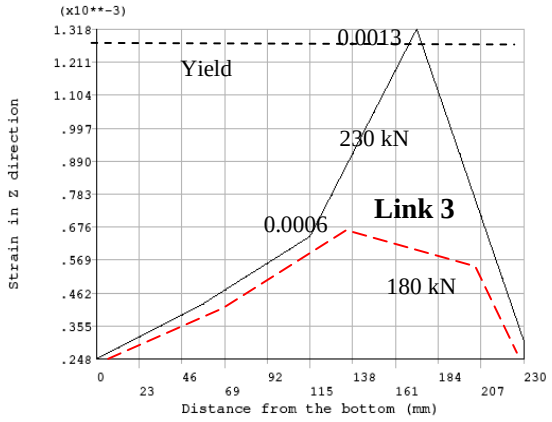

Figure 4.39: NSC3, Link 3 at 180 &230 kN loading

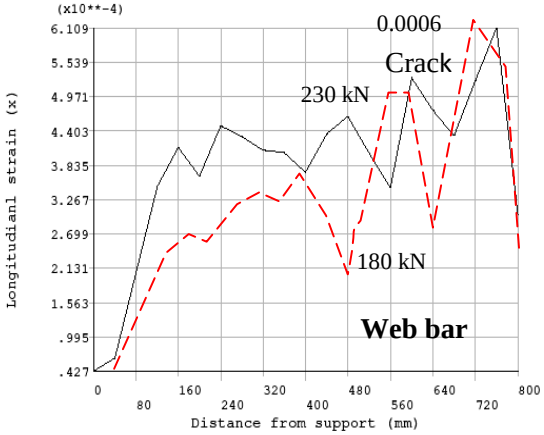

Figure 4.40: NSC3, Web bar at 180 &230 kN loading

Link 3 reaches its yield at 230 kN, for an increase in loading of 28%, and the maximum strain shifts to three quarters of the length of the link from bottom, Figure 4.39.

In spite of an increase in loading from 180 kN to 230 KN, or 28%, the maximum strain in the

HWB remains at 0.0006, indicating that HWB does not make any contribution during the final 30% load, therefore, does not contribute in improving the shear resistance of the beam, Figure 4.40.

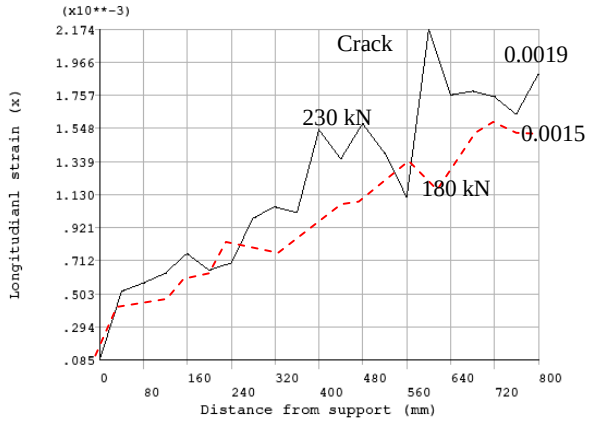

Figure 4.41: Tension bar at 180 kN and 230 kN in beam NSC

As loading increases by 28%, the strain on the tension bar is increased to 0.0019, or 26% , but remains 21% below its yield of 0.0023, Figure 4.41.

The load -strain plots at before failure for the FE numerical model at 180 kN in links 1, 2, and 3 show good agreement with experimental tests of beam NSC3 at 180 kN before failure at 200 kN.

4.5.5.3 Shear stress in XZ in NSC3

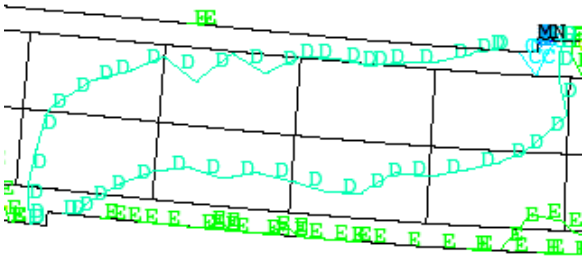

Loading (kN)	Tensile (-) shear stress N/mm^2		
	120	180	230
D	1.35	1.98	2.30
E	0.01	0.02	0.03

Figure 4.42: Shear stress in the shear span of beam NSC3 at loading up to 230 kN before failure

4.5.5.4 Comparison of deflection from FE and experimental test for NSC3

Direct displacement deflect meters were used to measure deflections for the experimental beams at mid-span at the centre of the bottom face of the beams. For the numerical model, deflections are measured at the same location as for the experimental beams.

In the linear range, the load deflection plot from the FE analysis is stiffer than the experimental results by approximately 38%. Other researchers using Ansys FE software [4-6] reached a similar conclusion.

The numerical model showed slightly more stiffness than the experimental model both in linear and non linear ranges as shown in deflection plot, Figure 4.43. This is due to micro cracking of concrete during the shrinkage cycle and bond slippage between reinforcement and concrete, and large cracks developed near failure which are not included in the FE analysis.

Load (kN)	Experimental NSC3 (mm)	FE NSC3 (mm)	Differ	%
60	-	1.7		
100	3.2			
120	4.1	3.7	- 0.4	9.7%
140	5.0	-		
160	5.9	-		
180	7.4	5.9	- 1.5	20%
230	-	7.8		

Table 4-6: Experimental and numeric load-deflection

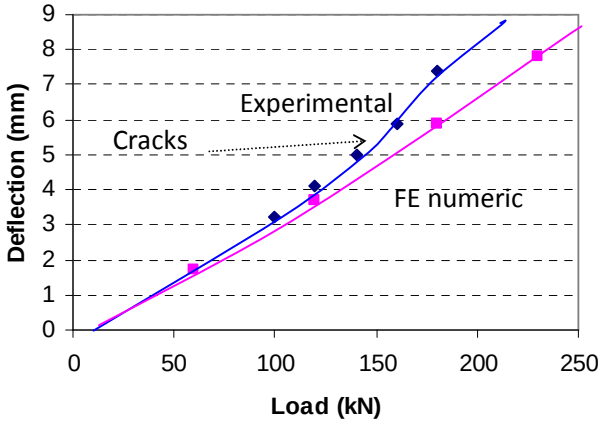

Figure 4.43: The load-deflection plots shows deflection of 5.9 mm for FE-NSC3 at 180 kN as compared to experimental test deflection of NSC3 at 7.4 mm.

4.5.5.5 Shear Strain XZ direction in beam NSC3

Figure 4.44 shows development of shear strain in XZ direction at three stages of loading from 120 to 230 kN.

It is notable that as the result of presence of HWB, just before failure at 230 kN the diagonal strut slightly deflects to improve the arch action.

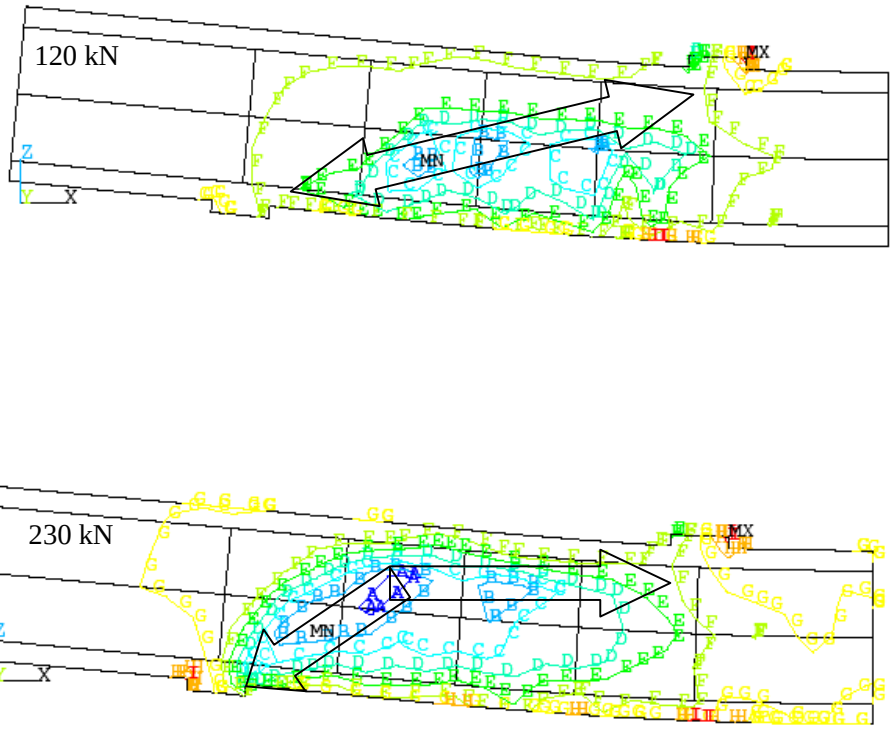

Load (kN)	Shear strain in XZ for NSC3 (N/mm^2)					
	A	B	C	D	E	F
120	1	0.9	0.7	0.5	0.3	0.1
180	1.7	1.4	1.1	0.5	0.3	0.1
230	2.4	2.0	1.6	1.2	0.8	0.4

Figure 4.44: Shear Strain XZ direction in beam NSC3 until 230 kN before failure.

4.5.5.6 Conclusion for model FE-NSC3

The estimate from the numerical analysis for strains in the centre of the links at 180 kN are within 33% for link 1, 7.7% for link 2, and 12% for link 3.

The deflection was 38% less for the numerical model than the experimental test because the numerical model shows slightly more stiffness than the experimental model both in linear and non linear ranges. The effects of bond slip between concrete and steel reinforcement and micro cracks occurring in the actual beams were excluded in the FE models, which resulted in higher stiffness for the numerical model.
The FE model describes the shear behaviour of beam FE-NSC3 in a reasonable approximation.

4.5.6 Numerical model for FE-HSC3

Beam HSC3, Table 3-8, Figure 2-5, which was modelled as FE-HSC3 is analogous to T-HSC3 which will be discussed in Chapter 7.

The significant improvement in shear resistance of HSC1 as a result of introducing 2-T20 will be modelled in this section. The failure load for FE-HSC3 is 290 kN.

4.5.6.1 Crack propagation of the beam FE-HSC3

Figure 4.45 shows the crack development in FE-HSC3 for up to 270 kN loading. The failure occurs at 280 kN.

The first inclined cracks in FE-HSC3 opened at 50 kN, and at 240 kN reaches the loading plate before failure. At 270 kN, failure is about to happen as crushing occurs under the loading plate, shown with a crossed circle, Figure 4.45.

At 180 kN, cracks in the shear span have extended just above half the depth, with the highest open crack shown in circle occurring in the third lower layer of concrete elements from top surface in comparison to open cracks across the complete depth of beam FE-NSC3, which has exactly the same reinforcement but with NSC.

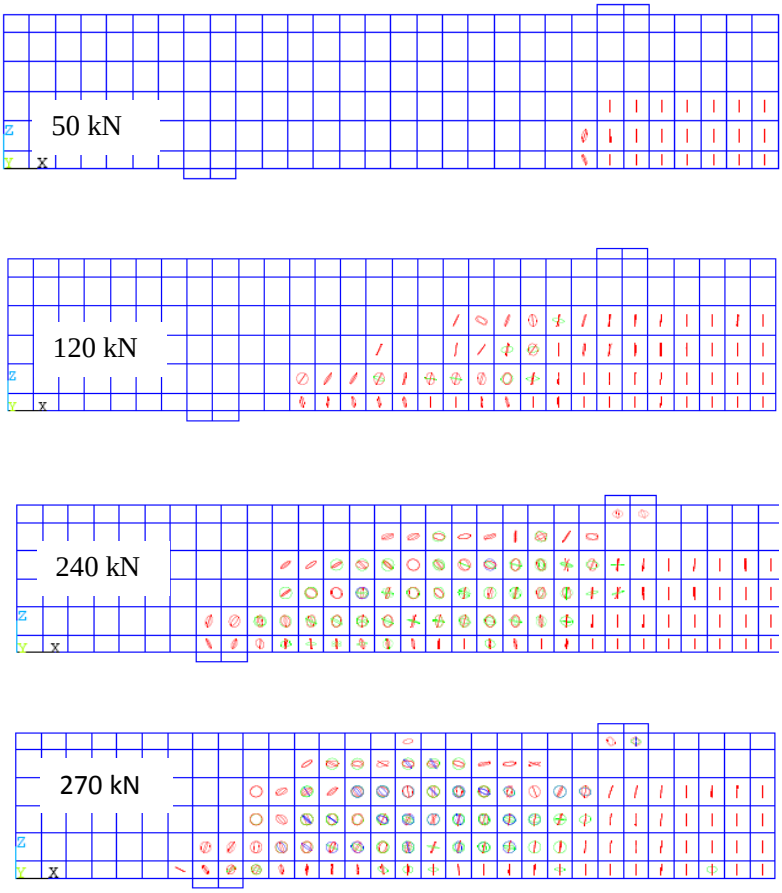

Figure 4.45: Crack propagation in FE-HSC3 .

.

4.5.6.2 Strain in tension bar at first crack in FE-HSC3

In beam FE-HSC3, the first loading of 50 kN has caused a strain of 0.42×10^{-3} at the mid-span of the beam which is close to the experimental recording for HSC3 at 50 kN of 0.41×10^{-3}. The tolerance between the model and the experimental test is 2.4%, Figure 4.46 and Appendix C.

At 270 kN, at link 1 of FE-HSC3 (close to the support) the maximum strain is 1.89×10^{-3} and occurs at the centre of the link. This can be compared with the experimental results for HSC3

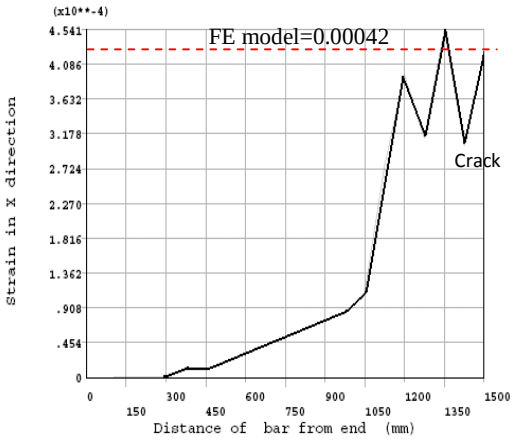

Figure 4.46: FE-HSC3, Strain in X direction in tension bar at 50 kN

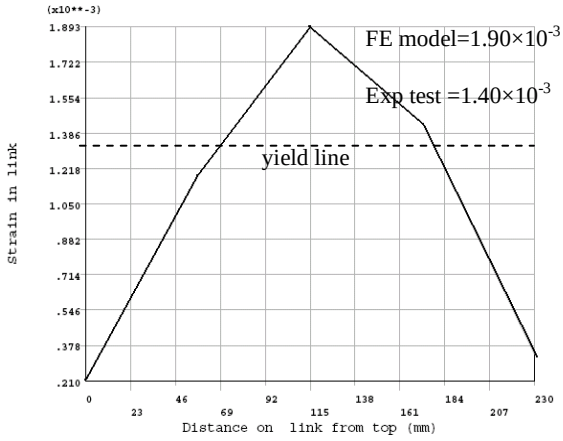

Figure 4.47: Link 1 of FE-HSC3 at 270 kN

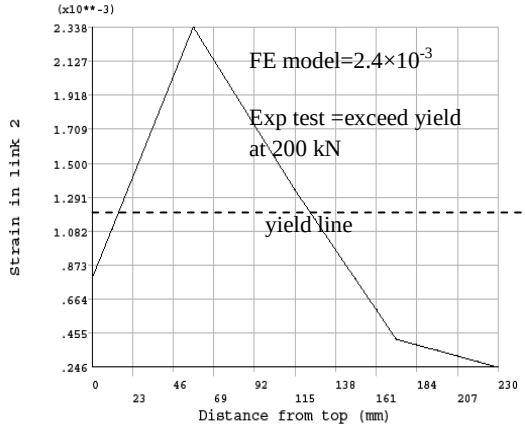

Figure 4.48: Link 2 of FE-HSC3, at the centre of shear span at 270 kN

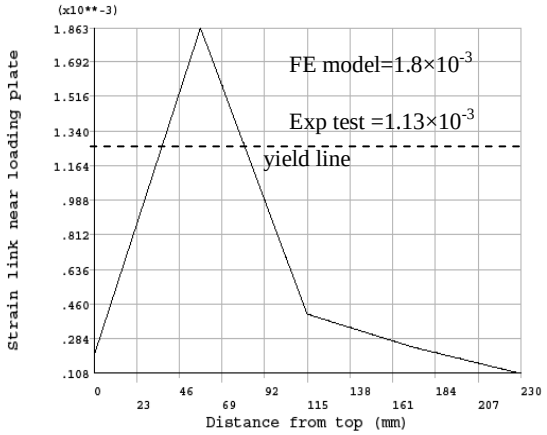

Figure 4.49: Link 3 close to loading plate at 270 kN at 270 kN

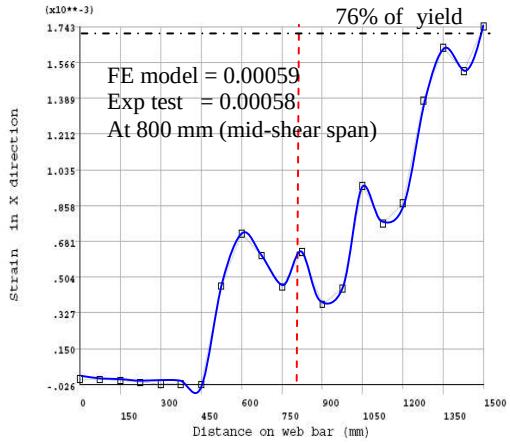

Figure 4.50: HSC3, at 270 kN, 2T20 HWB in x direction reach 76% of their yield at mid-flexural span.

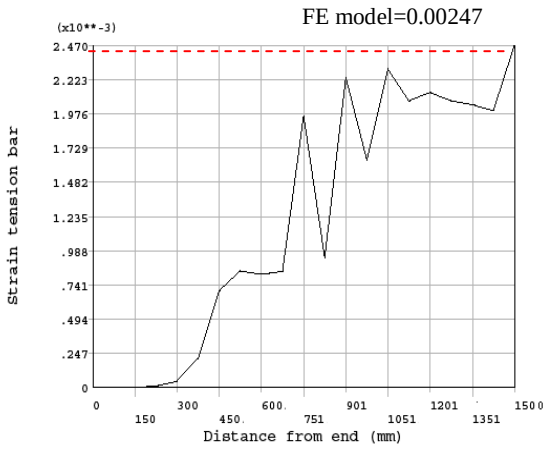

Figure 4.51: Strain in X direction in tension bar of HSC3 at 270 kN, 0.00247 compared to 0.0024 1 experimental

which is strained at 1.40×10^{-3} at the middle point of the link. However, at 270 kN, the maximum strain in FE-HSC3 is 2.34×10^{-3} in link 2, Figure 4.48, whereas experimental HSC3 is strained well beyond yield point (14.7×10^{-3}) at 200 kN at the middle point of the length of the link, Figure 2-36. The strain readings from the gauges demonstrates that in experiment after 200kN loading the middle stirrup has yielded and a significant shear crack has developed, Figure 2-14, however, the beam continues to resist shear forces for a further 80 kN up to failure load of 280 kN. The extra 80 kN of shear loading before failure is resisted by the HWB.

Link close to loading plate (link 3) reaches 75% of its yield. The presence of 2-T20 HWB delays this link from reaching its yield, Figure 4.49.

On the failing side of beam HSC3, the HWB strain recordings at 800 mm from centre are 1.49×10^{-3} at bottom and 3.24×10^{-3} on top which is 20% higher than its yield value of 2.7×10^{-3}. It is interesting to note that just before failure at the middle of shear span of beam NSC3 at 800mm away from mid-span of the beam the strain on the lower part of HWB, T-20, is 0.57×10^{-3} and on top is 0.86×10^{-3}, Appendix C.

There is a detailed analysis of moments produced on the HWB in Chapter 7 when the behaviour of dowel action for CVB which act similarly to HWB, is explained.

4.5.6.3 Strains in XZ direction in model FE-HSC3

The deflected inclined diagonal strut is developed in FE-HSC3 at 270 kN loading.

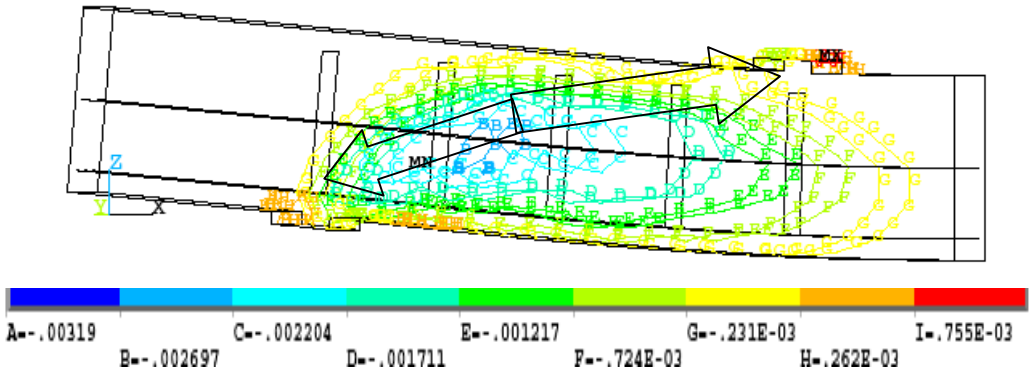

Figure 4.52: Strains in XZ direction in model FE-HSC3 at 270 kN

4.5.6.4 Displacement of FE-HSC3

Deflection increases linearly with load until 160 kN when a sudden increase in deflection occurs, due to cracking of the concrete beam. After this cracking the rate of deflection slightly increases as shown in Figure 4.54.

Small increase in loading from 270 to 285 kN or 15 kN results in 8% increase in deflection. This is less than 12.5mm deflection from experimental test at 250 kN loading, Appendix C.

Deflection of FE model is 34% smaller than corresponding experimental test for HSC3 because FE behaves stiffer because it does not model bond slippage of tension reinforcement or micro-cracking in the concrete due to shrinkage

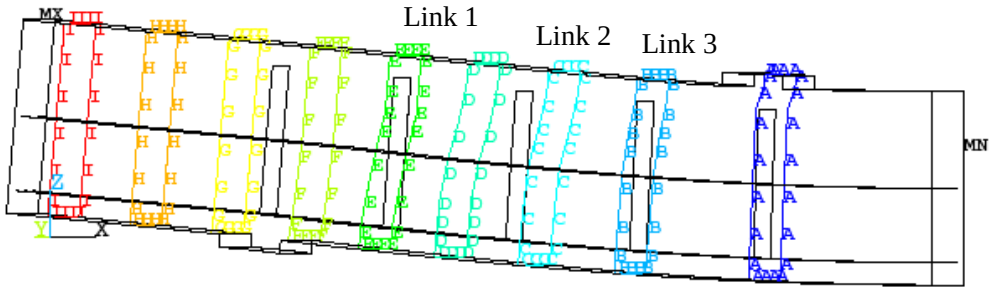

Load (kN)	Vertical displacement (mm)								
	A	B	C	D	E	F	G	H	I
270	-7.6	-6.3	-4.9	-3.35	-2.13	-0.8	0.6	2.0	3.4
285	-8.2	-6.7	-5.2	-3.7	-2.3	-0.8	0.7	2	3.6

Figure 4.53: Displacement of FE-HSC3 at 270 kN and 285 kN loading

4.5.7 The coefficient of closed and open cracks for HSC without HWB

Tolerances in convergence criteria should be carefully defined in a nonlinear analysis. With load adjustment, tolerances for both force and displacement criteria may need to be relaxed to avoid a diverged solution. After the load range that produces a diverged solution is revealed from a previous ANSYS trial run, either tolerance or load adjustments or both have to be made to prevail over the divergence problem at that loading level. In a nonlinear reinforced concrete analysis, the shear transfer coefficient must be assumed.

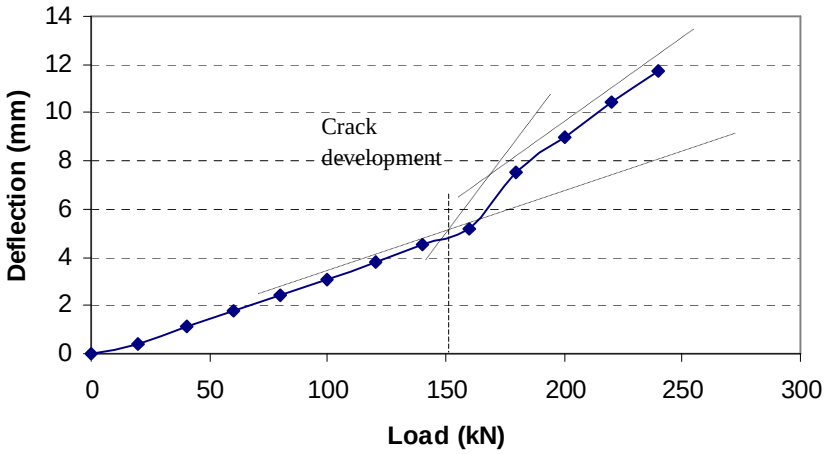

Figure 4.54: Experimental deflection shows that experimental test, HSC3, records 11mm displacement at 230 kN loading, whereas FE-HSC3 records 8mm at 270 kN.

For closed cracks, the coefficient is assumed to be less than 1.0, while for open cracks it should be in the range of 0.05 to 0.5 to prevent numerical difficulties [4-42] and [4-43]. In this thesis, for open cracks a value of 0.3 was used for NSC and 0.1 for HSC, and for closed cracks 0.1 for both NSC and HSC, which resulted in producing reasonably accurate predictions compared to the average results obtained from 3 repeated experimental tests on HSC1 .

However, the strain gauge recording differences on the top of the HWB in HSC3 at 800mm is 1.88×10^{-3} indicating there a significant moment on this section of web bar due to dowel action. This moment is produced when concrete is HSC and when stirrups are present to support the HWB, Appendix C.

The dowel action produced along 50mm length elements known as primary bearing length (PBL) by HWB resists a moment of 82.72 kNmm at link 1 near the support and a moment of 65.72 kNmm at link 3 near the loading point, Figure 4.56, compared to the maximum dowel action in NSC3 which reaches 37.56 kN at 230 kN before failure load, Figure 4.57.

4.5.8 Moment forces on HWB producing the dowel action

FE-HSC3 has no compression steel, and its strain recordings compare very well with the

strain gauge reading of HSC3 on the lower side of the HWB of 0.579×10^{-3} at a distance of 800mm from the centre, Appendix C, , and compares well with FE-HSC3 strain of 0.592×10^{-3}, Figure 4.50.

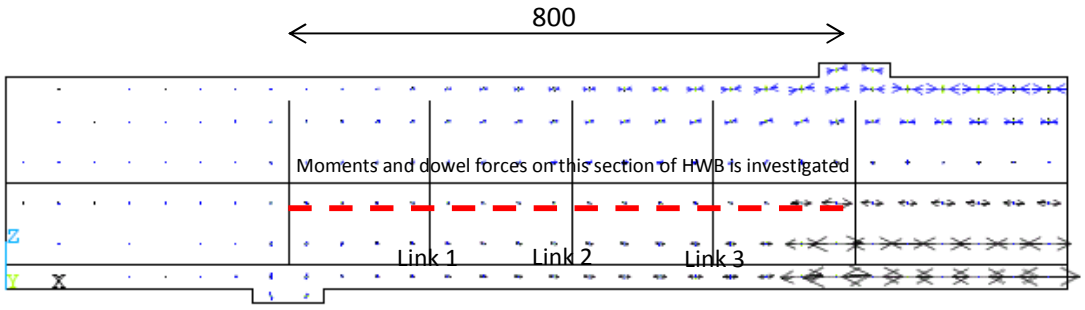

Figure 4.55: Location of HWB investigated are identified on principal strain vector at low loading prior to appearance of first inclined crack.

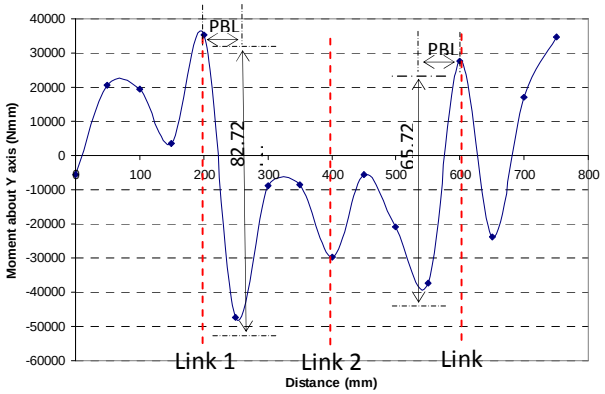

Figure 4.56: Moments producing dowel action in HSC3 on HWB length from centre of support to centre of loading plate as shown in Figure 4.55 before failure at 270 kN.

In general, FE models for HSC1, NSC3 and HSC3 predict reasonable results which compare well with the experimental results. Comparing the strains in the links, the tension in the main reinforcement and the deflection at the centre of the beam, it has been shown that the results are within 20% accuracy. Furthermore, the crack development in the FE model gives a reasonable indication of cracks developing in the experimental test.

Link	Node no	Distance (mm)	FE-HSC3 M_y Nmm 270 kN	FE-NSC3 M_y Nmm 220 kN	Link	Node no	Distance (mm)	FE-HSC3 M_y Nmm 270 kN	FE-NSC3 M_y Nmm 220kN
	1	0	-5477.7	8651.5		17	400	-29639	11212
	2	0	-20693	-8651.5	2	18	400	-5596.8	-11212
	3	50	20693	-35588		19	450	-5596.8	31069
	4	50	-19467	35588		20	450	21004	-31069
	5	100	19467	-22615		21	500	-21004	1637.5
	6	100	-3513.8	22615		22	500	37422	-1637.5
	7	150	+3513.8	-32918		23	500	-37422	-2425.8
	8	150	-32371	32918		24	550	7045.7	11147
1	9	200	35290	-17714		25	600	27691	1360.7
	10	200	47432	17714	3	26	600	-23955	-1360.7
	11	250	-47432	-25040		27	650	-23955	1360.7
	12	250	8689.3	25040		28	650	-17007	-1360.7
	13	300	-8689.3	-126		29	700	17007	37117
	14	300	8447.2	126		30	700	-34685	-37117
	15	350	-8447.2	-1013.4		31	750	34685	8651.5
	16	350	30107	-8395.9		32	750	-3271.7	-8651.5

Table 4-7: Location of moment about y axis producing the dowel force in z direction on the HWB from centre of support to centre of loading plate as shown in Figure 4.55.

4.6 Conclusion on beams of a/d=3.02

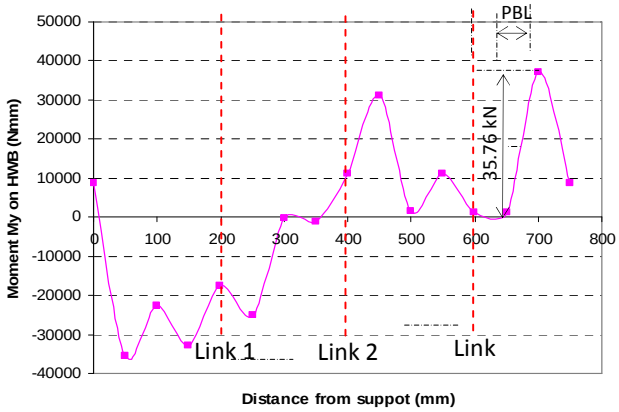

Figure 4.57: Moments producing dowel action in NSC3 on HWB length from centre of support to centre of loading plate as shown in Figure 4.55 before failure at 230 kN.

However, the unique performance of HWB resisting the applied load at the highest 40% loading increment could not be clearly demonstrated when strain on the links was investigated.

HWB displays a significant shear resistance when stirrups become totally redundant. In experimental testing of HSC3, Figure 3.39, this occurs at 200 kN and from that loading onwards the HWB resisted all shear forces until 285 kN failure load.

It has been demonstrated that for NSC3 (i.e. NSC1+HWB), the presence of HWB did not contribute to load capacity of the beam during the final 40 kN loading before failure, Figure 4.40. This may be due to the fact that stress distribution in the depth of the beam has changed after beam cracking.

Figure 4.48 shows that FE-HSC3 has reached maximum strain of 0.0024 in centre link . However, in the experimental test for HSC3, Figure 3.39(f) , strain recording for the same point exceeds well beyond yield point (14.7×10^{-3}) at 200 kN . This was similar for other beams HSC2 and HSC4 which demonstrates that the middle stirrup becomes totally obsolete after 200 kN but load bearing capacity continues to 270 kN for HSC2 and 300 kN for HSC4, Appendix C.

FE method does not simulate the model with actual elements separating. Therefore, after shear cracks occur, the actual opening of cracks is not taken into account, so the final deflection is after cracks have opened at 120 kN and for HSC1 the deflection at the centre of the beam is 4.6 mm, Appendix C, as compared to FE which is 3.9mm, Figure 4.28.

The 2-T20 web bars in x direction reach 76% of their yield at mid-span in HSC3 which has no compression steel. This reading compares very well with strain gauge reading of 0.579×10^{-3} at a distance of 800mm, Figure 4.50, Appendix C.

4.7 References

4-1 Balakrishnan, S., Elwi, A.E., Murray, D.W. 'Effect of modeling on NLFE analysis of concrete structure'. Journal of Structural Engineering, ASCE, 1988, Vol. 114, No 7, 1467-1487

4-2 Bresler, B., Scordelis, A.C. 'Shear strength of reinforced concrete beams'. J. Am. Concrete Institute, 1963, Vol 60, No. 1, 51—74

4-3 Vidosa , F.G, Kotsovos, M.D, Pavlovic, M.N, 'Three-dimensional non-linear finite element model for structural concrete.' Part 1 &2, Proc. ICE, Part2, 1991, Vol. 91, Sept, 517-560

4-4 Blaauwendraad, J., Zheng, P.W. 'Understanding brittle shear failure in concrete offshore structures' Patel, M. H. & Gibbins, R, Editors, Proceedings of the Sixth International Conference on Behaviour of Offshore Structures, 7-10 July 1992, Vols. 1, 2 and Supplement, 1358 pages, Bentham Press, Tavistock Place, London, ISBN-1-874612-02, 744-755

4-5 Seraj, S. M, Korsovos, M. D. and Pavlovic, M. N. 'Three-dimensional finite-element modelling of normal- and high-strength reinforced concrete members, with special reference to T-beams'. Computer & Structures Vol.44, No 4, pp 699-716, 1992

4-6 Kachlakev, D.I., Miller, T., Yim, S., Chansawat, K., Potisuk, T. (2001), 'Finite element modelling of reinforced concrete structures strengthened with FRP laminates,' California Polytechnic State University, San Luis Obispo, CA and Oregon State University, Corvallis, OR for Oregon Department of Transportation, May.

4-7 Zhang, S., Raoof, M. "Nonlinear finite-element analysis of shear characteristics of reinforced concrete beams". Internal report, South Bank University, London, 1992

4-8 Bhide, S. B. 'Reinforced concrete elements in shear and tension', PhD thesis , University of Toronto, 1986.

4-9 Kupfer, H.B., Gerstle, K.H. "Behaviour of concrete under biaxial stresses", Journal of Engineering Mechanics. Div, ASCE, 1973, Vol. 99, 853-866

4-10 Balakrishnan, S. Murray, D.W 'Finite element prediction of reinforced concrete behaviour'. Structural engineering report No. 138, Department of Civil Engineering, University of Alberta, Edmonton, 1986.

4-11 William, K. J. and Warnke, E. P., "Constitutive Model for the Triaxial Behavior of Concrete,"Proceedings, International Association for Bridge and Structural Engineering, Vol. 19, ISMES, Bergamo, Italy, pp. 174, 1975

4-12 Saenz, L.P, "Discussion of equation for the stress-strain curve of concrete", ACI Journal, 164, Vol 61, No 3, 1229-1235

4-13 Hu, H.T., Schnobrich, W.C. "Non-linear analysis of cracked reinforced concrete", ACI Structural Journal, 1990, Vol 87, No 2, 199-207

4-14 Soltani, M., 'Micro computational approach to post cracking constitutive laws of reinforced concrete and applications to nonlinear finite element analysis', Department of Civil Engineering, University of Tokyo, Ph.D Thesis, 2002.

4-15 Bangash, M, Y. H. "Concrete and Concrete Structures: Numerical Modeling and Applications". Elsevier Science Publishers Ltd, London , England, 1989

4-16 Parvanova, S., Kazakov, K., Kerelezova, I., Gospodinov, G., Nielsen, M. P.: Modelling the nonlinear behaviour of rc beams with moderate shear span and without stirrups using ANSYS, Proc. of International Conference, VSU "2005", pp. 1-65-1-70, 26-27 May, Sofia, Bulgaria, 2005

4-17 Houde, J., Mirza M.S., 'A Finite Element Analsis of Shear Strength of Reinforced Concrete Beams' Journal ACI Proceedings, volume 42, 1 January, 1974, pp.103-128

4-18 Gospodinov, G., Nielsen, M. P., Kerelezova, I., Kazakov, K., Parvanova, S., 'Developing new models for simulation of nonlinear behaviour of structures made from quasi-brittle materials like concrete, using fracture mechanics approach', Scientific report under contract № BN 51, UACEG, Sofia, Bulgaria, (2005)

4-19 Albajar, J. S. 'The influence of aggregate fracture on the shear strength of reinforced concrete beams'. Department of Civil & Environmental Engineering, Imperial College London, PhD thesis, September 2008

4-20 Sagaseta, J., Vollum, R., 'Non-linear finite element analysis of shear critical high-strength concrete beams'. AMCM 2008 Analytical models and new concepts in concrete and masonry structures, 6th International Conference Poland.

4-21 Hamadi, Y.D., Regan, P.E., 'Behaviour in shear of beams with flexural cracks'. Magazine of Concrete Research: Vol. 32, No 111: June 1980

4-22 Fanning, P., "Nonlinear Models of Reinforced and Post-tensioned Concrete Beams," Electronic Journal of Structural Engineering, University College Dublin, (2001) Earlsfort Terrace, Dublin 2, Ireland, 12 Sept..2001

4-23 Tavarez, F.A., "Simulation of Behavior of Composite Grid Reinforced Concrete Beams Using Explicit Finite Element Methods," Master's Thesis, University of Wisconsin-Madison, Madison, Wisconsin. 2001

4-24 Maekawa, K. Pimanmas, A. Okamura, H. 'NonLinear Mechanics of Reinforced Concrete', Spon Press, 2003.

4-25 Soltani, M., An, X., Maekawa, K., 'Computational model for post cracking analysis of RC membrane elements based on local stress-strain characteristics', Engineering Structures, vol 25, 2003: pp. 993-1007.

4-26 Task committee on finite element analysis of reinforced concrete structures of the structural division committee on concrete and masonry structures. Fini te element analysis of reinforced concrete. ASCE, New York, 1982.

4-27 Bangash, M. Y. H., 'Concrete and concrete structures'. Numerical modelling and applications. Elsevier Applied Science, 1989.

4-28 Elnashai, A.S. 'Nonlinear analysis of composite tubular joints'. PhD thesis, Imperial College, University of London, 1983.

4-29 Carroll, B.C., Behaviour of prestressed grout bond joints. PhD thesis, Imperial College, University of London, 1987.

4-30 Raoof, M., Lin,Z., 'Structural characteristics of RC beams with exposed main steel'. Proc. Instn Civ. Engrs Structs & Bldgs, 1997, 122, Feb., 35-51

4-31 Bedard, C.'Nonlinear finite element analysis of concrete Structures',.PhD thesis, Imperial College, university of London, 1983

4-32 Lin, J. J. Fafard, M., Beaulieu, D., and Massicotte, B. ,"Nonlinear analysis of composite bridges by the finite element method", Computers and Structures, 1991, Vol. 40, No.5, 1151-1167.

4-33 Kachlakev, D.I., McCurry, D., Jr., 'Simulated Full Scale Testing of Reinforced Concrete Beams Strengthened with FRP Composites': Experimental Results and Design Model Verification, Oregon Department of Transportation, Salem, Oregon, June 2000.

4-34 Gere, J. M. and Timoshenko, S. P., "Mechanics of Materials", PWS Publishing company, Boston, Massachussetts, 1997

4-35 Ramdane, K.E. ' Properties and structural behaviour of high strength concrete'. University of Westminster , PhD thesis. 2000

4-36 Al-Hussaini, A., Ramdane, K. 'Properties and creep of High Strength Concrete', Proceedings on an International Conference on Concrete, Tehran, Nov. 1992, pp. 762-779

4-37 ANSYS 11 'Instruction manual.'
http://www.ebookspdf.com/search/Ansys+11.0+Tutorial

4-38 Mindess, S. and Young, J. F., 'Concrete', Prentice-Hall, Inc., Englewood Cliffs, New Jersey,1981.

4-39 Shah, S. P., Swartz, S. E., and Ouyang, C., 'Fracture mechanics of concrete', John Wiley & Sons, Inc., New York, 1995.

4-40 Mphonde, A.G. and Frantz, G.C. ' Shear strength of high-strength concrete beams'. Report No . CE84-157, Department of Civil Engineering, University of Connecticut, 1984

4-41 Regan, P. E., Kennedy -Reid I. L., Pullen, A. D., Smith, D. A. 'The influence of aggregate type on the shear resistance of reinforced concrete' – The Structural Engineer, 6 December 2005

4-42 Huyse, L., Hemmaty, Y., and Vandewalle, L., "Finite element modelling of fibre reinforced concrete beams," Proceedings of the ANSYS Conference, Vol. 2, Pittsburgh, Pennsylvania, May 1994.

Chapter 5

The Strut and Tie Model

5.1 Introduction

Until the early 1990's, engineers assumed that the need for mechanical models had passed with the development of FE analysis programs and second order frame analyses. However it became clear that the errors inherent in the blind acceptance of computer output as discussed by Yankelevsky[5-1] can be significantly reduced by statically checking the model. Complex computer codes do not always predict adequately the response of complex engineering problems. Mechanical models are necessary to check the validity of results. STM is the design approach recommended by many international codes enabling the designer to clearly visualise the load path within the structural system.

This research extends the restriction of aspect ratio on application of the STM of beam-column joints for HSC columns with CVB with an aspect ratio of $3>h_b/h_c>2.5$. In general, STM is applicable to BCJ with $2>h_b/h_c>1$. In practice when aspect ratio is $h_b/h_c<1$, the joint is likely to fail in flexure. When $h_b/h_c>2$, it is recommended to use the variable truss method given in EC2 [5-18] which restricts the aspect ratio to 2.5.

HSC columns and transfer beams with aspect ratio $3>h_b/h_c>2.5$ are popular structural elements as described in Chapter 1. To this writer's knowledge, no other researcher has investigated the design of STM for HSC BCJ with CVB and aspect ratio $3>h_b/h_c>2.5$. This research investigates the presence of the strut in HSC columns with CVB and transfer beam connections with aspect ratio $3>h_b/h_c>2.5$, and after demonstrating that STM develops in a HSC beam with stirrups and HWB with span depth ratio of 3.02 the analogy is extended to HSC-BCJ with CVB with an aspect ratio of 3.

5.2 Aims and objectives

STM of reinforced concrete members are reviewed with the aim of improving knowledge of the behaviour of STM in HSC beams with $a/d\leq3$ with stirrups and HWB, and HSC exterior BCJ with stirrups and CVB of aspect ratio≤3.

The approach adopted includes an investigation into the background of the development of STM, exploring past research, code recommendations and STM design rules for structural discontinuities such as short beams and BCJ. The influence of HWB with stirrups in HSC beams of a/d=3 and TBCJ of aspect ratio 3 are introduced to develop STM of HSC beam with HWB and BCJ with CVB modelled in a new design approach.

This literature review will focus on both recent contributions related to STM and those past efforts most closely related to the present work.

STM for HSC beams with HWB of a/d=3 is developed by applying this writer's proposed empirical design rule for prediction of dowel resistance from Chapter 2. The predicted force acts to counter balance the deflected strut in STM.

The FE results on moments acting on HWB, described in Chapter 3 are converted to dowel force acting on HWB. This dowel force predicted by FE analysis is compared with predictions from empirical formulae for developing more accurate STM.

5.3 Background to the development of STM

The first mechanical model used to explain shear strength was the truss analogy described in 1899 and 1902, by the Swiss engineer Ritter and the German engineer Morsch [5-2]. The idea of the STM came from their analogy for the shear design of B regions. This method employs the truss model as its design basis which was used to idealize the flow of force in a cracked concrete beam.

In parallel with the increasing availability of experimental results and the development of limit analysis in plasticity theory, the truss analogy method has been validated and improved considerably in the form of full member or sectional design procedures.

In the 1970's Grob and Thurlimann [5-3] in Switzerland suggested a generalised truss model with variable strut inclination, introducing limits for the strut angles, based upon kinematic considerations.

Applying plastic analysis, Nielsen and his co-workers [5-4] in Denmark developed formulae for the stresses in reinforcement and in concrete struts. They presented a resolution for the strut angle when the shear resistance is determined by the simultaneous yield of stirrups and crushing of web concrete.

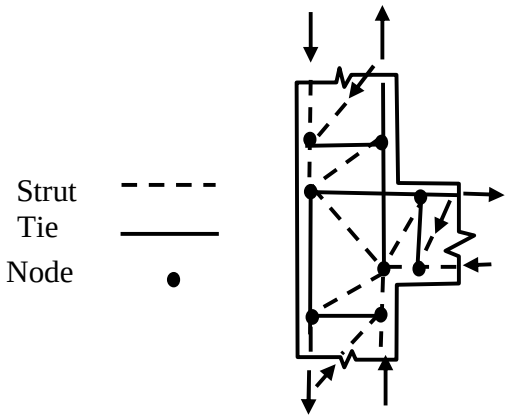

Figure 5.1: A basic STM showing the load path of struts and ties and forces in the boundary conditions of a BCJ with stirrups above and below the joint.

The conventional method of dimensioning sections subjected to flexure, shear and axial load - the beam theory - treats the structure section by section. However, the truss and STM show that shear (and torsion) are resisted by diagonal compressive stress fields in the concrete and so influence not only the section itself but a certain region on either side of it. Any calculation made on the basis of section by section design should be regarded as giving average values representative for a region around that section.
Therefore, the beam theory is suitable for the analysis of regular structure zones, i.e. zones with no geometric or static singularities, but not for the design of zones where 'average values' cannot be considered.

The STM developed by Marti [5-5] and Schlaich et al [5-6] promoted the use of the truss model in D regions. In 1982 and 1987, Schlaich [5-6] presented the concept of dividing structures into B (beam) and D (discontinuity) regions in the reinforced concrete structure. This has allowed the development of mechanical models for widely varying ranges of shear behaviour.

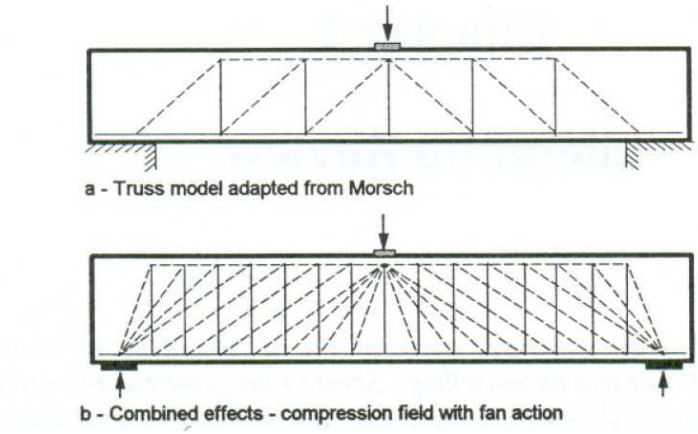

Figure 5.2 : Truss model combined with fan action

This approach reflects the differentiation of conventional structural analysis applying the Bernoulli hypotheses of plane strain distribution (B regions) and the analysis of special regions (D regions) where the beam theory does not apply.

STM has been developed to give general rules for the design of concrete structures, applicable to B and D regions, in a simple and practical way. However, in spite of recent developments in the STM, there are points that need more experimental evidence and more practical design proposals.

Briefly, a structure is divided up into D regions that extend the depth of the member each way from a reaction or discontinuity. The D regions are isolated and the stresses on their boundaries are resolved into a number of individual forces acting on the boundaries of a D region. STM are then used to design the D regions, Figure 5.3.

Thurlimann and colleagues [5-3] in Switzerland and Nielsen and his co-workers [5-4] in Denmark during 1970's analysed the shear and torsion problems more accurately through the theory of plasticity by using STM for the equilibrium solutions.

In 1984, MacGregor [5-7] wrote that the most important advances in reinforced concrete design would be the extension of plasticity based design procedures to shear, torsion, bearing

stresses, and the design of structural discontinuities such as joints and corners, allowing a designer to follow the forces through a structure.

5.3.1 Design background to STM

STM is an alternative or a complementary approach to either FE modelling or empirical methods for the design of BCJ as well as for deep beams, corbels, pile caps and squat shear walls. STM provides the structural analyst with some freedom of choice which can be used to make a cheaper, safer or optimised solution.

Modelling therefore requires some design experience to make a valid comparison of this method with an overall statical system which has developed from an empirical approach or a FE approach.The modelling process also requires considerable knowledge of detailing and therefore of practicable reinforcement layout; on the other hand, it is exactly in this field where STM replaces experience and guesswork with a more systematic and comprehensive design.

Before modelling of a D region begins, all the forces and reactions acting on the D region must be evaluated. The forces or stresses in sections bounded by D regions are taken from B region design. The elastic stress trajectories and distribution of elastic stresses within the D region is studied by tracing the flow of forces through the structure, developing systematically the 'load path' and the corresponding STM.

The stress diagrams of all the forces applied to the D region boundaries are subdivided in such a way that their individual stress resultants on opposite sides of the D region correspond in magnitude and can be connected by streamlined 'load paths' which do not cross each other. After sketching the load paths smoothly curved and replacing them by polygons, and after understanding the load path, for higher accuracy these curves are developed from FE model and further struts and ties can be added for transverse equilibrium.

Three main elements considered for practical use in STM of reinforced concrete structures are:

the uniaxially stressed steel ties, the uniaxially stressed concrete struts and the nodal zones, Figure 5.1. Considering the steel ties there is a general agreement that at the ultimate limit state, the ties can be stressed to the design yield strength of the reinforcement at points of maximum stress while it is important to clearly understand the mechanical effect of the longitudinal bars and stirrups in D regions.

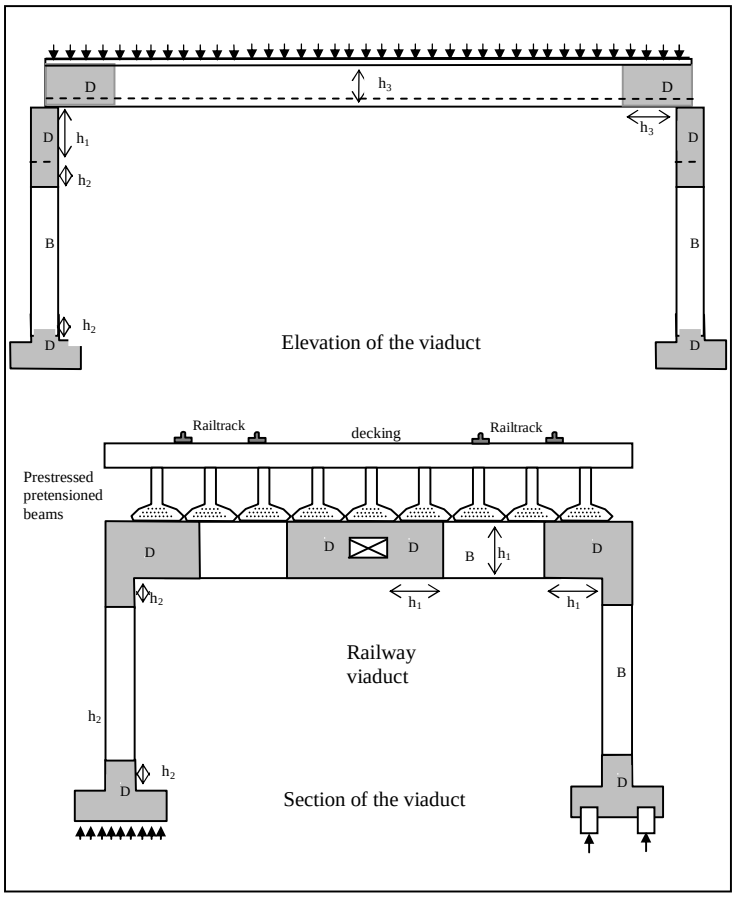

Figure 5.3: Structures are divided up into D regions that extend the depth of the member each way from a reaction or discontinuity and B regions, the parts of the structure between D regions. Isolated D regions are near concentrated load and reactions.

Some divergence exists on the stress limits and dimensions of the concrete struts and nodal zones. The role of the concrete tensile strength also needs attention [5-8]. To apply the general concepts of this method it is of paramount importance to have guidance on the shape and the strength of the struts and of the nodes of the trusses.

Schlaich and his team suggested that the size of a D region can be estimated using Saint

Venant' s principle. The D regions are assumed to extend roughly for a distance equal to the member's depth away from the discontinuous or disturbed section (zones with change in the geometry or under concentrated load or reaction). This principle is conceptual and not precise, however it serves as a quantitative guide in selecting the dimensions of the D region.

D regions as also assumed to fill the overlapping region common to two members meeting at a joint. This definition is used in the traditional definition of a joint region. Prior to any cracking, an elastic stress field exists which can be quantified with an elastic analysis, as well as a FE analysis. Cracking disrupts this stress field causing a major reorientation of the internal forces.

After cracking , the internal forces can be modelled with a STM consisting of concrete compression struts, steel tension ties, and joints referred to as nodal zones. If the compression struts are narrower at their ends than they are at mid-section, the struts may, in turn, crack longitudinally, leading to strut failure if no shear reinforcement is present. Failure may also occur by crushing, yielding of the tension ties, failure of the bar anchorage, or failure of the nodal zones. As usual, failure initiated by yield of tension bar ties is preferred because it could be more ductile.

5.3.2- Design approach using STM

Conditions required for STM

The overall structural analysis and B regions' design provide the boundary forces for D regions. The D regions are then modelled by struts and ties following the internal load path, with the struts following the flow of the compressive stresses and the ties representing the reinforcement in tension.

The struts and ties represent the stress fields by straight lines and the curvatures are concentrated in nodes, Figure 5.4. It must be pointed out that the STM of a D region does not have a unique solution. At the same time as giving some freedom of choice for the solution, some design experience is required to model the regions with practicable reinforcement layout and detailing.

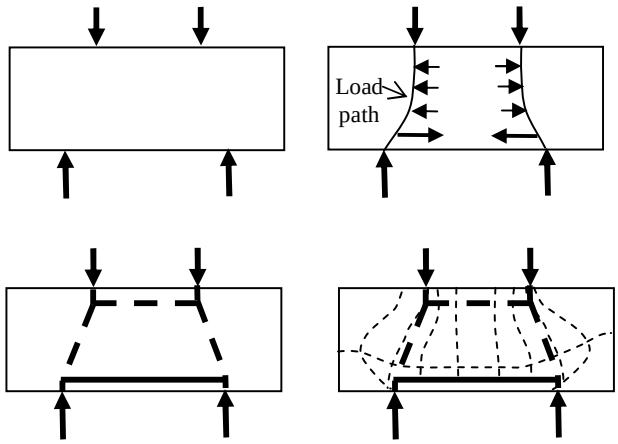

Figure 5.4: The load path developed in a short beam

STM is one of the segments of the structure that satisfies the following criteria:

a. it embodies a system of forces that is in equilibrium with a given set of loads;
b. the factored-member forces at every section in the struts, ties, and nodal zones do not exceed the corresponding design member strength for the same sections;
c. the lower-bound theorem of plasticity which states that the capacity of a system of members, support and applied forces that satisfies both (a) and (b) is a lower bound on the strength of the actual structure;
d. the structure must have sufficient ductility to make the transition from elastic behaviour to redistribute the factored internal forces into a set of forces that satisfy items (a) and (b).

The combination of factored loads acting on the structure and the distribution of factored internal forces is lower-bound on the strength of the structure, provided that no element is loaded or deformed beyond its capacity. STM should be chosen so that the internal forces in the struts, ties, and nodal zones are somewhere between the elastic distribution and a fully plastic set of internal forces.

5.3.3 Design process using STM

The design process using STM involves five major steps described below:

1) Define the boundaries of the D region and determine the boundary forces (the ultimate design forces) from the imposed local and sectional forces.

2)Sketch the truss, determine the equivalent boundary forces, and solve for the truss member forces.

3) Select reinforcing or prestressing steel to provide the necessary tie capacity and ensure that this reinforcement is properly anchored in the nodes.

4) Evaluate the dimensions of the struts and nodes such that the capacity of all struts and nodes is sufficient to carry the truss member forces.

5) Provide distributed reinforcement to ensure ductile behavior of the D region.

Since equilibrium of the truss with the boundary forces must be satisfied (step 2) and stresses everywhere must be below the limits (steps 3 and 4), one can see that the STM is a lower-bound (static or equilibrium) method of limit analysis.

Equilibrium should be satisfied at all nodes of STM. As a statically admissible stress field, STM has to be in equilibrium externally with the applied loading and reactions (the boundary forces) and internally at each node. In addition, reinforcing or prestressing steel is selected to serve as the ties and the concrete as struts, the effective width of each strut is selected, and the shape of each nodal zone is constructed such that the strength is sufficient. Therefore, only equilibrium and yield criterion need to be fulfilled for an admissible STM. The third requirement in solid mechanics framework, namely the strain compatibility, is not considered.

As a result of these relaxed requirements, there is no unique STM for a given problem. In other words, more than one admissible STM may be developed for each load case as long as the selected truss is in equilibrium with the boundary forces and the stresses in the struts, ties, and nodes are within the acceptable limits.

The lower-bound theorem guarantees that the capacity obtained from all statically admissible stress fields is lower than or equal to the actual collapse load. However, as a result of limited ductility in the structural concrete, there are only a small number of viable solutions for each design region.

5.3.4 Dimensioning of the Struts, Ties and Nodes

Once the STM for a region is chosen, the forces of the struts and ties are calculated satisfying equilibrium between applied loads and inner forces. The next task is the dimensioning of the struts, ties and nodes.

There is a general agreement about the dimensioning of the reinforcement ties. The reinforcement is considered stressed to the yield strength at the ultimate limit state.

Following the flow of forces in STM in detail frequently shows that the equilibrium can only be satisfied if concrete tensile forces can be accepted in places where reinforcement cannot be provided and the tensile strength of concrete must be utilized. However, it is more important to determine where the tensile strength of the concrete is utilised and then if possible to provide protection reinforcement, than to quantify the strength of the concrete ties. Schlaich and his colleagues [5-38] pointed out that more research work remained to be done concerning dimensioning of the concrete ties and struts.

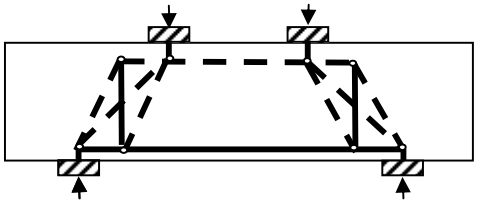

Figure 5.5: Shows STM for a short beam with stirrup

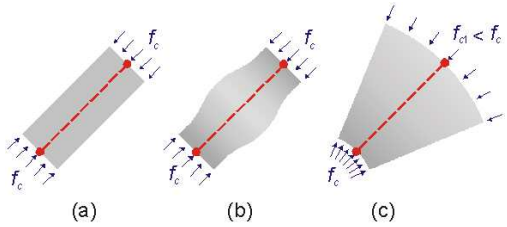

Figure 5.6: The compression stress fields are classified as 'prismatic' or 'parallel' stress fields(a), 'bottle-shaped'(b) and 'fan-shaped' (c).

The struts and nodes, representing compressed concrete zones, have different behaviour depending on the stress field and crack pattern. In the nodal zones the centre lines of the struts and ties and lines of action of any external loads (loads or reactions) must coincide, meaning that there are no moments in the nodes which are classified as 'smeared' or 'continuous' where wide concrete stress fields join each other or meet well distributed reinforcing bars, and 'singular' or 'concentrated' where concentrated forces (loads or reactions) are applied.

The compression stress fields are classified as 'fan-shaped', Figure 5.6(c), 'bottle-shaped' and 'prismatic', Figure 5.6(b), or 'parallel' stress fields, Figure 5.6(a). The fan-shaped zone is an idealisation of a stress field with straight struts converging to a point with negligible curvature or transverse stresses. The bottle shape is an idealisation of a stress flow where the compression stresses spread developing transverse stresses. The prismatic or parallel stress field occurs when the compression stresses are parallel and do not develop transverse stresses. The parallel stress fields are characteristic in B regions, where the stress trajectories are smoother than in D regions. The fan and bottle shaped stress fields are frequently found in D regions where concentrated forces spread out, or where geometric discontinuities cause large changes in the stress fields. The bottle-shaped field is normally not used because of its complexity and its reliance on concrete tensile strength. Schlaich et al [5-9] suggest that compressive struts should be orientated to approximate the flow of stress obtained from an elastic analysis. It is proposed that the ultimate limit state and serviceability in the cracked state should use one and the same model.

5.3.5 - Design factors for STM

Rogowsky and MacGregor[5-10] observed that if the chosen strut directions differed excessively from the elastic distribution, full redistribution might not occur and the strut could fail prematurely.

The strength of the struts and nodes are dependent on the multiaxial state of stress and are generally represented by $f_c^* = \nu f_c$ where ν is called the efficiency or effectiveness factor and f_c is the concrete compressive strength.

Schlaich and Schafer [5-9] suggest that the average compressive stresses at the node boundaries should be limited to $f_{cd}^* \leq 1.1 f_{cd}$ in nodes where only compression struts meet, creating a 2 or 3 dimensional state of compressive stresses;
$f_{cd}^* \leq 0.8\, f_{cd}$ in nodes where tensile bars are anchored and allowance in strength must be made for bond action.

For the strut stresses they suggest the following efficiency factors:

$f_{cd}^* \leq 1.0 f_{cd}$ for undisturbed and uniaxial state of stress;

$f_{cd}^* \leq 0.8 f_{cd}$ for compression fields with cracks parallel to the compression stresses;

$f_{cd}^* \leq 0.6\, f_{cd}$ for compression fields with skew cracks;

where f_{cd} is the concrete compressive design strength for uniaxial compression. The increased strength due to 2 or 3 dimensional states of compressive stresses may be considered if transverse compressive stresses are acting simultaneously.
Nielsen and colleagues [5-4] have proposed a web effectiveness parameter dependent on the concrete strength:

$f_c^* = [0.7 - (f_c/200)]\, f_c$ MPa

Marti [5-5] recommended an effective concrete compressive strength f_c equal to 0.6 f_c.
He suggested that if a refined assessment of f_c^* is desired, it should be based on a consideration of the strains associated with the assumed stress field.

Walraven and Lehwalter's [5-11] analysis showed that the capacity of the struts in short members without shear reinforcement strongly depends on the concrete quality, the width of the loading area and slenderness ratio a/d. They compared the capacity of the concrete struts, calculated for varying values of a/d and the ratio of loading plate width to effective depth, with the value 0.6 f_c as recommended as a stress limit in design calculations. They concluded that 0.6 f_c is a more reliable lower limit.

Collins and his co-workers [5-12] related the principal compressive stress in the concrete to both the principal compressive strain ε_2 and the principal tensile strain ε_1.

$f_{c2} = f_{c2max} [2 (\varepsilon_2/ \varepsilon_c') - (\varepsilon_2/ \varepsilon_c')^2]$ **5.1**

where

$f_{c2max}/ f_c = 1/ [0.8 - 0.34(\varepsilon_1/ \varepsilon_c')] \leq 1.0$ 5.2

with ε_c' the strain in concrete at peak compressive stress, usually considered equal to -0.002,

$f_{c2max} = 1/ (0.8+170\, \varepsilon_1)\, f_c \leq 1.0\, f_c$

Placas and Regan [5-13] carried out an extensive test programme for the investigation of the shear resistance of reinforced concrete beams. They observed that in beams provided

with stirrups there were two primary modes of shear failure: shear compression involving a criterion of compression failure in the concrete and shearing failure involving mainly vertical displacements across shear cracks. In the latter case it was observed that the interlock forces tend to produce flatter cracks until an inclination of around 26° when vertical stirrups are used and around 18° when 45° inclined stirrups are provided.
These values suggest the lower limits for the strut inclination. MacGregor [5-7] suggests that, in design, the value of θ should be in the range of 25° to 65°. Grob and Thurlimann [5-3] proposed limits for θ equal to 26.6° and 63.4°, whereas, instead of restricting limits of θ, Collins and Mitchell [5-14] related the strut angle to the concrete strength and the concrete strains.

5.3.6- Load spreading angle

Wight and MacGregor [5-35] recommend the load spreading angle is primarily a function of the ratio of the width of the loading plate, *a*, to that of the loaded member *b*.

Analysis [5-15] shows that the angle between the load and the inclined struts varies from 28° for a concentric load with *a/b* = 0.10, to 19° for *a/b* = 0.2, and down to about 12° for *a/b* = 0.5. As a result, the transverse tie in Figure 5.7 (b) would correspond to strut slopes from 1.9 to 1 for *a/b* = 0.1, to 2.9 to 1 for *a/b* = 0.2, and to 4.7 to 1 for *a/b* = 0.5. Similar values are obtained for other cases of load spreading, such as concentrated loads acting near one edge of a member or multiple, concentrated loads. A strut slope of 2:1 (longitudinal to transverse), as recommended by the ACI Codes, is conservative for a wide range of cases.

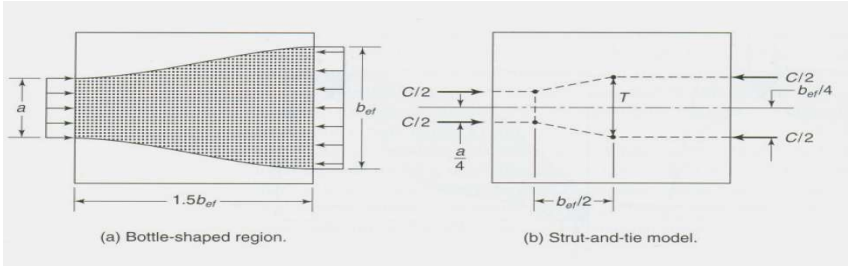

Figure 5.7: Spread of stresses in strut

Wight and MacGregor [2008][5-35]

The STM model should represent a realistic flow of forces from the loads through the D region to the reactions. Frequently this can be determined by observation. From an elastic stress analysis , such as a FE analysis, it is possible to drive the stress trajectories in an uncracked D region, as shown in Figure 5.8 (a) for a deep beam.

5.4 Review of design codes

STM design provisions consist of rules for defining the dimensions and ultimate stress limits of struts and nodes as well as the requirements for the distribution and anchorage of reinforcement. Guidelines in Comité Euro-International du Béton [5-16], FIP Commission 3, Practical Design of Structural Concrete [5-17] and Eurocode EC2 [5-18] for design by the STM have been developed for European practice.

Provisions for the STM have been incorporated in the Canadian Concrete Design Code [5-19] since 1984 and in the AASHTO LRFD[5-20] code since 1994. Another specific set of provisions has been developed to be included as an alternative design procedure in the 2002 ACI code [5-21].

Author or Code	Zutty [5-34]	ACI-ASCE [5-22]	ACI-318 [5-23]	Taylor [5-3]	BS8110 [5-24]	CAN 3 [5-25]	CEB-FIP 90 [5-16]
a/d Limit	2.5	2.0	2.2	2.0	2.0	3.	3

Table 5.1: Upper limit for a/d recommendations by codes and researchers for the development of sufficient arching action for development of STM

Table 5.1 shows that the majority of codes and past research recommend $a/d \leq 2.5$ in order to ensure the development of arch action. However, the Canadian code [5-25] recommends the angle of the strut $\theta \geq 15^{o}$ and CEB-FIP MC90 [5-16] limits the angle of the strut $\theta \geq 18.4^{o}$. EC2 [5-18] proposal is based , with some variations, on the CEB-FIP MC90 [5-16].

5.4.1 - CEB-FIP Model Code-90 [5-16]

In this code, discontinuity regions are defined as the regions near concentrated loads if

$a < z\cot\Theta$, where a is the shear span, z is the lever arm and Θ is the angle of the diagonal concrete strut to the chords, limited to $18.4^{\circ} \leq \Theta \leq 45^{\circ}$.

If $\Theta = 18.4^{\circ}$ is contemplated, the discontinuity regions are considered when a < 3 z. Considering z as approximately 0.9 d, the discontinuity regions occur at a < 2.7 d that is slightly higher than the shear span ratio adopted by other codes to define short beams. CEB-90 suggests, for short spans, the STM shown, Figure 5.9.

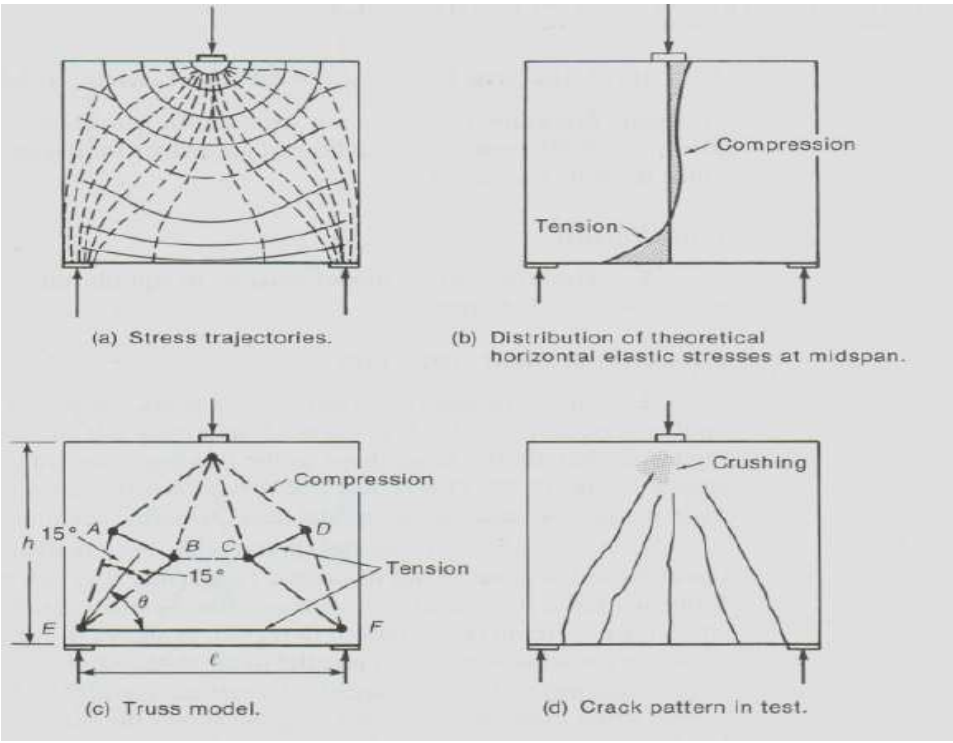

Figure 5.8: Single span deep beam supporting concentrated load
Source: Schlaich, J and Weischede, D [1982][5-15]

The CEB-FIP Model Code-90 [5-16] presents simplifications of the basic constitutive laws that are appropriate to use in STM. The design resistance of a zone under essentially uniaxial compression may be determined by means of a simplified uniform stress diagram over the full area of the strut considered. The average stresses recommended are as follows, with f_{ck} in MPa: for uncracked zones

$f_{cd1} = 0.85(1-f_{ck}/250)\ f_{cd}$ **5.3**

for cracked zones where the compressive resistance may be reduced by the effect of transverse tensile strains

f_{cd2}= 0.6(1-f_{ck}/250) f_{cd} **5.4 .**

The same concrete stress limits are considered for nodes - f_{cdl} for nodes where only compression struts meet or where the angle between the compression and the tie is more than 55°, and f_{cd2} for nodes where main tensile bars are anchored.

The inclination of the struts in the web of a beam resisting shear and axial action effects is said to be chosen freely in the range of 18.4° to 45°. It is not very clear in the code but it seems to refer only to B regions as in fan shaped stress fields, or D regions in general, where the cracks form from low values of θ to an almost vertical direction. Based on truss models and the limit stresses f_{yd}, f_{cdl} and f_{cd2}, CEB-90 presents equations to calculate the acting forces and the corresponding resisting forces in the ties and struts, according to the chosen angles of the concrete struts (θ) and of the transverse ties *(α)*- see CEB- 90 [5-16] - subsection 6.3.3.2.

The discontinuity regions are subdivided in two different zones - the discontinuity region itself, named D2, and the nearby transition region between B and D2 regions, named Dl. CEB-90 suggests the calculation of forces in transition regions D1 should be made as in B regions.

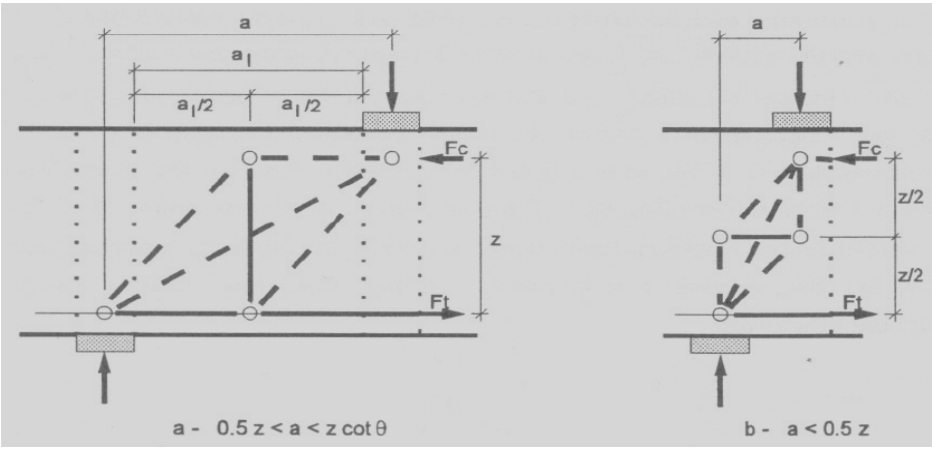

Figure 5.9: CEB-FIP MC90 [5-9] Standard Discontinuity Regions

Source: CEB-FIP MC90 [5-9]

5.4.2- The Canadian Code [5-25]

This code does not deal explicitly with 'short beams' but with discontinuity regions. Discontinuity regions in beams are defined as the regions near concentrated loads. The angle of the diagonal concrete strut to the chords is limited to $15^{\circ} \leq \Theta \leq 75^{\circ}$.

If $\Theta = 15^{\circ}$ is contemplated, the discontinuity regions are considered when $a < 2.8\ z$. z is approximately 0.9d, therefore, $a/d < 3.1$.

The series of 11 beams tested by this writer have d=265mm and a=800mm or a/d= 3.02 which lies within the allowable limits specified by the Canadian code.

In this chapter, the STM is used for shear analysis of this writer's experimental HSC beam which has stirrups and HWB and is defined as HSC3 and the results of these STMs are compared with those of numerical FE models from Chapter 4.

The Canadian Code [5-8] bases its recommendations on the equations derived by Vecchio and Collins [5-42] from tests of large scale panels subjected to uniform stress and strain fields.

The diagonal crushing strength of the concrete, f_{c2max},may be computed as

$$f_{c2max} = f_c \lambda\varphi_c / (0.8+170\ \varepsilon_1) \leq 1.0\ \lambda\varphi_c\ f_c \qquad \mathbf{5.5}$$

where λ is a factor to account for low density concrete, φ_c is the resistance factor for concrete and f_c is the cylinder compressive strength of concrete.
The effectiveness factor is a function of the transverse strain ε_1 which may be computed as

$$\varepsilon_1 = \varepsilon_x + [\ (\varepsilon_x + 0.002)/\tan^2\theta] \qquad \mathbf{5.6}$$

where ε_x is the longitudinal strain at mid-depth of the member (positive when tensile). In lieu of determining ε_x its value may be taken as 0.002 and, in this case, ε_1 is simply a function of the strut inclination θ . The angle θ may be chosen to have any value between 15° and 75°.

When a tension tie crosses a compressive strut the tensile strain ε_1 can be related to the average tensile strain of the bar, ε_s , and the angle between the tie and the strut, α_s,by

$$\varepsilon_1 = \varepsilon_s + [(\varepsilon_s + 0.002)/\tan^2 \alpha_s] \qquad \textbf{5.7}$$

The strain ε_s is suggested to be conservatively taken as f_y/E_s.
The concrete compressive stresses in the nodal zones are limited to

$0.85\varphi_c f_c$ in nodal zones bounded by compressive struts and bearing areas;
$0.75\ \varphi_c f_c$ in nodal zones anchoring only one tension tie;
$0.60\ \varphi_c f_c$ in nodal zones anchoring tension ties in more than one direction.

The Canadian Code[5-8] guidance is comparatively complicated for design use since the transverse strain ε_1 is not easy calculated and can not simply be presented as a function of ε_x and θ as explained above. Also if the value of ε_x is taken as 0.002, this will result in ε_1 becoming a function of angle θ. It has been suggested that ε_1 can be taken as a function of ε_s which is the average strain of the tie crossing the strut, and α_s. In discontinuous regions 'longitudinal strains'(ε_x) does not have a clear meaning.

Although STM can be designed for HSC beams with HWB and stirrups for $a/d \leq 3.1$ to the Canadian code [5-25], for the above reasons it is recommended to use stress trajectories from FE analysis, as will be shown in section 5.6.

5.4.3- ACI 318 Code [5-23] 2008 edition

Currently the American Concrete Institute (ACI) introduces the STM as a design method for D region problems. The provisions consist of five sections and are presented in Appendix A, and summarized as follows:

1. Rules in selecting STM

STM representing idealized load-transfer mechanism in the D region under consideration is to be selected (A.2.1). The selected STM should consist of struts, ties, and nodes (A.2.1) and has to be in equilibrium with the forces acting on the D region (A.2.2). The finite dimensions of

STM components, representing the stress fields of struts, ties, and nodes, should be considered (A.2.3). Tie stress fields can cross strut stress fields (A.2.4). To avoid severe strain incompatibility between struts and ties, the angle between a strut and a tie framing into a node cannot be smaller than 25 degrees (A.2.5).

2. Strength Requirements

The STM components must have sufficient capacity to resist the force demand such that (A.2.6)

$\varphi F_n \geq F_u$

where:

φ= strength reduction factor,

F_n=nominal strength of strut, tie, or node, and

F_u=factored force demand of the strut, tie, or node.

a) Strut Strength (ACI A.3)

The nominal strength of a strut, F_{ns} , is defined as

$F_{ns} = f_{cu} A_c$ **5.8**

where:

f_{cu} = effective compressive strength and

A_c = cross sectional area at the end of the strut.

The effective compressive strength, f_{cu} , is defined as

$f_{cu} = 0.85\beta_s f_c'$ **5.9**

where:

β_s = 1.00 for prismatic struts in uncracked compression zones,

βs = 0.40 for struts in tension members,

βs = 0.75 if struts may be bottle shaped and crack control reinforcement is included,

βs = 0.60 if struts may be bottle shaped and crack control reinforcement is not included, and

βs = 0.60 for all other cases.

The crack control reinforcement requirement is $0.003 \leq \Sigma \rho_{vi}$, where ρ_{vi} is the steel ratio of the i^{th} layer of reinforcement crossing the strut, and γ_i is the angle between the axis of the strut and the bars.

b) Tie strength (ACI A.4)

The nominal strength of a non-prestressed reinforcement tie, F_{nt}, is defined as

$F_{nt} = f_y A_s$ **5.10**
where:

A_s=area of steel reinforcement and

f_y=yield strength of steel reinforcement.

c) Node Strength (ACI A.5)

The nominal strength of a nodal zone, F_{nn} , is defined as

$F_{nn} = f_{cu} A_n$ **5.11**
where:

f_{cu} =effective compressive strength and

A_n =area of a nodal zone face in which the force is framing, measured perpendicular to the direction of the force.

The effective compressive strength, f_{cu}, is defined as

$f_{cu} = 0.85\beta_n f_c$'5.12
where:

β_n = 1.00 if nodes are bounded by struts and/or bearing areas,

β_n = 0.80 if nodes anchor only one tie, and

β_n = 0.60 if nodes anchor more than one tie.

3. Anchorage Requirements (ACI A.4.3)

The tie reinforcement must be properly anchored in the nodal regions at the ends of the tie such that the corresponding tie force can be developed at the point where the centroid of the reinforcement in the tie leaves the extended nodal zone which is a region bounded by the intersection of the effective strut width and the effective tie width.

4. Serviceability Requirements (ACI RA.2.1)

Design based on STM should satisfy the serviceability requirements. Provisions in the body of the code can be applied.

5.4.4- The Fédération Internationale du Béton FIP [5-26]

Recommendations published in September 1999 are based on the CEB-FIP Model Code 1990

(MC 90) to which frequent reference is made in the right-hand margins throughout the document. They also refer to later CEB Manuals as well as further FIP publications. For all types of structural concrete using normal weight aggregates, plain or reinforced, pre-tensioned or post-tensioned tendons, or combinations of all these types of reinforcement, they explain member design and detailing by means of STM.

Separate chapters deal with principles, material characteristics, technological details and durability requirements, strength of ties, struts and nodes of STM, ultimate limit state design, serviceability state design, and structural members. The former FIP Commission 3 wished this document to be of interest to consultants, contractors and authorities by enhancing the direct application of STM as a consistent design and detailing tool.

5.4.5- Eurocode 2: Design of Concrete Structures [5-18]

Design recommendation of Eurocode 2 for RC members is based on limiting the value of the angle θ of the inclined struts in a web as $1 \le \cot\theta \le 2.5$.
For members with stirrups , the shear resistance, V_{Rd} is the smaller value of:

$$V_{Rd,s} = \frac{A_{sw}}{S} Z f_{ywd} \cot\theta \qquad \textbf{5.13}$$

and

$$V_{Rd,\max} = \alpha_{cw} b_w z \nu_1 f_{cd} / (\cot\theta + \tan\theta) \qquad \textbf{5.14}$$

where

A_{sw} is the cross-sectional area of the shear reinforcement

s is the spacing of the stirrups

f_{ywd} is the design yield strength of the shear reinforcement

ν_1 is a strength reduction factor for concrete cracked in shear

α_{cw} is a coefficient taking account of the state of the stress in the compression

$$\nu_1 = 0.6\left[1 - \frac{f_{ck}}{250}\right] \qquad \textbf{5.15}$$

with f_{ck} in MPa is recommended
If the design stress of the shear reinforcement is below 80% of the characteristic yield stress $f_{ywk,}$ ν_1 is given as:

ν_1=6 for $f_{ck} \le 60$ MPa, in this case f_{ywd} should be reduced to 0.8 f_{ywd}

The recommended value of α_{cw} is as follows:

$\alpha_{cw} = 1$ for non-prestressed structures

$\alpha_{cw} = (1+\sigma_{cp}/f_{cd})$ for $0< \sigma_{cp}<0.25\ f_{cd}$

$\alpha_{cw} = 1.25$ for $0.25\ f_{cd} < \sigma_{cp}<0.5\ f_{cd}$

$\alpha_{cw} = 2.5(1- \sigma_{cp}/f_{cd})$ for $0.5\ f_{cd} < \sigma_{cp}<1.0\ f_{cd}$

where

σ_{cp} is the mean compressive stress, measured positive, in the concrete due to the design of axial force. This should be obtained by averaging it over the concrete section, taking account of the reinforcement.

The value of σ_{cp} need not be calculated at a distance less than $0.5d\cot\theta$ from the edge of the support.

The maximum effective cross-sectional area of the shear reinforcement , $A_{sw,max,}$ for $\cot\theta=1$ is given by:

$$\frac{A_{sw,\max} f_{ywd}}{b_w s} \le \frac{\alpha_{cw} \nu_1 f_{cd}}{2} \qquad \textbf{5.16}$$

The additional tensile force, ΔF_{td}, in the longitudinal reinforcement due to shear V_{ED} may be calculated from:

$\Delta F_{td}=0.5\ V_{ED}(\cot\theta)$ **5.17**

where $(M_{ED}/Z) + \Delta F_{td}$ should be taken as not greater than $M_{ED,\ max}/Z$, where $M_{ED,\ max}$ is the maximum moment along the beam.

5.4.6-Codes and past research guidance on the inclination of struts

When considering reduction factors for compressive struts, Nielson et al [5-**Error! Bookmark not defined.**] proposed a reduction factor of 0.45 to be taken for uncracked region of concrete of 50MPa instead of the factor of 0.6 which is the lower bound compressive strength recommended by most design codes. This difference in magnitude of the reduction factors suggests that further research for finding a more accurate value for reduction factors for HSC is needed.

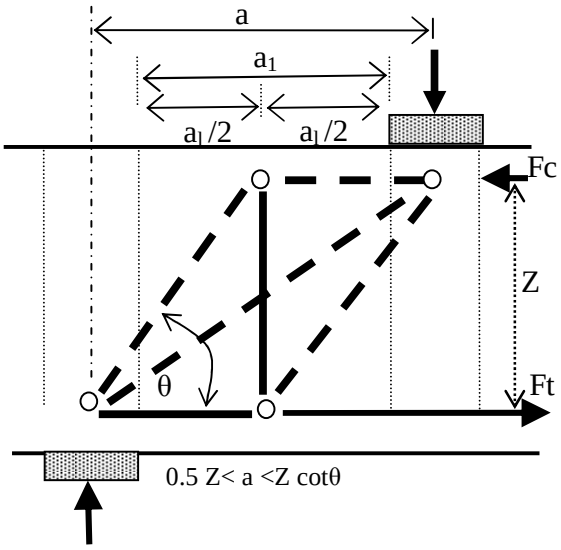

Figure 5.10: CEB-FIP MC90 standard discontinuity region, where 18.4º≤θ≤45º

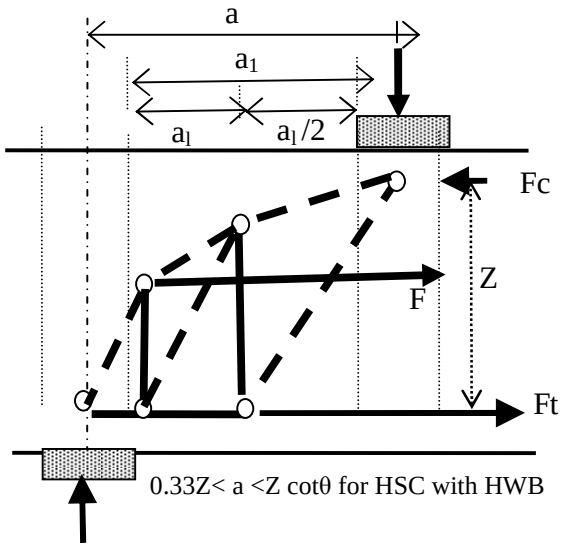

Figure 5.11: This writers' proposed model for HSC beams a/d≤3.02 with HWB and stirrups 18.4º≤θ≤45º

Code or researcher	Min θº	Max θº	Remarks
CEB-FIP-MC90[5-16]	15.0	45.0	The upper limit is for B region
ACI-318-08 [5-23]	19.7	-	General recommendation
EC2 [5-18]	21.8	45.0	General recommendation
CAN3-A23.3-M84[5-25]	15.0	75.0	General recommendation
Placas and Regan[5-13]	26.7	-	Slender beams with vertical stirrup
	18.3	-	Slender beams with 45º inclined stirrup
Rogowsky& MacGregor [5-10]	25.0	65.0	General recommendation
Grob and Thurlimann [5-3]	26.6	63.4	General recommendation
Collins et al [5-27, 28]	θ depends on concrete strength and strain		
Ortiz[5-42]	Min θ=25º, increase in max θ favorable to the node resistance		
This researcher	Min θ=18.5º, for HSC with HWB and stirrup and increase in max θ favorable to the node resistance		

Table 5.2: Minimum and maximum recommendations for the strut inclination

5.5 Literature review on short beams

The shear resistance of beams subjected to concentrated loads varies considerably with the shear span/effective depth ratio *(*a/d*).* Regan [5-29] described 'short beams' as supported beams subjected to a concentrated load on top and supported underneath within a distance of less than 2.5 d (a/d < 2.5).

Principal characteristics for short beams are:

- Shear cracks are not the product of flexural cracks but form independently near mid -height. There is generally only one dominant shear crack. Transverse forces can be supported directly by arching action in the concrete without causing shear stresses in the concrete at the head of the shear crack. The support at the bottom surface of the beam can restrain the concrete cover and considerable dowel action can develop.

- The failure of short beams occurs when the compression zone is crushed over the inclined cracks. This failure mode is referred to as shear compression failure. The inclined crack can extend high into the beam, reaching the loading zone, and local crushing of the concrete is likely to occur as well as crushing of the strut itself, see Figure 6-10a.

- The ability of short beams to carry load after the development of inclined cracks is due to the compressive resistance of the diagonal strut. In some cases the failure can occur when the inclined crack separates the strut into two parts, Figure 5.12b.

- Bond failure as a consequence of dowel action is possible. For a/d ratios over 2.0 (low Θ) the dowel effect at the inner side of the support can originate a splitting crack that runs along the reinforcement leading to a loss of bond, Figure **5.12**c.

Kani [5-30, 31& 32] developed 'The Rational Theory of Diagonal Failure', based on a large number of test results. The graphs of test results he obtained presented two different functions intersecting at a/d = 2.5. Each function represented a different failure mechanism.

He considered the cracked beam as a 'comb-like' structure increasing the loading of the tensile zone of the beam which is transformed into a series of vertical concrete teeth separated by cracks. He analysed the resistance of the beam considering the resistance of such concrete teeth. For a/d> 2.5 the diagonal failure occurred when the inclined cracks appeared as the capacity of the concrete teeth was reached.

In beams with a/d < 2.5 Kani observed the formation of an internal arch from the loading point to the support. These beams developed inclined cracks but still were able to carry additional load by the strut running from the load to the support.

Zsutty [5-33 &34] developed a combination of dimensional analysis and statistical regression analysis to provide an empirical basis for the separation of test beam behaviour into the arch action and the beam action of slender beams. With a large number of test data of reinforced concrete beams without shear reinforcement, he fixed the value of a/d = 2.5 as the means of separating the test beam results into arch action and beam action.

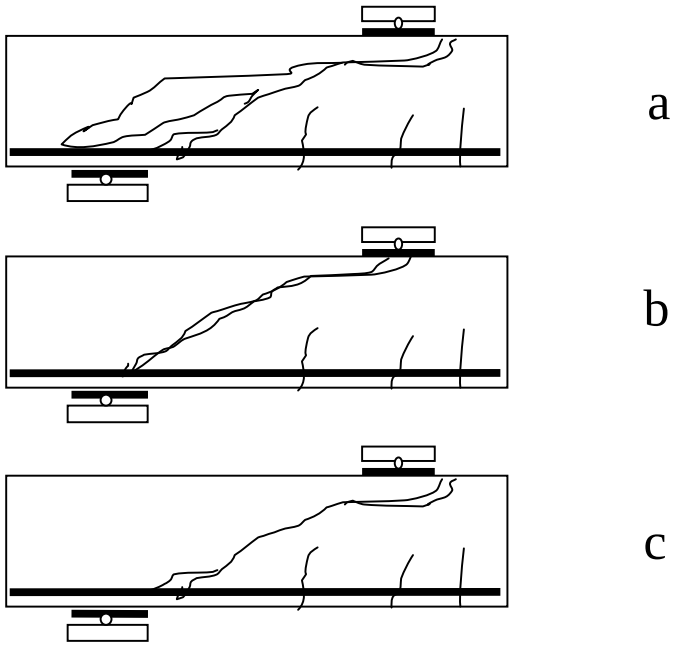

Figure 5.12: Shear failure in short beams
Source: Regan P.E, April 1971

He also suggested that the extra strength of arch action was only a function of beam properties but also depends on the manner of load application and beam support, and said that an accurate representation of the top and bottom pressures due to load and support conditions might be the dimensions of the load and support blocks or plates and their position in the short beam shear span.

Therefore, beams loaded on their top and supported at their bottom surfaces with a/d<2.5, where the arch action prevails, are called short beams .

5.5.1 - Influence of the width of the support plate on the node dimension

With STM the node dimensions can be decided in relation to the width of the support such as the strut model proposed by Ortiz for the short beam, Figure 5.13, which takes β= 56.3° or = atan (1.5) from experimental work.

Reviewing Ortiz' idealised support, it appears that β is larger than Θ resulting in a wider strut than Wight's model, Figure 5.15. Ortiz considers frictional force on the reinforcement along the short distance of 'C tan β', Figure 5.13, next to support plates to change the width of the strut. She assumes that tan β=1.5 and noted in her final conclusion that this assumption was based on experimental values, but does not specify the experimental measurements details, whereas Wight's approach resolves the forces at the support with a simplified direct struts.

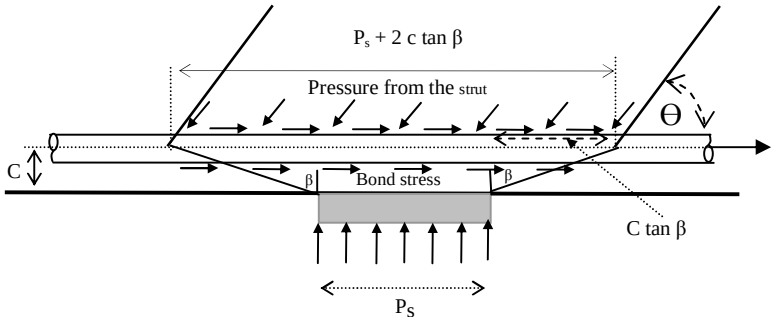

Ortiz' proposed Model

Figure 5.13: Idealised support node proposed by Ortiz [Error! Bookmark not defined.**]**

5.6 STM of beam due to arching

The arching action is dependent on the shear span to depth (a/d) ratio, presence of stirrups , strength of concrete and presence of HWB. In the following sections, the influence of these parameters on beams are discussed.

5.6.1- Beams with a/d ratio smaller than 2.5

When considering short beams of $1 \leq a/d \leq 2$, a direct inclined strut from loading to support plate is formed and this is demonstrated in an analysis of the experiments on two beams by Ortiz [5-42] in Chapter 7, data from which will be used for calibration of FE with STM models. STM models for beams of $1 \leq a/d \leq 1.5$ are shown in Figure 5.14.

When STM is for $2 \leq a/d \leq 2.5$ for beams with stirrups, the inclined deflected strut forms similar to that in Regan's model [5-42], Figure 5.16.

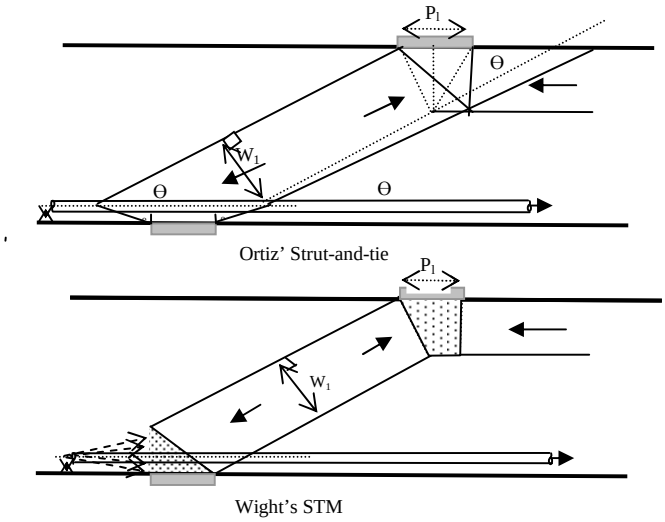

Figure 5.14: STM proposal by Ortiz [5-42] and Wight [5-35]

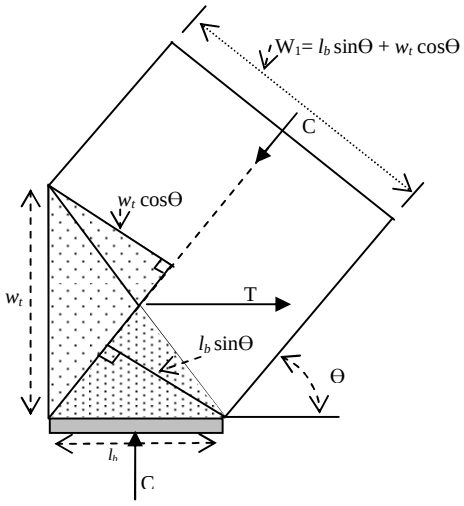

Figure 5.15: Width of inclined strut at node according to Wight's [5-35] proposal

Adopted from Wight [5-35], 2009

As suggested by Regan [5-29], the principal characteristic of short beams are shear cracks which are not the product of flexural cracks but form independently near mid-height. There is generally only one dominant shear crack. Transverse forces can be supported

directly by arching action in the concrete without causing shear stresses in the concrete at the head of the shear crack. The support at the bottom surface of the beam can restrain the concrete cover and considerable dowel action can develop.

As suggested by Regan [5-29], the principal characteristic of short beams are shear cracks which are not the product of flexural cracks but form independently near mid-height. There is generally only one dominant shear crack. Transverse forces can be supported directly by arching action in the concrete without causing shear stresses in the concrete at the head of the shear crack. The support at the bottom surface of the beam can restrain the concrete cover and considerable dowel action can develop.

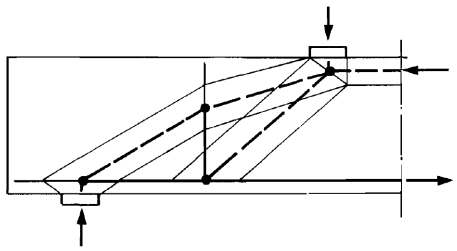

Figure 5.16: Combination of arch and truss effects in a detailed model of short shear span beams with stirrups as suggested by Regan [5-36].
Source: Regan [5-36]

Figure 5.22 shows that HSC beams with stirrups and HWB of shear span to depth ratio (a/d=3.05) have crack formation as that described for short beams by Regan [5-29] or beams of a/d≤2.5. However, the Canadian code [5-25], considers short beams to be a/d<3.05.

5.6.2 - Beams with the a/d = 3 with stirrups

In the STM approach for the cases when the beam is of HSC with stirrups and with HWB, the direction of the compression inclined strut developed in the beam 2.5 ≤ a/d≤3 is influenced by the presence of the HWB and this influence is also a function of the compressive strength of the concrete.

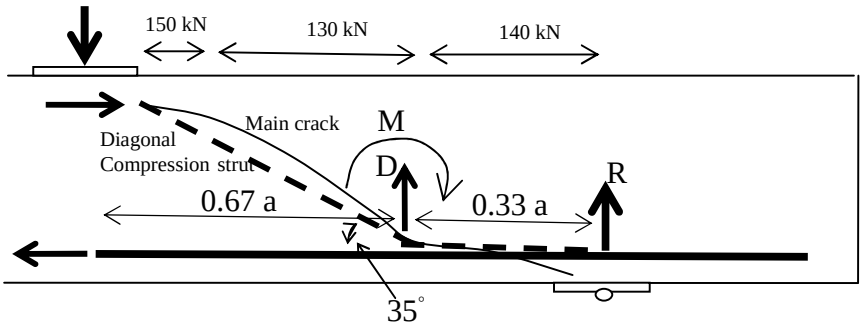

Figure 5.17: Beam NSC1 with stirrup and without HWB after failure.

When the beam is NSC1 of a/d=3.02, with stirrups and without HWB, the strut and tie action does not develop, Figure 3-18 and Figure 5.17. The upper part of the crack develops at 150 kN before the failure load of 160 kN which is due to the increased moment M from the dowel force D, activated at 140 kN after the dowel crack formed along the reinforcement .

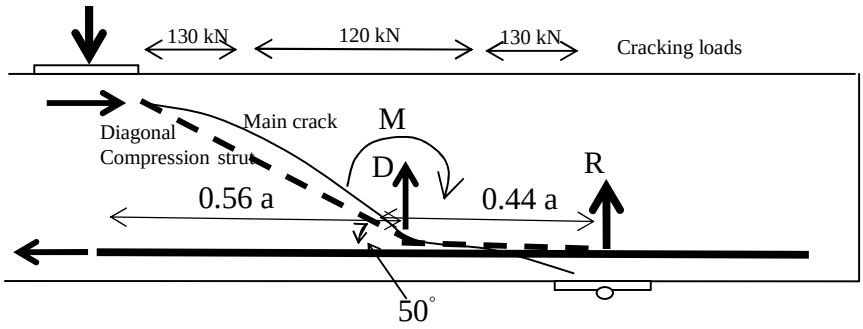

Figure 5.18: Beam HSC1 with stirrup and without HWB after failure

In HSC structures, shear cracking resistance will comparatively be low because of the weakness or the lack of aggregate interlock or aggregate type and for this reasons the shear resistance capacity in HSC may be lower than that in NSC.

For HSC1 of a/d=3.02 the strut and tie action does not develop, Figure 3-12 and Figure 5.18. Just before the failure load 140 kN, at 130 kN the upper part and the lower part of the crack develops. The maximum moment is shifted to 0.44d from support compared to 0.33a in the case of NSC1. The maximum moment from dowel action occurs close to mid shear span therefore producing the final failure cracks at the top as well as the bottom.

5.6.3- HSC Beams with a/d ratio of 3 with stirrups and HWB

In beam HSC4 of a/d=3.02 with 2T25 HWB, dowel resistance depends on concrete strength.

At an unknown location in the shear span on the HWB, where the maximum dowel moment develops from the dowel force D_{hwb}, this moment deflects the inclined strut, which improves the arching action and results in yielding of tension reinforcement, Figure 5.19.

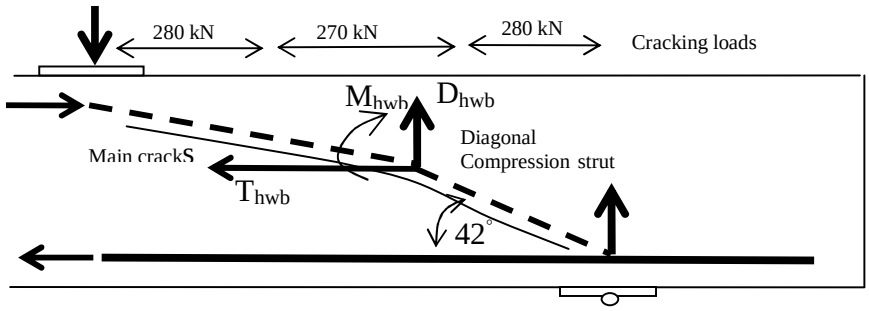

Figure 5.19: Inclined compression forces deflect in HSC4 beams with HWB of a/d ≈3.02 .

In beam HSC4, Figure 5.19, at 280 kN at the upper part of the crack and at 260 kN at the lower part of the inclined main cracks develop just before the failure load of 300 kN due to the moment M_{hwb} which is produced by dowel force D_{hwb} resulting in failure due to maximum moment after arching action has taken place.

At failure stage, presence of HWB produces many scattered cracks parallel or near to the main crack close to failure loading, which results in more ductile and gradual failure rather than sudden failure due to the formation of one main crack and the absence of HWB. When HWB is present, the energy from the increasing load is dispersed across the shear span in the form of numerous cracks, Figures 3-9 to 3-11 and Figures 3-13 to 3-15. The ductile failure due to the presence of HWB is in contrast with the sudden failure due to rapid transfer of energy from increased loading into a single large crack producing a brittle and sudden failure when no HWB is present, Figures 3-8 and 3-12.

It should be noted that when HWB was introduced in the HSC beam the load bearing capacity nearly doubled and the cracks width was restrained, allowing the development of full arching capacity of the structural system.

The action causing this deflection of the strut is demonstrated by investigating the strain gauge readings of the experimental results on top and bottom of the HWB within the shear span, near where the deflection of strut occurs, Figure 3.37, Appendix C.

The upper limit of a/d=3 may be increased for HSC beams with HWB, which has more effect on arching capacity than on shear cracking resistance. However, weak aggregate and/or weak aggregate interlock will significantly reduce the shear resistance capacity of HSC beams without HWB.

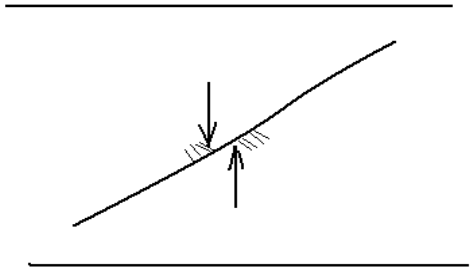

Figure 5.20: Contrary to the simple picture of performance of dowel action on flexural cracks, dowel forces are difficult to visualize at inclined cracks bearing on weak wedges of concrete

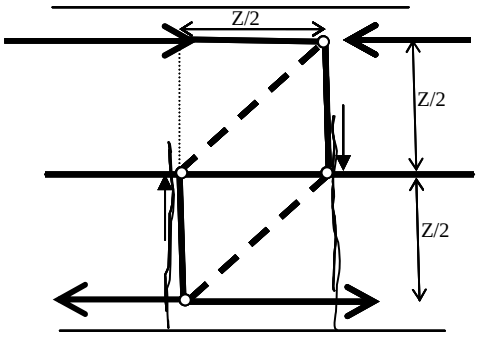

Figure 5.21: It is complicated to clearly envisage the dowel action within the main internal structural system comprising of stirrups and HWB and its transmission of forces on weak wedges of concrete

Dowel forces are reasonably easy to visualize at flexural cracks, but very complex to picture when they act on inclined cracks, Figure 5.20. It is difficult to propose actions by which they can be transmitted into the main internal structural system. Certain assumptions based on visualizing dowel actions on inclined cracks resembling dowel action in flexural cracks need to be introduced. Also the complex interaction of the dowel action from the HWB, diagonal compression from HSC and the tensile force in the stirrup need to be simultaneously

considered and visualized to understand their interactions, Figure 5.21.

The improved shear performance of HSC beams with stirrups and HWB of a/d=3.02 is mainly due to dowel forces from the HWB where they bear on strong wedges of concrete supported by the stirrups. The actions from these wedges are assumed to be transmitted into the main internal structural system to deflect the diagonal compression, Figure 5.21. This additional internal structural system within the length of 0.5z can be assumed to increase the STM action from the conventional a/z=2.5 to 3.

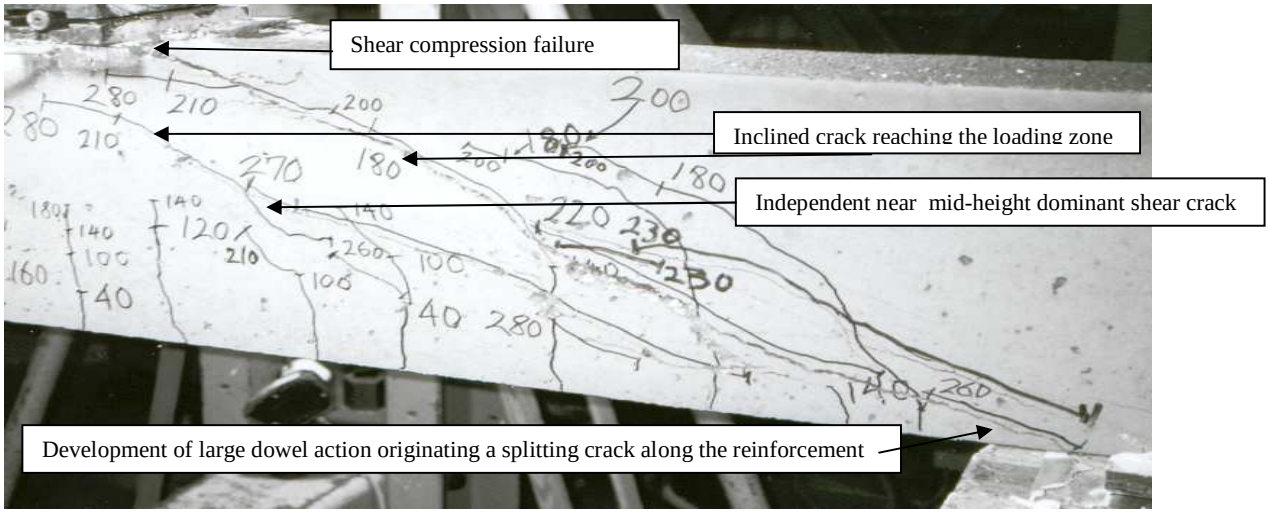

Figure 5.22: Beam HSC4 shows the characteristics identified by Regan [5-29] for short beams.

When the ratio of stirrups is low a load greater than the shear cracking load can often be resisted by a combination of arching effect and truss actions as long as a/d ≈3, Figure 5.19. The limit is not an exact one but tends to increase with increasing concrete strength, which has more effect on arching capacity than on shear cracking resistance. To propose a STM based on failure criteria is complex as STM is lower-bound plastic theory and does not have any compatibility condition.

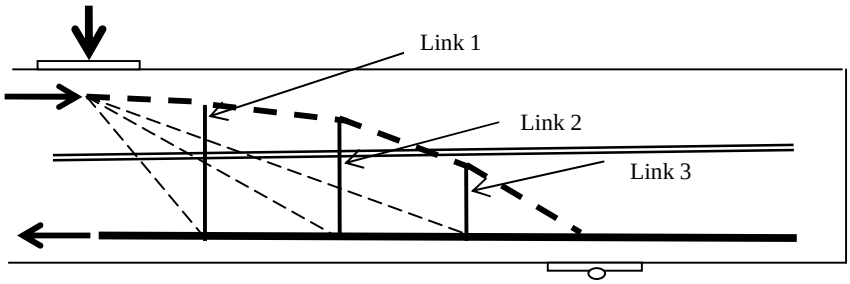

Figure 5.23: Combination of arch and truss actions as long as a/d ≈3. Forces produced by HWB are not shown.

HWB significantly affect the direction of the inclined compression strut in beams of a/d ≈3 when the strength of concrete is high and stirrups are present, Figure 5.23.

5.6.4-Codes' recommendation for upper limit of a/d

It is notable that all the codes give the value $\theta_{lim} \leq 3$, however, this research demonstrates that in HSC beams with shear reinforcement and HWB , if a simple truss model is used, θ_{lim} can be increased to 3.02. This is larger than the upper limit recommendations in all the codes. CEB-FIP90 [5-16] gives the closest prediction; however, it should be amended to give provision for HSC beams with HWB.

Code MC90 [5-16] imposes an upper limit of a/d=3 for STM. However, it will be demonstrated that for HSC beams with stirrups and HWB with a/d=3.02 the full STM action takes place with the yielding of the tension steel, Figures 3.24 to 3.26.

This upper limit of 3.02 is possible for HSC beams with stirrups and HWB, which has more effect on arch capacity than on shear cracking resistance. When beams are a/d=3, in the absence of HWB, the weakness in shear behaviour of HSC resulting from the absence of aggregate interlock and its low shear cracking resistance is apparent. However, many codes do not impose the necessary restrictions for possible shear weakness when $2.5 \leq a/d \leq 3$.

When HWB is introduced the shear cracking resistance significantly improves, the crack width is restrained and full arching capacity is developed. The proposed design rule for dowel action from Chapter 3 allows for prediction of the quantity of HWB in the beam (or CVB in

TBCJ) for shear reinforcement in HSC beams with HWB of a/d=3 or HSC- TBCJ with CV of aspect ratio ≈ 3. The proposed rule may be used with guidance from various codes to predict shear forces when HWB is present.

5.6.5-Location of the maximum moment due to dowel action from HWB

Figure 5.24 shows a variation of the bending moment due to dowel forces on the HWB in beam FE- HSC3 indicating the location of the point of maximum moment on the HWB. The quantitative value of the moments and forces on the reinforcement, HWB, are unrealistically small because full bond at concrete-steel interface is assumed rather than full slippage at the interface therefore the moment at the neutral axis of the RC beam is presented, Figure 5.24. However, the FE model provides valuable information on the location of the maximum moment in the shear span at HWB level. This information is essential for developing STM for the beam.

Future research may attempt to FE model the full slippage for the bond at the concrete-steel interface by introducing links as suggested in chapter 4 in order to obtain realisti values for the moment acting on the HWB after crack formation.

$F_1 \approx F_2 \approx 6620$ N

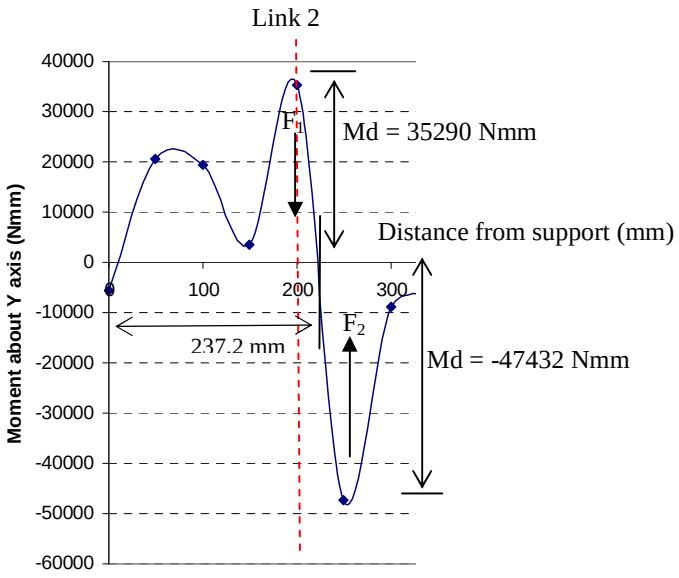

Figure 5.24: Location of maximum bending moment on HWB in beam FE- HSC3

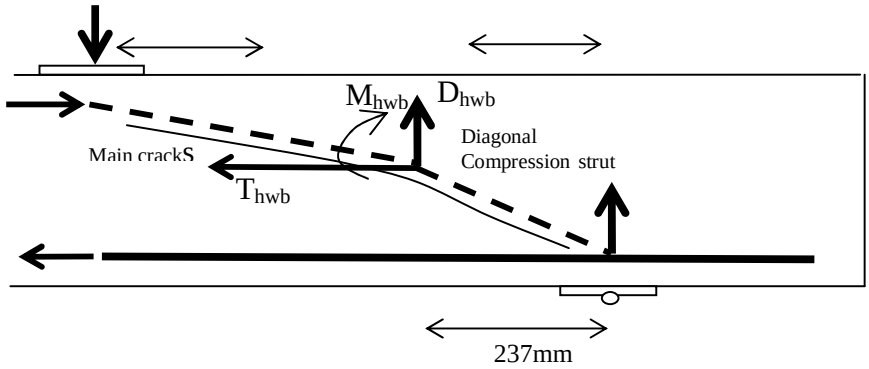

Figure 5.25: Location of maximum moment to deflect the inclined diagonal compression strut

Considering the bending moment diagram produced from the FE model for HSC with HWB in Figure 5.24, the distance from support to point of contra-flexure between the two largest moments acting in opposite directions is 237.2 mm, which is the point where maximum dowel action occurs within the shear span a= 800mm, and is close to 0.3a from support, Figure 5.27.

Compare the quantity of the dowel moments of the FE and the mechanical model the results from proposed dowel prediction rule Table 3.11 are used. The moment produced (M_{hwb}) is 20.7 (kN) x 237mm= 4.9 x10^6 Nmm, which is the moment on the HWB when full slippage at steel concrete interface occurs after the inclined crack is fully develops. The physical value for the moment from mechanical model is much higher than that provided by the FE model, Figure 5.24. This is due to full bonds assumed for the concrete-steel interface when the FE was modelled, however, the location of maximum moment presented is considered to be reasonable and will be used for further analysis and STM.

5.6.6 - Investigation of different load paths in STM

One option for STM of beam HSC3 is shown in Figure 5.26. The total force in the main strut from support of loading point is D_{wi} bearing θ to horizontal and its vertical component is $V_{wi,.}$ The force in the strut due to dowel action is D_{dow} bearing η to horizontal and its vertical component at support at the support is V_{dow}. The force in the strut due to stirrup is D_{ASV} bearing γ to horizontal and its vertical component at support at the support is V_{dow},

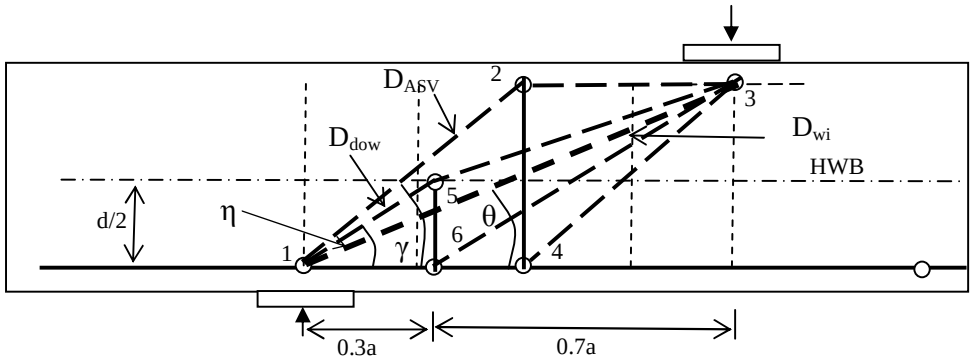

Figure 5.26: STM of HSC beam with HWB of a/d=3. Main strut, 1-3, at angle of θ, strut due to stirrups, 1-2, at angle of γ, strut due to dowel action from HWB, 1-5, at angle of η.

Another possible option for STM of HSC3 is shown in Figure 5.27, where strut 1-2 represents the resultant struts for the main strut from loading to support point 1-3 (not shown) and strut balanced by the stirrup (2-4). Considering resultant R representing force from stirrups and the main diagonal strut, the STM is simplified as shown in Figure 5.27.

$V_u = R\sin\beta + D_{dow}\sin\eta$ **5.18**

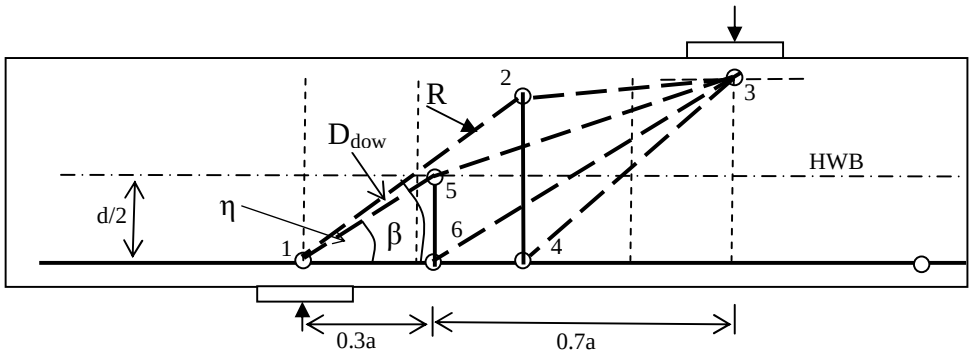

Figure 5.27: STM of HSC beam with HWB of a/d=3, showing the resultant of the main strut and the strut from stirrup as single strut 1-2, at angle β.

The third and most practical and realistic option for presenting the load path and STM for the beam HSC3 with HWB and stirrups of a/d=3.02 is by FE and experimental approach.

In FE approach, principal stress concentration where trajectories are produced, and to transpose the struts on the maximum stress line recorded for the concrete and the ties on

where reinforcement is positioned produces a rational STM.

In the experimental approach, maximum principal stresses produce tensile cracks, therefore transposing the main cracks for struts and the ties on where reinforcement is positioned develops a reasonable STM , Figure 5.28.

From above the data, the STM was developed, Figure 5.29, and the magnitude and direction of the internal forces inside the shear span of the beam is resolved.

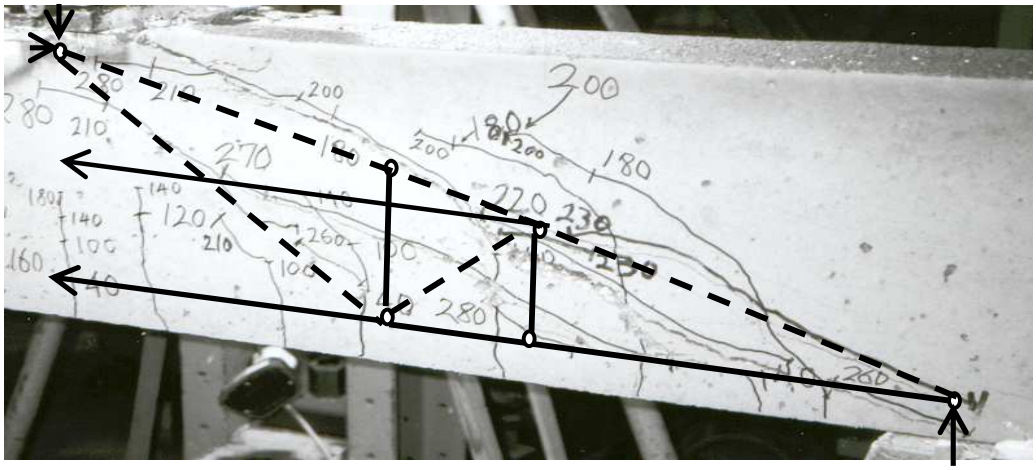

Figure 5.28: location of the STM in relation to position of the cracks of beam HSC4

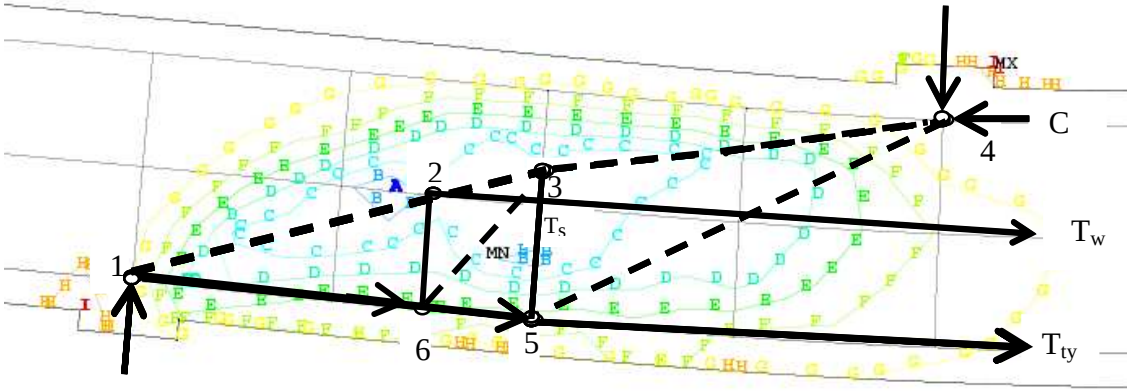

A	B	C	D	E	F	G	H	I
-0.0036	-0.0030	-0.0025	-0.002	-0.0014	$-0.89X10^{-3}$	$-0.36X10^{-3}$	$0.18X10^{-3}$	$0.7X10^{-3}$

Figure 5.29: Position of the STM in relation to the location of shear strain trajectories from FE analysis of beam HSC3

5.6.7- STM for beam HSC3

Location of node 2 is at 400+237=637 where the force resulting from a strain of 0.00058 is 72kN. Similarly, the strain gauge reading recorded experimentally on the web bar at the middle of the shear span, or at 800mm from the end of the beam for HSC3 was 0.000579 on the bottom side of web bar and 0.00188 on the top side of the bar indicating the local bending due to dowel action, Table 5.3, Appendix C.

On the other shear span where the failure occurs, the strain on top reached 0.00338 which is well over the yielding point, whereas the strain below the bar is 0.00177 which is well under yielding point, again indicating bending of HWB due to dowel action, Appendix C.

One simple approach is to apply the force predicted by the proposed empirical equation as the dowel force and develop the corresponding STM for beam HSC3.

$T_d = = 1.95 \times b_n \times d_b \times \sqrt[3]{f_{cu}}$

$b_n = b\text{-}2d_b$

where the breadth of the beam is b and d_b is the diameter of the HWB bars and f_{cu} is the cube strength of the concrete.

From the above

$T_d = 1.95 \times 110 \times 20\sqrt[3]{112} = 20.68$ kN

STM member	Strain gauge (10^{-3})	FE strain(10^{-3})
Web bar	0.579	0.610
Stirrup	Yield	yield
Tension bar	Yields to 2.8	Yields to 3.6

Table 5.3: Strain in HWB of STM compared to FE in beam HSC3

To check if the movement of cracks was correct for the mobilization of dowel action force T_d, reference was made to published measurements of vertical movements at flexural cracks which developed into shear cracks. It was clear that the movements are large enough for dowel resistance to be fully achieved as this movement is limited by the tensile strength of the

concrete, and a movement of about 0.1mm can adequately mobilize it. The significant difference in strain gauge readings on top and bottom of the web bar in the shear span confirms this movement has taken place, Figure 3-37.

Considering T_w is the tension in central bars, Figure 5.30, from the experimental strain gauge reading, FE analysis at 270 kN, Figure 5.30, at a distance ($L_{1\text{-}6}$ =237) 237+400= 637 mm from the end the strain gauge reading is shown to be 610 micro strain on 2T20 bars or tension of 579.9 micro strain is shown on the strain gauge glued to the lower part of the web bar at 800mm from the end which confirms tensile force of 72.5 kN. Therefore T_w= 72.5kN.

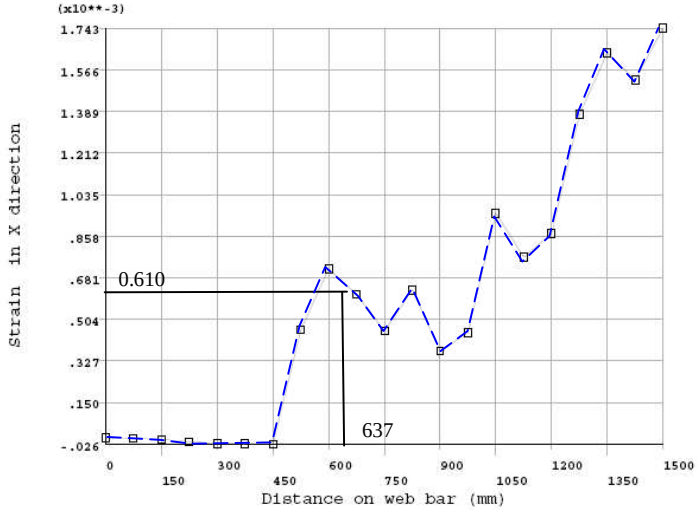

Figure 5.30: FE analysis of strain in X direction on HWB in beam HSC3 at 270 kN failure load on node 2.

Transposition of the model shows the lines of struts are approximately corresponding to crack formations, Figure 5.28.

T_{ty} is tension bars in beam which are 3T20 of f_{yw}= 460 kN at yielding. From experimental strain gauge reading, Figure 5.31, and FE analysis, it is demonstrated that 3T20 tension bars yield at the centre of the beam, as below:

$T_{ty} = 460 \times 3 \times \pi \times 10^2$ =433.54 kN

The dowel action force calculated from Baumann's modified equation from the proposed design rule in chapter 3 is:

$T_d = 1.95 \times b_n \times d_b \times \sqrt[3]{f_{cu}}$

$b_n = b\text{-}2d_b$

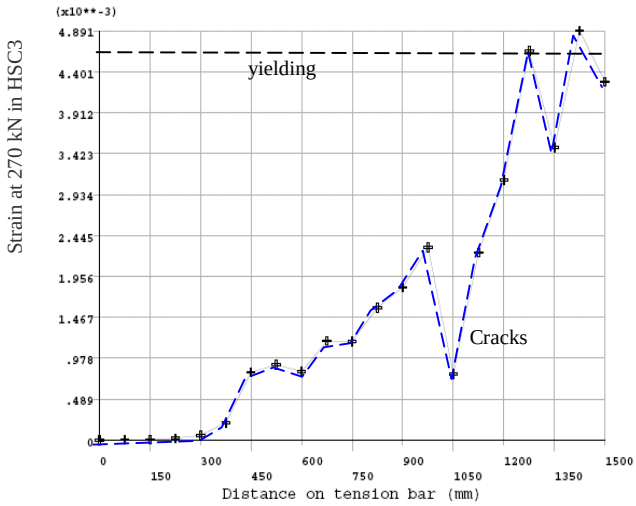

Figure 5.31: FE analysis of strain development on the longitudinal tension bars in beam HSC3 at 270 kN loading showing yielding of the tension steel at the centre of the beam

where the breadth of the beam or BCJ of concrete is b, d_b is the diameter of the HWB bars and f_{cu} is the cube strength of the concrete.

From the above

$T_d = 1.95 \times 110 \times 20 \sqrt[3]{112} = 20.68$ kN

As recorded from the strain gauges in the experimental tests and FE analysis the tension bars and stirrup in the middle of the shear span yielded of f_y= 250 MPa, we consider stress at 260 MPa to represent full yielding

$T_s = 260 \times 2 \times \pi \times 4^2 = 26.12$ kN

Considering external forces:

where W = 135 kN, d=265, a= 800, f_{yt} = 460 MPa and f_{ys}=240 MPa

recorded from strain gauges

T_w = 72.5 kN

The first step is to evaluate the compressive force along the horizontal compression strut from the equilibrium of the external forces and moments. This is done by taking moment for external forces :

$$T_w \times \frac{d}{2} + W \times a = C \times d \qquad \textbf{5.19}$$

or $T_w \times 115 + 135 \times 800 = C \times 230$

$\sum H = 0 \qquad C = T_w + T_{ty}$ or $C = T_w + 433.54$

From the above 2 equations

$230T_w - 115T_w = 800 \times 135 - 433.32 \times 230 \qquad \textbf{5.20}$

$T_w = 72.53$ kN

$C = 506$ kN

Dowel action which takes place in the direction node 2 to 6 is explained and discussed and shown in Figure 5.20.

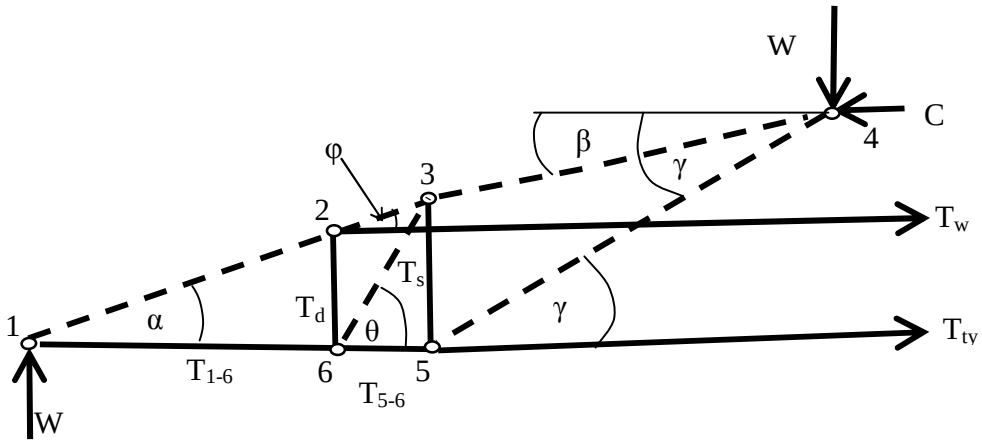

Figure 5.32: STM model of HSC beam with stirrup and HWB of a/d=3 analogous to HSC- BCJ with confinement bars and CVB with aspect ratio of 3

Start by resolving forces at node 5

$\tan\gamma = \frac{230}{400} = 0.58 \qquad \gamma = 29.9°$

$\sum V = 0 \qquad F_{4-5}\sin\gamma = T_s = 26.12$ kN $\qquad F_{4-5} = 52.4$ kN

$\sum H = 0 \qquad F_{4-5}\cos\gamma - T_{ty} + T_{5-6} = 0 \qquad T_{5-6} = 433.32 - 45.43 = 387.89$ kN

Resolve forces at node 6

$\sum V = 0 \quad T_d = 20.68 = F_{3-6}\sin\theta$

$\sum H = 0 \quad T_{5-6} - F_{3-6}\cos\theta + = T_{1-6}$

To find angle θ from the geometry

$\frac{l_{2-6}}{l_{3-5}} = \frac{l_{1-6}}{l_{1-5}} = \frac{20.68}{26.12}$

$$\frac{115}{l_{3-5}} = \frac{l_{1-6}}{400} = \frac{20.68}{26.12}$$

$L_{3\text{-}5}$ = 145.25mm, $L_{1\text{-}6}$ =316.69mm & $L_{5\text{-}6}$ =83.41mm

$$\theta = \tan^{-1}(\frac{145.25}{83.31}) = 60.16°$$

From equilibrium at node 6

$F_{3-6} = 23.84$ kN

$T_{1\text{-}6}$=377.6 kN

Resolve forces at node 1

$$\sum V = 0 \qquad F_{1-2}\sin\alpha - W = 0$$

$$\sum H = 0 \qquad F_{1-2}\cos\alpha - T_{1-6} = 0$$

$$\tan\alpha = \frac{W}{T_{1-6}} = \frac{135}{377.6} \qquad \alpha = 19.67° \text{ and } F_{1-2} = 401 \text{ kN}$$

Resolve forces at node 2

$$\sum V = 0 \qquad F_{1-2}\sin\alpha - T_d = F_{2-3}\sin\varphi \quad \text{or} \quad F_{2-3}\sin\varphi = 135 - 20.68 = 114.32$$

$$\sum H = 0 \qquad F_{1-2}\cos\alpha = F_{2-3}\cos\varphi - 72.53 \quad \text{therefore} \quad F_{2-3}\cos\varphi = 450.13$$

$$\tan\varphi = \frac{114.32}{450.13} \qquad \varphi = 14.25° \quad F_{2-3} = 464.42 \text{ kN}$$

Resolve forces at node 3

$$\sum V = 0 \qquad F_{2-3}\sin\varphi - 26.12 + F_{3-6}\sin\theta = F_{3-4}\sin\beta \quad \text{therefore}$$

$$F_{3-4}\sin\beta = 464.42\sin 14.25° - 26.12 + 23.84\sin 60.16° = 108.88$$

$$\sum H = 0 \qquad F_{2-3}\cos\varphi + F_{3-6}\cos\theta = F_{3-4}\cos\beta$$

$$F_{3-4}\cos\beta = 464.42\cos 14.25° + 23.84\cos 60.16° = 461.99$$

$$\tan\beta = \frac{108.88}{461.99} \qquad \beta = 13.26° \qquad F_{3-4} = 473.63 \text{ kN}$$

Resolve forces at node 4

$$\sum V = 0 \qquad F_{3-4}\sin\beta + F_{4-5}\sin\gamma = W = 135 \qquad \text{therefore} \qquad 108.88 + 26.12 = 135$$

$$\sum H = 0 \qquad F_{3-4}\cos\beta + F_{4-5}\cos\gamma = C = 506 \qquad \text{therefore} \qquad 460.97 + 45.43 = 506$$

The forces in the STM are in equilibrium internally as well as externally

5.6.8-Computing the strut and node dimensions for the STM

For node 1 and prismatic compression strut 1-2, side elevation of which is shown in Figure 5.15, the same bearing pressure is considered for each side of the node. This is a hydrostatic nodal zone because the in-plane stresses in the node are the same in all directions.

With STM, when the node dimensions can be decided in relation to the width of the support a strut-and- tie model can be easily developed. However, this is more complex with BCJ which does not have defined supports. As there is a tensile force from within tension reinforcement, the width of that side of the node is calculated from a hypothetical bearing plate on the end of the tie, which is assumed to exert a bearing pressure on the node equal to the compressive stress in the strut at that node. This is a C-C-T joint because this node is compressed in two directions and is anchoring a tie in one direction where strain incompatibility resulting from tensile steel strain adjacent to the compressive concrete strain reduces the strength of the nodal zone, therefore a reduction factor β_n will apply.

The effective compression stress for node 1 is :

The cylinder strength of the beam 90 MPa, from Table 17-1 of Appendix A of ACI318-08 [5-23] then from ACI section A.5.2.2, $f_{ce} = 0.85\beta_n f_c'$ where β_n=0.80

$$f_{ce} = 0.85 \times 0.8 \times 90 = 61.2 \text{ MPa}$$

For tension reinforcement ACI section A3.3 β_n=0.75

$$f_{ce} = 0.85 \times 0.75 \times 90 = 57.38$$

Using $\phi = 0.75$ to ACI Code section 9.3.2.6, the minimum cross-section for the node with axial force of 135 kN is an area of:

$$\frac{135 \times 1000}{0.75 \times 61.2} = 2941.18 \text{ mm}^2$$

The width of the beam is 150 mm. Therefore, the width of strut 1-2 is 19.61 mm.

Minimum dimension for node 1

This will control the base dimension of node 1 because strut 1-2 is a prismatic strut that can be designed by using β_s=1.0. Thus, the minimum base dimension of node 1 and width of strut 1-2 is :

$$w_{1-2} = \frac{401 \times 1000}{0.75 \times 61.2 \times 150} = 58.24 \text{ mm}$$

The support plate for the beams is less than 100mm so there is enough space for the node to fit on the plate.

At node 4 , ACI section A.5.2.1 in nodal zones bounded on all sides by struts and / or bearing areas, for $f_{ce} = 0.85\beta_n f_c^{'}$ recommends β_s=1.0

$f_{ce} = 0.85 \times 1 \times 90 = 76.50$ MPa

For node 4 subject to vertical load

$$w_{load} = \frac{135 \times 1000}{0.75 \times 76.50 \times 150} = 15.69 \text{ mm}$$

For node 4 subject to horizontal compression

$$w_{comp} = \frac{506 \times 1000}{0.75 \times 76.50 \times 150} = 58.79 \text{ mm}$$

The minimum height of node 1 is to be calculated for tie in $T_{1\text{-}6}$

$$w_{1-6} = \frac{377.6 \times 1000}{0.75 \times 57.38 \times 150} = 58.50$$

Axial tension in $T_{1\text{-}6}$= 377.6 kN

Area A_s required

$A_{s1-6} = \frac{377.6 \times 1000}{0.75 \times 460} = 1094 \text{ mm}^2$ > 3T20> 942 mm^2 because tension bars yielded 1.16 f_{yt}

Concrete strut width for 2-3

$$w_{2-3} = \frac{464.42 \times 1000}{0.75 \times 61.2 \times 150} = 67.45 \text{ mm}$$

Equivalent concrete strut tension in the HWB due to T_w

$$w_{TW} = \frac{72.53 \times 1000}{0.75 \times 57.38 \times 150} = 11.24 \text{ mm}$$

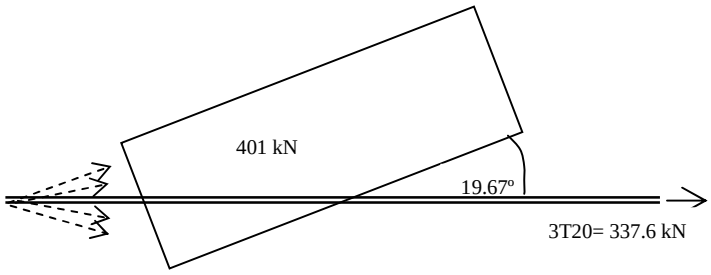

Figure 5-33: Force and width of the strut and tension in tie at node 1, struts are resolved into a resultant force to balance ties

Equivalent strut due to dowel action from HWB due to T_w

$$w_{Td(2-6)} = \frac{20.68 \times 1000}{0.75 \times 57.38 \times 150} = 3.2\,\text{mm}$$

Strut due to diagonal compression resulting from dowel action

$$w_{3-6} = \frac{23.84 \times 1000}{0.75 \times 61.2 \times 150} = 3.46\,\text{mm}$$

Equivalent strut due to tension in stirrup T_s

$$w_{TS(3-5)} = \frac{26.12 \times 1000}{0.75 \times 57.38 \times 150} = 4.05\,\text{mm}$$

Equivalent strut due to tension in stirrup $T_{5\text{-}6}$

$$w_{TS(5-6)} = \frac{387.89 \times 1000}{0.75 \times 57.38 \times 150} = 60.09\,\text{mm}$$

Equivalent strut due to tension in stirrup T_y

$$w_{ty} = \frac{433.54 \times 1000}{0.75 \times 57.38 \times 150} = 67.16\,\text{mm}$$

Maximum compression formed within the main strut along 3-4

$$w_{3-4} = \frac{473.63 \times 1000}{0.75 \times 61.2 \times 150} = 68.79\,\text{mm}$$

Maximum compression strut formed due to stirrup

$$w_{4-5} = \frac{52.4 \times 1000}{0.75 \times 61.2 \times 150} = 7.61\,\text{mm}$$

From calculations in the previous section the strut and node dimensions for the STM are shown in Table 5-5, Table 5-4 and Figure 5-35 to Figure 5-34

Strut	1-2	2-3	3-4	4-5	3-6
Angle	α	φ	β	γ	θ
Degrees	19.67º	14.25º	13.26º	29.90º	60.16º

Table 5-4: The angle each strut makes to horizontal

Member	Vertical component force (kN)	Horizontal component force (kN)	Axial force (kN)	Effective concrete strength f_{ce} (MPa)	Minimum width of strut or nodal zone w_s (mm)
Node 1	135.0	0.0	135.0	61.2	19.6
1-2	135.0	378.0	401.0	61.2	58.2
$T_{s(1-6)}$	0.0	378.0	377.6	57.4	58.5
2-3	114.0	450.0	464.4	61.2	67.5
$T_{d(2-6)}$	21.0	0.0	20.6	57.3	3.2
T_w	0.0	72.0	72.5	57.4	11.2
3-6	21.0	11.0	23.8	61.2	3.5
3-4	109.0	461.0	473.6	61.2	68.8
$T_{s(3-5)}$	26.0	0.0	26.1	57.4	4.1
4-5	26.0	45.0	52.4	61.2	7.6
Node 4	135.0	0.0	135.0	76.5	15.7
Node 4	0.0	506.0	506.0	76.5	58.8
$T_{s(5-6)}$	0.0	388.0	387.9	57.4	60.1
T_{ty}	0.0	433.0	433.5	57.4	67.2
INS 2	149.0	445.6	469.9	61.2	68.3
INS 3	134.8	461.7	481.0	61.2	69.9
INS 4	135.1	506.3	524.0	61.2	76.1

Table 5-5: Calculation of the forces in the STM of beam HSC3

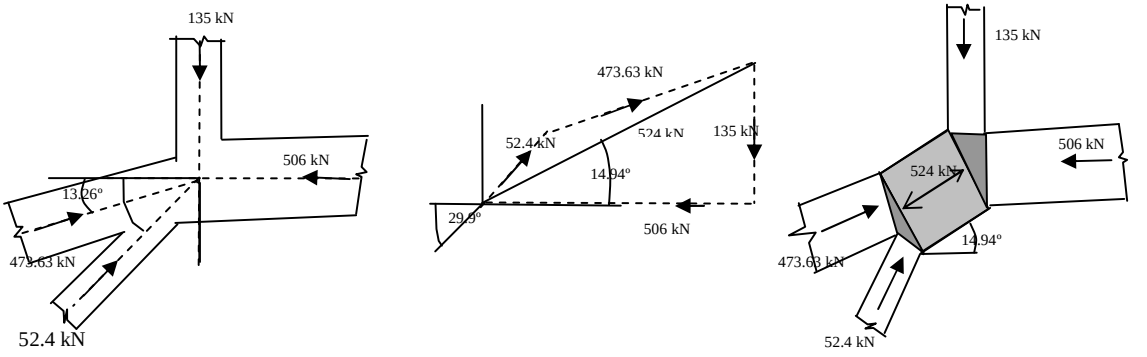

a) Four strut node 4 with replacing tension tie

b) Force polygon for node 4

c) Nodal zone 4 consisting of two hydrostatic subnodes and an internal strut

Figure 5-34: Resolution of forces acting on nodal zone 4 showing the type and dimension of nodes and struts

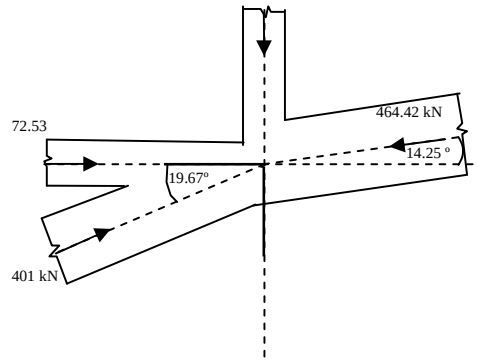

a) Four strut node 2 replacing tension ties with equivalent struts

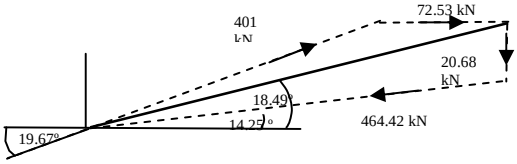

b) Force polygon for node 2

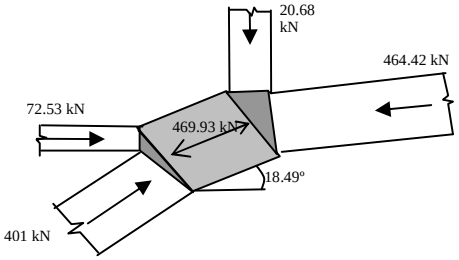

c) Nodal zone 2 consisting of two hydrostatic subnodes and an internal strut

Figure 5-35: Resolution of forces acting on nodal zone 2 showing the type and dimension of nodes and struts

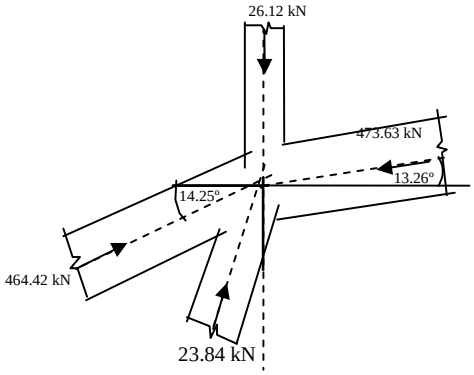

a) Four strut node 3 replacing tension ties with equivalent struts

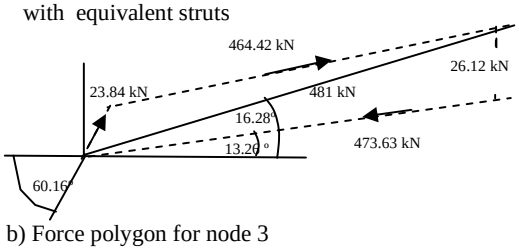

b) Force polygon for node 3

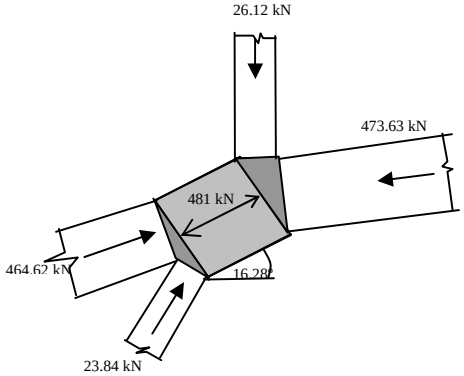

c) Nodal zone 3 consisting of two hydrostatic subnodes and an internal strut

Figure 5-36: Resolution of forces acting on nodal zone 3 showing the type and dimension of nodes and struts

From dimensions for nodes and struts the STM was developed for beam HSC3, Figure 5-37

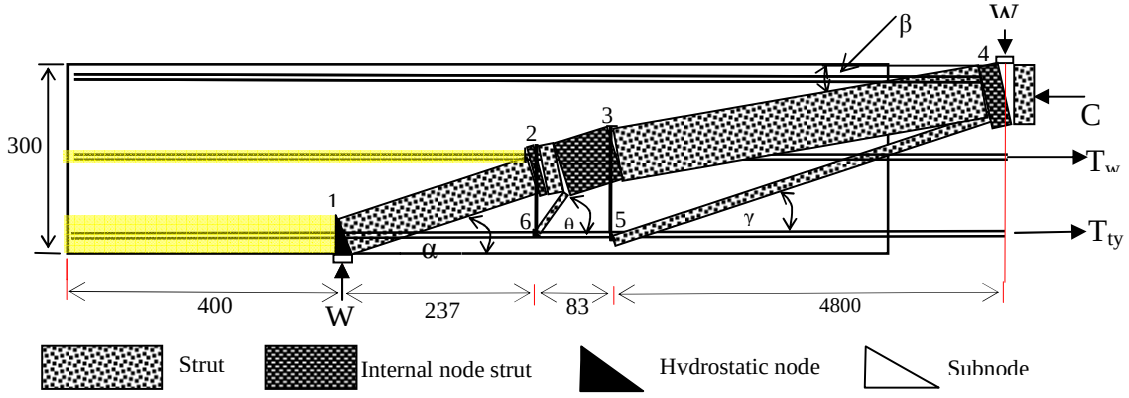

Figure 5-37: STM for HSC beam with HWB of a/d=3.02 with stirrups. The sum of the shear transmitted is counter balanced by vertical components of the deflected strut which has an improved arching action as well as the stirrups.

5.7 STM for BCJ

5.7.1- STM for TBCJ

It should be noted that STM of beam HSC3 is analogous to that of TBCJ with an aspect ratio of 3.

$$\frac{a}{d} = \frac{h_b}{h_c} = 3 \qquad \textbf{5.21}$$

where the applied support reaction on the beam, W, is analogous to tension in the beam bar at BCJ. Shear span, *a*, in beam is analogous to h_b which is the beam depth at BCJ. Depth of beam, *d*, is analogous to h_c which is the column depth at BCJ, as is the beam in Figure 5-37 to TBCJ, Figure 5-38.

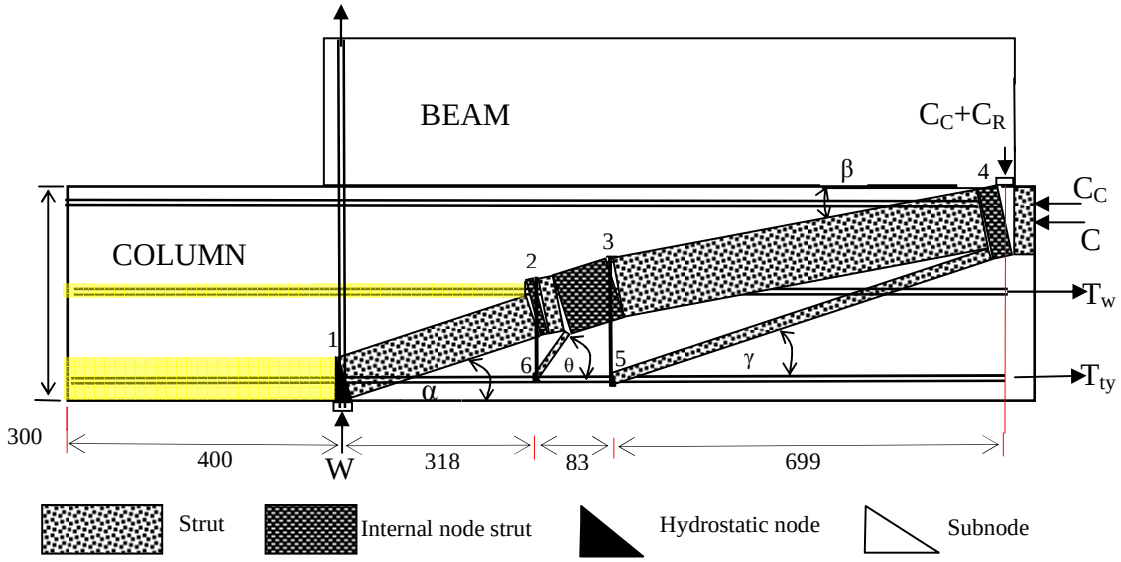

Figure 5-38: The proposed analogy of STM of HSC with HWB of a/d=3 to HSC-BCJ with apect ratio ≤3 with CVB.

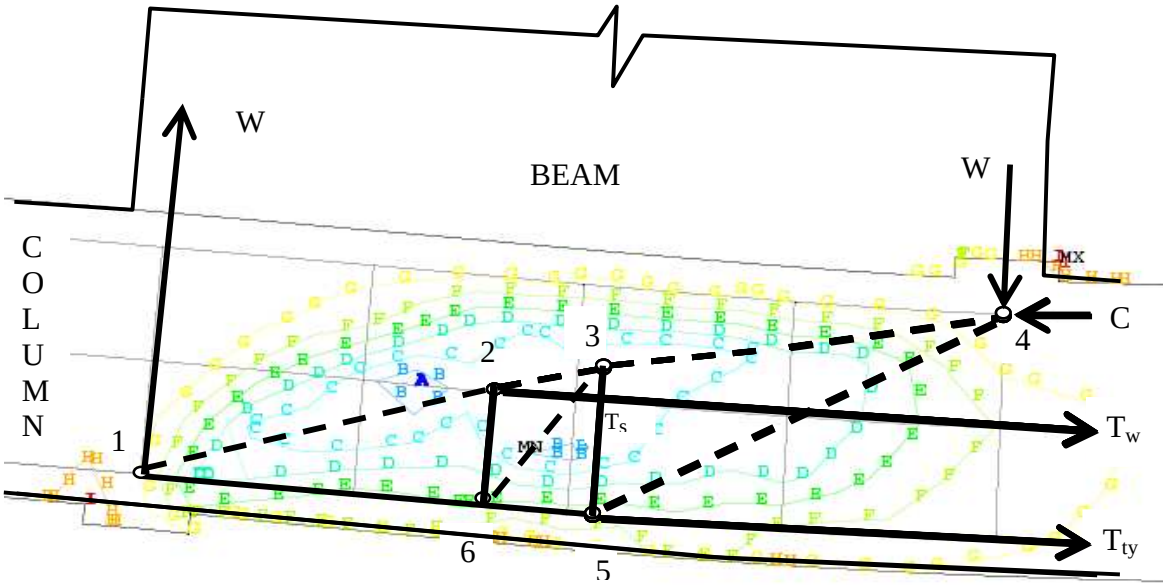

Figure 5-39: The STM for HSC- BCJ with confinement steel and CVB analogous to HSC beam with stirrups and HWB

Figure 5-39 shows the shear strain trajectory of BCJ analogous to the beam shown in Figure 5-33, where similar STM is applied to the TBCJ .

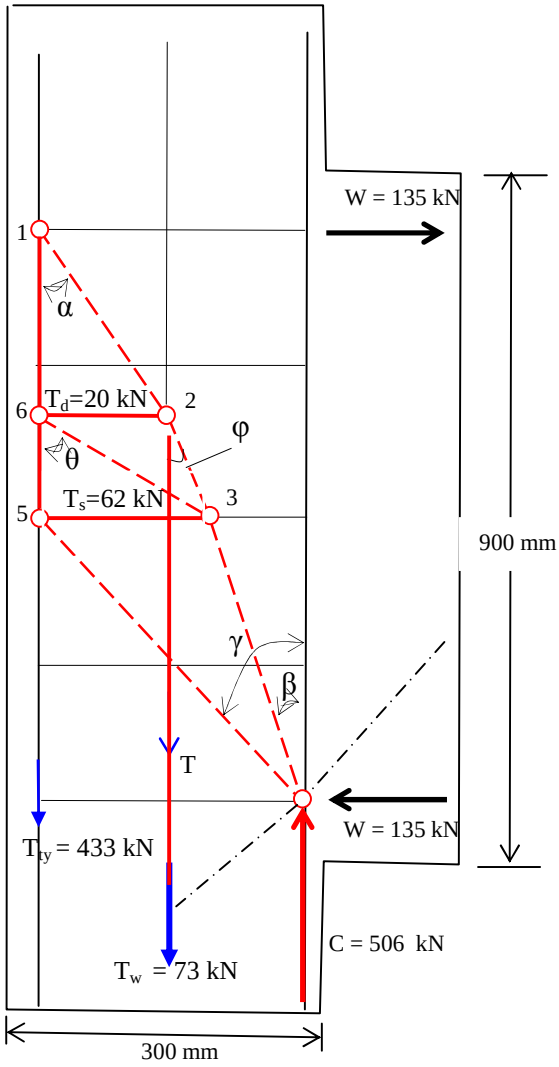

Figure 5-40: Forces acting within the HSC- BCJ with CVB of aspect ratio 3. It is assumed that forces shown as struts with dots and dashes are included in horizontal and vertical components W and C.

It is notable that for the purpose of showing the analogy in Figure 5-38 and Figure 5-39 the struts acting on the TBCJ from beam and from the lower part of the column is not shown. However, the presence of these two struts is shown in Figure 5-40, which also provides an indication of the magnitude of the forces in the ties and the angles of the struts.

5.7.2- Review of STM for BCJ

The model proposed by Pauley [5-37] is shown in Figure 5.41. Intermediate column bars are proposed for the model in order to equilibrate the vertical shear in the joint. No details such as the failure mechanisms, the geometry of the nodes and the cracked concrete strength were proposed for the model.

In a report published in 1984, a thorough critical review on BCJ was provided by Pauley and Park [5-38] which assumed the existence of two shear-resisting mechanisms: one involving joint shear reinforcement and the other consisting of concrete struts.

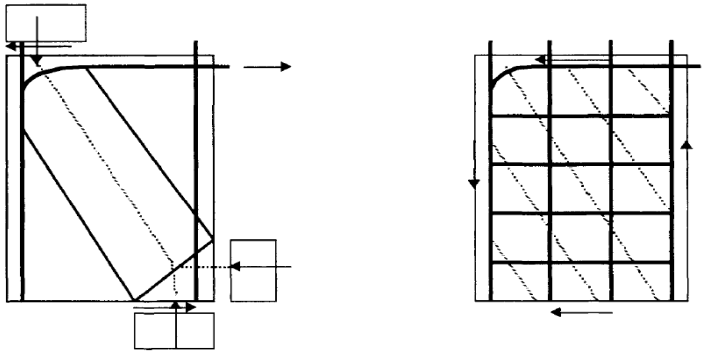

Figure 5.41 : The strut and tie model proposed by Paulay [5-38]

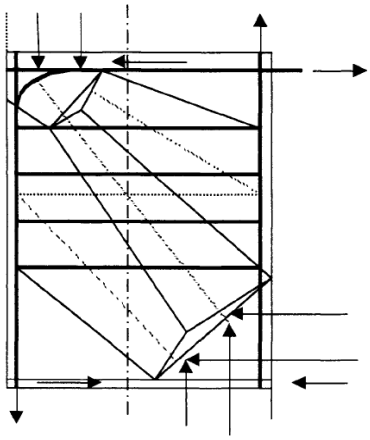

Figure 5.42: Vollum's original strut and tie model
Source: Vollum R. L, Newman J.B, [5-39]-1999

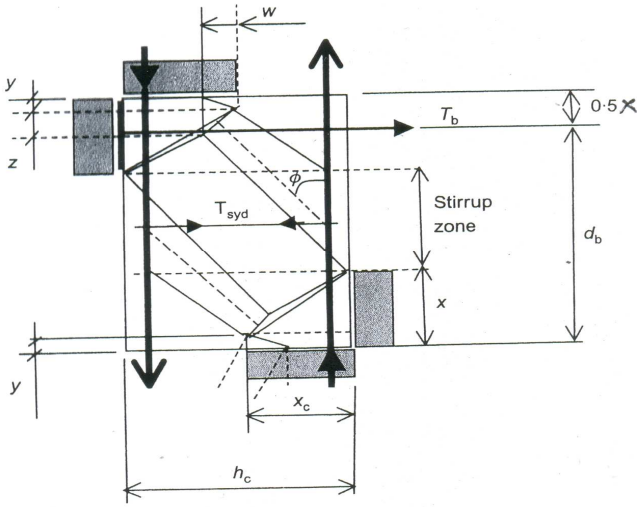

Figure 5.43: Vollum's revised strut and tie model
Source: Vollum R. L, Parker, D, [5-40]-2008

The STM developed by Vollum and Newman [5-39] appeared to be more complicated. However, Vollum and Parker [5-40] revised strut and tie model provides a comprehensive load path.

Vollum presented STM for joints with and without shear reinforcement. Similar parameters used previously by Ortiz [5-42] for developing STM for BCJ were employed .

Researcher	**Specimen**	**Detail**	Fc MPa	**Actual Failure Mode**	**Predicted Failure Mode**	P_{pred}/P_{fail}
Scott & Hamill [5-43]	C4ALN0	L Bar	42	P	J	0.94
	C4ALN1	L Bar	46	J	J	1.01
	C4ALN3	L Bar	42	J	J	1.26
	C4ALN5	L Bar	50	JS	B	1.20
	C4ALH0	L Bar	104	P	B	1.50
	C4ALH1	L Bar	95	B	B	1.43
	C4ALH3	L Bar	105	B	B	1.41
	C4ALH5	L Bar	98	B	B	1.29
	C6LN0	U Bar	51	J	J	1.46
	C6LN1	U Bar	51	J	J	1.63
	C6LN3	U Bar	49	JS	B	1.62
	C6LN5	U Bar	37	JS	B	1.25
	C6LH0	U Bar	101	J	J	1.11
	C6LH1	U Bar	102	JS	B	1.72
	C6LH3	U Bar	97	JS	B	1.52
	C6LH5	U Bar	100	B	B	1.23
Parker & Bullman [5-44]	4a	L Bar	39	C	C	1.72
	4b	L Bar	39	J	J	1.51
	4c	L Bar	37	J	J	0.94
	4d	L Bar	39	J	J	1.41
	4e	L Bar	40	J	J	1.40
	4f	L Bar	38	J	J	0.93
	5a	L Bar	42	C	B	1.63
	5b	L Bar	43	JS	B	1.49
	5c	L Bar	43	B	B	1.44
	5d	L Bar	43	C	C	1.54
	5e	L Bar	45	C	C	1.28
	5f	L Bar	43	C	C	1.23

Table 5.6: The predicted failure loads of Scott & Hamill's [5-43] and Parker & Bullman's [5-44] tests from Ortiz design rule.

Source: Tables adopted from Bakir and Boduroglu [5-41]-2001

Ortiz' proposal [5-42] for a design rule for BCJ failure was investigated [5-41] by predicting BCJ failure of two high strength BCJ which Scott & Hamill [5-43] tested to joint shear failure. This has demonstrated that Ortiz's design rule applied to the two HSC specimens (C6LH3 & C6LH1) to predict the joint shear failure load of specimens which were 51% and 72% higher than those of the test failure loads.

In general, Ortiz' proposed designed rule was not conservative when applied to beams tested by Scott & Hamill [5-43] and Parker & Bullman [5-44], Table 5.6. The abbreviations used for the failure modes in the table are: B: Beam failure, JS: Joint shear failure, P: Pullout of beam's bar, C: Column failure.

5.7.3-Basic approach to STM of BCJ of aspect ratio<2

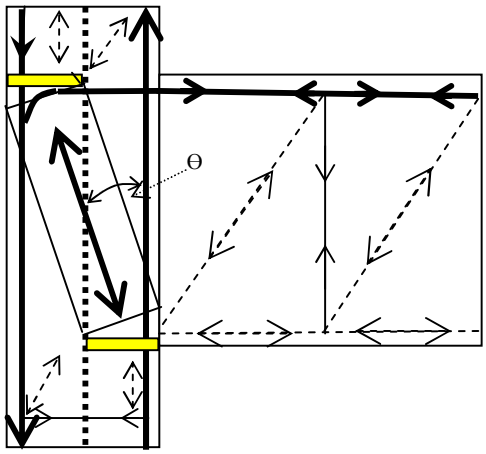

Figure 5.44: Basic STM for BCJ

STM are an idealization of the behaviour of cracked reinforced concrete. By reducing the continuum to a discrete STM, a simpler approach to concrete and reinforced concrete modelling is made possible. Since concrete structures bear the applied loads according to the way they are reinforced, an infinite number of STM are possible. All of them need to satisfy equilibrium and to respect yield criteria.

Some STMs are unsuitable because they would require high plastic deformations and force redistributions which are incompatible with the limited deformation capacity of concrete. Also, choosing an adequate STM for the ultimate limit state does not necessarily lead to satisfactory behaviour at the serviceability limit state.

Using STM with a geometry that follows the elastic flow of the internal forces in the uncracked state leads to solutions that have a more satisfactory behaviour in service. This

approach, however, is not always practical, because it would often require the reinforcement to be placed in diagonal directions with complex shapes.

A basic STM mechanical model can provide a clear guideline on shear performance of discontinuous joints in RC structures. More refined models are being evolved from STM in stress fields which is a positive step towards analysing more refined STM.

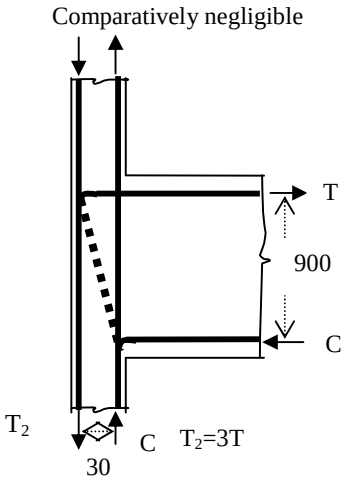

Figure 5.45: STM in the joint region forces in column bars in relation to beam bar

To this writer's knowledge no attempt has so far been made to propose a design method suitable for predicting joint shear of external transfer beams and HSC columns. This chapter is an effort to explore existing design rules to predict the joint shear resistance of HSC BCJ.

5.7.4-Formation of cracks in HSC-BCJ of aspect ratio=3 with CVB

A simplified proposed design method with stirrups and CVB is calculated as below based on modifying Ortiz' [5-42] design method.

The joint shear strength can be derived in terms of the node dimensions, Figure 5.47.

$D\cos\beta = F_v$ **5.22**

$D\sin\beta = V_j$ **5.23**

where D is the total force in the diagonal strut, F_v is the vertical force due to the applied load on top and bottom of the joint and V_j is the joint shear force.

Then let

w_i = width of diagonal strut without considering the stirrup or the CVB

D = Diagonal strut force at the joint just before cracking and it magnitude is

$$D = k \cdot b_c (1 - \frac{f_{ck}}{250}) f_{ck} \cdot w \qquad \textbf{5.24}$$

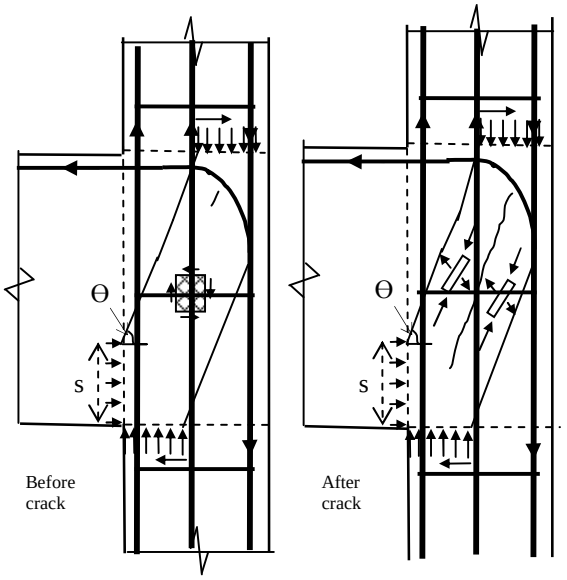

Figure 5.46: Principal stresses before crack formation and direction of tensile and compressive forces after the cracks are formed in the BCJ.

where b_c is the column breadth and w is the strut width

where γ_c is factor of safety for concrete which is given as 1.5, f_{ck} is the characteristic compressive strength of cylinder strength of 28 days, k = 0.6 for concrete struts in cracked compression zones, k = 0.85 for compression –tension nodes with anchored ties in one direction and k = 0.75 for compression-tension nodes with anchored ties in more than one direction. Hence, the diagonal strut force becomes

$$D = 0.6 \cdot b_c (1 - \frac{f_{ck}}{250}) f_{ck} \cdot w \qquad \textbf{5.25}$$

Hence the diagonal width is

$$w = \frac{D}{0.6 b_c (1 - \frac{f_{ck}}{250}) f_{ck}} \qquad \textbf{5.26}$$

For any increase in diagonal force will be represented as

$$\delta D = 0.6 \cdot b_c (1 - \frac{f_{ck}}{250}) f_{ck} \cdot \delta w \qquad \textbf{5.27}$$

Similarly the increase in diagonal force width is

$$\delta w = \frac{\delta D}{0.6 b_c (1 - \frac{f_{ck}}{250}) f_{ck}} \qquad \textbf{5.28}$$

The total diagonal force including the increase in loading is

$$D + \delta D = 0.6 \cdot b_c (1 - \frac{f_{ck}}{250}) f_{ck} \cdot (w + \delta w) \qquad \textbf{5.29}$$

The stirrups and CVB increase the shear force by

$$\delta V_j = T_s + V_d = A_{sv} f_y + 1.95 b_n d_b \sqrt[3]{f_{cu}} = \delta D \sin\beta \qquad \textbf{5.30}$$

From equation (5-22)

$$\delta V_j = \delta D \sin\beta$$

Substituting equation (5-24) gives

$$\delta V_j = \left(0.6 b_c (1 - \frac{f_{ck}}{250}) f_{ck} \cdot \delta w \right) \cdot \sin\beta \qquad \textbf{5.31}$$

Re-arranging and substituting equation (5-28)

$$\delta w = \frac{\delta V_j}{\left(0.6 b_c (1 - \frac{f_{ck}}{250}) f_{ck} \right) \cdot \sin\beta} = \frac{A_{sv} f_y + 1.95 b_n d_n \sqrt[3]{f_{cu}}}{\left(0.6 b_c (1 - \frac{f_{ck}}{250}) f_{ck} \right) \cdot \sin\beta} \qquad \textbf{5.32}$$

which is the increase in the diagonal strut width

w_i is the strut width when BCJ does not have any stirrups and its value is

$$w_i = \gamma W \qquad \textbf{5.33}$$

where the value of γ and β can be determined by from FE models indicating the point of deflection of the diagonal strut from moment concentration on HWB or CVB as suggested in Chapter 7 for TBCJ of HSC with CVB.

$W = h_c \cos\beta + s \sin\beta$ which is the maximum allowable width and γ is measured from the stress trajectories developed by FE model

The total diagonal strut width is found by substituting equations equations 5-32 and 5.33 into the following,

$$w = w_i + \delta w \qquad \textbf{5.34}$$

Which gives

$$w = \gamma W + \frac{A_{sv} f_y + 1.95 b_n d_b \sqrt[3]{f_{cu}}}{0.6 b_c (1 - \frac{f_{ck}}{250}) f_{ck} \sin\beta} \qquad \textbf{5.35}$$

Substituting into equation (5-25) gives the magnitude of the diagonal strut force which is

$$D = 0.6\, b_c \left(1 - \frac{f_{ck}}{250}\right) \cdot f_{ck} \cdot \left(\gamma W + \frac{A_{sv} f_y + 1.95 b_n d_b \sqrt[3]{f_{cu}}}{0.6 b_c (1 - \frac{f_{ck}}{250}) f_{ck} \sin\beta} \right) \qquad \textbf{5.36}$$

Substituting into equation (5-28), the total shear force in the joint is

$$V_j = 0.6\, b_c \left(1 - \frac{f_{ck}}{250}\right) \cdot f_{ck} \cdot \left(\gamma W + \frac{A_{sv} f_y + 1.95 b_n d_b \sqrt[3]{f_{cu}}}{0.6 b_c (1 - \frac{f_{ck}}{250}) f_{ck} \sin\beta} \right) \cdot \sin\beta \qquad \textbf{5.37}$$

Forces acting on the boundary of BCJ are investigated for failure analysis. It should be noted that the boundary regions are influenced by the joint and are typical transition zones, or D regions, where the strain distribution across the section do not follow the Bernoulli theory, and other stress distributions are taken into consideration to provide equilibrium, Figure 5.48.

Assuming that the depth of the beam chords is s, horizontal forces are $T_{bb,}$ R_t, F and joint shear force V_{jtest}; and considering Ortiz models as presented above, the Vertical equilibrium is achieved from the following equation modifying Ortiz equations

$F_v = F_{ti} + F_{bi} - F_{cvt} - F_{cvb} + C_{cb} - V_{be} = F_{te} + F_{be} + C_{ct}$ **5.38**

$D \cos\beta + V_{be} = F_{ti} + F_{bi} - F_{cvt} - F_{cvb} + C_{cb}$ **5.39**

where D is the total force in the diagonal strut, F_v is the vertical force introduced at each side of the joint and V_j is the joint shear force.

The treatment of the top node in this model which assumes that the tensile force in the beam reinforcement is treated as if it were transferred into the rear face of the column through a rigid plate, can lead to some controversy, as Hamil's specimens CAPLN0 and C4ALN0 were identical except that the beam reinforcement was anchored with a plate bearing onto the back face of the column in specimen C4PLN0 and failed at 20% higher load than C4ALN0.

However, pull tests by Jirsa demonstrate that anchorage of the beam bar to the rear face of the column through a rigid plate is almost identical to performance of L beam anchorage.

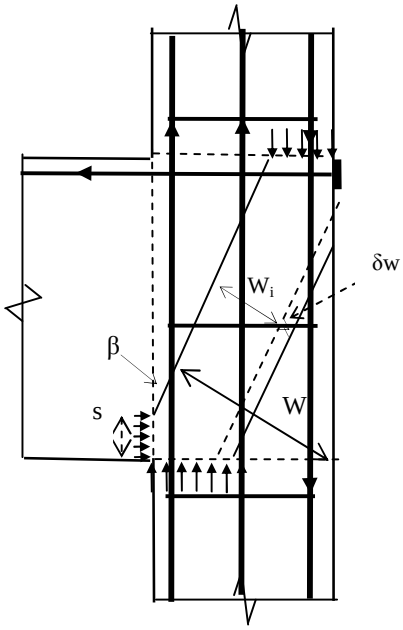

Figure 5.47: Diagonal strut definition

5.7.5-Performance of forces in BCJ reinforcement

The tests by Jirsa and Marques [46], details shown in Figure 5.51, demonstrate that if the restraints are not provided by column stirrups, the concrete under the bend of the beam steel fails in bearing and spalls off the side of the joint.

The loss of anchorage of the reinforcement, in particular in exterior connections, is undesirable because lateral shear can no longer be transmitted by the frame. Failure of the anchorage also causes a reduction in the energy-absorbing ability of the structural system.

The stresses and slip measured at points along a hook at a bar stress of 1.25 f_y in tests [5-45] with 90°, and 180°, hooks of a 22.2mm diameter bar are shown in Figure 5.50 to Figure 5.53. The arrows show magnitude and direction of the slip at A, B, and C. For the 180° hook, the slip measured at A was 1.75 times that measured at A in the 90° hook.

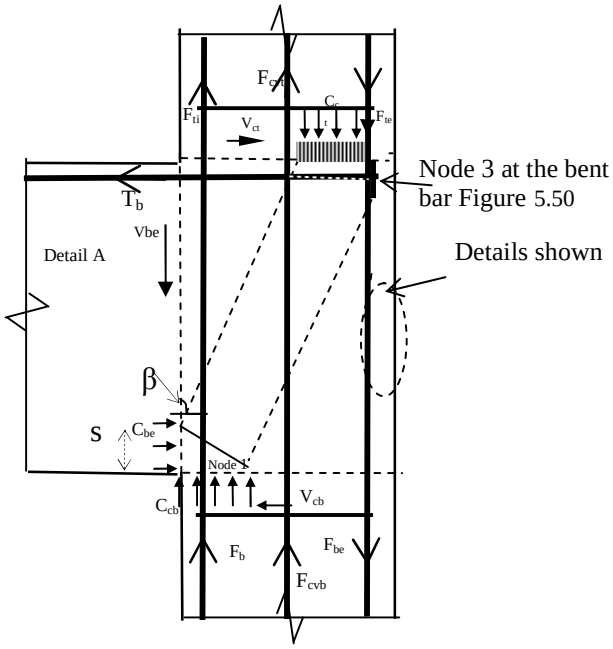

Figure 5.48: Simplified diagonal strut and boundary forces for aspect ratio= 3.

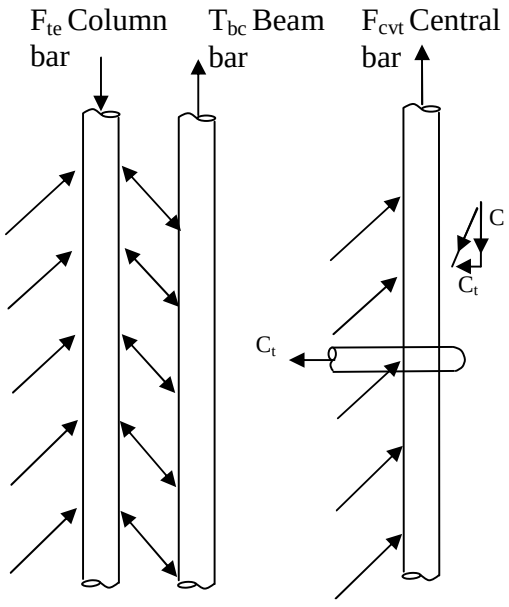

Figure 5.49: Detail A as in Figure 5.48, D = compression force from diagonal strut, C= compressive force from column and C_t= Concrete tensile force, T is tension on CVB

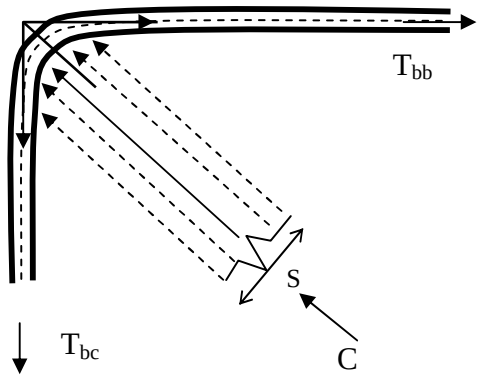

The tensile force in the beam bar in BCJ is assumed to be transferred into the back of the column through a rigid plate, whereas , in practice the beam reinforcement is anchored with a U or L bar.

Figure 5.50: Node anchored by bent bar. As shown in Figure 5.52 [5-46] Jirsa assumed that when T_{bb} yields, T_{bc} is negligible. This was overruled by Ortiz [5-42] as shown in Table 5.7

A 90° hook loaded in tension develops forces as shown in Figure 5.54. The stresses in the bar are resisted by the bond on the surface of the bar and by the bearing on the concrete inside the

hook. The hook moves inward, leaving a gap between it and the concrete outside the bend [5-45]. As the compressive force inside the bend is not collinear with the applied tensile force, the bar tends to straighten out, producing compressive stresses on the outside of the tail. Marques and Jirsa's concluded that when T_{bb} yields, then T_{bc} is negligible was based on two specimens only, J7-90-15-1-H and J11-90-15-1-H. They had 90º bend for the beam bar anchorage, Figure 5.50, and that was disputed by research completed by Ortiz [5-42] as shown in Table 5.7.

Ortiz [5-42] demonstrated that the tail stresses are 45% of the maximum stresses at the face of column. When the stress at the column face is 345 MPa, the tail stress is 210MPa. Table 5.7. This agrees with the none-linear FE analysis carried out in this research work and will be discussed further in Chapter 7 in the section discussing the strain on the beam bars.

Table 5.7 demonstrates the improved performance of L-shaped anchorage as compared to U-shaped, Figure 5.53 . This empirical design rule proposed in the next chapter will make provision for this.

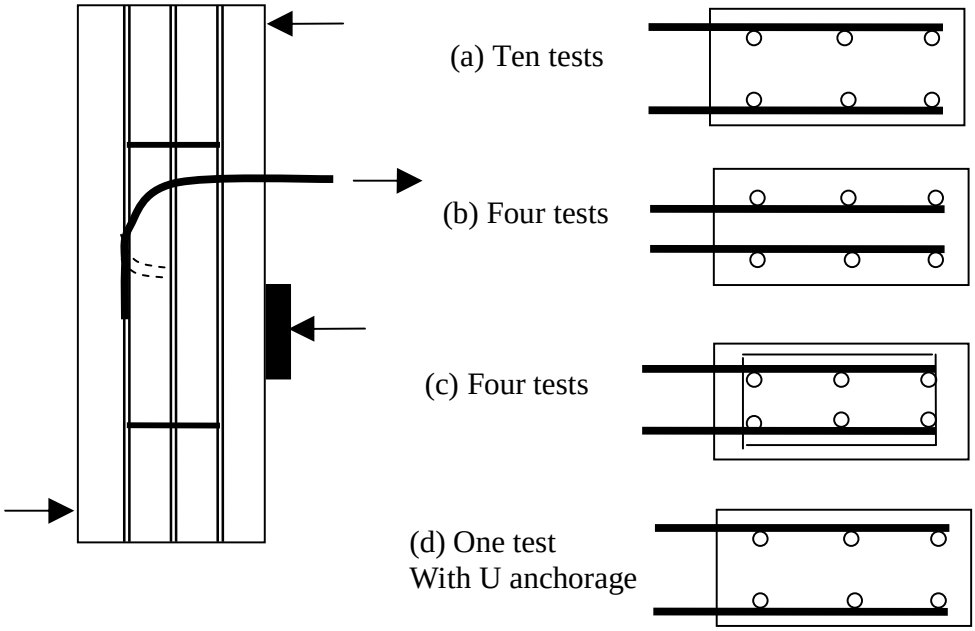

Figure 5.51: Detail of tests by Jirsa and Marques [5-46]

Similarly, it will be demonstrated in Chapter 7 that FE models of BCJ tested by Ortiz [5-42] disagrees with the data provided by Marques and Jirsa [5-46] as in their specimen J7-90-15-1-

H a major part of the bar forces (76%) was anchored in the lead length before the start of the bends, Figure 5.52. Contrary to their finding, Ortiz [5-42] demonstrates, Table 5.7, that on average, the percentage of forces anchored are 1.5% in lead, 43% in bend and 45% in tail.

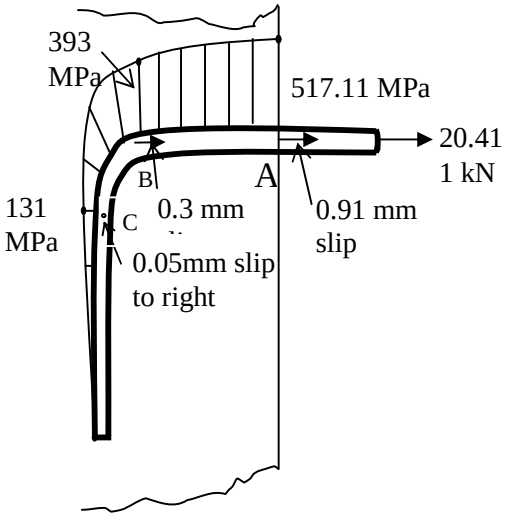

Figure 5.52: Stresses and slip - 90° standard hook at 1.25 f_y

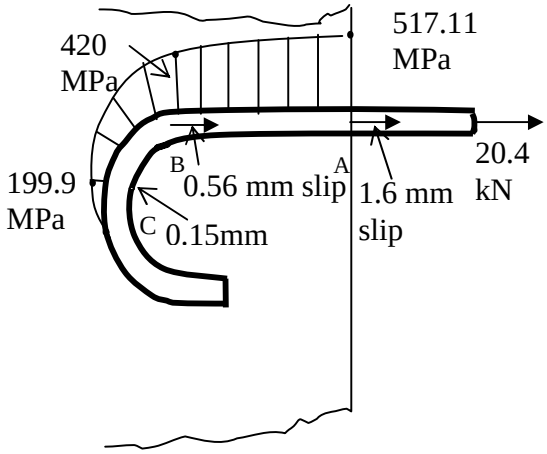

Figure 5.53: Stresses and slip -180° standard hook at 1.25 f_y

Ortiz [5-42] makes a comparison study for the bearing stresses inside the bends for the seven BCJ tested to failure from strain gauges readings positioned at the bend, with predictions from BS8110 [5-24] and CEB90 [5-16] for which factor α_1 with a reduction factor of 0.7 was considered.

It was concluded that BS8110 marginally underestimated bearing stresses for 2 out of 7 BCJ as no bearing failure was observed for those two specimens. All the bearing stresses were considerably higher than CEB 90[5-16] limits.

Ortiz's [5-42] results indicate that BCJ5 which had no confinement steel with a smaller bend radius of 4d with axial column load of 300kN showed signs of spalling of the concrete cover from the region inside the bend, which was recorded on the surface strain as the cover spalled. Its bearing stress was equal to the BS8110 [5-24] prediction when excluding γ_m .

BCJ7 loaded to the beam failure had a larger bend radius (8d) and the same column axial load

but did not experience spalling of cover under the bend region. This writer is of the opinion that the reason BCJ7 did not experience spalling of cover here is due to the presence of 4T10-100mm confinement steel with 2 stirrups within the bend compared with none in BCJ5, as Ortiz' tests demonstrate that increase in radius bend beyond 4d does not influence the joint shear force. The stirrups confining the bend and tail part of the rear reinforcement, Figure 5.54, prevented formation of the bend and tail gap which would have resulted in spalling the cover.

Spec no BCJ-	Stress at column face	% of face force anchored in		
		lead	bend	tail
1	350	-5	43	62
2	492	24	58	18
	370	34	48	18
3	415	-5	19	86
4	580	19	24	57
5	565	46	5	49
6	493	5	69	26
	447	5	40	55
7	660	6	56	38
	578	-6	65	41

Table 5.7: Ortiz' [5-42] recordings of % of face force anchored in lead, bend and tail for the seven BCJ specimens tested.

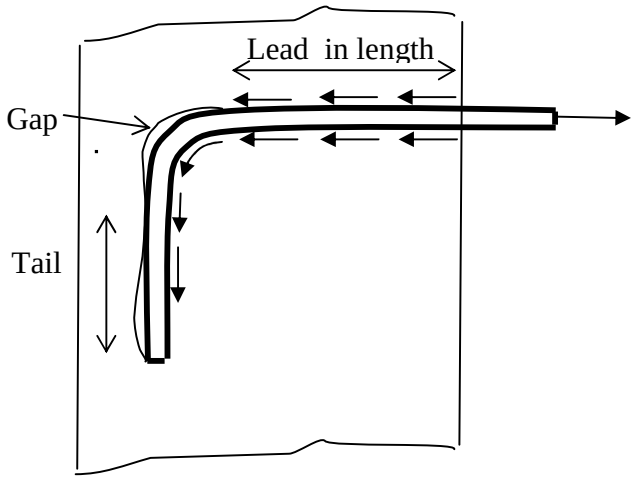

Figure 5.54: Forces acting on 90° standard hook

Source: Wight and MacGregor [5- 35]

With the load path showing the stabilising arching effect from CVB to consolidate the forces on the beam bar corner of the BCJ, these forces are counter balanced by C and C_b, Figure 5.61 . CVB is considered as an independent anchorage node subjected to tensile force T_4, which in this circumstance helps to develop the strut fully by improving the arching action and deflecting the main strut, Figure 5.61.

In practice, it could be difficult to position stirrups at the depth of the joint. A practical alternative for external BCJ with transverse beams is to use U bars ensuring that the legs of the U bars are perpendicular to the axis of the transverse beams encasing BCJ, however, for

corner columns in zones exposed to extreme loading conditions, L bar connections are preferable to U.

The beam reinforcement should be bent down into the column with adequate radius to avoid bearing failure and should be fully anchored in the column past the beginning of the bend with minimum length. Stirrups placed within the bend prevent spalling of the concrete at the cover.

It is often more convenient to anchor the beam reinforcement with U bars rather than L, however, it has been concluded [5-40] that joint shear strength of specimens with L bars is 20% more than those with U bars which have insufficient lap with the column bars, [5-40].

5.7.6-HSC or NSC BCJ with aspect ratio<2 with CVB

Rogowsky and MacGregor[5-10] have suggested that double strut action forms in deep beams, Figure 5.56. In this writer's opinion, this may occur when a/d <2, the main diagonal action reaches the upper truss at mid depth and makes the reinforcement (HWB) in the upper truss act in tension, Figure 5.55.

However when the aspect ratio is low the main diagonal strut will be fully develop, therefore CVB can not make much contribution to ultimate load capacity but still improves the ductility at .failure stage by producing larger number of smaller cracks distributed across the joint

It has been noted [5-47] that the influence of CVB to ultimate load capacity is very small when strength of the concrete is less that 50MPa and when aspect ratio is less than 2 the main diagonal strut fully develops and dilutes any influence from CVB. However, as was shown in Chapter 3 for beams with HWB, in a similar way the presence of CVB can produce distributed smaller cracks parallel to the main crack, which would dissipate the energy from ultimate loading, resulting in a ductile mode of failure rather than a brittle one when CVB is absent.

This research demonstrates that the main diagonal compression strut will deflect due to thepresence of HWB when a/d=3.02. This is in contrast to the model proposed by Rogowsky

and MacGregor [5-10], Figure 5.55, which is more suitable for NSC a/d≤2 or in shear walls or deep beams.

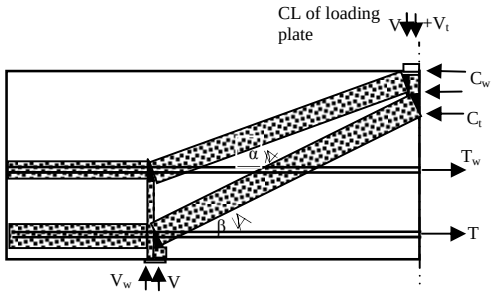

Figure 5.55: The above model for STM was proposed by Rogowsky and MacGregor[5-10] for the HWB.

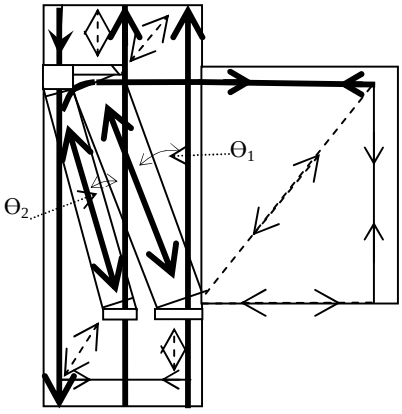

Figure 5.56: STM with CVB for aspect ratio < 2 . The CVB does not make as much contribution when aspect ratio < 2 .

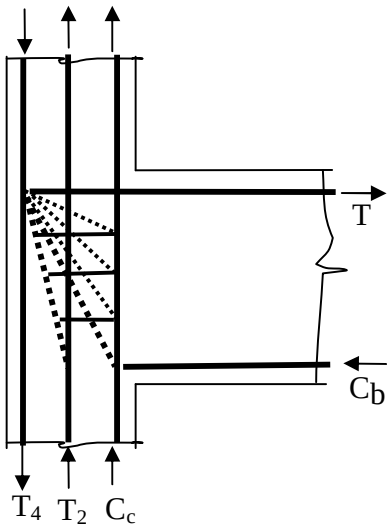

Figure 5.57:The load path in BCJ with CVB when aspect ratio is <2

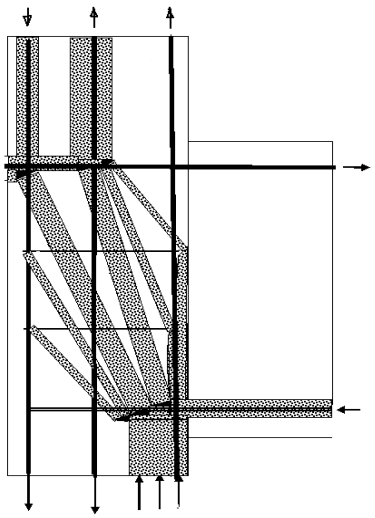

Figure 5.58: One possible STM for BCJ when aspect ratio is <1.2

5.7.7-HSC or NSC BCJ with aspect ratio<3 with CVB

Since St Venant's principle suggests that the localised effect of a disturbance dies out by about

one member depth from point of disturbance, it would be assumed that the member depth be considered as disturbed and there would be a comparatively shallow column extending to the upper and lower part of the beam. Therefore, the Bernoulli hypothesis of plane strain distribution would be valid at a third of the depth of the beam located at the middle of the depth of the beam in BCJ, .

The shear force at joint Vu (joint) at mid depth of the beam is resisted by the truss model from stirrups, Figure 5.61, and not by a single compression strut acting in diagonal direction as shown in Figure 5.56. This diagonal strut would have been resisting the shear force at the BCJ if the ratio of beam depth to column was less than 2. However, when this ratio is close to 3, the truss action under Bernoulli's principle would resist shear by stirrups.

As demonstrated in the experimental work in Chapter 3, HSC, in particular when it is made with limestone aggregate, failed in shear with a steeper angle of shear failure of about 55°, compared to NSC with an angle of about 45°. Therefore, when the spacing between stirrups is less than two thirds of the depth of the HSC member, then the shear cracks will travel between stirrups and as a result the member fails from a smaller shear force than in NSC.

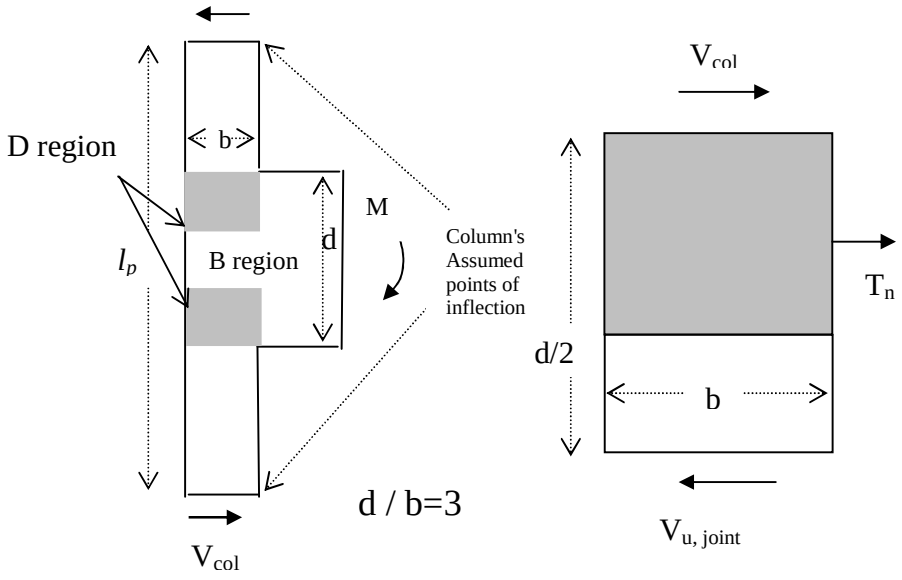

Figure 5.59: Free body diagram of the external BCJ with a transfer beam and a shallow column

Past research has demonstrated that change in the strength of concrete affects the monolithic property behaviour of the concrete in such way that if the difference in strength at the concrete joint between two concrete batches increases by more than 25%, the concrete mass from the two batches would not be behaving as a monolithic material. This would be the case for structures made with HSC columns of 80 to 100 MPa and NSC beams of 40 MPa. This phenomenon contributes to the idea that BCJ made with HSC columns act independently from the NSC in the beam. This adds to the argument that the shear in a column at BCJ would behave similarly to that in a beam, Figure 5.60.

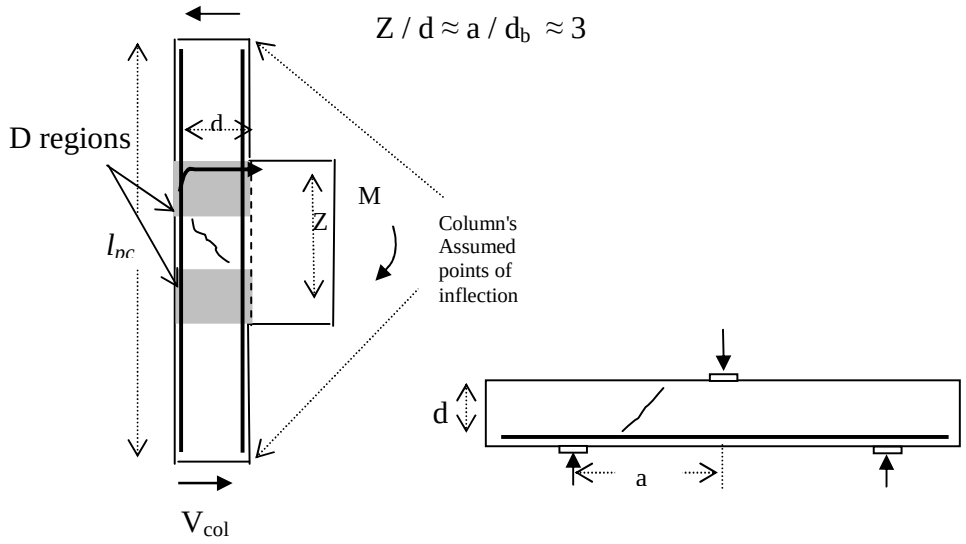

(a) Exterior BCJ (b) Analogous beam

Figure 5.60: Analogy between a BCJ made from a deep transfer beam and a shallow column and a beam of span to depth ratio of 3.

The presence of cold joints between column and beam near BCJ had been of concern until the recent ACI recommendation that the shear behaviour of BCJ determines the position of the cold joint between beam and the column, Figure 5.20.

The presence of CVB, Figure 5.61, deflects inclined compression forces proportionally depending on the strength of the concrete in the joint and the diagonal strut deflection throughout the depth of the joint to improve arching action. This is also due to the moment produced from dowel forces by CVB restricting propagation of flexural and inclined cracks.

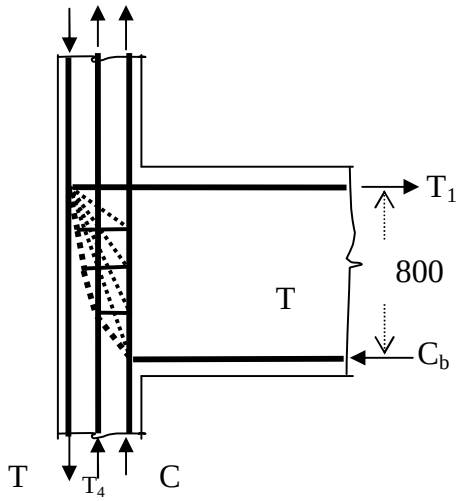

Figure 5.61: STM with stirrups and CVB, aspect ratio=3.

5.8 Discussion and conclusion on STM for beams and BCJ

HWB can deflect the inclined compression forces within the shear span of the HSC beam. When the concrete is of normal strength this deflection is not much and as a result the inclined compression forces are not that high, the diagonal strut is not wide and strong enough to demand the tension steel to yield, therefore full STM action with yielding of tension steel does not take place which is the case with beams NSC2, NSC3 and NSC4.

When the concrete is of high strength, and the HWB is present, the diagonal strut is deflected enabling it to become wider and stronger within the upper half of the beam and therefore enabling the beam to take more compressive force in the form of arching action which in turn would demand further performance and dissipation of energy from the tension bar to balance this force, resulting in tension reinforcement yielding. The action causing this deflection of the strut is demonstrated by investigating the strain gauge readings of the experimental results on top and bottom of the HWB within the shear span where the deflection of strut occurs.

When a HWB was introduced the shear cracking resistance is improved and the main crack width restrained, allowing the development of full arching capacity of the structural system, simultaneously develop smaller cracks parallel to the main crack due to presence of HWB which dissipate the energy from ultimate loading and produces a more ductile mode of failure.

The upper limit of a/d=3 may be increased for HSC beams with HWB, which has more effect on arching capacity than on shear cracking resistance. When beams are a/d=3, in the absence of HWB, the weakness in shear behaviour of HSC resulting from absence of aggregate interlock is apparent. However, when horizontal web reinforcement is introduced the shear cracking resistance is also improved and crack width is restrained, allowing development of full arching capacity of the structural system.

Dowel forces are reasonably easy to visualize at flexural cracks, but very complex to picture when they act on inclined cracks. It is difficult to propose actions by which they can be transmitted into the main internal structural system. Certain assumptions based on visualizing dowel action on inclined cracks resembling dowel action in flexural cracks were introduced. Also the complex interaction of the dowel action from the HWB, diagonal compression from HSC and tensile force in the stirrup needed to be simultaneously visualized.

When the ratio of web reinforcement is low a load greater than the shear cracking load can often be resisted by a combination of arch and truss actions as long as a/d ≈3, Figure 5.23. The limit is not an exact one but tends to increase with increasing concrete strength, which has more effect on arch capacity than on shear cracking resistance. To propose a STM based on failure criteria is complex as STM is lower-bound plastic theory and does not have any compatibility condition. In HSC due to absence of aggregate interlock shear, cracking resistance is comparatively low and may be less than NSC dependent on the type of the aggregate.

This research demonstrates that presence of the strut in the BCJ of HSC columns with CVB and transfer beams with aspect ratio $3>h_b/h_c>2.5$ solve the main problem in developing STM which is in determining the node dimensions for HSC-BCJ. CVB can deflect the inclined compression forces in beams of $2.5 \leq h_b/h_c \leq 3$ which will result in a new node at B. As the angle of the main diagonal strut α initially reduces to φ and finally β, the strut becomes wider, Figure 5-62. In HSC this wider strut contributes to a noticeable improvement in arching action and in combination with improved dowel action of CVB due to higher strength of concrete, a further improvement in shear is noticed.

In beams with shear reinforcement, if a simple truss model is used, there is a division and contradiction amongst all the codes regarding the limit to the angle of compression strut to horizontal θ_{lim} (cot θ_{lim}=a/d).

All the codes give $\theta_{lim} \leq 3$, however, this research demonstrates that in HSC beams with shear reinforcement and HWB , if a simple truss model is used θ_{lim} can be increased to 3.02 which is larger than the upper limit all the codes have so far recommended. CEB-FIP90 gives the closest prediction, however, it should be amended to give provision for HSC beams with HWB and after introducing this structural system, θ_{lim} is recommended to increase from $\theta_{lim} \leq 3$ to $\theta_{lim} \approx 3$.

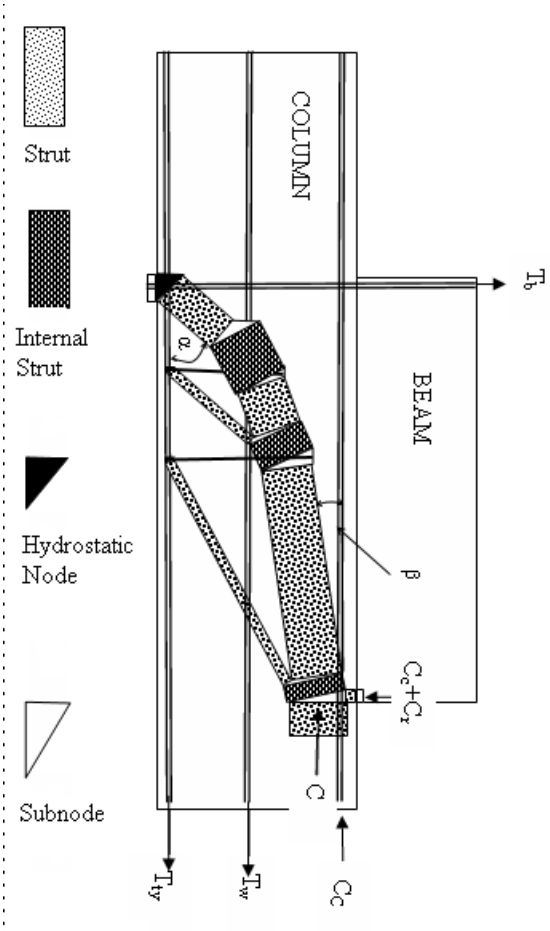

Figure 5-62: STM of the proposed HSC- BCJ with stirrup and CVB of aspect ratio=3

Placas and Regan [5-48] carried out an extensive test programme for the investigation of the shear resistance of reinforced concrete beams. They observed that in beams provided with stirrups there were two primary modes of shear failure: (1) shear compression involving a criterion of compression failure in the concrete, and (2) shearing failure involving mainly vertical displacements across shear cracks. In the latter case it was observed that the interlock forces tend to produce flatter cracks until an inclination of about 26° when vertical stirrups are used, and about 18° when 45° inclined stirrups are provided [5-48]. MacGregor [5-7] suggests that, in design, the value of θ should be in the range of 25° to 65°. Grob and Thurlimann [5-3] proposed limits for θ equal to 26.6° and 63.4°.

It was demonstrated that when designing HSC beams with stirrups and HWB of a/d=3.02 the

lower limits for strut inclination θ can be 19.67º reducing to φ=14.25º and finally β=13.26º, which is 26% lower than 18° suggested by Placas and Regan [5-48] , 20% less than MacGregor's [5-7] and 25% less than Grob and Thurlimann's [5-3] proposed lower limit.

ACI Code, Appendix B [5-23] makes a conservative recommendation for the slope of strut to be taken as 2:1 (longitudinal to transverse). However, this research demonstrates that when HSC beams with HWB or BCJ with CVB are being considered, this ratio can be extended up to the value of 2.78 :1 as demonstrated, with the lower limits for strut inclination being α=19.67º, reducing to φ=14.25º and finally β=13.26º for the specific cases, Figure 5-35 to Figure 5-34.

This research demonstrates that the main diagonal compression strut deflects due to the presence of HWB in short beams contrary to the model proposed by Rogowsky and MacGregor [5-10], Figure 5.55, although for reasons of simplifying design procedures in shear walls or deep beams their model may be considered as HWB do not seem to have a noticeable contribution when used with NSC.

When considering reduction factors for compressive struts, Nielson et al [5-4] proposed this factor to be taken as 0.45 for uncracked region of concrete of 50MPa compared to 0.6 which is the lower bound compressive strength recommendation of most codes. This difference suggests that further research for finding more accurate values for reduction factors for HSC is needed.

The position of the maximum moment from dowel action was identified by FE modeling the moment produced from transverse loading on the HWB. Concentration of dowel action was demonstrated to occur at 0.3 of length of shear span (a) from the support, Figure 5.30. The fan action produced by the dowel forces within the fan action produced by the stirrups in the HSC beam resulted in significant improvement in shear performance.

STM has been developed for HSC BCJ with CVB in the column and with the beam as transfer beams with aspect ratio $3>h_b/h_c>2.5$. The STM was used to solve the main problem in the TBCJ and to determine the node dimensions for HSC-TBCJ.

The deflected strut developed in HSC is wider than that of NSC and this contributed in better arching action in the beam, which together with the dowel action of HWB or CVB will result in significant improvement in the shear capacity of the beam of a/d=0.3 or the TBCJ.

It has been shown that the angle of the strut inclination developed in HSC beam (a/d=3) with stirrups and HWB is significantly smaller than the angle calculated by past research for NSC beams without HWB, Table 5.2.

In section 5.7.5, Performance of forces in BCJ reinforcement, a detailed investigation of anchorage of beam bars in BCJ demonstrates the significant stress transfer to the tail of the L bar, Table 5.7 and Figure 5.54.

5.9 References for Chapter 5

5-1 Yankelevsky, D. Z., 'Engineering Models and Computer Codes'. Journal of Professional Issues in Engineering, ASCE, V.114, No.2, Apr. 1988, pp.218-230

5-2 Morsch. E.: Der Eisenbetonau. 3rd ed (1908). Published in English as 'Concrete-Steel construction'. New York, Engineering News Publishing Co. 1909

5-3 Grob, J., Thurlimann, B. — "Ultimate Strength and Design of Reinforced Concrete Beams under Bending and Shear", IABSE - International Association for Bridge and Structural Engineering, Vol. 36-11, 1976, pp. 105-120.

5-4 Nielsen, M.P., Braestrup, M.W., Jensen, B.C., Bach, F. — "Concrete Plasticity -Beam Shear, Shear in Joints, Punching Shear", Danish Society for Structural Science and Engineering, Structural Research Laboratory, Technical University of Denmark, Special Publication, 1978.

5-5 Marti, P., "Basic Tools of Reinforced Concrete Beam Design," ACI Journal, Proceedings, Vol. 82, No. 1, January-February 1985, pp. 45-56.

5-6 Schlaich, J., Schäfer, K., and Jennewein, M., "Toward a Consistent Design of Structural Concrete," Journal of the Prestressed Concrete Institute, Vol. 32, No. 3, May-June 1987, pp. 74-150.

5-7 MacGregor, J.G. — "Challenges and Changes in the Design of Concrete Structures", Concrete International, Vol., No., Feb. 1984, pp. 48-52

5-8 Streit, W., Feix, J., Kupfer, H. — "Transverse Tension Decisive for Compressive Resistance of Concrete Cover", IABSE Colloquium - Stuttgart 1991, Vol. 62, pp. 761-766.

5-9 Schlaich, J., Schafer, K. — "Design and Detailing of Structural Concrete Using Strut-and-tie Models", The Structural Engineer, Vol. 69, No. 6, March 1991, pp. 113-125.

5-10 Rogowsky, D.M., MacGregor, J.G. — "Design of Reinforced Concrete Deep Beams", Concrete International - Design and Construction, Vol. 8, No. 8, August 1986, pp. 49-58.

5-11 Walraven, J.C., Lehwalter, N. — "The Bearing Capacity of Concrete Compression Struts in Short Members and Deep Beams", Darmstadt Concrete Annual Journal on Concrete and Concrete Structures, Vol. 3, 1988, pp. 117-128.

5-12 Vecchio, F.J., Collins, M.P. — "Stress Strain Characteristics of Reinforced Concrete in Pure Shear", Final Report, IABSE - Colloquium on Advanced Mechanics of Reinforced Concrete, Delft, 1981, pp. 211-225.

5-13 Placas, A., Regan, P.E. — "Shear Failure of Reinforced Concrete Beams", ACI Journal, Vol. 68, No. 10, October 1971, pp. 763-773.

5-14 Collins, M.P., Mitchell, D. — "Shear and Torsion Design of Prestressed and Non-Prestressed Concrete Beams", PCI Journal, Vol. 25, No. 5, Sept./Oct. 1980, pp. 32-100.

5-15 Schlaich, J, Weischede, D - "Detailing of Concrete Structures (in German)",Bulletin d'information 150, Comite Euro-International du Beton, Paris, March 1982, 173 pages.

5-16 Comité Euro-International du Béton, CEB-FIP Model Code 1990, Thomas Telford Services, Ltd., London, 1993, 437 pp.

5-17 FIP Commission 3, Practical Design of Structural Concrete, Fédération Internationale de la Precontrainte, Laussane, Switzerland, September 1999, 114 pp.

5-18 Eurocode 2: Design of concrete structures, Part 1-1, General rules and rules for buildings, BS EN 1992-1-1:2004, British Standards Institution, London, Dec 2004

5-19 CSA Technical Committee A23.3, Design of Concrete Structures CSA A23.3-94, Canadian Standards Association, Rexdale, Ontario, December 1994, 199 pp.

5-20 AASHTO LRFD Bridge Specifications, American Association of State Highway and Transportation Officials, 2nd ed., Washington, DC, 1998, 1116, pp

5-22 ``ACI-ASCE Committee 426 – "Suggested Revision to shear Provisions for Building Code", American Concrete Institute, Detroit, 1977,99 pp

5-23 ACI Committee 318, Building Code Requirements for Structural Concrete (ACI 318-08) and Commentary (ACI 318R-08), American Concrete Institute , Formington Hills, MI, 2008, 465 pp

5-24BS 8110: Structural Use of Concrete, Part 1.Code of practice for design and construction, British Standards Institution, London, 1985

5-25 Canadian Standards Association – CAN3-A23.3-M84 – 'Design of Concrete Structures for Buildings', Concrete Design Hand book, Canadian Portland Cement Association, 1985

5-26 FIP Report September 1999 ' Practical design of structural concrete' FIP Report September 1999, ISBN:978-1-874266-48-8

5-27 Collins, M.P, "Towards a rational theory for RC members in shear", ASCE Journal of the structural division, Vol. 104, No. ST4, April 1978, pp.649-666

5-28 Collins, M.P, Mitchell, D. "A rational approach to shear-1984 Canadian Code Provision", ACI Journal, Vol. 83, No. 6, Nov./Dec. 1986, pp. 925-933

5-29 Regan, P.E. – ‘Shear in Reinforced Concrete – An Analytical Study’, Report to the Construction Industry Research and Information Association – CIRIA, April, 199pp

5-30 Kani, G.N.J. — "Riddle of Shear Failure and its Solution", ACI Journal, Vol.61, No. 4, April 1964, pp. 441-467.

5-31 Kani, G.N.J. — "Basic Facts Concerning Shear Failure", ACI Journal, Vol. 63, June 1966, pp. 675-692.

5-32 Kani, G.N.J. — "Kani on Shear in Reinforced Concrete", Department of Civil Engineering - University of Toronto, Canada, 1979.

5-33 Zsutty, T.C. — "Beam Shear Strength Prediction by Analysis of Existing Data", ACI Journal, Vol. 65, Nov. 1968, pp. 943-951.

5-34 Zsutty, T.C. — "Shear Strength Prediction for Separate Categories of Simple Beam Tests", ACI Journal, Vol. 68, No. 2, February 1971, pp. 138-143.

5-35 Wight K.J, MacGregor J.G. 'Reinforced Concrete Mechanics & Design'. Pearson International Edition, fifth Edition 2009.

5-36 Regan, P. E. 'Research on shear: a benefit to humanity or waste of time?'. The Structural Engineer/Volume 71/No 19/5 October 1993.

5-37 Park, R. and Paulay, T. 'Reinforced Concrete Structures' John Wiley and Sons: 1975, 767 pp.

5-38 Paulay, T. and Park, R., "Joints in Reinforced Concrete Earthquake Resistance", Research Report 849, University of Canterbury, Christchurch, 1984, 71 pp.

5-39 Vollum R. L , Newman J.B., ‘Strut and tie models for the analysis /design of external reinforced concrete beam-column joints’. Magazine of Concrete Research, 1999, 51, No. 6, pp 415-425

5-40 Vollum, R and Parker, D. “External beam-column joints: design to Eurocode 2”, Magazine of Concrete Research, 2008, 60, No7, September , pp 511-521

5-41 Bakir, P.G, Boduroglu, H..M. ‘The review of strut-and-tie models suggested for exterior beam column connections’. Transactions on the Built Environment, Vol 57, 2001

5-42 Reys de Ortiz, I. ‘STM of reinforced concrete short beams and beam column joints’. PhD thesis, 1993, University of Westminster.

5-43 Scott, R.H, Hamill, S.J. “Connection zone strain in reinforced concrete beam column connections”, Proceedings of the 11th International Conference on Experimental Mechanics, Oxford, UK, 1998. pp. 65-69.

5-44 Parker, D.E, Bullman, P.J.M. Shear strength within reinforced concrete beam column joints. The Structural Engineer 1997; 75(4):pp 53–7

5-45 Marques J. L. G., Jirsa J. O., “A study of Hooked Bar Anchorages in Beam-Column Joints,”.ACI Journal, Proceeding s. Vol 72, No. 5, May 1975, pp. 198-209

5-46 Jirsa, J.O., Marques, J. L. G., "A study of hooked bar anchorages in beam-column joints,” Austin, University of Texas at Austin, Department of Civil Engineering, July 1972. Final report project 33

5-47 Atta, A.E. Taher, S.E.F, Khalil, A.H.A, El-Metwally S.E ‘ Behaviour of reinforced high-strength concrete beam column joint. Part 1: Experimental investigation’. Structural Concrete.2003.4.No4

48 Placas, A., Regan, P.E. — "Shear Failure of Reinforced Concrete Beams", ACI Journal, Vol. 68, No. 10, October 1971, pp. 763-773.

Chapter 6

Influence of Central Vertical Bar on Shear Performance of Beam Column Joint

6.1 Introduction

It has been recognised in industrialised countries located in seismic zones that BCJ can be critical regions in reinforced concrete frames and should be as strong or stronger than the members framing into them, which is why joint shear design for BCJ has been the subject of numerous research projects over the past three decades.

The shear design of BCJ is normally assessed in seismic countries where reports following earthquakes have identified BCJ as a critical part of the reinforced concrete frame structure.

Many tall reinforced concrete frames are built with transfer beams to provide clear spaces in their entrance halls. With the advantages of HSC, many such buildings are made with HSC columns. The external BCJ made up of transfer beam and HSC columns have a unique shear behaviour which, to this writer's knowledge, has not yet been investigated by any other researchers.

This chapter investigates the shear behaviour of external HSC BCJ with transfer beams exposed to monotonic loading. Transfer beams are comparatively deep and their beam to column aspect ratio can be as high as three.

This writer's experiments on 12 beams produced surprising results on the shear behaviour of HSC beams with and without HWB. The experiments demonstrated that the shear resistance of HSC beams with limestone aggregate could be less than that of NSC beams when shear span to depth ratio is three. However, the presence of HWB reverses the situation and significantly improves the shear resistance in HSC beams due to stabilising arching affect.

The analogy between the shear resistance in HSC beams with HWB of a/d≤3 subjected to the stabilising arching affect from dowel action and the joint shear resistance in HSC-BCJ with CVB for BCJ with aspect ratio $3 \geq h_b/h_c \geq 2.5$ is discussed in Chapter 1.
In Chapter 5 it was demonstrated that HSC beams of shear span a/d≤3 with HWB behave similarly to short beams of shear span 2≤a/d≤2.5 which are mainly dependent on arching affect for their shear resistance and since the shear behaviour of short beams is analogous to BCJ, similarly HSC beams of shear span a/d≤3 with HWB are analogous to HSC –BCJ with CVB and aspect ratio≤3.

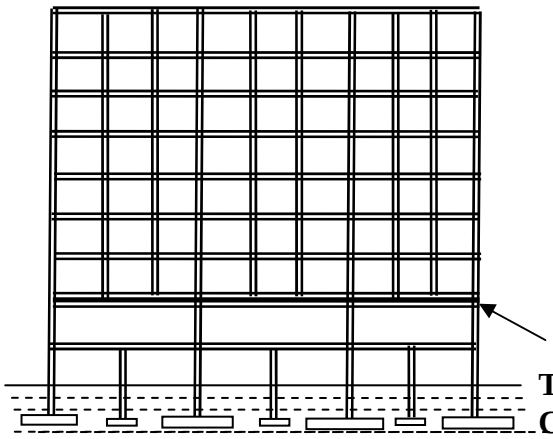

Figure 6.1: A multi storey building with transfer beams of aspect ratio $3 \geq h_b/h_c \geq 2.5$

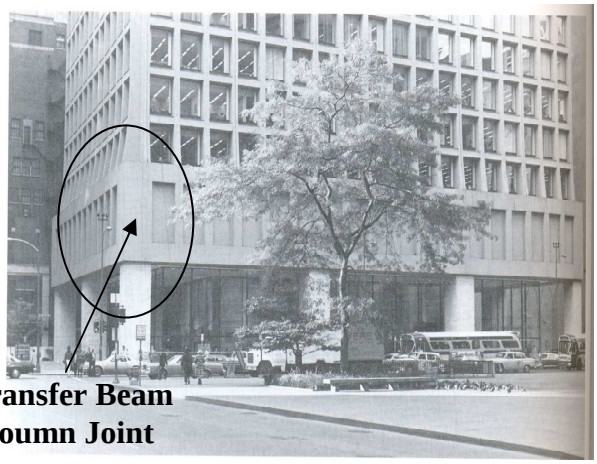

Figure 6.2: External TBCJ at Brunswick building, Chicago, USA

In this chapter, after an extensive literature review and analysis of past experimental work, an empirical design rule is developed to predict the joint shear resistance of HSC-BCJ of joint aspect ratio≤3 with CVB. In addition, a design rule for predicting the amount of shear stirrup in BCJ is proposed. This will be presented in the following order:

- Design approach for shear, anchorage, beam reinforcement and detailing of connection bars in BCJ.

- Comparison of Eurocode 2 [6-1] and ACI 318 [6-5] for the design of anchorage reinforcement, and of Eurocode 8 [6-20] and ACI 352 [6-22] for design of joint shear in BCJ.

- Investigation of Taylor's [6-2] design rule for crack formation in BCJ and choosing correct relation of tension to compression for concrete in this design rule.

- Introduction to the behaviour of external TBCJ of HSC, and the influence of dowel action from CVB on this type of joint

- Proposal for a design rule applicable to BCJ in general and HSC transfer beam and column joints in particular when CVB are present.

- Verification of the proposed design rule and comparison of its accuracy with rules from Eurocode 2 [6-1] and ACI 352 [6-22].

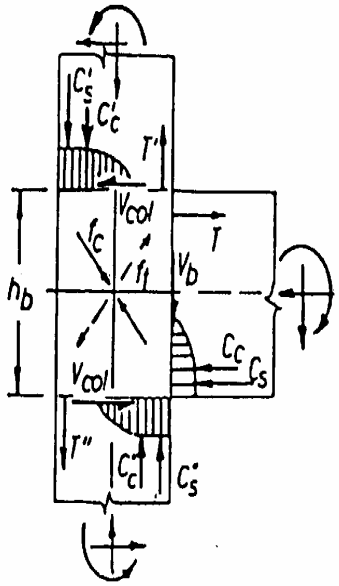

Figure 6.3: Internal forces on BCJ when no CVB is applied in NSC aspect ratio less than 2

Figure 6.4: External BCJ failure in the 1985 Mexico earthquake.
Source: Cheung, Pauly, Park [6-3] [1993]

6.2 Design of reinforced concrete BCJ

Design standards in the 1960s and earlier gave no attention to detailing BCJ of moment resisting reinforced concrete frames. With improvement in the detailing of the adjacent beams and columns, the consequence of the lack of attention to the shear strength of BCJ

has been demonstrated by the severe diagonal tension cracking in that region observed in many laboratory tests and structures during earthquakes.

The consequence of the diagonal tension cracking is a significant increase in flexibility of the frame and joint shear failure that has often led to collapse or unrepairable damage to the structure, Figure 6.4.

However, seismic design codes differ significantly in their design approaches to BCJ, and this remains probably the most controversial aspect of the seismic design of reinforced concrete moment resisting frames at present [6-4], hence there are considerable differences in design procedures for transverse reinforcement in BCJ in the various seismic codes of the world.

In this chapter, the influence of various parameters on the joint shear from the past BCJ experiments is reviewed and the existing recommendations on the influence of various parameters on joint shear are discussed.

Following a review of the EC8-NA [6-20] and ACI352 [22] design methods and the past experimental research on BCJ, an empirical design equation is proposed for the joint shear of BCJ introducing the shear resisting contribution of dowel action from the vertical bars located in the centre of the depth of the column at the joint. This predicted joint shear from the proposed design rule is compared with the guidelines from the existing codes.

A proposed design rule for joint shear in relation to prediction of quantity of CVB in the column as shear reinforcement in HSC BCJ with large aspect ratio will be introduced.

Finally, the joint shear contribution is investigated of vertical reinforcement at half the column depth or in layers within the depth of the BCJ as additional reinforcement or part of the column longitudinal reinforcement contribution to the joint shear resistance Vc at the BCJ of HSC columns and transfer beams.

6.2.1 The loading of exterior joints

The behaviour of BCJ can be explained by using a free body including the joint and extending between points of contra flexure at half storey height. Generally, the shear load input into an exterior BCJ is less than that encountered with interior joints since only one beam frames into the column, as shown in Figure 6.5, from the internal stress resultants, Figure 6.3, it is evident that the horizontal shear force is:

$V_j = C_c + C_s - V_{col}$ **6.1**

or,

$V_j = T - V_{col}$ **6.2**

$T = \frac{M}{Z}$ ***6.3***

where, V_j is the joint shear, C_c is the concrete compressive force in the flexural compression zone, C_s is the compression force in the compression reinforcement, V_{col} is the horizontal shear force across a column, T is tension force in tension reinforcement, M is the beam moment at the column face where beam connects to it, and Z is the flexural lever arm. Figure 6.5.

Generally, the theoretical joint shear force is dependent on the assumption used to calculate M and Z. In this section M is taken as:
M= P (L+d') not including the self weight of the beam.
L= Distance from the load to the face of the column facing the beam.
d'= The column cover and radius of the column reinforcement nearest to the beam.
The tensile force in the beam reinforcement was calculated by section analysis assuming linear strain distribution. The stress block from EC2 [6-1] was used for concrete with the assumed maximum stress value of 0.8 f_{cu} at a compressive strain of 0.002. In the analysis of BCJ, the beam width is taken as the width of compressive stress block.

The reinforcement elastic modulus was taken as 200GPa as an elastoplastic stress-strain response was assumed for it. No safety factor for the material was applied.

The value of the tension force in the above is either $f_s A_s$ or $\lambda f_y A_s$, depending on whether an elastic beam section or the critical section of a plastic hinge is being considered at the face of the column. λ is the steel strength factor of 1.25.

From consideration of moment equilibrium with respect to point C, the average column shear may be calculated by

$$V_{col} = \frac{2 \cdot M_n + h_c \cdot P}{\ell_c + \ell_c^{'}} \qquad \textbf{6.4}$$

where the magnitude of M_n depends on the value of beam tension force, T. ℓ_c and $\ell_c^{'}$ are the column heights measured from the beam centreline.

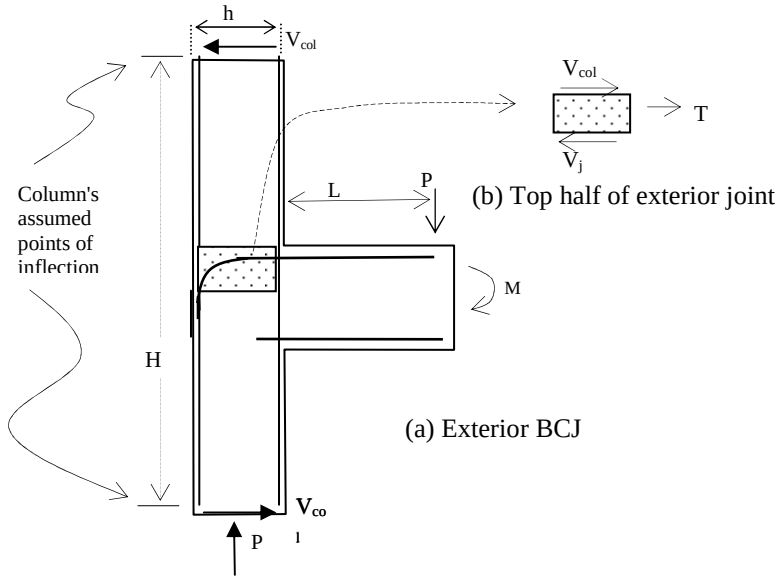

Figure 6.5: Forces acting on external BCJ

$$V_j = T - V_{col} \qquad P \times (L + \frac{h}{2}) = V_{col} \times H \qquad T = \frac{M}{Z} = \lambda A_s f_y$$

V_j	joint shear	V_{col}	horizontal shear force across the column
P	beam load	T	tension force in tension reinforcement
Z	flexural lever arm	M	beam moment at the column face
L	beam length	h	depth of column
A_s	area of beam steel	f_y	Steel yield stress
λ	strength factor = 1.25		
H	Height of column between points of inflection		

Furthermore, the vertical joint shear force from the equilibrium of the stress resultants i.e.,

$$V_{jv} = T^{''} + C_c^{'} + C_s^{'} \qquad \textbf{6.5}$$

or,

$$V_{jv} = T^{'} + C_c^{''} + C_s^{''} - V_b \qquad \textbf{6.6}$$

where $T^{'}, T^{''}$ are tension forces in tension reinforcement, $C_c^{'}$, $C_c^{''}$ are the concrete compressive forces in the flexural compression zone, $C_s^{'}$, $C_s^{''}$ are compression forces in the

compression reinforcement and V_b is the beam induced shear force at the face of the column, Figure 6.3.

.

However, by taking into account the distance between the various stress resultants and the member dimensions, an approximation for the vertical joint shear force for most design situations is computed with adequate accuracy as

$$V_{jv} = \frac{h_b}{h_c} \cdot V_j \qquad \textbf{6.7}$$

$$v_j = \frac{V_j}{b_e h_c} \qquad \textbf{6.8}$$

where, h_b is the depth of beam and h_c is the overall depth of the column in the direction of the horizontal shear to be considered.

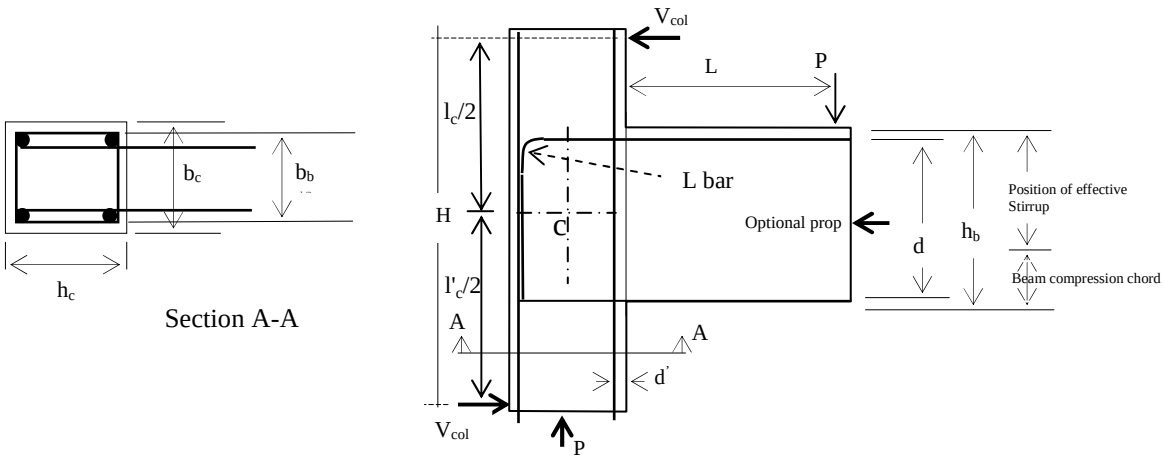

Figure 6.6: Notations used for the BCJ. L bar connections between beam and column improve joint shear by 10% to 20% [6-34] .

6.2.2 The design criteria of BCJ

Eight main concerns for the design of BCJ are as follows:

1. The strength of joint should not be less than the maximum strength of the weakest member with which it connects.
2. The strength capacity of a column should not be jeopardized by possible strength degradation within the joint or from anchorage failure.
3. The joint should be considered as an integral part of the column.
4. The joint reinforcement necessary to ensure satisfactory performance should not cause construction difficulties.

5. Cold joints above and below the joint must have the same strength capacity as the column and the joint.
6. Connection bars between beam and column with regards to type whether L or U and radius of bend of the bar should be designed and detailed. The area of connection steel should not exceed $1.25f_yAs$ of the steel required for the beam connection.
7. The area of reinforcement required in the top of the beam should be based on the bending moment at the face of the column and it is not good practice to design the beam tension steel for the moments at the centre of the column.
8. Design of large aspect ratio HSC-BCJ should satisfy the design proposal given in this chapter and should include CVB to ensure satisfactory joint shear resistance.

6.2.3 General design Guidance from EC2 [6-1], EC8 [6-20] and ACI 318 [6-5]

European Code EC2 [6-1] section 9.9 recommends that regions with discontinuity in geometry or action (D regions) should normally be designed and detailed with STM according to section 6.5 and detailed according to the rules given in Section 8. It recommends that the reinforcement , corresponding to the ties, should be fully anchored by an anchorage of l_{bd} according to section 8.4.

Annex J.2.2 recommends a STM for $h_c/h_b < 2/3$ for a limited range of $\tan\theta$. The value of $\tan\theta$ in a country may be found in its National Annex .

EC2 [6-1] has a conservative design rule to calculate the shear strength of columns and makes recommendation to use a diagonal strut mechanism for shear design at discontinuities.

European Code EC2 [6-1] allows use of concrete of up to 90MPa for BCJ. Both EC2 [6-1] and BS8110 [6-10] recommend standard methods to calculate the shear strength of the column which is also applied as a means of calculating shear in BCJ if the structure is not subjected to seismic loading.

EC8 [6-20] guidance for BCJ recognizes the importance of vertical bars between column corners at both depth and width of the BCJ but does not provide a shear design rule for the bars between column corners within the depth of column. EC8 [6-20] design guidelines

does not allow for the contribution of the stirrups and connection reinforcement detailing to joint shear.

The ACI 318 Code [6-5] covers BCJ design in several sections:
1. ACI 318 Code [6-5],, Section 7.9, requires enclosure of splices of continuing bars and of the end anchorages of bars terminating in connections of primary framing members, such as beams and columns.
2. ACI 318 Code [6-5], Section 11.10.2, requires a minimum amount of lateral reinforcement (ties or stirrups) in BCJ if the joints are not restrained on all four sides by beams or slabs of approximately equal depth. The amount required is the same as the minimum stirrup requirement for beams (ACI Equation (11-13)).
3. ACI 318 Code [6-5], Section 12.12.1, requires negative-moment reinforcement in beams to be anchored in, or through, the supporting member by embedment length, hooks, or mechanical anchorage.
4. ACI 318 Code [6-5], Section 12.11.2, requires that in frames forming the primary lateral load-resisting system, a portion of the positive-moment steel should be anchored in the joint to develop the yield strength, f_y' in tension at the face of the support.
The above sections do not give specific guidance for design. Design guidelines can be obtained from [6-6], [6-7], [6-8], [6-9] and ACI-ASCE Committee 352 [6-22].

In the following sub-sections we study the existing design equations for external BCJ subjected to monotonic loading.

6.2.4 Code design guidance for bent anchorages and bearing stress

Bends are used to provide additional anchorage when there is insufficient straight length available to develop a bar. Most codes prescribe a minimum radius of bend. It is important to note that the actual minimum size of the bend is frequently critical in detailing a structure.

EC2 [6-1] recommends that the minimum diameter to which a bar is bent shall be such as to avoid bending cracks in the bar, and to avoid failure of the concrete inside the bend of the bar.

In order to avoid damage to the reinforcement the diameter to which the bar is bent (Mandrel diameter) should not be less than $\phi_{m,min}$ the value of which may be found in the National Annex in the country of use. The recommended value is given in Table 6-1.

The mandrel diameter needs to be checked with the following expression to avoid concrete failure if the bar is positioned at the plane of bend close to concrete face and there is a cross bar with a diameter$\geq \phi$ inside the bend

$$\phi_{m,\min} \geq F_{bt}((1/a_b)+1/(2\phi))/f_{cd}$$

The value of f_{cd} should not exceed the value for concrete class C55/67

Code	Bar diameter	Minimum mandrel diameter for bends, hooks, and loops
EC 2	$\phi \leq 16$mm	4ϕ
	$\phi > 16$mm	7ϕ
ACI 318	25.4mm$\geq\phi\geq$9.55mm	6ϕ
	35.81mm$\geq\phi\geq$28.65mm	8ϕ
	57.33mm$\geq\phi\geq$43mm	10ϕ

Table 6.1: Minimum mandrel diameter to EC2 and [6-1] ACI 318 [6-5]

BS-8110 [6-10] gives the following equation to calculate the design bearing stress:

$$\sigma_{be} = \frac{F_{bt}}{r\phi} \leq \frac{2f_{cu}}{1+2(\phi/a_b)} \qquad \textbf{6.9}$$

where

F_{bt} is the tensile force due to ultimate loads in a bar or group of bars in contact at the start of a bend

r is the internal radius of the bend

ϕ is the size of the bar

a_b for a given bar is the centre to centre distance between bars perpendicular to the plane of the bend; for a bar adjacent to the face of the member, a_b should be taken as the cover plus ϕ .

This equation includes an allowance for a partial safety factor γ_m= 1.5 for concrete strength.

CEB-90 [6-11] gives the following equation in order to avoid cracking or crushing under local compression.

$$f_{cc}^{*} = f_{cc}\sqrt{\frac{A_2}{A_1}} \leq 4 f_{cc} \qquad \textbf{6.10}$$

where

f_{cc}^{*} is the bearing capacity of concrete under local compression

f_{cc} is the compressive strength of concrete under uniaxial stress, where the reduction factors α_1 and α_2 are also applicable

A_1 is the loaded area; $A_1 = \acute{o}\pi r/2$

A_2 is the cross section of the surrounding concrete into which the stress field develops

$A_2 = (c+\acute{o}+e/2)\ \pi r/2$ where c is the cover and e is the clear distance between the bars. The strength f_{cc}^{*} equals 1.24 $\alpha_1 f_c$ or 1.24 $\alpha_2 f_c$ according to the region. Near failure the region inside the bend is cracked and the factor α_2 should apply as long as the bearing stresses occurs in the radial direction and the angle between the cracks and the compression field is variable.

In ACI318 [6-5], the design process described in Section 12.5.1 does not distinguish between 90º and 180º or between top and bottom bar bends. The development length of a bend, l_{dh}, Figure 6.7, is calculated by using the following formulae:

$l_{dh} = [(0.02\psi_e\ f_y / \lambda\sqrt{f_c'})]d_b \times$ (applicable factor from ACI Code Section 12.5.3 varies from 0.7 to 1)

ψ_e = 1.2 for epoxy coated bars or wires and 1.0 for galvanized and un-coated reinforcement, and λ is the lightweight aggregate factor given in ACI Code Section 8.6.1. Values of l_{dh} for uncoated bars in normal-weight concrete are given in Tables A-8 and A-8M.

The factors from ACI Code Section 12.5.3 account for the confinement of the hook by over and stirrup. Confinement links reduce the possibility of the concrete between the hook and the concrete surface spalling off, resulting in premature failure of the hook.

ACI Code Section 12.5.3(a) gives minimum dimensions for 90º and 180º hooks as follows: For 180º hooks on 35.8 mm and smaller bars with side cover normal to the plane of the hook, not less than 63.5 mm$\times$0.7. For 90º hooks on 35.8 mm and smaller bars with side cover normal to the plane of the hook, not less than 63.5 mm and cover on the bar extension (tail) beyond the hook not less than 50.8 mm$\times$0.7.

The multipliers in ACI Code Section 12.5.3(b) and (c) reflect the confinement of the concrete outside the hook. 12.5.3(b) for 90º hooks on 35.8 mm and smaller bars that are enclosed within stirrups parallel to the bar being developed, spaced not greater than 3 d_b along the length of the tail extension of the hook plus bend.

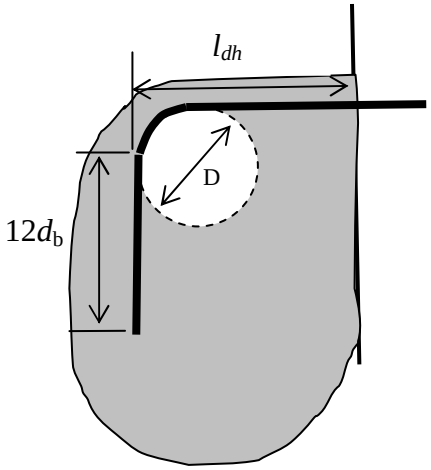

Figure 6.7: Standard 90º hook – ACI Section 7.1 and 7.2.1

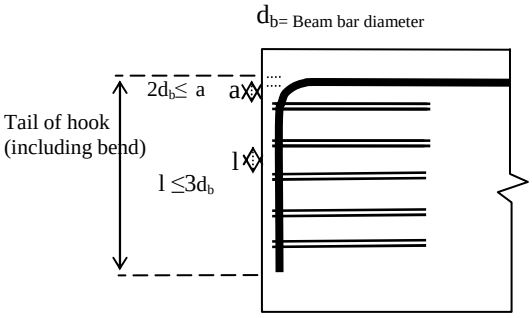

Figure 6.8: Confinement of hooks by stirrups with applicable factor from ACI

6.3 Literature review on shear behaviour in BCJ

As will be shown in this literature review, there is little agreement over the parameters which influence the shear behaviour of external BCJ amongst the past researchers.

6.3.1 Taylor's prediction for the diagonal cracking

Taylor [6-2] assumed that for external BCJ the philosophy of the column to be loaded with its working load and the beam to be loaded to ultimate is realistic, and this was used in his tests. He made a total of 26 tests on exterior BCJ of which aspect ratio of 20 specimens were 1.4 and 1.25, Figure 6.9. All were subjected to monotonic loading. In these tests, apart from the first specimen, the beam-ends were horizontally propped so that the joint could continue to carry increasing moment after the failure of its opening side. Nine of Taylor's specimens failed in joint, Figure 6.9.

Failure of a hook almost always involves crushing of the concrete inside the hook. If the hook is close to a side face, the crushing will extend to the surface of the concrete, removing the cover from that face. Rarely, the concrete outside the tail will crack, allowing the tail to straighten.

Tests on bars hooked around a corner bar have demonstrated that tensile stresses can

develop at a given end slip that are 10 to 30% larger than if the hook does not contain a bar.

The specimens were $^{3}/_{4}^{th}$ of a normal prototype size. The columns were instrumented with a series of points for a demountable mechanical Demec gauge close to the edge of the column. Three inclinometers were used, one on the beam, one on the column above and one below the joint to measure the rotations of the opening and closing corners separately.

In Taylor's tests the detailing of the steel was in accordance with Code of Practice CP110 [6-12] with the exception that the bearing stresses under the bends of the beam steel were not calculated. The bends were all with radius 3d. The beam bars were allowed to bend and run next to, and touching , the column bars to CP110. A link was provided in the column at the centre of the joint in all specimens, other than specimen B3/41/24 which had 3 links.

Loading took place in two stages. Initially the column and beam were loaded to their working load of 240 kN, then while column load was kept constant the beams was loaded incrementally up to failure. After reaching the ultimate load, the beam test was continued by applying increments of displacement to the end of the beam and taking the load cell readings until the condition of the specimen in the rig appeared to be too dangerous to continue.

The theoretical flexural moment (M_{flex}) for the beam section was calculated by using stress block proposed by Hognestad et al [13]and compared with the diagonal cracking moment (M_d) and ultimate moment of the joint (M_u) from the experiment. The moment equilibrium equation was checked from the experimental results by taking all the moments about the centre of the joint.

The general pattern of crack development was such that the first cracks were flexural ones in the beam and appeared at 84% of the test ultimate moment when the diagonal crack moment of the joint was reached. Failure of the joint occurred when the beam steel at the face of the column yielded. The column crushed along a line parallel to the inclined crack as failure was reached. From the load-cell and the inclinometer readings it is possible to

calculate the moments carried by the column above and below the joint as well as the rotations of the two halves of the joint.

The tests were designed to investigate parameters including beam steel percentage, column ties within the joint, beam steel detail, column load and the beam thrust. The conclusion of Taylor's investigations are described and compared with conclusions from other researchers.

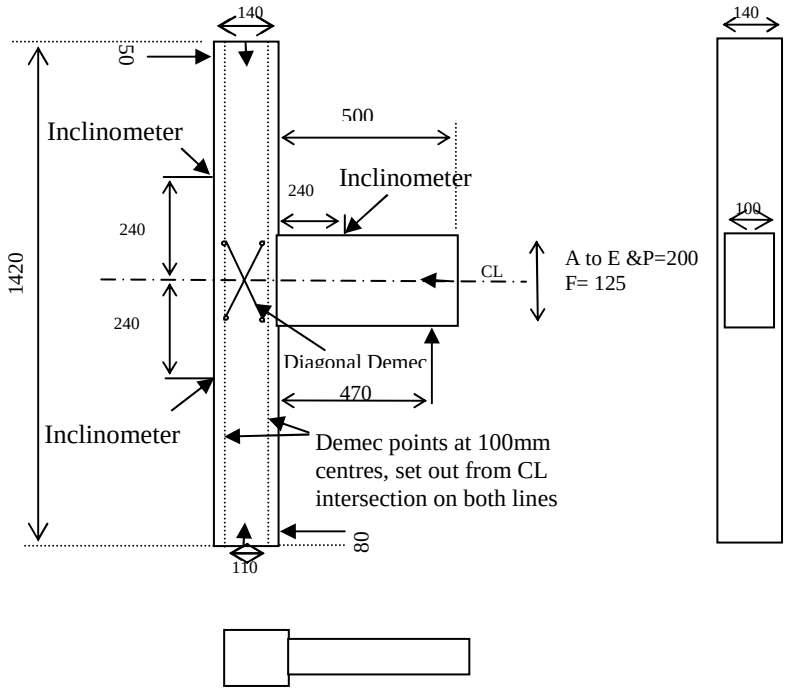

Figure 6.9:Geometry and position of test instruments in Taylor's tests (dimensions in mm)

Taylor investigated the moment of the diagonal cracking of the joint as a ratio of the theoretical flexural moment of the beam and concluded from his tests that the diagonal cracking at the working load is likely to occur in joints when beam steel percentage is more than 2.0. Even though the widths of the diagonal cracks immediately after forming were not greater than the criteria given by CP110, he recommended to design these areas so that diagonal cracking is prohibited at the working load.

Taylor developed an approximate theoretical approach to predict diagonal cracking of the joint based on principal stress analysis. From his test results he concluded that diagonal cracking initiates from the centre point of the joint, and proposed an empirical formulae to

predict the occurrence of the first crack at the centre of the joint from a principal tensile stress analysis.

Considering a uniform column stress due to the normal force, $\sigma_c = N_c /(b_c \cdot h_c)$, a uniform stress due to the beam thrust, $\sigma_b = N_b /(b_b \cdot h_b)$, and a parabolic distribution of shear with a maximum stress $1.5 \cdot v_c$; $v_c = V /(b_c \cdot h_c)$, Taylor predicted the diagonal cracking from a principal tensile strength analysis. As a result, the shear cracking stress is expressed as:

$$v_{cr} = 0.67 \cdot \sqrt{f_t^2 + \sigma_c \cdot f_t + \sigma_b \cdot f_t} \qquad \textbf{6.11}$$

where f_t is the tensile strength of the concrete.

However, after the analysis of the test data, the effect of the beam thrust was found to be small at cracking and was ignored. Therefore, the equation adopted to give a lower bound to diagonal cracking shear stress is written as:

$$v_{cr} = 0.67 \cdot \sqrt{f_t^2 + \sigma_c \cdot f_t} \qquad \textbf{6.12}$$

where $v_{cr} = V_{cr} /(b_c \cdot h_c)$ and with V_{cr} equal to the beam bars' force.

Furthermore, Taylor [6-2] with Clark [6-14] formulated a BCJ failure analysis by analogy to the behaviour of short beams as shown in Figure 1-5. From the British code, BS-CP110 [6-12], the ultimate shear stress of short beams was given as:

$$\frac{v_u}{v_c} = \frac{2 \cdot d}{a} \qquad \textbf{6.13}$$

where v_c is the concrete shear strength of a normal beam (table 5 of CP110). By considering the above equation and making a variable change ($z_b = a$) and ($d_c = d$), Taylor et al. established a lower bound solution for BCJ given by:

$$\frac{v_u}{v_c} = 3 + \frac{2 \cdot d}{a} \qquad \textbf{6.14}$$

where z_b is the lever arm of the beam at failure a is the shear span of short beams, dc is the effective depth of the column and d is the effective depth of the beam.

Taylor et al did not present any recommendations for the calculation of joint stirrups, but suggested the limitation of the beam steel percentage as the most convenient way to guarantee the strength of the BCJ. The limit of the steel ratio in the beam was given by:

$$\rho_b = \frac{A_s}{b_d \cdot d_b} = \left(3 + \frac{2 \cdot d_c}{z_b}\right) \cdot \frac{b_c \cdot d_c}{b_d \cdot d_b} \cdot \frac{\beta \cdot v_c}{0.87 \cdot f_y} \qquad \textbf{6.15}$$

where A_s is the area of the beam reinforcement, f_y is the yield strength of the steel and β is a factor accounting for the redistribution of the bending moments from the beam (β = 1-ratio of distribution). The figure of 0.87 is based on the CP110 simplified stress block approach which recommends that for a singly reinforced beam the ultimate moment of resistance is $M_u=0.87f_yA_sZ$ where A_s is the area of tension steel and Z is lever arm.

Taylor suggested that the column section below the joint should be designed to carry at least 70% of the moment supplied by the beam, in order to ensure the ability for the column to resist the extra moment imposed on it by the beam thrust. In addition, the column section above the joint should be designed to carry 50% of the beam moment.

6.3.2 Analysis of the available test data

Review and analysis of BCJ tests in experiments conducted by Taylor [6-2] in 1976, Kordina [6-15] in 1984, Sarsam [6-39] in 1985, Scott [6-16] in 1992, Ortiz [6-17] in 1993, Parker & Bullman [6-18] in 1994, Scott & Hamill [6-19] in 1998, Wilson [6-23] in 1998, and Vollum [6-35] in1999 are discussed in the analysis of available data in the following section. All these experiments were completed in the UK other than Kordina's which was performed in Germany.

Numerous tests of BCJ under cyclic loading simulating earthquakes have been performed by other researchers. In this writer's opinion, such tests have so much joint reinforcement that they are of little use for static load analysis, therefore, in this analysis, BCJ experiments exposed to incremental monotonic loading are investigated.

There is a general lack of agreement over the variable parameters such as concrete strength, column loading, joint aspect ratio, joint stirrups, beam thrust, beam reinforcement and column vertical bars which influence the joint shear behaviour of the external BCJ. In this chapter each of these parameters are investigated.

EC 8-NA[6-20] and ACI-ASCE Committee 352 [6-22] codes give design methods suitable for external BCJ.

As shown in Figure 6.6, a brief review on the calculation of joint shear force is that $V_{jh} = T - V_{col}$, where V_{jh} is the joint shear, V_{col} is the horizontal shear force across the column and T is the force in the tension reinforcement of the beam which is given by $T_n = M_n/z$, where M is the beam moment at the column face and z is the flexural lever arm.

The theoretical joint shear force is dependent on the assumptions used to calculate M and z. M is taken as shown in Figure 6.5, where L is the distance from the load P to the face of the column and d' is the distance from the face of the column to the centroid of the column reinforcement as shown in the Figure 6.6.

The tensile force in the beam reinforcement is calculated by section analysis assuming that plane section remains plane. The rectangular-parabolic stress block defined in EC2 [6-1] is used for the concrete.

The stress is assumed to reach a maximum value of $0.8f_{cu}$ at a compressive strain of 0.002. The width of the compressive stress block is taken as the beam width in the analysis of the BCJ. An elasto-plastic stress-strain response is assumed for the reinforcement with an elastic modulus of 200 GPa. No material factors of safety are applied in the tables. The proposed design rule was developed after 56 specimens were compared with results from shear index $V_j/b_c h_c f_c^{2/3}$ and $V_j/b_c h_c \sqrt{f_c}$ and stirrup index $A_{sje} fy/b_c h_c f_c^{2/3}$ from EC8-NA[6-20] for L and U beam connection bars.

6.4 Effective joint width and influence of transverse beams

The horizontal joint shear stress is defined as $v_j = V_j/b_e h_c$ where b_e is the effective joint width, taken as follows:
if $b_b < b_c$, b_c = least of $0.5(b_b+b_c)$ or $b_h+0.5h_c$
if $b_b > b_c$, b_c = least of $b_c+0.5h_c$ or b_b.

There is general agreement that the effective joint width is less than the column width if the column is wider than the beam [6-25]. In this case, the effective joint width is commonly taken as the average of the beam and column widths for a symmetrical joint.

No directly relevant test results related to a beam wider than the column are available, However, past test results from cyclically loaded, external BCJ with transverse beams can give some guidance [6-21].

The available data shows that joint shear strength increases due to the presence of transverse beams, and this is dependent on the loading on the transverse beams and their cross-sectional dimensions. The increase in joint shear strength is dependent on both the effects of confinement and resistance of joint shear stresses by concrete within the transverse beams to either side of the column [6-21]. This latter effect corresponds to an increase in effective joint width and suggests that this is greater than the column width if the beam is wider than the column.

No common agreement has been reached in various design code recommendations on either the definition of effective joint width, if the beam is wider than the column, or the effect of transverse beams. ACI/ASCE Committee 352 [6-22] limits the effective joint width to the column width, but increases the design joint shear strength of external BCJ by 33% if transverse beams frame into each side of the joint, as long as certain dimensional restrictions are met.

Contrary to ACI/ASCE Committee 352 [6-22], NZS 3101:1995[6-24] does not increase joint shear strength if transverse beams are provided, but allows the effective joint width to be taken as greater than the column width if the beam is wider than the column. In this case, the effective joint width is limited to the column width plus half the column depth, which is the same definition for EC8-NA [6-20] if the beam is wider than the column and this recommendation is applied for this chapter.

A failure analysis was carried out to determine a relationship between concrete strength and joint shear strength for the specimens. The analysis showed that joint strength has a closer relation to $(f_c')^{2/3}$ rather than $\sqrt{f_c'}$. Rigorous analysis of past experiments demonstrates (see p-329) that for this reason EC8-NA [6-20] is a safer design guidance than ACI/ASCE Committee 352 [6-22]. According to the above discussion the influence of concrete strength on joint strength is therefore taken in this thesis as $(f_c')^{2/3}$ rather than$\sqrt{f_c'}$. compressive strength to develop the proposed design rule .The cylinder strength is taken as

$f_c'=0.81f_{cu}$ **6.16**

where f_c' is tested on cylinder of 152x305 and f_{cu} on cubes of 100x100

fcu(150)= 0.95 fcu(100) **6.17**

where $f_{cu(150)}$ is tested on cubes of 150x150 and $f_{cu(100)}$ on cubes of 100x100

6.5 Code design guidance for external BCJ

The ACI Committee 352 [6-22] report on the design of reinforced concrete BCJ divides into two groups depending on the deformations the joints are subjected to:
a) Structures not apt to be subjected to large inelastic deformations which do not need to be designed according to ACI, Chapter 21, are referred to as non-seismic structures. Such structures have Type-1 BCJ.
b) Structures that must be able to accommodate large inelastic deformations and the result must satisfy ACI, Chapter 21, are referred to as seismic structures. Such structures have Type 2 BCJ.

The existing design methods ACI-ASCE Committee 352 [6-22] and EC 8[6-20] give design recommendations suitable for monotonically loaded, external BCJ which are expressed as follows:
ACI-ASCE Committee 352 [6-22] for joint shear of BCJ without transverse beams recommends:

$V_{jd} = 1 .058\ b_e h_c \sqrt{f_c'}$ **6.18**

EC 8-NA [6-20] Ductility Class Low DCL for joint shear recommends:

$V_{jd} = 0.525\ b_e h_c (f_c')^{2/3}$ **6.19**

Two different material factors of safety are used in the equations. Both methods calculate the joint shear force on the basis that the beam tensile steel yields. EC 8 [6-20] assumes that only two-thirds of the area of beam reinforcement should be included in the calculation of shear force. EC 8 [6-20] states that the factor of 2/3 be introduced to account for the fact that part of the inclined bond forces flow sideways out of the joint core. Volumn [6-41] points out that this seems reasonable if transverse beams are provided, but is open to discussion for corner joints and cases where the beam is wider than the column.

Both design codes specify minimum stirrup requirements, which are higher than the amount BS8110 recommends [6-10]. However, it will be shown that they do not make provision for joint strength to be increased by stirrups, even when joint strength is increased by stirrups, Figure 6.10 and 6-11. Neither of the equations predicts the agreed dependence of joint shear strength on joint aspect ratio.

From Figure 6.11, it is observed that when the stirrup index $0.2 \leq A_{sje}fy/b_c h_c f_c^{2/3} \leq 0.4$ the joint shear prediction is conservative. When stirrup index increases from 0.4 to 0.45, no increase in shear resistance is recorded. Therefore, this writer's design rule for amount of $A_{sje}f_y$ in the joint is limited to $0.2 \leq A_{sje}f_y/b_c h_c f_c^{2/3} \leq 0.4$.

6.6 Parameters that influence joint shear behaviour

Tests on monotonically-loaded, external BCJ , performed by Taylor[6-2], Ortiz[6-17], Scott[6-16], Scott Hamill[6-19], Parker & Bullman[6-18], Wilson [6-23], Vollum[6-35] and Kordina[6-15] are reviewed and influence of various parameters on shear behaviour of BCJ is investigated .

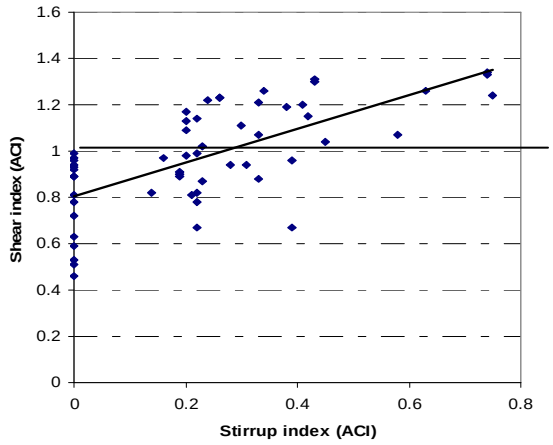

Figure 6.10: Joint shear index at line $V_j/b_c h_c \sqrt{f_c} = 1.058$ ACI 352 [6-22]. Stirrup index $A_{sje}fy/b_c h_c f_c^{1/2}$ slope

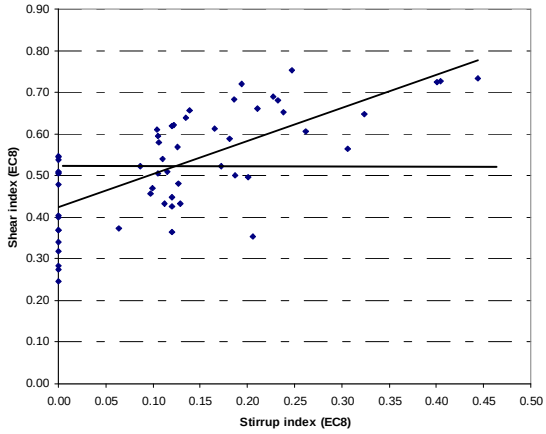

Figure 6.11: Joint shear index $V_j/b_c h_c f_c^{2/3} = 0.525V$ Stirrup index $A_{sje}fy/b_c h_c f_c^{2/3}$ for EC8-NA [6-20]

6.6.1 Relation of shear strength to concrete strength and shear index to stirrup index

A failure analysis is carried out by this writer. This analysis shows that joint strength is closer to the $(f_c')^{2/3}$ rule in EC8-NA [6-20] than the $\sqrt{f_c'}$.rule in ACI/ASCE Committee 352 guidelines [6-22] .

According to EC8 -NA [6-20] analysis, the average value of the shear index of 56 BCJ tests is 0.525 , which was chosen as the empirical value for joint shear design guidelines. All the specimen below the lines for shear index of 0.525 indicate the design guidelines over-estimate the joint shear, Figure 6.10.

The analyses of both ACI 352[6-22] and EC8-NA [6-20] are shown in Figure 6.11 and 6-12 which indicate that for all the results below the horizontal line the codes overestimate the joint shear.

Ignoring minimum reinforcement requirements, the number of safe predictions are 28 out of 56, or 50%, for EC8-NA [6-20], Figure 6.11, whereas ACI 352[6-22] overestimates most of the specimens without confinement steel and the number of safe predictions are 23 out of 56, or 41%, Figure 6.10. The slope indicates that improvement in joint shear is proportional to the increase in the area of confinement bars with the limit of $A_{sje}f_y/b_ch_cf_c^{2/3} \leq 0.42$ for EC8-NA [6-20] and $A_{sje}f_y/b_ch_cf_c^{1/2} \leq 0.8$ for ACI 352[6-22]. Both codes overestimate the joint shear for most of the specimen without confinement steel.

From failure analysis, it is shown that the experimental joint shear strength is closer to the EC8-NA [6-20] prediction compared to that of ACI/ASCE Committee 352 [6-22].

The influence of concrete strength on joint strength in this writer's proposed design rule is therefore taken as proportional to $(fc')^{2/3}$ with empirical figures for detailing of reinforcement connecting beam to column .

The average value of 56 tests for shear index = $V_{jd} / (f_c)^{2/3} b_e.h_c$ $MPa^{1/3}$ is 0.525, which is the empirical value chosen for EC8-NA [6-20] joint shear design guidelines.

In 56 BCJ specimens experimentally tested to failure, when investigating $V_j/b_ch_cf_c^{2/3}$ against $A_{sje}f_y/b_ch_cf_c^{2/3}$, the mean value for L reinforcement detail is 0.54 and for U is 0.49 and the mean value for all the tests is 0.525 which is taken as the empirical value for design equation EC8-NA [6-20].

Experiments on monotonically-loaded, external BCJ were performed by Taylor[6-2], Kordina[6-15], Sarsam [6-39]. Scott[6-16], Ortiz[6-17], Parker & Bullman[6-18], Scott Hamill[6-19], Wilson [6-23], and Vollum[6-35] and test data indicates that the existing design methods can be unsafe when applied to HSC BCJ. There is lack of agreement between EC8-NA [6-20] and ACI 352 [6-22] codes as well as with past researchers on the parameters that influence joint shear behaviour.

6.6.2 Main column vertical reinforcement in BCJ

The New Zealand Code of Practice [6-24] and Bertero [6-25] argued there is a positive contribution of vertical reinforcement to the joint shear whereas test experiments on joints without vertical reinforcement by Park [6-26] and Lee et al [6-27] resulted in satisfactory performance under severe seismic loading which led to the assumption that additional vertical joint reinforcement does not contribute to shear resistance of the joint.

The analysis of specimens 4a and 4d of Parker and Bullman [6-18] with identical parameters except for their column longitudinal reinforcement ratios of 1.09% for 4a compared to 4.38% for 4d, demonstrate that specimen 4a failed due to column failure at beam loading of 118 kN whereas specimen 4d failed at 150 kN beam loading. In spite of a column reinforcement increase of 400%, a comparatively small load increase of 27% was achieved.

Ortiz [6-17] increased column reinforcements, Table 6.2, of identical specimen BCJ1 and BCJ6 without shear stirrups. BCJ1 had the minimum recommended radius of bend of 4d [6-12]. BCJ6 had a larger radius of bend of 130mm (8d) but in spite of increasing column reinforcement by 33% and 67%, no improvement in joint shear shows that the ultimate joint moment increase for BJ6 compared to BCJ1 is only 1%.

The experiments demonstrate that column reinforcement does not have a significant influence on joint shear, however, the joints that have low column longitudinal reinforcement ratios and column axial stresses are more likely to fail by column hinging.

It should be noted that if column reinforcement is distributed in layers across the depth of the column as CVB their contribution to shear resistance is treated independently in this chapter. To this writer's knowledge, this influence has not been investigated in the past even though intermediate column bars are recommended in EC8 [6-20] for ductility class DCM. Neither has there been any research with direct emphasis on the joint shear contribution of CVB in layers near the centre of the depth of the column in HSC BCJ.

6.6.3 Influence of vertical reinforcement at the centre of the depth of column in BCJ

This section explores column reinforcement distributed in layers across the depth of the column as CVB and their independent contribution to joint shear resistance.

With regards to direct influence of CVB on the joint shear, the most related research available is an experimental programme by Atta, Taher, Khalil and El-Metwally [6-28 &29] which included a comparative study of BCJ which had CVB at half depth as recommended by EC8 [6-20]. The results of these tests are shown in Table 6.3.

Specimen	Column bars A_s / bd % ρ_c	Beam load at failure P (kN)	Joint moment M_n (kNm)	Column axial load N (kN)	Beam load to joint centre (mm)	Comments
BCJ1	2.01	118	141.6		1200	Radius of bend 65mm
BCJ3	2.68	118	147.5		1250	Radius of bend 130mm
BCJ6	3.35	115	143.8	300	1250	Radius of bend 130mm

Table 6.2: Influence of main column reinforcement on ultimate joint moment. Comparison of the significant increase of 67% in column reinforcement of BCJ6 compared to BCJ1, resulting in less than 1% increase in ultimate joint moment.

The variables studied were the grade of concrete in beam and column joint (group G1), the shape and reinforcement ratio of stirrups in the joint (group G2), and reinforcement in beam, column and joint (group G3).

This writer analysed a group of G3 specimens with concrete of cylinder strength of 65 MPa, joint aspect ratio of 2 and column reinforcement distribution of 8 bars in specimen G3-F, 6 bars in specimen G3-E, and 4 bars in specimen G3-C, Figure 6.13. The higher strength and aspect ratio and presence of CVB resemblances the behaviour of HSC-BCJ of aspect ratio=2 with CVB.

Ten specimens of reinforced concrete BCJ were tested. Nominal yield stress of reinforcement was 360 and 240 MPa for main steel and stirrups. The mix proportions for 1 m^3 of concrete of cylinder strength 60-70 MPa tested at around 45 days consisted of 600 kg ordinary Portland cement, 1175 kg granite, 600 kg sand, 156 kg water and 12 kg super plastisizer or W/C=0.28. The normal-strength concrete mix had the same proportions but with a water/cement ratio of 0.5 and with no super plastisizer. The specimens were moist-cured for 10 days.

An axial load of 400 kN was applied to the column and kept constant throughout the test. A hydraulic jack loaded the beams by applying upward load by increments of 10kN up to failure.

Group	Type	Concrete f_c (MPa)		Beam bar		Column bars	Joint stirrup	Failure Load (kN)	Load at Joint stirrup yield (kN)
		Beam	Column	Bottom	Top				
I	G1-A	67	67	3-T16	2-T10	4-T16	2-R8	128	92
	G1-B	36	36	3-T16	2-T10	4-T16	2-R8	100	61
	G1-C	33	65	3-T16	2-T10	4-T16	2-R8	118	73
II	G2-B	60	60	3-T16	2-T10	4-T16	-	103	-
	G2-C	65	65	3-T16	2-T10	4-T16	3-R8	127	96
III	G3-B	62	62	3-T16	2-T10	4-T16	1-T10	128	90
	G3-C	68	68	3-T16	2-T10	4-T16	2-R8	124	94
	G3-D	64	64	3-T16	2-T10	8-T16	5-R8	138	102
	G3-E	68	68	3-T16	3-T16	4-T16	2-R8	144	110
	G3-F	62	62	3-T16	2-T10	8-T16	2-R8	168	115

Table 6.3: Description of reinforcement, concrete strength, failure, cracking and joint stirrup yield load for experimental tests.

It can be noted that the beam reinforcement in the G3-F experiments was not sufficient for developing full joint shear failure. If beam reinforcement of 4-T16 instead of 3-T16 with bend radius of 4d were used, joint shear failure would have occurred at higher beam load for G3-F which had 8-T16 column reinforcement. This would have demonstrated the contribution of CVB to the joint shear.

Specimen G3-F has 2-T16 located at half the depth of the column and has U joint connection detailing which has 10% less joint shear resistance than G3-E, with L connection, whereas the failure load for G3-F is 168 kN compared to 144 kN in G3-E, which is further demonstration that the presence of CVB produces higher joint shear resistance despite weaker connection detailing.

Atta's specimen G3-F fails from beam flexural failure at 168kN and specimen G3-E fails from joint shear at 144kN. This shows that the joint shear resistance would have been higher if premature flexural failure had not taken place.

There is insufficient information on the spacing and type of reinforcement used as shear stirrups in the beam, therefore since the available diagram did not provide dimensions of spacing, using scale rule measurement it was assumed that links of 8mm diameter of 240 MPa nominal yield were spaced at 200mm.

In conventional design methods, $\lambda f_y A_s - V_{col}$ is used to predict joint shear failure. Considering specimen G3-F with λ=1.2, f_y=360 MPa, A_s= 602 mm^2. When the plastic hinge is being considered, the predicted joint shear failure is169.5 kN (260.4-91= 169.5 kN) with 3-T16 tension bars in the beam. From Figure 6.14 it can be seen that the failure occurs in the beam at about 200mm away from opening corner of the joint, and as the load is applied from the bottom the beam failure appears.

G3-E which failed in joint shear at 144 kN is identical to G3-F which had beam failure at 168 kN, the only difference being that G3-F has 2-T16 additional CVB which improve the beam load capacity by 17%. In addition, G3-E has L detailing rather than the U detailing of G3-F. The L detailing improves joint shear by 13%, therefore the presence of additional 2-T16 CVB in G3-F improves its joint shear by 17%+13%=30%. If G3-F had a larger quantity of tension steel in the beam and was designed to fail in joint shear, the beam load capacity would have further increased and the contribution of CVB would have been demonstrated to be greater.

Ten electrical resistance strain gauges were mounted on the reinforcement cage within the joint zone for each specimen. The position of 8 gauges are identified in the published paper although reading for gauges 5 to 8 are not provided.

The presence of a CVB deflects inclined compression forces proportionally to the strength of the concrete in the joint and the strut providing the compression force becomes wider making an effective compression strut throughout the depth of the joint. It is also due to dowel forces from CVB restricting propagation of flexural and inclined cracks.

Parametric investigations by this writer into the influence of CVB and HSC in the parametric model of BCJ-4 made of HSC with 2T12 CVB, Figure 6.12, showed 43% improvement in load bearing capacity, 198.13 kN, compared to BCJ-4 with NSC and without CVB of 138 kN.

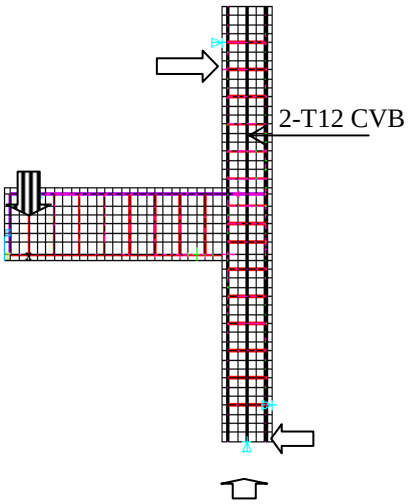

Figure 6.12:The meshed FE model of BCJ4 but of HSCwith 2T12 CVB .

A detailed FE parametric investigation on the influence of CVB and HSC will be carried out in Chapter 7.

6.6.4 Cracking load prediction

From diagonal cracking analysis for specimens in the horizontal reaction at the column top support, Rt = V_{col} was predicted conventionally by taking moment about the centre of the base of column, Figure 6.13.

$$P\ (L+\frac{h_c}{2}) = V_{col} \times H_c \qquad \textbf{6.20}$$

$$T_n - V_{col} = V_{jh} \qquad \textbf{6.21}$$

Considering BS8110 simplified stress block

$T_n = 0.87\ f_y A_s$ **6.22**

$$T_n = 0.87\, f_y A_s = 0.87 \times 360 \times 3.14 \times 3 \times (8)^2 = 188.8 \text{ kN}$$

The cracking analysis is checked to Taylor's approach, from equation in section 6.3 with $v_{cr} = V_{cr}/(b_c \cdot h_c)$ and V_{cr} equal to the beam bars force

$v_{cr} = 0.67\ \sqrt{(f_t^2 + \sigma_c\ f_t + \sigma_b\ f_t)}$

$$\sigma_c = \frac{400000}{200 \times 200} = 10 \text{ MPa}$$

where f_t is the tensile strength of concrete, $\sigma_b = N_b/(b_c h_c)$, N_b which is the horizontal thrust is zero,$\sigma_c = N_1/(b_c h_c)$ and N_1 is the vertical load on the column then $v_{cr} = 0.67\ \sqrt{(f_t^2 + \sigma_c\ f_t)}$. Results from Taylor's design rule for prediction of the first joint crack formation with

Taylor's, CEB[6-11] and this writer's proposed equations for predicting tensile strength of concrete are shown in Table 6.4.

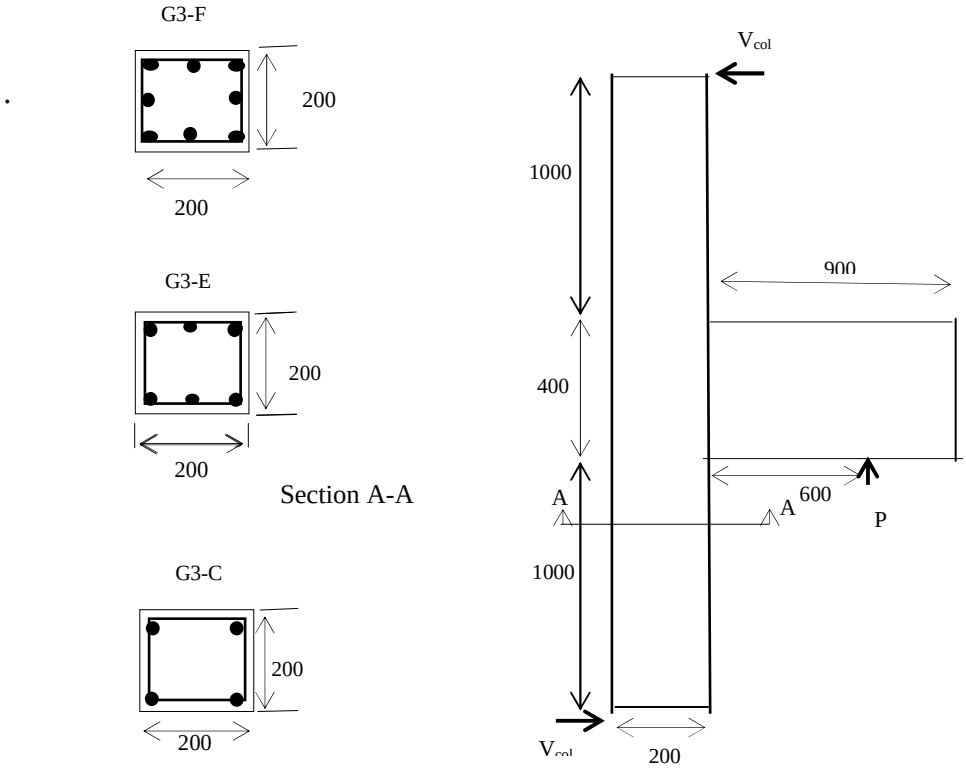

Figure 6.13: Geometry of beams tested by Atta et al [6-28]

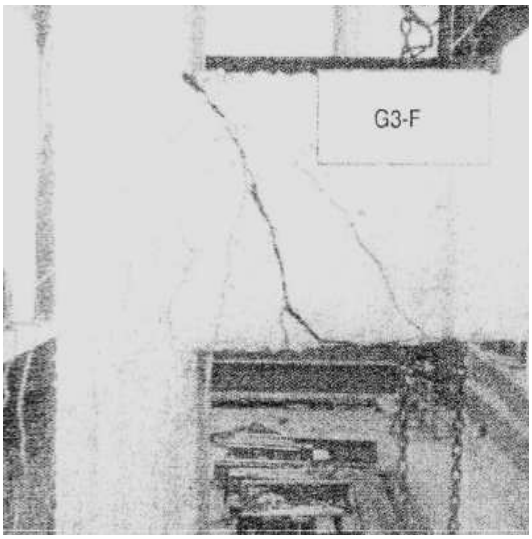

Figure 6.14: BCJ G3-F, which has 2-T16 CVB at the centre of depth of the column, had a failure in the beam at the flexural ultimate beam load of 168 kN .
Source: Atta et al [6-28], 2003

The experimental tests by Atta et al [6-28] indicate that the predicted values for this first joint shear crack, Table 6.4, for NSC are reasonably accurate, however, with HSC, Taylor's design rule over-estimates the joint shear strength by up to 57%, Figure 6.16.

Taylor's empirical design rule, $f_t = 0.1 f_c$, based on the 26 BCJ tests he conducted were of average concrete strength F_c= 37.27 MPa, as a result, for Atta et al's NSC test number 2 (G1-B) the prediction value is 9% larger than the experimental . However, for higher strength concrete of between F_c = 60 to 70 MPa the prediction is on average 57% higher.

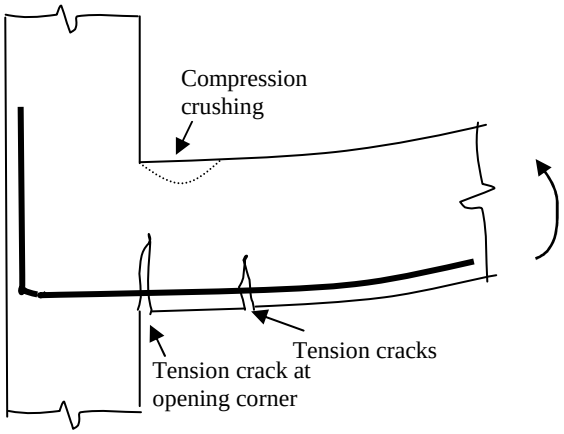

Figure 6.15: Flexural mode of failure for the beam at BCJ

CEB's recommendation ($f_t = 0.3 f_c^{2/3}$) for tensile strength of concrete gives predictions of average value with NSC at 3% higher strength than the experimental and for the average value with HSC the prediction is 32% higher than experimental values.

This writer's empirically calculated recommendation $f_t = 0.47\sqrt{f_c}$ gives the closest of all three methods of predictions of experimental value with NSC with 6% margin of safety and with HSC an average prediction of 12% higher than experimental values.

As demonstrated in Figure 6.16**,** this writer's proposed empirically calculated relation of $f_t = 0.47\sqrt{f_c}$ gives the most realistic results.

6.6.3 Joint aspect ratios

Meinheit & Jirsa's [6-31] test results on cyclically loaded internal BCJ with joint aspect

Test No	Specimen teste	Column $f_{c\,(MPa)}$	Cracking load (P) (kN)	Beam bars force T_n (kN)	Reaction (V_{col}) (kN)	Shear force $V_{u,joint}$ (kN)	CEB Code Ft= 0.3 (Fc) $^{2}/_{3}$	CEB Code/ Experiment	This writer's Ft=0.47$\sqrt{Fc}$	This writer/ Experiment	Taylor's a Ft=0.1 Fcu	Taylor's/ Experiment
1	**G1-A**	67	45	188.8	18.8	170.1	232.67	1.37	195.6	1.15	283.5	1.67
2	**G1-B**	36	40	188.8	16.7	172.1	177.89	1.03	161.1	0.94	187.5	1.09
3	**G1-C**	65	40	188.8	16.7	172.1	229.55	1.33	193.7	1.13	277.5	1.61
4	**G2-B**	60	45	188.8	18.8	170.1	221.54	1.30	188.9	1.11	262.6	1.54
5	**G2-C**	65	45	188.8	18.8	170.1	229.55	1.35	193.7	1.14	277.5	1.63
6	**G3-B**	62	45	188.8	18.8	170.1	224.78	1.32	190.8	1.12	268.6	1.58
7	**G3-C**	68	45	188.8	18.8	170.1	234.22	1.38	196.5	1.16	286.4	1.68
8	**G3-D**	64	50	188.8	20.8	168	227.97	1.36	192.8	1.15	274.6	1.63
9	**G3-E**	68	50	188.8	20.8	168	234.22	1.39	196.5	1.17	286.4	1.71
10	**G3-F**	62	55	188.8	22.9	165.9	224.78	1.35	190.8	1.15	268.6	1.62
Average value of ratio of prediction compared to experimental value								1.32		1.12		1.57

Table 6.4: Joint shear forces predicted cracking load comparing Taylor's, CEB and this writer's proposed method of calculating tensile strength of concrete in order to predict the first joint crack from Taylor's proposed method.

ratios of 1 and l.4 agree with the EC 8 [6-20] and ACI/ASCE[6-22] Committee 352 assumption that joint shear strength is independent of joint aspect ratio. However, design methods based on STM in ACI318 Appendix B [6-5] and Eurocode 2 [6-1] or Taylor's analogies with shear behaviour [6-2] conclude that shear forces in BCJ are dependent on beam column aspect ratio. Taylor restricts his analogy of beams to BCJ up to joint aspect ratio of 2.

The joint shear design equations proposed by Sarsam [6-39] and Vollum [6-35] are also based on STM and are dependent on joint aspect ratio. STM have been proposed by Ortiz [6-17], Parker &Bullman [6-18], and Vollum [6-35] for the design of joints with and without stirrups. All their models predict that joint shear strength is dependent on aspect ratio.

Therefore, joint shear design equations based on STM are limited to an aspect ratio of up to 2.5 and Vollum [6-35] recommends shear design for aspect ratio higher than 2.5 to be designed by use of the variable truss angle method for shear design recommendations in

EC2 [6-1]. This research, however, attempts to demonstrate that the use of CVB in the joint produces a stabilising arching affect and develops double strut action which results in increasing the limit for STM to the joint aspect ratio of 3.

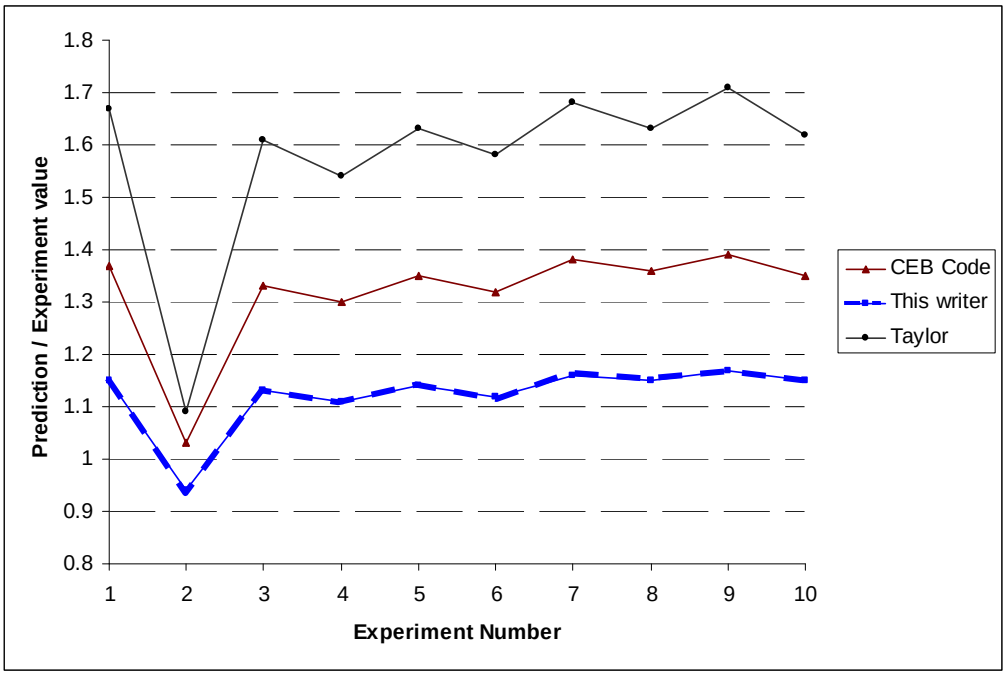

Figure 6.16: Prediction of first crack using Taylor's rule with different empirical rules for relation between tensile and compressive strength of concrete.

As noted earlier, this writer's experiments on 12 beams demonstrated a reduction of shear resistance in HSC compared to NSC in beams of shear span to depth ratio of 3. The situation was reversed by introducing HWB in the beam due to the stabilising arching affect which results in the beam performing in a similar way to short beams , considering Taylor's [6-2] analogy of beams shear behaviour to that of BCJ. Although Taylor restricted his analogy to beam column aspect ratio≤2, the stabilising arching affect due to dowel action from CVB on HSC BCJ of higher aspect ratio with a CVB could make this analogy possible for joint aspect ratio ≤3.

However, the shear resistance of HSC BCJ with aspect ratio of 3 and CVB could be analogous to HSC beams with HWB with a shear span to depth ratio of 3, because the dowel action of the central bar develops a stabilizing arching affect. This may suggest in the same manner that a HWB makes a contribution to the shear resistance of the HSC beam a/d=3, as CVB would also contribute to the joint shear of HSC BCJ of aspect ratio h_b/h_c=3.

It is interesting to note that in Kordia's experiments, specimen RE10 and RE7 have similar

$A_{sje}f_y / (f_c)^{1/2} b_e.h_c$ but RE7 has 18% higher shear index [$Vjd / (f_c)^{1/2} b_e.h_c$] because the joint aspect ratio of RE10 is 1.56 compared to RE7 with an aspect ratio of 1.4.

Consideration of the inclined stress field model proposed by Scott et al [6-30] suggests that the maximum joint shear strength should be related to the joint aspect ratio.

6.6.6 Beam thrust

Taylor[6-2] applied beam thrust to his entire specimens except for specimen P1/41/24. When there is absence of beam thrust, the opening and closing moments are identical, however, when beam thrust is applied as failure of the opening corner occurred, the closing side was able to carry more moments until its strength was drained. As a result, in the absence of beam thrust, failure occurs as the opening corner reaches its peak moment whereas when a prop is provided the opening corner is able to continue to carry moment, even down a falling branch while the moment in the closing side is increasing.

In the presence of beam thrust, the beam moment is not carried by the column in equal proportions above and below the joint; the closing corner of the joint may be carrying as much as 75% of the beam moment when the joint fails. The column, in the case of the test with beam thrust, was sharing the beam moment in the opening and closing sides in the proportions of 1:2 at failure.

6.6.7 Column axial compression

Meinheit et al[6-31] subjected BCJ to deformation to establish basic shear behaviour. Specimens were designed using recommendations of ACI-ASCE Committee 352 [6-22] and were proportioned so that shear stress in the joint would determine the maximum loads rather than the yielding of flexural members. From analysis of the test data and mode of failure, design recommendations for basic joint shear strength were made with emphasis that column axial load does not contribute to shear resistance of the joint.

Ortiz [6-17] tests on BCJ demonstrated that when 300 kN axial loads were applied to the column of the joint (BCJ6) without confinement reinforcement the joint shear was 315 kN compared to 322 kN of the same specimen without axial load (BCJ3). Her tests indicate that joint shear reduces by just 2% due to the presence of axial load of 300 kN which may be interpreted as no improvement for increased axial loading.

Kordina [6-18] investigated the influence of column axial forces by increasing the axial column load on the joints in his two matching specimens but the one exposed to a higher axial load had U connection bars and compared with the L connections on the joint with lower axial load, the U connection has 10% less joint shear resistance. Kordia concluded that presence of column load did not contribute to joint shear resistance.

Scott [6-16], investigated column axial loading by increasing the loading from 50 kN to 275 kN on each of his specimens. He concluded that column axial loading does not contribute to joint shear resistance. Scott & Hamill [6-19], tested their specimens at 50 kN and 100 kN column axial loading. The comparison demonstrated that the BCJ shear does not increase with increase in axial loading.

Parker and Pullman [6-18], made an in depth investigation into the affect of axial load on joint shear for BCJ by testing 11 specimens exposed to zero, 300 kN and 600 kN axial loadings. They concluded that column axial force in the BCJ contributes to the joint shear resistance and therefore proposed the following design rule for the joint shear V of a member without confinement links:

$$V=(A_{sc}f_y + N) \tan\Theta_{crit} \qquad \mathbf{6.23}$$

where A_{sc} is the total area of tension reinforcement on each face of the member and Θ_{crit} is the critical inclination of the compression strut relative to member axis. N is the axial column load.

Vollum [6-35] investigated the influence of column load on joint shear and observed that most other researchers had concluded joint shear strength does not increase with column axial load. However, he proposed the following design rule:

$$V_j = V_c + (A_{sje}f_y - \alpha b_e h_c \sqrt{f_c'}) \quad 6.24$$

where α is conservatively taken as 0.2 $MPa^{0.5}$ and is dependent on factors depending on concrete strength, joint aspect ratio and column axial load.
A number of past researchers argued that increase in column axial force Nu does improve the shear capacity of BCJ therefore it can be seen in terms of axial stress (N_u / A_g) where N_u is the column load and A_g is the gross cross-sectional area of the column at the joint, and this is implemented in some international codes of practice.

Researcher	Influence of axial load on joint shear	comment
Meinheit	No increase	Displacement loading
Ortiz	Minor increase 2%	300 kN load
Kordina	10% increase	L bar compared to U
Scott	No increase	275 kN load
Parker and Pullman	N $\tan\Theta_{crit}$	600 kN load
Vollum	Included in α	From other research

Table 6.5: Research performed on the influence of axial load on joint shear

6.6.8 Influence of compressive strength of concrete on shear resistance of BCJ

The only HSC BCJ specimens with concrete of $f_c' \geq 95$ MPa exposed to monotonic loading were the six with cylinder strength close to 100 MPa and joint aspect ratio of 1.4 tested by Scott & Hamill [6-19]. Their specimens C4ALHO of HSC and C4ALNO of NSC with aspect ratio of 1.36 were investigated for the influence of concrete cylinder strength on the joint shear. These two specimens were chosen because their geometry and material properties other than strength of concrete were the same. The column axial load and concrete were 100 kN and 104 MPa for C4ALH0 and 50 kN and 42 MPa for C4ALN0 and none had stirrups. C4ALHO had 37% higher shear resistance compared to C4ALNO. The results demonstrated that for the low aspect ratio (1.36) the higher strength of concrete could improve the load bearing capacity of the compression strut and therefore have improved joint shear resistance.

For 8 tests [6-19] of aspect ratio 1.4, 4 HSC and 4 NSC, it was noted that the average shear stress is 8.7 MPa for HSC of average f_c=101.5 MPa and 6.2 MPa for NSC of f_c=48.25 demonstrating that an increase in concrete strength of 110% results in an increase in shear resistance of BCJ of 40%, or a ratio of 1: 2.75. When aspect ratio is increased [6-28] to 2, an increase in compressive strength of 86% results in 27% increase in shear resistance or a reduced ratio of 1:3.2.The difference in shear resistance is not proportionally high when considering the increased compressive strength of 24%, ie. 110%-86%.

As the joint aspect ratio increases to 2, the difference in joint shear performance of BCJ of G1-A and G1-B at 67MPa and 33MPa subjected to column axial loading of 400 kN, Table 6.3, becomes comparatively smaller at failure loading of 128 kN and 100 kN, which is a 28% increase.

	Researcher	Aspect ratio	f_c (MPa)	N_u kN	% Increase in Shear
C4ALHO	Scott & Hamill's[6-19]	1.36	104	100	37%
C4ALNO			42	50	
G1-A	Atta et al [6-28]	2.0	67	400	28%
G1-B			33	400	

Table 6.6: Reduction of increase in joint shear with increase in aspect ratio

Vollum produced a graph, Figure 6.17, showing that the relation between joint shear and cylinder concrete strength is 0.9√fc' and based on this relation he proposed his design rule:
Vj = Vc + (Asjefy - αbehc √fc') **6.24**

It is of concern that as shown in Figure 6.18, the shear resistance of beams tends to decrease as concrete strength and beam depth increase**.** The graph is restricted to d≤ 100mm and f_{cu}≤ 100 MPa.

Table 4: Results of tests by Motamed and comparisons with equations (2) and (4)

Beam no.	ρ'_l (%)	a/d	f_{cu}	f_c	V_u (kN)	$V_{u/VRk,eqn\ 4}$	$V_u/V_{Rk,c\ eqn\ 2}$
NSC1	1.58	3.02	43.2	34.6	80	1.08	1.44
HSC 1-1	0.14	3.02	109.0	94.0	65	0.69	0.86
HSC 1-2	0.14	3.02	101.2	86.2	70	0.76	0.95
HSC 1-3	0.14	3.02	106.6	91.6	80	0.85	1.06
BJ-2	1.58	4.15	118.1	103.1	71	0.74	0.90

Notes: 1) b = 150mm d = 265mm h = 300mm ρ_l = 2.37%
2) $\rho_w f_{yw}$ = 0.47N/mm² (for f_{cu} = 100N/mm², $\rho_w f_{ywk}$ min = 0.74N/mm² according to EC2 and 0.84N/mm² according to the Concrete Society recommendations)
3) Values of V_{Rk} and $V_{Rk,c}$ have been calculated ignoring the limitations on f_{cu} and $\rho_w f_{ywk}$
4) Aggregate: 20mm gravel in NSC-1, 10mm limestone in all other beams
5)All beams failed in shear.

Table 6.7: Demonstration of the potential problem with high strength limestone aggregate concrete. N.B: Equations 2 and 4 are discussed in chapter 2.

Source: Regan, 2005, [6-32]

Similarly, this writer's experimental tests demonstrated that when the amount of shear reinforcement used in the HSC beams of a/d= 3 was below the minima of both EC 2 and the Concrete Society recommendations, which are $\rho_w f_y \geq 0.08$and $\rho_w f_y \geq 0.039$, the ultimate shear to the characteristic resistance reduces significantly when calculated by the BS 8110 equation without a limit on f_{cu} and ignoring the requirement on $\rho_w f_y$ which was as

low as 0.69 in one test. The ultimate strengths of three of the four HSC beams were below both that of a reference beam, with gravel aggregate, and normal value of f_{cu}, Table 6.7.

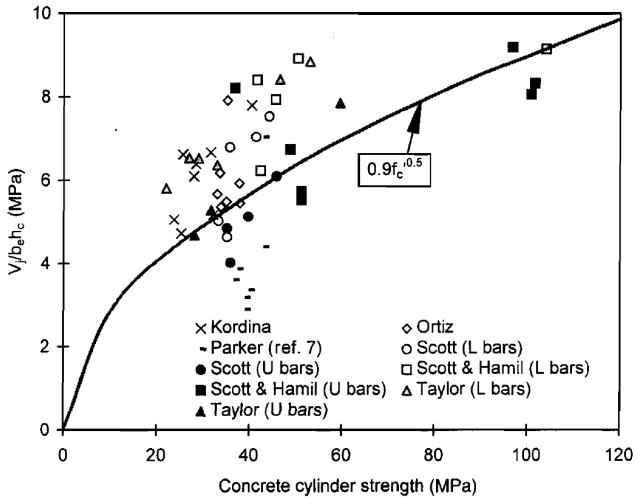

Figure 6.17: Vollum's graph indicating joint shear strength is proportional to the square root of the concrete cylinder strength

Source:Vollum 1999, [6-33]

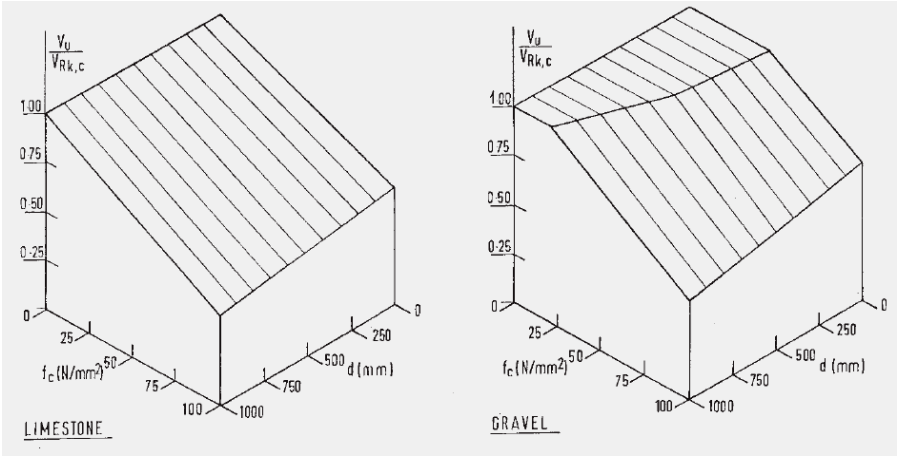

Figure 6.18: Relation between $V_u/V_{Rk,c}$ (equation 2-1), f_c and depth of beam d

Adopted from Regan, 2005, [6-32]

The comparison shows that as aspect ratio increases from 1.5 to 2 this does not improve the shear resistance at the same rate. If this increase had happened at the same rate, the shear resistance would have improved by 32% instead of 27% when aspect ratio increased to 2. Unfortunately, to this writer's knowledge, there are no other tests for investigating the influence of concrete strength on the shear resistance of BCJ in relation to increase in aspect ratio.

Therefore Vollum's design rule is dependent on the strength of concrete although it imposes a limit on the maximum predictable shear based on BCJ7 of Ortiz' beam which is $1.33 b_e h_c \sqrt{f_c}$. When designing for HSC-BCJ with large aspect ratio the equation may over-estimate the joint shear.

This writer introduces a design rule that included shear improvement due to dowel action from CVB for HSC BCJ with large aspect ratio. As demonstrated, HSC beams with a/d=3 with central web bars produce improved shear resistance resulting from arching action which is analogous to HSC BCJ with large aspect ratio 3.

6.6.9 Influence of beam tension reinforcement on joint shear

ACI 318 [6-5] and EC8 -NA [6-20] calculate joint shear force on the basis that the beam tensile steel yields, but EC8-NA [6-20] assumes that only $^2/_3{}^{rd}$ of the area of beam reinforcement should be included in the calculation of shear force. EC8-NA [6-20] states that the factor of $^2/_3$ is introduced to account for the fact that part of the inclined bond forces flow sideways out of the joint core. This is reasonable if transverse beams are provided, but needs further investigation for corner joints, [6-41.

Taylor investigated the moment of the diagonal cracking of the joint as a ratio of the theoretical flexural moment of the beam and concluded from his tests that the diagonal cracking at the working load is likely to occur in joints when beam steel percentage of more than 2.0 is used. Although the widths of the diagonal cracks were not greater than the criteria given by CP110[6-12] immediately after they formed, he recommended to design these areas so that diagonal cracking is prohibited at the working load.

Parker and Bullman's [6-18] specimens 5f and 5b both had identical parameters except for beam reinforcement ratios. Beam 5f had a reinforcement ratio of 1.4% and 5b one of 0.9%, therefore an increase of 56% in beam reinforcement resulted in an increase of joint shear strength of 36%.

Scott's [6-16] specimens C4AL and C1AL had similar concrete strength with only 3 MPa difference and the rest of the parameters were identical except for the beam reinforcement ratios. The joint shear strength of C4AL had a reinforcement ratio of 2.1% compared to

that of C1AL which was 1.1%. This 91% increase in beam reinforcement resulted in an increase in joint shear of around 27%.

Researcher	BCJ - $\rho_{b\%}$	BCJ - $\rho_{b\%}$	Increase in $\rho_{b\%}$	Increase in shear
Parker et al [6-18]	5b – 0.9%	5f – 1.4%	56%	36%
Scott's [6-16]	C1AL – 1.1%	C4AL – 2.1%	91%	27

Table 6.8: Influence of increase in beam reinforcement on joint shear of BCJ

It is concluded that this increase in reinforcement ratio in beams results in an increase in BCJ shear resistance. However, this increase in joint shear is not as high as the increase in beam reinforcement. Further investigation is needed to explore the relation between beam reinforcement percentage and compressive and tensile strength of concrete as well as to the joint shear stirrups.

6.6.10 Influence of eccentricity on the joint shear

Vollum and Newman [6-33] tested ten external BCJ where one of the beams is eccentric to the column. The tests were designed to investigate the strength of the joints under combined loading and to develop a design rule to predict connection strength. The effect of eccentricity and reinforcement detailing on connection strength, cracking and deformation was also explored.

The tests showed that such connections could be used in practice as long as the torsional capacity of the joint is not exceeded. However, BCJ failure can occur in five modes for such connections; 1, column flexure; 2, uniaxial joint shear; 3, torsion in the concentric beam without yielding of its longitudinal steel; 4, biaxial joint shear; and 5 yield reinforcement.

Failure modes 2 to 4 result in column failure and can be prevented by making sure that the maximum possible torsional strength of concentric beams exceeds the applied torsion and the design action should lie within the lower bound to the biaxial joint shear strength given by

$$\left(V_{jc}/V_{jo}\right)^2+\left(V_{je}/V_{jo}\right)^2\le 1 \qquad 6.25$$

where V_{jo} is the uniaxial joint shear strength, Vjc is the joint shear force due to beam loading at failure and Vje is the joint shear due to beam load.

6.6.11 Influence of anchorage detailing on the joint shear

Vollum [6-33] plotted a graph for tests completed by the past researchers to demonstrate the influence of joint stirrups on joint shear strength in relation to L bars and U bars .

He introduces [6-33] factor β in his design equation with β= 1 for connections with L bars and 0.9 for connections with U bars. However, his more recent paper [6-34] recommends that his previous research [6-35] indicated that the joint shear strength of U bar was 20% less than that of similar specimens with L bars.

It is worth noting that in his tests Taylor concluded that his 3 specimens of U bars connections gave very similar results to those of the tests with L bars anchorage. As shown in Table 6.1 the radius of bend when larger than 3d (48mm) makes a significant difference to joint shear when increased from 65mm to 130mm.

From this writer's detailed investigation of the 56 BCJ specimens it was concluded that the detailing of the anchorage of the beam bar to column using L bars performed 10% better in joint shear compared to U bars.

6.6.12 Influence of joint stirrups

It has been concluded by Ortiz [6-17] that stirrups are able to increase joint strength only if positioned above the flexural compressive zone of the incoming beam and below the main beam reinforcement within the upper $^{5}/_{8}$ of the beam depth below the tensile reinforcement in the beam and she found the most efficient location for the stirrup to be above the centre line of the beam, Figure 6.6.

This conclusion follows the yielding of stirrups in Ortiz' specimen BCJ4 [6-17] and then Vollum[6-35] considering the same region as the effective region for joint stirrups. This writer's FE numerical model STM agrees with this approach. However, the parametric investigation , by this writer, demonstrates that the stirrup located 50 mm above the beam prevents buckling of the column front reinforcement and improves the joint load bearing capacity by 17%.

Also the parametric investigation on short beam B1analogous to BCJ, Figure 6.23, for beam with a stirrup near support in flexural span failed at 540 kN compared to model for B1 without this stirrup which failed at 460 kN, indicating that the presence of a link above opening corner of similar BCJ can improve load bearing capacity of the joint by 17%.

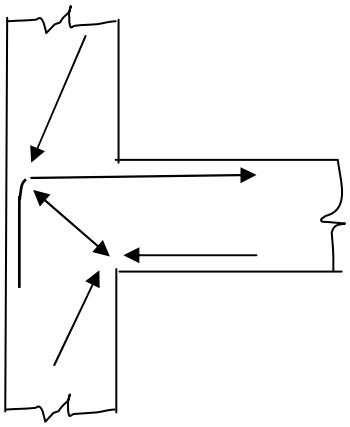

Figure 6.19: Internal forces in joint allowing development of strut with an L bar anchorage

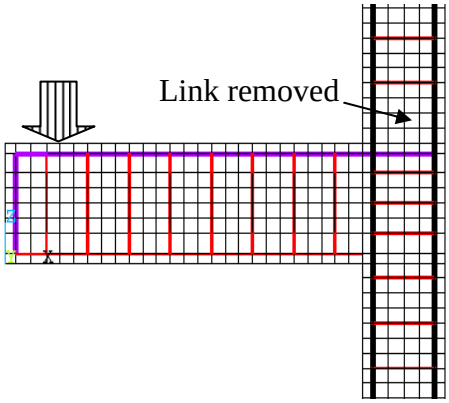

Figure 6.20: Parametric investigation of FE model of BCJ4 with the link above opening corner removed

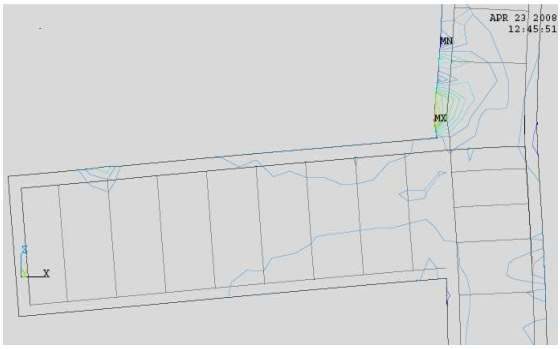

Figure 6.21: At failure load of 118 kN with stirrup just above opening corner removed from mdel of BCJ4.

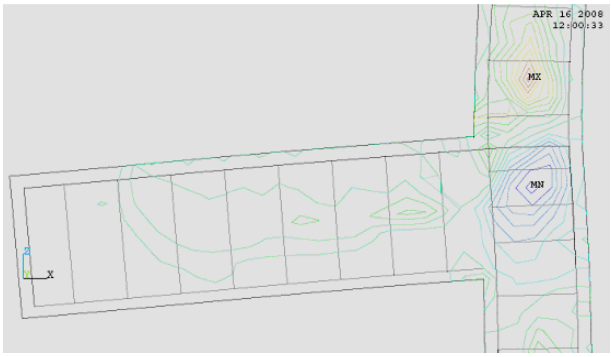

Figure 6.22: The maximum compressive strain develops at the centre of the diagonal compression strut in BCJ when stirrup is present above opening corner in FE model of BCJ4

This investigation was extended by parametrically modelling BCJ-4 with removal of the stirrup above opening corner. Comparing FE models, it was demonstrated that removing the stirrup above opening corner reduces the load bearing capacity of the model from 138 kN to 118 kN or results in 17% drop in load bearing capacity of the model BCJ-4, Figure

6.20. Presence of the stirrup above the opening corner results in shear failure of the diagonal compression strut in the joint at 138 kN, Figure 6.22.

Absence of stirrups above the opening corner resulted in crushing of the concrete above opening corner at 118 kN, Figure 6.21, Figure 6.25. Principal strain vector just before failure load at 110 kN loading shows the strain concentratation above the opening corner resulting in crushing of the concrete, Figure 6.24.

Beeby and Fathibitaraf's [6-36] approach to the design of reinforced concrete frames was that the most significant effect of the membrane forces on the structural behaviour was the bending moment imposed on the columns.

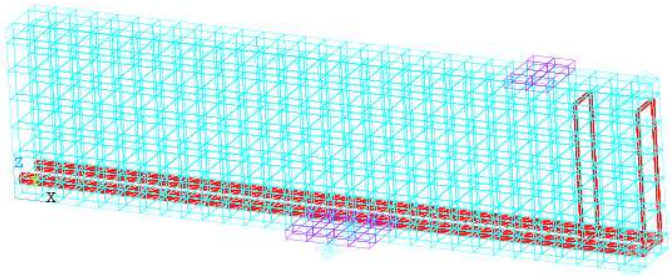

Figure 6.23: Parametric model for beam B1 with a stirrup near support outside shear span failed at 540 kN compared to model for B1 without this stirrup which failed at 460 kN

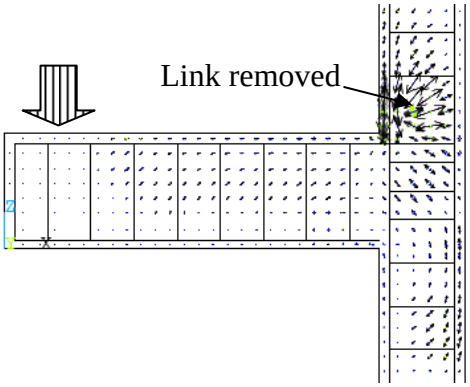

Figure 6.24: Principal strain vector at 110 kN in BCJ-C. with top link removed from BCJ-B.

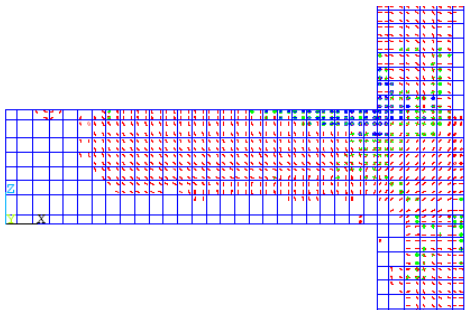

Figure 6.25: Compression failure above the opening corner of the model with link removed from this point

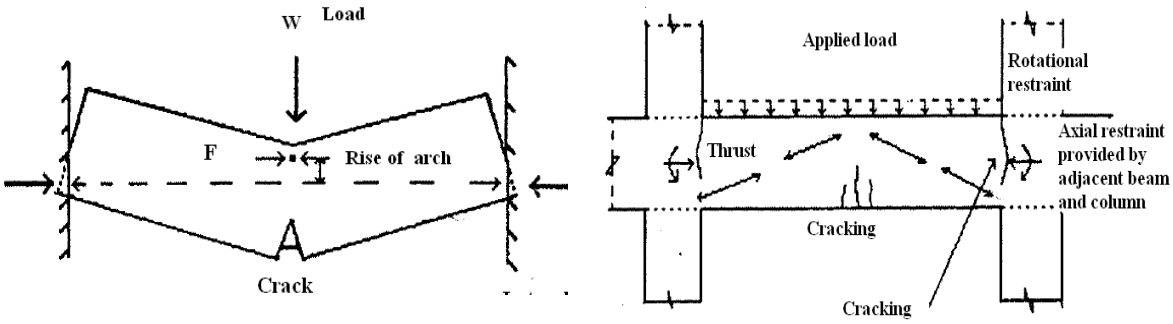

a) A reinforced concrete beam after deformation under load

b) Development of membrane forces in a frame

Figure 6.26: the cracking on the beam as the axial force led to crushing and on the column due to the lateral force from the beam, followed with crushing of concrete in the compressive zone of the beam, and failure of the column or beam.

Source: Beeby, A.W., and Fathibitaraf, F., [6-37] 1997

At the Construction Hall of the University of Westminster, Farjamand [6-38] experimentally tested 3 beams and 7 H frames of NSC to investigate compression membrane action effects in reinforced concrete frames. This phenomena explores the arching action of the beam along its diagonal compression strut due to column restraints on the movement corresponding to the beam's deflection at the ends of the beam below its neutral axis. This force results in additional forces acting on the column at BCJ near the soffit of the beam, therefore producing plastic hinges in the columns from extreme loading.

The test specimens were devised to model an end span in a multi-panel reinforced concrete frame. From the experimental and analytical study of frames presented in the thesis, it can be concluded that the compressive membrane forces act on the beam within the frames, are more pronounced in higher stages of loading and are affected by stiffness of the columns. This writer's investigation of H frames loading at failure shows that they are close to the loading recorded on the fully developed shear diagonal crack at BCJ, with the exception of one H frame which has axial load of 180 kN applied to the columns.

Crack investigations on columns and on BCJ demonstrate that on average, near ultimate load flexural cracks do not propagate after 69% of ultimate loading whereas shear cracks at BCJ develop full diagonal cracks up to 91% and could have continued propagation to failure.

H Frame	1	2	3	4	6	7	Mean	% of load
Ultimate load (kN)	140	136	144	136	124	124	134	
BCJ shear crack (kN)	132	128	132	124	100	116	122	91
Column flexural crack (kN)	0	108	84	128	116	116	92	69

Table 6.9: The flexural and shear cracking loads in relation to the ultimate loads

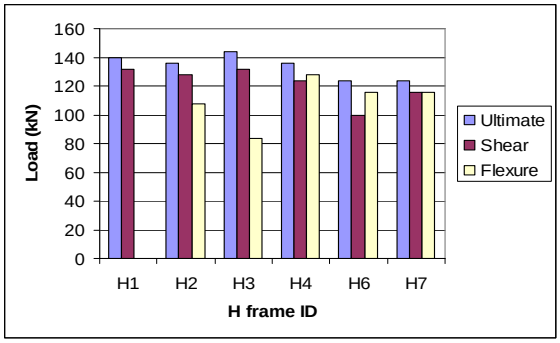

Figure 6.27: Comparison of shear cracking load and flexural cracking load in relation to failure load.

The stirrups are located above or below beam level where you have a cold joint. At the top of the column, 100 mm below soffit of the beam, the pour is stopped for the next pour including beams and at the bottom of the column, 100mm above the beam, the kicker concrete is placed for supporting the shuttering for the above floor columns. Therefore, additional stirrups within the distance of the depth of the column above and below the beam in BCJ ensure the integrity of the concrete cold joints while requirements for discontinuity of the joint to St Venant's rule is fulfilled.

Figure 6.28: a) ACI 318 [6-5], Marti and Sarsam's proposed stirrup detailing at BCJ. b) This writer proposes detailing for external corner BCJ for torsion stirrups only when the structure is exposed to extreme loading which produce torsion at the joints.

Sarsam's proposed 135º stirrups with legs extending a≥110mm [39] into the core of BCJ may obstruct the poker vibrator from compacting core of the concrete resulting in poor quality honey-combed concrete, Figure 6.28 a.

The type of stirrup suggested would normally be used when element is subjected to torsion which may also be used to resist large shear load in the corner external BCJ to allow unobstructed access for the poker vibrator to achieve full compaction at the core of the BCJ, Figure 6.28 b.

The extreme loading is produced due to torsion on the joint resulting from gyrational forces on the unsymmetrical structure. In practice, all buildings have either unsymmetrical plan or distribution of loading on the plan is uneven, therefore gyrational forces from extreme loading produce torsion in the corner BCJ.

A detailed investigation of the strain development in BCJ in the column above the opening corner and below the closing corner is in Chapter seven of this thesis.

Vollum [6-33] plotted a graph for tests completed by past researchers .The influence of joint stirrups on joint shear strength is shown for L bars and U bars, where the normalised joint shear strength $Vjd / (f_c)^{1/2} b_e.h_c$ MPa$^{1/2}$ of the specimens is plotted against stirrup index $= A_{sje}f_y / (f_c)^{1/2} b_e.h_c$ MPa$^{1/2}$, where A_{sje} is the effective area of joint stirrups, defined as the area of stirrups placed within the upper $^5/_8$ of the beam depth below the tensile reinforcement in the beam.

Vollum's graph does not fully take aspect ratio into account. His lower limit for aspect ratio is achieved by restricting his design rule with the empirical value of $0.97(f_c)^{1/2} b_e.h_c$ which is from tests by Wilson [6-23].

Taylor tested one specimen, B3/41/24, with additional joint reinforcement which did not show joint strength beyond that achieved in his other tests which mostly had one stirrup at the centre. Taylor assumed that this was probably because the mode of the joint was firstly diagonal cracking and then crushing of the strut of concrete parallel to the diagonal cracks, Figure 6.19. The failure mode is similar to the diagonal compression failure of short beams over-reinforced in shear, then additional reinforcement in column links beyond one link in the centre of the joint is not likely to enhance the strength of the joint, only to increase its ductility by holding the concrete and stopping it from bursting.

Taylor assumed that the reason that additional linking reinforcement is provided in joints of structures subjected to earthquake loading is because the binding steel holds the joint together and enhances the strength of the second and subsequent load cycles, rather than to give more strength in the first cycle.

The definition of A_{sje} for the effective area of joint stirrups generally varies depending on the researcher. As an example, this writer for his proposed design rule defines A_{sje} as the area of stirrups placed within the length of $(2h_c + h_b)$ in the column at equal distance from the centre of beam in BCJ.

The equation $(V_j = V_c + A_{sje}f_y)$ overestimates the contribution of the stirrups indicating as extremely low value for V_c. This was also demonstrated by Meinheit & Jirsa [6-31] from their experiment on cyclically loaded BCJ. This equation is not conservative at high stirrup indices because joint shear failure occurs before yielding of stirrups.

The graphs show that joint shear strength is increased by stirrups only if the stirrup index exceeds a critical minimum value of about 0.2% which is the amount recommended by BS8110 [6-10]. Figure 6.10 and Figure 6.11.

This writer investigated the yielding of the stirrups of BCJ4 of Ortiz in which the two stirrups within the upper $^5/_8{}^{th}$ of the beam depth below the tensile reinforcement in the beam, yield. However, from FE models and investigation of the BCJ specimen, on the frames discussed in this section, it is concluded that within the discontinuous region of BCJ , Figure 4-1, which extends from the depth of the column (h_c) below soffit to above the top of the beam in BCJ, to confine the diagonal compression struts.

6.7 Comparison of experimental test data with the code guidance

In this section, the experimental data from 56 specimens tested by a group of researchers are compared with prediction from code guidance.

6.7.1 Comparison of EC8 [6-20] with tests

EC8-NA [6-20] gives design recommendations for monotonically loaded, external BCJ expressed as follows:

$Vjd = 0.525\ (f_c)^{2/3}\ b_e.h_c$ **6.26**

For EC -NA [6-20] ductility class low (DCL) .

Material factor of safety is included. EC8 calculates the joint shear force on the basis that the beam tensile steel yields. From Table 6-11 the empirical value of 0.525 was determined from the mean of the experiments.

EC8 -NA [6-20] design methods specify minimum stirrup requirements greater than those of BS 8110 [6-10]. EC 8-NA [6-20] and ACI/ASCE Committee 352 [6-19] do not take into consideration dependence of joint shear strength on joint aspect ratio.

In the graphs Shear index = $V_{jd} / (f_c)^{2/3} b_e.h_c$ MPa$^{1/3}$ is plotted against Stirrup index = $A_{sje}f_y / (f_c)^{2/3} b_e.h_c$ MPa$^{1/3}$, Figure 6.29. The graphs demonstrate the stirrups contribution to joint shear.

The average of 56 tests gives a shear index of 0.525 which was chosen as the empirical value for EC8 -NA [6-20] joint shear design guideline. All the specimens below this line demonstrate that the EC8 NA [6-20] design guide overestimates the joint shear . Ignoring minimum reinforcement requirements, the safe predictions are 28 out of 56, or 50%.

Ortiz' results are close to the EC8-NA [6-20] design rule. The aspect ratio is 1.33 and cylinder concrete strength is between 33 and 38 MPa .Tests demonstrate that the joint shear index increases linearly with the increase in the amount of stirrups, Figure 6.29: Compare research for relation Shear index V Stirrup index.Figure 6.29. Kordia's experiment demonstrates an improvement in shear index with an increase in stirrup index and safe prediction to the EC8-NA [6-20] guideline. Tests demonstrate that above shear index $0.5(f_c)^{2/3} b_e.h_c$ increases linearly with the increase in amount of stirrups. The specimens were of aspect ratio of 1.4 to 2. The specimen RE2 with f_c= 25MPa and aspect ratio of 2 had no confinement steel, and specimen RE4 with aspect ratio of 1.5 with minimum confinement steel had the lowest joint shear, Figure 6.29.

Taylor's specimen B3/41/24, in spite of a significant increase in stirrup index and shear index, has not increased compared to other specimens with less than half the stirrup index. The experimental results are safe to the EC8-NA [6-20] design guidelines. The tests were performed on NSC with aspect ratio of 1.43, Figure 6.29.

Scott's experiments had a small variation in stirrup index, therefore do offer clear evidence on the influence of aspect ratio. Six of the experimental results below the dotted line are unsafe to the EC8-NA [6-20] design guideline. The specimens C7 and C9 with aspect ratio of 2 and lowest beam reinforcement of 1.4% had the lowest joint shear. All the specimens had a similar quantity of confinement steel. The specimen C4AL with the smallest aspect ratio of 1.4 with maximum confinement and beam steel had the highest joint shear. Figure 6.29.

The graphs in Figure 6.29 demonstrate that EC8 overestimates the joint shear design of HSC BCJ. C4ALH0 has a shear index of 0.4, or 31% overestimation. The aspect ratio for all BCJ is 1.4. The predicted shear index to EC8-NA[6-20] is low for HSC-BCJ.

All specimens were of aspect ratio of 1.4. HSC beams C4ALH0 (L, 104 MPa,), C6LH0 (U-101 MPa), C6LH1(U-102 MPa) and C6LH3 (U- 97 MPa) had joint shear indices of 0.4, 0.37, 0.37 and 0.43. The identical normal strength specimens C4ALN0 (L-42 MPa), C6LN1(U-51 MPa), C6LN0 (U-51Mpa) and C6LN3 had joint shear indices of 0.51, 0.40, 0.46 and 0.50 demonstrating that EC8-NA[6-20] design rule over estimates joint shear by 19% for HSC compared to NSC, Figure 6.29. The numbering at the end of BCJ name indicates the number of stirrups and the numbering after the first letter indicates the type of anchorage, i.e: 6 means U and 4 is L.

Parker's and Bullman's [6-18] test had failing at the bearing plate therefore a very low shear index. 4a, 5a, 5d and 5e had column flexural failure, and are not included. Most of the experimental results, other than 5f, which had a stirrup index of 0.3, had low joint shear.

Minimum stirrups were used in Vollum's two specimens. Both Sarsam's and Wilson's specimen had no confinement steel, Wilson's joint aspect ratio is 1 compared to Sarsam's of 1.5. Wilson's low aspect ratio improves its joint shear comparable to EC8-NA [6-20] recommendation with minimum stirrups.

EC8-NA [6-20] does not take into consideration the joint shear contribution of the stirrups or different detailing L and U for the beam bar connections.

There is a need for a new design rule which takes into consideration the importance of CVB, joint stirrups, detailing the beam bar connections, joint aspect ratio and the strength of concrete.

6.7.2 Comparison of ACI Committee 352 with tests

The shaded area of Figure 6.5 represents the upper half of the external joint regions in BCJ in reinforced concrete frames. (b) shows free body diagrams of the portions of the joints above the neutral axes of the beam entering the beam-column joint and (a) shows the horizontal shear at the mid-height of the joint given by:

$$V_{u,\,joint} = T - V_{col} \qquad \textbf{6.27}$$

where the joint shear is equal to the nominal force in the top steel in the joint, minus the shear in the columns due to sway. The column shears, V*col,* can be obtained from a frame analysis; for most practical cases, they are estimated from the free-body diagram, where points of contra flexure are assumed at the mid height of each story. The force T_n is the tension in the reinforcement in the beam at its nominal capacity. Thus,

$$T = \alpha A_s f_y \qquad 6.28$$

The factor α is intended to account for the fact that the actual yield strength of a bar is larger than the specified strength in most cases. It is taken to be at least 1.0 for Type-l frames, where only limited ductility is required, and at least 1.25 for Type-2 frames, which require considerable ductility.

The ACI Committee 352 [6-22] design procedure for Type-l (no seismic) joints consists of three main stages:

1. To provide confinement to the joint region by means of beams framing into the sides of the joint or by a combination of the confinement, from the column bars and from the ties in the joint region. The confinement allows the compression diagonal to form within the joint and intercepts the inclined cracks. For the joint to be properly confined, the beam steel must be inside the column steel.
2. To limit the shear in the joint.
3. To limit the bar size in the beams to a size that can be developed in the joint.

For best joint behaviour, the longitudinal column reinforcement should be uniformly

distributed around the perimeter of the column core. For Type-l joints, ACI Committee 352 [6-22] recommends that at least two layers of transverse reinforcement (ties) be provided between the top and the bottom levels of the longitudinal reinforcement in the deepest beam framing into the joint. The vertical centre to centre spacing of the transverse reinforcement should not exceed 12 in (304mm) in frames resisting gravity loads and should not exceed 6 in (152.4 mm) in frames resisting non seismic lateral loads. In non seismic regions, the transverse reinforcement can be closed ties, formed either by U-shaped ties and cap ties or by U-shaped ties lap spliced within the joint.

The ACI Committee 352 [6-22] design procedure still applies the 45° truss analogy. This calls for caution for HSC-BCJ because the diagonal crack is steeper in HSC due to absence of aggregate interlock.
Kordia's [6-15] specimens had an aspect ratio of 1.4 to 2. The specimen RE2 with aspect ratio of 2 without confinement steel and specimen RE4 with aspect ratio of 1.5 with minimum confinement steel of stirrup index 0.19 had lower joint shear than predicted by ACI 352[6-22]. However, the rest of the specimens with a stirrup index higher than 0.25 had a predicted shear index higher than ACI 352[6-22]. Figure 6.10.

When comparing Taylor's [6-14] experimental results for joint shear with ACI 352 prediction, specimen B3/41/24 with a large amount of confinement steel has stirrup index of 0.75 and a shear index of 0.73 compared to specimen A3/41/24 with a stirrup index of 0.34 and a shear index of 0.72. Specimens C3/41/24 and C3/41/137 have shear indices of 0.94 and 0.88, which fail below ACI 352[6-22] prediction. These two specimens have U connections to beam reinforcement. All specimens were of aspect ratio of 1.43.

Scott's [6-16] specimens C7 and C9 with aspect ratio of 2 had the lowest beam reinforcement, 1.4%, and as a result had the lowest joint shear. The specimen C4AL with the smallest aspect ratio of 1.4 with maximum confinement and beam steel had the highest joint shear. Only specimens of aspect ratio of 1.4, with the largest beam reinforcement of 2.1%, had a joint shear index higher than that predicted by ACI 352[6-22] because it does not include aspect ratio in its design rule.

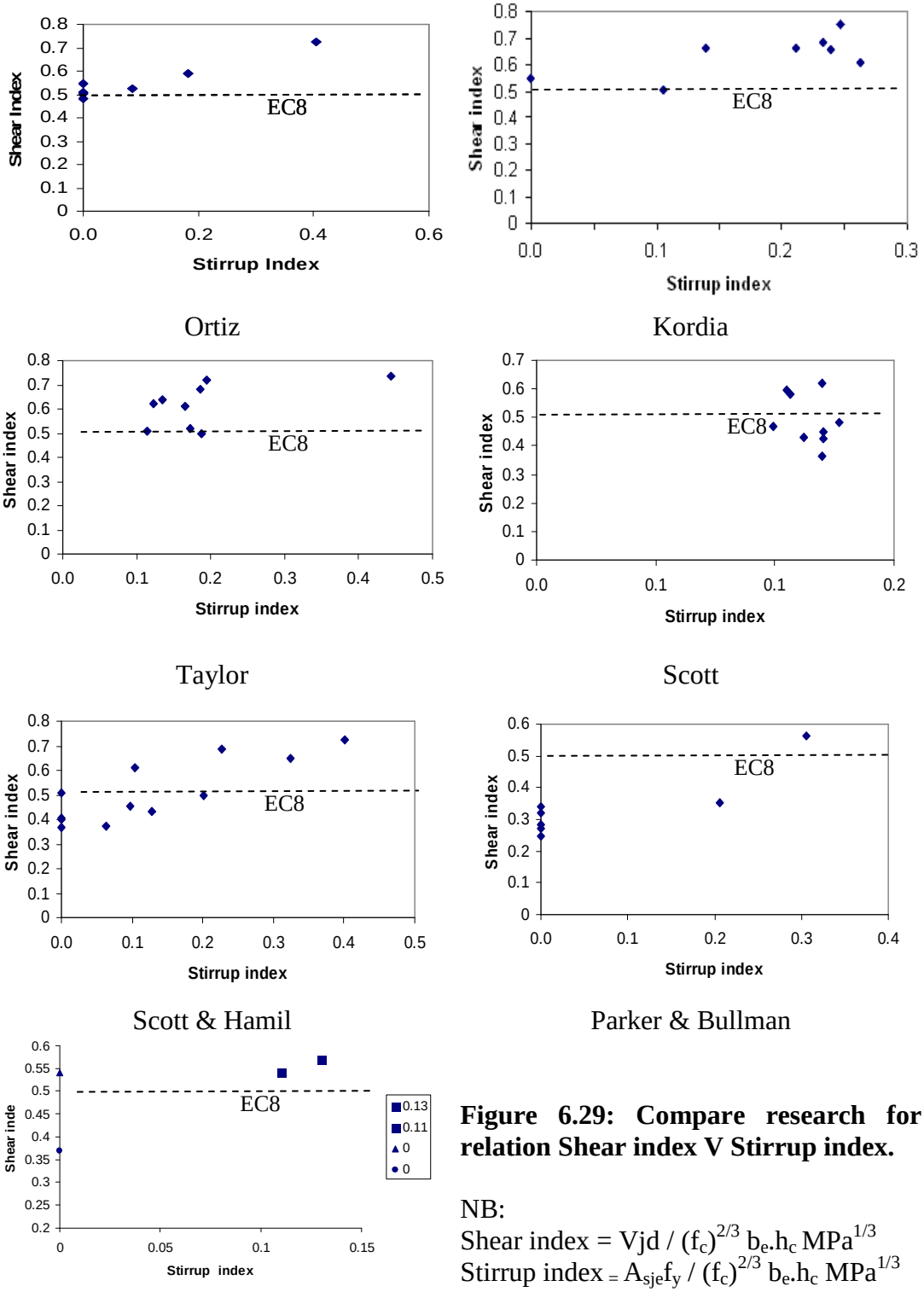

Figure 6.29: Compare research for relation Shear index V Stirrup index.

NB:
Shear index = $Vjd / (f_c)^{2/3} b_e.h_c$ MPa$^{1/3}$
Stirrup index = $A_{sje}f_y / (f_c)^{2/3} b_e.h_c$ MPa$^{1/3}$

Vollum (0.13, 0.11), Wilson (0.54) Sarsam 0.375

Scott and Hamill's [6-19] specimens included HSC and NSC material but all other properties and amount of beam, column reinforcement were the same. All HSC joints failed at lower joint shear than predicted by ACI 252. All specimens had an aspect ratio of 1.4. HSC beams C4ALH0 (104 MPa) with L detailing, C6LH0 (101 MPa), C6LH1(102

MPa) and C6LH3 (97 MPa) with U detailing had joint shear indices of 0.89, 0.81, 0.82 and 0.94. The identical normal strength specimens C4ALN0, C6LN0, C6LN1 and C6LN3 had joint shear indices of 0.96, 0.78, 0.89 and 0.96 demonstrating that the ACI 352[6-22] design rule overestimates by 4% for HSC compared to NSC.

Specimen EX2 tested by Sarsam [6-39] had the lowest joint shear index of 0.7. Neither Sarsam nor Wilson [6-23] used joint stirrups, and their joint aspect ratio was 1.5 and 1. This difference in aspect ratio could be the main reason for a 35% increase in joint shear index for the two specimens. ACI 352[6-22] design rule does not consider joint aspect ratio.

6.8 Design equations proposed by other researchers

In this section we review empirical design equations proposed by other researchers for the prediction of joint shear strength for exterior BCJ subjected to monotonic loading.

6.8.1 Design equation of Sarsam and Phillips [6-39]

Their design equation for monotonically loaded exterior BCJ consists essentially of two parts. The first is similar to the proposal by Zsutty [6-40] for the ultimate shear strength of beams with low a/d ratio (≤2.5). Instead of d/ a, the column/beam effective depth ratio, d_c/d_b, is used to obtain a formula with a built-in strength reduction for design purposes. The second part is the multiplier $(1+0.29\ N_u/A_g)^{0.5}$, which accounts for the column compression proposed in the superseded version (July1976) of ACI 352[6-5].

$$V_{col} = 5.08(f_{cu}\rho_c)^{0.33}(d_c/d_b)^{1.33}\ (1+0.29N_u/A_g)^{0.5}\ b_c d_c \qquad \textbf{6.29}$$

where V_{col} is the column shear force at the column-joint interface (N); f_{cu} is the concrete cube strength (MPa); ρ_c is the column longitudinal reinforcement ratio $\rho_c=A_{so} / b_c d_c$ where A_{so} is the area of the layer of steel furthest from the maximum compression face in a column (mm^2); A_g is the gross cross-sectional area of the column at the joint (mm^2); N_u is the axial column load (N); d_c is the effective depth of the layer of steel furthest away from the maximum compression face in a column (mm); d_b is the effective depth of beam tension reinforcement (mm); d_c is the width of column section at the joint (mm).

The shear force resisted by the links is calculated in a similar manner to the New Zealand approach [6-24] as:

$V_{sd} = 0.87A_{js}f_{yv}$ **6.30**

$V_{ud} = V_{cd} + V_{sd}$ **6.31**

where A_{js} is the total area of horizontal link reinforcement crossing the diagonal plane from corner to corner of the joint between the beam compression and tension reinforcement (mm^2); f_{yv} is the tensile strength of the link reinforcement (MPa); V_{sd} is the design link shear force resistance (N); V_{cd} is the design shear force resistance of concrete in a joint (N); V_{ud} is the design ultimate shear capacity of joint (N). All the joint stirrups are considered to be effective in increasing the joint shear capacity.

Sarsam and Phillip's [6-39] equation ignores the effect of detailing of beam anchorage and their proposal is dependent on the axial load on columns which has been demonstrated to have no influence. Sarsam applies the New Zealand approach [6-24] as $V_{sd} = 0.87A_{js}f_{yv}$ which gives too much weight to stirrup contribution to joint shear while reducing the significance of the contribution of the concrete.

Sarsam's design rule depending on concrete contribution of $(f_{cu})^{0.33}$ underestimates the contribution of concrete to joint shear. As demonstrated, Figure 6.19, the closest estimate to contribution of NSC joint shear is $(f_c)^{2/3}$.

6.8.2 Design equation of Vollum and Newman [6-41]

Vollum and Newman [6-33] completed extensive investigation on past research and as a result proposed their design recommendations for exterior BCJ as follows:

$V_j = V_c + (A_{sje}f_y - \alpha b_e h_c \sqrt{f_c'})$ **6.32**

$V_c = 0.642\beta\,(1+0.555(2-h_b/h_c))b_e h_c\sqrt{f_c'}$ **6.33**

The maximum joint shear strength should be limited to:

$V_j < 0.97b_e h_c\sqrt{f_c'}(1+0.555(2-h_b/h_c)) < 1.33\, b_e h_c\sqrt{f_c'}$

Their design rule depends on $\sqrt{f_c}$ gives reasonable predictions, this writer's proposed equation depends on $(f_c)^{2/3}$, Figure 6.11 compared to Figure 6.10, which also gives a closer estimate of the joint shear of the specimen of NSC and HSC to predicted joint shear.

The maximum joint shear is limited to 1.33 $b_e h_c \sqrt{f_c'}$. Their empirical figure is based on the results obtained from specimen BCJ7 by Ortiz where maximum joint shear was achieved with maximum amount of links. However, if $\sqrt{f_c'}$ with HSC in large aspect ratio is applied this 1.33 $b_e h_c \sqrt{f_c'}$ will overestimate the joint shear.

Their maximum joint shear is also required to be less than $0.97 b_e h_c \sqrt{f_c'}(1+0.555(2-h_b/h_c))$. This empirical number $0.97 b_e h_c \sqrt{f_c'}$, is based on Wilson's [6-23] test with a very low aspect ratio of 1, which would result in an underestimation of joint shear if HSC is used as the compression strut in short aspect ratio would fully develop.

Vollum [6-35] reached the conclusion that axial load has insignificant influence on joint shear. His recommendations are limited to BCJ of aspect ratio 2.5, and he recommends designers to refer to the variable truss approach recommended by EC2 [6-1] for designing BCJ of aspect ratio≥2.5.

However, in the last chapter it was demonstrated that STM was developed for HSC beams with HWB of a/d=3 which is analogous to HSC BCJ of aspect ratio 3 with CVB, therefore, STM was developed for the TBCJ.

6.8.3 Design equations of Ortiz [6-17] and Parker &Bullman [6-18]

Ortiz developed a method for predicting the shear strength of the column in a reinforced concrete BCJ. The method was assessed using the results of seven tests on beam column specimens of which three have shear stirrups.

Parker &Bullman [6-18] developed a method for predicting the shear strength of the column in a reinforced concrete BCJ. The method was assessed using the results of tests on 12 beam column specimens.

Both methods overestimate the influence of joint stirrups on joint shear strength because they calculate joint strength using the following equation:

$V_j = V_c + A_{sje} f_y$

where V_c is the joint shear strength without stirrups and $A_{sje}f_y$ is the effective capacity of joint stirrups. This common assumption overestimates the contribution of joint stirrups and undervalues the contribution of the concrete. Neither recommend an upper limit for $A_{sje}f_y$.

6.9 This writer's proposed design equation

Both design codes ACI 352[6-22] and EC8-NA[6-20] specify minimum stirrup requirements. The BS 8 110 [6-10] recommendation for minimum reinforcement at spacing 12 times the diameter of the column reinforcement is the lowest requirement when compared with ACI352[6-22] and EC8-NA [6-20] recommendations and there is no provision made for joint strength to be increased by stirrups in the codes mentioned.

The design recommendations of ACI352[6-22] and EC 8-NA[6-20] fail to predict the observed dependence of joint shear strength on joint aspect ratio, the influence of HSC and detailing of the reinforcement of anchorage of the beam reinforcement to column. In addition, the recommended amount of stirrups is not enough to provide sufficient joint shear strength when shear forces are high.

Sarsam and Phillips' [6-39] equation ignores the effect of detailing of beam anchorage and puts too much emphasis on axial load on the column, and joint shear being proportional to $f_{cu}^{1/3}$is an underestimation of the contribution of concrete to joint shear.

A comparison of joint shear dependence on concrete was examined for $f_{cu}^{1/2}$.and $f_{cu}^{2/3}$. Looking at the convergence of the experimental results without shear stirrups when joint shear is designed by considering contribution of concrete to be $f_{cu}^{2/3}$, the values of shear index are over a range of 0.25 to 0.55, or a tolerance of 0.3, Figure 6.11, whereas this increases over a range of 0.45 to 1.05, or tolerance of 0.6 when considering concrete contribution of $f_{cu}^{1/2}$, Figure 6.10, therefore it can be assumed that with the contribution of concrete to be $f_{cu}^{2/3}$ it is within smaller tolerance and is more accurate.

Vollum and Newman's [6-34] design rule has joint shear directly proportional to the contribution of concrete $f_{cu}^{1/2}$ .Vollum and Newman refer designers to the EC2[6-1] variable truss angle method when joint aspect ratio is larger than 2.5. When the EC2[6-1] design rule was used for shear design of HSC beams of a/d=3 which is analogous to aspect

ratio of 3, although the amount of shear reinforcement used in the beams was below minima of EC2[6-1] recommendation $\rho_w f_y \geq 0.08$, the ultimate shear to the characteristic resistance was as low as 0.86, Table 6.7.

As joint aspect ratio exceeds 2.5 in cases of transfer beams, the shear resistance of HSC particularly with limestone aggregate may become similar or less than NSC, therefore the existing proposals prove unsafe for transfer beams with HSC columns, Figure 6.18.

Therefore, there is a need for design equation for TBCJ which includes the shear contribution of CVB. A suitable design rule for transfer beams when joint aspect ratio exceeding 2.5 with CVB is introduced in Chapter 7. However, for conventional BCJ with aspect ratio less than 2.5 the following proposed equation provide the most accurate prediction as shown in Table 6-11 and Figure 6.30.

From equation this writer's derived equation for a beam in section 3.5, equation 3.12, $1.64\, b_n\, d_b\, f_{cu}^{1/3} (n)^{1/4}$, is proposed for the analogous BCJ, which is

$$V_{du} = 1.64\, h_c\, d_b\, f_{cu}^{1/3} (n)^{1/4} = 1.64\, (b_e - n d_b)\, d_b\, f_{cu}^{1/3} (n)^{1/4} \qquad \textbf{6.34}$$

$$V_{jd} = V_c + 1.64\, h_c\, d_b\, f_{cu}^{1/3} (n)^{1/4} + (A_{sje} f_y - 0.1 b_e h_c f_c^{2/3}) \qquad \textbf{6.35}$$

where $0 \leq A_{sje} f_y / (f_c)^{2/3}\, b_e.h_c - 0.1 b_e h_c f_c^{2/3} \leq 0.2 b_c h_c f_c^{2/3}$

$$V_{jd} = \gamma (f_c)^{2/3}\, b_e.h_c + 1.64\, h_c\, d_b\, f_{cu}^{1/3} (n)^{1/4} + (A_{sje} f_y - 0.1 b_e h_c f_c^{2/3}) \qquad \textbf{6.36}$$

whereL bar $\gamma = 0.54$ or U bar $\gamma = 0.49$

Limits on each parts of the equation based on Table 2-7 is as follow:

$$V_{jd} = \gamma (f_c)^{2/3}\, b_e.h_c + 1.64\, h_c\, d_b\, f_{cu}^{1/3} (n)^{1/4} + (A_{sje} f_y - 0.1 b_e h_c f_c^{2/3}) < 0.35 b_c h_c f_c^{2/3}$$

$$0 \leq (A_{sje} f_y - 0.1 b_e h_c f_c^{2/3}) < 0.15 b_c h_c f_c^{2/3}$$

$$0 \leq 1.64\, (b_e - n d_b)\, d_b\, f_{cu}^{1/3} (n)^{1/4} \leq \eta b_c h_c f_c^{2/3}$$ where $\eta = 0.05$ for HSC and $\eta = 0.02$ for NSC

where

V_{jd} total joint shear resistance

h_c is the section depth of the column (mm)

f_c' is the concrete cylinder strength (MPa);
b_e is the average of the beam and column widths (mm)

The proposed design rule is based on refining the EC8 design rule by using γ factor for beam detailing and the dowel action from the central bar within the depth of the column.

The reason $(f_c)^{2/3}\, b_e.h_c$ was taken for concrete contribution is as a result of comparison with the ACI 352 recommendation for $(f_c)^{2/3}\, b_e.h_c$. The accuracy of EC8 for predictions compared to experiments was 50% , whereas ACI352 was 41%, Figure 6.10.
V_c is from the strut action in concrete depending on the beam reinforcement detailing,

$V_c=0.54f_c^{2/3}b_eh_c$ **6.37**

for L detailing and

$V_c = 0.49\, f_c^{2/3}b_eh_c$ **6.38**

for U detailing.

This writer's also recommends that guidance on the minimum stirrup guidance in EC8 for DCM (Ductility class medium) [6-42] needs to be compared and taken into account when designing to recommendations in EC8-NA[6-20]DCL (Ductility class low) [6-20].

When f_c>50 MPa then V_{du} needs to be taken into account and CVB of A_{du}> 1% should be utilised to maximise the joint shear contribution of dowel action in HSC BCJ. This figure is demonstrated to be effective in this writer's experimental tests on HSC beams with HWB.
Using Baumann's dowel cracking expression,
The dowel force causing cracking is:
V_{du} =Dcr = $1.64\, h_c d_b\, f_{cu}^{1/3}(n)^{1/4}$
or for two CVB at mid depth of the column

V_{du} =Dcr = $1.95\, h_c d_b\, f_{cu}^{1/3}$ **6.39**

Researcher	Identity	H_c mm	L mm	h_c mm	d_c mm	b_c mm	h_b mm	d_b mm	b_b mm	ρ_b Beam
Vollum [6-41]	EBCJ6	2000	450	200	167	200	300	257	200	0.008
	EBCJ8	2000	450	200	167	200	300	257	200	0.012
Wilson[5.23]	J1	3000	850	300	269	154	300	257	154	0.017
Scott &Hamill [6-19]	C4ALN	1700	750	150	117	150	210	177	110	0.021
	C4ALN	1700	750	150	117	150	210	177	110	0.021
	C4ALN	1700	750	150	117	150	210	177	110	0.021
	C4ALN	1700	750	150	117	150	210	177	110	0.021
	C4ALH	1700	750	150	117	150	210	177	110	0.021
	C6LN0	1700	750	150	117	150	210	177	110	0.021
	C6LN1	1700	750	150	117	150	210	177	110	0.021
	C6LN3	1700	750	150	117	150	210	177	110	0.021
	C6LN5	1700	750	150	117	150	210	177	110	0.021
	C6LH0	1700	750	150	117	150	210	177	110	0.021
	C6LH1	1700	750	150	117	150	210	177	110	0.021
	C6LH3	1700	750	150	117	150	210	177	110	0.021
Parker & Bullman [6-18]	4b	2000	850	300	245	300	500	445	250	0.009
	4c	2000	850	300	245	300	500	445	250	0.009
	4d	2000	850	300	245	300	500	445	250	0.009
	4e	2000	850	300	245	300	500	445	250	0.009
	4f	2000	850	300	245	300	500	445	250	0.009
	5b	2000	850	300	245	300	500	445	250	0.009
	5f	2000	850	300	245	300	500	445	250	0.014
Ortiz [6-17]	BCJ1	2000	1050	300	267	200	400	367	200	0.011
	BCJ2	2000	1100	300	267	200	400	367	200	0.011
	BCJ3	2000	1100	300	267	200	400	367	200	0.011
	BCJ4	2000	1100	300	267	200	400	367	200	0.011
	BCJ5	2000	1100	300	267	200	400	367	200	0.011
	BCJ6	2000	1100	300	267	200	400	367	200	0.011
	BCJ7	2000	1100	300	267	200	400	367	200	0.011
Scott [6-16]	CIAL	1700	750	150	117	150	210	179	110	0.011
	C4	1700	750	150	117	150	210	177	110	0.021
	C4A	1700	750	150	117	150	210	177	110	0.021
	C4AL	1700	750	150	117	150	210	177	110	0.021
	C7	1700	750	150	117	150	300	267	110	0.014
	C3L	1700	750	150	117	150	210	177	110	0.021
	C6	1700	750	150	117	150	210	177	110	0.021
	C6L	1700	750	150	117	150	210	177	110	0.021
	C9	1700	750	150	117	150	300	267	110	0.014
Sarsam[5.39]	EX2	1536	1422	204	172	157	305	272	152	0.010
Kordia [6-15]	RE2	3000	1000	200	167	200	400	365	200	0.009
	RE3	3000	1000	200	167	200	400	265	200	0.018
	RE4	3000	1000	200	167	200	400	265	200	0.012
	RE6	3000	1000	200	167	200	400	265	200	0.012
	RE7	3000	975	230	217	230	350	315	230	0.013
	RE8	3000	975	230	217	230	350	315	230	0.013
	RE9	3000	975	230	217	230	350	315	230	0.013
	RE10	3000	975	230	217	230	350	355	230	0.012
Taylor [6-2]	P1/41/2	1290	470	140	110	140	200	170	100	0.024
	P2/41/2	1290	470	140	110	140	200	170	100	0.024
	P2/41/2	1290	470	140	110	140	200	170	100	0.024
	A3/41/2	1290	470	140	110	140	200	170	100	0.024
	D3/41/2	1290	470	140	110	140	200	170	100	0.024
	B3/41/2	1290	470	140	110	140	200	170	100	0.024
	C3/41/2	1290	470	140	110	140	200	170	100	0.024
	C3/41/1	1290	470	140	110	140	200	173	100	0.024
	C3/41/2	1290	470	140	110	140	200	170	100	0.024

Table 6-10: Geometry and beam reinforcement for BCJ.

Researcher	Specimen	Detail	Fc MPa	$A_{sje}f_y/b_c h_c f_c^{2/3}$ $MPa^{1/3}$	$V_j/b_c h_c f_c^{2/3}$ $MPa^{1/3}$	V_{jcal}/V_{jec8}	$V_{jcal}/V_{jpropose}$
Vollum [6-41]	EBCJ6	U Bar	26	0.13	0.57	1.08	1.2
	EBCJ8	U Bar	33	0.11	0.54	1.03	1.1
Wilson[5.23]	J1	L Bar	32	0.00	0.54	1.03	1.0
Scott & Hamill [6-19]	C4ALN0	L Bar	42	0.00	0.51	0.97	0.9
	C4ALN1	L Bar	46	0.10	0.61	1.16	1.1
	C4ALN3	L Bar	42	0.23	0.69	1.31	1.3
	C4ALN5	L Bar	50	0.32	0.65	1.23	1.2
	C4ALH0	L Bar	104	0.00	0.40	0.77	0.7
	C6LN0	U Bar	51	0.00	0.40	0.76	0.8
	C6LN1	U Bar	51	0.10	0.46	0.87	0.9
	C6LN3	U Bar	49	0.20	0.50	0.94	1.0
	C6LN5	U Bar	37	0.40	0.73	1.38	1.5
	C6LH0	U Bar	101	0.00	0.37	0.70	0.8
	C6LH1	U Bar	102	0.06	0.37	0.71	0.8
	C6LH3	U Bar	97	0.13	0.43	0.82	0.9
Parker & Bullman [6-18]	4b	L Bar	39	0.00	0.25	0.47	0.5
	4c	L Bar	37	0.00	0.32	0.61	0.6
	4d	L Bar	39	0.00	0.27	0.52	0.5
	4e	L Bar	40	0.00	0.28	0.54	0.5
	4f	L Bar	38	0.00	0.34	0.65	0.6
	5b	L Bar	43	0.21	0.35	0.67	0.7
	5f	L Bar	43	0.31	0.56	1.08	1.0
Ortiz [6-17]	BCJ1	L Bar	34	0.00	0.51	0.96	0.94
	BCJ2	L Bar	38	0.09	0.52	1.00	0.97
	BCJ3	L Bar	33	0.00	0.55	1.04	1.01
	BCJ4	L Bar	34	0.18	0.59	1.12	1.09
	BCJ5	L Bar	38	0.00	0.48	0.91	0.89
	BCJ6	L Bar	35	0.00	0.51	0.97	0.94
	BCJ7	L Bar	35	0.40	0.73	1.38	1.35
Scott [6-16]	CIAL	L Bar	33	0.13	0.48	0.91	0.9
	C4	L Bar	41	0.11	0.58	1.10	1.1
	C4A	L Bar	44	0.11	0.59	1.13	1.1
	C4AL	L Bar	36	0.12	0.62	1.18	1.1
	C7	L Bar	35	0.12	0.43	0.81	0.8
	C3L	U Bar	35	0.12	0.45	0.85	0.9
	C6	U Bar	40	0.11	0.43	0.82	0.9
	C6L	U Bar	46	0.10	0.47	0.89	1.0
	C9	U Bar	36	0.12	0.36	0.69	0.7
Sarsam[5.39]	EX2	L Bar	52	0.00	0.37	0.70	0.7
Kordina [6-15]	RE2	L Bar	25	0.00	0.54	1.04	1.01
	RE3	L Bar	40	0.14	0.66	1.25	1.22
	RE4	L Bar	32	0.11	0.50	0.96	0.93
	RE6	L Bar	32	0.21	0.66	1.26	1.22
	RE7	L Bar	26	0.25	0.75	1.43	1.39
	RE8	L Bar	28	0.24	0.65	1.24	1.13
	RE9	U Bar	28	0.23	0.68	1.30	1.39
	RE10	U Bar	24	0.26	0.61	1.15	1.24
Taylor [6-2]	P1/41/24	L Bar	33	0.17	0.61	1.17	1.13
	P2/41/24	L Bar	29	0.19	0.68	1.30	1.26
	P2/41/24A	L Bar	47	0.14	0.64	1.22	1.18
	A3/41/24	L Bar	27	0.19	0.72	1.37	1.33
	D3/41/24	L Bar	53	0.12	0.62	1.18	1.15
	B3/41/24	L Bar	22	0.44	0.73	1.40	1.36
	C3/41/24BY	L Bar	32	0.17	0.52	0.99	1.1
	C3/41/13Y	U Bar	28	0.19	0.50	0.95	1.0
	C3/41/24Y	U Bar	60	0.11	0.51	0.97	1.0

Table 6-11: Comparison of accuracy of proposed design rule and EC8 [20] for all the BCJ excluding provision for stirrups.

The above equation was applied to 56 laboratory BCJ specimens monotonically loaded to failure. As Table 6-11 shows, the results from this proposed design rule are compared to those from EC8-NA [6-20] , and a slight improvement in safety of 0.04% is recorded due to the replacement of the general figure of 0.525 with the more relevant figures of 0.54 for L detailing and 0.49 for U detailing of the beam bar.

A comparison of the predictions of the proposed design rule without including provision for stirrups, with the EC8-NA rule demonstrated in graphs in Figure 6.30, show that for the 56 specimen tested, EC8 only gives a more economical and safer prediction for 12, or 21% of the specimens. The proposed design rule offers a safer and more economical design rule for 44 specimens, or 79%, of the tests.

1. The graph shows a comparison of the proposed design rule's joint shear prediction to EC8 when no shear stirrups are used in the specimen.. The proposed design rule offers higher accuracy.

2. When minimum reinforcement is applied, if the average is considered for all specimens, $V_{jcal}/V_{jpropose}$ =1 and V_{jcal}/V_{jec8}=0.98 which indicates that the proposed rule is safe but EC8-NA [6-20] is slightly unsafe. However, if only the NSC specimen is considered $V_{jcal}/V_{jpropose}$ =1 and V_{jcal}/V_{jec8}=1, indicating both rules are equally safe. When HSC samples are considered, $V_{jcal}/V_{jpropose}$ =0.85 and V_{jcal}/V_{jec8}=0.77, indicating that the proposed rule is 8% safer than EC8-NA [6-20].

3. For all specimens with $A_{sje}f_y/ b_c h_c f_c^{2/3} \leq 0.1$, the average value for normal strength $V_{jcal}/V_{jpropose}$ =0.79 and V_{jcal}/V_{jec8}=0.8. For HSC $V_{jcal}/V_{jpropose}$ =0.8 and V_{jcal}/V_{jec8} =0.75 .

4. All specimens with $A_{sje}f_y/ b_c h_c f_c^{2/3} = 0.2$ are predicted safely to EC8 recommendations for DCM rather than EC8 -NA [6-20] for DCL.

The minimum amount of stirrups EC8-NA [6-20] recommended for ductility class DCL is not sufficient to provide a safe prediction for non-seismic regions. From the tests, it is demonstrated that for BCJ1, BCJ5, BCJ6, C6LN0 and C4ALN0 which are NSC the EC8-NA [6-20] design prediction is unsafe at 76% to 97% compared to the experimental results.

6.10 Conclusion and the proposed design rule for BCJ

A design method has been developed, based on statistical data of 56 published test results, to calculate the shear resistance in HSC and NSC BCJ, Figure 6.30.

The proposed equation is a function of aspect ratio and the magnitude of shear force in BCJ and lower-bound theorem of plasticity are maintained.

The results given by the proposed design equation are closer to 79% of the total actual experimental data while only 21% of the predictions by EC8-NA[6-20] are closer to the actual experimental results.

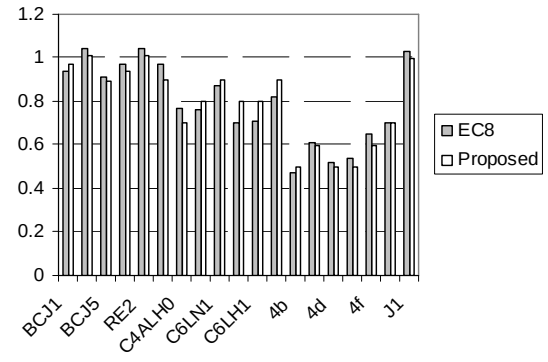

1) No shear stirrups in the specimen

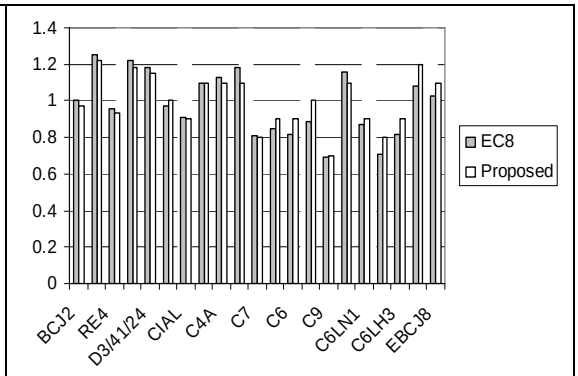

2) Asjefy/ $b_c h_c f_c^{2/3} = 0$.

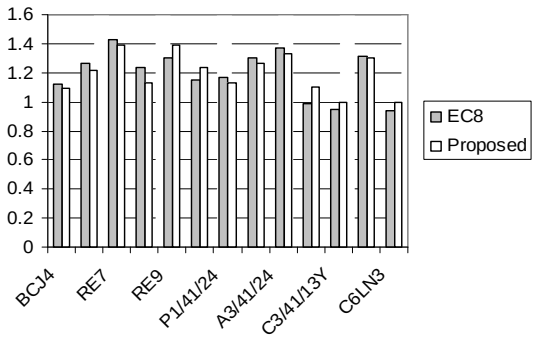

3) Asjefy/ $b_c h_c f_c^{2/3} = 0.2$

Figure 6.30: Comparison of prediction of joint shear of proposed equation with EC8. Provision to allow for stirrups in the proposed equation is not included.

An investigation of past experiments for specimens with monotonic loading indicates the design guidelines from EC8-NA[6-20] for DCL need to be refined for this equation for L and U connection bars while including a provision for the shear contribution of stirrups.

The proposed design rule accounts for the shear contribution of CVB, the detailing of anchorage reinforcement as well as the confinement stirrups leading to a more accurate prediction.

As there are considerable differences in design procedures for transverse reinforcement in BCJ in the codes, a design rule for shear reinforcement as an alternative to the minimum transverse reinforcement proposed by EC8-NA[6-20] for DCL is needed. This thesis proposes such a design rule to filling this void, while giving special attention to shear contribution of CVB in HSC-BCJ with large aspect ratio.

When considering BCJ without shear reinforcement, the proposed design rule from EC8 NA[6-20] for DCL are unsafe. Therefore, adherence to provide stirrups to recommendations of EC8 [6-20] for DCM is recommended. When the quantity of stirrup reinforcement is compliant to requirements of EC8 [6-42] for DCM, a safe and optimised prediction is achieved.

To this writer's knowledge, no experimental tests on HSC-BCJ of aspect ratio>2 have taken place. The performance of HSC- TBCJ of aspect ratio>2.5 needs to be experimentally tested . Therefore, use of the proposed design rule to supplement CVB in addition to recommendations for stirrups from EC8 [6-20] for DCM offers a reasonable prediction for joint performance when designing HSC-BCJ with aspect ratio>2.5.

The proposed design rule is based on practical detailing approach at BCJ to maximise shear resistance while introducing an easier method of construction by minimising congestion of the stirrups in the column at TBCJ .

Presence of CVB contributes to producing many smaller thiner cracks parallel to the main crack at ultimate load before failure, these smaller cracks dissipate the energy from ultimate load by producing many distributed cracks across the joint, resulting in a ductile and eventual failure.. When CVB is absent the main crack at the ultimate load would be suddenly formed which would be comparatively thicker and would result into sudden failure of the joint in a less ductile manner compared to when CVB is present.

Both design codes ACI 352 and EC8-NA specify minimum shear stirrup requirements, however, they do not give provision for the joint strength to be increased by the stirrups.

The design recommendations of these codes fail to predict the observed dependence of joint shear strength on the joint aspect ratio, as well as the influence of HSC and detailing of the anchorage on the behaviour of BCJ. In addition, they do not provide any recommendation if the amount of stirrups is not adequate in order to provide sufficient shear strength at BCJ when the shear forces are high.

As noted above, HSC beams may be weaker in shear than NSC beams when span depth ratio is 3. It can also be deduced that HSC-BCJ will be weaker than NSC-BCJ when the joint aspect ratio exceeds 2.5.

The traditional approach to predict joint shear strength is as follows:
shear strength is given by

$V_j = V_c + A_{sje}f_y$

where V is the joint shear strength without stirrups and $A_{sje}f_y$ is the yield capacity of the effective joint stirrups. From investigation into the performance of stirrups in experimental tests [6-17] for specimen BCJ4, it was shown that with stirrup index= $A_{sje}f_y / (f_c)^{2/3}\ b_e.h_c$= 0.2 $MPa^{1/3}$ two stirrups above the flexural compressive zone of the incoming beam and below the main reinforcement within the upper $^5/_8$ yielded, however, when stirrup index was increased to 0.4 non of the stirrups yielded.
Based on experiment results shown in Figure 6.29, this writer's proposed equation for the stirrup is $A_{sje}f_y - 0.1b_ch_cf_c^{2/3}$ within the joint which is restricted to $0.2 \le A_{sje}f_y / (f_c)^{2/3}\ b_e.h_c \le 0.4$ based on past experiments, Figure 6.29. The factor $0.1b_ch_cf_c^{2/3}$ depends on concrete strength and joint aspect ratio.

Experimental tests by this writer on 12 beams demonstrated that for the design of HSC beams with a/d=3, HWB produced superior shear capacity due to the development of dowel action which in turn enhanced the stabilising arching affect in the beams.
Using Baumann's modified dowel cracking expression, the dowel force causing cracking is:

V_{du} =Dcr = 1.64 $h_cd_b\ f_{cu}^{1/3}(n)^{1/4}$ (for n number of bar in the beam)
V_{du} =Dcr = 1.95 $h_cd_b\ f_{cu}^{1/3}$ (for n = 2 i.e. bar at mid-depth, BCJ with HWB)

where d_b= diameter of the dowel bars and n is number of bars, V_{du} = dowel force**,** and f_{cu}= cube crushing strength of concrete of 150 mm cubes in N/mm^2.

The stabilising arching effect in the HSC beam of a/d = 3 with HWB makes the beam perform like a short beam $2 \leq a/d \leq 3$ and is analogous to HSC - BCJ with aspect ratio of 3 with CVB.

For BCJ with CVB and stirrups in HSC column, the shear resistance is

$V_j = V_c + V_{du} + (A_{sje}f_y - 0.1b_ch_cf_c^{2/3})$ where $0.2 \leq A_{sje}f_y / (f_c)^{2/3} b_e.h_c \leq 0.4$

$V_c = \gamma(f_c)^{2/3} b_e.h_c$ is joint shear resistance due to concrete

where $\gamma = 0.54$ or 0.49 for L-bar, or U-bar for beam connection

In section 2.4.6 of Chapter 2, the spacing between links of $400(f_{cu})^{-0.16}$ mm was demonstrated to be reasonable for beams of a/d=3.02 in order to allow for the change in the angle of shear crack which is dependent on the strength of concrete, for the purpose of calculating the spacing of stirrups. This limit for spacing of stirrups is proposed for analogous BCJ.

As the next chapter demonstrates, the diagonal compression strut in the TBCJ strains the stirrups along the mid-length through which the strut passes. Struts located below the neutral axis of the beam in TBCJ are mainly strained within the half depth of the column close to the beam and struts located above the neutral axis of the beam in BCJ are mainly strained within the half depth of the column away from the beam. Placing stirrups in such aconfiguration can improve the robustness of the structure.

6.11 References for Chapter 6

6-1 Eurocode 2: Design of concrete structures, Part 1-1, General rules and rules for buildings, BS EN 1992-1-1:2004, British Standards Institution, London, Dec 2004

6-2 Taylor, H.P.J. 'The Behaviour of In Situ Concrete Beam column Joints', Cement and Concrete Association, May 1974, Technical Report no. 42492, 33p.

6-3 Cheung P. C., Paulay T, Park R, "Behviour of BCJ in seismically- loaded RC frames". The Structural Engineer, Volume 71, No.8, 20 April 1993

6-4 Park, R.: "Some considerations in the seismic design of reinforced concrete interior beam column joints of moment resisting frames", Journal of the Structural Engineering Society of New, Zealand, Vol. 15, No. 2, September 2002, pp. 53-64.

6-5 ACI Committee 318, Building Code Requirements for Structural Concrete (ACI 318-08) and commentary (ACI 318R-08), American Concrete Institute , Formington Hills, MI, 2008, 465 pp

6-6. Balint and Harold P. S, Taylor P. J, 'Reinforcement Detailing of Frame Corner Joints with Particular Reference to Opening Corners', Technical Report 42.462, Cement and Concrete Association, London, February, 1972, 16 pp.

6-7 Ingvar H. E. Nilsson and Anders Losberg, "Reinforced Concrete Corners and Joints Subjected to Bending Moment," Proceedings ASCE, Journal of the Structural Division, Vol. 102, No. ST6, June1976,pp.1229-1254

6-8 William D. Cook and Denis Mitchell, "Studies of Disturbed Regions near Discontinuities in Reinforced Concrete Members," ACI Structural Journal, Vol. 85, No.2, March-April 1988, pp. 206-216.

6-9 Schlaich, J, Weischede, D, Detaining of Concrete Structures (in German), Bulletin d'Information 150, Comite Euro-International du Beton, Paris, March 1982, 163 pp

6-10 BS 8110: Structural use of concrete, Part 1.Code of practice for design and construction, British Standards Institution, London, 1985

6-11 Comité Euro-International du Béton, CEB-FIP Model Code 1990, Thomas Telford Services, Ltd., London, 1993, 437 pp.

6-12 British standard institution. CP 110:1972. "The structural use of concrete. Part 1: Design, materials and workmanship". pp. 154

6-13 Hognestad, E. , Hanson, N.W and McHenry, D. "Concrete stress distribution in ultimate strength design". Journal of the american Concrete Institute. Proceedings Vol. 52, No 10. December 1955. pp.455-479

6-14 Taylor, H.P.J., Clarke, J.L., "Some Detailing Problems in Concrete Frame Structures," The Structural Engineer, Vo1.54, No.1, January 1976, pp.19-32.

6-15 Kordina, K. “Bewehrungsfuhrung in Ecken und Rahmenendknoten”, Deutscher Ausschuss fu¨r Stahlbeton, Heft 354, 1984

6-16 Scott, R.H. “The effects of detailing on RC beam column connection behaviour.” The Structural Engineer 1992;70(18):318–24.

6-17 Reys de Ortiz, I. ‘STM of reinforced concrete short beams and beam column joints’. PhD thesis, 1993, University of Westminster.

6-18 Parker, D.E, Bullman, P.J.M. Shear strength within reinforced concrete beam column joints. The Structural Engineer 1997;75(4):53–7

6-19 Scott, R.H, Hamill, S.J. “Connection zone strain in reinforced concrete beam column connections”, In: Proceedings of the 11th International Conference on Experimental Mechanics, Oxford, UK, 1998. pp. 65-69.

6-20 Eurocode 8: “Design provisions for earthquake resistance of structures”, London, British Standard Institution , 1995

6-21 Eshani, M.R, Wight, J.K. "Effect of transverse beams and slab on behaviour of reinforced concrete beam-to-column connections', ACI Structural Journal, 82, March-April 1985, p188

6-22 ACI-ASCE Committee 352, 'Recommendations for Design of Beam-Column Joints in Monolithic Reinforced Concrete Structures'. ACI Journal Proceedings: Part 3, Detroit, American Concrete Institute 1998

6-23 Wilson, I. D.: 'SIFCON joints in precast concrete structures', 8th BCA Annual Conf. on Higher Education and the Concrete Industry, Southampton, July 1998, p227

6-24 Standard association of New Zealand Standard Code of practice for the design of concrete structures, Wellington. DZ3101 : Parts 1 and 2: 1995

6-25 Bertero, V.V "Overview of the State-of-the-Art in Earthquake-Resistant Reinforced Concrete Building Construction". US National Conference on Earthquake Engineering August 22,1979 PP 838-852

6-26 Park, R . and Thompson K,J. "Cyclic load tests on prestressed and partially prestressed beam-column joints". Journal of the prestressed Concrete Institute. vol. 22, No. 5. September -October 1977.pp. 84-110

6-27 Lee, D. L. N, Wight, J.K and Hanson, R.D. "Reinforced Concrete beam-column joints under large load reversal". Proceedings of the American Society of Civil Engineers. Vol 103, No. ST12. December 1977. pp.2337-2350

6-28 Atta, A.E. Taher, S.E.F, Khalil, A.H.A, El-Metwally S.E ‘ Behaviour of reinforced high-strength concrete beam column joint. Part 1: Experimental investigation’. Structural Concrete.2003.4.No4

6-29 Atta AE, Taher SEF, Khalil AHA, El-Metwally S.E ‘Behaviour of reinforced high-strength concrete beam column joint. Part 2: Numerical Simulation’. Structural Concrete.2004.5.No3

6-30 Scott, R. H., Feltham I., and Whittle, R. T. 'Reinforced concrete beam-column connections and BS8110,'The Structural Engineer, 72, No. 4, February 1994, p55

6-31 Meinheit, D. F.; Jirsa, J.O. 'The Shear strength of reinforced concrete beam-column joints' CESRL report no. 77-1, Department of Civil Engineering, The University of Texas at Austin, 1977-01 (500 U582 77-1)

6-32 Regan, P. E., Kennedy -Reid I. L., Pullen, A. D., Smith, D. A. ‘The influence of aggregate type on the shear resistance of reinforced concrete’ – The Structural Engineer. 6 December 2005

6-33 Vollum R. L and Newman J.B ' Towards the design of reinforced concrete eccentric beam-column joints'. Magazine of Concrete Research, 1999, 51, No. 6, Dec pp397-407

6-34 Vollum, R. Parker, D ‘External beam-column joints: design to Eurocode 2’. Magazine of Concrete Research, 60, No 7 September , 511-521, 2008

6-35 Vollum, R.L ‘Design and analysis of beam-column joint’, PhD thesis, University of London , April 1998

6-36 Beeby, A.W., and Fathibitaraf, F., 1997. ‘Membrane Effects in Reinforced Concrete Frames- aproposal for change in the design of Framed Structures. Innovation in Civil and Structural Engineering’, Civil -Comp press Publications, Edinbyrgh, PP 135-145

6-37 Beeby, A.W., and Fathibitaraf, F., 1997. ‘Membrane Effects in Reinforced Concrete Frames- aproposal for change in the design of Framed Structures. Innovation in Civil and Structural Engineering’, Civil -Comp press Publications, Edinbyrgh, PP 135-145

6-38 Farjamand, M. ‘ Compressive membrane effects in reinforced concrete frames’. PhD thesis, University of Westminster, 2007

6-39 Sarsam, K.F., Phillips, M.E. ‘The shear design of insitu reinforced beam-column joints subjected to monotonic loading’. Magazine of Concrete Research 1985;37(130):16–28.

6-40 Zsutty, T.C. — "Shear Strength Prediction for Separate Categories of Simple Beam Tests", ACI Journal, Vol. 68, No. 2, February 1971, pp. 138-143.

6-41 Vollum, R. L, Newman, J. B. 'The design of external , reinforced concrete beam-column joints'. The Structural Engineer, Volume 77/Nos 23 & 24, 7 December 1999.

6-42 Eurocode 8: “Design of structures for earthquake resistance”. Part 1: General rules, seismic actions and rules for buildings. 1998-1:2003, 30 Oct 2003

Chapter 7
Validation of FE analysis of Short beams and Beam Column Joint

7.1 Introduction

STM models and empirical shear design methods for beams and BCJ were discussed in Chapters 5 and 6. In this chapter the behaviour of short beams and BCJ experimentally tested [7-1] will be investigated numerically by using a nonlinear FE computer programme in order to develop accurate models to compare with two short beams and two BCJ specimens tested in the Construction Hall at the University of Westminster.

Developing an accurate FE model is essential for investigating the various factors and parameters which influence the behaviour of BCJ and transfer beam column joint **(**TBCJ).

7.2 Aims and objectives

The aim of this chapter is to verify and validate the FE models for short beams and BCJ specimens with experimental tests [7-1] in order to use this data to carry out numerical parametric investigations of factors affecting the behaviour of TBCJ and in particular to investigate the influence of CVB on TBCJ in Chapter 8.

7.3 Methodology

This chapter is divided into two parts: the first to develop accurate FE models of the experimental tests in order to analyse and investigate the behaviour of short beams and analogous BCJ; the second to validate the accuracy of the developed FE models in order to continue FE parametric investigation for TBCJ in the next chapter.

7.4 Calibration of short beams without stirrups

Object of this section is to verify and validate FE modelling of the shear behaviour of beams with shear span/depth ratio of 1.5 by comparing the results with those obtained from experiments.

Initially, two reinforced concrete short beams B1 and B2 with a/d=1.5 with flexural

reinforcement and without stirrups were FE modelled and analyzed to failure and their analytical results were compared with those of experimental results obtained by Ortiz [7-1], which are used to calibrate the parameters for later analyses. The only difference between B1 and B2 is the length of the steel plate at the support. The lengths for B1 and B2 are 240 mm and 140 mm respectively, Figure 7.5.

Based on the results obtained from the calibrated FE models the deflections, stresses and cracking of the beams were analyzed at different key points along the lengths of the beams. The FE analytical results as well as the parametric investigation were discussed and conclusions regarding the shear behaviour of HSC beam with HWB are reached and recommendations for further research are made.

7.4.1 FE approach the beams B1 and B2

General information regarding FE approach to predict shear in short beams including material behaviour and material models for concrete and steel, crack modelling and other fundamental information are discussed in details in sections 4.1 to 4.4 of chapter 4.

The FE mesh adopted for one half of the span for beams B1 and B2 without shear links consisted of 450 elements (30× 5×3) above the reinforcement and 150 elements (50×3) for the cover.

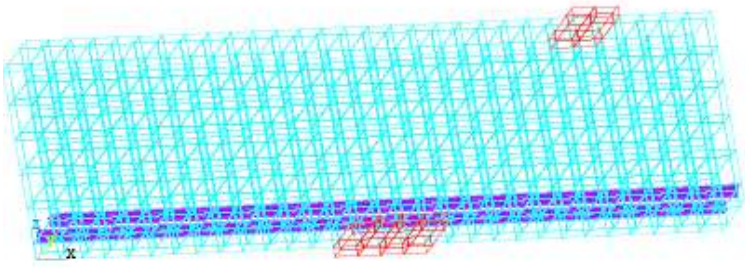

Figure 7-1: Half of Beam B1 with large support plate without link in 3D modelled by symmetry

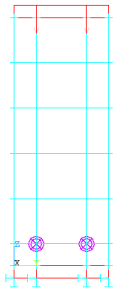

Figure 7-2: Sections of B1 and B2 with restraints

The initial cracking of beam B1 in the FE model corresponds to a load of 120 kN that creates stress just beyond the modulus of rupture of the NSC of 4.9 MPA. (Appendix A).

The experimental work completed by Ortiz [7-1] on two NSC short beams will be considered to develop, calibrate and verify similar nonlinear FE models for these beams.

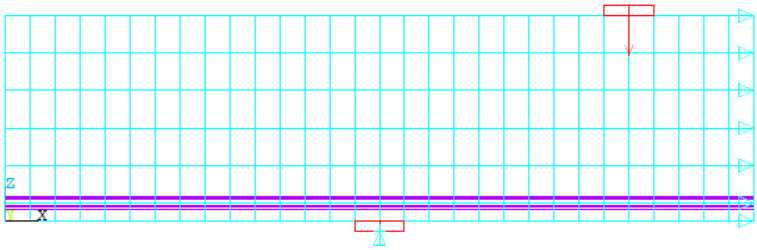

Figure 7.3: Elevation of B2 with restraints under the small support plate and load applied to loading plate. Centre of the beam is restrained in X direction to simulate symmetry around mid-span section.

Experimental strains in the tension steel were recorded by using strain gauges in order to obtain qualitative information on the struts and ties formed up to failure load the experimentally tested B1 and B2 failed at 560 kN and 440 kN.

The dimensions of the beams and detailing of the tension reinforcement provide sufficient anchorage length for the reinforcements by extending beyond support points. The geometry of beams B1 and B2 as well as their reinforcement is shown in Figure 7.4. Beams were 3000mm long with supports located 750mm from each end of the beam allowing a simply supported span of 1500mm. Flexural steel reinforcements were designed to BS4449 with yield stress of steel (f_y) of 500 MPa using 2-T25 bars with a section area of 982 mm^2. The percentage of tension steel is 1.8% and no shear reinforcement was used. Cover for the rebar was 25 mm and the shear span/depth ratio is 1.52 for both B1 and B2.

The 28 days compressive cylinder strength of concrete for beam B1 and B2 is fc =51 MPa, and fc =36 MPa respectively.

No mid-span deflection was recorded in the experimental work, however, FE numerical models prediction of mid-span deflection just before failure is found to be 3.7mm for beam B1 and 3.5mm for beam B2. This means that the effect of the 42% reduction in the size of the steel plate at the support has resulted in only 5% reduction in the vertical deflection at the mid-span.

However, the size of the steel plate influences the width of the main strut at the support, as restraining the concrete cover develops dowel action depending on the size of the support plate which in turn increases the width of the diagonal compression strut.

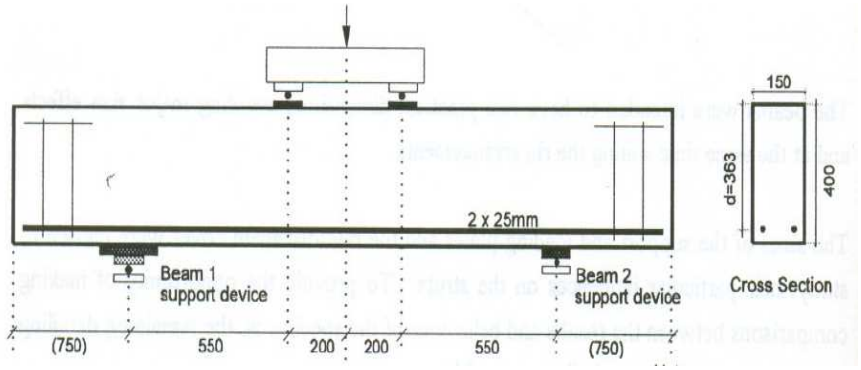

Figure 7.4: Geometry, reinforcement and loading for beams B1 and B2. All dimensions are in mm. NB: B1 has larger support plate compared to B2.

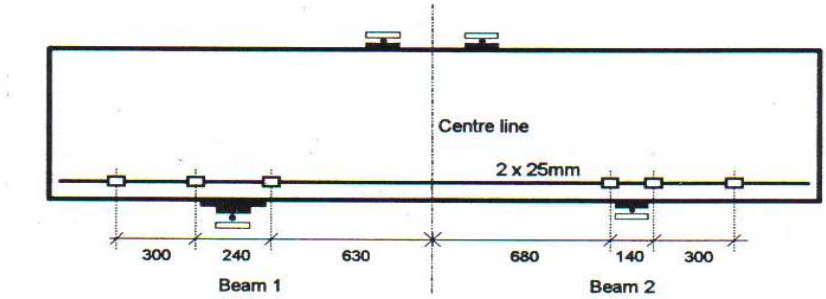

Figure 7.5: Location of strain gauges in beams B1 and B2 provided on the longitudinal bars, fixed in pairs, one gauge on top and another on the bottom.

Source: Reys de Ortiz, June 1993 [7-1]

Beam	Width b mm	Depth d mm	Cover c mm	Shear span a mm	a/d	Pl mm	Ps mm	ρ %
B1	150	363	37	550	1.52	100	200	1.80
B2	150	363	37	550	1.52	100	100	1.80

Table 7-1: Dimensions and reinforcement ratio of Ortiz's beam B2. All data apply to B1 other than support plate (Ps) which is 200 mm for B1 instead of 100mm.

Source: Table reproduced from Reys de Ortiz, June 1993 [7-1]

7.4.2 Experimental beam B1

This beam failed when the reinforcement yielded near the support. As presented, strain measurements in the reinforcement showed values higher than the yielding point. From the middle of the span to the left hand support, the diagonal crack reached the horizontal strut provoking local crushing.

Cracks reached the region under the loading plates and the horizontal strut. At 470 kN (shear force of 235 kN) the right hand horizontal strut crushed from the outer side of the loading plate to the shear crack at the lower side of the diagonal strut. The original crack opened wide near the support. Some crushing of the concrete in the horizontal strut was observed.

The sudden change in strain is not shown in the graphs obtained from the experiment because of the complexity of instrumentation and the cost involved. However, the FE method can be used to predict such detailed information.

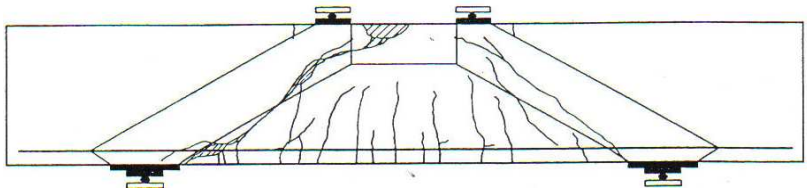

Figure 7.6: Crack propagation in the beam B1, experimentally tested by Ortiz in relation to the assumed diagonal and horizontal struts at 560 kN.

Source:Ortiz. 1993 [7-1]

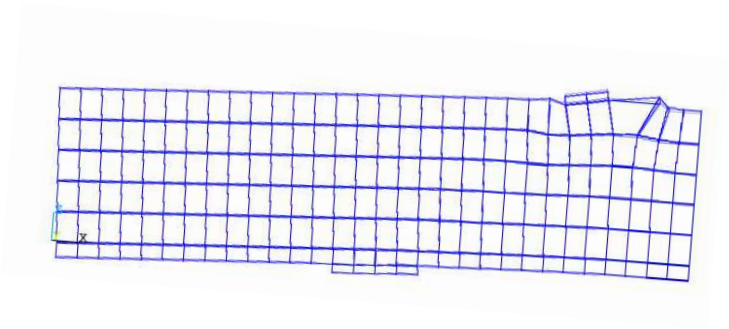

Figure 7.7: Numerical representation of beam B1 at 470 kN with sudden and brittle failure of the concrete at horizontal strut simulating the experimental failure.

7.4.3 Experimental beam B2

It is notable that the reinforcement at this failure load, by FE analysis, reaches 78% of its yield, whereas in the experiment the yield recorded by use of strain gauges is at 87% of the yield. ANSYS predicts this failure load at 100% of the experimental values, i.e. failure load 460kN.

The following conclusions can be made based on the evaluation of the analyses of the calibration of reinforced concrete beams:

- Strain in steel at the centre line along with initial and progressive cracking of the FE model compare well to hand calculations as shown in the Appendix A, when the first crack appears.
- The experimental strain in x-direction (ε_{xx}) on the tension reinforcement at the mid-span of the beams will be used to calibrate the FE models.

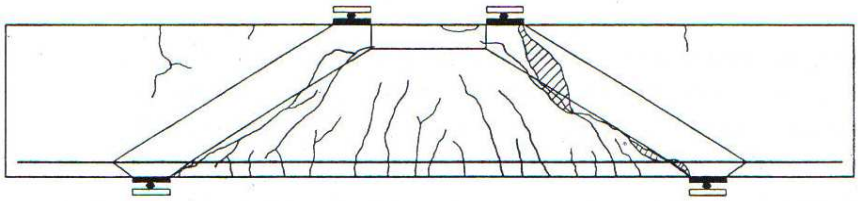

Figure 7.8: Crack propagation beam B2, experimentally tested by Ortiz in relation to the assumed diagonal and horizontal Strut. Failure occurring at diagonal Strut.

Source: Ortiz.1993 [7-1]

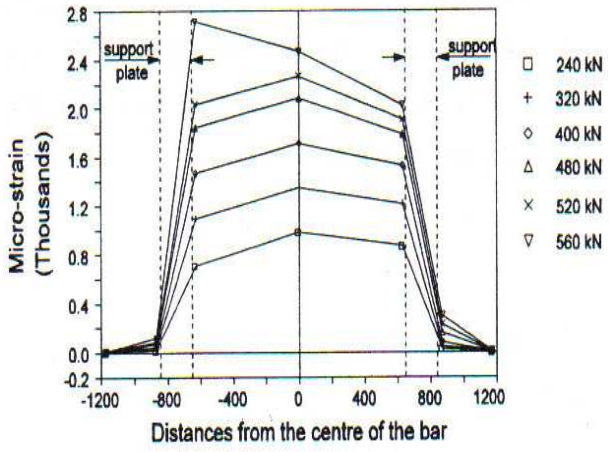

Figure 7.9: **Strain in the longitudinal bar at failure loads**

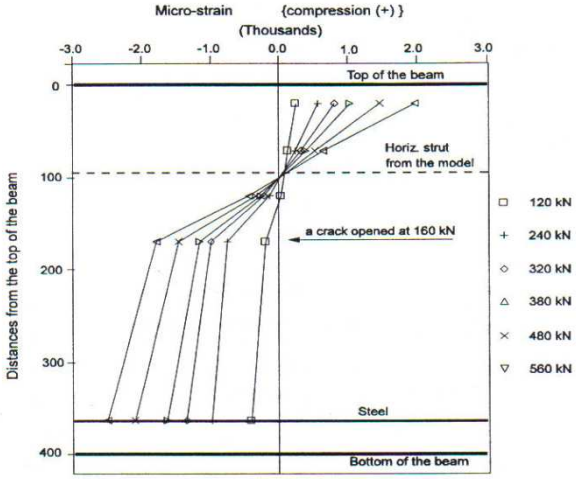

Figure 7.10: Beam 1: Strain in the middle of span at section 7

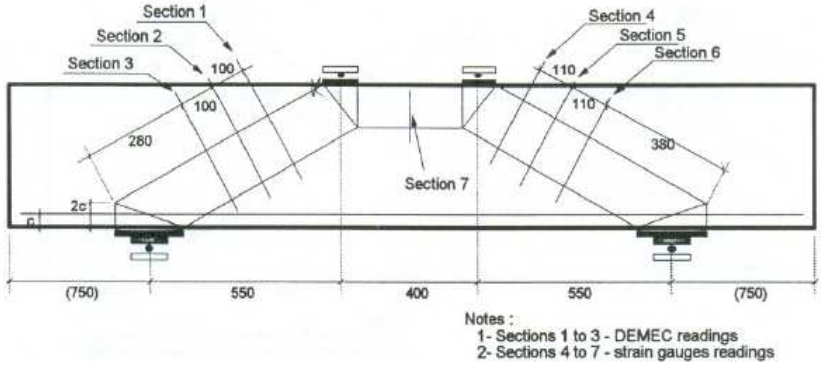

Figure 7.11: Beam 1 - Considered struts and instrumented sections

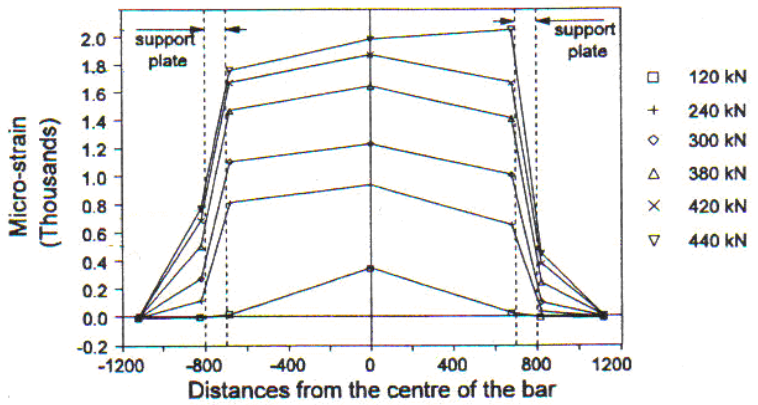

Figure 7.12: Experimental strains in longitudinal tension reinforcement of beam B2

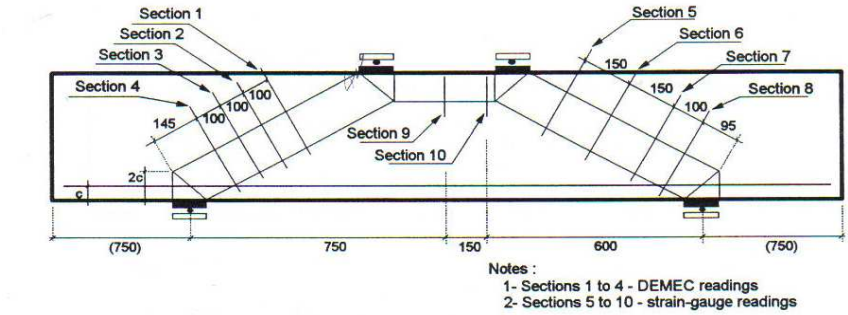

Figure 7.13: Ortiz Beam 2- Considered Struts and Instrumented Section

Source: Ortiz I. R.1993 [7-1]

Type of Beam	Failure Load P (kN)	Shear Force V (kN)
Experimental B1	560	280
Experimental B2	440	220
FE Model B1	470	235
FE Model B2	440	220

Table 7-2 : Failure load P and ultimate shear force

FE idealisation of the experimental beams, B1 & B2

In this section material and element modelling , meshing and evolution of crack patterns for FE analysis of the beams B1 and B2 is discussed.

7.4.4 FE modelling and calibration for beams B1 and B2

The behaviour of two RC beams with similar geometry, reinforcement and loading plate

under comparable incremental loadings with span/depth ratio 1.52 is studied. The support plates for B1 were 200mm wide compared to those for B2 which was 100mm wide. In this section crack propagation, shear strains, shear stresses, principal strain vectors, strain and stresses along the tension reinforcement in X direction, and strain across the cross section of the beam for FE model of B1 and B2 is investigated and the results are compared with the experimental test results for the corresponding beams.

7.4.4.1 FE meshing for model B1

In this section plots of FE results for beam B1 are analysed and compared. The FE mesh adopted for one half of the span for beams B1 and B2 without shear links consisted of 450 elements (30× 5×3) above the reinforcement and 150 elements (50×3) for the cover.

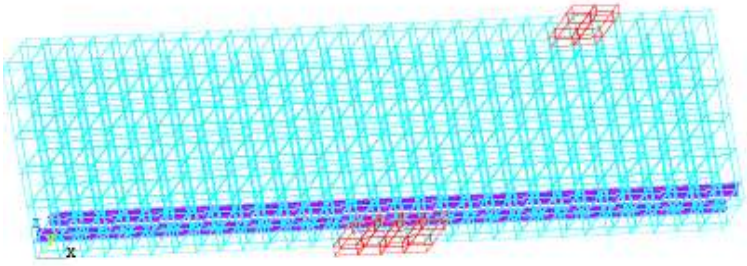

Figure 7.14: Half of Beam B1 with large support plate without link in 3D modelled by symmetry

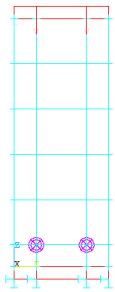

Figure 7.15: Sections of B1 and B2 with restraints

7.4.4.2 Crack propagation for beam B1

In this section crack propagation of beam B1 with an increase in incremental loading up to failure stage is investigated.

The main stages of the progressive cracking process for beam B1 under increasing load are shown in Figure 7.16 to Figure 7.18. Such a cracking process is typical for crack formation and extension which eventually transform the short beams into STM. In short beams, collapse always occurs as a result of failure of the arch, which is preceded by near-horizontal splitting of the compressive zone of the beam.

At 120 kN the first vertical tension crack at the centre span appears, Figure 7.16. The strain in tension bar resulting from this initial loading for the formation of the first crack compares well with hand calculation by elastic theory (Appendix A), Table 7-5 and Table 7-6, Figure 7.42**.**

At 270 kN, integration points in the form of 45° diagonal cracks gradually rise in the shear span . At 360 kN, integration points are inclined in the shear span to form into an arch. If the point has opened and then closed, the red circle outline will have an X through it. At 410 kN integration points spread wider on top, and compression cracks appear in the elements under the loading plate.

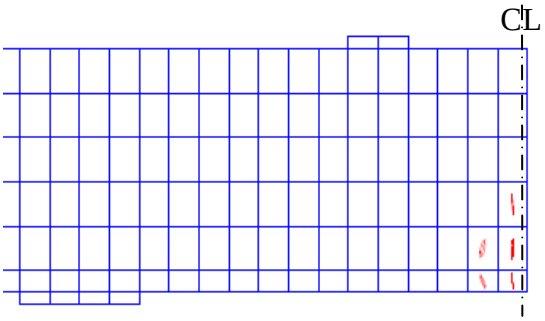

Figure 7.16: **At 120 kN the first vertical tension crack in beam 1**

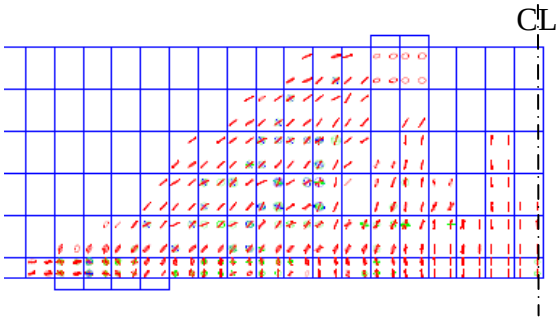

Figure 7.17: At 460 kN the width of the arch increases in beam 1

At 460 kN, the width of the arch increases further at higher levels near the loading plate with integration points in the form of short lines sloping at 450 kN which travel through the complete ellipse of the diagonal strut and spread toward the horizontal strut in the form of compression cracks under the loading plates, Figure 7.17.

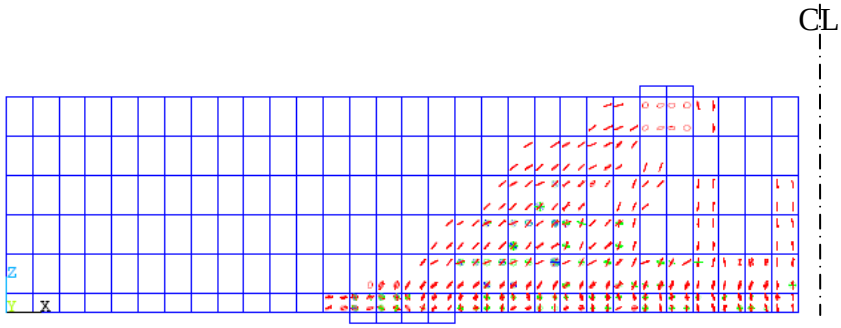

Figure 7.18: At 470 kN cracks extend eventually transforming the beam into a tied arch. Collapse occurs as a result of horizontal splitting of the compressive zone of the beam in the horizontal compression strut near loading plate.

7.4.4.3 Strain in XZ direction in beam B1

In this section shear strain in XZ direction is investigated at incremental loading to failure. At failure stage further details of stress behaviour are investigated in X and Z directions.

In this section shear stress in XZ direction is investigated at incremental loading to failure, the base of the strut is on the inner half of the support plate towards the mid span in the bottom and almost outside of the loading plate in the shear span on top, Figure 7.19. This demonstrates a larger angle of diagonal strut to horizontal in the FE model as compared to

Ortiz's STM which has its diagonal strut extending from centre of the support plate to the centre of loading plate.

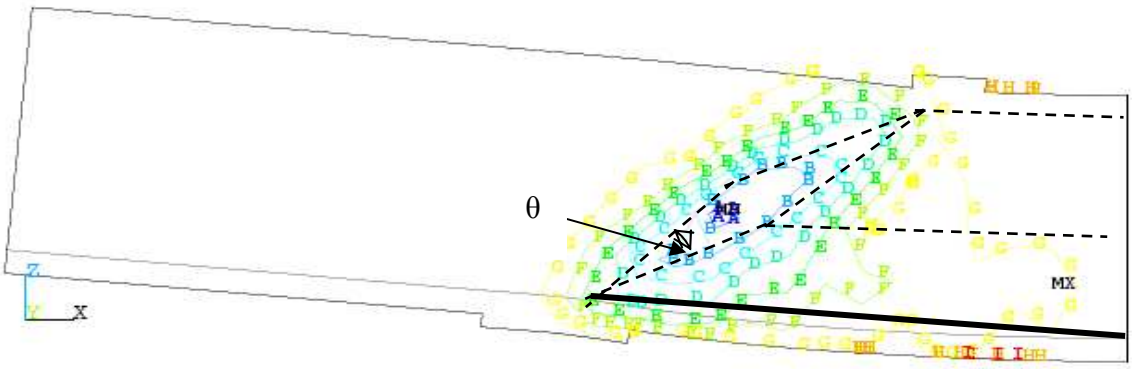

Contour	B	C	D	E	F	G	H	I
Strain $\times 10^{-3}$	-4.1	-3.4	-2.6	-1.8	-1.1	-0.3	0.4	1.2

Figure 7.19: At 450 kN the strain in XZ direction fully develops.

Maximum tension appears near the centre of tension steel where cracks appear, and maximum compression occurs in the middle of the diagonal strut. The angle between the inclined compression struts coinciding with strain line -4.1×10-3 is 15° 28' for B1 with support plate of 200mm long. This is a smaller angle than in B2, with 100mm long support plate. This indicates B1, therefore has higher shear resistance, Figure 7.19.

7.4.4.4 Principal strain vector plot for beam B1

Development of the principal strains in relation to an increase in incremental loadings are recorded. At120 kN vector plot tensile strains develop at the bottom in the centre. At 200 kN vector plot principal, strains deflect at 45° angle in the shear span. At 270 kN there are much higher principal tensile strains at the bottom compared to the top, therefore the beam continues to deflect. At 460 kN, Figure 7.20 full inclined diagonal compression strut develops. At 470 kN failure occurs with horizontal and inclined tensile stress producing compression at right angle which causes crushing near loading plate.

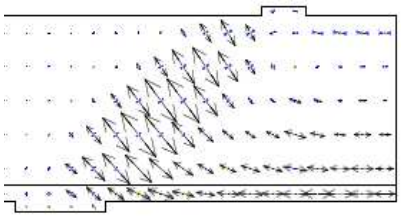

Figure 7.20: At 460 kN vector plot

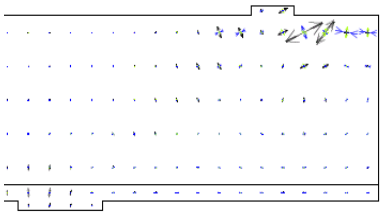

Figure 7.21: At 470 kN after compression failure

7.4.4.5 Strain and stresses along the tension bar in beam B1

The strain along the longitudinal tension bar at incremental loading is recorded from the FE model of the beam, and a graph comparable to the experimental graph shown in Figure 7.9 was produced. These strains from the experimental and FE models are compared in the graph shown in Figure 7.42.

At 460 kN stress in XZ, the diagonal strut becomes wider on top as Ortiz' model indicates, and becomes narrower near the support plate. By geometric scaling, it is shown that the angle of Strut is = tan-1(0.6) as compared to Ortiz' proposal of tan-1(0.55), Figure 7.23.

At 460 kN vector plot, horizontal compressive principal strains on top are more or less of the same magnitude of tensile principal strains at the bottom. This indicates that this over-reinforced beam does not allow further development of principal strains in the bottom and the energy is therefore transferred to the top with stress build up from this strain exceeding the level of allowable concrete stress, Figure 7.20.

At 470 kN after compression failure, energy is transferred to the top with stress build up from the strain exceeding the allowable concrete stress, therefore crushing below top surface level from dilation of concrete results in tension vectors forming the compression failure near the loading point, Figure 7.21.
There are several possible explanations for what causes the FE models to have higher stiffness than the experimental test, as follows:

<u>Micro cracks</u>
Shrinkage of the concrete during curing and handling of the beam cause micro cracks in the concrete during curing and experimental, which make the experimental beam less stiff compared to FE which does not model micro cracks.

<u>Bonds</u>

It is assumed that there is perfect bond between the concrete and steel reinforcement in the FE model, however, bond slip occurs and the composite action between the concrete and steel reinforcing is reduced. The overall stiffness of the experimental beams is expected to be lower than for the FE models.

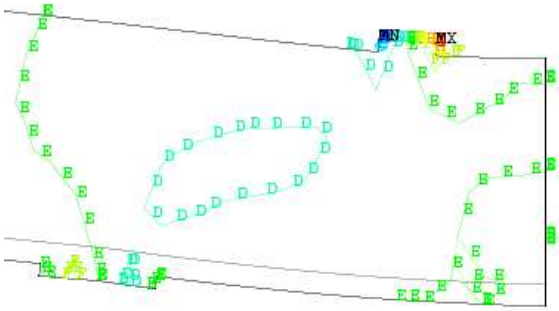

Figure 7.22: At 120 kN stresses in XZ direction

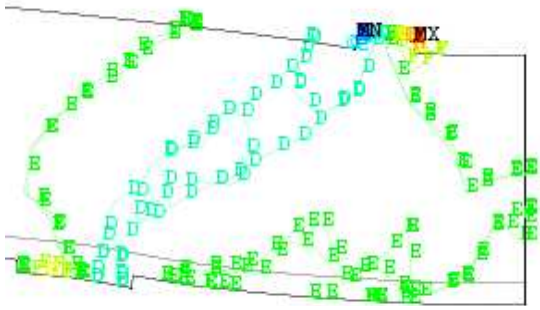

Figure 7.23: At 460 kN stress in XZ.

Load	Stress MPa								
	A	B	C	D	E	F	G	H	I
120	-5.07	-3.81	-2.55	-1.30	-0.04	1.22	2.48	3.74	4.99
460	-22.1	-16.7	-11.3	-5.90	-0.49	4.93	10.3	15.7	21.2

Table 7-3: Stresses in XZ direction in the form of ellipse in compression in the middle of the diagonal strut at the shear span.

Element separation

At later stage of loading when cracks are wide, elements separation occurs after which the FE strains recorded are significantly less that the experimental results as FE does not simulate element separation and behaves like rubber rather than brittle non-homogenous concrete.

Maximum Load (kN)	120	240	320	380	400	460
FE numeric Strain ×10-3	0.4	0.99	1.73	1.92	2.46	2.62
Experimental Strain ×10-3	0.40	0.97	1.30	1.60	1.73	2.0

Table 7-4: Maximum strain recorded at the centre of longitudinal bar at various loads.

7.4.4.6 Strain in cross-section at mid-span for beam B1

The strain in the middle section in X direction at incremental loading is recorded from the FE model of the beam, and a graph comparable to the experimental graph is produced.
At 120 kN, the strains are small across the whole section and evenly distributed across the section, apart from the centre of the span at the bottom of the steel and concrete where the first crack of only 100mm length develops. At 320 kN loading with a significant tension crack of about 100mm deep, the tensile strain remains more or less the same along that depth, however tensile strain significantly drops above the closed end of the crack.

At 400 kN, both tensile stresses in the steel and compressive stresses in the concrete are well below the material strengths. At this loading the neutral axis is at mid depth of the beam.

At 460 kN strain in tension bar at 1050mm from end, mid shear span, rises to 1.940×10^{-3} as the shear crack has opened, Figure 7.24, exhibiting a drop in the strain. This strain change happens because of the presence of cracks which form next to the loading plate just before compression failure. The tension crack at centre of span has widened with a jump in strain due to horizontal strut compression failure**.**

7.4.4.7 Deformation of beam B1 with Loading

The failure of the horizontal strut in FE model B1 results from splitting of the compressive zone and can occur only as a result of the development of tensile stresses induced by volume expansion of the concrete in regions subjected to large compressive stresses.

The tension crack at the centre widens significantly within its 73mm depth at the bottom. The neutral depth is between 73mm to 219mm from the bar. The compression on the concrete is at 50mm from the top. The compression from concrete acts at 268 mm from the bar, Figure 7.26a.

At 460 kN load, the tension steel has just began to yield whereas the compressive strain in the concrete on top near the loading plate at 1.31 micro strain is close to the cylinder crushing strength of 1.48 micro strain of the concrete, Figure 7.26b . However, the failure of the horizontal compression strut is due to dilation of the concrete next to the loading plate which results in principal tension strain vectors causing cracks and failure in the horizontal strut, Figure 7.21.
When the maximum load exceeds 460 kN, the compression failure results, Figure 7.25, tensile crack formations between 120 kN and 160 kN result in fluctuations in displacements.

7.4.5 FE analysis for model B2

In this section plots of FE results for beam B2 are analysed and compared with the experimental test.
Strain in tension bar, deflection at mid-span, and strain in horizontal direction across the mid-span section are investigated.

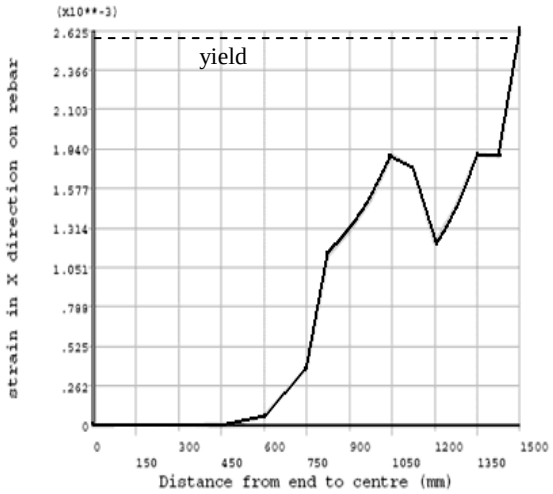

Figure 7.24: Beam B1, at 460 kN. Strain in tension bar

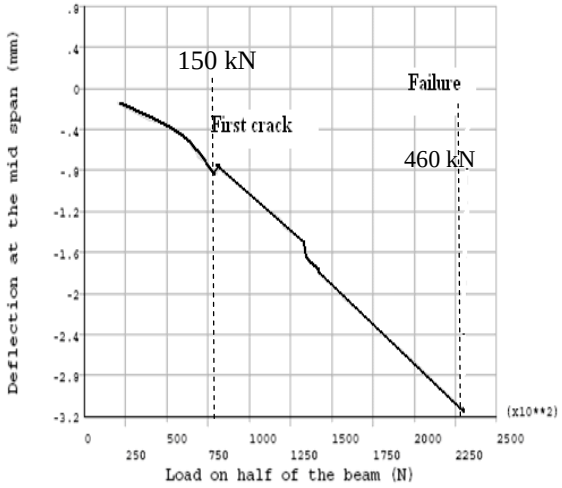

Figure 7.25: Load V deflection for B1. First crack at 150 kN

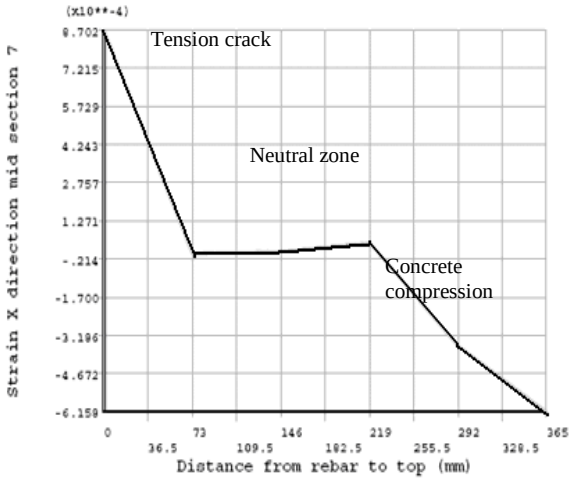

a) Strain at section in X direction, 240 kN

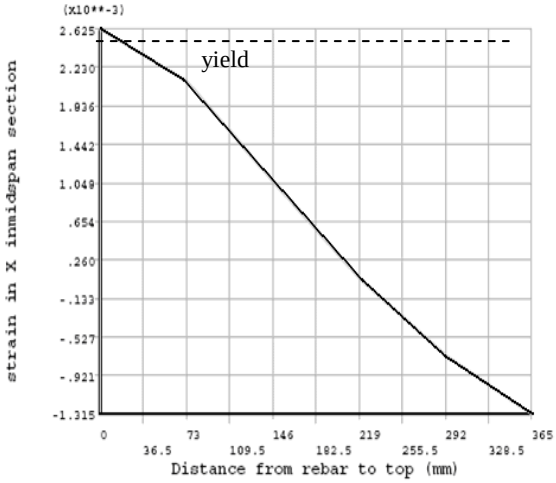

b) Strain at section in X direction 460 kN

Figure 7.26: Strain in X direction at mid-section v distance from tension bar upward

7.4.5.1 Crack propagation for beam B2

The main stages of the progressive cracking process that beam B2 undergoes under increasing load are shown. Such a cracking process is typical for crack formation and extension which eventually transform the short beams into a tied arch. In short beams collapse always occurs as a result of failure of the arch, which is preceded by near-horizontal splitting of the compressive zone of the beam.

At 160 kN, vertical cracks extend towards the supports and turn inclined in the shear

span. At 200 kN, the first diagonal tension cracks in the form of 45° lines appear rising in the shear span.

At 360 kN loading the distribution of cracks happens within a wider diagonal strut compared to beam B1.

When there is a sudden change in strain in the shear span, severe cracking inevitably occurs. The location and the crack width obtained from the FE model confirms this. This sudden change in strain is not shown in the graph obtained from the experiment because of the complexity of instrumentation and the cost involve. However, the FE method can be used to predict such detailed information.

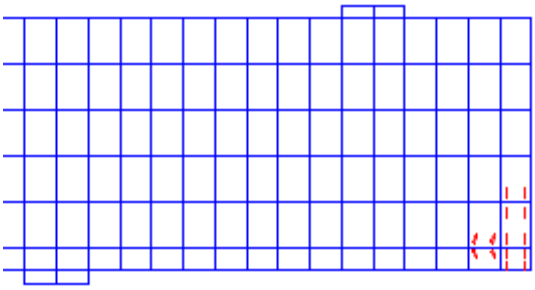

Figure 7.27: Beam B2 at 120 kN the first vertical tension crack at the centre span appears. This initial loading for the formation of the first crack is hand calculated by elastic theory (Appendix A).

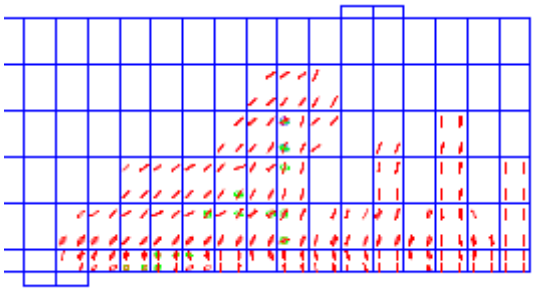

Figure 7.28: At 320 kN when the crack has opened and then closed, the circle outline will have an X through it. The circle represents the second opening of cracks in the integration point.

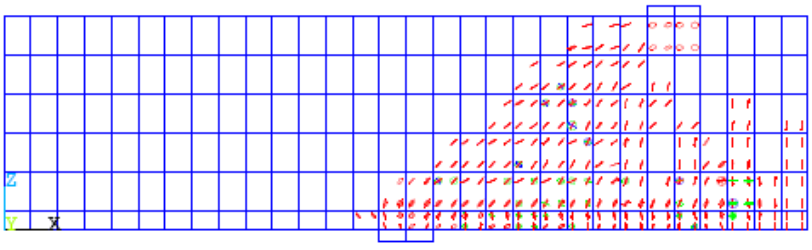

Figure 7.29: At 440 kN loading, crushing of integration points marked blue, X in the circle, at the centre of diagonal strut indicate failure in shear span starting near neutral axis heading towards the outer side of the loading plate with compression cracks extending under loading plate.

7.4.5.2 Nodal strain and stresses in XZ direction for beam B2

Nodal strain in XZ direction shows the gradual development of the diagonal compression Strut.

Comparing the angle of crack of B2 and B1, there are larger tension tie forces in B2 as the angle of compression struts to the tie is 79° 59' as compared to B1 which is 82° 16', therefore higher force on the tie at half the depth results in reaching tensile strength of concrete sooner, producing shear cracks and lower shear resistance. Figure 7.31.

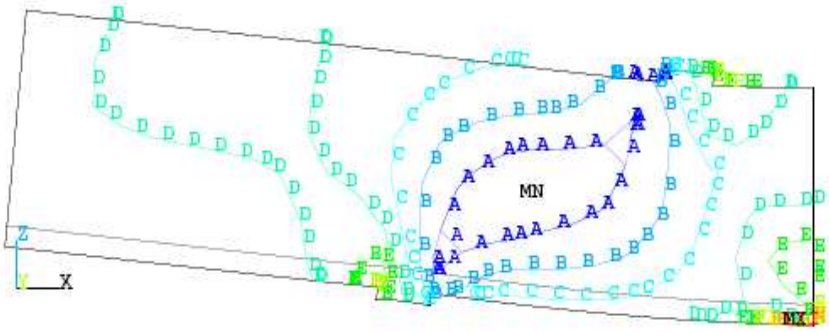

Contour	A	B	C	D	E
Strain×10-4	-1.0	-0.7	-0.4	0.1	0.4

Figure 7.30: Nodal strain at 120 kN in XZ direction shows comparatively higher strains in the shear span near the diagonal Strut region.

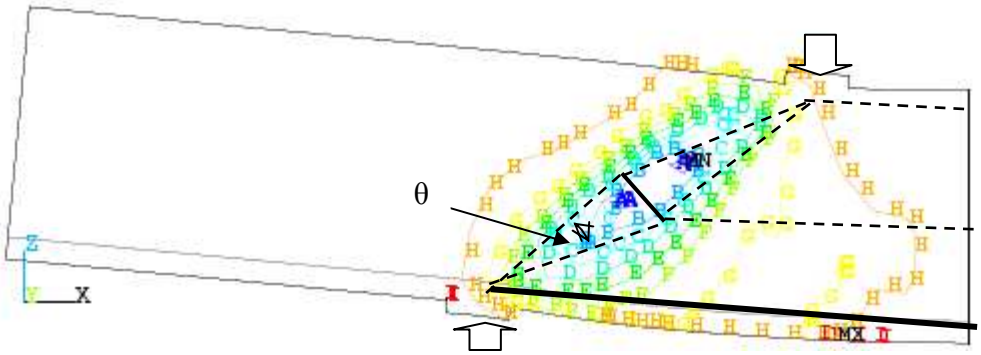

Contour	A	B	C	D	E	F	G	H
Strain×10-3	-5.2	-4.5	-3.8	-3.1	-2.3	-1.6	-0.9	-0.2

Figure 7.31: Strain in XZ direction at 440 kN. The angle between the inclined compression struts coinciding with strain line -4.1×10^{-3} is 20° 9' for B2 with support plate of 100mm long.

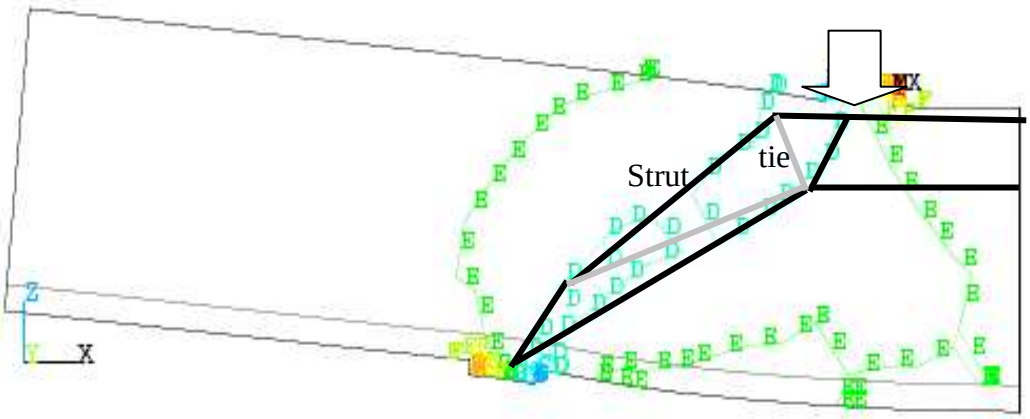

Contour	D	E
Stress Mpa	-5.63	-0.57

Figure 7.32: Stresses in XZ direction at 440 kN. Minus sign indicates compression. Model for nonlinear STM based on FE of shear stress development in the beam.

7.4.5.3 Principal strain vectors at incremental loadings for beam B2

At 120 kN principal strain vectors are tensile and horizontal, concentrated near the tension bar at the centre of the beam.

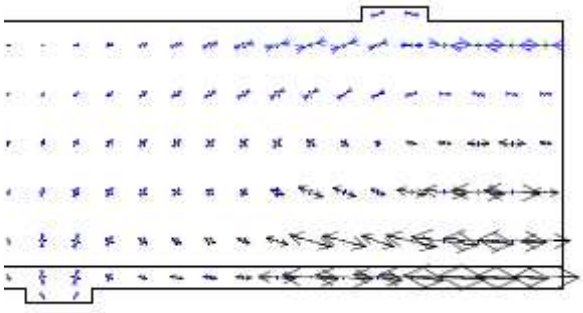

Figure 7.33:At 160 kN principal tensile strain vectors begin to deflect at a modest angle in the shear span.

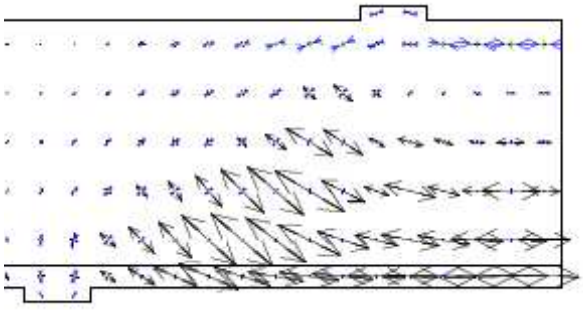

Figure 7.34: At 240 kN, principal tensile strain vectors deflect at 45°.

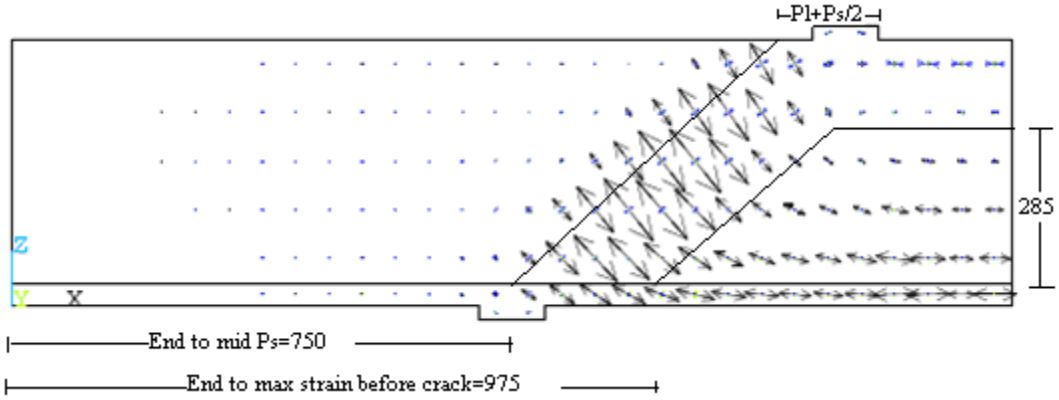

Figure 7.35: Principal strain vectors at 440 kN spread into the diagonal compression Strut, just before failure.

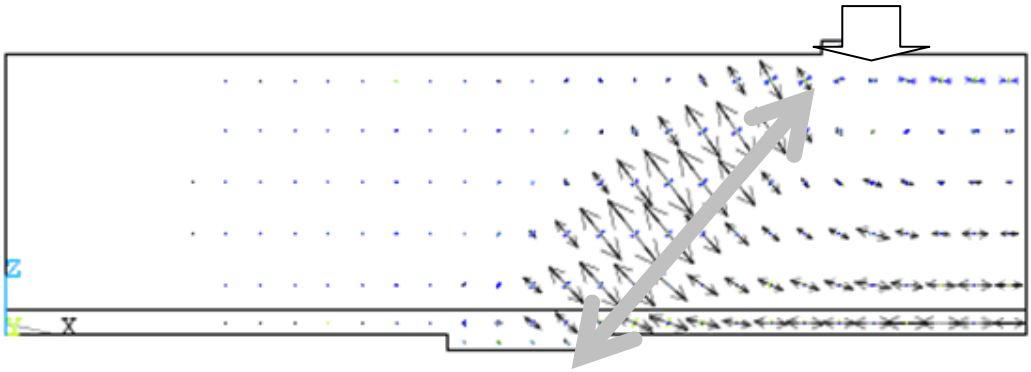

Figure 7.36: The concentration of stress vectors indicate that the angle of the non linear diagonal compression Strut is greater when the size of the support plate is larger.

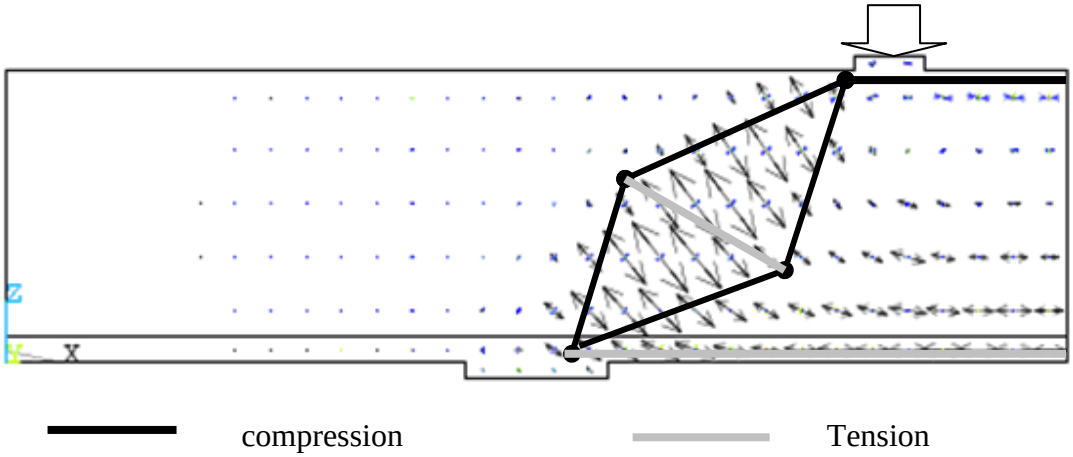

Figure 7.37: The STM in nonlinear analysis of STM in beam B1, based on the assumption that principal stress are distributed in oval form.

7.4.5.4 Strain in X direction in the tension reinforcement in beam B2

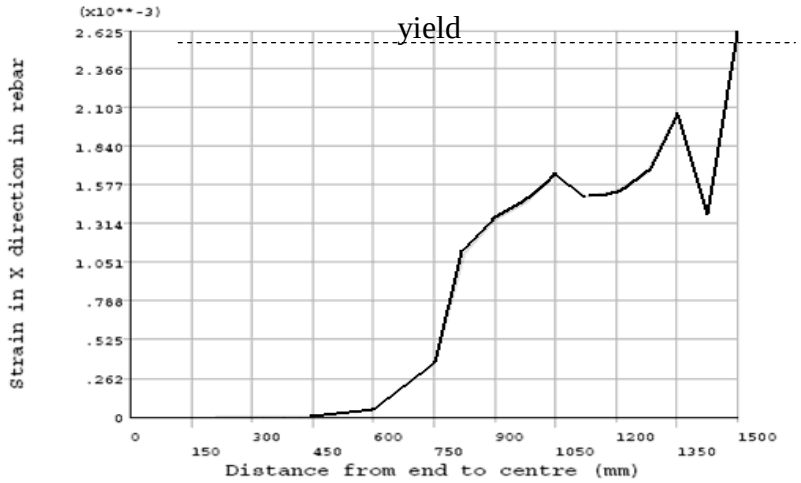

Figure 7.38: Beam B2 at 440 kN long bar loading strain in X direction along the tension bar. The tension crack at the centre of the beam contributes to the yielding of tension steel

7.4.5.5 Strain in X direction mid span section in beam B2

Graphically, from strain concentration, the dimensions of diagonal compression strut and horizontal compression strut when the tension bar has yielded can be estimated. The width of the diagonal compression strut is 225 cos 45° and the width of horizontal compression strut is 80mm, Figure 7.35.

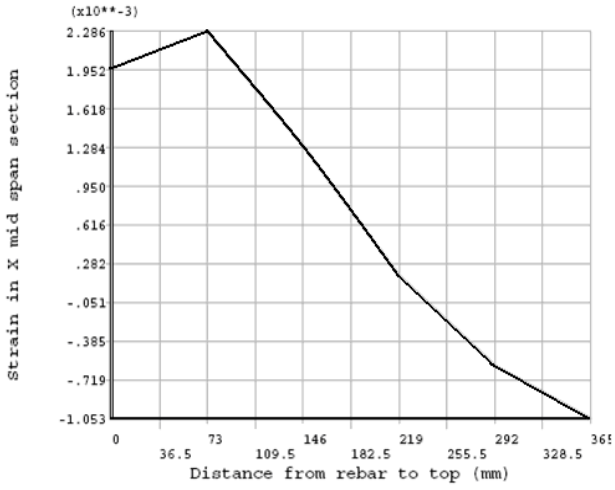

Figure 7.39: 380 kN strain in mid span section across the depth in X direction before yielding of the tension steel.

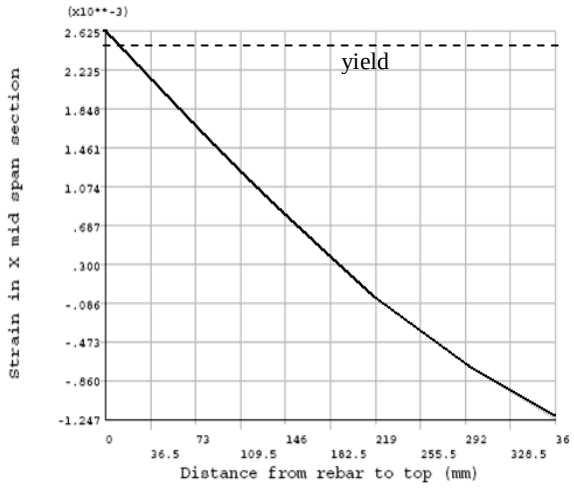

Figure 7.40: At 440 kN at mid span section.

At 440 kN at mid span section, the tension steel just begins to yield. The compression on top is about 33 N/mm^2 less than limit of 41 N/mm^2, Figure 7.40.

7.4.5.6 Load v deflection relation for beam B2

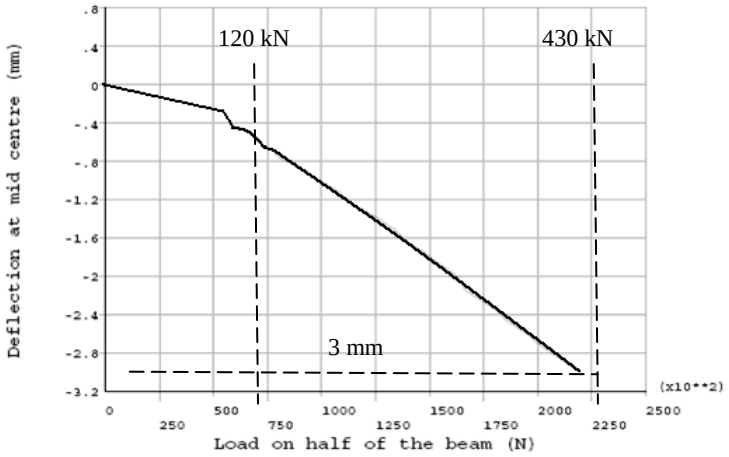

Figure 7.41: Deflection against load. At 60 kN load on half the beam, equivalent to 120kN full load on beam

There is a sudden increase in deflection of 0.3mm at 120 kN caused by the formation of the first cracks. Deflection at first crack is 0.3mm which is comparable to linear stress calculations, Appendix A.

The final deflection of B2 is 3.2mm which is similar to that of B1, Figure 7.25. The first crack in B1 develops at 150 kN compared to that of B2 which occurs at 120 kN. This could possibly be partly due to larger support plate in B1.

Deflection for beams B1 and B2 were not recorded in the experimental tests.

7.4.6 Comparison of numerical models B1 and B2

The numerical models for beams B1 and B2 simulate the experimental model reasonably accurately with a factor of safety of 1.2.

In both beams, FE model prediction is closer at lower load, however, as loading increases the prediction becomes more conservative, Figure 7.42.

	Strain×10^{-3}	
Load(kN)	FE B1	Exp B1
240	0.993	0.970
320	1.731	1.360
400	2.463	1.727
460	2.625	
480		2.065
520		2.250
560		2.460

Table 7-5: The loads and strains recorded by experiment and FE modelling for beam B1

	Strain×10^{-3}	
Load(kN)	FE B2	Exp B2
120	0.411	0.335
240	0.993	0.940
300		1.23660
380	1.960	1.630
400	2.310	
420		1840
440	2.625	1970

Table 7-6: The loads and strains recorded by experiment and FE modelling for beam B2 with small support plates

7.4.6.1 Progressive cracks in beams of shear span/ depth ratio of 1.5

The stages of the progressive cracking as incremental loading increases for the two RC beams are plotted. Such a cracking propagation is quite typical for all RC structural beams investigated where crack formation and extension eventually transform the beam into a tied arch. Collapse always occurred as a result of failure of the arch, which was preceded by near-horizontal splitting of the compressive zone of the beam with B1 actually failing from horizontal compression failure, Figure 7.7.

Such a mode of failure is compatible with the failure mechanism proposing that splitting of the compressive zone can occur only as a result of the development of tensile stresses induced by volume expansion of the concrete in regions subjected to large compressive stresses. This failure mechanism implies that structural behaviour is independent of the strength characteristics of concrete in compression; hence, a failure criteria describing the conditions for failure under combined compression-tension should, in practice, be sufficient for the purpose of analysis.

The main stages of the progressive cracking process that beam B1 undergoes under increasing load are shown in Figure 7.18 for beam B1, and in Figure 7.27 for beam B2. The failure of the horizontal strut in FE Model B1 results from the splitting of the compressive zone and can occur only as a result of the development of tensile stresses induced by volume expansion of the concrete in regions subjected to large compressive stresses.

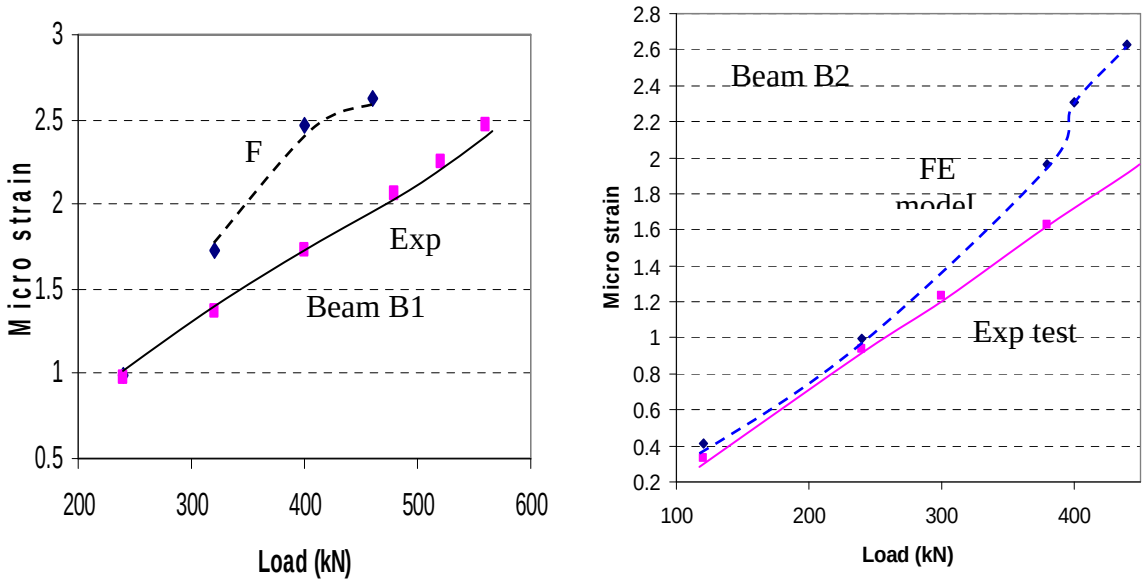

Figure 7.42: The graph shows values of the load against the strain in X direction in the tension bars at the centre of the beams for FE models and the strain recording from experimental test for beams B1 and B2.

Beam B1's shear failure load at 470 kN is 7% greater than beam B2 which failed at 440 kN. The only difference between these two beams is the larger support plate of 200mm for beam B1 compared to that of 100mm for beam B2. This shows that dowel action at the support can restrain the concrete cover where a considerable dowel action develops, therefore delaying failure. This is demonstrated in the larger principal inclined vectors near the support for beam B1 in Figure 7.44 than those for beam B2 in Figure 7.43.

This tied arch response of an RC short beam also lends support to the compressive force path (CFP) concept, which hypothesizes that the causes of beam failure are associated with the development of tensile stresses in the region of the path along which the compressive force is transmitted to the supports and not, as is widely considered, with the stress conditions in the region below the neutral axis [7-2].

On the basis of this hypothesis, the absence of shear reinforcement in the case of short beams subjected to two-point loads should cause eventual collapse as a result of the failure of the compressive zone in the middle span and in the region adjacent to the load point. This mode of failure is accurately predicted by the programme, as can be seen in FE model failure of beam B1, which shows the collapse condition of a short beam without shear reinforcement , after the formation of the last crack just inside the middle span as shown in Figure 7.18.

Ortiz'[7-1] STM for the short RC beams without shear reinforcement subjected to two-point loading is developed by considering crushing mode of failure when the applied load increases to the level at which the diagonal crack that forms within the shear span at an earlier load stage penetrates into the compressive region towards the loading point.
However, such a crushing mode of failure in the region of the loading point is unlikely since the multi-axial compressive state of stress that exists there will cause a local increase of concrete strength [7-3] Instead, it is proposed that the diagonal crack will branch almost horizontally toward the compressive zone of the middle span of the beam in order to by-pass this high-strength region, Figure 7.44.

The path of crack branching should be that of a compressive stress trajectory which, as indicated by the change in the direction of the CFP, is characterized (for local equilibrium purposes) by the presence of a resultant compressive force where, bearing in mind the deflected shape of the beam before failure, the load path is the minimum distance between the loading and support points of the inner half of the loading plate to the outer part of the support plate. This could also be an additional reason for the delay in failure of B1 compared to B2 when the support plate is larger which increases the angle of the CFP.

The corrected STM can be developed from the FE model showing the strain path between loading and supporting points. The implication of this proposal failure mechanism is that the angle Θ proposed by Ortiz as the angle of diagonal strut to the horizontal should be increased in order to simulate the correct STM.

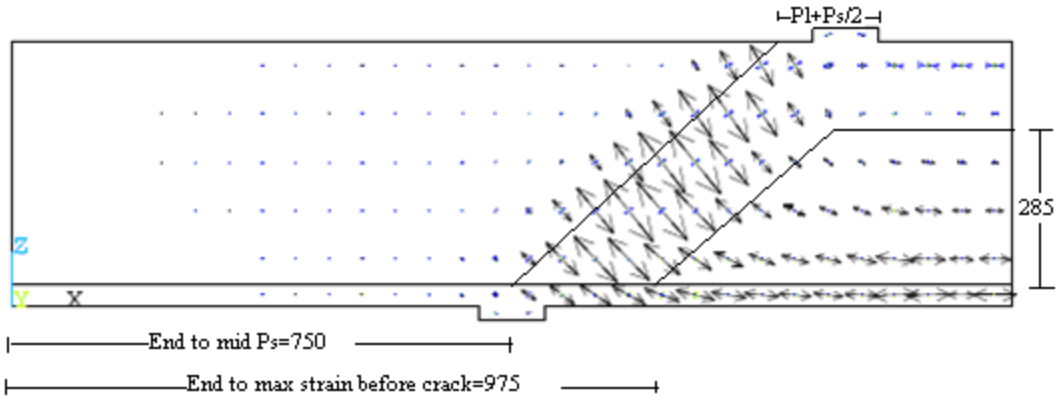

Figure 7.43 : The principal strain vectors give an indicative profile of the diagonal and horizontal compression struts and the tensile forces along the steel tie. The angle of strut is = tan-1 {d/[3-550-(PL+PS)]}

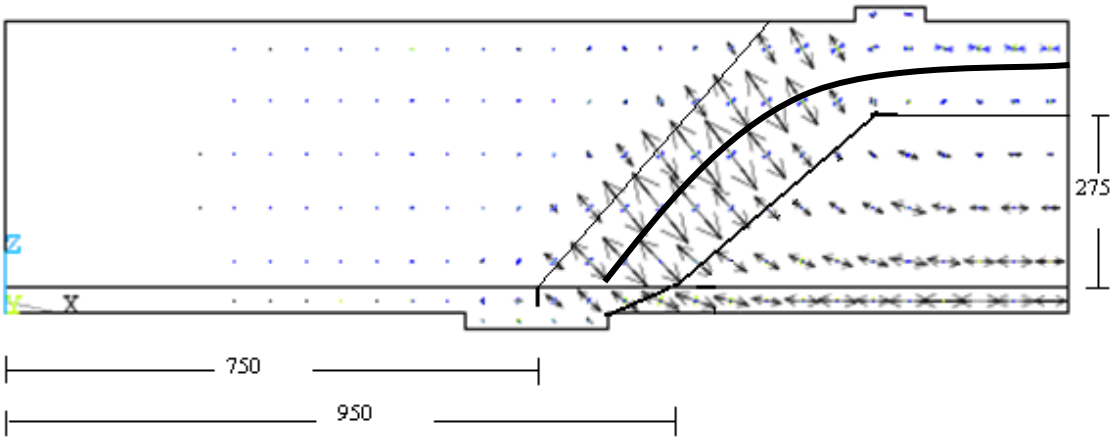

Figure 7.44: Load path is minimum distance between loading point and support point of inner half of loading plate to outer part of support plate.

This does not happen in B1 experimental or FE model, although the longitudinal bar near the support yields at 0.0027 with the failure in experiment, Figure 7.9, but the actual maximum tensile strain of 0.0026 just yields in the tension bar at mid span, Figure 7.24. It should be noted that the predicted values of both the maximum load and maximum strain in the longitudinal bars should be considered as lower-bound values since any triaxial compressive stress conditions that may develop when the ultimate-strength capacity is approached cannot fully be allowed for by the plane-stress analysis employed. However, since such triaxial stress conditions are set up only once the collapse load is practically attained, they should affect only the plastic or near-plastic deformational behaviour rather than the strength characteristics of a beam. Nevertheless, the predicted strain in X direction in the centre of longitudinal bar in Ortiz' [7-1] model is still useful for the purpose of comparison.

7.4.6.2 Bond and anchorage in beams of shear span/ depth ratio of 1.5

The influence of the bond stresses over the supports is considered, and nodes and struts are defined. FE models are developed and the analysis of their behaviour is compared to that of the struts analysed by Ortiz. The FE modelling was compared with the experimental results.

The test data exhibited in Figure 7.24 and Figure 7.38 show that at high loads the stress in the longitudinal bars is practically constant over the clear span and reduces drastically just over the support plates. Table 7-7 presents the bond stresses obtained on the basis of the difference of the bar stresses between the two strain gauged sections nearest to the edges of the plates. These values are compared with the British Standard and the CEB-90 [7-4] recommendations , excluding the safety factors.

The design ultimate anchorage bond stress , f_{bu} recommended by BS8110 [7-5] section 3.12.8.4, is $f_{bu}=\beta\sqrt{f_{cu}}$.

where β is a coefficient related to the type of reinforcement and includes a partial safety factor, γ_m, of 1.4. For beams with minimum stirrups $\beta = 0.50$ for deformed bars, but for beams without shear reinforcement BS recommends $\beta = 0.28$.

The design value of bond stress, f_{bd}, given by CEB, Section 6.9.3, is:

$f_{bd}= \eta_1 \eta_2 \eta_3 f_{ctd}$ **7.1**

where

η_1 considers the type of reinforcement $\eta_1 = 2.25$ for ribbed bars,

η_2 considers the position of the bar during concreting $\eta_2 = 1.0$ for bottom bars, η_3 considers the bar diameter $\eta_3 = 1.0$ for $\Phi \leq 32$ mm, f_{ctd} is the design value for concrete tensile strength.

f_c is cylinder concrete crushing strength

Disregarding the safety factors and taking $f_{ctd}=0.30f_c^{2/3}$,

$f_{bu}=0.675f_c^{2/3}$ **7.2**

From Section 6.9.5 of CEB the effect of confinement by the concrete cover (coefficient $\alpha 3$) and the effect of the transverse pressure (coefficient $\alpha 5$) are taken into account and the bond strength is considered as:

$f_{bu(p)} = 0.30f_c^{2/3}/(\alpha_3\alpha_5)$ **7.3**

$\alpha_3= 1 - 0.15\{(c_d - \Phi)/\Phi\}$ **7.4**

$0.7 < \alpha_3 < 1.0$, with c_d = lesser of minimum cover and half clear spacing of bars,

$\alpha_5= 1- 0.04\sigma_p$ **7.5**

$0.7 < \alpha_5 < 1.0$, with α_5 the pressure transverse to the plane of the bars, and $0.7 \leq \alpha_3\alpha_5 \leq 1.0$

Comparing the ultimate anchorage bond stress of the British Standard and CEB-90 recommendations, there seem to be considerable discrepancies, but the British Standard guidance uses a low value for the coefficient β (related to the type of reinforcement) when the beam does not have stirrups. In addition, it probably leans on the safe side for the bottom bars as no account is taken of the difference between top and bottom bars. CEB does consider the good bond conditions of the bottom bars.

From Table 7-7, it can be seen that the reinforcement developed anchorage bond stresses far larger than the limit values given by the British Standard and also above those of the CEB if the influence of transverse pressure is ignored, but less than or equal to the CEB

values when the transverse pressure is considered. Only beam B2, at the right hand side support, presented a maximum bond stress and horizontal cracking over the support when the shear loading was 10% smaller than that at failure, but even beyond this loading, the anchorage was still reliable.

	f_{bu}(N/mm^2)			
Beam type	Experiment	FE model	BS8110	CEB-80
B1	10.3	9.3	3.1	9.3
B2	10.2	7.4	2.6	7.4

Table 7-7: Bond stresses over the supports - Anchorage bond stresses - Comparison with codes . The transverse pressures used in the CEB equation for σp are calculated as σp =R ⁄(bl_1) where R is the reaction and l_1 is the distance between the gauges

In the FE model the reinforcement developed anchorage bond stress 20% less than the experimental value which is comparable to the CEB-90 prediction and far more optimistic than the BS8110 prediction.

Referring to graphs in Figure 7.38, for longitudinal tension steel, produced by FE model, it is shown that reinforcement strain continued to decrease rapidly beyond the support plate, suggesting that the transverse pressure improved the bond beyond the support plate. This was also confirmed experimentally as recorded by the gauge placed beyond the plate.

7.4.7 Discussions on FE models of beams B1, B2

Numerical models for B1 and B2 were developed to predict the dowel action produced by tension reinforcement as a result of pressure from the larger support plate. The FE models for the beams were successfully verified and validated.

According to CEB-90 [7-4] recommendations, the shear failure prediction with diagonal Struts considered as uncracked zones is 564 kN for B1 and 424kN for B2, and 510 kN for B1 and 296 kN for B2 when considering diagonal struts as cracked zones.
The CEB-90 recommendation for uncracked zones predicts yielding of tension reinforcement. The experimental graph produced indicates yielding of the reinforcement for B1. Yielding in tension reinforcement occurred in both FE models B1 and B2.

Beam B1's larger support plate contributed to higher dowel resistance at the support and therefore higher shear resistance of the beam. The numerical model recognised this dowel

action and predicted an improvement of only 6.8%, whereas in experiment the larger support plate contributed an additional 17% to shear resistance.
A number of secondary cracks occur in the shear span as shear cracks propagate. These cracks probably occur due to the shear retention factor (SRF).

Although it appears that no relevant shear strains should take place within the flexural span, the presence of even small SRF stiffens such Gauss points and, therefore, attracts stresses that gradually build up and exceed the failure stress envelope in tension. However, such occurrences take place just before failure and hence have a negligible effect on load prediction.
For B2 at 500 kN, it should be noted that cracking affects suddenly the region where the compressive-force path changes direction, compared to the predicted crack pattern at 320 kN. Diagonal cracks initialise and subsequently propagate towards the loading point. When divergence of the iterative procedure takes place at total load, multiple cracking occurs in the region of support.

7.4.8 Conclusion on FE Models for beams B1 and B2

The load-strain plots for selected locations from the FE analysis show fair agreement with the test data. For the load-tensile strain plots for the main steel reinforcing at midspan, the strains from the FE analysis and the experimental data correlate well in the linear range, and the trends in the nonlinear range are generally comparable.

- The general behaviour of the FE models represented by the load-strain plots at midspan shows good agreement with the test data from the full-scale beam tests. However, the FE models show slightly more stiffness than the test data in both the linear and nonlinear ranges. The effects of bond slip (between the concrete and steel reinforcing) and microcracks occurring in the actual beams were excluded in the FE models, contributing to the higher stiffness of the FE models.

- The final loads from the FE analyses are 15% lower than those from the experimental results which is probably due in part the effects of the dowel action of the tension reinforcement resulting from a larger support plate being ignored, and using assumed materials properties values instead of measured values.

- The crack patterns at the final loads from the FE models correspond well with the observed failure modes of the experimental beams. The load predicted for the initial crack from the numerical method agrees with the hand calculation presented in Appendix A.

When strut and tie are overlapped on the corresponding numerical models for beams B1 and B2, the angle between the inclined compression struts which coincides with strain contours -4.1×10^{-3} is 15° 28' for B1 with support plate of 200mm long. This is a smaller angle than for B2, where the corresponding angle between the inclined compression struts is 20° 8', Figure 7.19, with 100mm long support plate. This indicates smaller tension tie force between the compression struts for B1, therefore higher shear resistance. This is a smaller angle than for B2, with the corresponding angle between the inclined compression struts of 20° 8', Figure 7.32.

7.5 FE validation of beam column joints

The two FE models BCJ-A and BCJ-B had beam and the column depths of 400 mm and 300 mm respectively, therefore their aspect ratio is = $\frac{400}{300}$ = 1.33

Aspect ratio is defined as the ratio of depth of beam to the depth of column, i.e.

$$\text{Aspect ratio} = \frac{depth\,of\ beam}{dpeth\,of\ column} = \frac{d_b}{d_c}$$

This will be carried out in two stages as follows:

1. to develop a correct FE model for BCJ based on laboratory tested structures for which full data and their experimental results are available. Two FE models were developed to represent the BCJ specimens tested. The models are BCJ-A without stirrups and BCJ- B with shear stirrups to conform with experiment specimens BCJ-1 and BCJ-4.
2. to verify and validate the FE models BCJ-A and BCJ-B by using the experimental strain gauge recordings on column bars and stirrups of experimental specimens BCJ-1 and BCJ-4.

Two experimentally tested specimens [7-1], BCJ1, Figure 7-46 and BCJ-4, Figure 7-59 with aspect ratio 1.33, are identical in all properties, geometry and set up except that BCJ-4 has 3 additional shear links positioned at the centre of the joint and has 2 T16 in each of the column corners compared with BCJ1 which has 1 T16 (Table 7-8). BCJ-1 was modelled as BCJ-A , Figure 7-48 to Figure 7-51 and BCJ-4 as BCJ-B, Figure 7-61 to Figure 7-64**.**

Experimental test	No of beam bar & diameter (mm)	Total area (mm^2)	Anchorage length (mm)	No of column bar & diameter (mm)	Total area (mm^2)	Beam load (kN)
BCJ-1	4-T16	804	367	6-T16	1206	118
BCJ-4	4-T16	804	492	10-T16	2010	130

Table 7-8: Detailing of beam and column reinforcement for BCJ-1 and BCJ-2

Having demonstrated that the FE numerical model reasonably predicts the correct behaviour of experimental tests in the laboratory, FE modelling approach adopted is validated and verified.

7.5.1 Geometry, material properties of FE models

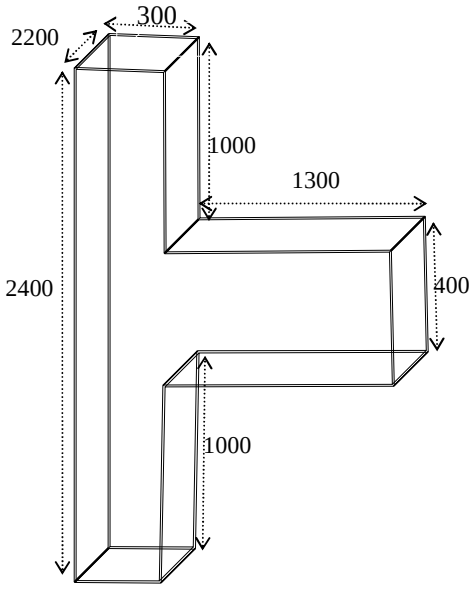

Figure 7-45:FE BCJ model of aspect ratio 1.33

Two BCJ with aspect ratio 1.33 Figure 7-45 have concrete cube strength for NSC models as 42 MPa. The average values for the cube strength for experimental specimens BCJ-1 and BCJ-4 with concrete properties are shown in Table 7-9.In the FE analysis for NSC the shear coefficient for closed cracks is assumed to be 1.0 or less, and the suggested range for open cracks is taken as 0.05 to 0.5 to prevent numerical difficulties [7-6], [7-7] and [7-8]. In this thesis the coefficient for NSC is assumed to be 1.0 for closed cracks and 0.3 for open cracks.

Both beams and columns were reinforced with hot-rolled round deformed bars. The details of BCJ reinforcement for the experimental tests used for validation and verification are shown in Table 7-8 and the reinforcement used in the FE models is shown in Table 7-10.

Experimental specimens	Cube Strength f_{cu} MPa	FE Model's Average value f_{cu} MPa	Cylinder Strength f_c MPa	FE Model's Average f_c MPa	Splitting Strength f_{sp} MPa	FE Model's Average f_{sp} MPa
BCJ-1	42.3		34.0		2.77	
BCJ-4	42.0	42	34.0	34	2.98	2.87

Table 7-9: **Concrete properties used for NSC in the experiments on BCJ. The averages of these properties were used in FE model analysis.**

For the analysis in part 1, FE model BCJ-A and BCJ-B were developed to idealize the experimental model BCJ-1 and BCJ-4. FE idealization considers similar geometrical and material properties to the experimental model. However, assumptions were made in order to simplify the FE model to obtain accurate results, which are as follows:

i. The bent-bars linking the top main beam reinforcement to the rear column reinforcement were idealized as L-shape bars. According to past research [7-10] this will have a nominal affect on the behaviour of the BCJ, but will significantly simplify the analysis of BCJ.

ii. The top reinforcements in the beam 4T16, Figure 7-47.

The reinforcement in the column of BCJ-4 of 10T16 comprising of 4 double T16 in corners and 2-T16 at centre changed to the equivalent area of 4T22.6 in corners and 2T16 at centre for BCJ-B, Figure 7-64**.**

The anchorage of the beam bar for BCJ extended to the length of effective depth of beams, ie. 330mm

FE model Identity	Aspect ratio	No & diameter (mm)	Total area A_s (mm^2)	Reinforcement ratio A_s/bd %	Anchorage length (mm)	Cube Strength f_{cu} MPa	Beam load (kN)
BCJ-A	1.33	4T16	804	1.1	330	42	129.5
BCJ-B							138

Table 7-10: Failure loads, concrete property and beam reinforcement for numerically analysed BCJ. Yield strength for all beam reinforcement is $f_{y=}$ 720 MPa. Beams and columns were reinforced with hot-rolled round deformed bars

FE model Identity	Number & Diameter (mm)			Area A_s (mm^2)	% Steel A_s/bd
	Corner	Centre	CVB		
BCJ-A	4-T16	2-T16	0	1206	2.01
BCJ-B	4-T22.63		0	2010	3.35

Table 7-11: Column reinforcement. The column corner bars have yield strength f_y= 720 MPa.

7.5.2 Loading of the specimen

General information on the position of loading points for BCJ of aspect ratio 1.33 is shown in Figure 7-51.

At the early stage of modelling BCJ with aspect ratio of 1.33, the computer processing power was limited to Pentium (R) 4CPU, 2.66 GHz with496 MB of RAM, and the software was an older version of ANSYS which required certain provisions to be introduced in order to perform the FE analysis. The size and number of the elements for the BCJ model was chosen according to past research recommendations [7-9], there were 4900 elements and 5200 nodes. Displacement load was applied to the models to produce reactions equivalent to force loads at loading point.

Model	No of BCJ joint stirrups	No of column stirrups	No of beam stirrups	Joint Stirrup diameter mm	Joint stirrup yield strength f_y MPa
BCJ-A	----	12	8	T8	571
BCJ-B	3	12	8		

Table 7-12: Shear reinforcement in FE models.

7.5.3 Validation of FE model BCJ-A with the experimental test BCJ-1

In this section FE model for BCJ-A is validated by comparing the strain gauge readings on column and beam reinforcement with those of strain gauge recordings for BCJ-1.

Reinforcement detailing of the experimental specimens and FE models are shown in Figure 7-47 to Figure 7-52.

The model BCJ-A failed at beam load of 129 kN compared to 118 kN for BCJ-1, or 9.3% higher load.

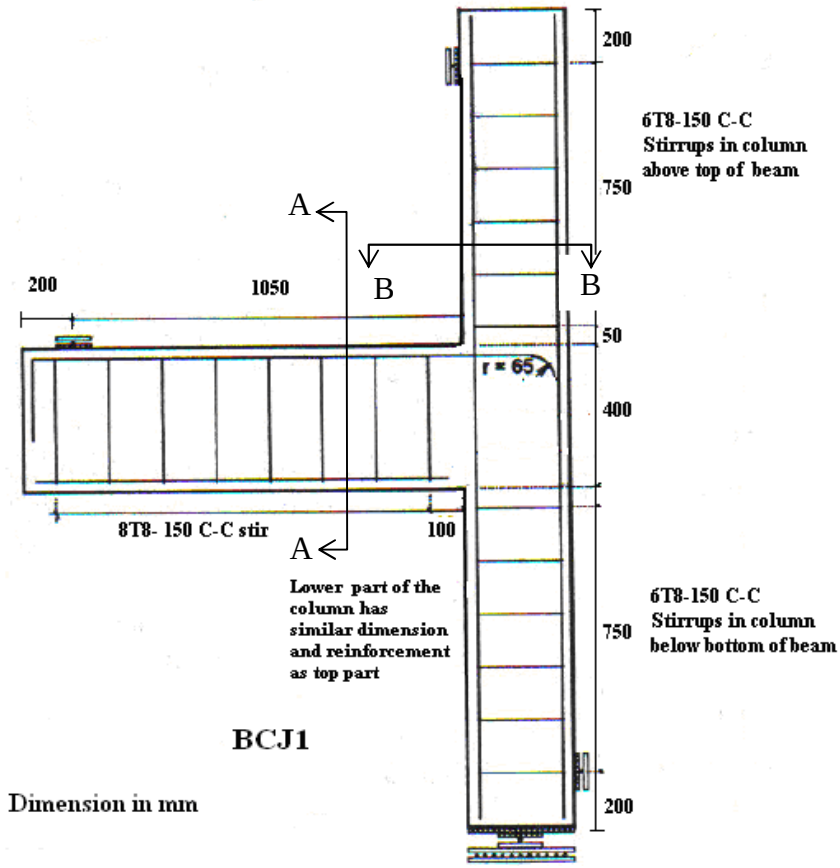

Figure 7-46: **Reinforcement detailing of experimentally tested BCJ-1.**

An investigation was completed to confirm that the displacement load applied produces similar behaviour to force loads. It was then concluded that displacement load would be employed for the numerical analysis of BCJ of aspect ratio 1.33 to compensate for limited computation facilities.

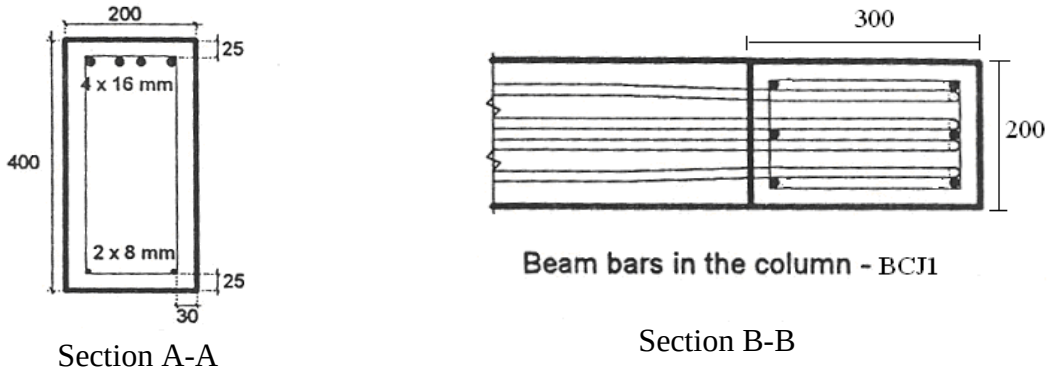

Figure 7-47: Reinforcement in the cross sections for beams and column for BCJ-1.

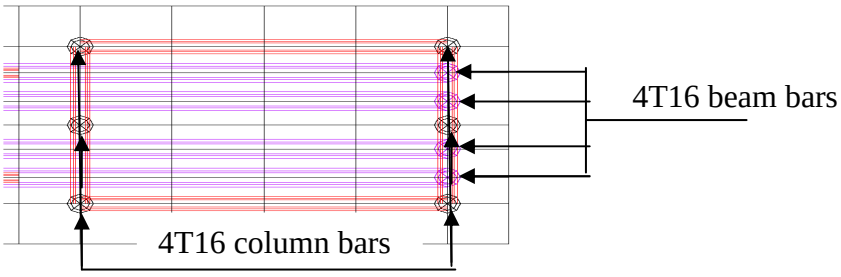

Figure 7-48:Main reinforcement in the column section of the FE model for BCJ-A showing 4 T20 beam bars with 6T16 for column reinforcement

In Chapter 7, for FE modelling a TBCJ with aspect ratio of 3.11, it was not possible to continue with the above limitations because the number of elements had nearly tripled, therefore the software was upgraded to a higher version of ANSYS, and the hardware was upgraded to Pentium D CPU, 3.2 GHz with 0.99 GB of RAM. This made it possible to apply incremental monotonic force loading to TBCJ by the step loading approach.

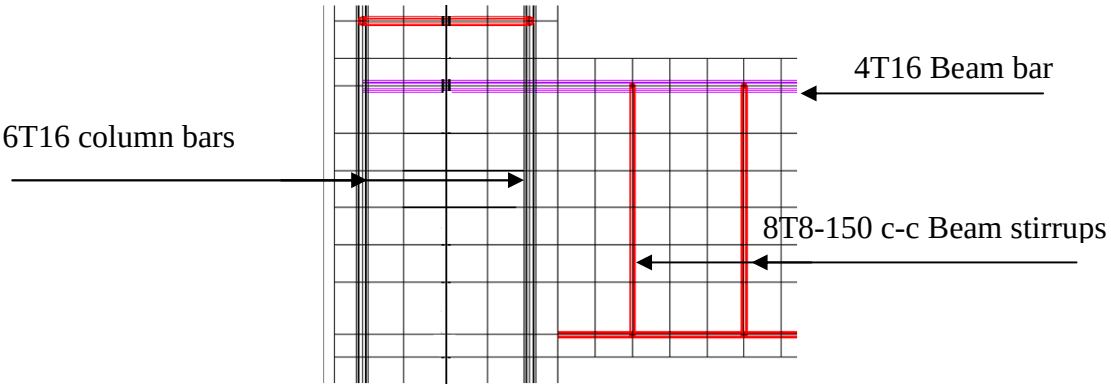

Figure 7-49: Side elevation for the concrete element and the reinforcement cage for the model of BCJ-A

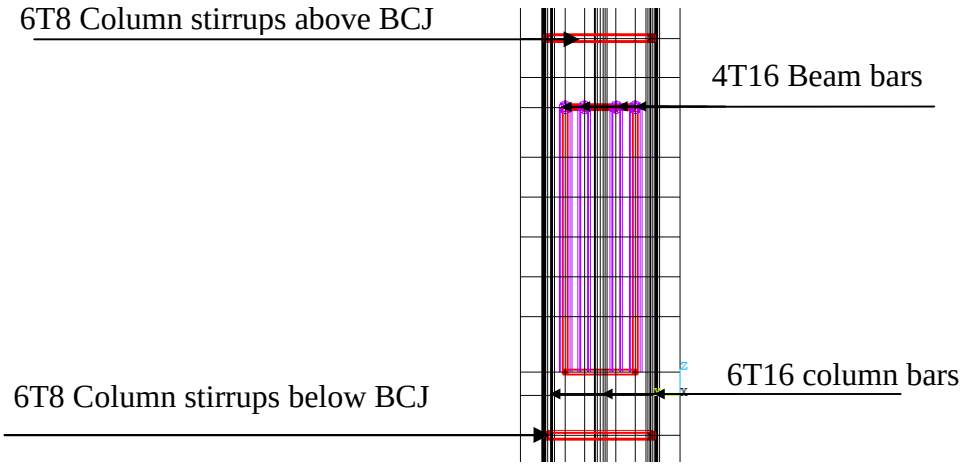

Figure 7-50: Beam cross section showing the concrete element and the reinforcement cage for column joint BCJ-A

7.5.4 Comparison of the strain recordings of BCJ-A with BCJ-1

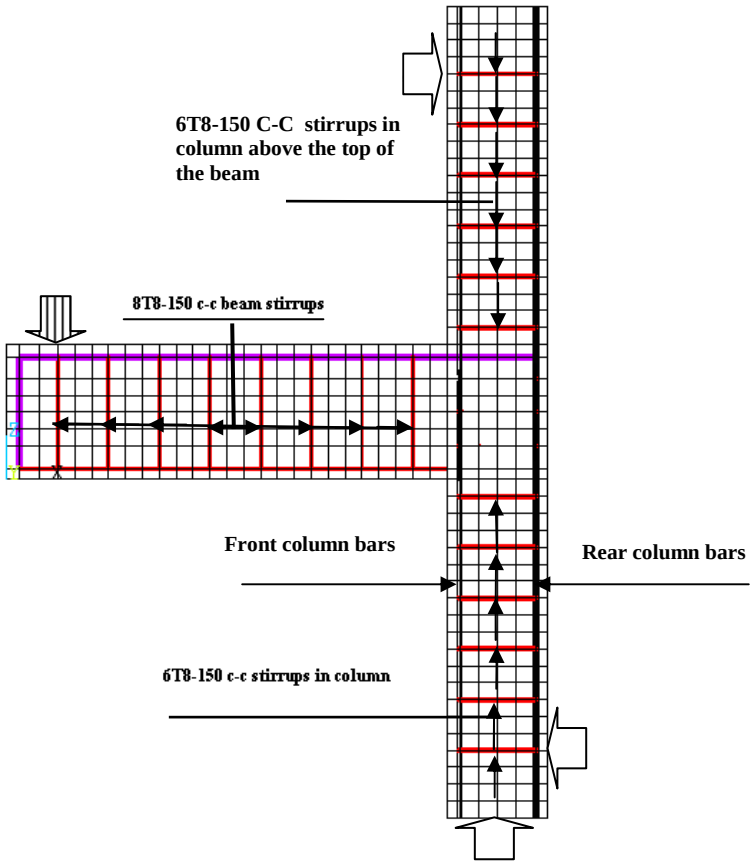

Figure 7-51: Elevation of the BCJ-A showing stirrups in beam and column. For sections refer to Figure 7-50 for beam and Figure 7-48 for column

From these results it can be noted that predictions of the FE model are good and reasonably accurate. However, the FE model predicts cracks on the front column bar because of its ability to record strains linearly, but the experimental strain gauges do not record this crack, Figure 7-53. Table 7-13 indicates reasonable accuracy of the FE analysis when compared with the test results. The large cracks at the opening corner at 40 mm above the beam in column front face represent a sudden change in strain as shown in the FE numerical analysis results.

Figure 7-53 shows the change in strain of the front column reinforcement on strain gauges A, B, C, D and E, and Figure 7-52 within the depth of the beam. Strain gauges readings on the front column reinforcement for the model and experiment are within 14% tolerance of one another, in spite of only 2.5% difference in loading, Table 7-13.

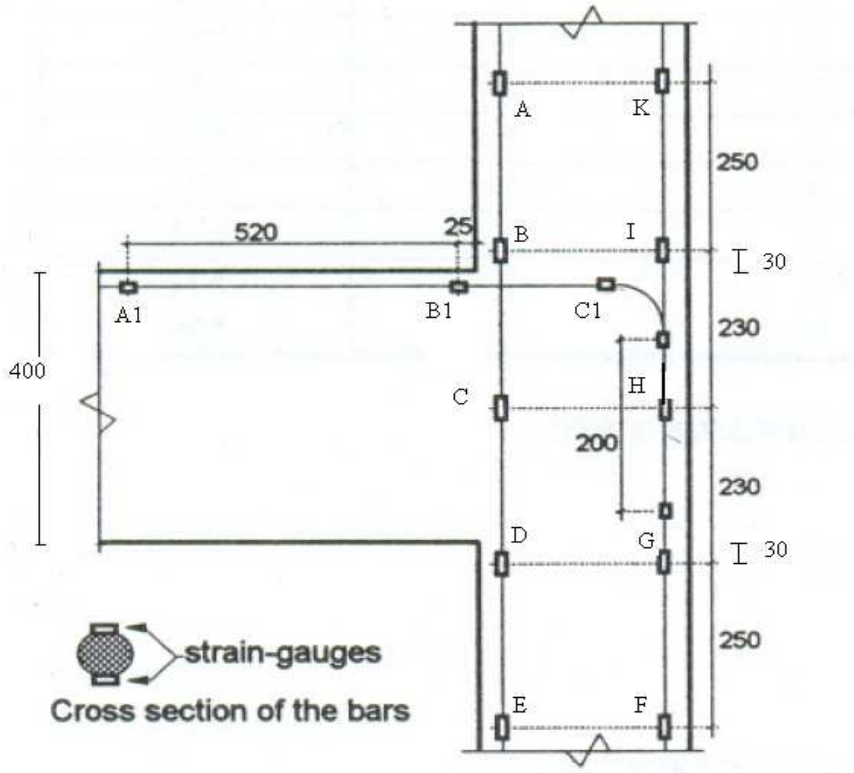

Figure 7-52: Typical arrangement for strain gauges on reinforcement of BCJ 1

Similarly, strains in the rear column bar were compared and the results are shown in Figure 7-54 and, in general, there is a good agreement between the two results, however, some cracks developed between the positions of the strain gauges which were not recorded in the experimental results as gauges only record strains at preset points. Strain gauge readings on the rear column reinforcement for the model and experiment are within 13% tolerance of one another, in spite of only 2.5% difference in loading, Table 7-13.
The axial strains in the main column bars were measured and plotted from Table 7-13 for front column bar and Table 7-14 for rear column bar, Figure 7-57. Maximum strains developed in the front and rear bars in the FE model of 0.0017 and 0.00035 compared to 0.0015 and 0.0004in the experimental test, which is within 14% tolerance. The position of these maxima is as shown and they are associated with development of cracks at these locations.

The strains from FE analysis on the horizontal part of the beam bar of BCJ-A at 73 kN loading in comparison to strains in beam reinforcement recorded by the strain gauges in the experimental test for specimen BCJ-1 at 75 kN show a negligible 2.6% difference in loading.

Strain gauge readings on the horizontal part of beam reinforcement for the model BCJ-A and experiment BCJ-1, are within 6% of one another in spite of there being only 2.5% difference in loading, Figure 7-56**.** The strain from FE analysis on the horizontal part of the beam bar of BCJ-A at 73 kN loading was transposed on the graph provided for beam reinforcement recorded by the strain gauges for specimen BCJ-1.

The strain readings of the front column reinforcement were obtained by (1) experimentally using the strain gauges and (2) analytically using FE model. Good agreement between the two results are shown in the circles where the strain gauges provide readings. More details of the strain in the bar are shown by the FE results which indicate development of cracking in the concrete at those position (max strains).

Strain gauge readings in reinforcement recorded from experimental model BCJ-1 and strain results from FE model BCJ-A are plotted, and indicate a reasonable closeness to one another.

Strain gauge	A	B	C	D	E
FE model	0.0011	0.0017	0.00065	-0.0004	-0.00035
Experiment test	0.00095	0.0015	0.0007	-0.00045	-0.0004
Difference %	14%	12%	8%	13%	14%

Table 7-13: Results obtained experimentally from BCJ-1 and by FE analysis of BCJ-A on the column front reinforcement at 75 kN loading

7.5.5 Conclusion on validation and verification of the numerical model BCJ-A

To validate and verify the structural behaviour of FE model BCJ-A developed to predict the behaviour of the experimental model structure BCJ-1 the strains in three critical reinforcement of the structure were considered and compared, ie. in front column bar, rear column bar and in the horizontal part of beam reinforcement.

Strain gauge	K	I	H	G	F
FE model	-0.00028	-0.00010	0.00065	0.0004	0.00035
Experimental test	-0.00025	-0.00011	0.0007	0.00045	0.0004
Tolerance	0.11	0.10	0.07	0.11	0.13

Table 7-14: Strain readings of rear column reinforcement for the model and experiment are within 13% tolerance, Figure 7-54.

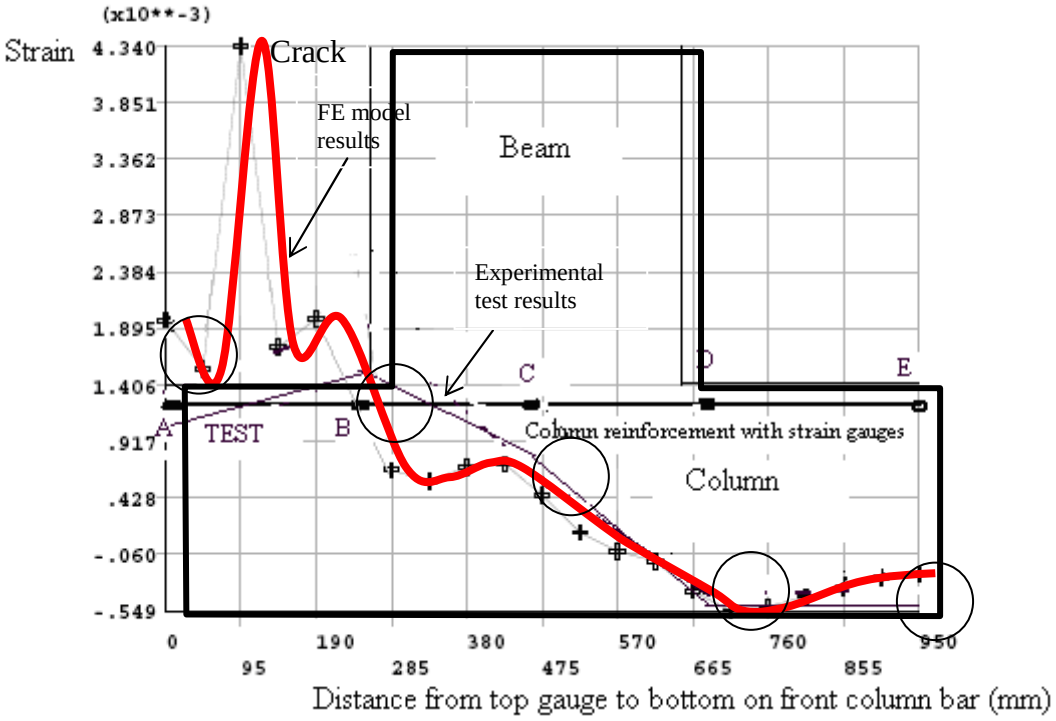

Figure 7-53: The longitudinal strain in the front column bars (Figure 8-9) from the numerical model BCJ-A at 73 kN (7mm displacement load) compared to experimental tests for BCJ-1 at 75 kN loading.

The results obtained by FE analysis for BCJ-A with 75 kN at A1, B1 and C1 Figure **7-51,** are also shown. These coincide with the mid-point strain between experimental results of BCJ-1 strains between 70 and 80 kN.

Strain gauge	A1	B1	C1
FE Model	0.00085	0.00095	0.00090
Experimental test	0.00090	0.0010	0.00085
Tolerance	0.06	0.05	0.06

Table 7-15: Strain gauge readings on the horizontal part of beam reinforcement for the model BCJ-A and experiment BCJ-1 are within 6% of one another, Figure 7-55 .

The experimental specimen BCJ-1 was modelled into an FE model, BCJ-A, which has been analysed for equivalent boundary and loading conditions, the strain recording results differ by only 2.5% and as shown in the graph, Figure 7-56, indicate the following points:

1. Generally the overall strains which developed in the front and rear column reinforcement for experimental specimen BCJ1 and for FE model for BCJ-A are in

agreement. This indicates that the idealization of the BCJ is correctly and appropriately modelled and that the predicted behaviour represents an accurate behaviour of the real structure.

2. The magnitude of the strains in the FE model and those measured by the strain gauges experimental model at the position of the strain gauges are in good agreement which indicates accurate FE modelling and analysis of BCJ-1.

3. The FE model shows a number of peak results in the strains at various points along the length of the bars. These represent cracking in the concrete which occur during the loading. However, these sudden increases in strains and the crack development are not recorded by the experimental results in BCJ-1 because the cracks occurred in areas between the strain gauges, therefore they have failed to be recorded by the strain gauges, whereas FE results record linear changes in strain between these preset points.

4. It has been shown that at 7mm displacement-load (equivalent to 73 kN force-load) the analysis of FE model of BCJ-A is a reasonable comparison with experimental results for BCJ-1 with loading of 75 kN.

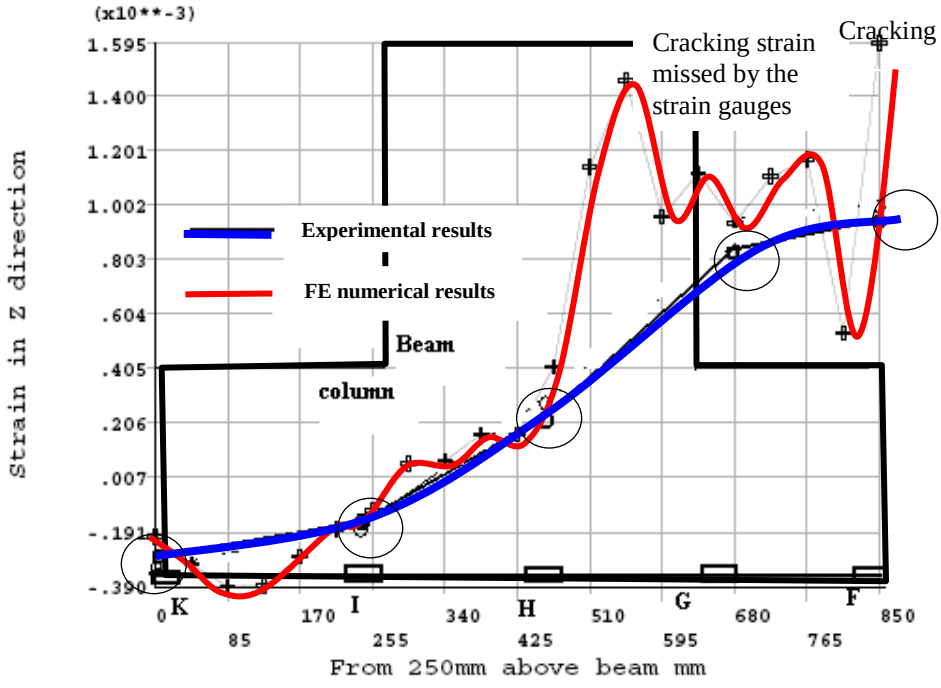

Figure 7-54: The strain gauge reading for the rear column reinforcement bars.

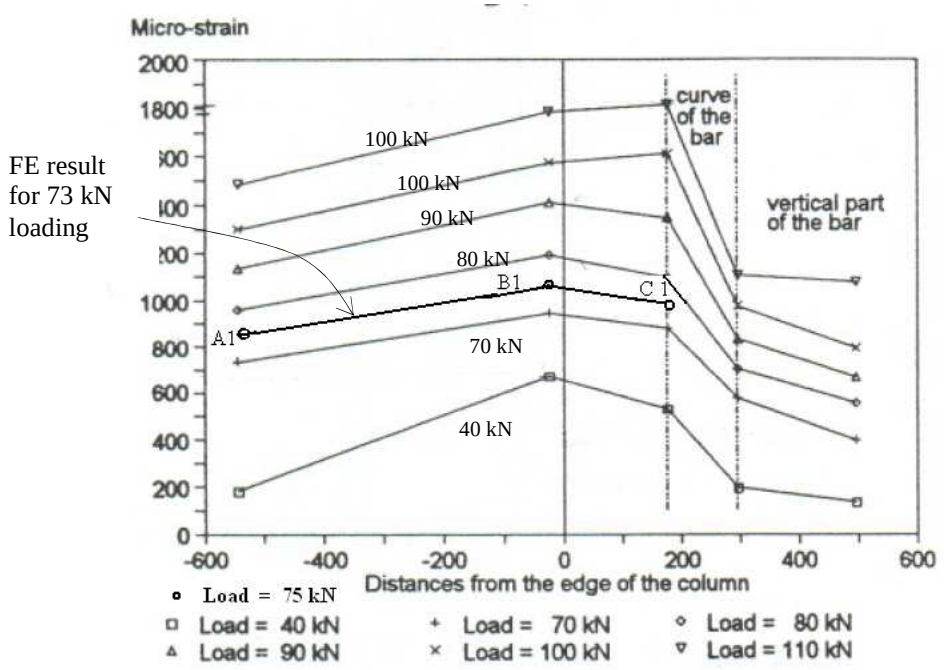

Figure 7-55: Strains in beam reinforcement recorded by the strain gauges (experimental test) for specimen BCJ-1 at incremental loads of 40 kN to 110 kN.

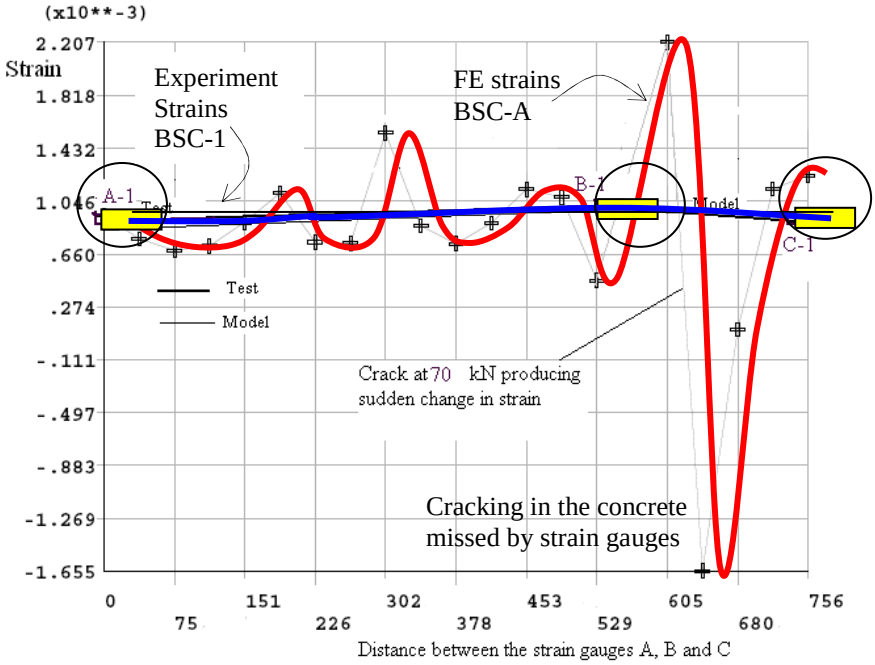

Figure 7-56: Experimental Strain gauge readings on horizontal part of the beam reinforcement; model BCJ-A is displaced 7mm at 73 loading kN. The strains are shown at locations A1, B1 and C1 (Figure 7-52). FE strains were also plotted for the same bar and good agreement at the point of gauge measurement (circled)

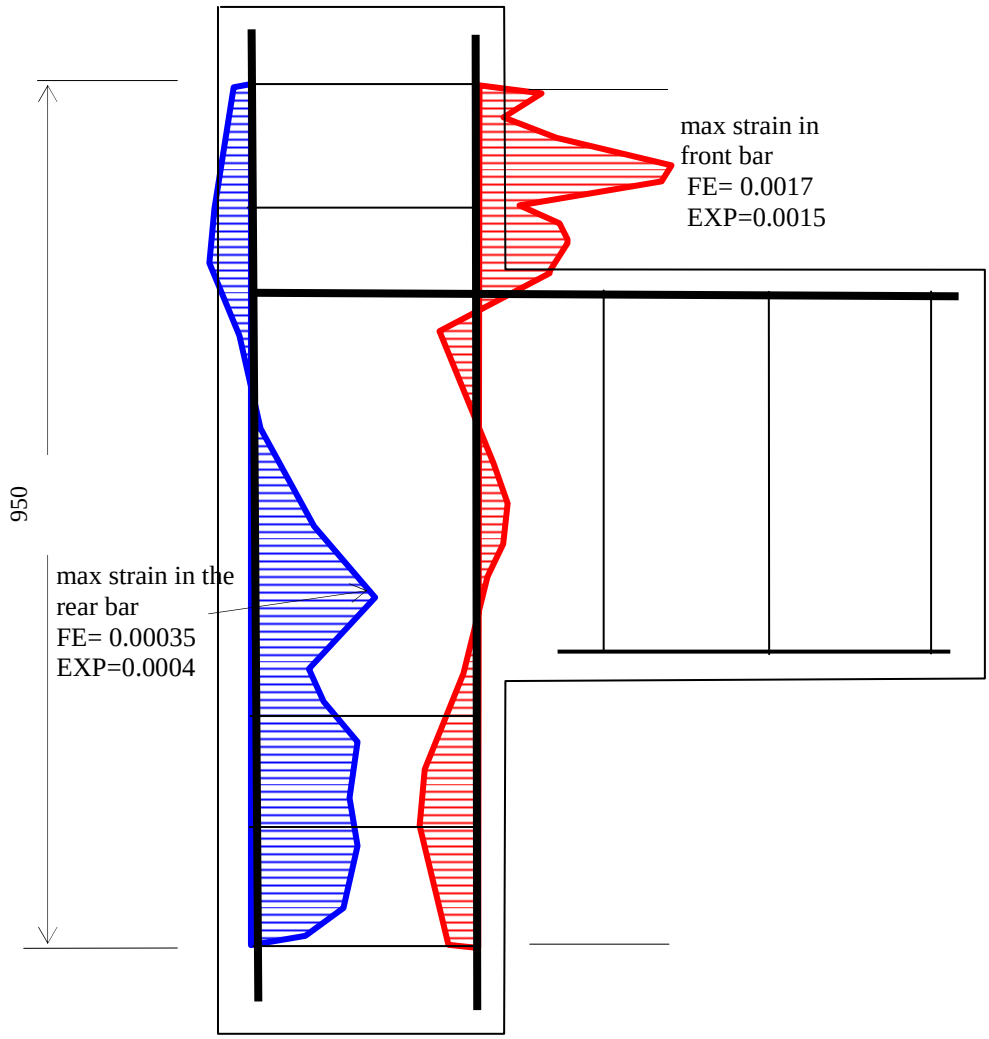

Figure 7-57: Axial strains in the main column bars along the length of the bars. Maximum axial strain developed in the front and rear compare well between experimental test (EXP) and FE model (FE)

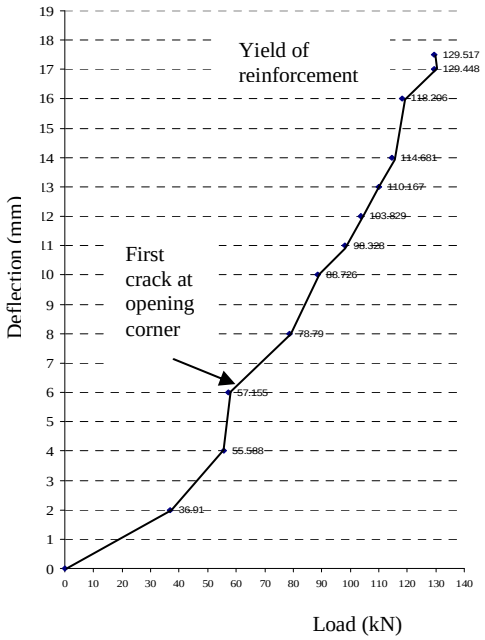

Figure 7-58: Model BCJ-A, the graph shows displacement corresponding to loads.

7.6 Comparison of FE model BCJ-B with experimental test BCJ 4

BCJ-B, Figure 7-61, is the FE model for experimental specimen BCJ-4, Figure 7-59, and

has the same geometry, material properties and beam reinforcement as BCJ-A. However, BCJ-B has 3 additional stirrups in the joint,

Figure 7-63, and has 4 external corner bars of T22.63, Figure 7-64, as compared to BCJ-A with 4-T16 mm.

Details of reinforcement for BCJ-4 are shown in Figure 7-59 and Table 7-8. The beam reinforcements are 4-T16 on top and 2-R8 at bottom, the distance between the centre of the beam's corner top bars is 124mm to provide for distribution of 4-T16 bars with a cover of 30 mm, Figure 7-60, and column reinforcements are 10-T16. The column reinforcement for the model BCJ-B is 4-T22.63 and 2-T16, Figure 7-61. The model failed at beam load of 138 kN compared to 130 kN for BCJ-4, ie. 6.1% higher.

In FE modelling, the concrete mesh sizes [7-9] are chosen to be around two or three times the size of the aggregate. Since 20mm aggregate is used, the size of mesh chosen is 65mm.

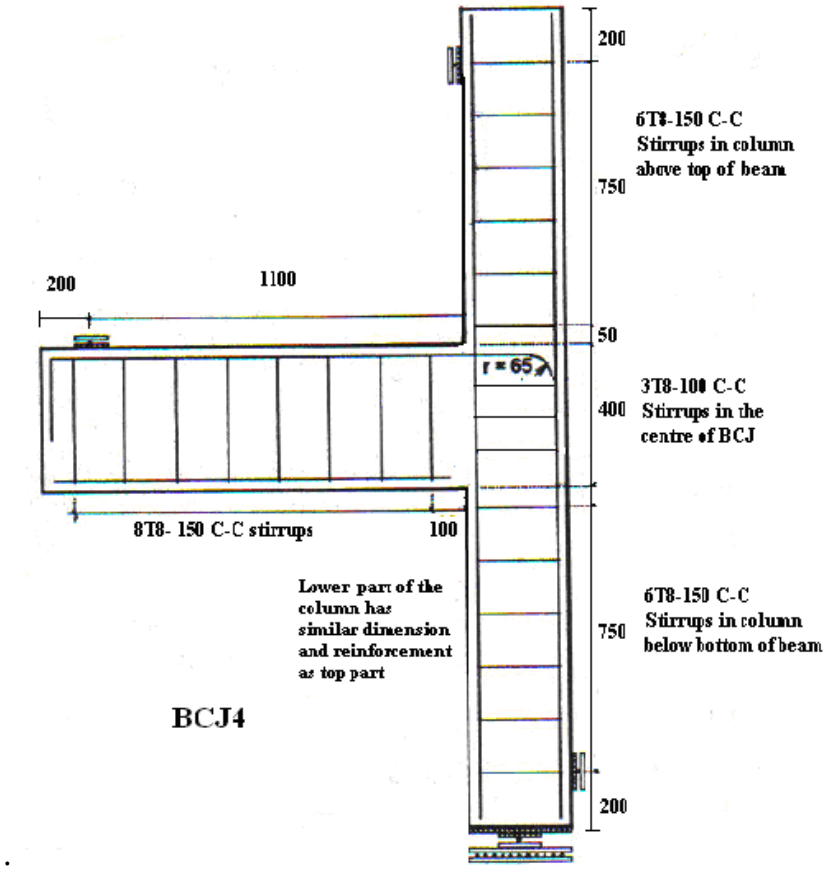

Figure 7-59: Reinforcement detailing of experimentally tested BCJ-4.

The column corner reinforcement in BCJ-4 of 2-T16 placed in the four corners, Figure 7-60, are assumed to be replaced with a single bar of T22.63 with the same total area As=2010 m^2 or percentage As / bd = 3.35% in the column, Figure 7-61. All main reinforcements in BCJ-B have yield strength f_y=720 MPa. All stirrups are T8 and bottom reinforcement of the beam are T8 and have yield strength of f_y=571 MPa.

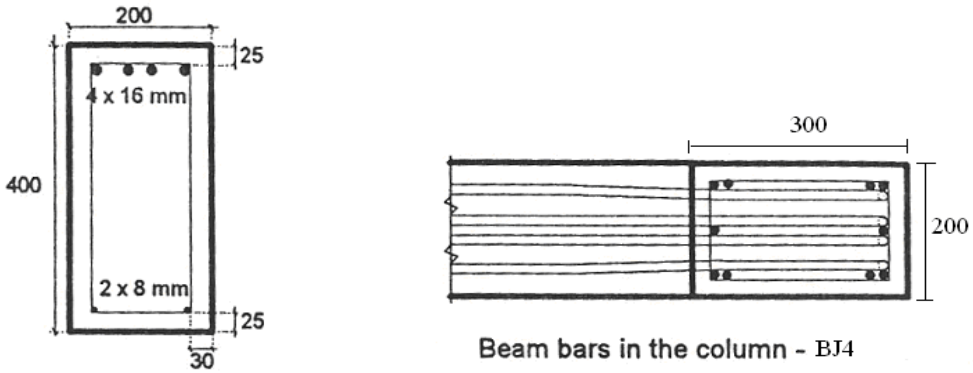

Figure 7-60: Column and beam cross sections for experimental test BCJ-4

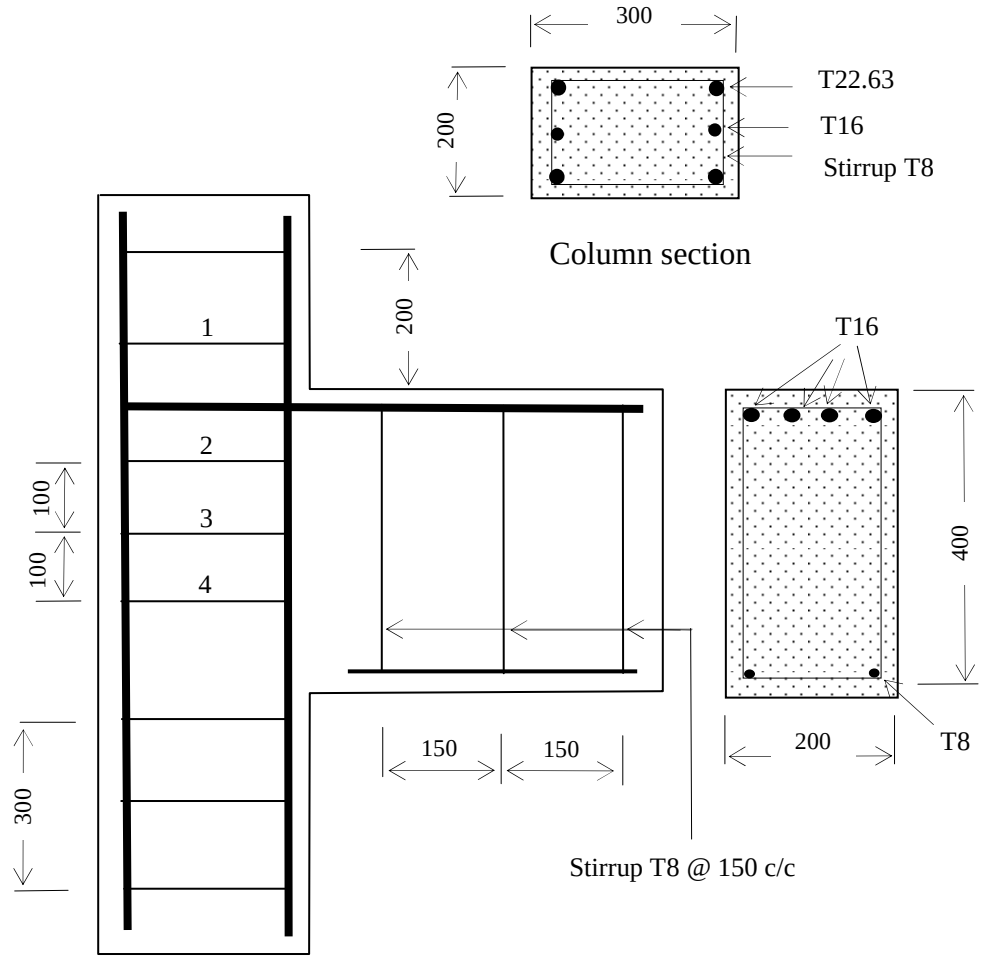

Figure 7-61: Details of idealized FE model, BCJ-B, representing the experimental model BCJ-4. The dimensions and position of the four shear links investigated in the column are numbered as shown.

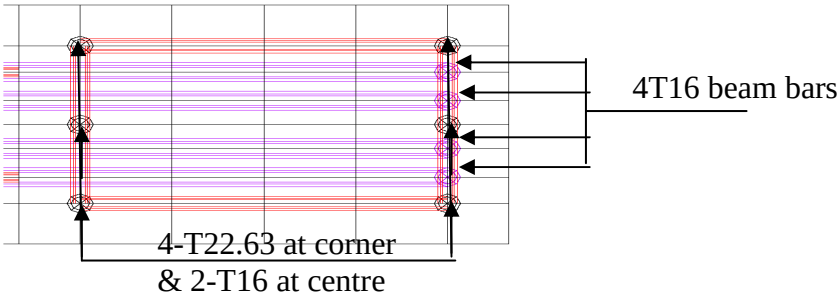

Figure 7-62: Cross section B-B of the column for numerical model of BCJ-B . Main beam bars (purple), column reinforcement (black), links and the 8mm bar to hold the links in the cage (red).

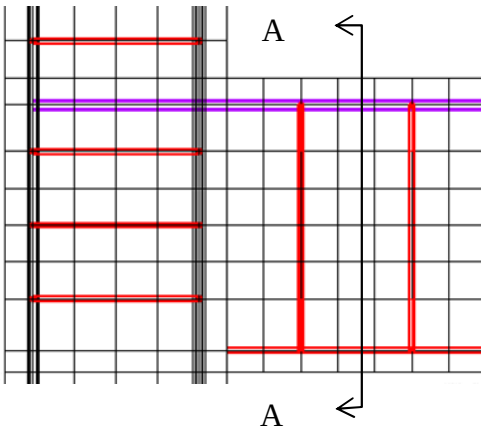

Figure 7-63: Elevation view of the numerical model of the experimental BCJ-B. Purple bars are the main beam reinforcement, black are column reinforcement, red bars are links and 8mm bar at the bottom which holds the links in place.

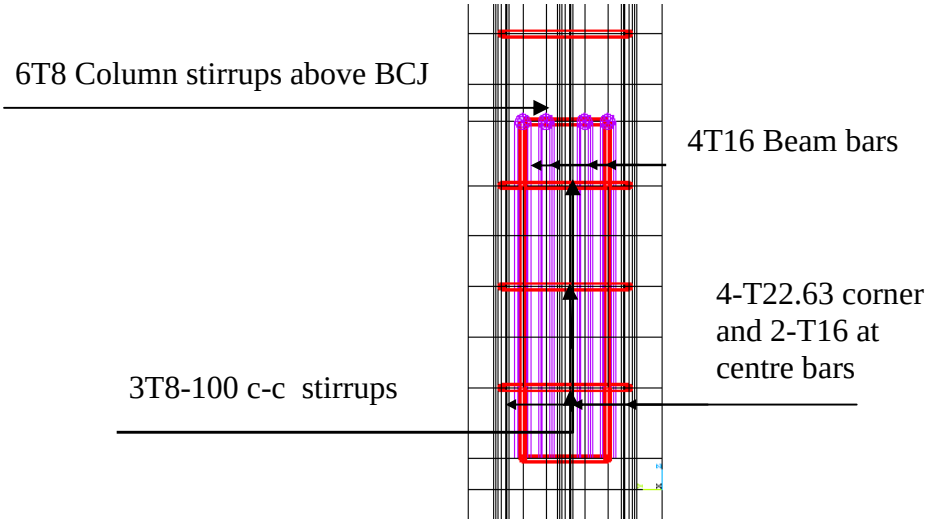

Figure 7-64: Section A-A of the numerical model of beam column connection showing the cross section of the beam at BCJ for BCJ-B

The effect of the radius of bend for beam bars at beam column connection in BCJ-4 was not considered in the model BCJ-B since test data from monotonically loaded connections is inconclusive. For example, varying the radius of bend between 4 and 8 bar diameters and past research has suggested no significant effect on joint shear strength [7-10].

7.6.1 Cracks comparison of BCJ-4 to FE model BCJ-B

The reported crack formation for experimental work, Figure 7-65, indicates that BCJ1 fails at opening corner with spalling of concrete cover on the column reinforcement

because yielding occurred above the opening corner. In comparison to BCJ-1, the BCJ-4 specimen beam bar has a smaller anchorage length at the beam end.

Experimentally it was recorded that at 50 kN loading the first crack opened below the central stirrup. At 60 kN another crack ran parallel to the expected diagonal compression strut direction. From this stage onward the cracks formed diagonally parallel in the assumed direction. The crack below the central stirrup was only 0.10 mm wide up to failure. At 100 kN loading, the widest joint crack was 0.20 mm and at 120 kN it was 0.42 mm wide.

The failure is reported to have occurred by widening of diagonal crack and anchorage. However, on investigating the strain it was found that the final yielding occurred at 138.3 kN, repeated crushing and failure occurs within the diagonal inclined compression strut of the joint (Figure 7-66). The numerical model crack formation reasonably simulates the experimental tests (Figure 7-65) .

The failure occurred by wide opening of the diagonal cracks and cracks parallel to column bars on the external (rear) side and above the joint. Two stirrups, one at the centre of the joint and another above the centre, yielded. At failure, the concrete spalled off at the internal (beam) side of the joint, near the column bars at closing corner.

The joint stirrup near the beam bars shared some of the stresses with the beam bars. The other joint stirrups had a rise in the strain gradient after cracking .

In the FE model of BCJ-B, initial cracks formed at 36.9 kN loading and flexural cracks started from the top of the beam towards the column at the opening corner and extended vertically downwards half the depth of beam at BCJ in a similar pattern to the experimental test BCJ-4 at 40 kN . Diagonal tensile cracks which appear in the model for BCJ-B, Figure 7-66, resemble the diagonal cracks recorded at 40 kN in BCJ-4 as shown in Figure 7-65.

Some crushing of the elements along the diagonal near the opening corner appear in the form of circles, Figure 7-66. As loading increases to 76.2 kN, the cracks appear in the lower exterior (rear) column face of the BCJ, these are tensile cracks but just below half the depth of beam they become diagonal tensile cracks.

At 138.3 kN, repeated crushing and failure occur at the closing corner of BCJ-B, Figure 7-66. The numerical model crack formation reasonably simulates the experimental tests (Figure 7-65) .

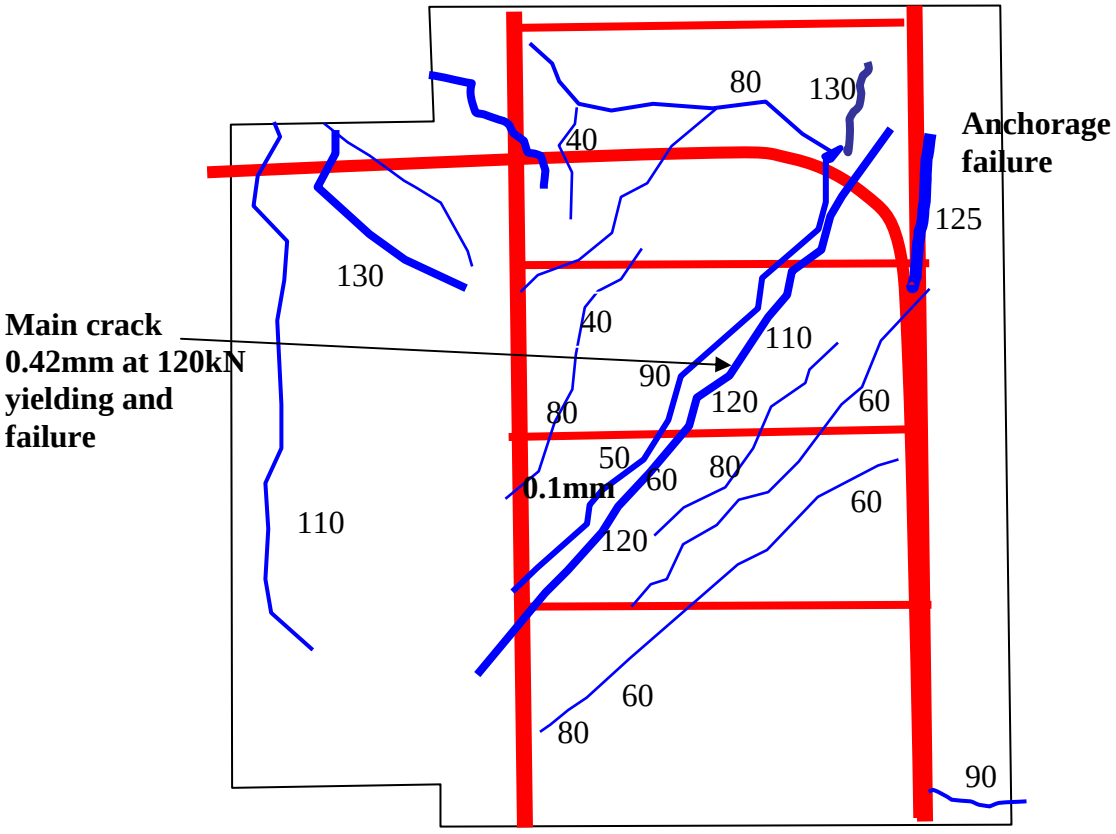

Figure 7-65: Sketch drawn from the photograph of the experimental cracks formed on BCJ-4 just before failure at 130 kN.

When the applied load increased to 138 kN nearing BCJ-B failure point, Figure 7-66, three areas of major stress distribution can be noted as follows:

- Major bending crack path in the beam starting close to the opening corner, continuing downwards parallel to the edge of the column.

- Major compressive diagonal crack path in the centre of the joint starting from the top of the joint close to the rear face and expending downward toward the closing corner.

- Significant bending cracking at lower part of the rear column face at closing corner level.

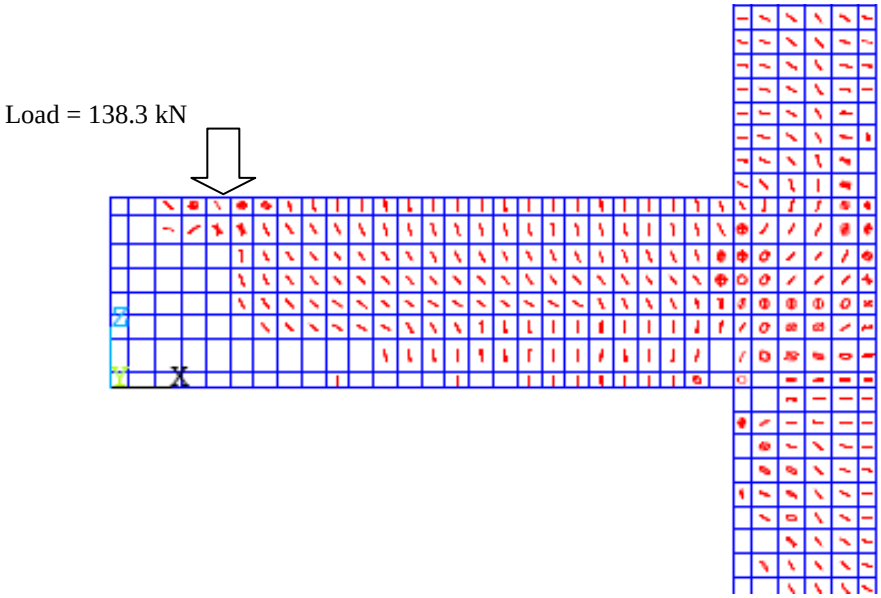

Figure 7-66: At failure load of 138.3 kN, crushed elements (circles) develop in diagonal direction at BCJ resulting in diagonal shear failure of BCJ-B. The lines of cracks are a duplicate of the crack lines from the experimental test at failure.

Experimental results from BCJ-4 gave the following information:

i. The width of the first diagonal crack reached 0.1 mm, however, other diagonal cracks reached 0.2 mm at 100kN and 0.42 mm at 120 kN loading.

ii. Failure occurred at 130 kN.

iii. From the strain gauge results, it has been noted that the upper and the central shear links yielded just before failure.

iv. At failure, the concrete at the closing (compression) corner spalled off and the concrete crashed.

7.6.2 Comparison of strain in reinforcement for BCJ-B and BCJ-4

Strain in column reinforcement and links for FE model BCJ-B and tested specimen BCJ-4 will be compared in this section.

In Figure 7-67, when cracks open, strains in reinforcement suddenly increase depending on the depth of the crack.

The line passing through circles represents strain gauge readings in the experiment as compared to the numerical model recording. The large crack appears in the front column

bar above the opening corner, Figure 7-65 compare with FE model, Figure 7-66 and strains recording shows the cracks along rear and front column bars Figure 7-67**.**

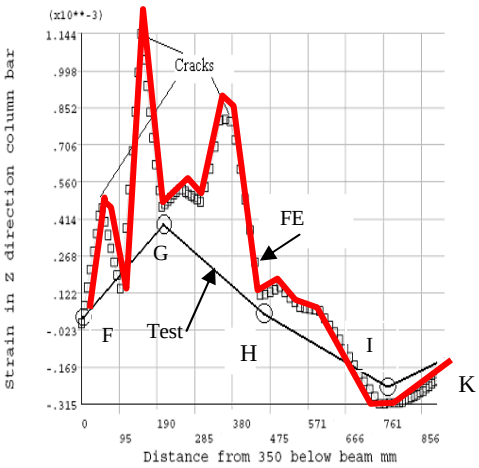

a) Strain along the rear column bar from (0.0) 280mm above opening corner

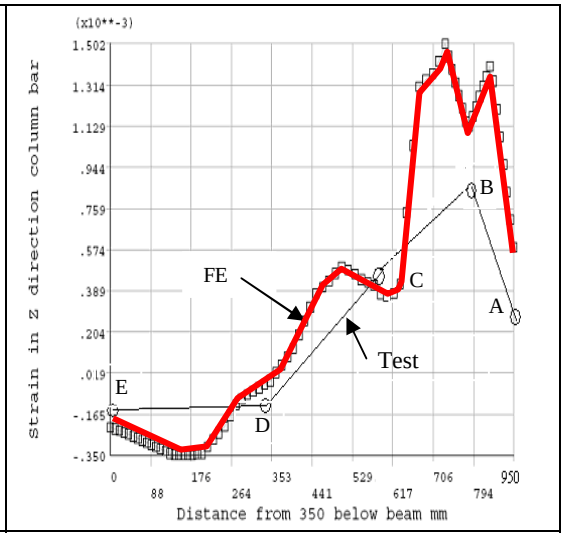

b) Strain along the front column bar from (0.0) 280mm below closing corner

Figure 7-67:Comparison of strain recordings from FE and tests along the front and rear column bar at 55.6 kN. Position of the gauges are shown in Figure 8-9.

Maximum strain	At failure at stirrup		At 55.6 kN in column bars	
	Link A	Link B	Front	Rear
BCJ-4 specimen	0.003	0.0012	0.0008	0.0004
BCJ-B model	0.0023	0.0014	0.0011	0.00041
Tolerance	30%	14%	37%	2%

Table 7-16: Strain recording for FE model prediction and experimental test.

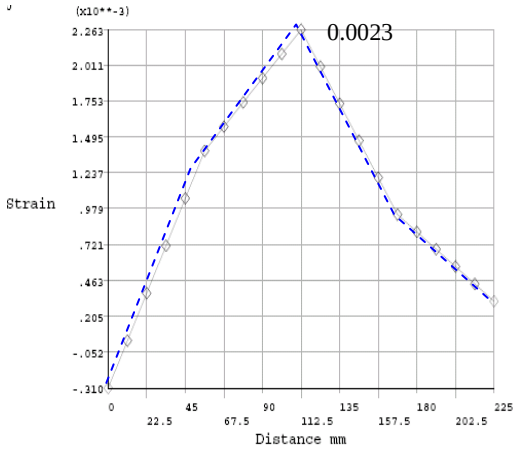

a) Middle link A - FE 0.0023 compared to experiment of 0.003

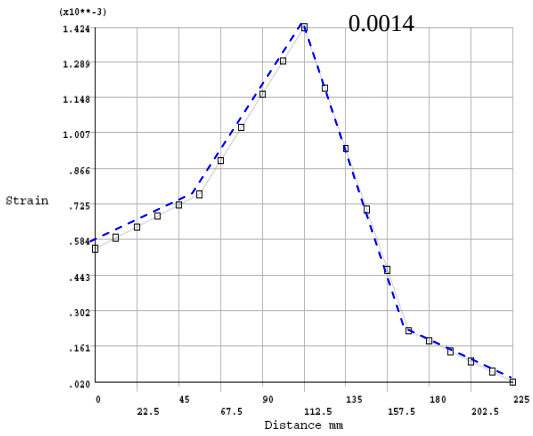

b) Lower link B –FE 0.0014 compared to experiment of 0.0012

Figure 7-68: The FE beam load of 138 kN compared to experimental beam load of 130 kN.

7.6.3 Comparison of FE model BCJ-B experimental test BCJ-4

In this section failure loads, crack propagation, deflection, strain in column reinforcement and links for FE model BCJ-B will be compared to tested specimen BCJ-4.

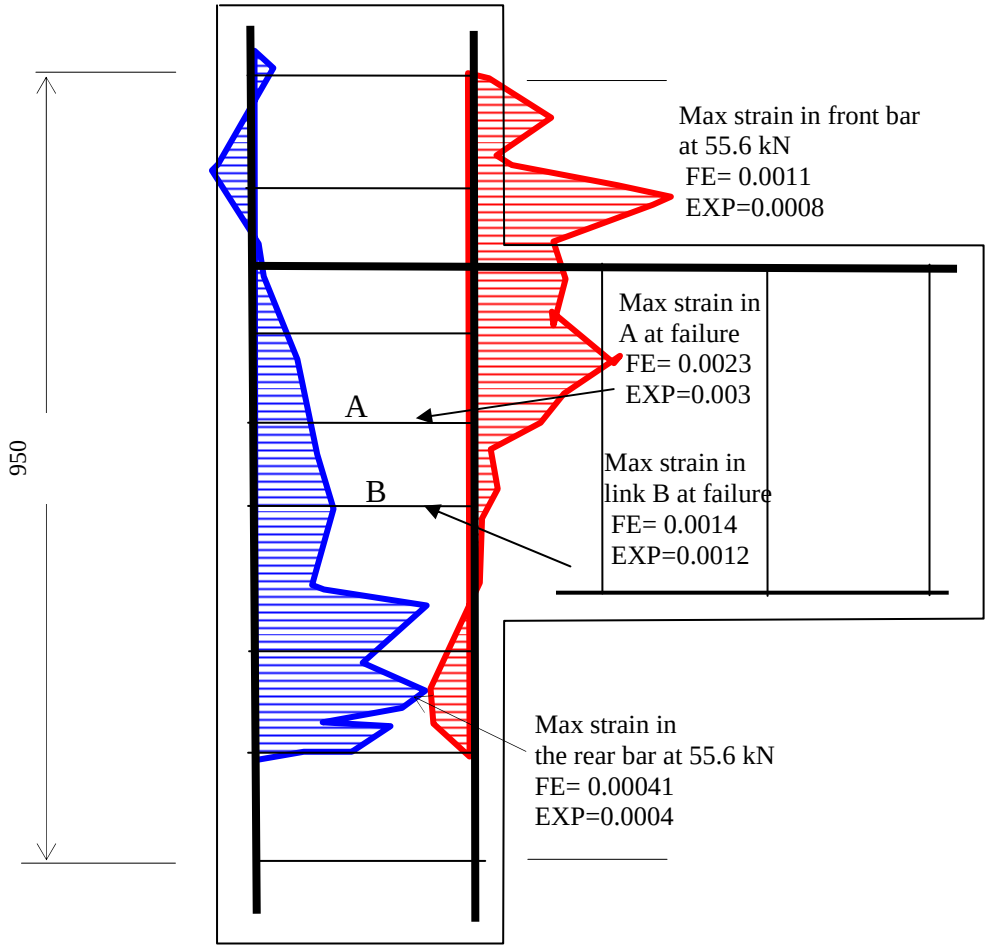

Figure 7-69: Comparison of maximum strains in front and rear column bars for BCJ-4 and BCJ-B at 55.6 kN.

Failure beam load of 138 kN for the model BCJ-B compares well to 130 kN beam load for experiment BCJ-4, with a 6.4% difference.

Table 7-16 indicates reasonable accuracy of the FE analysis when compared with the test results. The large cracks at 40 mm above the beam in column above opening corner represent a sudden change in strain. Figure 7-67 (b) shows the change in strain of the front column reinforcement on strain gauges A, B, C, D and E within the depth of the beam. Strain gauge readings on the front column reinforcement for both the model and experiment are within 37 % tolerance of one another at 57 kN loading, Table 7-16.

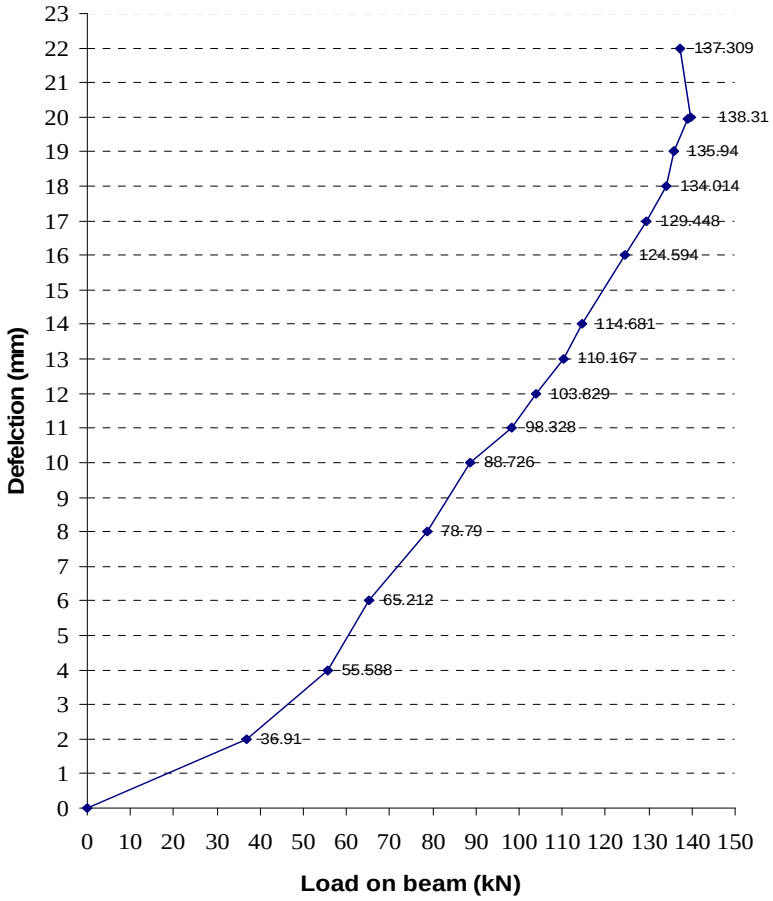

Figure 7-70: Load applied at the end of the beam, against deflection at loading point for BCJ-B numerical model up to failure at 138.3 kN loading

Similarly, the strains in the rear column bar were compared and the results are shown in Figure 7-69 and, in general, there is a good agreement between the two results. However, some cracks which developed between the positions of the strain gauges were not recorded in the experimental results as gauges only record strains at preset points and these are shown in FE results. Strain gauge readings on the rear column reinforcement for the model and experiment are within 2% tolerance of one another at 57 kN loading, Table 7-16.

Maximum strains developed in the front and rear bar at 57 kN and in links A and B , Figure 7-69.

7.6.4 Load-Deflection behaviour of BCJ-A compared to BCJ-B

Investigation of the load-deflection behaviour of BCJ-4 with 3 additional shear links at the centre of the joint will be carried out in a similar way to the study of BCJ-1 with no shear links in model BCJ-A, Figure 7-58 and Figure 7-70. The aim of this section is to investigate the influence of shear links on the overall behaviour of BCJ.

The vertical deflection under the point of the applied load was evaluated for various loading magnitudes and these were plotted against the applied load. In both joint types, the behaviour of load-deflection is similar in both BCJ type, ie. BCJ-A without shear link in the joint, and BCJ-B with the addition of 3 shear links.

However, the joint without shear links, BCJ-A, developed larger cracks than the model with the shear links. This indicates that the shear links provide greater strength for the joint, but most importantly increases the joint ductility. Maximum load carried by BCJ-A is 129 kN at 17 mm deflection, while the failure load of model BCJ-B is 138 kN at 23 mm deflection, which is only a 7% increase in loading but an 29% increase in deflection.

7.6.5 Comments on BCJ anchorage

Theoretically, the design of stirrups required in the BCJ region should be provided between the beam tensile reinforcement and the top of the flexural compression zone in the beam which can be assumed to equal 3/8ths of the beam depth. However, in practice, cold joints 50mm above and below the beam in the column can be venerable locations. In this writer's FE parametric investigations, as the stirrup located 30mm above beam in specimen BCJ-B is removed, a reduction in BCJ shear resistance of 14% was recorded. Similarly as discussed the shear influence was due to compression membrane failure below the beam in section. It is recommendable to have stirrups 50mm above to 50mm below the beam at BCJ, bearing in mind that at weaker column concrete sections where the cold joints are located and FE analysis and compression membrane theory confirm this recommendation.

It is essential that a minimum area of joint shear reinforcement be provided in all external BCJ as recommended in ACI 318-05 [7-11] . It is proposed that there should be minimum area of shear reinforcement in beams as proposed by EC2 [7-12] as shown below be used:

$$\frac{A_{sw}}{b_c s} = \frac{0.8 f_{ck}^{0.5}}{f_{yk}}$$

where A_{sw} is cross sectional area of shear reinforcement, b_c is overall width of the column, s is spacing between the links, f_{ck} is 28 days characteristic compressive cylinder strength, and f_{yk} is characteristic yield strength.

In practice, it could be difficult to position stirrups at the depth of the joint. A practical alternative for external BCJ with transverse beams is to use U bars while ensuring that the legs of the U bars are perpendicular to the axis of the transverse beams encasing BCJ, however, for corner columns U bars should be avoided and only stirrups with hooks similar to should be used in corner BCJ.

The beam reinforcement should be bent down into the column with adequate radius to avoid bearing failure and should be fully anchored in the column past the beginning of the bend with minimum length .

It is often more convenient to anchor the beam reinforcement with U bars rather than L, however, it has been demonstrated that joint shear strength of specimen s with L bars are 20% more than U bars which have insufficient lap with the column bars

7.6.6 Conclusion on validation of FE models of BCJ

The structural behaviour of FE model BCJ-A was developed to predict the behaviour of the experimental model structure BCJ-1, and strains in the critical locations of front column bar, rear column bar and beam bar were compared.

The experimental model BCJ-4 was modelled into an FE model BCJ-B, which has been analysed for equivalent boundary and loading conditions, and the results shown in the graphs indicated the following points:

1. Generally the overall strains which developed in the front and rear column reinforcement for FE model BCJ-A are in agreement with the experiment results obtained for BCJ-1. The magnitude of the strains in the FE model and those measured by the strain gauges from the experimental specimens at the critical locations of the reinforcement are in agreement, which demonstrates accurate FE modelling and analysis of BCJ-1.

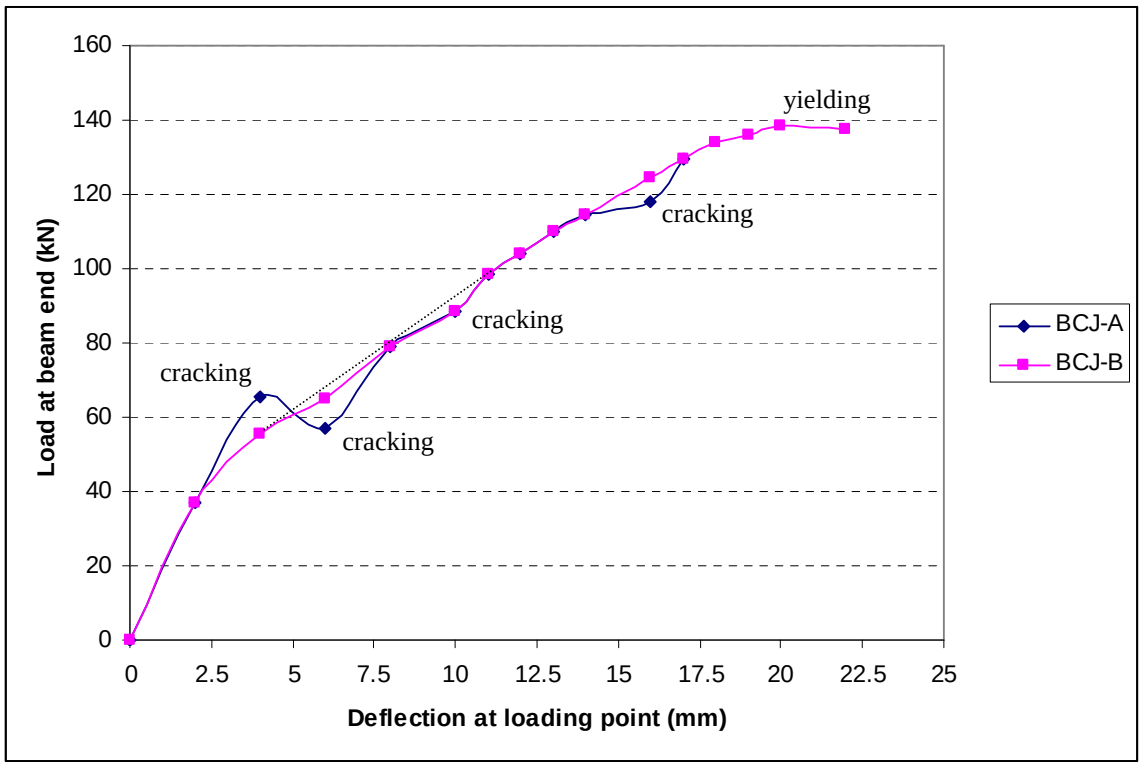

Figure 7-71: Comparison of deflection to corresponding load for models BCJ-A and BCJ-B

2. The FE results show a number of peak results in the strains at various points along the length of the front and rear bars. These represent cracking in the concrete which occurs during the loading. However, these sudden increases in strains and the crack development are not recorded by strain gauges for the experimental specimen BCJ-4 because the cracks occurred in areas between the strain gauges, whereas FE results record linear changes in strain between these preset points.

3. It has been shown that the results of 4 mm displacement-load (equivalent to 56.6 kN force-load) used for the analysis of the FE model of BCJ-B is the reasonable value to use for comparison with experimental results for BCJ-1 with loading of 60 kN.

Therefore, this chapter which covers the validation and verification for the two FE models BCJ-A and BCJ-B of experimentally tested BCJ1 and BCJ4 is completed successfully.

The results produced demonstrate that numerical and experimental results compare well, the software is validated and the FE method of analysis is verified.

7.7 References for Chapter 7

7-1 Reys de Ortiz, I. 'STM of reinforced concrete short beams and beam column joints'. PhD thesis, 1993, University of Westminster

7-2 Kotsovos, M.D. 'Compressive force path concept: basis for reinforced concrete ultimate limit state design.' ACI Struct. Journal, 1988, 85, 68-75

7-3 Kotsovos, M.D. 'Mechanisms of 'shear' failure'. Magazine of Concrete. Research, 1983,35, 99-106

7-4 CEB-FIP Model Code 1990-CEB-FIP International Recommendations – Final draft, 1992

7-5 BS 8110: Structural use of concrete, Part 1.Code of practice for design and construction, British Standards Institution, London, 1985

7-6 Kachlakev, D.I., Miller, T., Yim, S., Chansawat, K., Potisuk, T., "Finite Element Modeling of Reinforced Concrete Structures Strengthened With FRP Laminates," California Polytechnic State University, San Luis Obispo, CA and Oregon StateUniversity, Corvallis, OR for Oregon Department of Transportation, May 2001.

7-7 Huyse, L., Hemmaty, Y., and Vandewalle, L., "Finite Element Modeling of Fiber Reinforced Concrete Beams," Proceedings of the ANSYS Conference, Vol. 2, Pittsburgh, Pennsylvania, May 1994.

7-8 Najjar, S., Pilakoutas, K., and Waldran, P., "Finite Element Analysis of GFRP Reinforced Concrete Beams." Proceedings of the Third International Symposium, Sapporo, Japan, 2, 519-526, 1997.

7-9 Bedard, C. "Non –linear finite element analysis of concrete structures", University of London, 1983, PhD Thesis.

7-10 Vollum, R.L., Newman J.B., "Discussion on paper published in Magazine of Concrete Research," 1999,51,No. 6,415-425- Strut-and-tie models for analysis/design of external beam column joints. Magazine of Concrete Research, 2001, 53, No.01, February, 63-66

7-11 ACI Committee 318, Building Code Requirements for Structural Concrete (ACI 318-08) and commentary (ACI 318R-08), American Concrete Institute , Formington Hills, MI, 2008, 465 pp

7-12 Eurocode 2: Design of concrete structures, Part 1-1, General rules and rules for buildings, BS EN 1992-1-1:2004, British Standards Institution, London, Dec 2004

Chapter 8
High Strength Concrete Transfer Beam Column Joint With Central Vertical Bar

8.1 Introduction

In this chapter the behaviour of HSC and NSC TBCJ with and without CVB will be investigated numerically by using a nonlinear FE computer programme in order to develop accurate models to compare four FE models of TBCJ specimen with analogous beams tested experimentally in the Construction Hall at the University of Westminster under the supervision of the advisor of this current research work.

8.2 Aims and objectives

The aim is to carry out parametric FE numerical investigations of factors affecting the behaviour of TBCJ of aspect ratio 3.11 in order to investigate the influence of the material property of HSC, in presence of CVB and column and beam bar reinforcement and shear links on TBCJ.

A TBCJ for a one storey industrial building is designed to ACI 352 [8-1], Appendix B, and predictions from proposed empirical design rules for the TBCJ designed to ACI 352 [8-1] will be compared with those obtained from the FE models. Both empirical and FE predictions are compared with the data from analogous beams tested experimentally.

The simplified STM model for TBCJ is compared with FE models and the load path for its struts and tie is determined.

8.3 FE analysis and parametric investigation of TBCJ

The FE parametric investigation on four TBCJ with aspect ratios 3.11, with and without CVB made with HSC or NSC are completed and the results are compared with analogous beams NSC1, NSC3, HSC1 and HSC3 of a/d=3.02 as detailed in Table 3-4 of Chapter 3. The following FE models were developed:

- T-NSC1(Figure 8.2): TBCJ without CVB made of NSC with aspect ratio similar to span depth ratio of experimentally tested NSC1 beam which has no HWB.
- T-HSC1(Figure 8.2): TBCJ without CVB made of HSC with aspect ratio similar to span depth ratio of experimentally tested HSC1 beam which has no HWB.
- T-NSC3 (Figure 8.10): TBCJ with CVB made of NSC with aspect ratio similar to span depth ratio of experimentally tested NSC3 beam which has HWB.
- T-HSC3 **(**Figure 8.10**):** TBCJ with CVB made of HSC with aspect ratio similar to span depth ratio of experimentally tested HSC3 beam which has HWB.

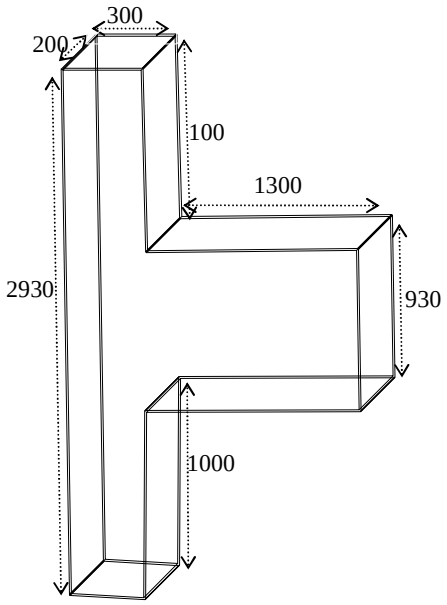

Figure 8.1: Four FE T BCJ models with aspect ratio 3.11 were modelled for parametric investigation

8.4 Material properties and loading of FE models

TBCJ with aspect ratio of 3.11 have a 930mm deep beam and 150mm width throughout.

This particular depth of the beam was chosen because when moment distribution of 20% is considered, the distance from the centre of compression stress block to beam bar is 800mm which is equal to the shear span of the beams experimentally tested.

The concrete cube strength for NSC models is 42 MPa and for HSC is 110 MPa. The average values for the cube strength of tests BCJ-1 and BCJ-4 for NSC and beams HSC1, HSC2, HSC3 and HSC4 were considered, Table 8.1.

Both beams and columns were reinforced with hot-rolled round deformed bars. The details of BCJ reinforcement for the experimental tests used for validation and verification are shown in Table 8.2**.**

Type	Model	Cube Strength f_{cu} MPa	Average f_{cu} MPa	Cylinder Strength f_c MPa	Average f_c MPa	Splitting Strength f_{sp} MPa	Average f_{sp} MPa
BCJ	BCJ-1	42.3	42	34.0	34	2.77	2.87
	BCJ-4	42.0		34.0		2.98	
Beams	HSC1	106.0	110	84.8	8.8	4.21	4.52
	HSC2	109.3		87.4		5.20	
	HSC3	112.5		90.0		4.34	
	HSC4	112.5		90.0		4.34	

Table 8.1: **Concrete properties used for NSC in the experiments on BCJ [and for HSC on beams, Table 2-5. The averages of these properties were used in FE model analysis.**

FE idealization considers similar geometrical and material properties to the experimental model. However, assumptions were made in order to simplify the FE model to obtain accurate results, which are as follows:

The top main beam reinforcement to the rear column reinforcement were idealized as L-shape bars. According to past research [2] this will have a nominal affect on the behaviour of the BCJ, but this will significantly simplify the analysis of BCJ.

In the FE analysis, the reinforcement was chosen for TBCJ with minimum quantities of stirrups, beam and column reinforcement so that the strains in all reinforcement such as stirrups, beam bar, front column bar and CVB could be fully developed . The reinforcement requirement for beam bars with aspect ratio for TBCJ of 3.11 predicted as ACI 352 [8-1] is equivalent to the area of 4-T20 which are simplified to the equivalent area of 3T23 for numerical modelling, , Figure 8.2. The column bars for TBCJ of aspect ratio 3.11 are 4-T20.

Both beams and columns were reinforced with hot-rolled round deformed bars with the exception of shear stirrups in TBCJ which are mild steel reinforcement **(**Figure 8.2**).**

The anchorage for the beam bar of TBCJ was 560mm**.**

FE model Identity	Aspect ratio	No & diameter (mm)	Total area A_s (mm^2)	Reinforcement ratio A_s/bd %	Anchorage length (mm)	Cube Strength f_{cu} MPa	Beam load (kN)	Comment
T-NSC1	3.11	3-T23	1246	0.67	560	42	220	Figure 8.2
T-HSC1						110	260	
T-NSC3						42	260	Figure
T-HSC3						110	340	

Table 8.2: Failure loads, concrete property and beam reinforcement for numerically analysed BCJ. Yield strength for all beam reinforcement is $f_{y=}$ 720 MPa.

FE model Identity	Number & Diameter (mm)			Area A_s (mm^2)	% Steel A_s/bd
	Corner	Centre	CVB		
T-NSC1	4-T20	0	0	1257	3
T-HSC1	4-T20		0	1257	3
T-NSC3	4-T20		2-T20	1257	3
T-HSC3	4-T20		2-T20	1257	3

Table 8.3: Column reinforcement. The column corner bars have yield strength f_y= 720 MPa and CVB have f_y= 563 MPa. CVB are not included in the percentage of column reinforcement.

8.5 Loading of the specimen

With the anticipation that FE analysis of TBCJ requires a much larger processor, arrangements for obtaining higher processing power hardware and an improved version of the software were put in place at a later stage when analysis of TBCJ was about to take place. This allowed the application of incremental monotonic step force loading to TBCJ. Four FE models of TBCJ with aspect ratio (beam depth /column depth) of 3.1 were developed. A general description of the geometry, stirrup detailing and size of the elements for TBCJ models is shown in Figure 8.2.

Model	BCJ joint stirrups	Column stirrups	Column Stirrup below beam	Joint stirrup	Comment
T-NSC1	8-T8-150cc	6-T8-150cc	6-T8-150cc	6-R6-200cc	Only 5 stirrups in BCJ are mild
T-HSC1					
T-NSC3					
T-HSC3					

Table 8.4: Shear reinforcement in FE models. TBCJ have mild R-6 for stirrups in the joint. All column and beam stirrups are T-8 of f_y=571 MPa

When applying step loading for the TBCJ models, initial loading of 60 kN with load steps of 20 kN was used until failure occurred. After failure the last load step was repeated with a smaller load increment of 10 kN in order to produce more accurate results.

8.6 FE model idealisation of TBCJ

Types of element used and the characteristics of the elements needed are shown in Figure 8.2 to Figure 8.6 with the following element dimensions:

For Column: Depth 300 mm = 6 elements,
Width 200 mm = 6 elements,
Height above the beam 1000 mm = 20 elements,
Height beneath the beam 1000mm = 20 elements

For Beam: Depth 930 mm = 11 elements,
Length 1600mm = 32 elements

The total number of concrete elements , Figure 8.2, used for the column section above and below beam in TBCJ is 1440 elements (40x6x6), and for the beam including the joint the total element is 3648 elements(32x6x19). This means that a total of 5088 concrete elements of "Solid 65" material from the ANSYS programme were used in the analysis of each TBCJ considered above. This excludes the elements used to idealise the reinforcement.

TBCJ for NSC and HSC have similar detailing as shown in Figure 8.2**.** T-NSC3 and T-HSC3 have additional 2-T20 CVB at the centre of the depth of column, Figure 8.10**,** where the location of structural loading and constraints for all TBCJ are also shown.

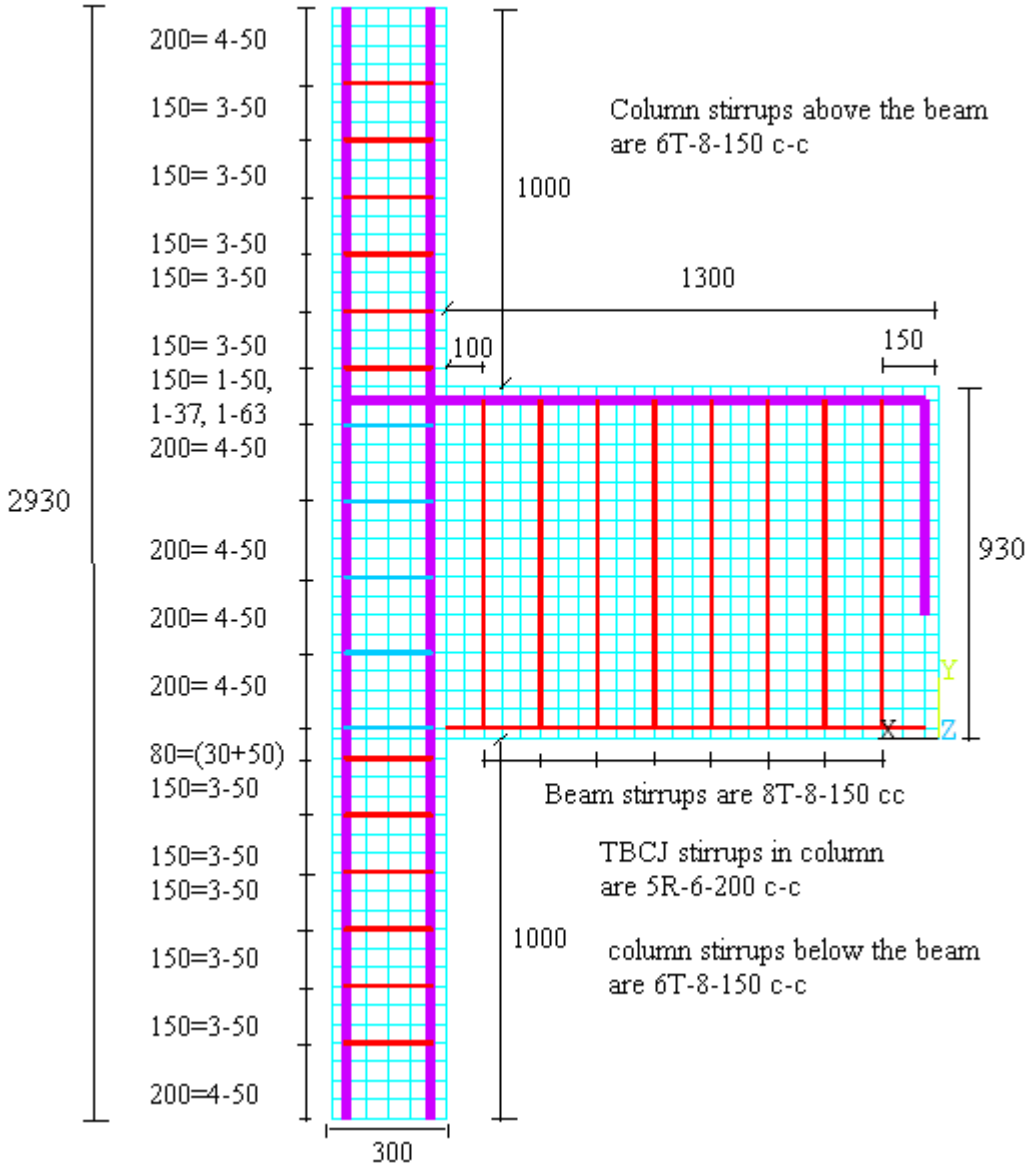

Figure 8.2: Side elevation of T-NSC1 & HSC1 with column width of 200mm and beam depth of 930mm. Detailing and location of the column and beam stirrups. Column element sizes are shown. (All dimensions are in mm).

The number of elements along the length of beam and depth of column is 19 within depth, 32 along the length of the beam and 6 within width of column including TBCJ, a total of 3648 concrete elements. The column parts above and below the beam have 2 x 20 x 6 x 6 = 1440 concrete elements. Total number of concrete elements (Solid 65) is 5088. Each element has 6 degrees of freedom (DOF) therefore the total DOF is 244,200.

Beam bar vertical anchorage after bend is 563mm for all specimens.

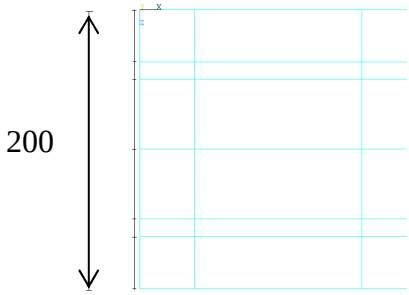

Figure 8.3: The total width of TBCJ is 200mm and is divided into six elements .

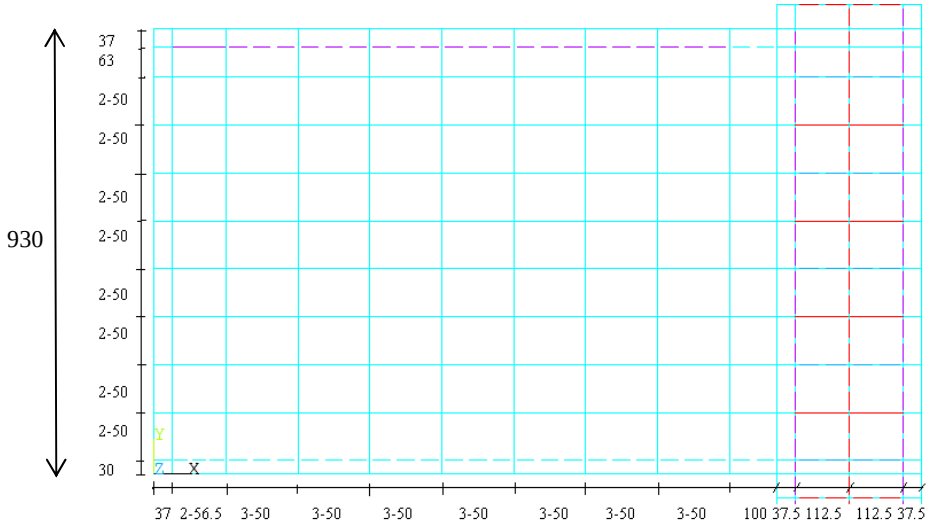

Figure 8.4: **The beam length (1300mm) plus column depth (300mm) at TBCJ total 1600mm and depth of the beam is 930 mm. The division of elements between beam stirrups , e.g 3-50 means 3 elements of 50mm within 150mm spacing.**

The size and number of the reinforcement elements correspond to their surrounding concrete elements.

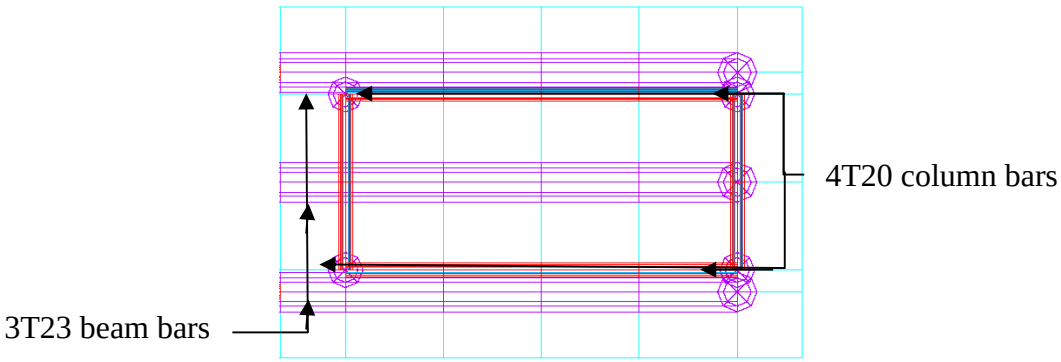

Figure 8.5: Column section at T-NSC1 & T-HSC1 (no CVB) just above the beam bar showing 4T20 column reinforcements and 3 T23 beam bars in horizontal view. The beam is anchored to BCJ.

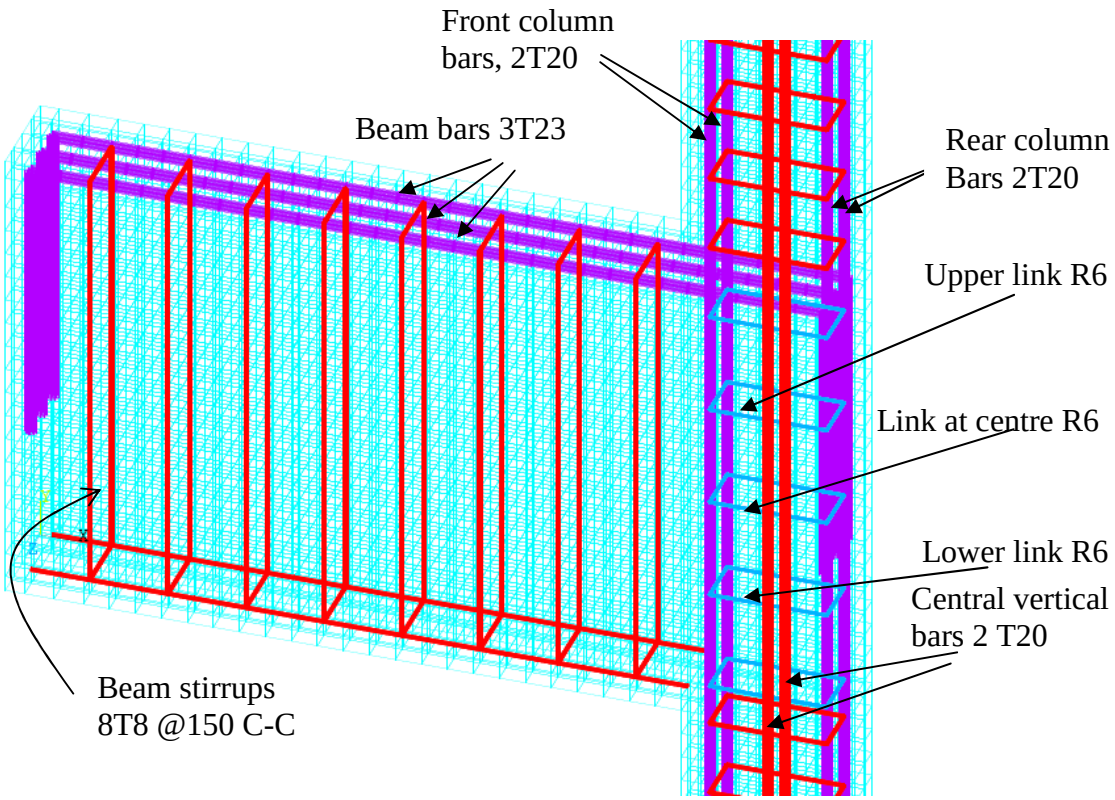

Figure 8.6: Specimens T-NSC3 and T-HSC3, in addition to the column and beam reinforcement, have 2T-20 placed at half the depth of the column as CVB. The strain in the above identified reinforcement is analysed in detail and graphs are produced for the variation of strain along the shown reinforcement in the following sections.

The beam bars are 3-T23 which are equivalent to 4-T20 (design details in Appendix B). It was assumed that this reinforcement would be sufficient to yield at joint shear failure.

A TBCJ was designed and details given in Appendix B. It has been noted that the beam required 4-T20 reinforcement bars at the top. However, this would have caused a complex FE meshing problem for the model, so these 4-T20 were changed to an equivalent total cross-sectional area of reinforcement which of 3-T23.3 diameter bars, giving a more appropriate FE element size and better FE meshing for more accurate analysis. Lower reinforcements are 2-T8 and beam shear reinforcements are 8T8 at 150 C-C.

TBCJ shear reinforcements are 5 R6 at 200 C-C, chosen as being the same shear reinforcement used in the analogous beams tested experimentally, Table 3-4..

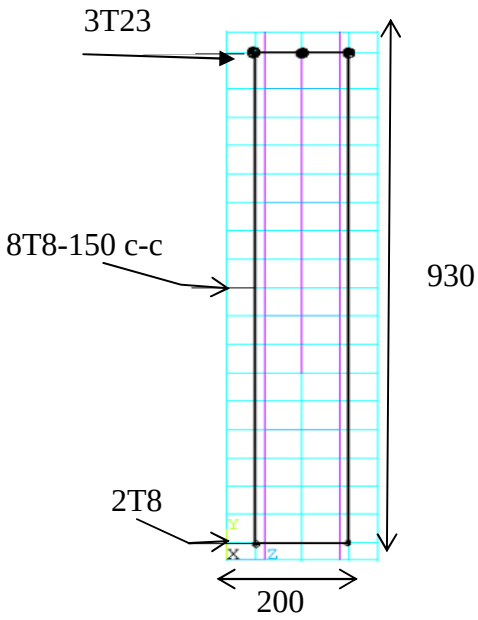

Figure 8.7: **Beam cross section.**

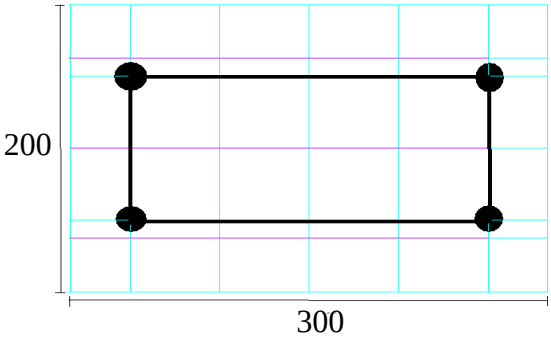

Figure 8.8: Column with 4T20 and no CVB

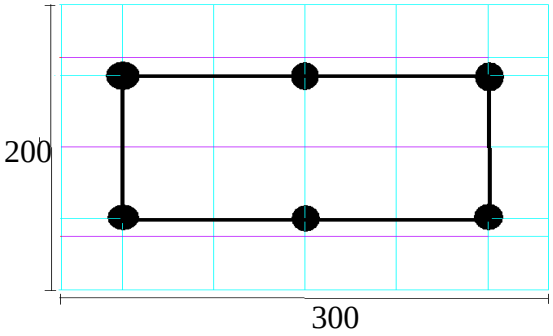

Figure 8.9: Column with 4T20 and 2T20 CVB

8.7 Influence of HSC and CVB on the load bearing capacity of TBCJ

The TBCJ models were set up as shown in Figure 8.10 **and loading was applied at 10 kN increment starting from 60 kN. The following results were obtained:**

1.	T-NSC1	no CVB concrete strength is 42 MPa	failed at 220 kN
2.	T-HSC1	no CVB concrete strength is 110 MPa	failed at 260 kN
3.	T-NSC3	with CVB	failed at 260 kN
4.	T-HSC3	with CVB	failed at 340 kN

Increase in strength of concrete from 42 MPa to 110 MPa, or 175%, resulted in improvement in load bearing capacity from 220 kN to 260 kN, or 18%.

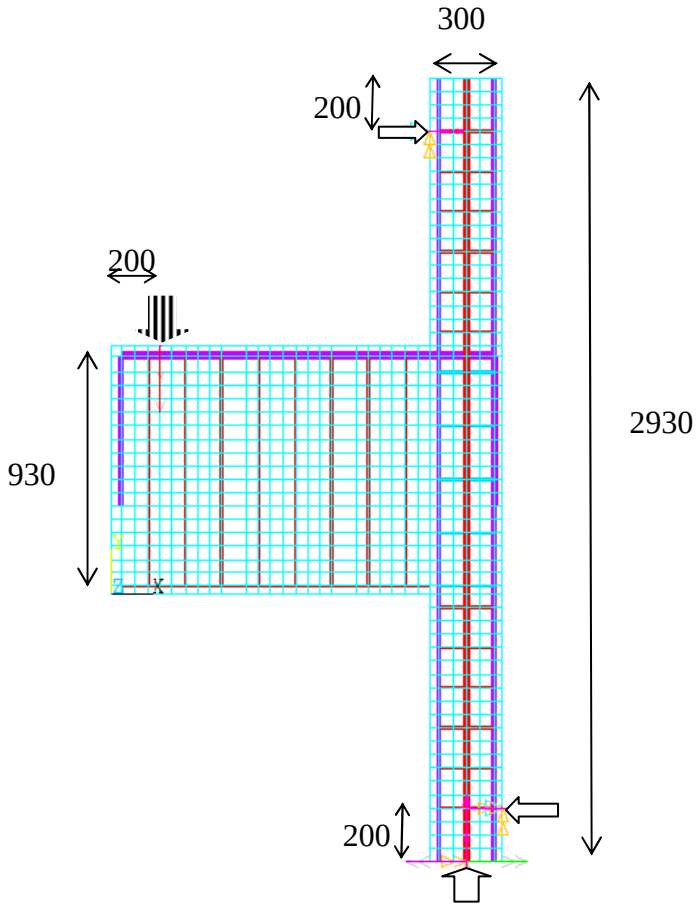

Figure 8.10: Position of the applied load, reactions and constraints of TBCJ with CVB. Figure 8.2 shows same elevation without CVB.

When CVB is added, the load bearing capacity of T-NSC1 increases from 220 to 260 kN in T-NSC3 or 18%. The greatest increase occurs when the concrete strength is increased to HSC and CVB is present in T-HSC3 when load bearing capacity increases from 260kN for T-HSC1 to 340 kN for T-HSC3 or an improvement of 31% .

8.8 Crack development

The distribution of cracks is more widespread on the T-NSC3 specimen . This widespread distribution of cracks in NSC results in premature mobilisation of dowel cracks along the CVB for NSC compared to HSC, therefore less lateral strain on the CVB in HSC compared to NSC.

In the final section of this chapter the moments about z axis on CVB will be determined as these moments are higher in NSC which results in early formation of cracks in T-NSC3 as compared to T-HSC3.

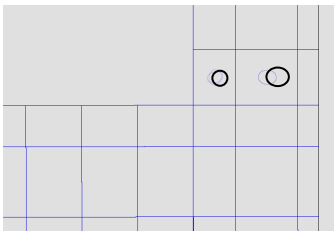

Figure 8.11: In T-NSC1 the first crack appears in the two elements in the column just above the opening corner. The circle indicates the crack and the octagon represents crash

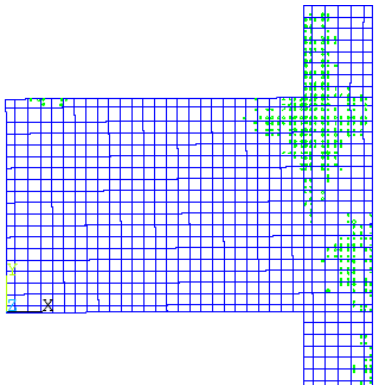

Figure 8.12: At 140 kN cracks appear near the opening corner and on the column rear of the closing corner.

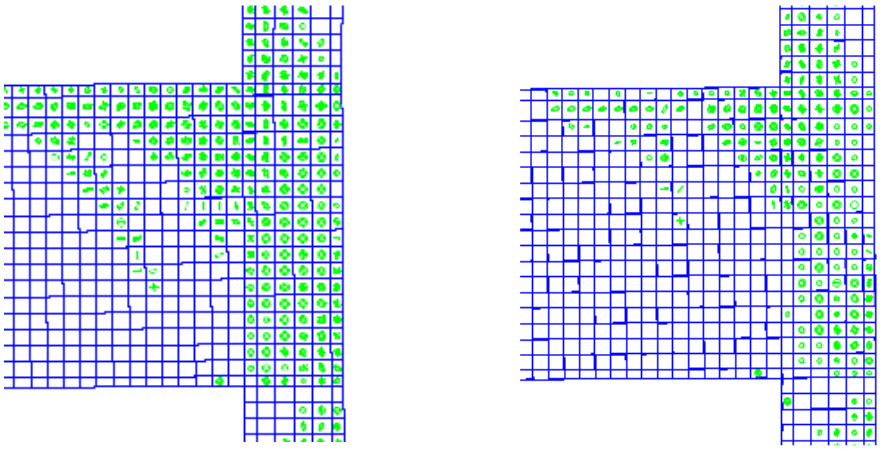

a) T-NSC3 **:** 200 kN b) T-HSC3 : 200 kN

Figure 8.13: Comparing the amount cracks produced on T-NSC3 and T-HSC3 at 200 kN .

8.9 Deflection of models

Deflection is measured at the loading point level at the end of the beam and it was assumed relationship between load and deflection are approximately linear as shown in Figure 8.14.

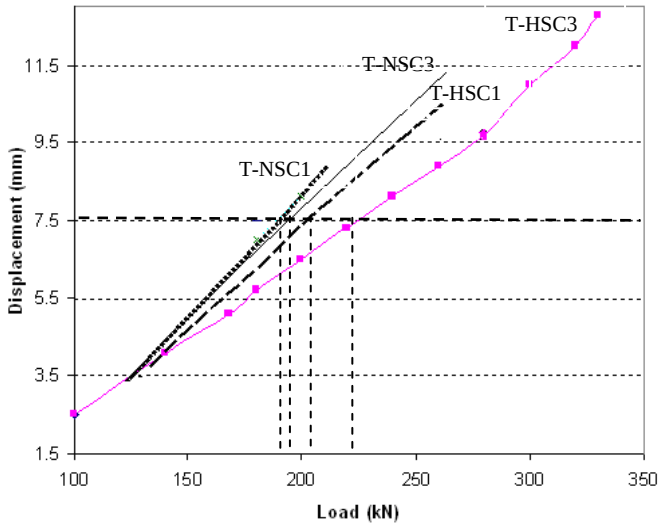

Figure 8.14: Displacement of end beam

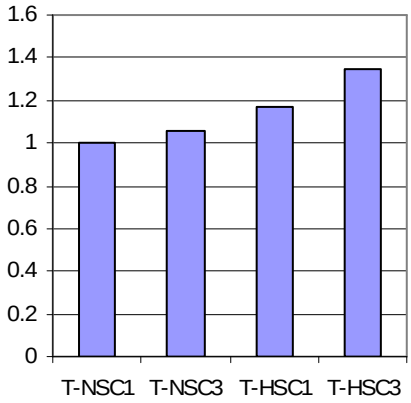

Figure 8.15: Deflection Comparison

Specimens	T-NSC1	T-NSC3	T-HSC1	T-HSC3
Load (kN)	210	250	250	330
Deflection (mm)	9	11.5	10	13

Table 8.5: Ultimate deflection at 10 kN before failure load

	Loading at 7.5 mm deflection			
Specimens	T-NSC1	T-NSC3	T-HSC1	T-HSC3
Load (kN)	178	188	208	241
Specimen/ T-NSC1	1	1.06	1.17	1.35

Table 8.6: Comparison of loading corresponding to 7.5mm deflection

Table 8.6 shows the load required on each specimen to produce 7.5mm deflection. The table compares the increase in deflection due to concrete strength and presence of CVB. The following conclusion for deformation of the specimen is concluded:

- T-NSC3 has added CVB compared to T-NSC1 but material property is the same resulting in reduction of deflection by 6%

- T-HSC1 has no added CVB compared to T-NSC1 but its material property is improved from NSC to HSC resulting in reduction of deflection by 17%
- T-HSC3 has added CVB and has improved concrete strength compared to T-NSC1 resulting in reduction of deflection by 35% .

8.10 Analysis of the strain development in the reinforcement

In this section a rigorous investigation on the stain development along critical length of the reinforcement cage of the TBCJ is carried out at incremental loading up to failure in order to demonstrate the influence of CVB and HSC in TBCJ.

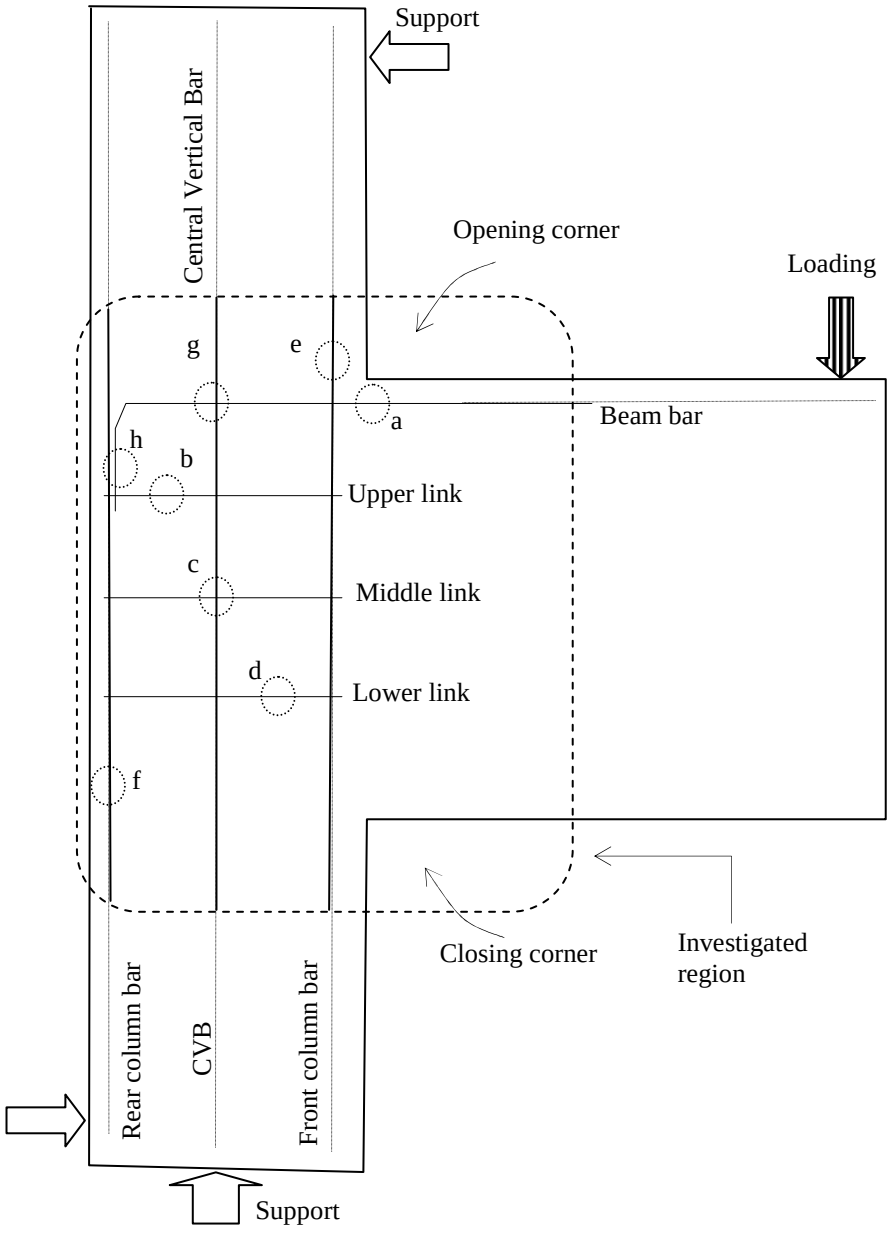

Figure 8.16: Key diagram for TBCJ showing critical locations of maximum strain on the reinforcement

The investigation into strain development is focused on locations shown along the reinforcements detailed in Figure 8.16. The location and the length of each reinforcement under investigation is shown in Figure 8.17 and Figure 8.18**.**

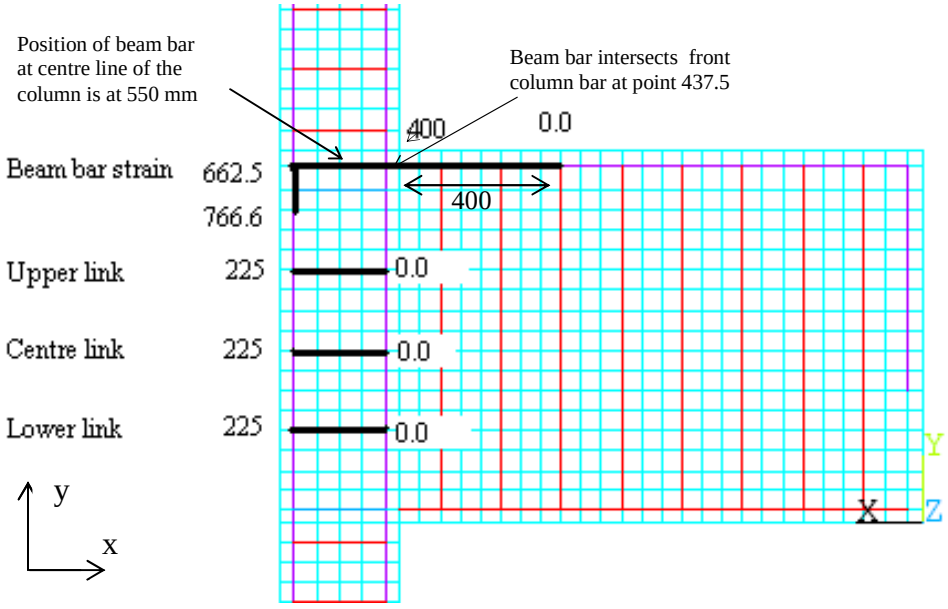

Figure 8.17: TBCJ with positions of strains investigated. The strain of the beam L shaped bar is measured at a point 400mm away from the face of column. TBCJ link strains investigated for 3 links as shown.

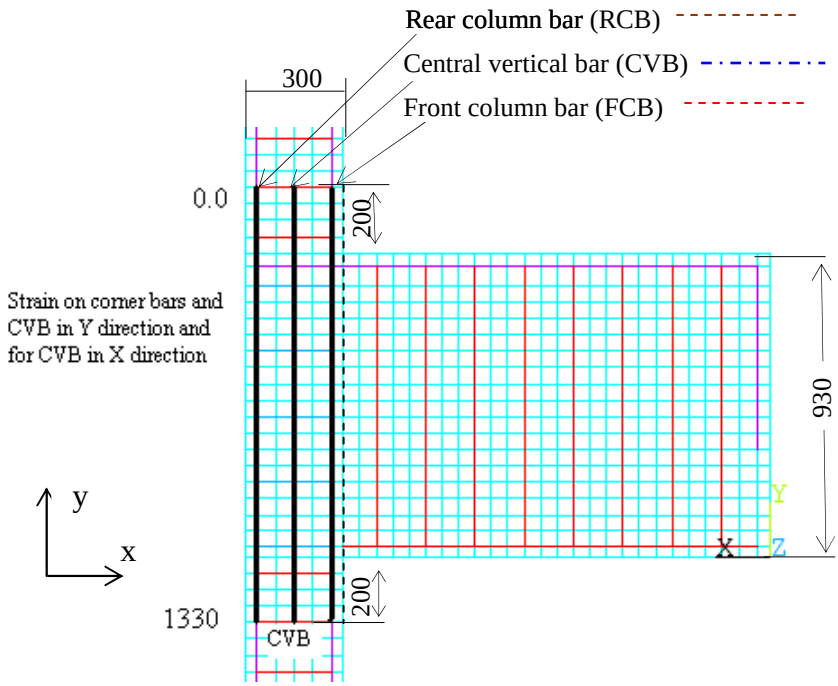

Figure 8.18: Position of strain merged in Y direction along the critical part of the column bar starting at point 0.0 which is 200mm above the top of the beam in front column bar (beam side).

8.10.1 Strain along the L shaped beam bar

The position of beam bar in TBCJ considered in the discussion is shown in Figure **8.17**. The total length of this section is 766.6 mm which is considered as the critical location of interest where strain in the beam bar develops to its maximum.

The radius of bend is not included in the beam bar length as past research [8-2] has suggested that the radius of bend does not play a dominant role in determining the ultimate joint behaviour in BCJ. However, this is an assumption to simplify FE modelling, in practice the minimum radius of bend must be minimum as shown in Table 6-1.

The maximum strain in the beam bars of the four specimens are investigated from graphs starting from Table 8.7, comparing strain in NSC and HSC models, T-NSC1 and T-HSC1, in a horizontal (X) direction for beam reinforcement.

When the applied load is increased to 200 kN, the maximum strain in NSC is 0.0023 and occurs at the opening corner, but in HSC the maximum strain is greater than 0.0028 and occurs at the bent corner of bar, Figure 8.19a, which is 22% greater than NSC.

With T-NSC1 compared to T-HSC1at 200 kN, strain on the beam bar for T-HSC1 at the point of entering the column increases by 8% and its bent reinforcement (f_y=720) reaches 87% of its yield. The strain on the tail part part of anchorage 0.0014, Figure 8.19b. The strain at tail for T-NSC1 at 200 kN, just before failue is 61% of strain in lead. This compares well with BCJ1 which had 62% and BCJ4 57%, Table 5-4.

At 210 kN load, before failure at 220 kN T-NSC1 with 10 kN (5% increase in loading), the strain on the tail anchorage increases from 0.0014 to 0.0026 (86% increase), Figure 8.19a.

At 210 kN, T-NSC1 fails as a result of the strain in the vertical tail anchorage part of the beam bar, whereas in T-HSC1 at 220 kN strain concentration is as the bend yields, Figure 8.19d.

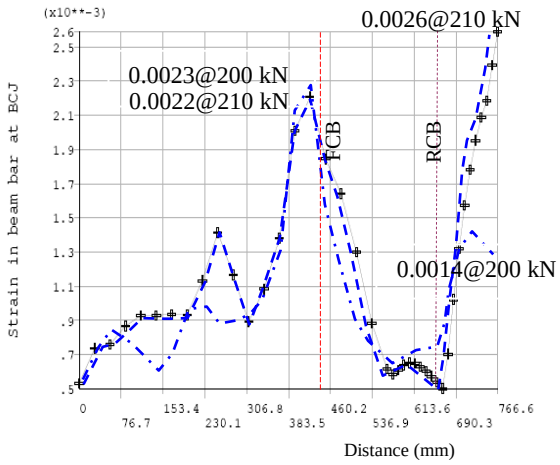

a) T-NSC1 strain at 200 &210 kN

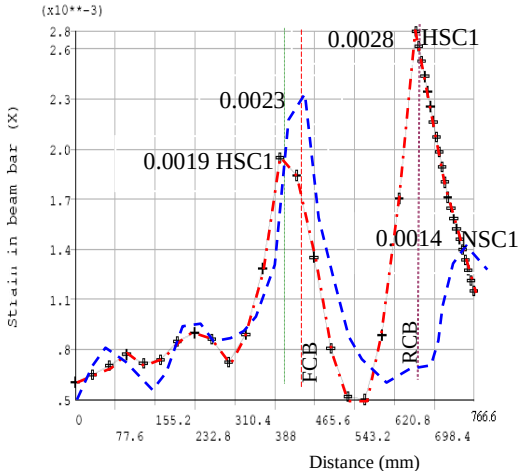

b) T-NSC1& HSC1 strain at 200 kN

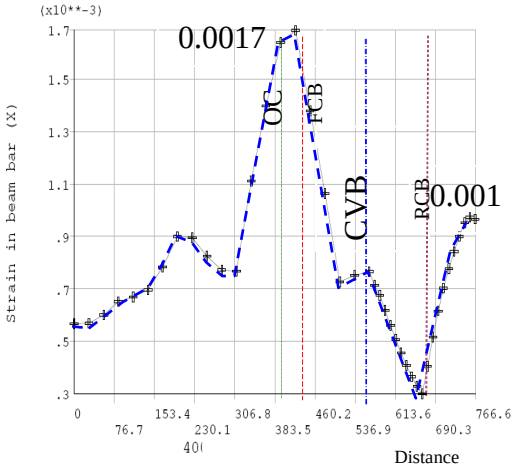

c) T-NSC3 with CVB is strain at 200 kN

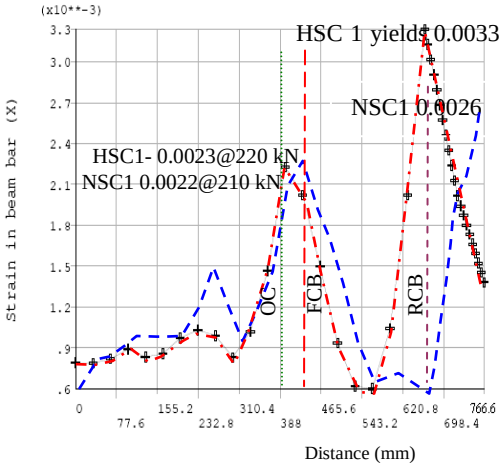

d) T-HSC1 strain at 220 kN & T-NSC1 strain at 210 kN.

Figure 8.19: Comparison of strain in beam bar

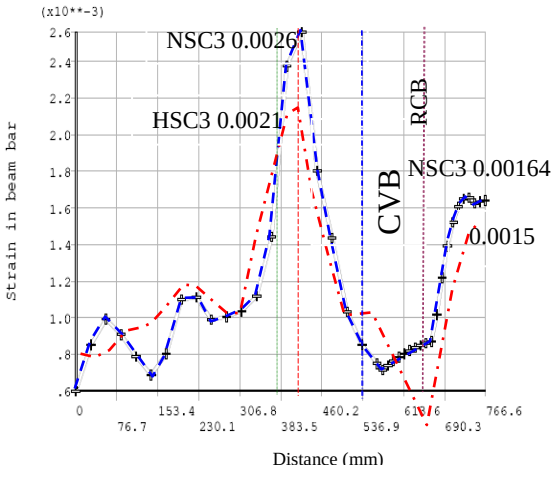

Figure 8.20: T-NSC3& HSC3 Strain at 240 kN

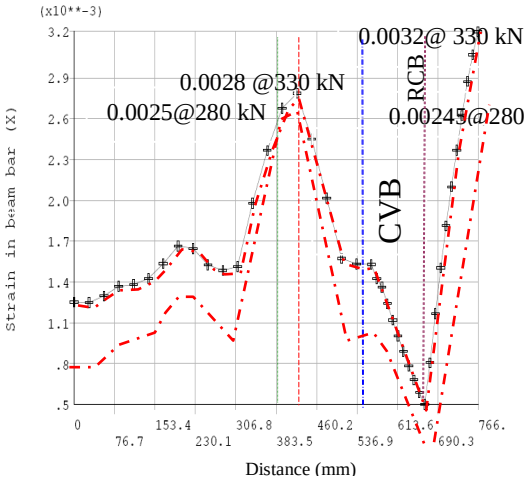

Figure 8.21: T-HSC3 up to 330 kN.

A comparison of beam bar strain in T-NSC3 and T-HSC3 at 240 kN load, Figure 8.20, shows that the position of maximum strain is the point at opening corner for both cases with HSC3 strained to 0.0021 and NSC3 to 0.0026, a reduction in strain of 24% due to the material property. At 240 kN, strain in tail for T-NSC3, and T-HSC3 are 63% and 75% of strain in lead, Figure 8.20.

In beam reinforcement in T-HSC3, Figure 8.21, up to 280 kN strain is the maximum at opening corner at 0.0025, which changes to 0.0028 as load increases to 330 kN. The maximum strain is 0.0032 at the tail anchorage just before failure.

For T-NSC3 at failure, the strain in the region near the opening corner reaches 0.0026 whereas at the end of anchorage bar it reaches 0.0016, Figure 8.20. Therefore, the introduction of CVB in NSC results in increasing strain at the opening corner by 13% and a reduction in strain at anchorage tail of 42%, Figure 8.20.

The presence of CVB in HSC results in a significant drop in strain at the bent corner of the bar. The concentrated strain in the bent reached 0.0033 in HSC specimens without CVB at 220kN load, Figure 8.19d, however, the presence of CVB ensured that strain at bent corner does not increase more than the very small and insignificant figure of 0.0005. Presence of CVB in HSC reverses the situation in the anchorage by by bringing the tail to yield of 0.0032.

	Beam bar strain without CVB (10^{-3})				Beam bar strain with CVB (10^{-3})			
Load	Opening corner		Anchorage		Opening corner		Anchorage	
(kN)	HSC1	NSC1	HSC1	NSC1	HSC3	NSC3	HSC3	NSC3
140	0.99	1.4	0.81	0.63	1.2	1.5	0.5	0.9
168						1.9		1
200	2.0	2.3	2.8	1.4	1.7		1	
210		2.3		2.6				
220	2.3		3.3					
240					2.1	2.6	1.5	1.65
260					2.3		1.9	
280					2.5		2.5	
320					2.85		3.1	
330					2.85		3.2	

Table 8.7: The results from graphs for TBCJ. Load against strain in the beam reinforcement indicates maximum strain fluctuation at opening corner and anchorage. NB: Anchorage failure for HSC1 is at the bent corner as compared to HSC3 which occurs at the end of the anchorage bar and not the corner.

For specimen without CVB, HSC has 40 kN or 18.2% higher load bearing capacity than NSC, but as Figure 8.22b shows, HSC specimens have a higher ratio of strain in bent at anchorage to strain in opening corner compared to NSC, Figure 8.22a, which is not a desired characteristic as this shows that the T-HSC1 failure occurs at the bend and is less ductile than T-NSC1. This situation reverses when CVB is present in HSC, Figure 8.21, when the strain on the bend is reduced and the beam bar and the tail are strained at 0.0025 and 0.0024 up to 280 kN, and just before failure at 330 kN the strain in tail reaches 0.0032 when beam bar strain is 0.0028 and failure occurs due to slippage at the tail.

For NSC at equal loading of 200 kN, comparing Figure 8.19(a&c), at opening corner (OC), CVB reduces the strain on the bar from 0.0023 to 0.0017 or by 29%, and reduces the strain on the tail of the anchorage from 0.0014 to 0.001 or by 40%.

The influence of CVB in NSC significantly reduces the strain on the anchorage as loading passes 200 kN. T-NSC3 at 240 kN has beam bar strain of 0.0026 at opening corner, with strain at tail of 0.0006, Figure 8.20, whereas at 210 kN has beam bar strain 0.0022 at opening corner, with strain at tail of 0.0026, Figure 8.19a.

For T-NSC1, the gradient for increase in strain with loading is a ratio of 1.6 micro strain to 100 kN, whereas this is reduced to 1 micro strain to 100 kN loading when CVB is present, demonstrating that the presence of CVB in NSC reduces the possibility of tail anchorage failure.

When CVB is present in TBCJ- HSC3, the failure occurs at the end of the anchorage bar as compared to failure of T-HSC1 with no CVB which occurs at the bent corner of the anchorage which is more critical.

The highest improvement in joint shear resistance occurs with T-HSC3 when HSC and CVB are present. The failure load of T-HSC3, with CVB reaches 340 kN as compared to T-HSC1, without CVB, which failed at 250 kN. This improvement of 36% was achieved due to the contribution of CVB to HSC.

The strain on the beam bar at failure for HSC specimen just before failure, 330kN, at the tail, yield at 0.0033 when CVB is present, and at the opening corner it is 0.0028. Figure 8.21

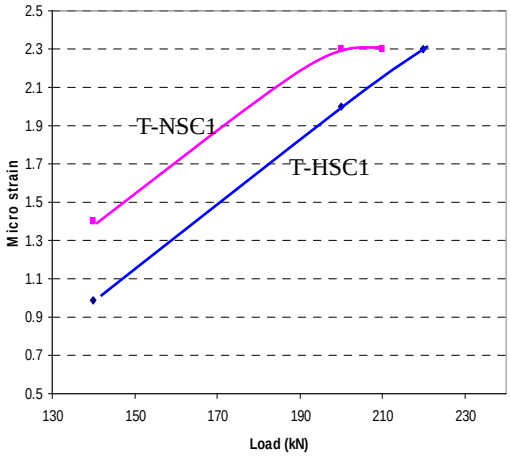

a) Beam bar strain for T-NSC1 & HSC1 without CVB at opening corner

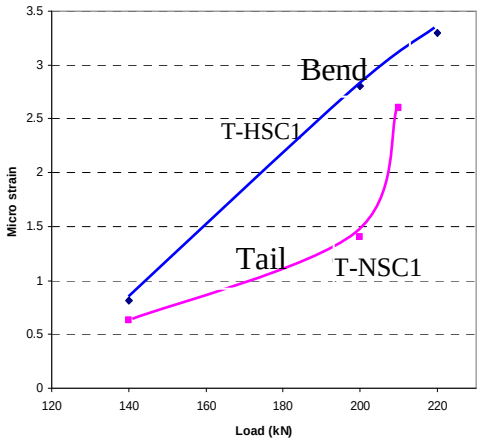

b) Beam bar strain for T-NSC1 & HSC1 without CVB. NB: HSC1 maximum at the bent whereas NSC maximum at tail

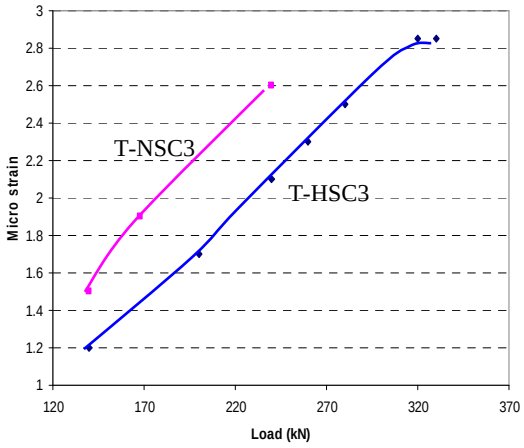

c) Beam bar strain for T-NSC3 & HSC3 with added CVB at opening corner

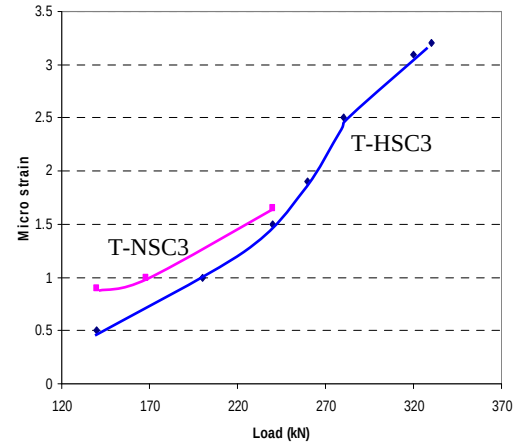

d) Beam bar strain for T-NSC3 & HSC3. NB: HSC3 fails at the at tail of the anchorage bar and not at bent corner

Figure 8.22: The graphs obtained from Table 8.7 on comparison of strain development on beam bar for TBCJ made with NSC and HSC with or without CVB at maximum strain locations of opening corner and anchorage.

When CVB is present in NSC, at 240 kN, before failure load of 260 kN, the strain in the beam bar is 0.0026 and the strain in anchorage is reduced to 0.00164. Again, the presence of CVB in NSC reduces strain on the anchorage and allows the beam bar to develop higher

strain.

Similarly, in HSC models without CVB, at 220 kN, the maximum strain in beam bar at the opening corner is 0.0023 and at the bent is 0.0033, Figure 8.19d. When CVB is present in HSC, at 240 kN, the strain in the beam bar at the opening corner is 0.0021 and the strain in the tail is 0.0015. As before, this indicates that the presence of CVB in HSC significantly reduces strain on the anchorage bend and allows the beam bar to develop higher strain at the opening corner until failure at the tail of the anchorage.

Observation of the strains results of L beam bar are as follow:

A. Comparison between NSC and HSC in TBCJ

NSC:

- Maximum strain develops at the opening corner at early stages of loading up to 200 kN, but at 210 kN it occurs at tail of anchorage, Figure 8.19a.
- Strain reaches 0.0026 for NSC at tail of anchorage which is below yield (0.0036) at 210 kN, Figure 8.19a.

HSC:

- Maximum strain at opening corner is lower than in the NSC model. However, higher strain almost reaching yielding load occurs at bent corner of anchorage, leading to brittle and sudden failure. The bent corner is strained at 0.0033 at 220 kN, Figure 8.19b. This could also be due to delay in crack development at the opening corner.

B. Comparison of influence of CVB on the behaviour of NSC and HSC of TBCJ

NSC + CVB (T-NSC3)

- Loading capacity of the BCJ increases by 18%.
- Maximum strain develops at the opening corner at 0.0026 (yielding occurs at 0.0038).
- Pull out occurs at the anchorage end due to strain of 0.0016 which is 62.5% less compared to when there is no CVB. Presence of CVB results in more ductile failure.

HSC + CVB (T-HSC3)

- Increase in load bearing capacity from 260 to 340 kN.

- Prevents failure at the bent corner and delays pull out of lead anchorage until after 280 kN loading. At 280 kN, strain in opening corner is higher than strain at the end of anchorage. The failure from pull out of anchorage occurs at 330 kN.
- More ductility to the structural frame, higher possibility of forming plastic hinge at beam near opening corner, because at failure the beam bar at opening corner strain is 0.0028 compared to 0.0023 when CVB is absent.

8.10.2 Strain in the upper shear link in TBCJ

The strain along the length of the upper link in horizontal (X) direction is investigated, see location of upper link in Figure 8.17. The fluctuation of strains corresponding to incremental loading according to the development of strain along the length of the leg of stirrup which is 225mm long, is also investigated.

T-NSC 1

i. Yielding develops in the link as early as 140 kN loading, Figure 8.23a.
ii. Position of maximum strain occurs initially at centre of the link for T-NSC1,
iii. Figure 8.23 c, but by increasing the load to 200kN, the position will be at 50mm on the length of the link from the rear of the column bar.
iv. Position of the maxima indicates that the centre of the link, where the experimental strain gauges are located, does not experience the greatest strain values at higher loads.
v. Maximum strain at failure is 0.0027 and the load is 220 kN. This value is 2.16 times the yield strain.
vi. Maximum strain increases from 0.0013 to 0.0027 due to increase of loading from 140 kN to 220 kN. This indicates 100% increase in strain as the result of the 57% increase in loading.

T-HSC 1

i. No yielding takes place until the loading is equal and greater than 200 kN.
ii. Maximum strain occurs at 50mm on the length of the link from the rear of the column bar from lower loading up to failure, Figure 8.23a.
iii. Maximum strain at failure is 0.0036 and the load is 250 kN, which is 2.88 times the yield strain, Figure 8.24b.

iv. Maximum strain increases from 0.001 at 140 kN to 0.0036 at 250 kN, 3 times the yield value just before failure. However, it does not reach its yield until 168 kN loading.

v. This indicates 260% increase in strain as a result of 79% increase in loading.

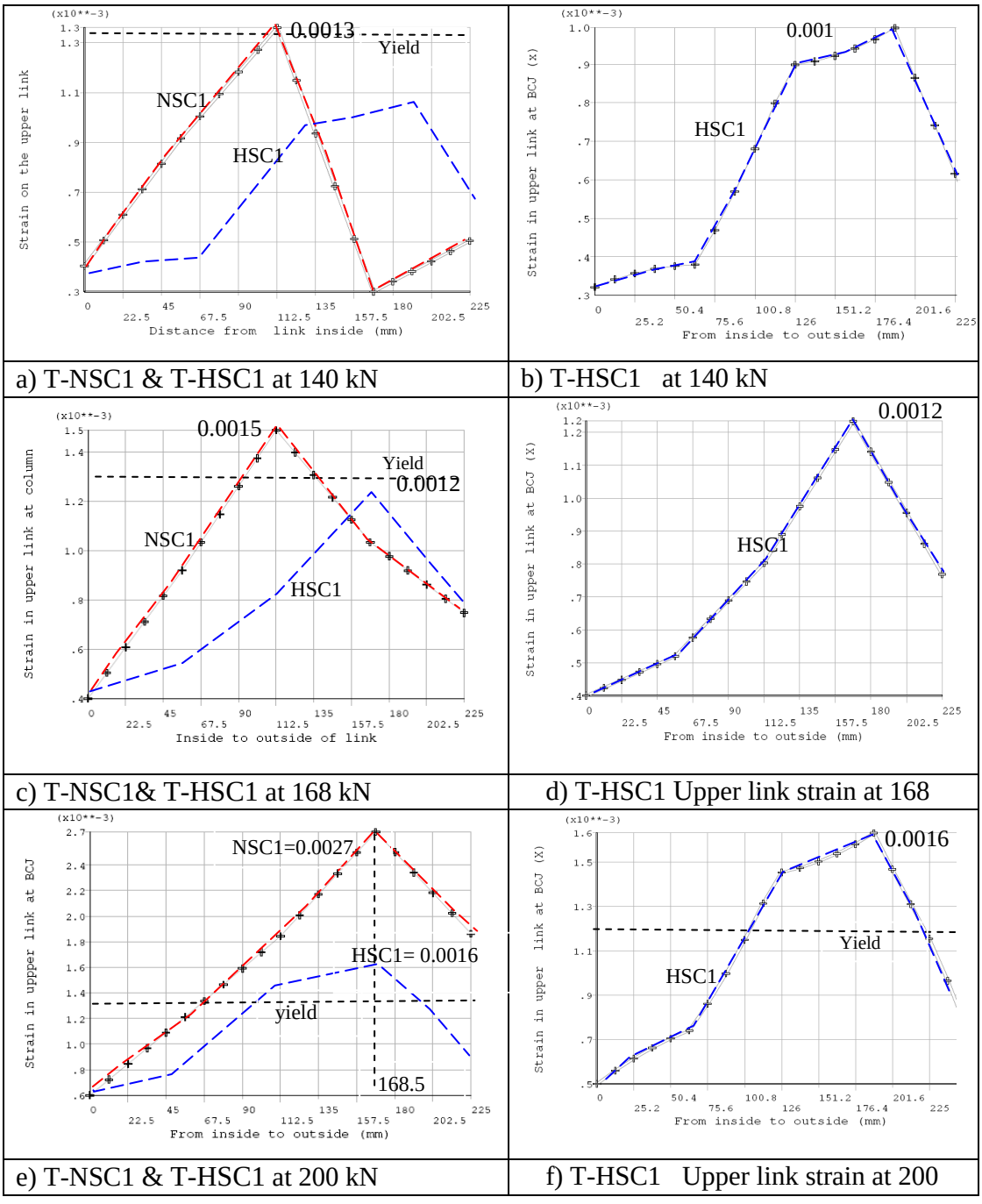

Figure 8.23: Upper link strain T-NSC1& HSC1 just before failure of T-NSC1 at 220kN.

From the above it can be concluded that, in the upper shear link, HSC1 experienced 160% more shear strain and 14% more loading capacity to failure compared to NSC1.

Figure 8.24 shows that generally HSC reduces the magnitude of the strain at the centre by 25%.

NSC + CVB (T-NSC3)

i. Yielding occurs as early as 140 kN loading.
ii. Maximum strain occurs at 50mm on the length of the link from the rear of the column bar from lower loading, all the way up to the failure load..
iii. Maximum strain at 240 kN (just before load failure of 250 kN) is 0.0027. This is 2.16 times the yield strain of the link and it is exactly the same as for the NSC1 model, which indicates that CVB did not change the amount of the maximum strains in the link and resisted the additional shear load of 30 kN on its own
iv. Maximum strain increases from 0.0014 to 0.0027 due to increase of loading from 140 to 240 kN. This is a 93% increase in strain due to 71% increase in loading.

	Maximum strain		**Maximum strain from end (mm)**		**Strain at ends**	
Load (kN)	**NSC (10^{-3})**	**HSC (10^{-3})**	**NSC**	**HSC**	**HSC (10^{-3})**	**NSC (10^{3})**
140	1.3	0.94	112.5	169	0.3	0.4
168	1.5	1.2	112.5	169	0.75	0.8
200	2.3	1.6	169	169	0.95	0.55
240		3.0		169	2.0	
250		3.6		169	2.6	

Table 8.8: Maximum strain within the leg of the upper link for T-NSC1 and T-HSC1

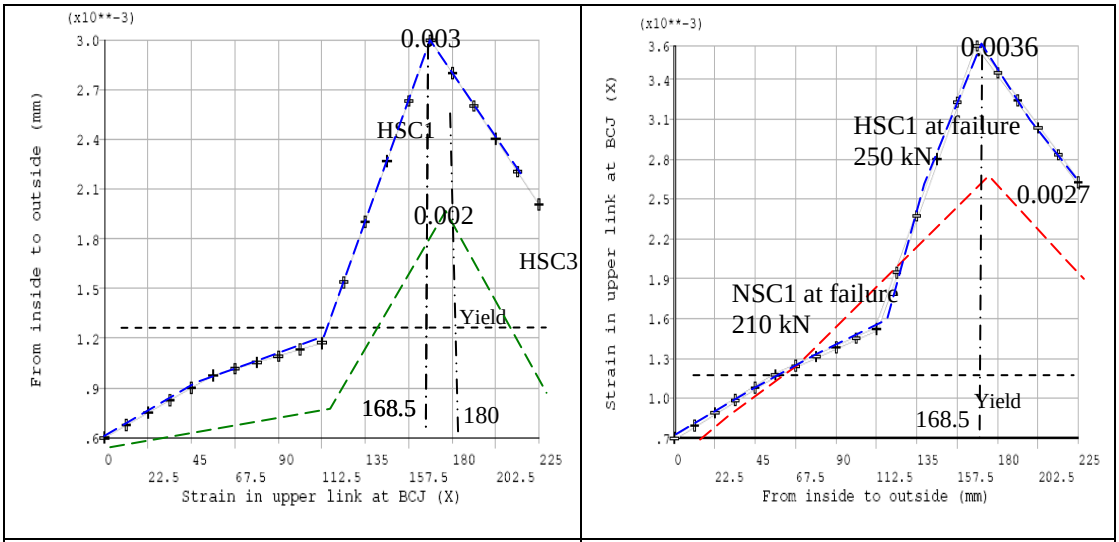

a) At 240 kN, T-HSC1 is compared to T-HSC3

b) Comparison of NSC1, 210kN & HSC1, 250 kN before failure load

Figure 8.24: Development of strain in upper link of T-HSC1 up to failure load 260 kN. Position of maximum strain is point b, Figure 8.16

HSC + CVB (T-HSC3)

i. No yielding takes place until 200 kN loading.

ii. Maximum strain always occurs at 36mm on the length of the link from the rear of the column bar from lower loading,

iii. Maximum strain at 330 kN (just before failure of 340 kN) is 0.0034. This value is 2.72 times the yield strain of the link.

iv. Maximum strain increased from 0.0011 to 0.0034 due to increase in loading from 140 to 330 kN. This 209% increase in strain is due to 136% increase in loading.

Comparing the behaviour of the upper links in NSC3 and HSC3 it can be concluded that the maximum shear strain developed in the link of HSC3 model is 125% greater than that developed in NSC3. Also maximum loading capacity of the model of HSC3 increased by 93% compared to that of NSC3.

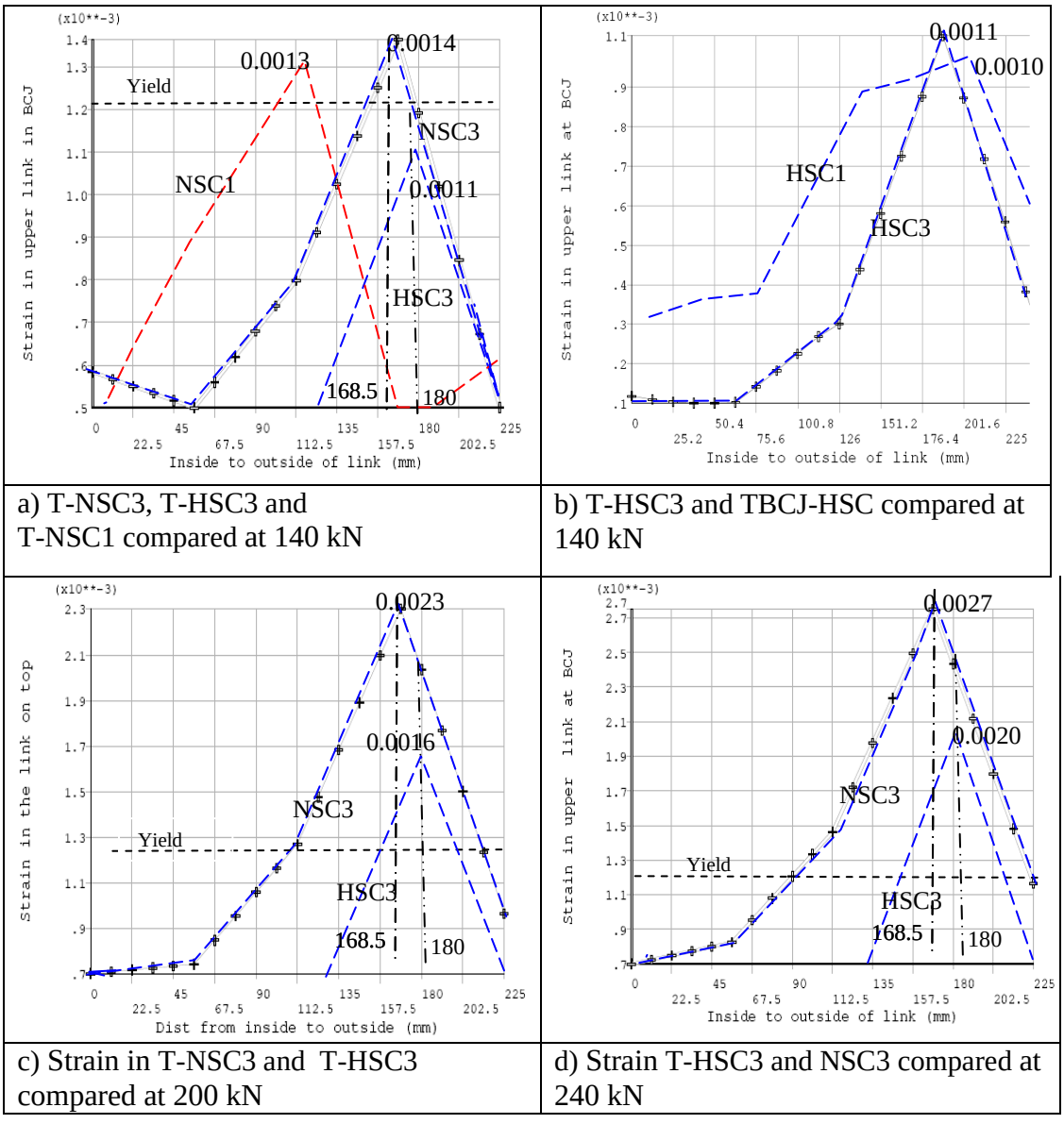

a) T-NSC3, T-HSC3 and T-NSC1 compared at 140 kN

b) T-HSC3 and TBCJ-HSC compared at 140 kN

c) Strain in T-NSC3 and T-HSC3 compared at 200 kN

d) Strain T-HSC3 and NSC3 compared at 240 kN

Figure 8.25: Comparison of strain in upper link of T-NSC3 & T-HSC3 before failure of T-NSC3 at 250 kN. Position of maximum strain is shown as point b in Figure 8.16.

Summary of influence of HSC material on the behaviour of upper shear link

i. Considering T-NSC3 and T-HSC3 indicates that HSC3 reduced the strain/unit load developed in the link by 22% without CVB and 39.8% with CVB.

ii. Consideration of NSC1 & HSC1 indicates that HSC increases the strain per unit load in the link by +12% for model with no CVB.

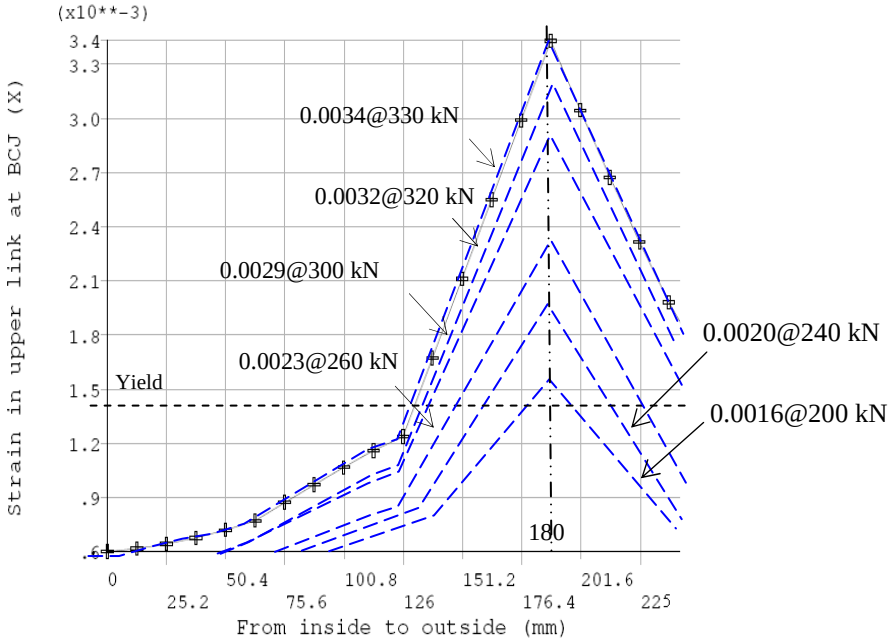

Figure 8.26: Strain in the upper link for T-HSC3 up to failure load of 340 kN. Position of maximum strain is point b, Figure 8.16

Load (kN)	Strain NSC Maximum (10^{-3})	Strain HSC Maximum (10^{-3})	Strain end of HSC (10^{-3})	Strain end of NSC (10^{3})	Fig No	NSC	HSC
140	1.4	1.1	0.6	0.22	8.25	a	b
200	2.3	1.6	0.95	0.55		c	d
240	2.7	2	1.15	0.6		e	f
260		2.3		0.8	8.26	a	b
280		2.7		1.1		c	d
300		2.9		1.4	8.26		b
320		3.2		1.45		c	
330		3.4		1.7			d

Table 8.9: Maximum strains in upper link and at the end in T-NSC3 & T-HSC3 .

	Initial strain at 140 kN (a)	Max failure load (just) kN (b)	Distance of Max strain from rear column bar mm (c)	Max strain at failure (d)	% increase in strain (d-a)/a	Strain/ unit load 10^{-6} N (a/b)
T-NSC1	.0013	210	50	.0027	108%	12.9
T-HSC1	.0010	250	50	.0036	260%	14.4
T-NSC3	.0014	240	50	.0027	93%	11.25
T-HSC3	.0011	330	36	.0034	210%	10.3

Table 8.10: Conclusive data from strain recordings at upper link

Summary of influences of CVB on the behaviour of upper shear link

i. CVB does not significantly influence the magnitude of strains developed in the link, neither at the initial loading of 140 kN nor at failure load for both NSC and HSC models.

ii. CVB caused the reduction of strain per unit load: 16% for NSC and 40% for HSC. This indicates that CVB increased the confinement and shear resistance of the BCJ which resulted less strain per unit load on the link. Therefore, it can be concluded that CVB is more effective in HSC structures.

iii. In HSC with CVB, the position of maximum strain is at 36mm from the rear column bar as compared to 50mm for all other models.

Summary of strain-load relationship for upper shear link

For models without CVB it can be seen that the relationship of strain and applied load on the model is relatively linear for T-NSC1. However, for T-HSC1 the relationship is slightly different as when the load reaches 240 kN there is sudden increase in the strain in the link due to the formation of a crack in the model after the yielding of steel which occurs at 240 kN, Figure 8.24.

Discussion of strain behaviour in the upper shear link

When comparing NSC1 with NSC3 the maximum strain developed in NSC1 in the upper link is 0.0027 at 210 kN, Figure 8.23e**.** However, when analysing a model for a similar joint but with the addition of CVB, i.e. NSC3 model, the maximum strain is the same 0.0027 but the load increases to 240 kN, Figure 8.25d. This is an appreciable 14% increase in loading capacity with constant strain in the link. This additional 14% shear resistance in TBCJ is supported by the CVB.

In Appendix C, strain gauge recordings from experimental tests for beams NSC2, NSC3 and NSC4 with HWB of T12, T20 and T25, and strain gauge readings in stirrups (No 25 & 27) are analogous to the upper link yields when exceeding 200 kN loading . Failure immediately occurs and the presence of HWB does not resist any additional shear forces and shear failure immediately follows at 210 kN.

Similarly, comparing the results in HSC1 and HSC3 it can be noted that the maximum

strain which develops in HSC1 in the upper link is 0.0036 at 250 kN, Figure 8.24b. However, when testing a similar joint in HSC3 model but with the addition of CVB, the maximum strain remains relatively the same at 0.0034 but the load increases to 330 kN, Figure 8.26. This is a 32% increase in loading capacity with relatively the same strain (only 5% difference) in the link.

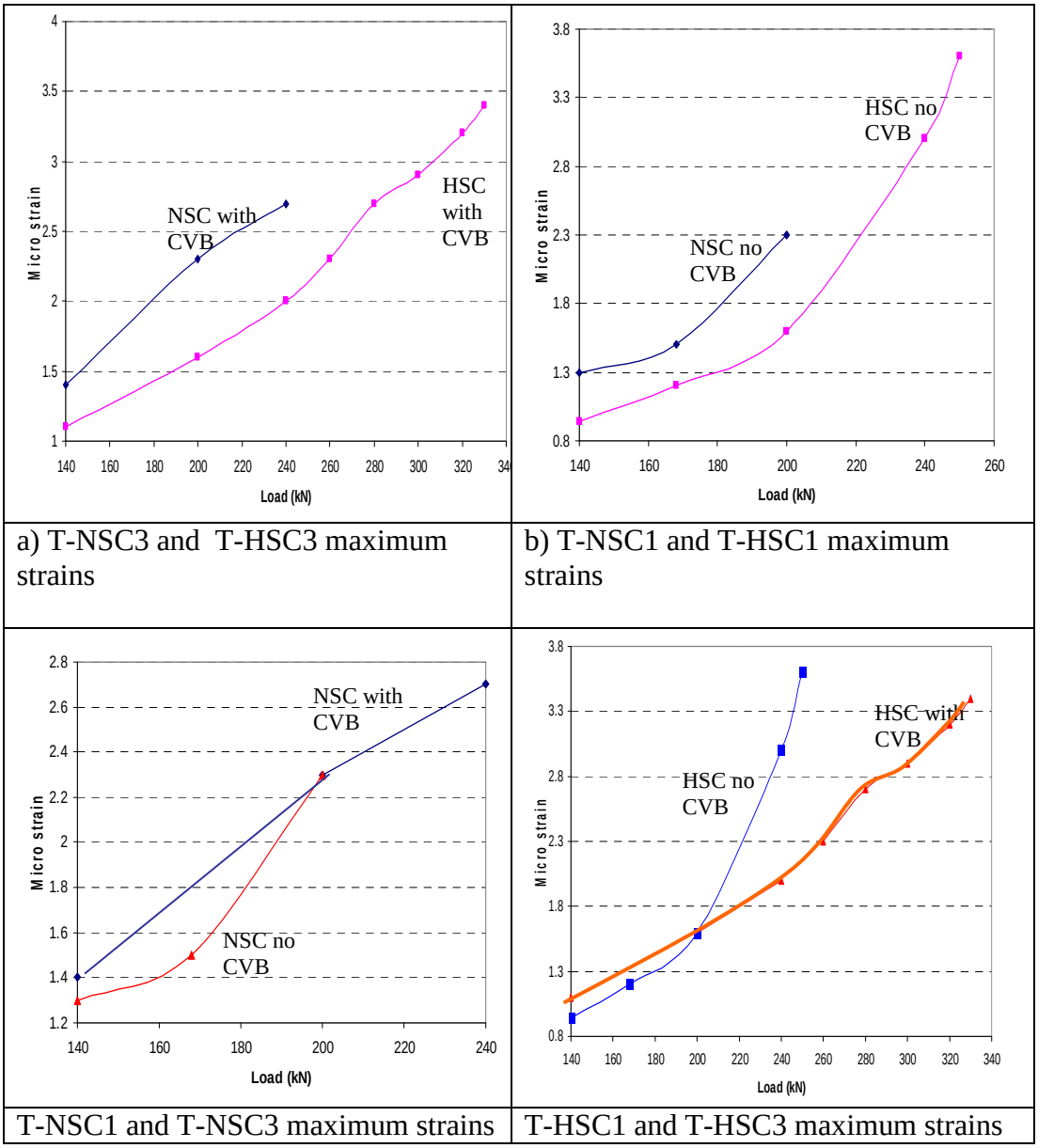

a) T-NSC3 and T-HSC3 maximum strains

b) T-NSC1 and T-HSC1 maximum strains

T-NSC1 and T-NSC3 maximum strains

T-HSC1 and T-HSC3 maximum strains

Figure 8.27: Maximum strain fluctuation in the upper link for all TBCJ models

It can be concluded that CVB has a limited influence on the confinement (14%) in TBCJ-NSC models, however, it has a good influence on the confinement of the HSC joint (32%), in T-HSC models.

This activation of strain within the region of development of the diagonal compression strut in T-NSC3 is due to presence of CVB which improves the load bearing capacity for T-NSC3 to 260 kN, compared to 220 kN for T-NSC1. This increase of 18% in load bearing capacity in NSC is modest compared to 55% for T-HSC3 of failure of 340 kN.

As shown in Appendix C, from strain gauge recording of experimental tests on the analogous HSC beams with HWB (similar to CVB for TBCJ), as loading is increased, when the links exceed their yield cracks are formed, then HWB begins to resist shear forces for the additional loading.

Strain gauge readings in Appendix C show that for beam HSC4 which has HWB of T25, in stirrups (Links no. 25 & 27) analogous to upper link after 260 kN yield beyond 0.01 when all other stirrups also exceed their yield value significantly, but presence of HWB resists shear forces up to failure load of 300 kN.

Discussion on strain developments on the upper shear link

The main cracking developed in NSC and HSC were at 168 kN and 200 kN respectively, Figure 8.23 (c& e), whereas, tensile strength of NSC and HSC are 2.9 and 4.5 MPa respectively, Table 8.1. This means 19% larger cracking load in spite of 55% higher tensile strength for concrete.

CVB resulted in reduction of maximum strain in upper shear link . For 140 kN, maximum strain reduced in NSC and HSC by 8% and 10% respectively, Figure 8.25(a&b) whereas for 200 kN maximum strain reduced in NSC by 17% while HSC strain behaviour does not change. Figure 8.23e and Figure 8.25c.

HSC without CVB has a strain per unit load gradient of 0.014 kN^{-1} compared to with CVB of 0.01 kN^{-1} at loading of 140 kN to 240 kN. This gradient increase for HSC with CVB as load increases from 240 to 320 kN to 0.015 kN^{-1}, from 320 to 330 kN to 0.02. This shows CVB comes to full action at final loading stage, Figure 8.25.

8.10.3 Behaviour of strain at lower link of TBCJ

The strain along the length of the lower link in horizontal (X) direction is investigated. The location of lower link strain from 0.0 point is shown in Figure 8.17**.**

The fluctuation of strains corresponds to incremental loading (according to the development of strain) along the length of the stirrup which is 225mm long, located 700mm below the top of the beam.

Comparison of the strain in lower link for T-NSC1 and T-HSC1

The strain distribution is concentrated at the centre of the links (112.5mm) for T-NSC1, and as the load increases this concentration is transferred to the quarter span point (56.3mm), Figure 8.28, but the strain is almost distributed to the inner half of the column in T-HSC1, for up to 220 kN loading. However, as the load exceeds 240 kN, the strain concentration is at quarter span point (56.3mm) up to failure load . This distribution of strain in the lower link of the TBCJ demonstrates development of a diagonal strut in the zone close to the inner side of the lower link for T-NSC1 & HSC1.

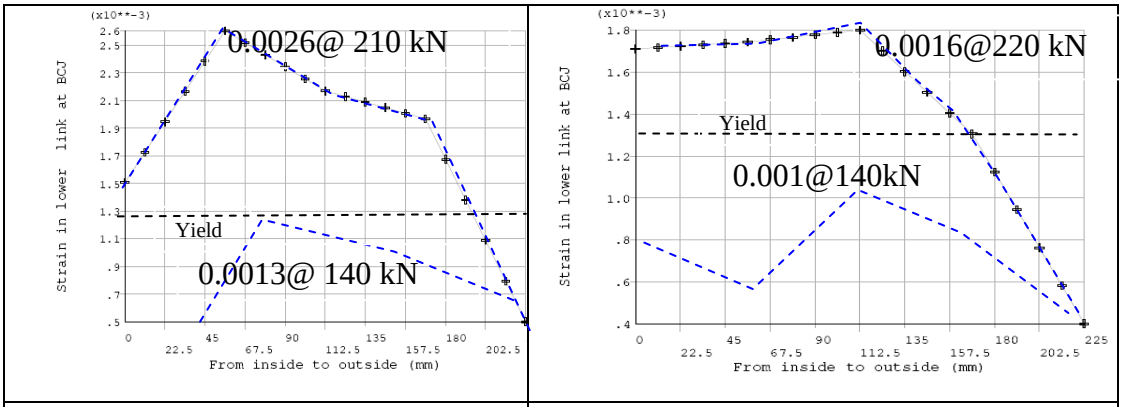

a) T-NSC1 Strain at 140& 210 kN | b) T-HSC1 Strain at 140& 220 kN

Figure 8.28: Comparison of strain at lower link for T-NSC1 and HSC1

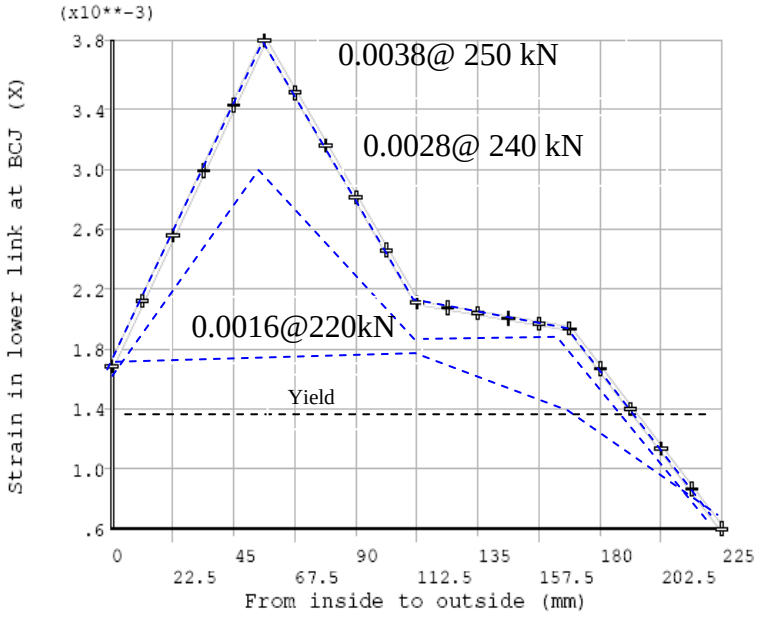

Figure 8.29: T-HSC1 Strain at 250, 240 and 220 kN in lower link

The total maximum strain for all specimens is recorded for corresponding failure loading . This maximum strain is at quarter span of link at 56.3mm from the inner end of the stirrup for both NSC and HSC. At the inner end of the stirrup just before failure of T-NSC1, strain develops to 0.0015 for T-NSC1, Figure 8.28a, and 0.0017 for T-HSC1, Figure 8.29, which indicates that presence of the diagonal compression strut in the BCJ not only shifts the maximum strain to the quarter span of the column depth, it also from the outset initiates proportionally higher strain on the end (0.0 mm), whereas at the other end (225.0mm) where there is no influence of diagonal compression strut the strain is very small.

With T- NSC1 up to loading of 140 kN, the maximum strain of 0.0013 develops at the centre (75mm) of the link, Figure 8.28**a**. However, by the time loading reaches 200 kN and strain develops to 0.0026 , the maximum strain occurs at a quarter of its length (56.3m) in the location where the diagonal compression strut develops at the lower part of the T-NSC1 and this continues until failure at 210 kN loading, Figure 8.28a**.** In T-NSC1 the stirrup starts its yield at 140 kN loading with a strain of 0.0013 (f_y=250 MPa), Figure 8.28, but in T- HSC1 this does not occur until after 168 kN loading when strain is 0.0012 , the maximum strain occurs at a quarter of its length (56.3mm) in the location where the diagonal compression strut develops, Figure 8.29, at the lower part of the T-HSC1 until failure of the strut at 260 kN loading.

	Maximum strain		Distance from end (mm)		Strain at ends	
Load (kN)	NSC (10^{-3})	HSC (10^{-3})	NSC	H SC	HSC (10^{-3})	NSC (10^{3})
140	1.3	1	112.5	112.5	0.75	0.3
168	1.6	1.2	112.5	112.5	1.2	0.6
200	2.1	1.6	56.3	112.5	1.5	1.45
210	2.6	1.7	56.3	112.5	-	1.5
220		1.8		112.5	1.7	
240		2.8		56.3		
250		3.8		56.3		

Table 8.11: Strain performance of lower link located in T-NSC1 and T-HSC1

This change in location of the maximum strain in lower link at T-HSC1 to a quarter of the length within the region of diagonal compression strut is of special significance as in the experimental tests it is always assumed that the mid-length of stirrup would be exposed to the maximum strain and therefore strain gauges are mistakenly placed at the centre of leg of links. Compared to the reading at its centre of 0.0016 at 220 kN, Figure 8.37b as loading is increased to 250 kN the maximum strain is 0.0038 compared to the reading at its centre of 0.0021, Figure 8.29, increasing by 81% in the zone where the diagonal compression strut is active.

Similarly, in T-NSC1 the strain at quarter span at 200 kN is 0.002 compared to the reading at the centre of 0.0014, Figure 8.28 , a 186% increase, and as loading is increased to 210 kN it is 0.0026 compared with the reading at the centre of 0.0021, a 124% increase.

	Maximum strain		Distance from end (mm)		Strain at ends	
Load (kN)	HSC (10^{-3})	NSC (10^{-3})	NSC	HSC	NSC (10^{-3})	HSC (10^{3})
140	0.81	1.2	56	56	0.3	0.07
200	1.2	2.1	56	56	0.63	0.45
240	1.5	2.4	56	56	0.7	0.58
260	1.6			56		0.62
280	1.9			56		0.75
300	2			56		0.86
330	2.3			56		1.05

Table 8.12: Comparison of strains in horizontal direction in the lower link of T-HSC3 and T-HSC3 up to failure of T-HSC3. Maximum strain occurs at 56mm from end, close to the beam.

This maximum difference just before failure of 81% for T-HSC1 at 250 kN and 24% for T-NSC1 is due to development of the compression diagonal strut in that zone on the link. It is recommended that in future experimental research work positioning of the strain gauges on links be determined based on the direction of the diagonal compression strut above and below the centre of BCJ.

Discussion of strain analysis in the lower link

T-NSC1 has a maximum strain of 0.0026 at 210 kN and failure load of 220 kN in lower link, Figure 8.28 **.** T-NSC3 developed maximum strain of 0.0024 at 240 kN and its failure load is 260 kN, an increase in loading of 40 kN due to the presence of CVB, Figure 8.30**.**

The strain for NSC at lower loading up to 220 kN is the same for both with and without CVB, Figure 8.31d**.** This increase of 18% in load bearing capacity in NSC is modest compared to the 42% increase for HSC, Figure 8.31c. This demonstrates that the proposed Baumann's modified design rule which is based on dowel action being dependent on concrete strength for dowel or shear resistance is verified by this numerical model.

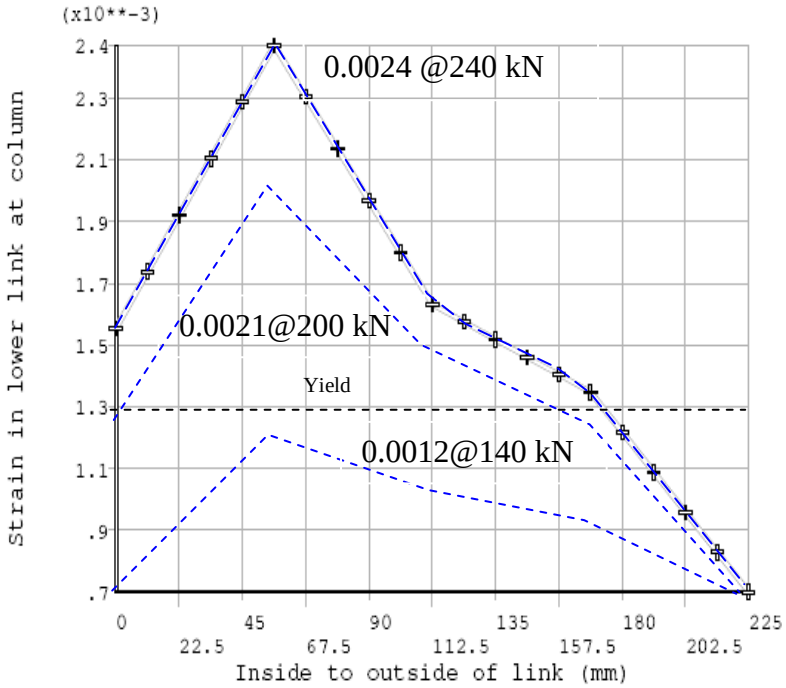

Figure 8.30: T-NSC3 in the lower link until failure load of T-NSC3. Position of maximum strain is point d

Contrary to the lack of influence of CVB on strain development in NSC up to 210 kN, in

HSC the contribution of CVB to strain development is significant when loading is above 140 kN. **Figure** 8.31c.

8.10.4 Comparison of strain in centre link for TBCJ

The strain variation corresponds to incremental loading along the length of 225mm of the central stirrup shown in Figure 8.32.

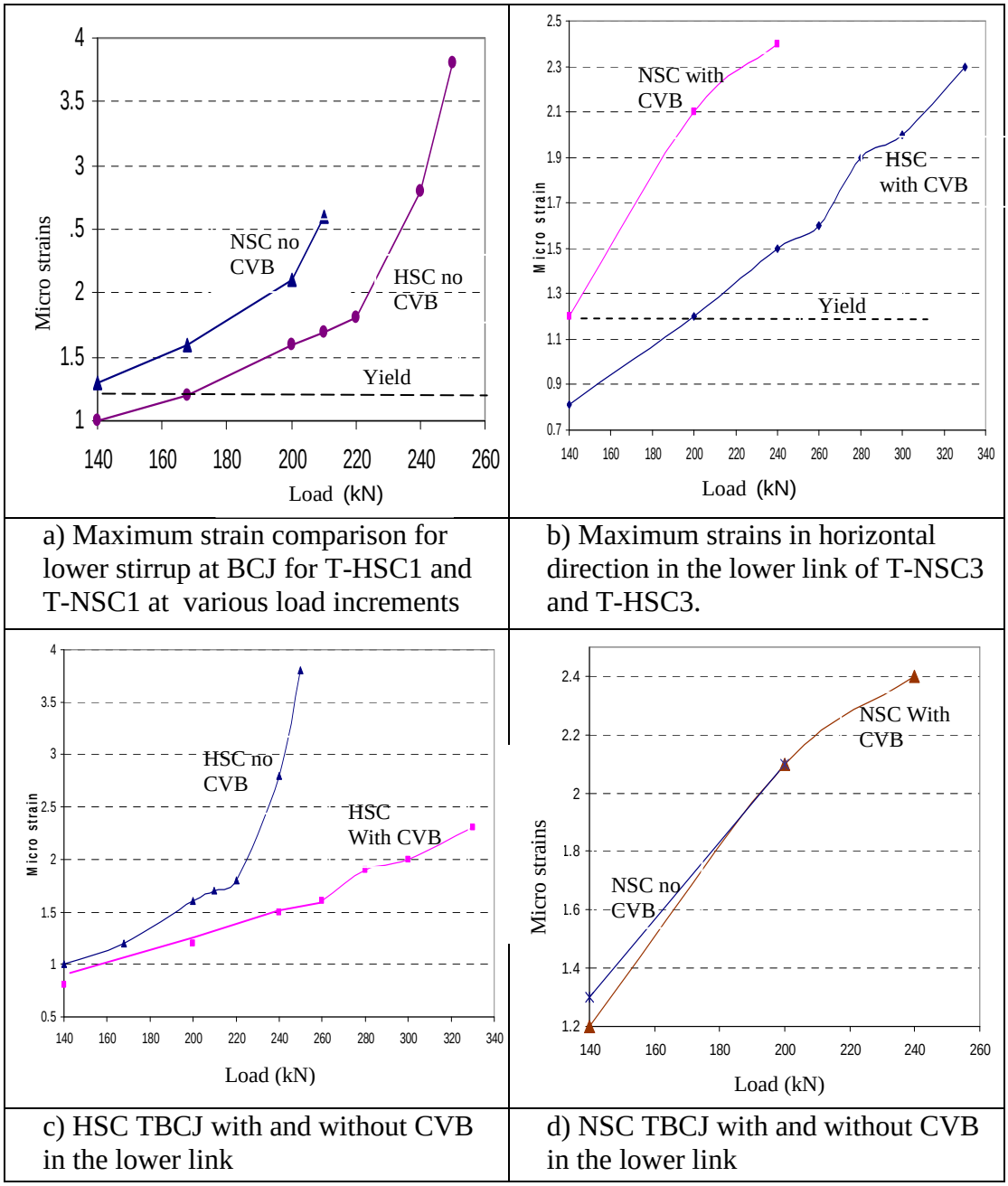

a) Maximum strain comparison for lower stirrup at BCJ for T-HSC1 and T-NSC1 at various load increments

b) Maximum strains in horizontal direction in the lower link of T-NSC3 and T-HSC3.

c) HSC TBCJ with and without CVB in the lower link

d) NSC TBCJ with and without CVB in the lower link

Figure 8.31: Maximum strain comparison for lower stirrup

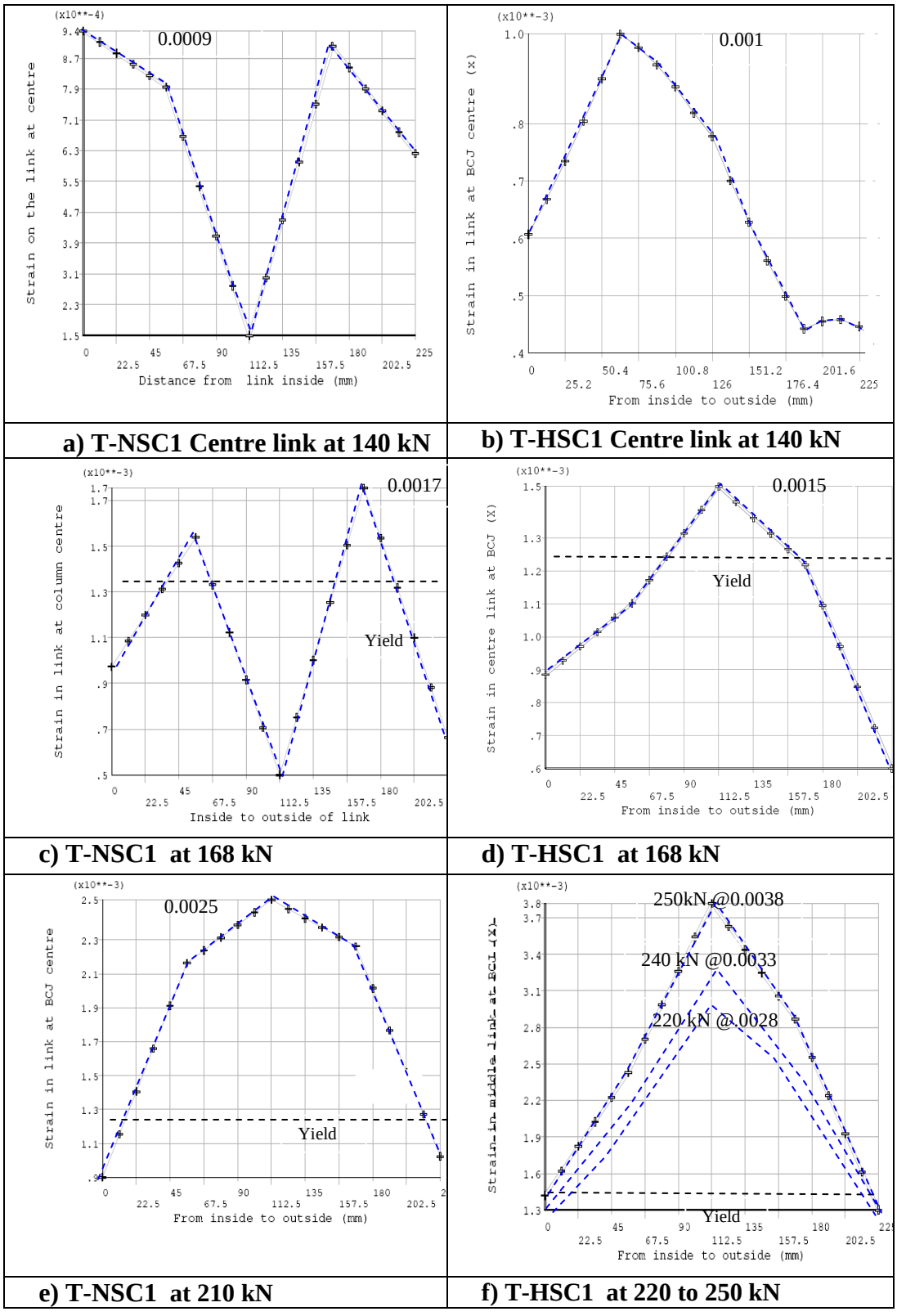

Figure 8.32: Comparison of strains for centre links for T-NSC1 &HSC1

Both NSC and HSC specimen without CVB pass their yield values at 168 kN, Figure 8.32 (c &d). , T-HSC1. Figure 8.32 show the strains in centre link for T-NSC1 and T-HSC1

and indicates the fluctuations in strain as loading increases to before failure up to 250 kN. Figure 8.32 (e) shows that at 210 kN for T-NSC1 strain is distributed across the length of link as compared to T-HSC1, Figure 8.32, where strain is concentrated at the centre of link. This distribution of strain at 210 kN before failure causes the development of a wider strut at centre part of TBCJ, where the link strain is 0.0025 compared to 0.002 in T-HSC1.

Figure 8.34a shows that when no CVB is present in NSC the centre link is strained at the steady and consistent rate of 2.14×10^{-3} per kN all the way to failure, whereas in HSC without CVB at an early stage up to load of 160 kN the rate of 2.14×10^{-3} per kN similar to NSC suddenly drops to a strain of 1.79×10^{-3} because higher concrete strength demonstrates its contribution up to 220 kN when cracks in the concrete make it ineffective, and the abrupt and sudden jump of rate of strain increase per kN is from 1.79×10^{-3} to 6×10^{-3} for 40kN and then failure, demonstrating the brittle and sudden failure behaviour of HSC with no CVB, Figure 8.34a.

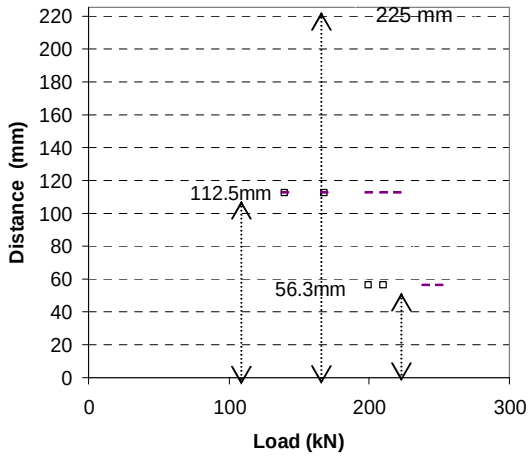

Figure 8.33: Distance where point of maximum strain develops for T-HSC1 and T-NSC1 on the stirrup from the inner end to its outer end

Notes on the slope gradients:

θ_1 is very high strain rate indicating rapid yielding and very little contribution from concrete strength. θ_2 is high strain rate indicating rapid yielding and contribution from concrete strength and reasonable confinement. θ_3 is low strain rate indicating slow yielding and good contribution from concrete strength and good confinement, Figure 8.34d.

The mode of failure of T-HSC1 gives little warning of cracks which widen up to 220kN and

then in the last 40 kN the cracks open suddenly with no warning. FE does not simulate element separation and demonstrates failure as if concrete was behaving like rubber to failure point. It is possible that if alternative methods such as Finite Difference or Applied Element methods were applied for this structural system, element seperation could have been recorded for the centre link at 220 kN, instead of 6×10^{-3} strain increase per kN.

Figure 8.34b shows that TBCJ of NSC both with and without CVB have the same gradient or rate of increase in strain of 2.14×10^{-3} per kN, but surprisingly the average strain in NSC with CVB is around 14% higher from start up to failure load for T-NSC1. Experimental tests on analogous beams NSC1 and NSC3, Figure 3-39, confirm the same strain distribution as in Figure 8.34.

Load (kN)	**T-NSC1 (10^{-3})**	**T-HSC1 (10^{-3})**	**T-NSC3 (10^{-3})**	**T-HSC3 (10^{-3})**
140	0.15	1	1.5	1
168	0.5	1.5		
200			2.8	1.2
210	2.5			
220		2		
240		3.3	3.1	1.6
250		3.8		
260				1.8
280				1.9
300				2.1
320				2.2
330				2.3

Table 8.13: Comparing centre link maximum strain for T-NSC1 and HSC1 up to failure of T-HSC1 at 260 kN

This 14% increase in strain is due to CVB straining straining the link . This is contrary to the behaviour for HSC, Figure 8.34d, when the presence of CVB reduces the strain in the link. HSC surrounding CVB produces significant dowel resistance to the extent that from an early loading stage this dowel shear resistance takes a larger proportion of the applied shear load.

Discussion on the strain analysis in centre link

The FE model shows that the strain in the centre link, Figure 8.34, for T-NSC1 at 210

kN without CVB is less than the strain for T-NSC3 which has CVB, demonstrating that the centre bar for T-NSC3 is strained from 2.8×10-3 to 3.1×10-3 during the final 40 kN loading or 0.75×10-3 per kN, or 10% increase in strain for 20% increase in loading, showing that the dowel action in CVB is absorbing most of the additional shear forces produced by the increased loading.

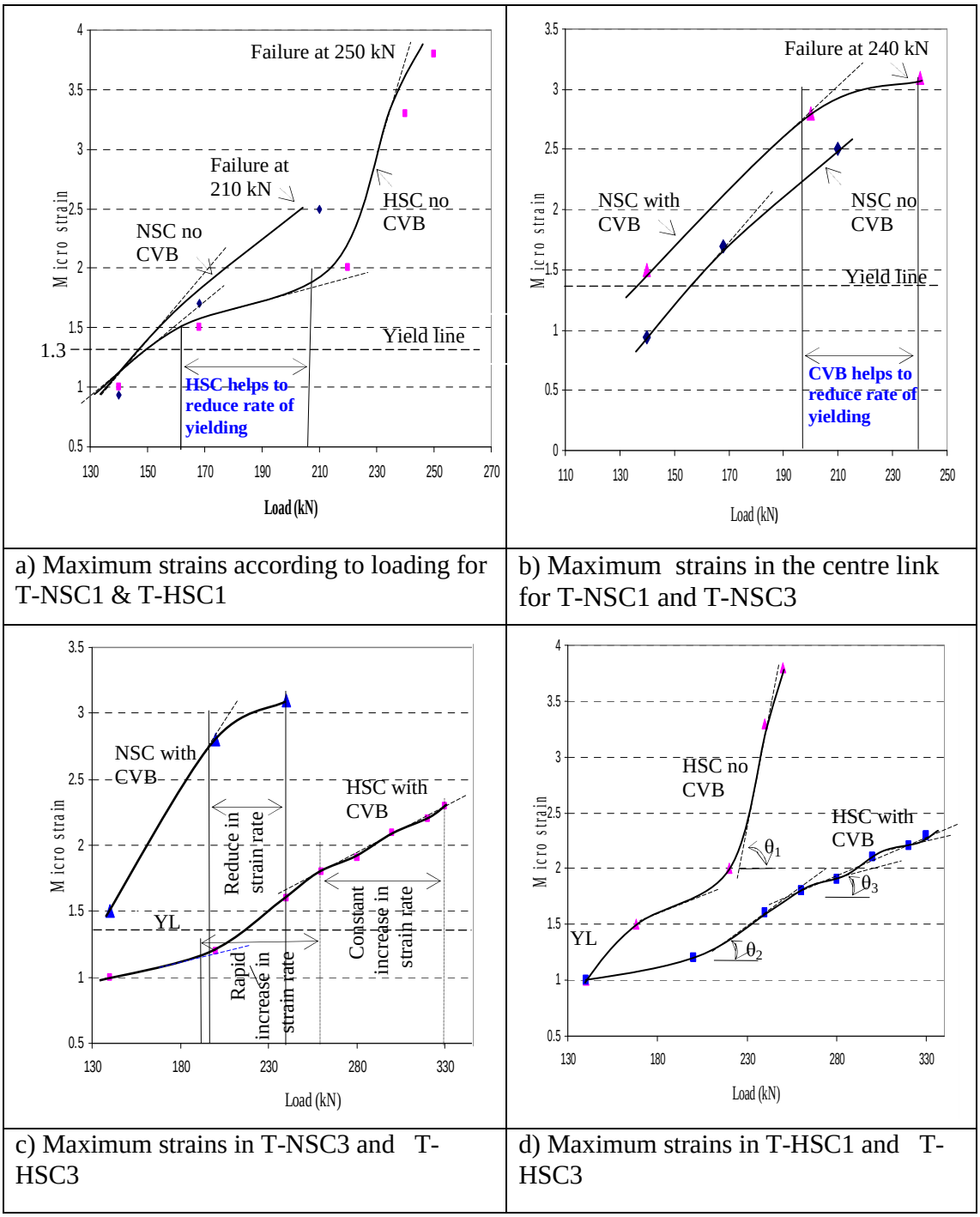

a) Maximum strains according to loading for T-NSC1 & T-HSC1

b) Maximum strains in the centre link for T-NSC1 and T-NSC3

c) Maximum strains in T-NSC3 and T-HSC3

d) Maximum strains in T-HSC1 and T-HSC3

Figure 8.34: Comparison of longitudinal strains on the centre link for T-NSC1, T-HSC1, T-NSC3, and T-HSC3. These graphs compares well with analogous beam shown in Figure 3-39 chapter 3.

Comparing FE model strain recordings for T-NSC1 and T-HSC1 in Figure 8.34, model HSC has a strain gradient of 0.0179×10^{-3} per kN up to 170 kN loading, after which the high strength of concrete contributes to restricting a rapid increase in strain. As a result, the strain gradient is reduced to 0.01×10^{-3} per kN from 170 kN to 220 kN. At 230 kN shear cracks developing close to centre link increase the strain gradient to 0.06×10^{-3} per kN from 220 kN to failure at 250 kN.

The comparison of the behaviour of T-NSC3 with HSC3 in Figure 8.34 (c) can be compared to the behaviour of the analogous beams NSC3 and HSC3, (Figure 2-36c in Chapter 2), where the influence of HSC in reducing strain on the centre link is clearly apparent. From Figure 2-36d in Chapter 2, it was recorded experimentally that after HSC3 has passed its yield value of 1.3×10^{-3} several times over reaching 9.9×10^{-3} at 200 kN, a significant shear crack has made the centre link obsolete, but the dowel action from HWB is the only means of resisting the shear forces from 200 kN to 280 kN. This demonstrates that only dowel action from HWB was resisting the final 80kN (40%) loading.

The presence of CVB increases the load bearing capacity of T-HSC3 to 340 kN compared to 260 kN T-HSC1, Figure 8.34 (d). Just before failure of T-HSC3 at 330 kN the strain is 0.0023, Figure 8.35d, which is less than 0.0038 for T-HSC1 at 250 kN, Figure 8.32f. The dowel action in the CVB takes up a significant proportion of the shear in such way that in spite of more than a 30% increase in load the strain on the centre link is reduced by 65%.

The maximum strain in all TBCJ acts at the centre span (112.5 mm) of the leg of the centre link which is close to the centre of the inclined diagonal compression strut in the joint.

The presence of CVB in NSC specimens does not make a significant contribution to strain reduction on the centre link. The CVB makes a modest contribution of 0.0004 difference in strain reading in comparison with the specimens without CVB and this difference remains unchanged as the applied load increases, Figure 8.34 (b)**.**

For similar beams the presence of HWB in NSC specimens does not make much difference in strain on the centre link until 120 kN, (Figure 2-36d, Chapter 2). After this loading

NSC1 which has no HWB has a very high strain increase at 0.033×10^{-3} until its failure. The strain reaches 9.3×10^{-3} (more than 700% yield) after 140 kN, and the dowel action from HWB resists shear until failure load of 170 kN.

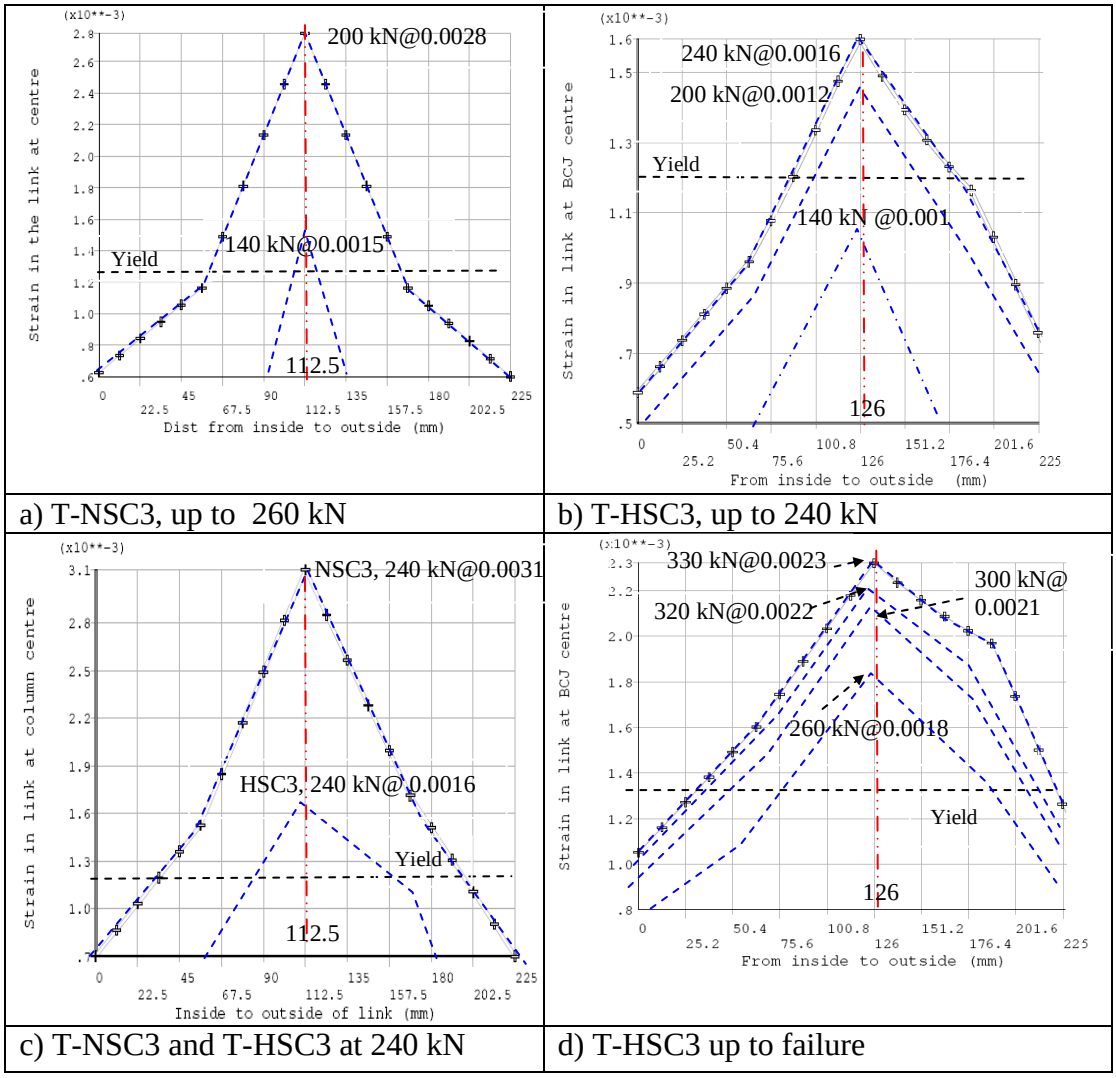

Figure 8.35: Comparison of strains in axial direction in the centre link for T-NSC3 and T-HSC3.

The presence of CVB in HSC specimens makes a significant contribution to strain reduction on the centre link and this increases exponentially as the applied loading increases, Figure 8.34 (d). At 250 kN loading, the maximum strain in centre link of HSC model without CVB is 0.0038, or 300% of its yield value, compared to 0.0017, 42% above yield, when CVB is absent. The maximum strain on centre link in HSC with CVB is 0.0023, 92% above its yield, at 330 kN loading. Failure load is 340 kN.

The experimental results for beams HSC3 and HSC1 show that after 120 kN as the strain in centre link of HSC1 reaches 1.8×10^{-3} or %138 its yield value, the beam abruptly fails. However, when HWB is present the strain in the centre link remains as little as 0.17×10^{-3}, 13 % of its yield value , up to 180 kN loading. However, due to formation of large shear cracks, the centre link reaches strain of 9.9×10^{-3} (760% of its yield) at 200 kN, but at this stage the HWB independent of any other material resists the shear forces for another 80kN or a further 40% increase in loading, Figure 2-36, Chapter 2.

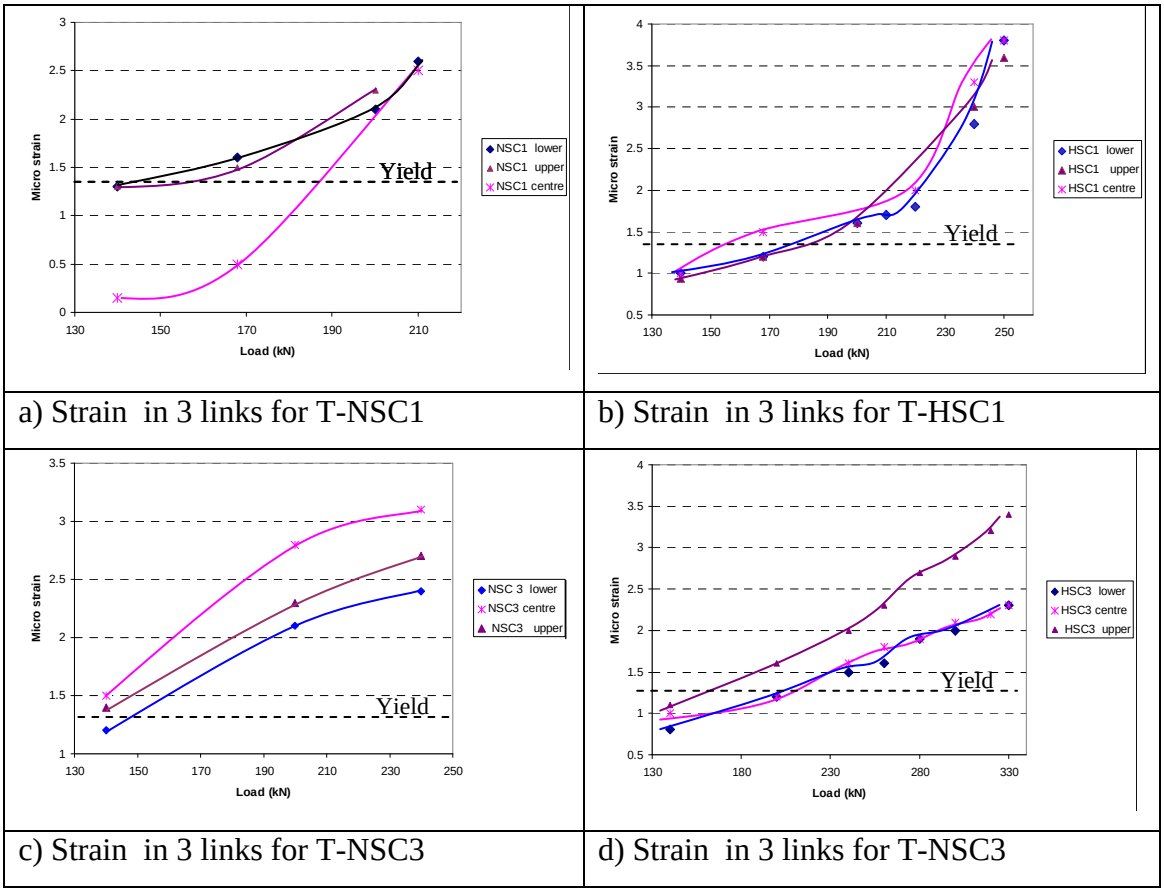

a) Strain in 3 links for T-NSC1

b) Strain in 3 links for T-HSC1

c) Strain in 3 links for T-NSC3

d) Strain in 3 links for T-NSC3

Figure 8.36: Strain in 3 links located at the centre of the TBCJ..

Conclusion on behaviour of all links

T-NSC1, Figure 8.36a

- Central link experiences much smaller deformations compared to the upper and lower links but it develops similar strain at failure.
- Generally the strain in the links increases gradually when the rate of strain/load is constant which indicates normal concrete mode of failure.
- Failure occurs at 210 kN when the strain is 2.0 times the yield strain.

T-HSC1, Figure 8.36b

- All the three links experience similar strain behaviour, which indicates that there is better stress distribution when using HSC.
- There is rapid strain increase in all the three links after 210 kN which indicates a brittle mode of failure.
- Failure occurs at 250 kN when the average strain is 2.9 times the yield strain.

T-NSC3 (T-NSC1+CVB), Figure 8.36c

- Central link carried maximum strain behaviour compared to the upper and lower links. This is the reverse behaviour of NSC1 (without CVB), which shows the influence of CVB on the behaviour of the joint.
- Generally the strain in the links increases rapidly with the rate of strain/load maximum at initial loading and this reduces with further increase in loading. This represents a more ductile mode of failure compared to NSC1.
- Failure occurs at 240 kN when the maximum strain is in centre link of 2.5 times the yield strain.

T- HSC3 (T-HSC1+CVB), Figure 8.36d

- A new location for maximum strain on the upper link compared to the other three models is due to presence of CVB in HSC.
- Similar behaviour to T-HSC1 (without CVB) except the rate of strain/load is half that of HSC1 which indicates a more ductile mode of failure.
- The upper link experienced greater strain behaviour compared to lower and centre links which probably due to the cracks which developed at back of the column near anchorage bar.
- Just before failure at 350 kN when the maximum strain is in upper link with a value of 2.3 of the yield strain.

Summarising the joint behaviour in these three links, three main points can be noted which are:

1. The position of maximum strain in the upper link from the rear column reinforcement is 50 mm for T-NSC1, T-NSC3 and T-HSC1. Presence of CVB in T-HSC3 deflects the position of maximum strain on the upper link to 36 mm from the rear column bar.

2. By using HSC for BCJ, the ductile behaviour of the joint changes to brittle mode of failure. Therefore it is not advisable to use HSC alone for TBCJ.
3. By using CVB, the joint increased its confinement and become more ductile. However, the greatest improvement developed when CVB was used with HSC where the confinement of the joint increased and the ductility also improved compared to NSC, concluding that it is strongly advisable to use CVB with HSC for TBCJ.

8.10.5 Front column reinforcement

Strain along the front column reinforcement in vertical (Y) direction is analysed in this section. Location of maximum strain from the 0.0 point on the front reinforcement is shown in Figure 8.18.

The maximum strain in the front column bar occurs at the opening corner of the BCJ because the flexural tension is highest at this point.

Strain development along the front column bar in all four specimens is investigated and compared. Longitudinal strain in front column bars in T-NSC1and T-HSC1 is a maximum distance of 200mm which coincides with the point of the opening corner shown in Figure 8.10. This maximum strain is due to the flexural behaviour of the column due to tensile force from the main beam bar. This flexural behaviour is such that the column behaves in bends at that particular point thereby producing tensile strain in the front column bar. This tensile strain is reduced by 18% for corresponding load in T-HSC1, compared to T-NSC1 at 140 kN, Figure 8.37a.

When CVB is added to the specimen, the crack width at critical position is reduced, Figure 8.37a. In NSC models under 140 kN loading the maximum strain recorded which occurs at the opening corner is 0.0039. When CVB is added to this specimen the strain at the same location is reduced to 0.0033. This reduction indicates that when CVB is not present, the front column bar just passes yield and first cracks appear, however, when CVB is present under the same loading the maximum strain at the same location is only 0.0033 which is under the yield value therefore no cracks appear.

Similarly in HSC models under 140 kN loading, Figure 8.37b, the maximum strain recorded which occurs at the opening corner is 0.0033. When CVB is added to this specimen, the strain at the same location at 200 kN is also 0.0033. This indicates that when CVB is not present, the front column bar passes yield and comparatively large cracks appear at 180 kN, however when CVB is present under the loading of 200 kN the maximum strain at the same location is only 0.0033, which is under the yield value, therefore no cracks are formed, Figure 8.37d.

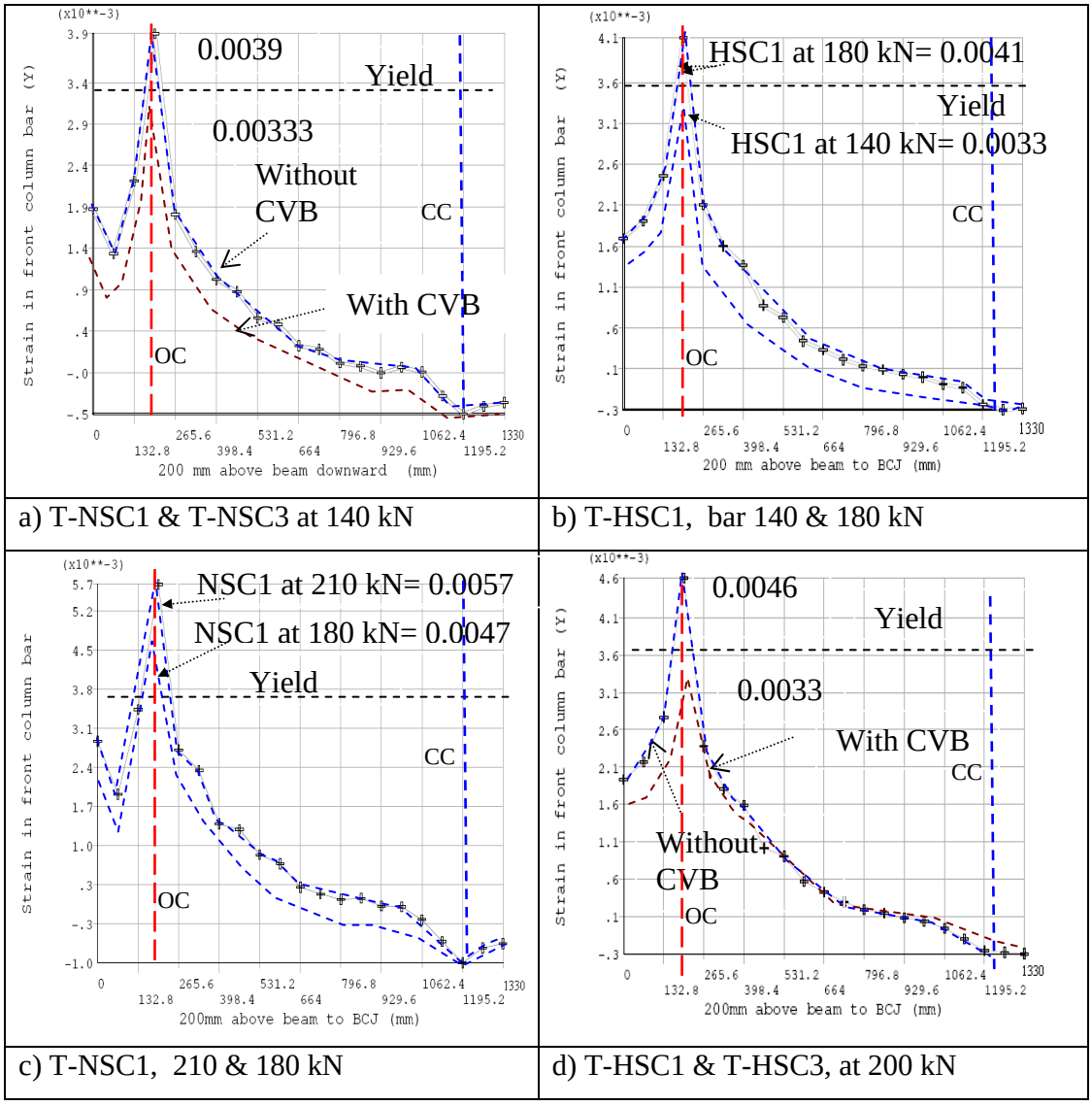

a) T-NSC1 & T-NSC3 at 140 kN

b) T-HSC1, bar 140 & 180 kN

c) T-NSC1, 210 & 180 kN

d) T-HSC1 & T-HSC3, at 200 kN

Figure 8.37: Longitudinal strain in front column bar in T-NSC1and TBCJ- HSC1 up to failure of T-NSC1. NB:OC= Opening corner, CC= Closing corner

Discussion on the investigation of strain development in front column bars

In the front column bars for T-NSC1 at 210 kN loading, the maximum longitudinal strain

at the level of the opening corner is 0.0057, Figure 8.37c, or 158% of the yield strain of 0.0036. When concrete strength is improved to HSC in T-HSC1, the yield at 200 kN load at the same strain reduces to 0.0046 which is 28% higher than yield but 24% less than NSC due to the higher strength of the concrete, and is similar to the load bearing capacity of T-NSC1 at 180kN, Figure 8.37c.

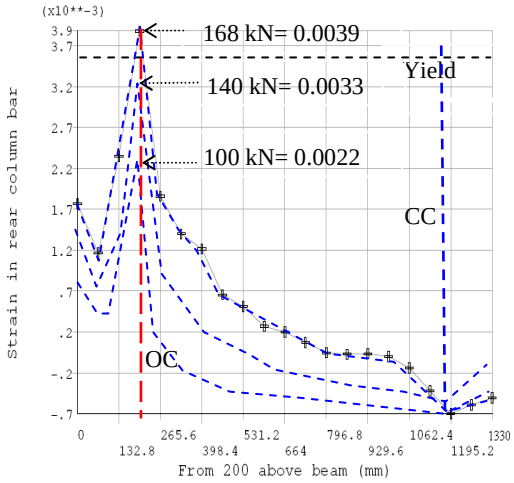

a) T-NSC3, 168 kN

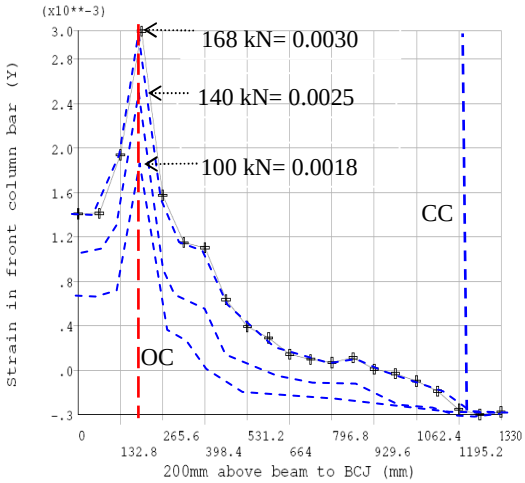

b) T-HSC3, at various loadings

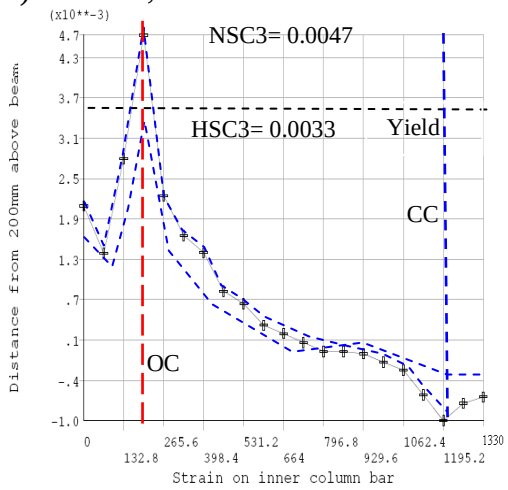

c)T-NSC3, T-HSC3, 200 kN

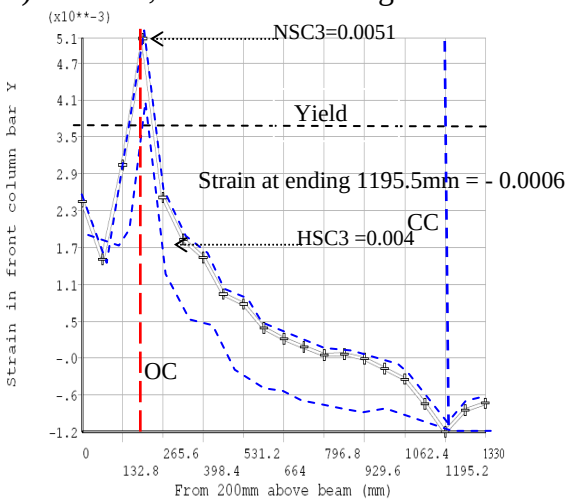

d) T-NSC3& T-HSC3, 220 kN

Figure 8.38: Longitudinal strain in front column bars, TBCJ- **HSC3, up to 220 kN. Position of maximum strain is point e. NB:OC= Opening corner, CC= Closing corner**

The introduction of CVB to TBCJ causes a reduction of 21% in the maximum strain developed in the front bar in T-NSC3 at 200 kN, Figure 8.38c, compared to T-NSC1 at 210 kN, Figure 8.37c. The yield in the presence of CVB reaches 0.0047 for 200kN, Figure 8.38a, which is comparable to 180 kN loading for T-NSC1 without CVB, Figure 8.37c. When comparing maximum strains 0.0047 for T-NSC1, and 0.0041 for T-HSC1, at

180 kN there is an improvement of 15% due to material improvement from NSC to HSC, Figure 8.37b.

Surprising results appear when CVB is present in HSC for T-HSC3, demonstrating its significant contribution in increasing the load bearing capacity to 300 kN when the front column bar is strained at 0.0057, Figure 8.39, which is the same strain for T-NSC1 at 210 kN loading, Figure 8.37c, or an increase of 43% in loading at the same level of maximum strain on the front bar only due to the use of HSC material rather than NSC, and the presence of CVB.

Cracks develop at the same position in both T-NSC3 and T-HSC3, however, they are smaller in HSC by an average of 27%. At 220 kN loading when CVB is present the maximum cracking strain in NSC is 0.0051 whereas in HSC it is only 0.004, Figure 8.38d.

Load (kN)	**TBCJ Strain (10^{-3})**			
	T-NSC1	**T-HSC1**	**T-NSC3**	**T-HSC3**
100			2.2	1.8
140	3.9	3.3	3.3	2.1
168			3.9	3
180	4.7	4.1		
200			4.7	3.3
210	5.7	4.6		
220				4
240			5.1	4.4
260				4.8
280				5.2
300				5.7
320				7.2
330				8.9

Table 8.14: Comparison of strain in front column bars for all TBCJ specimens

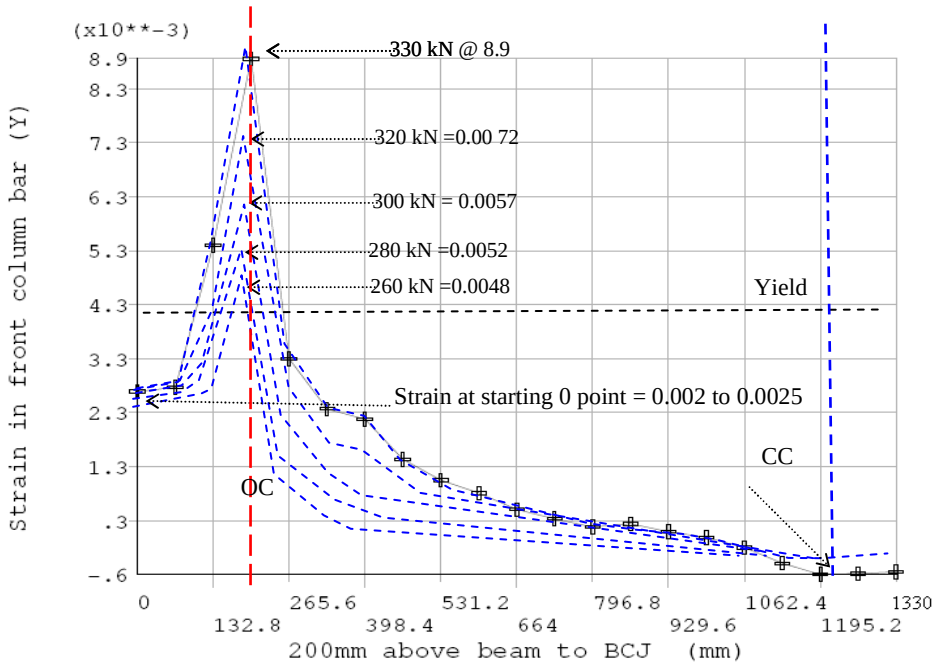

Figure 8.39: T-HSC3- front column bar 240 kN to 330 kN. NB:OC= Opening corner, CC= Closing corner

A. Influence of HSC on the behaviour of TBCJ

1. The influence of HSC on TBCJ joints without CVB is as follow:

- Considering T-NSC1 & HSC1, at 210 kN and 200 kN when the concrete splitting strength increased from 2.87 N/mm^2 (NSC) to 4.52 N/mm^2 (HSC), Table 8.1, the tensile strain in the front column bar was reduced from 0.0057 to 0.0046. This represents a 24% reduction which is relatively small compared to the 57% increase in material splitting strength, Figure **8.37**ure 7.38 c &d.

- The maximum failure load capacity of TBCJ was increased by 18% after increasing the material strength of the concrete.

2. The Influence of HSC on TBCJ joints designed with CVB is as follows:.

- The tensile strains which developed in the front bars at 220 kN for T-NSC3 & HSC3 are 0.0051 and 0.0040 respectively, Figure 8.38d. This again represents a relatively small reduction in strain in relation to a large increase in concrete

strength. Also it can be noted that CVB did not significantly influence the amount of strain developed in the front bars, Figure 8.37c.

- The maximum failure load capacity increased from 260 kN (NSC3) to 340 kN (HSC3), which represent 31% increase in maximum load capacity of TBCJ due to the increase of concrete materials.

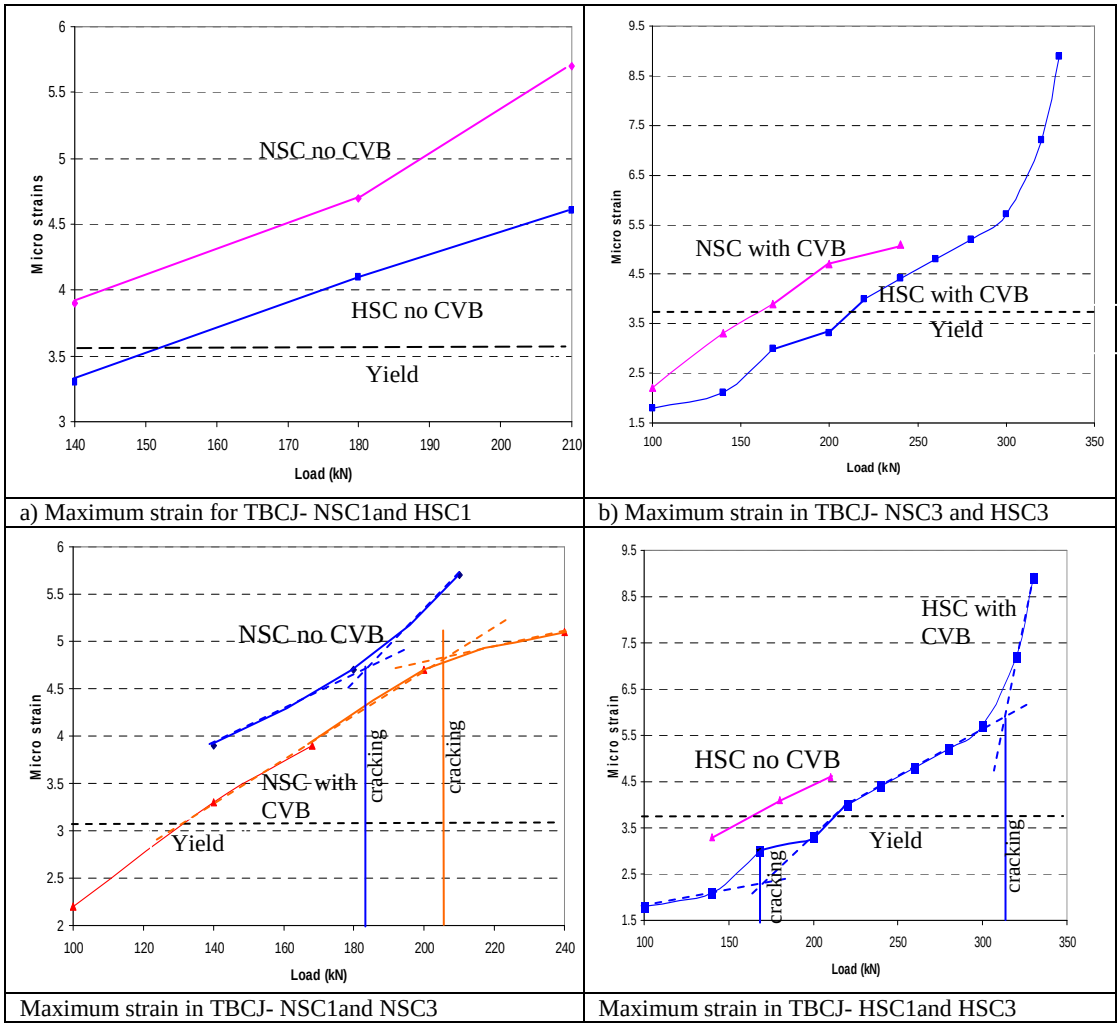

a) Maximum strain for TBCJ- NSC1and HSC1

b) Maximum strain in TBCJ- NSC3 and HSC3

Maximum strain in TBCJ- NSC1and NSC3

Maximum strain in TBCJ- HSC1and HSC3

Figure 8.40: Comparison of maximum strain in front column bars for all TBCJ specimens

Maximum tensile strains in front bars of TBCJ NCS3 & HSC3 were 0.0051 and 0.0089 respectively, Figure 8.40. This represents a 75% increase which means the joint with higher strength develops a larger crack above opening corner level before failure. This high yield in the column front bar is of concern when compared with strain at the same

loading in the beam bar of 0.0029. Therefore, column failure is the mode of failure for all the TBCJ models.

However, if 200 kN loading is considered, the strain in the front column bar for T-HSC3 is 0.0033, and the strain in beam bar T-NSC3 is 0.0047, Figure 8.38. This demonstrates that the plastic hinge would occur in NSC3 column before HSC3.

B. Investigation into the effectiveness of CVB on the behaviour of TBCJ

- The influence of CVB on the behaviour of TBCJ joints constructed with NSC is investigated. At 140 kN the maximum yield for NSC1 is 0.0039 compared to 0.0033 in NSC3 or 18.2% increase in yield, Figure 8.28a, and at the higher load of 210 kN, NSC1 yields at 0.0057 compared to 0.0051 in NSC3, about 12% increase, Figure 8.38d.

- At 210 kN loading, NSC1 columns without CVB would form the plastic hinge before NSC3 and HSC3 as its front bar would yield at 0.0057, Figure 8.28c.

- The tensile strains which in the front bars for TBCJ HSC1 & HSC3 at 220kN were 0.0033 and 0.0021 is a 57% reduction which indicates that CVB increased the rigidity of the joint by 57%.

8.10.6 Comparison of strain in rear column bars

In this section strain along the rear column reinforcement in the vertical (Y) direction is investigated. Location of maximum strain from the 0.0 point on the rear reinforcement is shown in Figure 8.18**.**

Maximum tensile strain in the rear column bar occurs near the level of the closing corner of the T-BCJ, because the flexural tension is highest at this point. This maximum strain is due to the flexural behaviour of the column due to compressive force from the lower part of the beam. This flexural behaviour is such that the column bends at that particular point, thereby producing tensile strain in the column bar.

It can be noted that the strain in T-HSC1 compared to T- NSC1 at 210 kN is 47% less, Figure 8.42.

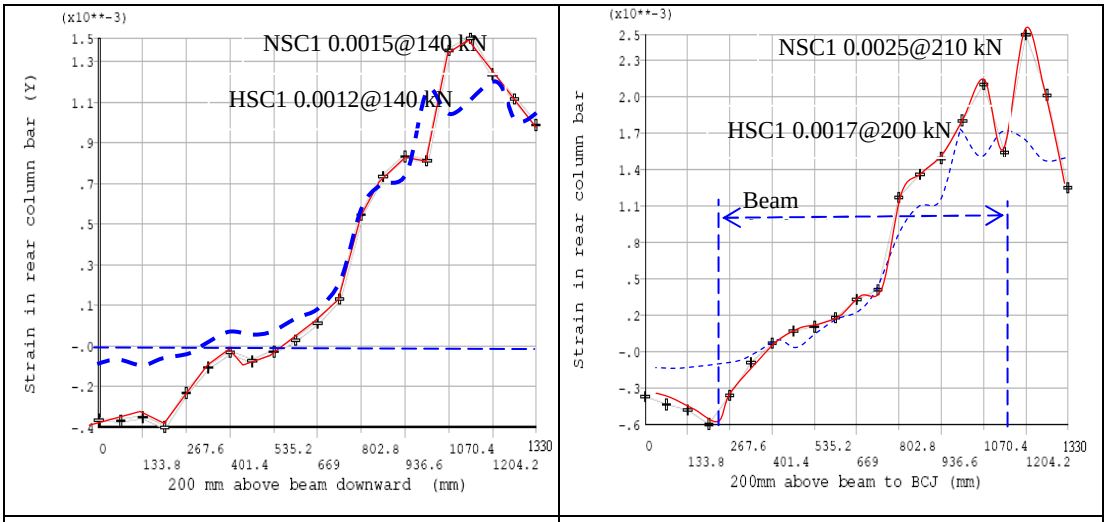

a) T-NSC1, and T-**HSC1** rear bar 140 kN loading

b) TBCJ- **NSC1**, rear bar at 210 kN loading and T-HSC1 at 200 kN

Figure 8.41: Longitudinal strain in y direction in rear column bar in T-NSC1 and T-HSC1 up to failure of T-NSC1 at 220 kN. Maximum strain is point f. Figure 8.17 _____ NSC and ---------- HSC

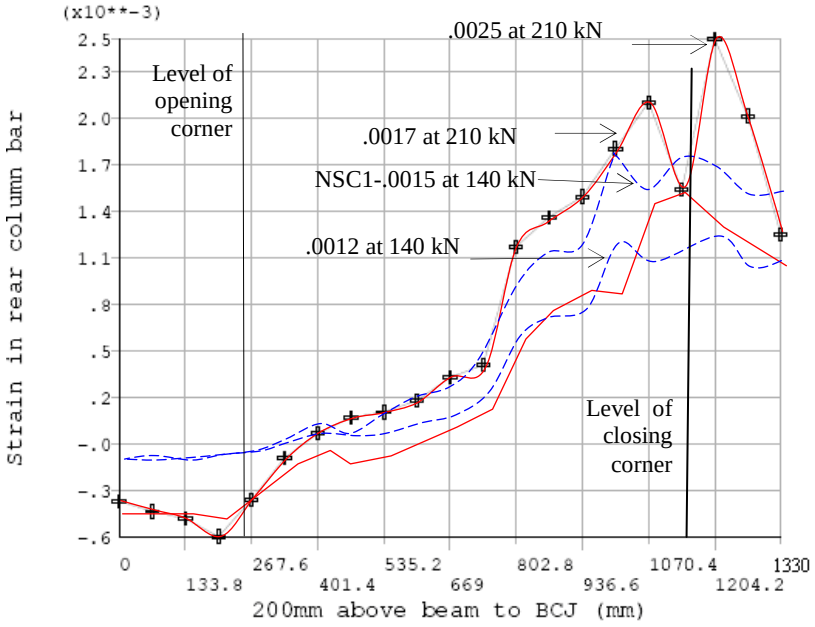

Figure 8.42: Axial strain in the rear bar of the main column reinforcement _____ NSC1 and ---------- HSC1

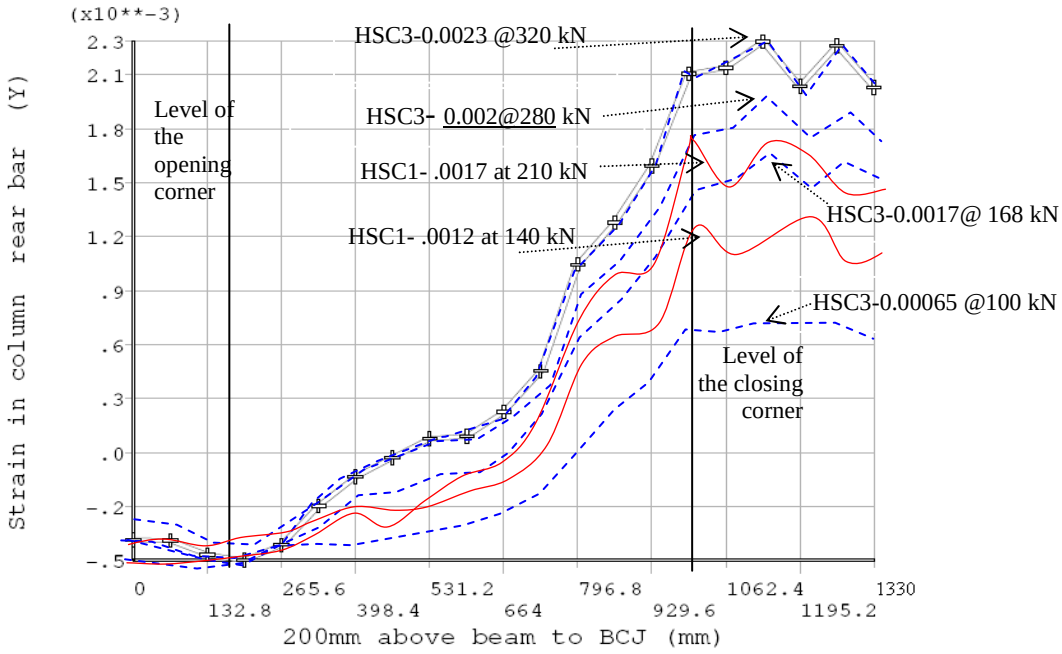

Figure 8.43: Strain in the rear column bar T-HSC1 and T-HSC3.
_____ HSC1 and ---------- HSC3

`

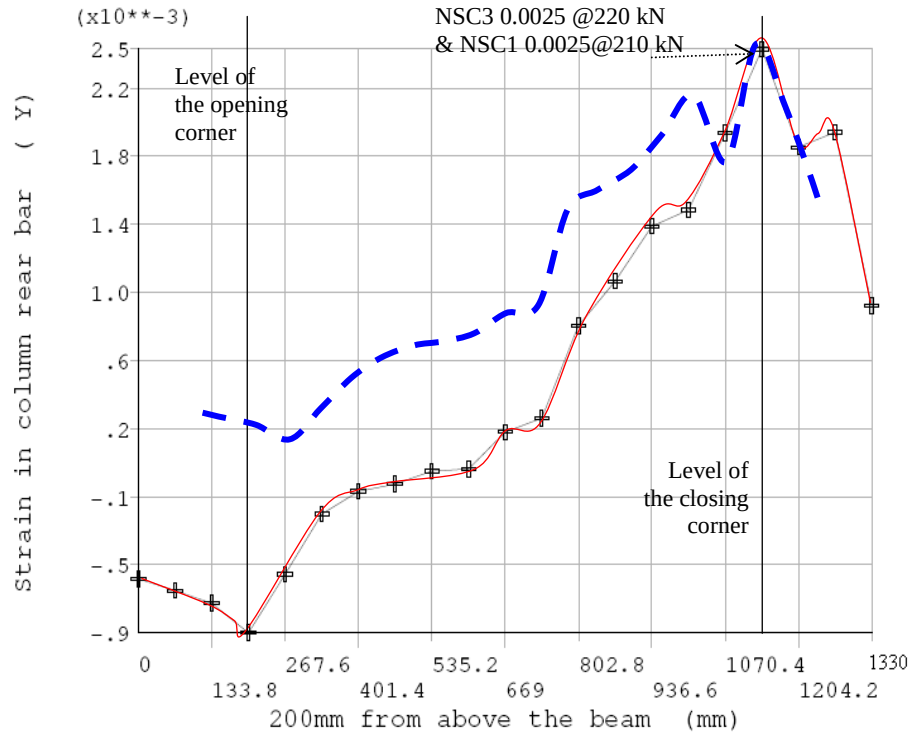

Figure 8.44: Axial strain in the rear bar of the main column reinforcement
_____ NSC1 and ---------- NSC3

In HSC, the presence of CVB reduces the maximum strain on the rear reinforcement at the critical location at the level of closing corner by 25% . A load application of 168kN produces strain of 0.0017 in T-HSC1, but when CVB is present 210kN produces the same strain of 0.0017 in T-HSC1, Figure 8.43.

In NSC , the presence of CVB does not make much contribution to ultimate load bearing capacity. At 210 kN loading NSC1 is at strained 0.0025 which remains the same when CVB is present at 220 kN in T-NSC3, Figure 8.44. Similarly at 140 kN loading the strains in T-NSC1 and NSC3 are 0.0015 or 0.0016 which is a negligible strain, **Figure** 8.42 and Figure 8.44.

As the graphs for strain in the rear column reinforcement show, the maximum strain just before failure in all cases is 0.0025 for T-NSC1 and T-NSC3 or 0.0024 for T-HSC3, Figure 8.43, which are all below the yield value and occur near closing corner level.

Rear column bars are exposed to a small amount of compressive strain near the level of the opening corner but this strain is comparatively small and the maximum value 0.0009 occurs in T-NSC3 just before failure load at 220 kN, Figure 8.44. This is mainly due to eccentricity in loading on the external BCJ which results in high tensile strains in the front column bar opening corner. As shown in Figure 8.45c, when CVB is added to NSC there is small reduction of 6% in the strain in rear column bar. However, when the material is improved to HSC the rear column bar is strained 32% less than NSC, Figure 8.45b, with CVB. The strains in NSC with and without CVB are very close, Figure 8.45. When CVB is present there is only 0.0003 less strain in the maximum strain location. The location of maximum strain remains almost the same and is shown as point f in Figure 8.16.

8.11 Strain behaviour in CVB at (Y) direction

In this section, strains along the CVB column reinforcement in (Y) direction are investigated. Location of maximum strain from the 0.0 point on the CVB reinforcement is shown in Figure 8.18. It can be noted that the behaviour of CVB in HSC beam-column models is such that :

- Maximum axial strain in CVB occurs at the level of the opening corner and the second maximum value occurs just above the axes of the closing corner which is similar to CVB behaviour in NSC models.

- Minimum axial strain in CVB occurred approximately around the mid-depth of the beam.

Specimen	Load (kN)	Strain (10^{-3})	
		HSC	NSC
Without CVB	140	1.5	1.2
	210	2.5	1.7
With CVB	100	1.2	0.65
	140	1.6	0.93
	168	1.9	1.2
	220	2.5	
	240		1.7
	260		1.8
	280		2
	300		2.2
	320		2.3
	330		2.4

Table 8.15: Strain fluctuations with incremental loads for the rear column bar

The influence of HSC on the axial deformation of CVB is as follows:

- Overall behaviour of CVB is similar in both NSC and HSC models except that the HSC model with CVB develops 33% higher loading capacity.

- The strain at failure of NSC is 0.0019 is similar to that in HSC, whereas HSC failure load is 280 kN and NSC at 240 kN,

- Maximum strain value occurs at the level of the opening corner and the second maximum strain occurs at the level just above the closing corner.

The strain development along the CVB indicates that this happens at the same section as where the front column bar is strained. The action of CVB is also part of the double truss action.

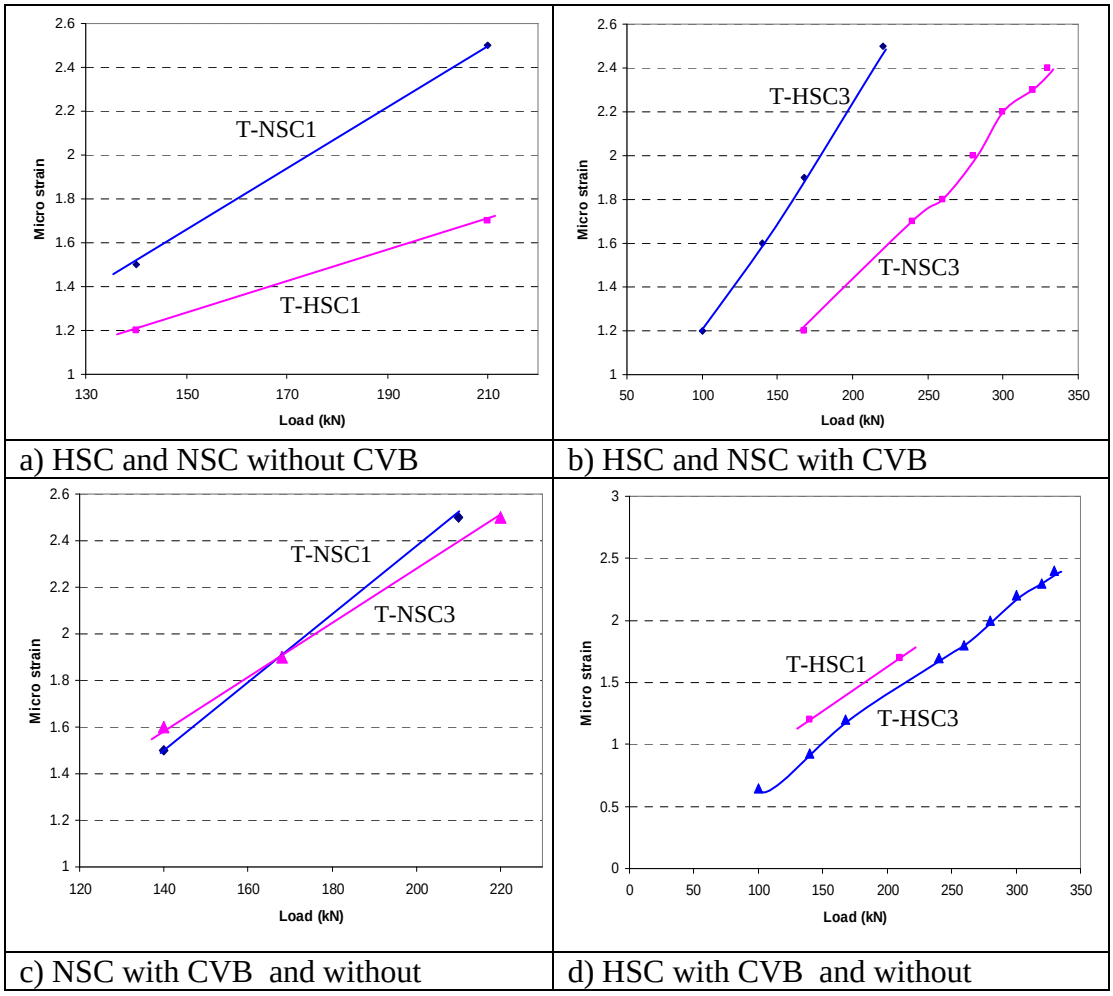

Figure 8.45: Strain fluctuations with incremental loads for the rear column bar

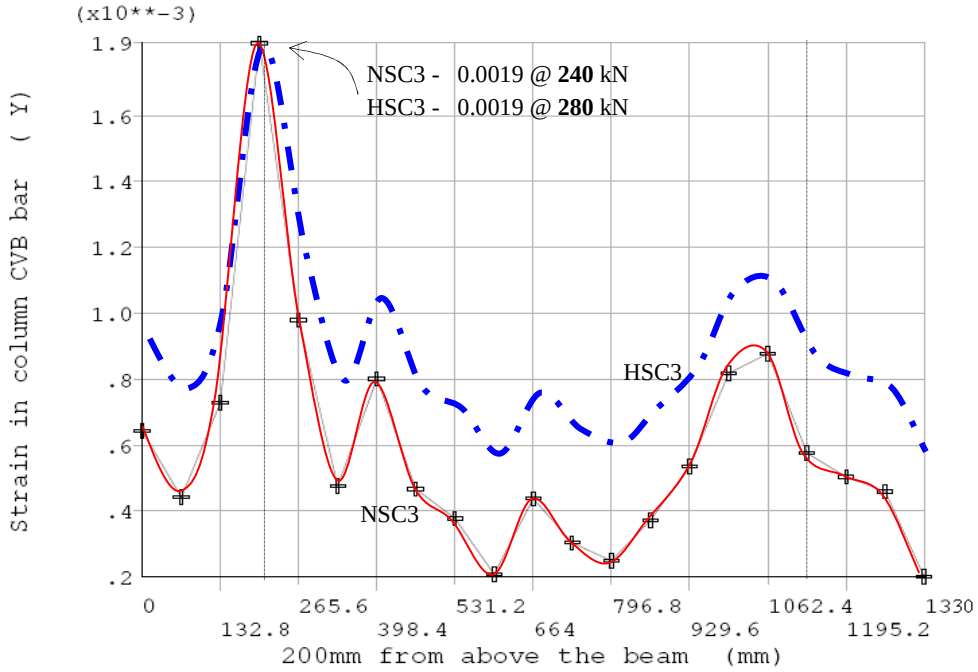

Figure 8.46: Comparison of T-NSC3 and HSC3 at equal strains

8.12 Strain in X and Y direction on CVB

Cracking behaviour was presented in the form of graphs of moment M_z against length of CVB for TBCJ. The graphs show overall characteristics for a TBCJ with links and shows a detail for change in moment due to the presence of link, the post-cracking behaviour being given by the values of the dowel force corresponding to the dowel force on the CVB and the tensile force absorbed in the the stirrup.

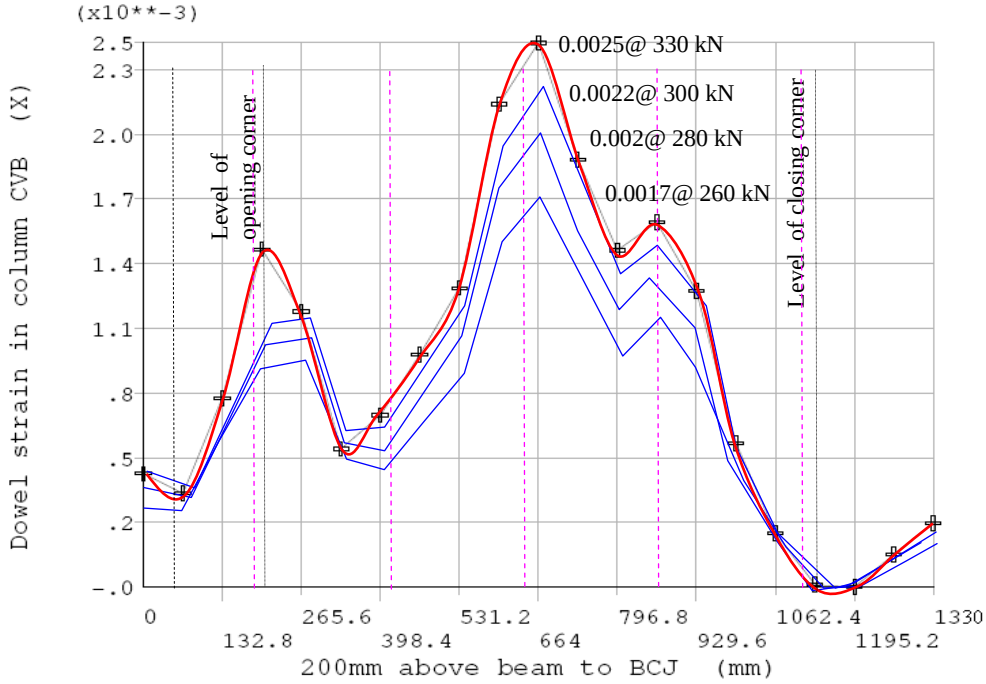

Figure 8.47: Horizontal (x-direction) strain in CVB for T-HSC3

Load (kN)	TBCJ			
	NSC3, Y	HSC3, Y	NSC3, X	HSC1 X
168		1.1		
200	1.7	1.3	2.8	1.3
220	1.8	1.5	3.3	1.4
240	1.9	1.6	3.8	1.6
260		1.7		1.7
280		1.9		2
300		2		2.2
320		2.4		2.3
330				2.5

Table 8.16: Strain development in CVB in dowel, horizontal (X) direction and in longitudinal, vertical (Y) direction.

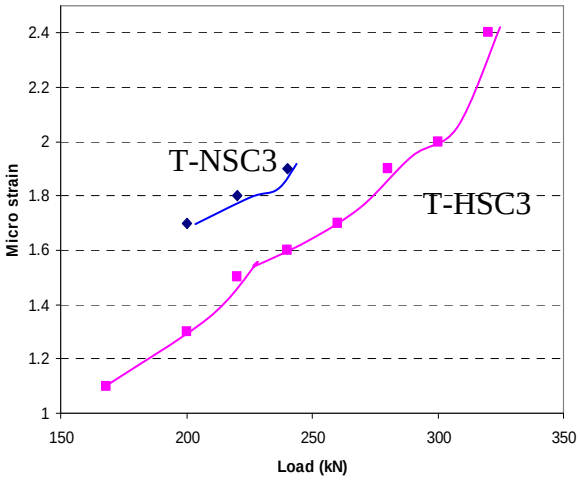

Figure 8.48: Longitudinal strain on CVB for T-NSC3 and T-HSC3

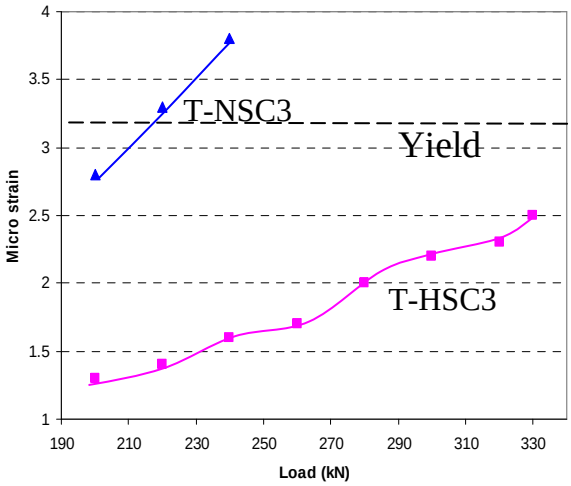

Figure 8.49: Strain in horizontal direction on CVB, T-NSC3 and HSC3.

8.13 Moment about Z axis acting on CVB

The maximum dowel action on CVB occurs at the point of its intersection with the beam bar, which is the location where the end of the inclined diagonal compression strut is restrained just above Link 7, the most critical location within the beam BCJ which causes the failure crack.

In this section a diametrical presentation of the moments acting about z axis which produce the dowel actions and the corresponding dowel forces are investigated in detail on the elements of the CVB along its critical length of 1330mm, Figure 8.51.

The moments M_z transfer between the two elements of the CVB (the dowelaction) when no links are of equal magnitude and in opposite direction. This would be the case for an element shown in Figure 8.53. However, when this element is adjacent to an element with astirrup positioned at its node, Figure 8.53, the moments are distributed between the elements and the stirrup and the moments M_z is of different magnitude and their direction is determined by the moment contribution from the link.

In all moment diagrams the largest positive moment is at opening corner where the upper node for diagonal compression strut forms. In NSC model T-NSC3, the largest negative dowel moment to develop is at the lower end of the inclined diagonal compression strut with the dowel action just above link 3, Figure 8.54. These two points coincide with the end of the diagonal compression strut in the TBCJ. The horizontal resultant of these large forces from the end of the diagonal compression strut on its top and bottom ends are mostly counter balanced by the dowel action on the CVB.

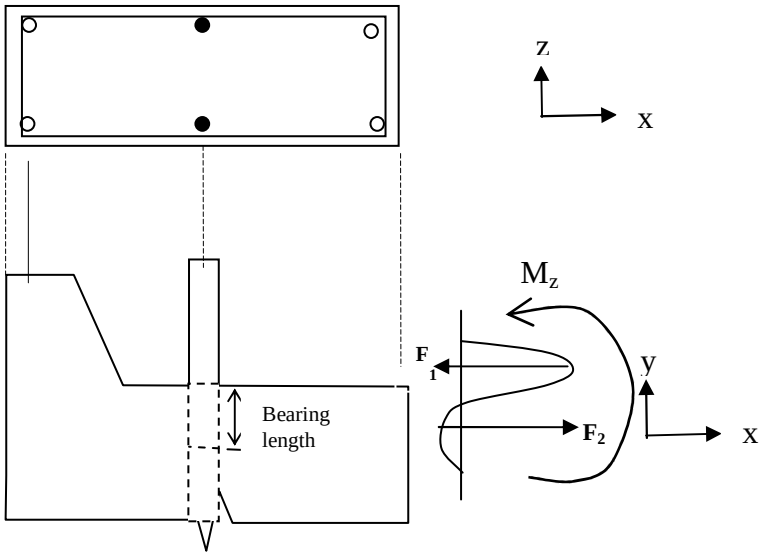

Figure 8.50: Forces F1 and F2 which produce moments Mz about z axis.

In T-HSC3 at 168 kN loading the highest positive moment following the largest M_z at intersection with the beam bar occurs at link 8, located just above the opening corner which is 73,058 Nmm, Figure 8.54, this is repeated at 240 kN loading with the moment 106,110 Nmm and at 330kN with 171,490 Nmm, Figure 8.57. It is notable that the quantity of moments are very small. This is due to FE model assuming full bond interface between concrete and steel. In reality, full slippage occurs to develop moments on the steel. This issue is discussed in details in chapter 4. However, the object of this practice is to find the location where the maximum moment occur on the CVB.

Figure 8.53, represents the direction of the moments and interaction of the moments at nodes where a stirrup intersects the CVB. However, in the graphs produced for analysis such details are omitted and only changes in the moments Mz are presented

In T-NSC3 the largest negative moment develop at the point above link 3, which is the level of support for the lower end of the inclined diagonal compression strut which is 35,786 Nmm at 168 kN and 57,009 Nmm at 240 kN just before failure load of 260 kN, Figure 8.57.

Figure 8.54 to Figure 8.57 show the Moment Mz on the CVB for various loading and material on node i with vertical dotted lines representing stirrups in Figure 8.51. acting on element top node end (i), Figure 8.52.

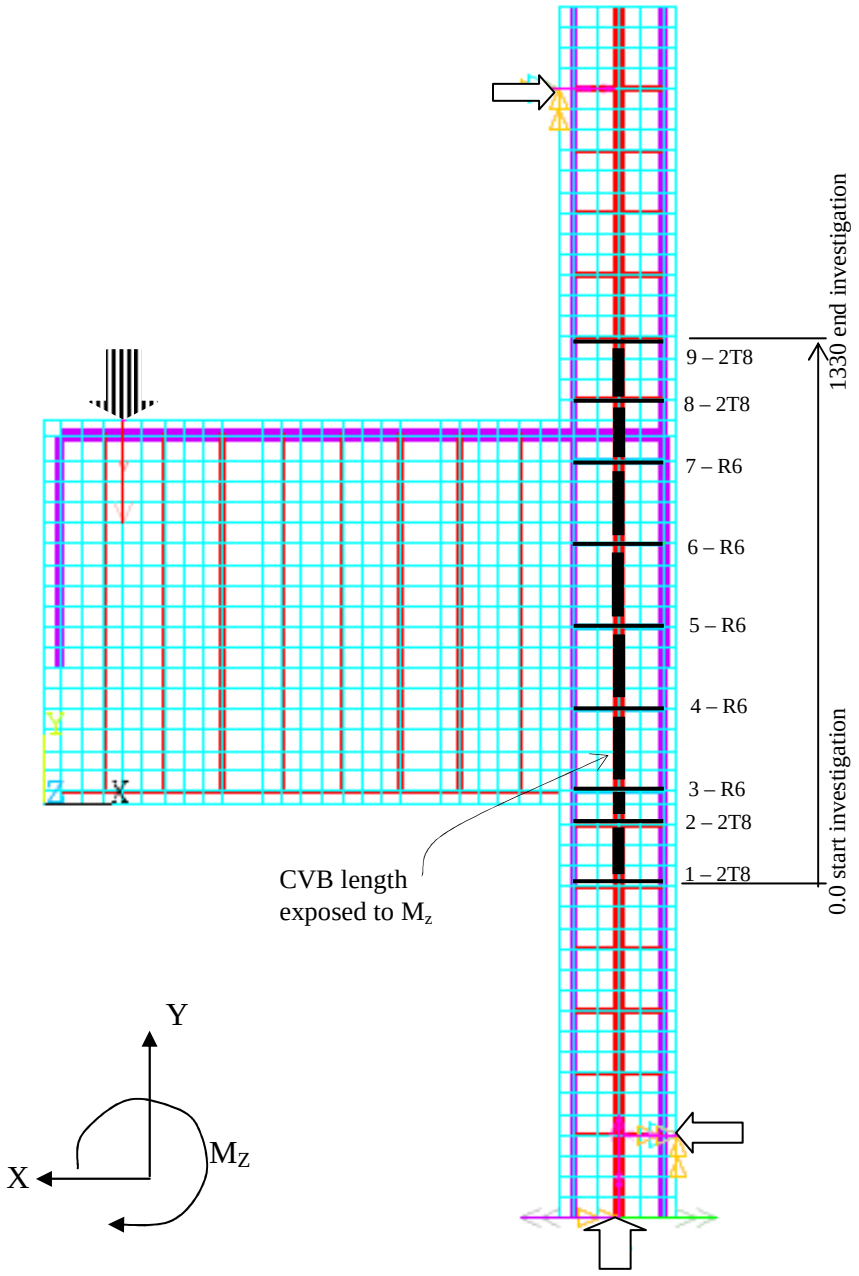

Figure 8.51: The diagram shows the position of CVB in thick dotted line and stirrups in thin dotted lines for which moment M about z axis are plotted in the following graphs. Dimensions are in mm.

Index No	1	6& 7	12& 13	20& 21	28& 29	36& 37	44& 45	48& 49	54
Link No	9	8	7	6	5	4	3	2	1

Table 8.17: Link position is numbered in Figure 8.51 in relation to Index (Node) shown on Table 8.18.

At 240 kN, the loading dowel moment is 106,110 Nmm on T-HSC3 compared to 153,840 Nmm for T-NSC3 which is its dowel moment just before its failure load of 260 kN as compared to 171,490 Nmm for T-HSC3 at 330 kN loading which is just before its failure load of 340 kN. Figure 8.55 to Figure 8.58.

Figure 8.52: Node ends for elements are identified as node i for the top and node j for bottom. Moment and force diagrams represent moments at node i whereas tables show moments at top node i and bottom node j

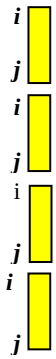

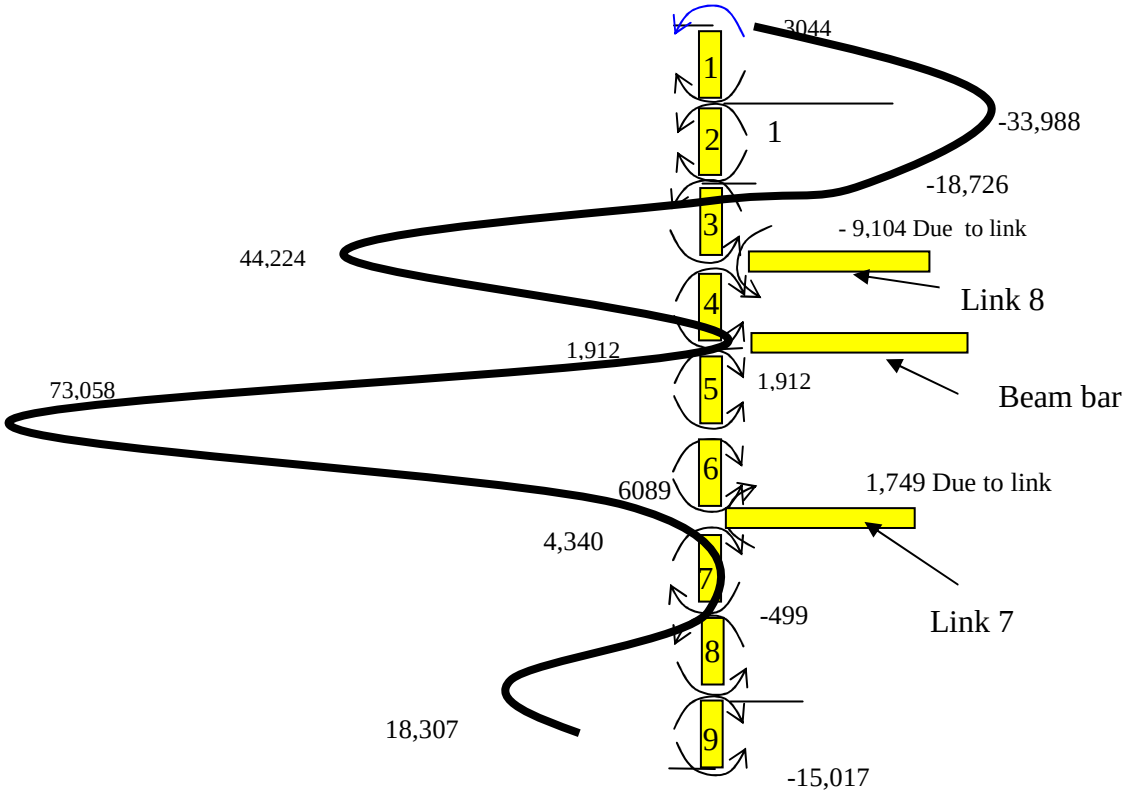

Figure 8.53: Diagrammatical presentation of the moments acting on the top 9 elements.

8.14 Discussion on strain analysis of CVB in TBCJ

From the numerical modelling of beam columns in this chapter of the thesis, it is demonstrated that the presence of CVB delays increase in the width of the cracks in TBCJ from. Figure 8.59, the difference in maximum and minimum moments which act along the primary bearing length exposed to dowel action is significantly less when HSC is used.

The quantity of moments recorded by FE are very small. This is due to FE model assuming full bond interface between concrete and steel, whereas full slippage occurs in reality to develop moments on the CVB. Chapter 4 deals with this issue in details. The object is to find the location where the maximum moment occur on the CVB in order to develop a STM for the TBCJ.

Link	Node No	Distance CVB mm	Mz Nmm	Link	Node No	Distance CVB mm	Mz Nmm	Link	Node No	Distance CVB mm	Mz Nmm
T89	1	1328	-3044.8		19	878	15017	R64	37	428	-4723.3
	2	1278	33988	R66	20	828	2479.7		38	378	20997
	3	1278	-33988		21	828	-1991.5		39	378	-20997
	4	1228	18726		22	778	-8321.8		40	328	10517
	5	1228	-18726		23	778	8321.8		41	328	-10517
T88	6	1178	-35120		24	728	10739		42	279	28323
	7	1178	44224		25	728	-10739		43	279	-28323
	8	1128	-1912		26	678	-8159	R63	44	230	10261
	9	1128	1912		27	678	8159		45	230	-14018
	10	1091	-73058	R65	28	628	4370		46	200	17793
	11	1091	73058		29	628	-137.38		47	200	-17793
R67	12	1028	-6089.5		30	578	12359	T82	48	150	14514
	13	1028	4340.5		31	578	-12359		49	150	-16892
	14	978	498.59		32	528	-1949.7		50	100	10067
	15	978	-498.59		33	528	-1949.7		51	100	-10067
	16	928	-18307		34	478	-3211.2		52	50	19465
	17	928	18307		35	478	3211.2		53	50	-19465
	18	878	-15017	4	36	428	5317.9	1	54	0	3084.5

Table 8.18: T-HSC3 at 168 kN loading. The first column section lightly shaded represents the 18 nodes corresponding to 9 elements shown in Figure **8.53.**

Element no	Mz at node I of CVB	Mz at node j of CVB	Mz at node j of link	Comment
1	-3044	33988		
2	-33988	18726		
3	-18726	-35120		
			-9104	Link moment
4	44224	-1912		
5	1912	-73058		
6	73058	-6,089		
			1749	Link moment
7	4340	499		
8	- 499	-18307		
9	18307	-15017		

Table 8.19: T-HSC3 at 168 kN loading, the table shown shows how much moment about z axis acts at the nodes of the elements. The readings are then presented in Figure 8.54.

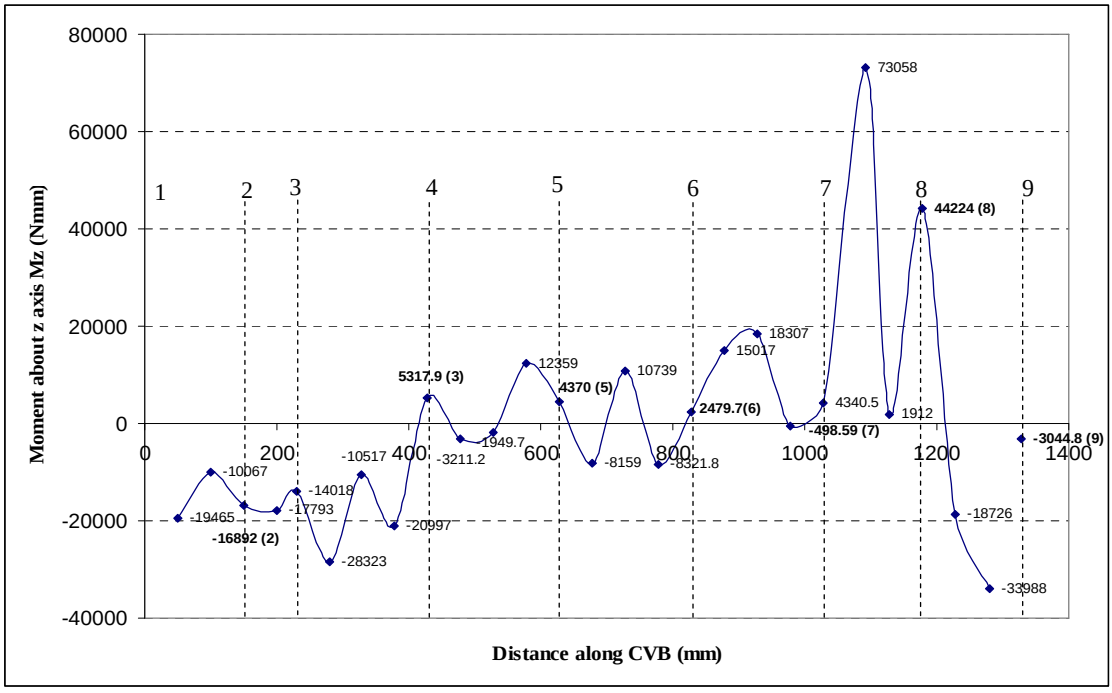

Figure 8.54: Moment Mz on the CVB for T-HSC3 at 168 kN

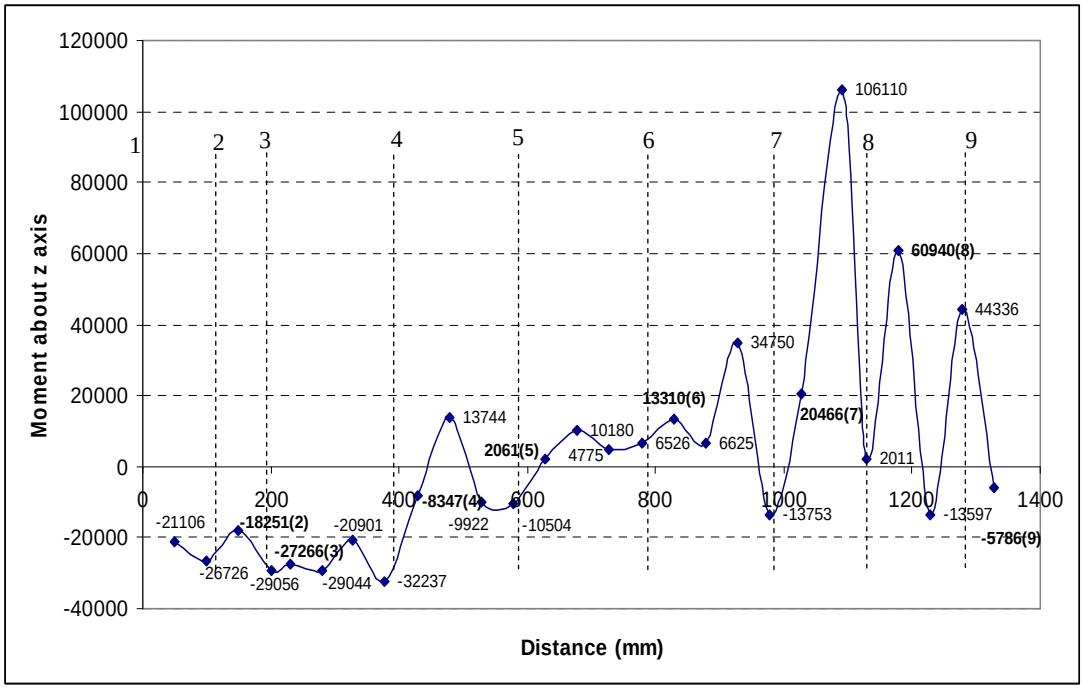

Figure 8.55: Moment about z axis (Mz) on CVB for T-HSC3 at 240 kN.

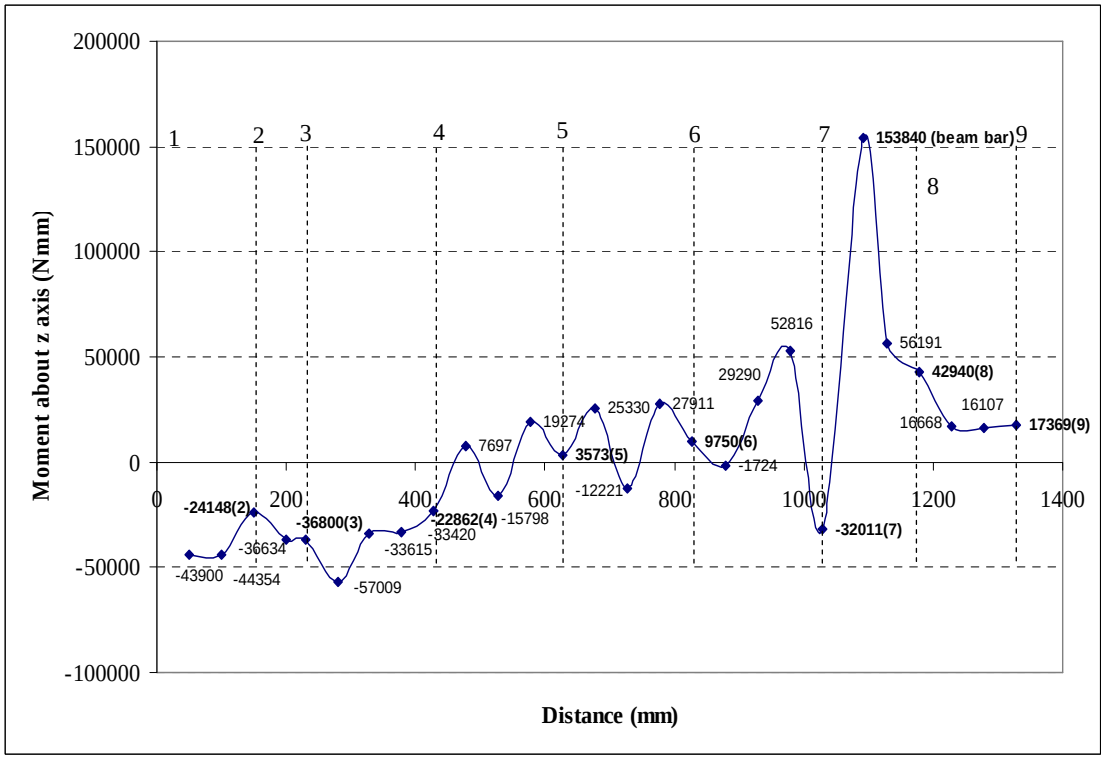

Figure 8.56: Mz T-NSC3-240 kN loading

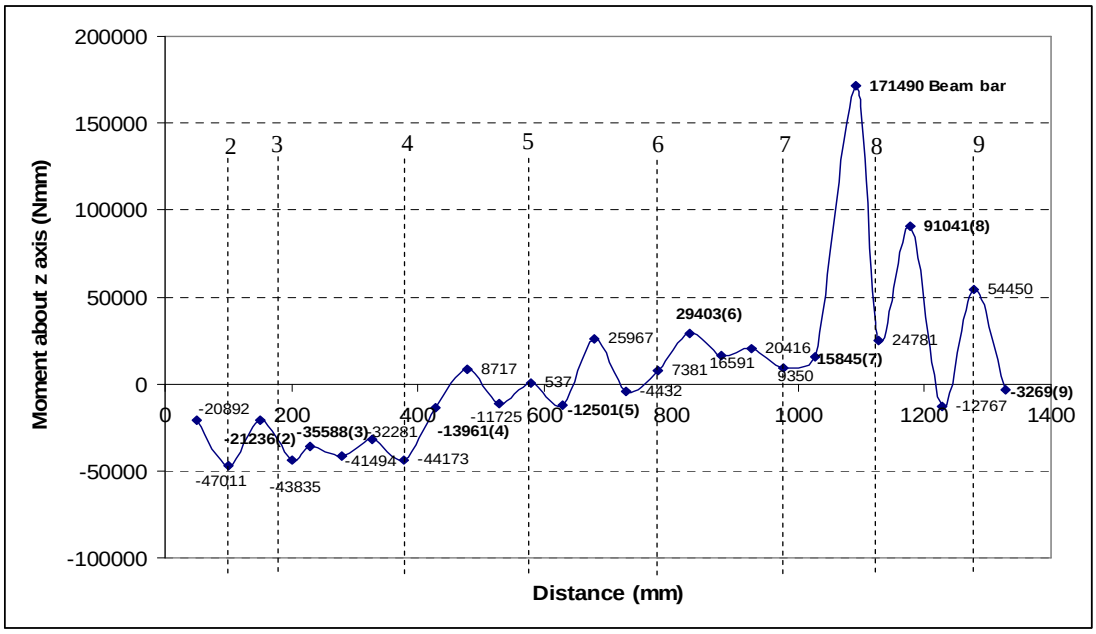

Figure 8.57: Moments about Z axis on CVB of T-HSC3 at 330 kN

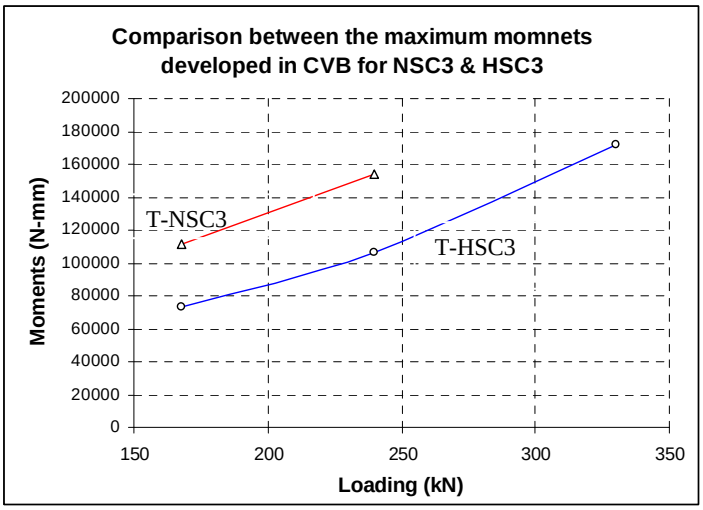

Figure 8.58: Comparison between the maximum moments for NSC3 & HSC3 developed in tested length of CVB, 1300 mm at BCJ.

It is noted that:

i. NSC3 developed greater maximum moments compared to HSC3

ii. Increased loading increases the maximum moment

Investigating the maximum moments acting on CVB at 240 kN, the moment produced on CVB is 45% more in NSC, Figure 8.56, compared to HSC, Figure 8.55. At the same loading the minimum moment for NSC is 77% less in NSC than HSC. Larger difference

between maximum and minimum moments means larger moment acts on CVB, making it produce wider cracks leading to failure.

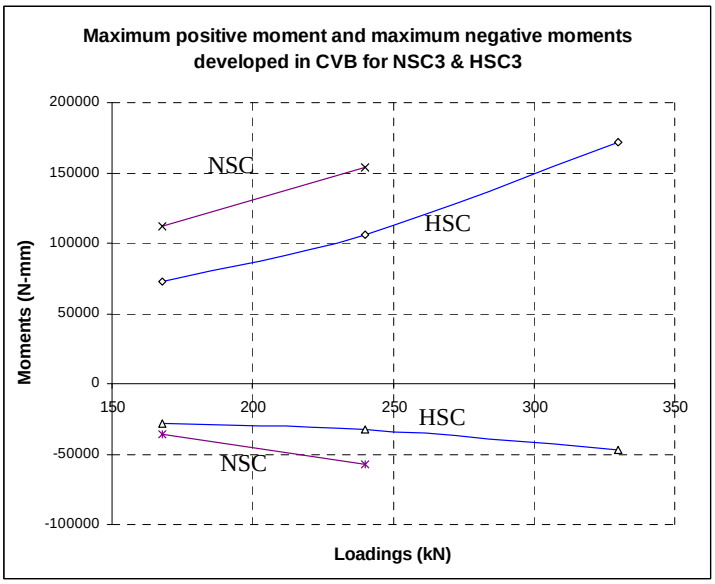

Figure 8.59: Comparison between maxima and minima moments for NSC3, HSC3 of the investigated length of CVB, 1330 mm at the beam column join (see Figure 8.51)

The minimum moment in TBCJ occurs closer to link 4 in HSC than in NSC which has its minimum close to link 3, indicating that diagonal compression strut is deflected in T-HSC3 at ultimate load.

The difference between maximum and minimum moments in HSC just before failure at a load of 330 kN in TBCJ is 215.7 kNmm compared to 210.8 kNmm in NSC at 240 kN, demonstrating that the presence of HSC has resulted in increasing load resisting capacity by 37.5% while supporting CVB so that the moment on CVB is almost the same.

At 260 kN, T-NSC1 fails in the diagonal compression strut whereas T-HSC1 fails at 260 kN. When CVB is added, T-NSC3's load bearing capacity improves to 260 kN, an increase of 18% compared with that of T-NSC1. The greatest increase occurs when HSC is used which increases the T-HSC3 load bearing capacity to 340 kN, an improvement of 31% compared to T-HSC1 and T-NSC3.

The TBCJ has the deep beam covering the front column bar. Therefore, the material properties of HSC does not behave in the same way as in the analogous HSC beam of

shear span to depth ratio of 3.05 which had premature failure due to initiation of tensile shear cracks which developed in the cover at early loading stage. In TBCJ –HSC1 presence of the deep beam acts as a large cover preventing early formation of initial shear crack in the joint.

The results confirm the existing analogy between beams of span ratio 3.02 with analogous TBCJ of aspect ratio 3.11. In experimental tests on beams from chapter 2, NSC3 and HSC3, presence of 2-T20 HWB resulted in increasing failure loads to 200 kN for NSC3 and 280 kN for HSC3, an increase in shear resistance of 25% for NSC and 90% for HSC. In TBCJ, the presence of 2-T20 CVB resulted in increasing failure load to 260 kN for NSC and 340 kN for HSC an increase in shear resistance of 18% for NSC and 31% for HSC. 55% increase in ultimate load bearing capacity for T-HSC3 compared to T-NSC1.

TBCJ Failure Load (kN)	Beams Failure Load (kN)
T-NSC1=220	NSC1=160
T-HSC1=260	HSC1=148
T-NSC3=260	NSC3=200
T-HSC3=340	HSC3=280

Table 8.20: Table of failure loads for the experimentally tested beams and numerically modelled TBCJ.

8.14.1 Proposed empirical design rule for TBCJ

For HSC when $60 \leq f_{cu} \leq 120$

$$V_{jd} = V_c + 1.64\,(b_e - nd_b)\,d_b\,f_{cu}^{1/3}\,(n)^{1/4} + (A_{sje}f_y - 0.1b_e h_c f_c^{2/3}) \qquad \textbf{8.1}$$

where $0 \leq A_{sje}f_y / (f_c)^{2/3}\, b_e.h_c - 0.1b_e h_c f_c^{2/3} \leq 0.1b_c h_c f_c^{2/3}$

$0 \leq 1.64\,(b_e - nd_b)\,d_b\,f_{cu}^{1/3}\,(n)^{1/4} \leq \eta b_c h_c f_c^{2/3}$ where $\eta = 0.12$ for HSC and $\eta = 0.04$ for NSC

$$V_{jd} = \gamma(f_c)^{2/3}\,b_e.h_c + 1.64\,h_c\,d_b\,f_{cu}^{1/3}(n)^{1/4} + (A_{sje}f_y - 0.1b_c h_c f_c^{2/3}) < 0.7b_c h_c f_c^{2/3} \qquad \textbf{8.2}$$

For L bar $\gamma = 0.13$ or U bar $\gamma = 0.11$

h_c is the section depth of the column (mm)

f_c' is the concrete cylinder strength (MPa);

b_e is the average of the beam and column widths (mm)

For T-HSC3

Taking moment about the bottom reinforcement of the beam.

$T_b \times (930 - 37 - 30) = P \times 1150$ P= 340 kN

$$V_{col} = \frac{1300 \times 260}{2} = 221 \text{ kN}$$

$$V_{jdfe} = T_b - V_{col} \qquad 8.3$$

T_b = 453 kN $V_{jd\ fe}$= 232 kN

Similarly for T-NSC3 with P= 260 kN

T_b = 346.5 kN $V_{jd\ fe}$= 177.5 kN

Beam	**HSC2**	**HSC3**	**HSC4**	**NSC2**	**NSC3**	**NSC4**
f_{CU} N/mm^2	109.3	112.5	112.5	41	47.7	43.3
V_S kN	18.7	18.7	18.7	18.72	18.72	18.72
Vc kN	114.9	117.1	117.1	59.8	66.1	62.0
Web Steel	12	20	25	12	20	25
V_{dow} kN	14.1	20.7	23.5	10.2	15.6	17.1
$V_{jd\ Beam}$ kN	129.0	137.8	140.6	59.8	66.1	62.0
$V_{Beam\ test}$ kN	132.5	140	150	101.5	100	105
$V_{Beam\ test}/V_{jd\ Beam}$	1.03	1.02	1.07	1.45	1.22	1.33
ρ_b%	0.5	1.4	2.2	0.5	1.4	2.2

Figure 8.60: Prediction of proposed formulae compared to beam experiments for HSC beams with HWB

8.14.2 Strut and tie model for TBCJ

From analysis of strain in the direction of shear force or in axial direction on the leg of stirrups, it was concluded that the maximum strain on upper link known as link 6 in Figure 8.51 for T-HSC3 is at 36mm from the rear column reinforcement. This compares to this location being 50mm for other 3 models.

Similarly at the centre or link 5 in Figure 8.51 the point of maximum strain is at 125mm from the front column reinforcement.

BCJ	T-HSC3	T-NSC3
f_{CU} N/mm^2	110	42
V_S kN	18.7	18.7
Vc kN	117.1	66.1
Web Steel	20	20
V_{dow} kN	20.7	15.6
$V_{jd\ beam}$ kN	137.8	66.1
V_{fe} kN	232	177.5
V_{fe} /$V_{jd\ T\text{-}HSC3}$	1.68	2.68

Table 8.21: Prediction of proposed formulae compared to TBCJ experiment results for T-HSC3 beams with HWB

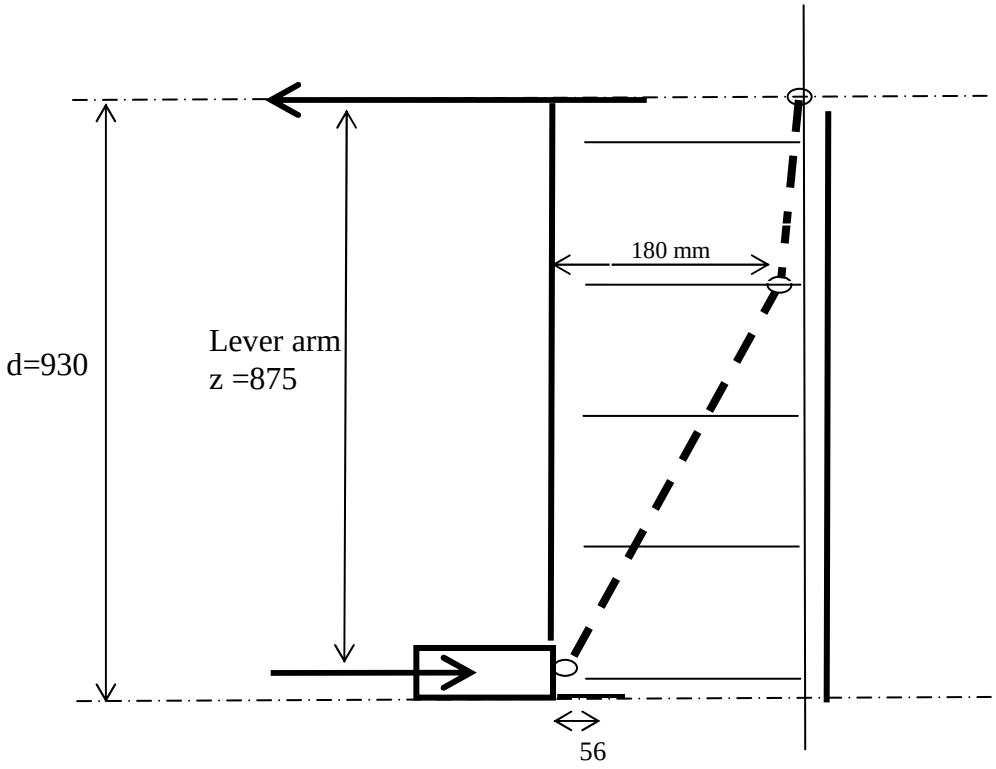

Figure 8.61: STM developed for T-HSC3

The force on the tension bar is = $0.78\times720\times3\times\pi\times(\frac{23}{2})^2$ =699.6 kN

$V_j= T_{bb}-V_{ct}= C_{be}-V_{cb}$ **8.4**

where

T_{bb} is the total force in the beam bar

V_{ct} is the shear force above the column

C_{be} is the force in the beam's compression chord

V_{cb} is the shear force in the column below the joint

$V_{ct} \times (2930 - 400) = 340 \times (1300 - 150 + 150)$

V_{ct}= 174.7 kN

V_j= 699.6-174.7=524.9 kN

V_{ct}= V_{cb}

C_{be}= 524.9- 174.7=350.2 kN

8.15 Conclusion on contribution of CVB to HSC in TBCJ

- Influence of HSC materials with no CVB

From the results of models. T-NSC1 and T-HSC1, it can be noted that an increase in concrete strength of 162% results in an increase in maximum failure load of 18%. This indicates that the significant increase in concrete strength has little influence on the increase in load bearing capacity of TBCJ.

- Influence of CVB in NSC TBCJ

Considering models T-NSC1 and T-NSC3, it is noted that while the NSC remain the same the loading bearing capacity of the TBCJ increases by 18% due to the use of CVB. Again this is a comparatively small increase when considering the increase in reinforcement . Therefore, the use of CVB in NSC TBCJ does not influence the load bearing capacity significantly.

However, the analogous beams tested by the writer demonstrated that presence of HWB results in producing numerous small cracks parallel to the main crack before failure load. This means the structure failed in a more ductile manner compared to when HWB was absent, the same principal may apply to TBCJ with CVB.

- Influence of CVB in HSC TBCJ

Considering models T-HSC1 and T-HSC3, it is worthy of attention that while HSC remains the same, the loading capacity of the TBCJ increases by 31% due to the presence of CVB. This is a significant increase as a result of using CVB in HSC TBCJ. Therefore, the use CVB in HSC TBCJ is favourable.

The analogous beams in chapter 3 demonstrated that presence of HWB results in producing numerous small cracks parallel to the main crack before failure load. This means the structure failed in a more ductile manner compared to when HWB was absent. In HSC, absence of HWB resulted in sudden and brittle failure of the beam at ultimate loading less than similar beam made of NSC. The same principal may apply to HSC TBCJ with and without CVB.

- Influence of CVB and HSC on behaviour of TBCJ

Comparing T-NSC3 and T-HSC3, when the concrete strength has been increased and CVB was added to TBCJ, it can be noted that the loading capacity of the TBCJ increases by 31%. This is the same percentage as obtained with the use of CVB only and without the effect of material properties of concrete. Presence of CVB results in more ductile mode of failure for both NSC and HSC.

Summing up these results it can be noted that the load bearing capacity of TBCJ significantly increases when CVB is used with HSC, and neither CVB nor HSC by themselves improve the load capacity of TBCJ.

An empirical design equation was proposed for HSC TBCJ with HWB which was also applied to the analogous beams experimentally tested. The equation produced reasonable prediction compared to FE and experimental results.

A detail investigation of strain within the critical location in the reinforcement cage was completed. Data obtained from strain development in the beam bar and links were used to identify the location of deflection of the diagonal compression strut n order to develop a STM.

The beam failure loads of TBCJ were compared with the predicted load from the proposed design equation for TBCJ. The equation was applied to analogous beams which had been experimentally tested.

8.16 Reference

8-1 ACI-ASCE Committee 352, 'Recommendations for Design of Beam-Column Joints in Monolithic Reinforced Concrete Structures'. ACI Journal Proceedings: Part 3, Detroit, American Concrete Institute 1998

8-2 Vollum, R.L and Newman J.B . “Discussion on paper published in Magazine of Concrete Research,” 1999,51,No. 6,415-425- Strut-and-tie models for analysis/design of external beam column joints. Magazine of Concrete Research, 2001, 53, No.01, February, 63-66

Chapter 9
Conclusion and Suggestions for Future Work

9.1 Introduction

HSC is widely used for many multi-storey commercial and residential buildings in the industrialised world. There are numerous economical and technical advantages in using HSC, however, there are still many uncertainties about its structural behaviour, one of the most important of which is the shear performance of BCJ in multi-storey buildings. This is because structural members were designed for shear according to codes developed for NSC.

It has so far been proven that for beams with span/beam ratio of a/d=3.02, the shear resistance is equal to, and in some cases less than, NSC. For this reason, further research work and design recommendations regarding the shear behaviour of HSC were suggested in most of the reviewed literature.

It was experimentally demonstrated, Table 2-5, that HSC beams with HWB when designed using this writer's suggested design rule in addition to BS8110, Table 2-10, developed greater shear capacity in the beam with the following ratio

$$\frac{ultimate\ shear\ force}{characteristic\ shear\ performance} = 1.2\ to\ 1.26$$

This is greater than that of the test results for similar beams without HWB which only developed a ratio of 0.69, Table 2-1.

In chapter 3, HSC and NSC beams with and without HWB of span to depth ratio of 3.02 were experientially tested, Chapter 4 verified and validated the adopted FE numerical analysis approach by calibrating FE models to the experimental tests from Chapter 3, Chapter 5, discussed STM for beams tested in chapter three and further discussed STM for BCJ and analogous TBCJ with HWB and gave a proposal for STM for BCJ.

Chapter 6 investigated the empirical equation and code guidance for design of BCJ and TBCJ and gave proposed design rule for BCJ, Chapter 7 combined the information in chapter 4 on

FE validation and verification of the tested beams with the calibration of beams and BCJ from Chapter 6 which verify and validate FE modelling for BCJ in order to parametrically investigate the performance of CVB in TBCJ made of HSC

In chapter 8, the behaviour of HSC and NSC TBCJ with and without CVB was investigated by using a nonlinear FE computer programme, the data obtained from the analysis was used to demonstrate the influence of CVB in TBCJ. Empirical design rule for designing HSC TBCJ with CVB was proposed.

9.2 Reviews

The literature on shear behaviour of beams, in particular influence of dowel action to resist shear was reviewed and experimental tests on HSC beams, beams with HWB and BCJ was studied.

A review of FE analysis was carried out together with factors associated with numerical modeling HSC beams with HWB.

Past research work on STM for beams and BCJ was discussed. Various STM design proposals were compared and studied for their suitability for HSC BCJ.

A review of FE analysis of BCJ was carried out for factors associated with numerical modelling of HSC TBCJ.

Methods of improving the shear capacity of beams and BCJ as well as design code recommendations were studied.

8.1 Proposed design rule for concrete indirect tensile strength (f_t)

From experimental tests on NSC and HSC, it is proposed that $f_t = 0.47\sqrt{f_{cu}}$ gives a more accurate prediction of indirect tensile strength (f_t) for corresponding cube compression tests (f_c) compared to design rules recommended by BS1881 Part 117 or CEB's recommendation ($f_t = 0.3\, f_c^{2/3}$), Tables 2-3 and 2-4.

9.3 Horizontal Web Bars (HWB) and Central Vertical Bars (CVB)

Past experimental work by this writer demonstrated that the shear capacity in HSC beams with span/depth ratio of a/d=3.02 is less or equal to the shear of NSC beams of the same geometry and with the same reinforcement, Table 3-1.

However, the situation reverses when HWB are placed at the centre of the depth of the beam. The shear which developed in this model was twice the shear resistance of the same HSC beam with no HWB. However, little difference was noted when HWB were used in NSC beams. This is because, in NSC, the stirrups will yield and fail regardless of the presence of HWB. Therefore HWB have limited influence on NSC, whereas it is a very effective influence when used in HSC beams, Table 2-5.

It has been noted that, in general, HWB located towards the centre of the beam improves the shear resistance of the beams significantly. This supports the experimental results obtained previously by this writer. The results in beams with HWB (beam HSC4) compared with those without (beam HSC1) indicate a significant increase in shear resistance in HSC beams of around 130%,.

At failure stage, presence of HWB produces many scattered cracks parallel or near to the main crack close to failure loading. This results in more ductile and gradual failure compared to sudden failure due to formation of one main crack and sudden failure in the absence of HWB. When HWB is present, the energy from the increasing load is dispersed across the shear span in the form of numerous cracks, Figures 3-9 to 3-11 and Figures 3-13 to 3-15. The ductile failure due to presence of HWB is in contrast with the sudden failure due to rapid transfer of energy from increased loading into a single large crack producing a brittle and sudden failure when no HWB is present, Figures 3-8 and 3-12.

Development of shear strain on the reinforcement cage in HSC beams investigated shows that the influence of HWB is more effective at the final stage of loading. It was noted that the final 40% of the applied load is mainly resisted by the shear performance of HWB since the shear stirrups have yielded several times their yield value. In the initial 60% of the total applied load

the stirrups resisted shear forces. However, HWB in NSC have little influence on shear improvement of the beam because as the stirrups yield and become plastic, the beam fails regardless of the presence of HWB, Figure 2-36.

HWB can also provide added ductility and resistance to accidental, blast and seismic loading on beams and BCJ. For design purposes, when considering fire exposure in particular, their location being protected by the surrounding concrete would be of some advantage.

Dowel action from HWB did not make any contribution to shear resistance in NSC beams without transverse reinforcement and made only a small contribution when stirrups are present with HWB. This is because the maximum shear performance from dowel action is dependent on support from the stirrups and the tensile strength of concrete. Dowel action is not fully developed in NSC with stirrups because of the limited tensile strength of concrete.

Comparing tests of NSC beams with HWB without stirrups to the similar beams but with stirrups, it is shown, Table 2-19, that $V_{test} / V_{Bau\ (Mot)}$ is 14% larger than $V_{test} / V_{Bau\ (Hej)}$, indicating that this increase is due to the presence of the stirrups used in this writer's tests on NSC where there were none used. Therefore, presence of stirrups improves dowel action and the shear resistance by 14%, Table 2-19.

HSC beams with HWB of a/d=3 are analogous to HSC TBCJ of aspect ratio 3 with CVB. In such structural systems CVB has similar properties and advantages in TBCJ as HWB in beams, Figure 1-5.

9.4 FE model

FE models were developed for beams and BCJ to investigate the influence of HWB and CVB as well as HSC on the shear behaviour of these structures and the results were compared with those of previous experimental work carried out by this writer as well as published experimental results by other researchers.

The FE model usually predicts a greater failure load and a smaller deflection than experimental tests. However, the differences are greater in NSC and smaller in HSC, because

HSC has lower shrinkage because the water cement ratio (W/C) was 0.25 for HSC beams as compared to 0.6 for NSC. This significant reduction in W/C for HSC means much smaller shrinkage or micro cracking for HSC, and higher tensile strength for HSC means less slippage at bond between concrete and reinforcement.

The FE does not model material properties such as micro- cracking or bond slippage effect, it therefore models NSC as a stiffer structure compared to the experiment, whereas in HSC because of lower micro-cracking and slippage, the FE model gives a closer prediction to the experimental results.

In the experimental work, HWB comes into action resisting shear loads during the final 40% of the loading of the HSC3 beam. The experimental gauge recorded that after the initial 60% loading was applied, all 3 centrally located stirrups in the shear span had yielded more than three times their yield value, demonstrating that significantly wide cracks had occurred in the shear span. This was demonstrated in the FE model by showing yielding of the same stirrups at around double the yield value The FE model shows deformation of the structural system as if it is made of a rubber rather than brittle and non-homogenous HSC and after wider cracks develop element separation is not modeled by FE.

The shrinkage of concrete experimental beams which results in micro cracking, bond slippage between reinforcement and concrete, honey combing, and element separation at final stages of loading when cracks are wide are not included in the FE model, this results in making the structural system behave more rigid.

FE models of beams with and without HWB as well as BCJ with and without CVB were carried out to idealize a number of past experimental model results accomplished by this researcher and others. The results were compared and good agreements were achieved between the experimental and the numerical, FE, results.
The FE method was used to develop numerical models which were verified and validated with the experimental works for beams of 3> $\frac{a}{b}$ >1.5 and for BCJ with aspect ratio of 1.33 and was successfully applied for parametric investigation of TBCJ, 3.11= $\frac{d_b}{d_c}$

9.5 Strut and tie (STM)

HWB can deflect the inclined compression forces within the shear span of the HSC beam of a/d≈3, Figure 4.50, producing a wider and stronger diagonal compression strut at the supporting plate resulting in yielding of the tension reinforcement, from the full aching action produced by the inclined strut, Figure 2-27, therefore full STM development, and in similar manner CVB deflect the inclined compression forces within the analogous TBCJ, Figure 4.48.

When the concrete is of normal strength, this deflection is not much and as a result the inclined diagonal compression forces is not a strong concrete and wide, and is not deflected enough to bring the tension bar to yield, therefore the inclined diagonal strut is not wide or strong enough to produce sufficient arching action to strain the tension steel to yield. As a result, full strut and tie action with yielding of tension steel does not occur, as demonstrated with beams NSC2, NSC3 and NSC4, Figures 2-16, 2-17 and 2-18.

Higher strength of concrete contributes to improved arching action more than on shear cracking resistance. The upper limit of a/d≤2 for STM can therefore be increased for HSC beams with HWB to a/d≈3. When beams are a/d=3, in the absence of HWB, the weakness in shear cracking resistance of HSC resulting from absence of aggregate interlock, in particular limestone, is apparent, Table 2-1. However, when HWB was introduced the shear cracking resistance was significantly improved and crack initiation was delayed and its widening was restrained, allowing the development of full arching capacity in beams or analogous BCJ. Figure 2-36.

When the ratio of web reinforcement was low, a load greater than the shear cracking load could be resisted by a combination of arch and truss actions. As long as a/d ≈3, the limit is not an exact one but tends to increase with increasing concrete strength, Figure 4.27, which has more effect on arch capacity than on shear cracking resistance. This is the same as with TBCJ.

To propose a STM based on failure criteria is complex as STM is a lower-bound plastic theory and does not have any compatibility condition. However, it was attempted by FE modelling to find the angle of deflection of the diagonal compression strut at its intersection with HWB,

Figure 3-86 or with CVB, Figure 7-59, by calculating the moments produced on them by dowel action. This data ws used to develop a STM for TBCJ, Figure 7-63.

It has been shown that the idealization of STM of HSC beams with HWB with a/d≈3 developed in this investigation is analogous to STM model of HSC – TBCJ with CVB of .

As STM was developed to represent the characteristics of the stress paths in HSC beam with HWB of shear span/depth ratio 3.02. Figure 4.47. This model was extended to represent the stress path behaviour in TBCJ with CVB of aspect ratio of 3.11. Figure 4.48.

Strut and tie mechanical models were developed and analysed for beams with span/depth ratios of $\frac{a}{b} = 3.02$ and for TBCJ of aspect rations of $\frac{d_b}{d_c} = 3.11$ with and without HWB and CVB. Figure 7-63**.**

9.6 The coefficient of friction for FE model for open cracks in HSC

Since the coefficient of friction for closed cracks in HSC is similar to that of NSC and past research has demonstrated its value to be equal to 1, FE models for HSC1 beams tested by this writer were developed and the coefficients of friction for open cracks in HSC1 without HWB within the allowable range values for the friction of 0.1 to 0.3 were calibrated these with the experimental results. This investigation was similarly extended to HSC beams with HWB in order to determine the coefficients of friction of open cracks when HWB is present. It was concluded that the coefficients of friction for open cracks can be taken for HSC made with limestone with HWB as 0.15 and for NSC with HWB as 0.3 respectively.

9.7 Design recommendation for TBCJ

Design recommendations of codes ACI 352 and EC8-NA for HSC BCJ fail to show the dependence of the joint ‘shear strength’ on the joint ‘aspect ratio’, as well as the influence of HSC and detailing of the anchorage of beam bar on the behaviour of BCJ, and do not provide

any recommendation if the amount of stirrups is not adequate in order to provide sufficient shear strength at BCJ when the shear forces are high. Their specified minimum shear stirrup requirements, however, do not give provision for the joint strength to be increased by the stirrups.

The assumption that the stabilising arching effect in the HSC beam of $a/d \approx 3$ with HWB makes the beam perform like a short beam of $1 \leq a/d \leq 2.5$ and is analogous to HSC - TBCJ with aspect ratio of around 3 with CVB was found to be reasonable and provides good idealisation for the structural behaviour of HSC TBCJ.

Baumann's modified design rule for shear prediction including the dowel action of the web bar is safe as the diameter of the web bar increases. Baumann's approach proposing that dowel action from the web bar is related to the strength of concrete is a rational one, therefore his design rule was modified by making provision for the number of dowel bars and to improve its reliability and is proposed for shear design.

CVB contributed significantly to the shear capacity of HSC transfer BCJ. It was also shown that if CVB is not used, then this results in a strain concentration at the anchorage corner bend of the L-shaped beam-bar in HSC TBCJ. This is undesirable in the design of BCJ. Therefore, the use of CVB is beneficial to prevent strain concentration at the bend.

9.8 Future research

In the light of FE numerical results presented in this study, the following research topics are suggested:

- Experimental tests on beams identical to HSC beams HSC2, HSC3 and HSC4 but without the stirrups are recommended, to demonstrate the contribution of stirrup support to HSC beams with HWB.

- Shear resistance of HSC beams of span depth ratio 3.02 made of lime stone aggregate were less or equal to NSC, although FE modelling showed that this is not the case for TBCJ model T-HSC1. It is recommended to investigate these findings by experimental tests.

- In beams with shear reinforcement, if a simple truss model is used, there is a division and contradiction amongst all the codes regarding the limit to the angle of the diagonal compression strut to the horizontal θ_{lim} ($\cot \theta_{lim}=a/d$). All codes give $\theta_{lim}\leq 3$, however, this research demonstrates that if in HSC beams with shear reinforcement and HWB a simple truss model is used θ_{lim} can be increased to 3.02 which is larger than the upper limit all the codes have so far recommended. CEB-FIP90 gives the closest prediction, however, it could be amended to give provision for HSC beams with HWB and further research is required to confirm an increase of $\theta_{lim}\approx 3$.

- Extreme loadings such as blast, impact and seismic produce significant gyrational forces, HSC has a economical potential for multi-storey RC frames as light frames made of HSC reduce gyrational, in addition to the economic benefits of using HSC.

- HWB and CVB improves the fire resistance of RC frame.

- FE concrete models do not include the influence of micro-cracking due to shrinkage. There is a significant difference inthe water cement ratio applied to NSC (0.6) and HSC (0.25). Further research is proposed to include the influence of micro-cracking due to shrinkage in NSC and HSC, and to model bond slippage between reinforcement and various strengths of concrete.

- It is suggested that finite difference and applied element methods to model element separation be applied to the experimental tests on HSC2, HSC3 and HSC4 beams to compare strain developments in the centre links with those recorded in Figure 2-36. FE does not model element separation whereas the large strain in the central links indicate element separation.

- Further experimental tests are required to investigate the effect of side cover on CVB in TBCJ of HSC with different cover thickness as cover plays an important part before and after spalling off.

- The influence of gauge length and its location in confinement bars should be investigated as it was demonstrated in the FE models of both beams and BCJ that past experimental tests failed to catch the strain localisation at peak strain.

- The spacing between shear links is proposed to be taken as $400(f_{cu})^{-0.16}$ mm in order to allow for the change in the angle of shear crack which is dependent on strength of concrete. Although this proposed rule is an improvement to the exiting limit of 200mm proposed by BS8110.

- Research to investigate the optimized spacing between stirrups when HWB or CVB is used in HSC beams or TBCJ could provide a solution for the maximum allowable spacing for which the support from stirrups is fully utilized to initiate the dowel action for HWB or CVB. When this maximum allowable spacing is determined, the data would be used to provide a design rule to give the minimum number of required stirrups and maximum amount of HWB or CVB. An optimized design rule would help reduce congestion of stirrups at location of high shear in the HSC structural member.

- Coefficients of friction of open and closed cracks for HSC beams or BCJ with HWB or CVB need to be experimentally and numerically investigated and modelled by using fracture mechanics. Walraven has performed extensive experiments on shear transfer in cracks in concrete, however, to this writer's knowledge crack propagation in HSC structural systems with dowel bars resisting shear has not been investigated. This can be an area for future research.

- Future research is required to FE model the full slippage for the bond at the concrete-steel interface by introducing links as suggested in chapter 4 in order to obtain realistic value for the quantitative value of the moments acting on the HWB in HSC beams of a/d=3 after crack formation.

Appendix A

Calculation of load at first tension crack

Ortiz' beam B1

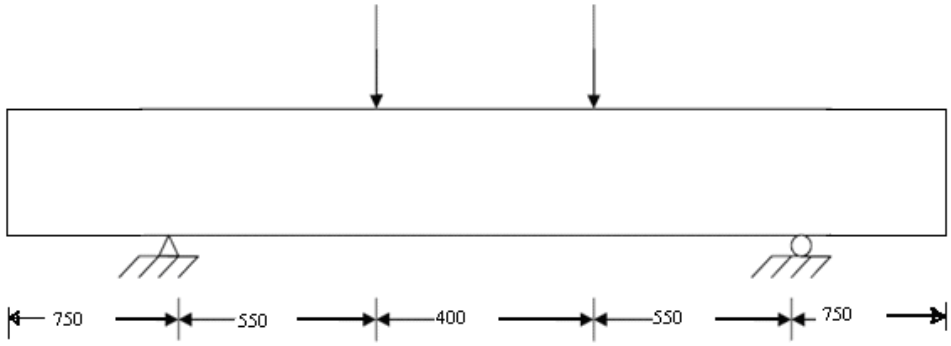

Figure A-1: Dimensions in Elevation and location of supports and loading points

Maximum Moment
The moment that occurs from the existing forces

$M_{max}=(60000N)(550mm)=33\times10^6$ Nmm

Material ProperTies
The gross moment of inertia

$I_G = (1/12)(bh^3)= 8\times10^8$

The modulus of elasticity of the concrete
E_c = 31,000 MPa
Modulus of rupture
$f_r= 0.6\sqrt{f_{cu}} =$ 4.68 MPa

Stresses in Concrete and Steel
The stresses at the extreme tension fiber are calculated using a transformed moment of inertia of the concrete and steel reinforcement

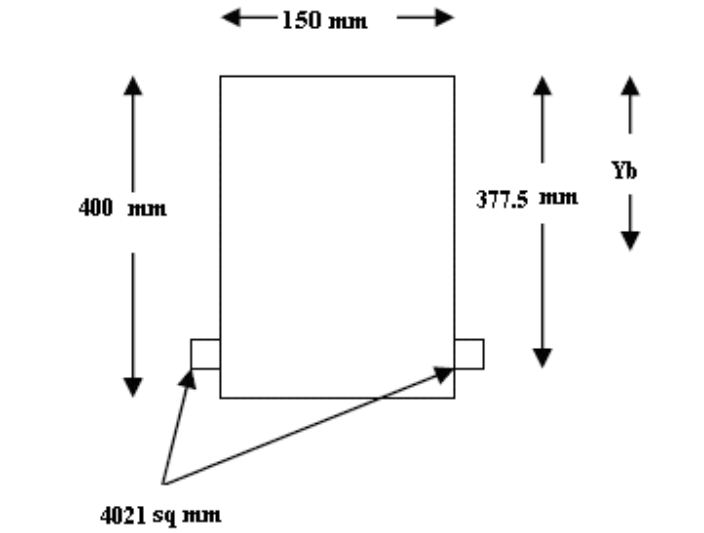

Figure A-2: Transformed Cross-Section for beam HSC1

Transformed area of steel

$(A_s)_t = 8.2As = 4021$ mm^2

2119 mm^2 distributed on each side of the concrete cross-section

Calculate the distance from the top fiber to the neutral axis of the transformed moment of inertia

$$\bar{y} = \frac{A_1 y_1 + A_2 y_2}{A_1 + A_2}$$

=221 mm

The transformed moment of inertia

$$I_{tr} = \left[I_G + Ad^2 \right]_{Concrete} + \left[Ad^2 \right]_{Steel}$$

= 9.9×10^8 mm^4

The stress at the extreme tension fiber is then calculated

$$f_{ct} = \frac{My_b}{I_{tr}}$$

= 4.95 N/mm^2

The stress in the steel at this point is calculated

$$f_s = \frac{My_b}{I_{tr}}\eta$$

= 4.95×8.2= 40.64 N/mm^2

Strain in steel = 0.0002

Loads

The load at first cracking

P=120,000 N

This writer's beam HSC1

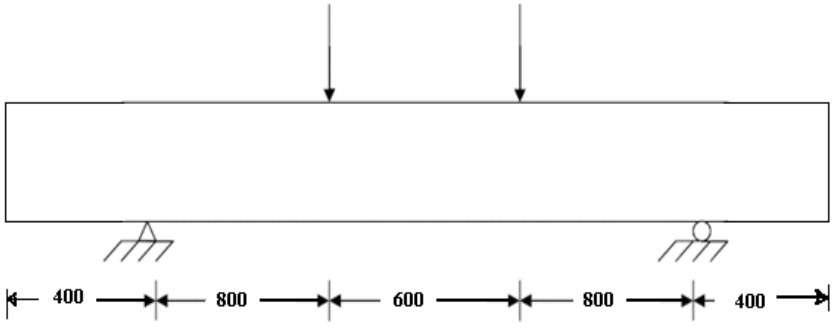

Figure A-3: Dimensions in Elevation and location of supports and loading points

Maximum Moment

The moment that occurs from the existing forces

$M_{max}=(20000N)(800mm)=16\times10^6$ Nmm

Material Properties

The gross moment of inertia

$I_G = (1/12)(bh^3)=$

The modulus of elasticity of the concrete
E_c = 33,400 MPa
The modulus of rupture
f_r= 5.2 MPa

Stresses in Concrete and Steel
The stresses at the extreme tension fiber are calculated using a transformed moment of inertia of the concrete and steel reinforcement

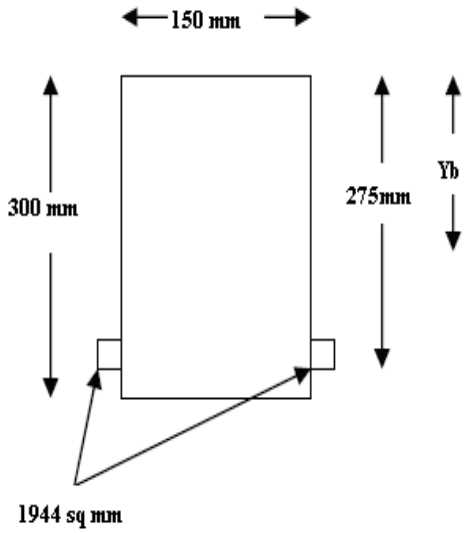

Figure A-4: Transformed Cross-Section for beam HSC1

Transformed area of steel

$(A_s)_t = 4.13As = 3889$ mm^2

2119 mm^2 distributed on each side of the concrete cross-section

Calculate the distance from the top fiber to the neutral axis of the transformed moment of

inertia

$$\bar{y} = \frac{A_1 y_1 + A_2 y_2}{A_1 + A_2}$$

=159.1 mm

The transformed moment of inertia

$$I_{tr} = \left[I_G + Ad^2 \right]_{Concrete} + \left[Ad^2 \right]_{Steel}$$

= 369×10^6 mm^4

The stress at the extreme tension fiber is then calculated

$$f_{ct} = \frac{My_b}{I_{tr}}$$

= 6.1 N/mm^2

The stress in the steel at this point is calculated

$$f_s = \frac{My_b}{I_{tr}} \eta$$

= $6.1 \times 4.13 = 25.18$ N/mm^2

Deflections

The deflection at the centerline of the high strength concrete beam HSC1 at load 40 kN.

$$\Delta_{max} = \frac{Pa}{24EI_{tr}}(3l^2 - 4a^2)$$

= 0.65 mm

Loads

The load at first cracking

$$f_{ct} = \frac{My_b}{I_{tr}}$$

6.1 N/mm^2 = [P× 800mm × (300mm-159.1mm)]/ 369×10^6 mm^4

P=20,000 N

Appendix B

Design of a transfer beam column joint to ACI 352

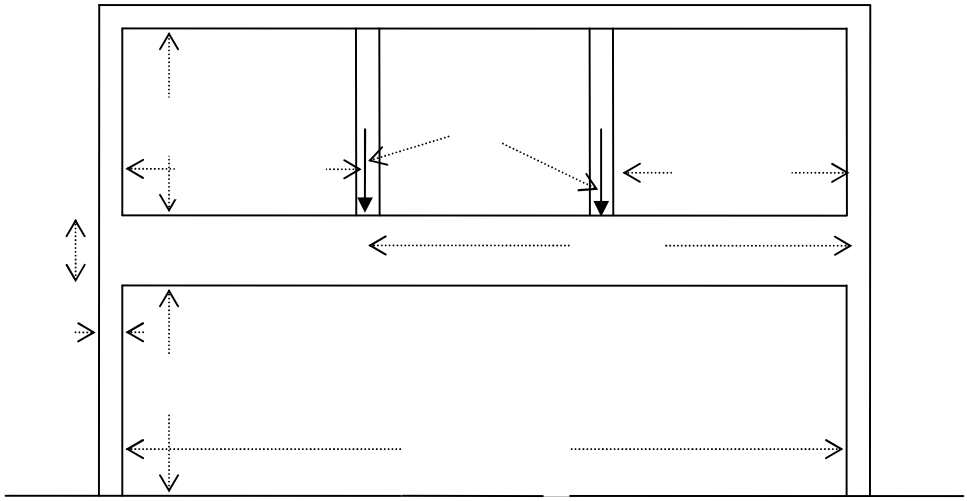

Figure B-1: A commercial or industrial RC frame with open industrial space at ground floor and office on the first floor. The frame is repeated at 4m spacing designed with spandrel beams in between frames.

The structure represent a typical ground floor column free show room or industrial space for fork lift manoeuvre with 2 columns at 5m spacing supported by a 900X130 mm transfer beam.

The perimeter columns have cross section of 300X150 mm.

First live office loading is 3 kN/$m^{2.}$

Load on the transfer beam /m from ground floor

The loads are not factored.

W= L.L (4 X 3) +D.L(4 X 1.5)+ Self wt of beam (1 X.0.225) X2.8 = 18.6 kN

The loading on the roof is 0.75 kN/m2 . The load on each internal column is

P=P1= P2= L.L(5 X 4 X 0.75) + D.L(5 X 4 X 1.5)=45 kN

Moment developing at the end of the transfer beam

$= Pa^2b/l^2 + Pab^2/l^2 + W l^2/12$

=[(45 X 10 X 25) / (15 X 15)] + [(45 X 100 X 5) / (15 X 15)]+[(18.6 X 15 X 15) / 12]

=50+100+348= 498 kNm

From Whitney's concrete stress block

$Mn= A_s f_y (d - xw/2)$ where xw = 0.54 d

As = 498 X 106/[460 X (950 -256)]=1562mm^2 or ≈ 3T26 or 1593 mm^2

For type 1 joint α=1

Tn=As.α. fy = 1593 X 1 X 460= 733 kN

Consider the free body diagram with l_{pc}= 4500mm

$V_{col}= M_n / 4500$ = 498700/4500= 110.8 kN

V_u (joint) = 733- 110= 622 kN

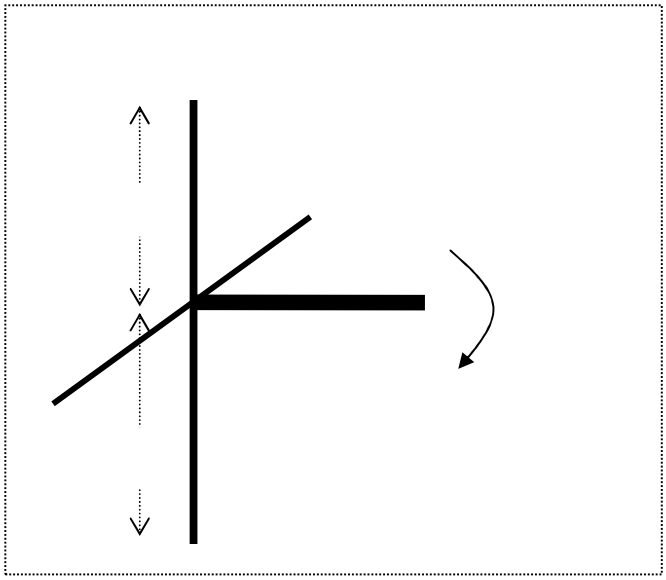

Figure B-2: Exterior joint - Classification of joints - ACI 352 (γ = 20 Value for type - 1 joints)

Check the shear strength of the joint:

Using b_j =(110+300)/2= 205 ≤ 130+150 . The thickness of the joint is, h_{col}, is equal to the column dimension parallel to the shear force in the joint. Use h_{col} = 400mm .

For an exterior joint, all the beams are at least 75% as wide as the corresponding column face and the shallowest beam is at least 75% depth of the deepest beam. Therefore for an exterior joint γ=20

fc' ≤42 MPa

Vn=0.083 X 20 X 262 X 300 X √42 =845 kN

must satisfy the normal strength requirement that $\varphi Vn \geq Vu$ where φ= 0.75 and V_u =622kN

φVn=633.75>622 OK

Design the column reinforcement, an initial design from Joint Institution Manual (IStructE & ICE), 'Manual for the design of reinforced concrete building structures'. section 3.7.4, table 5.

The load from dead and live load is 1251 kN, multiply by a factor of 2 as code recommends. Therefore, each column has 1251 kN loading. Table 5 recommends 1% area of steel or 900mm^2 for 300 X 300 column for 1213 kN loading. Therefore 4T20 in the corners.

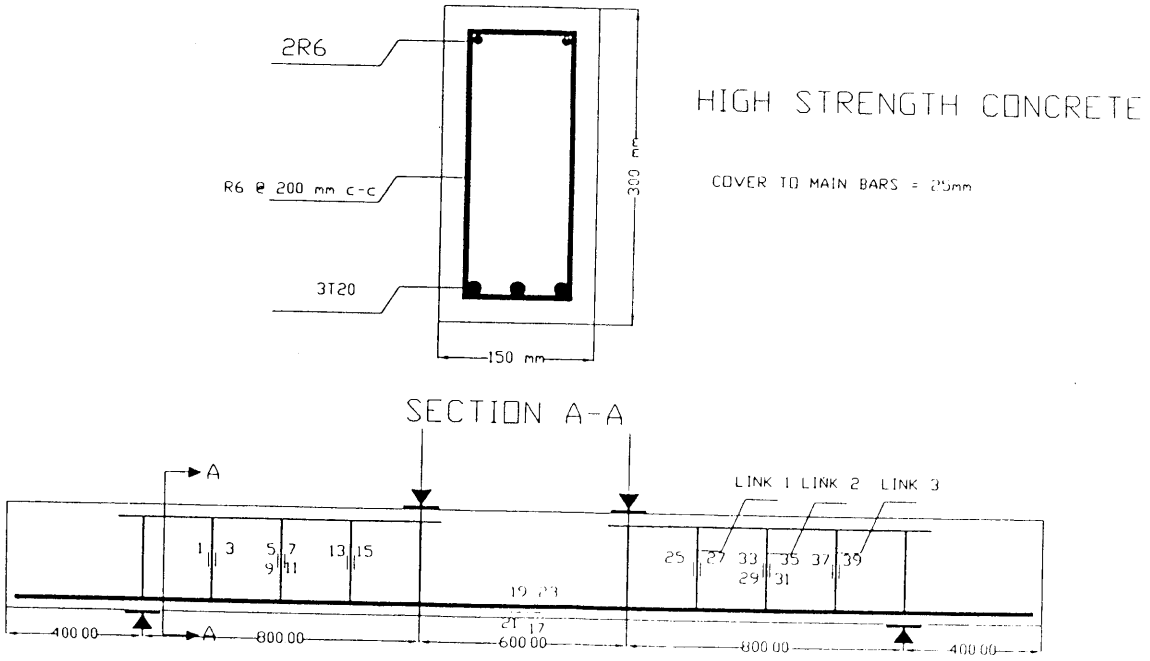

Beam HSC1

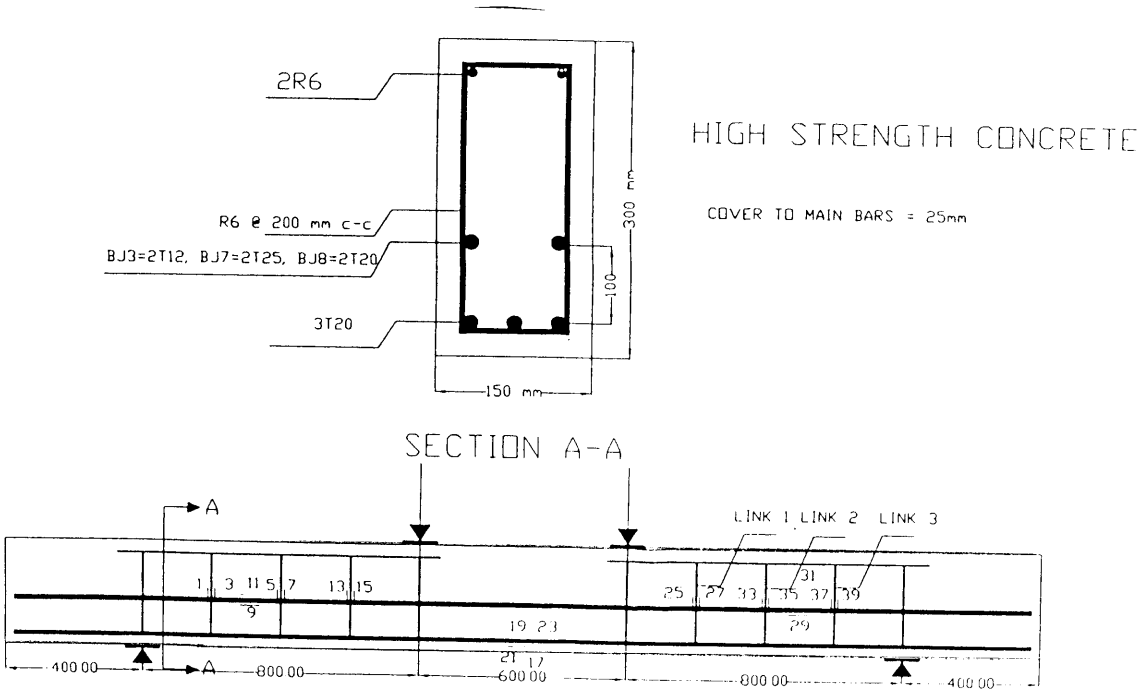

Beams HSC2, HSC3 and HSC4

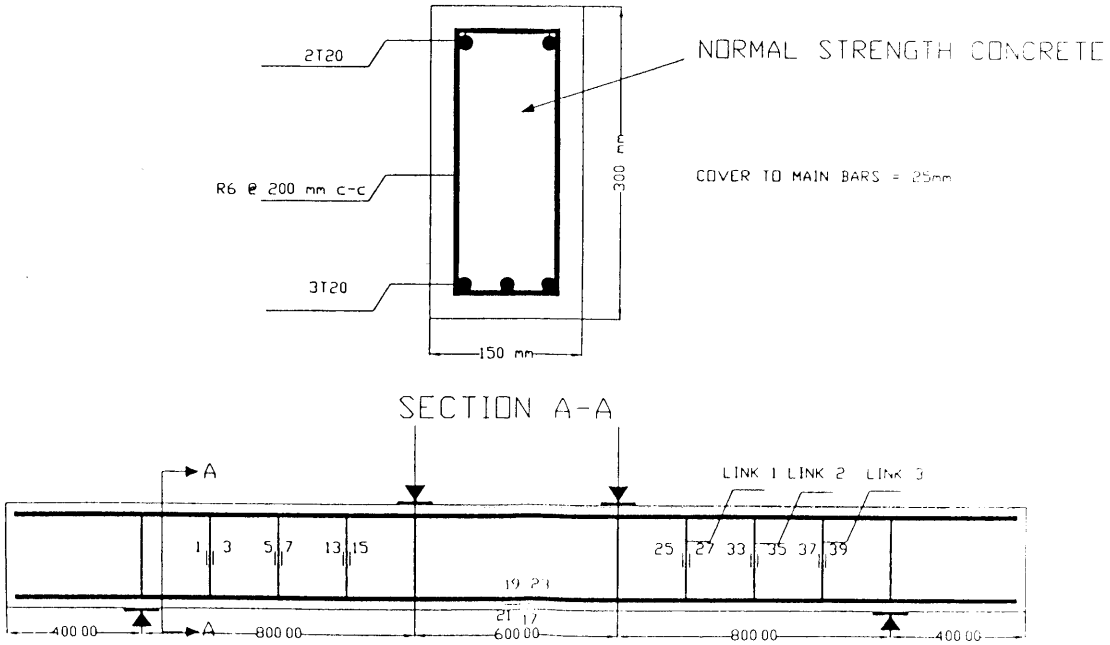

Beam NSC1

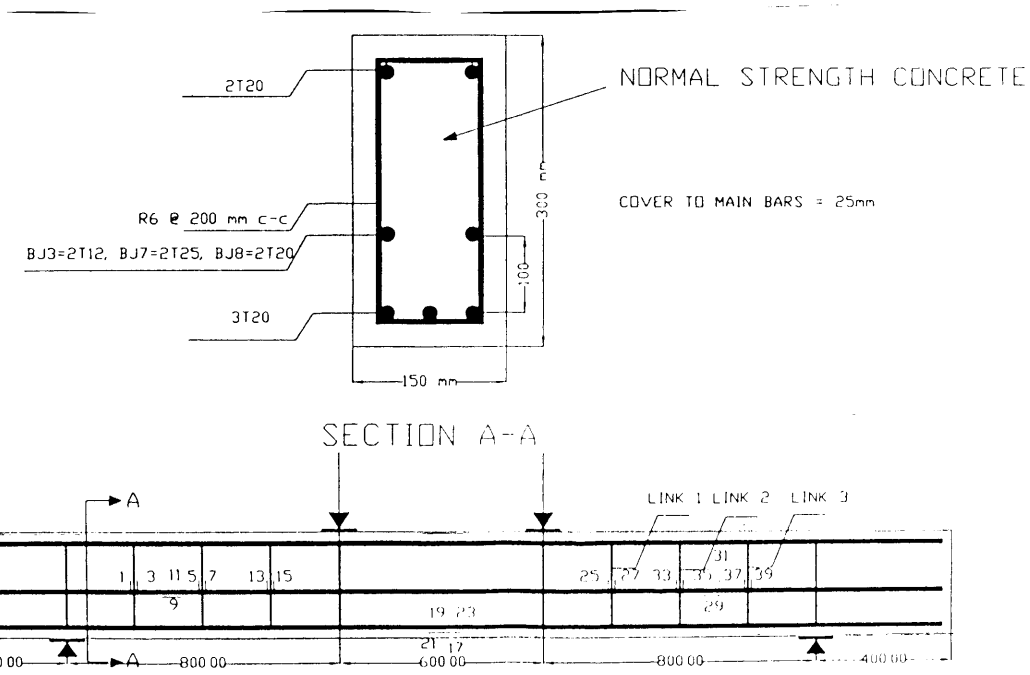

Beams NSC2, NSC3 and NSC4

LOAD	BJ1	BJ2	HSC2	HSC1	NSC2	NSC3	HSC4	HSC3	NSC4	NSC1
0	0.0	0.0	0.0	0.0	0.0	0.0	0.0	0.0	0.0	0.0
20	0.4	0.3	0.3	0.3	0.4	0.4	0.4	0.4	0.4	0.4
40	1.0	1.0	1.0	1.0	1.1	1.1	1.0	1.1	0.9	0.9
60	1.8	2.0	1.7	1.7	1.8	1.8	1.7	1.8	1.5	1.7
80	2.6	2.9	2.4	2.5	2.6	2.5	2.3	2.4	2.1	2.5
100	3.4	3.9	3.1	3.2	3.4	3.2	3.0	3.1	2.7	3.3
120	4.5		3.9	4.6	4.3	4.1	3.6	3.8	3.4	4.4
140	5.5	FAILURE	4.6	FAILURE	5.3	5.0	4.2	4.5	4.1	5.8
150	6.0		5.5		6.1	5.4	4.6	4.8	5.0	6.9
160	6.5		6.0		6.6	5.9	4.9	5.2	5.7	FAILURE
170	7.1		6.5			6.6	5.6	6.2	6.0	
180	7.6		7.6			7.4	6.5	7.5	6.6	
190	8.2		8.4			8.4	7.5	8.1	7.9	
200	8.9		9.1		FAILURE	FAILURE	8.0	9.0	9.5	
210	9.5		9.9				8.7	9.6	FAILURE	
220	10.1						9.2	10.4		
230	12.0		FAILURE				9.9	11.0		
240	12.7						10.5	11.7		
250	FAILURE						11.6	12.5		
260							12.3			
270							13.2			
280								FAILURE		
290										
300							FAILURE			

LOAD (KN) & DEFLECTIONS (MM) OF BEAMS

Load (kn)	Gauge 1	Gauge 3	Gauge 5	Gauge 7	Gauge 13	Gauge 15
0	0.0	0.0	0.0	0.0	0.0	0.0
20	9.5	8.4	7.2	12.1	7.7	12.7
40	11.7	9.9	7.8	16.1	8.1	15.8
50	12.7	11.3	12.0	21.0	23.7	35.6
60	16.4	13.2	12.9	24.1	31.3	52.9
80	26.4	23.1	20.1	31.9	106.0	139.1
100	39.9	36.8	334.2	162.6	250.2	368.6
120	84.3	85.4	953.1	396.3	467.0	641.7
130	95.0	95.4	5085.1	2243.8	553.8	746.3
140	117.4	114.8	10727.0	9614.1	615.5	802.4
150	137.2	147.0	12212.0	9843.1	676.1	857.9
160	275.3	302.2	17033.0	14622.1	774.7	968.8
0	E1 Ovrld	E1 Ovrld	E1 Ovrld	12567.1	7249.6	6604.2

Load (kn)	Gauge 17	Gauge 19	Gauge 21	Gauge 23
0	0.0	0.0	0.0	0.0
20	62.3	86.5	78.4	104.4
40	174.9	240.8	212.1	281.6
50	265.9	370.4	332.6	439.5
60	349.3	482.2	435.0	573.9
80	509.1	696.6	638.2	829.9
100	643.9	915.6	836.1	1090.5
120	785.0	1129.7	1027.9	1344.2
130	853.3	1245.7	1130.5	1481.8
140	927.7	1354.1	1224.6	1611.2
150	981.5	1466.3	1319.5	1745.5
160	1024.6	1543.3	1381.0	1838.8
0	64.6	217.1	200.3	256.6

Load (kn)	Gauge 25	Gauge 27	Gauge 33	Gauge 35	Gauge 37	Gauge 39
0	0.0	0.0	0.0	0.0	0.0	0.0
20	10.3	10.6	13.9	14.6	12.4	12.7
40	15.6	17.4	19.3	21.3	18.1	17.9
50	27.1	25.5	26.4	28.8	20.5	21.5
60	33.4	25.1	35.2	36.2	25.0	24.8
80	58.4	55.4	73.5	61.0	36.8	36.2
100	164.6	161.3	296.0	279.8	42.8	46.1
120	276.7	263.2	1708.0	1031.9	70.5	86.8
130	308.4	295.5	4252.4	11185.4	119.1	144.5
140	347.7	336.8	3126.9	13826.4	522.6	535.6
150	463.7	480.5	3203.2	14735.4	750.1	738.3
160	803.4	842.2	2923.2	21732.4	1101.5	1082.1
0	256.5	589.6	3703.3	16805.4	9240.9	4025.2

Beam NSC1

Load (kn)	Gauge 1	Gauge 3	Gauge 5	Gauge 7	Gauge 13	Gauge 15	Gauge 17	Gauge 19	Gauge 23
0	0.0	0.0	0.0	0.0	0.0	0.0	0.0	0.0	0.0
10	10.4	11.4	11.9	12.7	11.3	6.7	48.4	40.1	34.2
20	11.7	12.9	14.1	14.9	12.0	0.3	102.7	82.2	73.4
30	11.8	14.0	14.4	15.9	14.8	1.1	203.8	131.4	125.5
40	13.3	17.2	16.5	18.5	15.8	1.6	337.2	211.6	195.8
50	18.0	22.2	22.2	24.5	20.2	4.5	463.4	297.8	276.2
60	20.3	24.4	22.9	25.2	65.9	33.2	593.3	382.0	356.6
70	23.8	27.3	27.7	29.1	128.5	72.9	712.6	458.6	431.8
80	27.5	30.3	34.2	30.4	225.9	84.8	838.6	537.6	509.8
90	32.0	34.4	43.5	36.6	339.1	112.2	968.1	625.6	591.0
100	37.5	37.3	55.8	48.5	444.5	143.8	1086.1	708.5	670.2
110	42.1	41.0	70.1	57.5	565.6	220.0	1162.4	799.7	755.8
120	36.9	36.0	88.9	73.2	664.8	293.9	1217.1	875.9	828.0
130	105.3	61.8	148.1	122.3	817.9	393.1	1309.2	970.0	920.0
140	174.7	95.8	173.1	144.5	901.2	432.5	1387.7	1037.2	984.4
150	534.0	303.5	381.8	351.7	1032.8	488.2	1468.3	1115.7	1063.4
160	755.4	502.5	593.4	582.8	1167.0	565.6	1548.0	1198.5	1150.9
170	939.9	606.6	706.4	675.1	1293.0	667.9	1625.2	1285.7	1234.4
180	1064.1	686.6	737.6	709.0	1434.7	756.0	1664.6	1363.8	1307.4
190	1119.7	765.9	1133.1	1034.7	2048.9	1332.6	1627.4	1367.4	1313.2
195	1155.8	847.7	5341.0	2543.8	10995.0	8973.3	1739.5	1491.5	1424.9
200	1214.9	908.4	9678.0	8448.0	12727.0	12136.3	1770.8	1527.6	1459.8
0	379.9	303.6	7966.7	7478.0	13474.0	12316.3	377.5	176.5	186.8

Load (kn)	Gauge 25	Gauge 27	Gauge 29	Gauge 31	Gauge 33	Gauge 35	Gauge 37	Gauge 39
0	0.0	0.0	0.0	0.0	0.0	0.0	0.0	0.0
10	9.7	10.9	8.8	11.9	9.7	9.1	8.8	10.1
20	11.2	13.3	15.4	16.0	11.2	10.2	10.3	12.
30	11.8	12.8	26.8	21.9	11.8	11.0	10.3	14.
40	13.9	11.2	44.1	31.5	13.9	12.1	12.3	17.
50	18.5	12.7	62.5	42.0	18.5	14.9	16.2	22.
60	17.7	13.0	75.7	46.6	17.7	12.8	17.0	24.
70	17.8	16.0	105.0	60.0	17.8	12.6	19.1	26.
80	26.7	20.5	138.6	90.4	26.7	24.4	20.1	27.
90	44.1	24.8	158.3	109.1	44.1	41.7	22.2	32.
100	54.6	31.9	1223.5	134.5	54.6	53.2	29.2	39.
110	70.5	39.7	1282.4	160.1	70.5	67.3	36.6	48.
120	100.7	52.5	1321.6	190.5	100.7	98.6	43.7	57.
130	343.7	156.0	1381.6	238.3	343.7	341.5	74.9	86.
140	416.4	193.9	1401.2	256.1	416.4	411.9	88.3	100.
150	974.8	342.9	1420.3	260.9	974.8	972.0	874.5	970.
160	1131.0	424.4	1428.9	259.7	1131.0	1109.9	1148.5	1300.
170	1355.8	499.0	1471.4	300.1	1355.8	1331.0	1348.1	1407.
180	1417.9	581.4	1520.3	348.4	1417.9	1531.5	1470.8	1459.
190	1378.3	689.4	1571.4	406.0	1378.3	1902.8	3766.2	3682.
195	11127.2	834.1	1678.0	502.7	11127.2	4998.2	12317.9	11855.
200	15091.2	910.7	1752.9	567.9	15091.2	2752.6	12878.9	12120.
0	7956.2	#VALUE!	2124.0	-1068.0	7956.2	#VALUE!	#VALUE!	6493.

Beam NSC2

Load (KN)	Gauge 1	Gauge 3	Gauge 5	Gauge 7	Gauge 9	Gauge 11	Gauge 13	Gauge 15
0	0.0	0.0	0.0	0.0	0.0	0.0	0.0	0.0
10	4.2	6.5	8.1	5.1	7.2	9.2	5.1	3.9
20	5.0	6.9	7.6	4.7	11.8	18.0	6.0	3.8
30	6.2	8.6	8.9	4.9	17.2	27.9	8.8	7.0
40	6.8	9.9	14.2	9.0	21.1	39.5	14.5	8.4
60	12.0	15.9	14.3	11.7	37.3	75.1	15.4	-0.9
80	13.9	19.0	12.0	10.7	79.0	126.5	25.8	-7.0
100	11.7	19.3	21.6	21.3	146.3	162.5	58.6	40.3
120	9.6	19.2	60.8	62.9	245.8	208.2	80.1	72.4
140	48.4	37.2	150.4	184.8	333.0	232.6	136.0	128.1
160	695.5	567.2	229.4	262.3	434.8	236.6	349.7	290.6
170	1000.1	797.2	379.6	400.5	479.3	238.1	638.7	524.7
180	1084.5	859.4	552.0	556.7	530.8	271.3	841.2	712.8
190	1110.9	877.2	950.6	739.6	1120.8	137.2	1008.3	931.3
200	1125.3	897.9	1838.0	1147.1	1625.0	-229.8	1012.9	1314.4
0	310.0	226.4	647.0	552.4	1001.8	-535.3	53.7	336.6

Load (KN)	Gauge 25	Gauge 27	Gauge 29	Gauge 31	Gauge 33	Gauge 35	Gauge 37	Gauge 39
0	0.0	0.0	0.0	0.0	0.0	0.0	0.0	0.0
10	3.5	3.3	11.5	6.4	5.0	5.1	4.1	5.1
20	6.2	4.4	15.1	12.5	4.9	5.7	5.2	5.2
30	5.5	3.0	22.3	23.0	10.7	11.9	4.4	4.8
40	3.8	0.4	33.8	35.1	13.2	14.7	7.1	6.9
60	13.4	5.3	68.2	71.7	28.7	31.3	11.2	15.6
80	8.8	20.2	101.5	130.8	65.5	59.5	15.5	21.7
100	14.2	60.1	133.7	240.7	118.4	117.8	12.7	20.9
120	44.3	114.4	148.8	347.7	234.2	254.8	22.8	45.0
140	84.4	166.7	199.3	395.8	299.1	320.2	101.2	183.3
160	149.5	236.2	383.9	420.2	441.9	472.8	415.3	479.6
170	247.4	321.4	665.9	422.6	931.6	1078.6	646.9	722.1
180	428.1	484.5	793.1	438.7	1029.0	1208.7	703.0	784.8
190	673.9	680.8	962.3	418.3	1135.8	1504.2	758.4	848.3
200	1018.4	947.4	571.4	857.5	11628.5	12689.4	988.9	1139.1
0	1726.8	-583.1	-970.7	783.5	#VALUE!	#VALUE!	25536.1	#VALUE!

Load (KN)	Gauge 17	Gauge 19	Gauge 21	Gauge 23
0	0.0	0.0	0.0	0.0
10	43.9	44.3	63.6	44.5
20	93.0	100.3	122.3	101.2
30	165.8	183.9	199.6	186.9
40	259.7	284.0	292.4	295.3
60	430.6	468.2	494.1	499.7
80	606.2	655.6	691.5	707.8
100	783.5	846.4	887.2	921.0
120	971.0	1047.7	1091.4	1143.6
140	1149.4	1247.5	1288.6	1359.5
160	1323.5	1440.0	1476.8	1568.9
170	1423.0	1558.2	1590.7	1696.8
180	1505.5	1649.2	1681.9	1797.8
190	1582.7	1745.3	1777.4	1903.0
200	1652.9	1833.0	1857.8	1997.8
0	210.0	223.3	292.2	246.5

Beam NSC3

Load (kn)	Gauge 1	Gauge 3	Gauge 5	Gauge 7	Gauge 9	Gauge 11	Gauge 13	Gauge 15
0	0	0	0	0	0	0	0	0
20	21.3	22.2	22.7	27.6	38.3	41.4	28.2	24.4
40	25.7	27	24.6	31.1	57.1	65.7	31.5	27.6
60	29.1	28.9	28	35.7	79.4	98.1	23.6	22.3
80	33.2	34.5	34.5	42.2	105.8	143.7	29.1	23.5
100	37.4	40.5	57.2	73	147.2	219.9	55.1	37.8
120	38.9	42.2	105.7	112.2	196.1	309.3	89.1	57.1
140	60.3	54.1	191.5	207.7	248.3	383.6	126.8	82.9
160	114.3	80.7	507.5	559.1	430.5	451.7	267.6	173
170	175	129.6	1103.7	1193.1	518.4	623	574.8	413.7
180	236.8	183.7	1399.6	1528.4	516.8	727.1	787.1	574.9
190	384	312.7	1540.9	1556.8	487.8	859.8	913.9	675.6
200	1434.3	1087.4	3051.3	4241.7	337.8	1063.2	962.7	718.7
210	1480.4	1116.2	17337.3	16385.8	26.1	1533.7	985.7	741.8
0	-175.8	-213.4	14970.3	13477.8	-208.4	872.8	532.1	356.1

Load (kn)	Gauge 17	Gauge 19	Gauge 21	Gauge 23
0	0	0	0	0
20	97.5	94.7	93	100.2
40	236.1	247.1	237	258.5
60	410	442.2	391.5	447.5
80	584.2	640.7	554.8	639
100	754.3	834.5	716.6	817.6
120	933.5	1034.9	887.8	998.2
140	1103.4	1229.1	1044.4	1166.4
160	1283.5	1431.2	1208.8	1331.3
170	1393.9	1549.6	1295.5	1399.5
180	1486.6	1649.8	1375.4	1466.7
190	1577.5	1746.4	1449.7	1536.7
200	1653.7	1830.4	1518.5	1606.7
210	1751.9	1937.5	1595.5	1687.1
0	195.4	208	172.3	43.5

Load (kn)	Gauge 25	Gauge 27	Gauge 29	Gauge 31	Gauge 33	Gauge 35	Gauge 37	Gauge 39
0	0	0	0	0	0	0	0	0
20	26	21.3	52	32.5	21.9	26.9	26.2	32.7
40	29.8	22.2	61	50	24	32.1	30.5	42.3
60	35.6	24.6	99	79.5	29.5	38.9	33.6	48.7
80	53.7	44.4	138	136.5	33.7	44.6	37.2	50.2
100	190.6	83.2	210	198.3	56.8	66.1	46.2	58.9
120	428	215.5	304	278.4	167	120.1	55.4	61.3
140	661.1	389.9	399	334.3	345.3	213.7	76.9	65.6
160	1043.2	692.6	570	348.5	722	499.9	224.3	427.9
170	1209.7	885.2	804	333.1	1096.1	853	446.9	751.9
180	1209.3	1082.7	1064	279.9	1340.4	1083.8	723.1	1164
190	1259.3	1150.3	1238	242.6	1480.5	1318.7	959.6	1539.1
200	1372.3	1308.7	1251	299.3	1411.3	1472.9	1076.2	1615.6
210	2109.5	1852.5	601	1041.4	14824.5	7082.2	1176.2	1662.5
0	3780.1	3613.4	-351	650.6	E1 Ovrld	E1 Ovrld	1070.9	13517.2

Beam NSC4

Load (kn)	Gauge 1	Gauge 3	Gauge 5	Gauge 7	Gauge 9	Gauge 11	Gauge 13	Gauge 15
0	0.0	0.0	0.0	0.0	0.0	0.0	0.0	0.0
20	7.1	5.6	6.2	8.5	6.7	7.0	3.7	4.6
40	7.6	6.8	10.8	11.9	8.9	8.9	20.5	21.6
60	27.2	28.2	41.7	51.8	37.4	50.0	33.0	18.8
80	42.5	45.6	70.6	88.5	63.3	62.7	61.0	52.1
100	59.2	64.6	160.1	218.5	108.4	104.0	483.9	287.1
120	156.9	153.8	2469.2	3104.3	2943.0	5091.9	913.3	1483.8
130	695.3	715.4	13157.9	833.0	17398.4	1350.9	888.6	1501.8
0	701.7	731.1	9894.9	1120.8	13789.4	2293.8	322.1	356.0

Load (kn)	Gauge 17	Gauge 19	Gauge 21	Gauge 23
0	0	0	0	0
20	68.6	67.9	67.2	74.9
40	267	235.3	232.9	246
60	537.2	487	551.7	557.6
80	774.2	701.7	803.5	825.9
100	987.2	893.4	1027.8	1034.4
120	1186.5	1074.6	1226.4	1230.8
130	1305.7	1127.7	1344.1	1371.3
0	317.2	281.6	314.9	337.4

Load (kn)	Gauge25	Gauge27	Gauge29	Gauge31	Gauge33	Gauge35	Gauge37	Gauge39
0	0.0	0.0	0.0	0.0	0.0	0.0	0.0	0.0
20	4.6	8.3	10.0	7.6	6.8	7.1	6.4	5.9
40	9.8	13.4	9.0	10.0	7.7	9.1	7.8	8.6
60	83.7	84.0	52.0	48.4	42.4	44.2	30.4	25.8
80	143.0	175.1	79.0	52.5	78.6	48.2	44.9	38.9
100	254.5	355.9	167.0	137.4	133.3	143.6	79.5	51.7
120	348.3	464.2	1053.0	1021.8	794.8	799.0	98.7	91.0
130	334.4	448.4	18897.0	4842.3	8830.5	1281.2	783.2	788.0

Beam HSC1

Load (KN)	Gauge 1	Gauge 3	Gauge 5	Gauge 7	Gauge 9	Gauge 11	Gauge 13	Gauge 15
0	0.0	0.0	0.0	0.0	0.0	0.0	0.0	0.0
20	-0.2	3.4	2.4	4.1	16.9	14.6	5.9	6.0
40	0.2	5.2	2.3	6.7	36.2	29.9	30.1	27.6
60	2.6	15.3	30.3	45.8	192.2	127.7	48.4	89.1
80	13.1	21.7	60.3	75.6	289.7	179.9	74.9	113.6
100	22.9	32.8	124.5	125.7	417.0	245.5	117.0	124.6
110	41.6	51.9	162.3	178.9	469.4	272.5	172.3	163.9
120	49.2	59.5	179.1	213.2	470.2	265.5	202.3	189.2
130	62.3	66.9	191.7	226.2	467.7	259.4	239.0	220.3
140	78.7	95.0	94.9	227.6	481.8	265.9	280.5	262.3
150	98.6	88.4	211.1	243.1	493.9	273.7	326.6	315.3
160	157.4	121.5	226.4	257.8	508.3	284.4	363.6	357.9
170	1384.9	958.9	375.8	383.6	519.5	280.5	407.9	408.8
180	1621.6	1109.9	422.9	427.7	532.2	286.1	454.4	462.8
190	2076.1	1282.5	487.4	466.1	520.7	394.4	1519.4	1780.3
200	2538.4	1335.7	547.0	519.7	575.3	473.5	1681.6	1936.4
210	4398.4	1620.7	654.5	639.4	642.4	563.6	1755.5	1874.2
220	6535.3	2637.1	773.9	761.8	743.0	687.0	1773.6	1822.5
230	7916.4	3936.5	1065.4	1030.2	1090.1	1285.4	1796.4	1960.3
240	7891.4	4018.7	1246.6	1180.0	1257.2	2360.2	2186.1	2762.2
250	7950.4	4195.4	1299.2	1233.6	1280.7	2580.2	5942.3	6399.1
260	8107.4	4475.9	1349.5	1287.7	1312.0	2754.5	8830.9	4748.6
0	6647.0	2901.9	288.2	271.0	411.2	999.7	9599.9	3712.4

Load (KN)	Gauge 17	Gauge 19	Gauge 21	Gauge 23
0	0.0	0.0	0.0	0.0
20	75.9	76.7	85.7	74.5
40	237.8	252.8	265.5	231.1
60	520.5	502.8	581.6	476.0
80	725.8	704.3	811.8	679.6
100	902.4	883.3	1012.0	869.0
110	1003.0	979.7	1124.6	974.1
120	1103.9	1066.7	1243.1	1072.3
130	1200.1	1152.2	1352.3	1169.2
140	1298.5	1238.4	1459.3	1267.6
150	1391.5	1330.4	1588.7	1368.6
160	1486.4	1420.6	1674.4	1466.1
170	1581.3	1514.8	1783.3	1570.7
180	1678.0	1608.9	1893.5	1673.4
190	1761.7	1687.4	1985.5	1757.5
200	1856.0	1777.3	2094.8	1855.7
210	1942.9	1856.6	2193.5	1940.6
220	2035.5	1941.7	2296.5	2029.1
230	2116.0	2013.9	2382.7	2102.2
240	2220.4	2106.0	2495.1	2194.4
250	2315.3	2189.0	2598.0	2279.2
260	2401.2	2262.4	2684.5	2355.0
0	470.6	416.1	481.1	431.6

d (KN)	G No25uE	G No27uE	G No29uE	G No31uE	G No33uE	G No35uE	G No37uE
0	0.1	0.7	0	0	0	0	0
20	1.8	2.3	76	10.7	2.5	1.1	2.5
40	40.2	11.9	92	23.2	4.7	1.6	5.1
60	46.6	23.6	259	110.2	37.4	26.3	14
80	56.5	67.7	408	221.7	53.3	37.9	23.3
100	92.3	139.7	573	367.5	66.1	89.2	35.2
110	143.5	185.3	678	548.3	79.2	145.7	49.2
120	222.8	242.4	747	619.4	106.1	181.7	52
130	361.9	337.4	801	650.2	143.2	221.7	48.9
140	548.2	499	799	618.7	231.7	294.2	121.3
150	870.6	753	821	594.3	267.3	329.4	211.1
160	1018.7	895.8	838	596.5	276.5	340.1	879.5
170	1176.9	1057	889	619	285.5	349.9	1015.8
180	1353.5	1260.5	917	647.3	300.8	366.5	1090.2
190	1551.4	1496.7	980	677.4	337.5	410.9	1171.4
200	1572.2	1534.5	1035	698.9	616.3	730.5	1244.5
210	1865.2	1916.8	2779	549.7	11919	12716	1238.8
220	1959.1	2204.6	2955	466.9	12226	12947	1256.7
230	2041.8	2187.7	3084	444.8	12441	13078	1266.1
240	3249	2230.1	3199	402.4	13331	14200	1283.5
250	3565	9912	3297	384.7	14914	16044	1301.4
260	3065.5	15708	3416	423.5	16335	17743	1329.3

Beam HSC2

Load (kn)	Gauge 1	Gauge 3	Gauge 5	Gauge 9	Gauge 11	Gauge 13	Gauge 15
0.0	0.0	0.0	0.0	0.0	0.0	0.0	0.0
20.0	6.0	8.5	6.8	12.0	19.2	6.9	6.9
40.0	5.3	8.8	7.6	26.2	47.7	49.3	42.2
60.0	8.4	14.2	15.9	88.9	153.7	91.2	85.4
80.0	9.4	15.5	12.1	128.4	217.3	128.7	120.7
100.0	2.5	9.9	-4.7	149.3	285.7	141.1	144.6
120.0	15.7	25.2	0.4	188.7	345.7	183.6	207.5
140.0	31.7	36.9	31.2	212.8	419.3	251.8	312.0
160.0	107.6	96.2	69.5	227.6	448.7	369.8	516.0
180.0	126.8	152.6	98.3	289.6	484.3	569.5	870.0
200.0	182.3	212.3	318.1	1422.1	214.5	871.2	1101.3
210.0	209.8	250.3	1432.5	1561.1	186.8	912.1	1136.6
220.0	732.2	1036.4	4250.0	904.6	1342.3	1035.2	1326.1
230.0	762.7	1059.1	9773.8	789.5	1539.0	1086.7	1387.6
240.0	804.7	1085.4	11039.8	744.7	1619.3	1143.9	1481.2
250.0	877.1	1107.2	11143.8	697.9	1745.2	1220.0	1592.7
260.0	1423.8	1154.1	12366.8	606.7	1819.9	1321.0	1752.1
270.0	1622.6	1189.7	13072.8	579.9	1879.8	E1 Ovrld	1928.7
280.0	1795.7	1209.7	13678.8	953.3	1658.4	E1 Ovrld	2759.0
0.0	877.2	436.1	7259.7	358.6	10.1	E1 Ovrld	2909.8

Load (kn)	Gauge 17	Gauge 19	Gauge 21	Gauge 23
0	0	0	0	0
20	68.3	79.2	77.9	87.7
40	315.9	244.1	351.8	320.2
60	510.3	434.1	556.4	532.8
80	687.1	708.8	739.1	762.1
100	825.8	915.7	897.6	968
120	991.2	1134.5	1078.9	1182.8
140	1145.1	1335.3	1249.5	1385.8
160	1296.1	1525	1414.5	1578.4
180	1450.6	1722.8	1586.3	1781.6
200	1604.8	1921.7	1757.1	1985.1
210	1679.7	2017.7	1842	2084.7
220	1749.9	2107.5	1918.4	2178.6
230	1820.7	2200.1	1999.2	2271
240	1894.6	2296.1	2080.6	2367.5
250	1969.6	2395.1	2166.9	2466.9
260	2033.2	2480	2240	2550.1
270	2104.6	2573.7	2320.8	2642.3
280	2171	2661.3	2394.7	2724.6
0	324.4	402.1	372.5	393.3

Load (kn)	Gauge 25	Gauge 27	Gauge 29	Gauge 31	Gauge 33	Gauge 35	Gauge 37	Gauge 39
0	0.0	0.0	0.0	0.0	0.0	0.0	0.0	0.0
20	7.2	8.4	86.0	16.5	8.8	9.9	12.3	11.7
40	26.2	15.0	99.0	33.9	8.5	8.7	12.8	11.5
60	49.1	8.4	117.0	66.2	15.5	15.7	17.3	15.4
80	44.7	26.0	170.0	171.7	35.1	28.9	19.4	17.7
100	55.0	37.5	209.0	242.5	33.9	30.3	22.9	18.9
120	79.9	65.7	275.0	332.5	35.0	45.3	34.3	38.5
140	96.0	92.2	292.0	474.3	44.1	88.8	40.9	51.1
160	113.4	110.8	447.0	634.9	97.0	152.4	60.5	114.3
180	127.8	128.1	523.0	757.8	186.2	239.4	321.5	402.6
200	428.1	423.4	625.0	838.3	14795.8	14599.2	2065.1	1819.7
210	457.7	453.2	660.0	2091.0	16600.8	16545.2	2093.7	2453.0
220	489.5	486.5	843.0	2397.8	21428.8	20530.2	6494.8	5768.4
230	525.7	522.9	1088.0	2619.5	2338.8	22875.2	9701.7	7547.3
240	692.1	682.1	1168.0	2784.7	26999.8	31240.2	9462.5	7755.3
250	804.4	816.0	1218.0	2931.7	27627.8	33841.2	10137.2	8552.3
260	927.7	968.0	1341.0	3090.2	28470.8	37571.2	E1 Ovrld	7616.3
270	1105.0	1162.5	1491.0	3240.7	29331.8	40478.2	E1 Ovrld	5817.8
280	1796.9	1725.8	1778.0	3380.5	31918.8	43613.2	E1 Ovrld	4745.1
0	894.7	14054.0	-1167.0	1149.4	E1 Ovrld	28446.2	E1 Ovrld	3204.0

Beam HSC3

Load (kn)	Gauge 1	Gauge 3	Gauge 5	Gauge 7	Gauge 9	Gauge 11	Gauge 15
0	0	0	0	0	0	0	0
20	-23.4	-19.1	-23.2	-20.4	-18.9	-12.9	-22.4
40	-22.3	-16.1	-22.9	-18.3	-7.4	2.3	-4.4
60	-20.8	-13.4	-8.1	9.1	24.6	69.9	10.3
80	-18.6	-9.3	-28.1	44.8	66.7	147	1.3
100	-20.4	-6.2	-64.3	75.2	100.3	211.3	-3.7
120	-9.8	-2.2	-110.8	91.7	148.4	294.6	5.7
140	0.8	11.4	-108	100.5	200.8	363.6	33.1
160	12.4	32.2	-70.1	126.2	253.6	430.2	66.8
180	32.7	77	-31.6	148.6	289.5	473.4	87.7
200	93.8	183.4	14.6	210.1	321.9	549.3	101.7
210	197.9	313.8	123.4	416.7	316.5	637.7	115.5
220	1979.2	1473.8	14783.5	14684.5	-391.7	1652.5	321.2
230	2170.8	1520	16371.5	16414.5	-506.1	1818.8	435.9
240	3137.2	1739.9	17115.5	17827.5	-616.9	1981.2	554.1
250	5007.8	1888.2	22802.5	23358.5	-621.2	2065.7	694.7
260	5687.2	1943.9	23023.5	23591.5	-661.2	2151.1	1426.7
270	6822.8	2029.1	23258.5	23902.5	-724.3	2245.7	2316.6
280	7840.4	2027.6	23632.5	24493.5	-770.3	2328	6447.5
290	10327.7	2486.6	25921.5	26578.5	-256.2	2273.7	E1 Ovrld
300	11020.7	5955.6	28535.5	30156.5	70.7	2302.2	16397.4
0	9014.7	4196	23706.5	23616.5	-125.8	945.6	E1 Ovrld

Load (kn)	Gauge 25	Gauge 27	Gauge 29	Gauge 31	Gauge 33	Gauge 35	Gauge 37	Gauge 39
0	0	0	0	0	0	0	0	0
20	-12.3	-11.3	-25700	1.6	-9.3	-12.6	-7.2	-14.3
40	-14.2	-14	-25660	21	-6.3	-10.4	0.4	-12.2
60	-3.1	-16.5	-25890	145.6	13.4	2.2	10.4	-8.5
80	2.3	-15	-25820	211.1	10.3	7	18.5	-6.1
100	15.6	-16.8	-25700	277.1	1	12.9	37.2	-5.5
120	56.4	10.5	-25640	342.6	3	44.5	48	-14.1
140	78.3	38.7	-25550	391.6	40.9	87.2	74.1	-14.6
160	87.2	56.1	-25570	456.8	77.8	138.2	123.4	-9.4
180	100.5	80.6	-26430	602.7	277.9	401.5	530.7	203.4
200	134.8	149.3	-33760	744.8	982.9	1166	1772.9	1088.8
210	515.3	704.5	-34020	1553.4	1968.4	2049.5	1798.9	1368.6
220	939.6	1197.4	-34670	2118	11214.1	15429.2	1921.8	1484.4
230	1201	1525.9	-34930	2372.3	17995.1	22022.2	2082.7	1739.4
240	1332.2	1849.7	-35110	2577	18201.1	22422.2	2245.4	1856.1
250	1266.1	2088.7	-35610	2769.7	18519.1	22805.2	2553.7	2011.9
260	1281.4	2145.1	-36500	2932.6	19264.1	23621.2	3150.2	2159.8
270	10616	15911.1	-38060	1731.3	23681.1	26450.2	4581.5	2325.1
280	11173	17694.1	-39230	1642	24854.1	26845.2	1002.3	9226
290	11619	19732.1	-40140	1571.7	24658.1	27304.2	-1960.8	13518
300	12130	22615.1	-56570	1465.5	22152.1	28928.2	-775.8	15873
0	E1 Ovrld	E1 Ovrld	-85860	740.9	13392.1	E1 Ovrld	-1344.5	23159

Load (kn)	Gauge 17	Gauge 19	Gauge 21	Gauge 23
0	0	0	0	0
20	54.8	59.2	48.3	70.7
40	341	304.5	270.3	355.1
60	500.6	528.6	440.5	569.2
80	645	731.6	585.4	788
100	790.4	910.7	732.3	979.3
120	957.9	1081.7	890.8	1122.9
140	1118.9	1260.6	1049.6	1290.5
160	1277.4	1434.5	1204.1	1454.9
180	1436.6	1607.4	1357.5	1624.8
200	1590.1	1775.2	1506.6	1792.7
210	1646.2	1835.8	1562.5	1855.1
220	1747.7	1944.9	1660.2	1965.7
230	1819.9	2021.4	1729.5	2043.7
240	1895.5	2103.5	1802.4	2127.1
250	1969.9	2186.7	1875.9	2210.5
260	2040.2	2263	1941.6	2287.7
270	2110.6	2341.1	2009.9	2364.8
280	2183.9	2423.3	2078.8	2447.7
290	2256.7	2504.9	2149.6	2529.7
300	2310.4	2565.2	2203.3	2592.5
0	315.8	382.3	316.9	352.4